

stis SOIL-CROP MODEL

Conceptual framework, equations and uses

N. Beaudoin, P. Lecharpentier, D. Ripoche-Wachter, L. Strullu,
B. Mary, J. Léonard, M. Launay, É. Justes, editors



STICS soil-crop model

Conceptual framework, equations and uses

Beaudoin N., Lecharpentier P., Ripoche-Wachter D.,
Strullu L., Mary B., Léonard J., Launay M., Justes É.

Collection Update Sciences & Technologies

Public policies and food systems
in Latin America
J.-F. Le Coq, C. Grisa, S. Guéneau,
P. Niederle, coord.
2022, 446 p.

La santé globale au prisme de l'analyse
des politiques publiques
S. Gardon, A. Gautier, G. Le Naour,
O. Faugère, R. Payre, coord.
2020, 248 p.

Méthodes d'investigation
de l'alimentation et des mangeurs
O. Lepiller, T. Fournier, N. Bricas,
M. Figuié, coord.
2021, 244 p.

Manger en ville
Regards socio-anthropologiques d'Afrique,
d'Amérique latine et d'Asie
A. Soula, C. Yount-André, O. Lepiller,
N. Bricas, J-P. Hassoun, coord.
2020, 172 p.

Eating in the city
Socio-anthropological perspectives
from Africa, Latin America and Asia
A. Soula, C. Yount-André, O. Lepiller,
N. Bricas, J-P. Hassoun, coord., D. Manley
(traduction)
2021, 158 p.

This book was funded with support from the French National Fund for Open Science
(project AAPFNSO2019OPEN-STICS-13999) and from CIRAD.

It is licenced under CC-by-NC-ND 4.0.

For all requests for permission to reproduce or translate,
please contact stics@inrae.fr

To cite this book:

Beaudoin N., Lecharpentier P., Ripoche-Wachter D., Strullu L., Mary B., Léonard J., Launay M., Justes É., eds. 2023. STICS soil-crop model. Conceptual framework, equations and uses, Versailles, éditions Quæ, 516 p.

Éditions Quæ
RD 10, 78026 Versailles Cedex
France
www.quae.com www.quae-open.com

© éditions Quæ, 2023

ISBN papier : 978-2-7592-3678-7
ISBN pdf : 978-2-7592-3679-4
ISBN ePub : 978-2-7592-3680-0

Contents

Foreword	7
<i>Peter Thorburn</i>	
Dedication	11
Preface	13
<i>Nicolas Beaudoin, Patrice Lecharpentier and Dominique Ripoche-Wachter</i>	
The first book	13
A new book based on an innovative approach	14
Project funding.....	16
English revision.....	16
Chapter 1. Introduction	17
<i>Dominique Ripoche-Wachter, Nicolas Beaudoin and Eric Justes</i>	
1.1 History.....	17
1.2 Purpose.....	19
1.3 The STICS open book	20
1.4 Human-machine interfaces.....	22
1.5 Tools for STICS users.....	24
Chapter 2. Overall description of the modelled system	31
<i>Nicolas Beaudoin, Dominique Ripoche-Wachter, Marie Launay, Eric Justes and Nadine Brisson</i>	
2.1 Conceptual framework.....	31
2.2 STICS validity domain	35
2.3 Relationship and priority between processes.....	39
2.4 Model genericity.....	41
2.5 Parameterised crop species	45
Chapter 3. Development	47
<i>Nadine Brisson, Iñaki García de Cortázar Atauri, Marie Launay and Dominique Ripoche-Wachter</i>	
3.1 The importance of phenology on crop development.....	47
3.2 Simulated events.....	48
3.3 Main development processes	50
3.4 Emergence and initiation of crop development and growth	57
Chapter 4. Shoot growth	67
<i>Loïc Strullu, Alain Mollier, Jean-Louis Durand and Nadine Brisson</i>	
4.1 Leaf dynamics.....	67
4.2 Radiation interception.....	78

4.3 Biomass production.....	78
4.4 Stress indices	81
Chapter 5. Root growth.....	93
<i>Nadine Brisson, Nicolas Beaudoin, Alain Mollier, Florent Chlebowski, Marie Launay and Loïc Strullu</i>	
5.1 Introduction	93
5.2 Vertical root growth.....	94
5.3 Root length density production and root distribution.....	98
5.4 Turnover of root biomass and N content allocation.....	111
5.5 Calculation of root density for water and nitrogen absorption.....	114
Chapter 6. Nitrogen acquisition by plants	119
<i>Bruno Mary, Fabien Ferchaud, Loïc Strullu and Nadine Brisson</i>	
6.1 Nitrogen uptake by plants.....	119
6.2 Nitrogen fixation by legumes.....	126
Chapter 7. Biomass and nitrogen partitioning.....	131
<i>Loïc Strullu, Jean-Louis Durand, Bruno Mary, Nicolas Beaudoin and Nadine Brisson</i>	
7.1 Introduction	131
7.2 Identified organs and compartments.....	132
7.3 Vegetative organs.....	134
7.4 Remobilisation of reserves	141
7.5 Harvested organs.....	145
7.6 Roots.....	145
7.7 Biomass and nitrogen partitioning after cut of forages	146
7.8 N and C inputs to the soil from perennial crops.....	147
Chapter 8. Yield formation	149
<i>Nadine Brisson, Iñaki García de Cortázar Atauri, Françoise Ruget and Benjamin Dumont</i>	
8.1 Quantitative yield.....	150
8.2 Yield quality.....	162
Chapter 9. Canopy microclimate	167
<i>Nadine Brisson, Marie Launay and Gaetan Louarn</i>	
9.1 Introduction	167
9.2 Radiation interception.....	170
9.3 Energy budget and crop temperature.....	178
9.4 Canopy moisture	194
9.5 Climate under shelter.....	195
9.6 Correcting temperatures for high altitude climates.....	197
Chapter 10. Transfers in soil: water, nitrate and heat fluxes	201
<i>Joël Léonard, Bruno Mary, Guillaume Jégo, Nicolas Beaudoin and Nadine Brisson</i>	
10.1 Water and nitrate fluxes	201
10.2 Soil temperature	208

10.3 Modifications of surface conditions that influence water and heat transfer	210
Chapter 11. Water balance	215
<i>Nadine Brisson, Remi Vezy, Dominique Ripoche-Wachter and Patrick Bertuzzi</i>	
11.1 Background and conceptual framework	215
11.2 Soil evaporation.....	216
11.3 Potential crop water requirements.....	221
11.4 Physical soil surface conditions.....	224
11.5 Plant transpiration and derived stresses	229
11.6 Water balance.....	231
Chapter 12. Carbon and nitrogen transformations in soil and balances	233
<i>Bruno Mary, Fabien Ferchaud, Hugues Clivot and Joël Léonard</i>	
12.1 Organic and mineral C-N pools.....	233
12.2 Decomposition and mineralisation of organic matter	235
12.3 Nitrification	243
12.4 Denitrification	248
12.5 N ₂ O emissions.....	252
12.6 Ammonia volatilisation.....	256
12.7 Carbon and nitrogen balances	259
Chapter 13. Soil-crop management effects	263
<i>Nadine Brisson, Bruno Mary and Dominique Ripoche-Wachter</i>	
13.1 Introduction	263
13.2 Crop management.....	263
13.3 Crop operations and soil tillage.....	269
13.4 Soil water management.....	271
13.5 Nitrogen and carbon inputs in soil	273
Chapter 14. Ways of STICS use	281
<i>Nicolas Beaudoin, Julie Constantin, Anne-Isabelle Graux, Gatién Falconnier, François Affholder, Françoise Ruget and Laurent Ruiz</i>	
14.1 Defining the unit of simulation (USM)	282
14.2 Rotations and long-term simulations.....	284
14.3 Simulation over large spatial scales.....	295
14.4 Simulation with coupled models.....	302
14.5 Typology of STICS uses.....	308
14.6 Perspectives for model capacity extension toward agroecology.....	319
Chapter 15. Tools for smart use of the standard STICS model version	323
<i>Dominique Ripoche, Christine Le Bas and Nadine Brisson</i>	
15.1 Driving use options	323
15.2 Strategy use options	327
15.3 Model formalism options.....	331

STICS soil-crop model

15.4 Parameterisation.....	348
15.5 Tools for users	379
Chapter 16. Model capacity extension methods.....	383
<i>Samuel Buis, Guillaume Jégo and Eric Casellas</i>	
16.1 Introduction	383
16.2 Evaluating model performances.....	383
16.3 Adapting STICS to a new crop or cultivar	387
16.4 Tools and rules for model coupling.....	401
References	405
Chapter 17. Definition of symbols	437
17.1 Definition of parameters	437
17.2 Definition of output variables	472
17.3 Internal variables definition	504
Authors list.....	515

Foreword

PETER THORBURN

Cropping systems are complicated non-linear biophysical systems, made complex by drivers that can't currently be predicted, namely climate and management actions executed in response to numerous socio-economic-political drivers. How do we, agricultural scientists, make sense of these systems and help land managers meet their goals and the goals of the societies in which they live? Models are tools used by agricultural scientists to make sense of these systems for over 100 years. This 2nd edition of the "STICS red book" represents an important milestone in the evolution of cropping systems models over that period.

Models have evolved from simple equations of plant growth in the early- and mid-1900's to today's sophisticated cropping systems models (Keating and Thorburn, 2018). An important part of this evolution was the "leap" from crop models, which coupled models of growth of a single crop to models of soil processes, to "cropping system" models in the 1990's. Cropping systems models allowed realistic representation of crop rotations and so reflected more closely the way farmers viewed and managed their fields. As these models developed descriptions of them were published: A landmark was papers by the major modelling groups around the world in 2003 Special Issue of the *European Journal of Agronomy* (Volume 18, Issues 3–4) followed by updates in a Thematic Issue of *Environmental Modelling and Software* in 2014 (Volume 62). Overviews of STICS were included in both (Bergez *et al.*, 2014; Brisson *et al.*, 2003). However, journal papers come with length restrictions and the "overviews" of complicated tools like cropping systems models in those papers are inadequate resources for new and experienced users alike. To me, the 1st edition of the "STICS red book" represented the commitment of the STICS team to support those users and expose the detail of the concepts, structures and approaches in the model to their modelling peers.

The 2nd edition of the "STICS red book" shows how comprehensive the STICS cropping systems model has become. Long gone are the days (for STICS and other models) when simulating a "crop-fallow-crop" rotation was challenging and novel. This is now one of the first tasks given to students learning cropping systems modelling. Developments since the 1st edition of the "STICS red book" include the capability to address contemporary issues such as climate change impacts and adaptation, greenhouse gas (GHG) emissions and abatement, organic agriculture, spatial application, and coupling with other models (e.g. of hydrology, pest and diseases, etc.).

Some of these applications have indirect or direct links with government policy. Modelling in this context raises new challenges for model development and application coming from the increased scrutiny to which the results will be subjected (Moore *et al.*, 2014). In agriculture, models started as tools of scientific enquiry. For example, C.T de Wit's interest in modelling was sparked by the desire to know the potential yield of a crop (Keating and Thorburn, 2018). The scrutiny of such modelling was likely limited to scientific peers who likely understood and accepted the strengths and weaknesses of modelling [although this was not always the case; e.g. Passioura (1996)]. As models developed and modellers started using them to inform farmers how to improve their management, scrutiny expanded to include farmer stakeholders as well as scientific peers. However, in many farmer interactions the model (or simulation output) acted as a "boundary object" facilitating discussions between the modeller and farmer (Jakku and Thorburn, 2010). The modeller explaining to the farmer the simulation results and their meaning built trust in the farmer of the modeller (provided the explanations made sense to the farmer!). This was/is essentially a social process and the technicalities of the model application itself were not necessarily scrutinised – if the farmer trusted the modeller, she trusted the model. Further, the farmer was free to change farm management, or not, as a result of these interactions, and solely bore the consequences of any changes (whether positive or negative).

In public policy applications, the link between the modeller and (government) stakeholder is likely to be much less personal than between modellers and farmers or scientific peers. Further, the application of the policy will often create "winners" and "losers". It is natural for the "losers" to want to scrutinise the technical basis behind the policy impacting them. A recent example of this is the examination of modelling behind water quality policy for agricultural lands in New Zealand (Johnson *et al.*, 2021). The "losers", and other stakeholders, will likely ask questions about the quality of the science in the model, whether that is accurately implemented in the code (and for the specific version of the model used in the analysis) and whether the model was competently run. Publication in the peer reviewed literature is often the means of assuring the quality of the science. As a community, however, cropping systems modellers have less established methods of quality assurance for implementation and running models than some other communities. For example, just for calibration of phenology, an important but limited part of running a crop model, there is a huge diversity of approaches used by different modellers (Seidel *et al.*, 2018) and there will be benefits from having some consistency in the approach (Wallach *et al.*, 2021). Conversely, ensuring accurate implementation of science in model code, i.e. having good software development practices, has received less attention across cropping systems models (Holzworth *et al.*, 2015). It is therefore significant that this issue has been discussed in the 2nd edition of the "STICS red book".

What does the future hold for cropping systems models? That question has been addressed in a number of recent papers (Jones *et al.*, 2017; Keating and Thorburn, 2018; Silva and Giller, 2020) and their conclusions do not need repeating here. However, those authors agree that application of cropping systems models will be an important methodology in meeting the coming challenges faced by food and agricultural systems and the models will need to be further improved and developed. That development will necessitate increasing efforts in collecting data to underpin those developments.

Data availability has always been both a limitation and driver of model development: in many respects cropping systems models have been created to overcome the scarcity of data. As we enter the age of “big data”, data will increasingly be available from remote and proximal sensors. That raises the questions of how those data will aid model development and/or application, and how will they affect the relevance of cropping systems modelling? An example of the first question is the potential use of multi-year high resolution data on crop growth and development to inversely parameterise models, e.g. soil water (He and Wang, 2019) or phenology (Araya *et al.*, 2016) parameters, aiding subsequent application. The implications of the second question are less clear. With rich data, possibly less biophysical detail is needed in a model if it is designed for use in conjunction with those data (e.g. Donohue *et al.*, 2018). Even further, there may be no role for a biophysical model at all. However, this “struggle” between models and data for prediction and understanding is not new. An example is the prediction of the optimum rates of nitrogen fertiliser in the mid-west corn-belt of USA. Large datasets have been gathered and developed into a tool for forecasting the Maximum Return to Nitrogen (Sawyer *et al.*, 2006; <http://cnrc.agron.iastate.edu>). However, recently developed approaches based on cropping systems modelling are showing promise in increasing accuracy of those forecasts (Puntel *et al.*, 2018). And, unlike purely data-driven approaches, the cause of a result from a cropping systems model can be tracked down and understood, enlightening the modeller and their stakeholders. Thus, it is unlikely there will be a single “winner” in the “struggle” between models and data for prediction. What is clear however, is that modelling systems (structure and software) will need to evolve to be easily applied with these new sources of data. The STICS model is well advanced down that development road and thus will remain relevant for a long time. I forecast there will be a 3rd edition of the “STICS Red Book” in the future!

Dedication

This book is dedicated to Nadine Brisson... Nadine Brisson was an ever-enthusiastic captain of the STICS ship and kept her sights set far ahead. With her intelligence, energy, insightfulness, determination and presence, she was always able to bring people on board with her who would remain ever faithful. Her vessel covered great distances, towards the shores of all the continents, sometimes facing storms along the way but continuing cheerfully and steadfastly onwards, committed to fulfilling her pledge: to give the scientific community a tool to help tackle food security, climate change, agroecological transition and other major challenges. She would have been so pleased with this new edition, which is available at zero cost (free numeric version), in keeping with the values of Open Science that she promoted before the movement had even emerged. Her life ended much too soon, but it was full of professional and personal adventures. She became fast friends with nearly everyone she met, and this is how we will forever remember her.

To Nadine

Au rendez-vous des bons copains
Y avait pas souvent de lapins
Quand l'un d'entre eux manquait a bord
C'est qu'il était mort
Oui, mais jamais, au grand jamais
Son trou dans l'eau n'se refermait
Cent ans après, coquin de sort
Il manquait encore

When to a rendezvous they'd go
Not often was there a no-show
If one of them was not on board,
it means he was no more
But never could their friendship dim
as the deep seas closed ever him
A hundred years after the peal,
they mourn him still

Source: LyricFind

Parolier : Georges Brassens (1964)

Extrait des paroles de Les Copains d'abord © Universal Music Publishing Group

Preface

*NICOLAS BEAUDOIN, PATRICE LECHARPENTIER
AND DOMINIQUE RIPOCHE-WACHTER*

►► The first book

In 2009, the initial project team produced the book *Conceptual Basis, Formalisations and Parameterization of the STICS Crop Model* (Brisson *et al.*, 2009), often referred as the ‘STICS Red Book’, published by Editions Quæ.

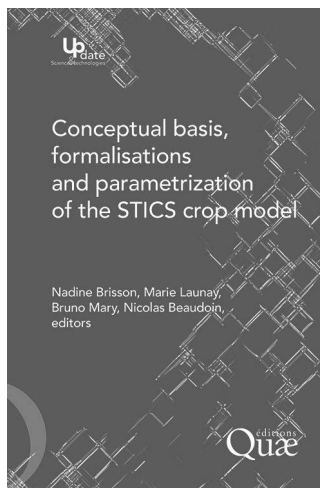


Figure 0.1. Cover of the first edition of the book.

The first edition of this book was written primarily by Nadine Brisson and was quite original in that synthesised scientific knowledge about cropping systems. The book covered the STICS model formalisms in an exhaustive way. But, more than ten years on, it was in need of a comprehensive update following the profound changes to the capabilities of the STICS model.

The following authors contributed to the original formalisations according to their affiliations:

– INRA (now INRAE): R. Antonioletti, N. Beaudoin, P. Bertuzzi, T. Boulard, N. Brisson, S. Buis, P. Burger, F. Bussi ere, Y.M. Cabidoche, P. Cellier, P. Debaeke,

F. Devienne-Barret, C. Durr, M. Duru, B. Gabrielle, I. García de Cortázar Atauri, C. Gary, F. Gastal, J.P. Gaudillère, S. Générumont, M. Guérif, G. Helloux, C. Hénault, B. Itier, M.H. Jeuffroy, E. Justes, M. Launay, S. Lebonvallet, G. Lemaire, B. Mary, T. Morvan, B. Nicolardot, B. Nicoullaud, H. Ozier-Lafontaine, L. Pagès, S. Recous, G. Richard, R. Roche, J. Roger-Estrade, F. Ruget, C. Salon, B. Seguin, J. Sierra, H. Sinoquet, R. Tournebize, C. Valancogne, A.S. Voisin

– ESA-Angers: Y. Crozat

– ARVALIS Institut du végétal: P. Gate

– CEMAGREF (now INRAE): B. Rebière, J. Tournebize, D. Zimmer

– CIRAD: F. Maraux

►► A new book based on an innovative approach

In 2019, ten years after the first book was published, the STICS project team decided to update it by integrating all the STICS skill extensions which have since been developed, evaluated and published. Several key changes deal with:

- the roles of carbon and nitrogen reserves in perennial crops,
- the biological destruction of mulch from crop residues,
- soil N₂O emissions,
- forage harvest management.

All of the STICS project team members worked together in a dynamic collaborative way to produce this new book.

Their work was supported by an innovative editorial approach, thanks to the involvement of Patrice Lecharpentier, who oversaw the feasibility study for the project, the design and finally the implementation of the writing workflow.

Another base part of the work is the bibliographic database management (under Zotero¹) the workflow is depending on. The STICS database organisation and maintenance was possible thanks to the support of Christine Le Bas.

This dynamic workflow aims to maintain a close link between changes in model formalisms (including associated data) and the book content with regular updates (Figure 0.2).

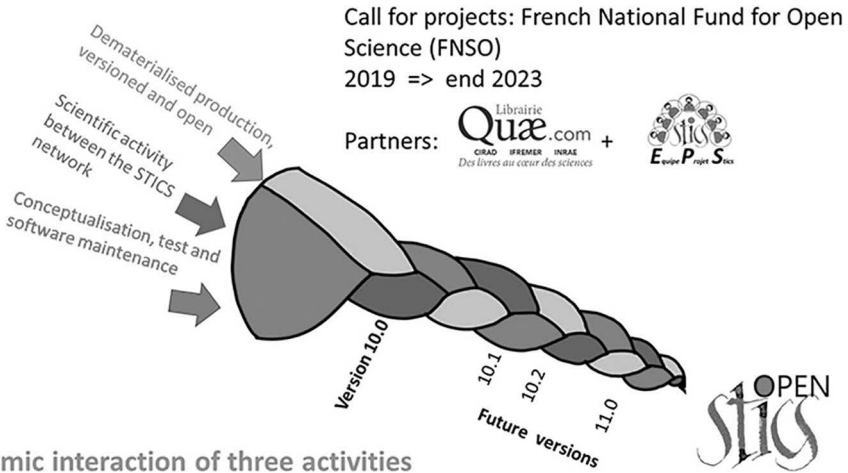
The collaborative dimension is crucial and based on the experience of the project team. The use of reproducible science tools is of the utmost importance.

The project, named 'Open-STICS', was selected for the 2019 French National Fund for Open Science (FNSO) call for projects, which is aimed at supporting such kind of open science editorial projects.

The main objectives were to offer the STICS user community a written, open access resource in English, with content that can be updated regularly according to the standard versions of the model.

Specific tools were chosen to produce the book in order to easily incorporate updates, including making corrections, adding new formalisms, modifying settings, extending application domains and adding new plants species.

1. <https://www.zotero.org/>



- Dynamic interaction of three activities
- Writing: collaborative approach

Figure 0.2. The workflow for the new book showing the dynamic interaction between the three activities of the STICS project team

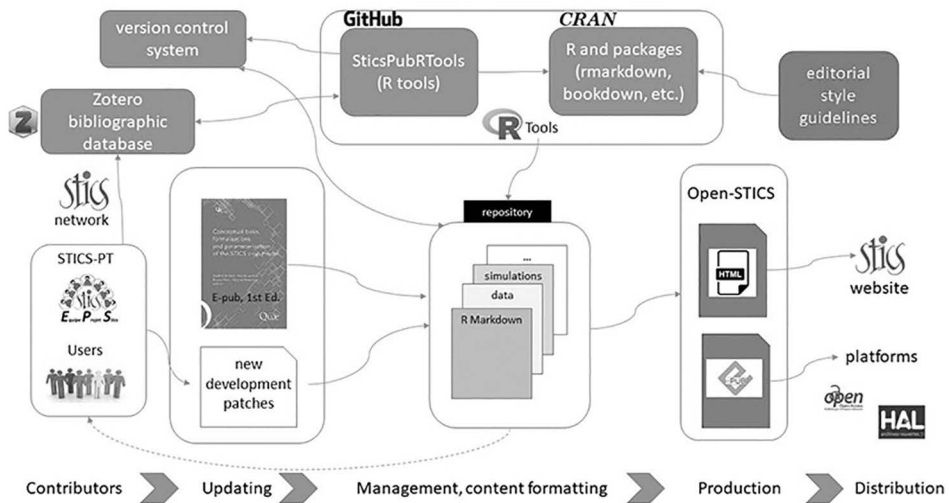


Figure 0.3. The technical workflow of the new book.

The book was produced using essentially R language (R Core Team, 2020) and a specific format for reproducible document writing, R Markdown (<https://rmarkdown.rstudio.com/>, Allaire *et al.*, 2021). The chosen configuration was based on the ‘bookdown’ package, which is designed for book or other document content formatting (<https://bookdown.org/yihui/bookdown>, ; Xie, 2016, 2021).

These packages are distributed under the GPLv3 licence and allow users to generate different output formats such as HTML, PDF, DOC, EPUB (Figure 0.3). The R Markdown format makes it easy to integrate lines of R code, for example, in order to generate illustrations (tables, graphs, etc.). Mathematical equations and literature references can be automatically formatted using specific syntaxes.

For a subset of these types of insertions and formatting, operations need additional R functions which have been developed separately from the packages used for this book (for equation implementation and plots), as well as data from simulations or observations, or which have been formatted in a specific way.

The book production is managed as a development project in the form of an RStudio project (RStudio Team, 2021, <https://www.rstudio.com/>). All necessary files (code, text and data) are managed using a version control system (Subversion, <https://subversion.apache.org/>) shared among all contributors (essentially STICS team members at the moment). This means that every author is able to maintain the content of the book project: they can save changes, get changes made by other authors, and finally produce the book or parts of it in different file formats. This package permits dynamic interaction between STICS book editions, scientific design activities and software maintenance (Figure 0.2).

▶▶ Project funding

This project was funded with the support of:

- **the French National Fund for Open Science (FNSO)**,
- **CIRAD**, and
- **the Agroecosystems Division of INRAE**.

▶▶ English revision

Teri Jones-Villeneuve (teri@jonesvilleneuve.com)

Throughout the revision process for the book, Teri offered helpful feedback by pointing out areas where additional clarity was needed and suggesting improvements. The entire STICS project team thanks her for her professionalism and are very grateful for this contribution to the book.

Chapter 1

Introduction

*DOMINIQUE RIPOCHE-WACHTER, NICOLAS BEAUDOIN
AND ERIC JUSTES*

REVIEWED BY: GUILLAUME JEGO AND PATRICE LECHARPENTIER

This introduction will outline the purpose and brief history of the STICS model, along with the general concepts. We will also discuss the collective dynamics of its development, evaluation and governance. Finally, we will introduce the different chapters of this book which describes the algorithms in the model. A list of user network services can be found at the end.

Some sections of this chapter come from the translation of the book chapter « Modélisation du fonctionnement des agro-écosystèmes: l'épopée STICS (Beaudoin *et al.* 2019), with the permission of QUAE Edition ».

►► 1.1 History

The model design started with a first meeting held in France in 1996, where the foundations of the key model principles were laid out. The aim was to create “a single model for different crops that integrated both specialist and generalist knowledge in order to be general, robust, simple, operational and flexible.” (Beaudoin *et al.*, 2019)

The specifications of STICS were co-developed by researchers and engineers from various disciplines in the fields of agronomy (*sensu lato*) and modelling, who recommended four main characteristics:

- A balance between the different compartments and interacting processes in the soil-plant-atmosphere system, in order to produce a generic soil-crop model, applicable to a wide variety of themes and contexts.
- Genericity of the plant functioning description, based on general ecophysiological concepts, guiding to the definition of a single model. The same basis applies to the simulation of soil functioning processes.
- Simple and uncomplicated input data, with easily accessible parameters that are not very sensitive to change of scale, which facilitates the model's operational use in real agricultural situations.
- Robustness of formalisms and their parameterisation, which ensures realism in a wide range of agro-environmental conditions, and including management practices.

An additional characteristic scalability has emerged over time. The original strategy was to work together to design a dynamic, functional, one-dimensional model, with a strong agro-environmental aim. This soil-crop model can perform simulations either at a plot scale (the model's aim) or at a macro-regional scale, but only in conjunction with other models or tools (e.g. software platforms).

STICS was developed at INRAE (formed following the merger of INRA and IRSTEA) in collaboration with other research and educational institutes such as the French agricultural research and cooperation organization CIRAD, the Graduate School-Ecole des Mines de Paris and the Laboratory for Sciences of Climate and Environment – LSCE, along with French professional institutes (ARVALIS, Terres Inovia, CTIFL, ITV, ITB, Agrotransfert), and few other partners.

The STICS model is open source (Licence CeCiILL C, v2.1, the French equivalent of a lesser general public license, or LGPL). Its code has been filed with the Agency for the Protection of Programs (APP), the European organisation for the protection of authors and publishers of digital creations, under the reference number: IDDN.FR.001.360007.000.S.C.2021.000.10000.

In the early STICS development stages, many well-known models were available (CERES: Ritchie and Otter (1985), ARCWHEAT: Weir *et al.* (1984), EPIC: Williams *et al.* (1989), SUCROS: van Keulen and Seligman (1987), among others) that were

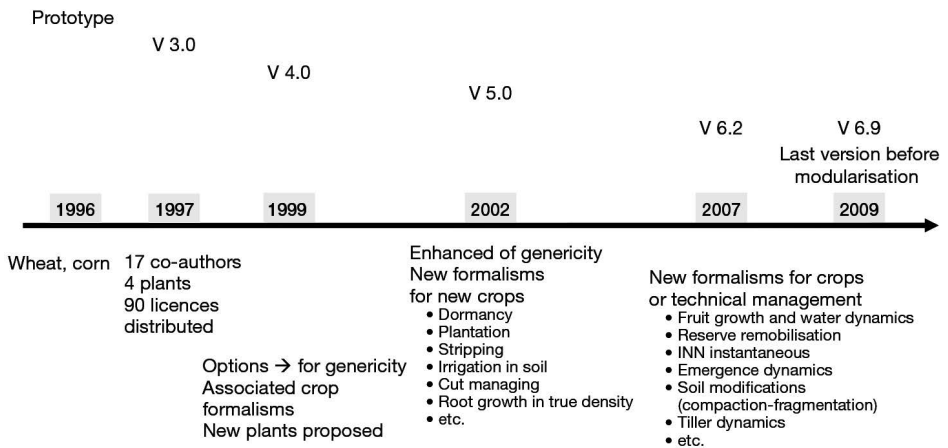


Figure 1.1. STICS versions before modularisation.

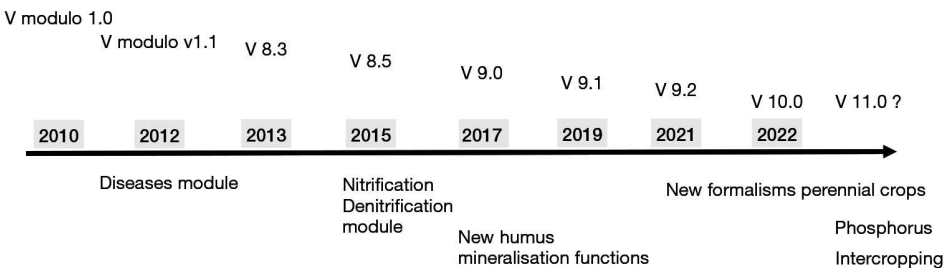


Figure 1.2. STICS versions since modularisation.

developed from the pioneering work of de Wit (1978) or Duncan (1971). However, new models appeared regularly in the literature (SSM: Amir and Sinclair (1991), CROPSIM: Hunt and Pararajasingham (1995), WANGRO: Rao Kanneganti and Fick (1991), GRAMI: Maas (1993), SHOOTGRO: McMaster *et al.* (1991); Teittinen *et al.* (1994), etc.). As Sinclair and Seligman (1996) explained, this is because there cannot be a single universal model can exist in the field of agricultural science and it is necessary to adapt system definitions, simulated processes and formalisations must be adapted to specific environments or to new problems (technical, genetic, environmental, etc.). It is also understandable that each modelling team wants to develop its own model in order to control the code and its development. These authors emphasize the heuristic potential of modelling, which was a crucial element in the STICS development. The work on STICS was firstly published in 1998 by Brisson *et al.* (1998b).

These timelines shown in Figures 1.1 and 1.2 describe the different versions that have been developed and the changes in formalisms and simulated processes.

►► 1.2 Purpose

The aims of the STICS model (the acronym stands for Scientific, Technical and Interdisciplinary simulator of soil-Crop System functioning) are similar to those of many existing crop models (Whisler *et al.*, 1986). However, STICS also takes into account cropping system diversity, including soil functioning. STICS is a soil-crop model, and not just a crop model, which runs at a daily time-step and using input variables related to climate, soil and the cropping system and its management.

According to Daniel Wallach *et al.* (2018), STICS can be defined as a deterministic process-based model. It can continuously simulate successions of various crop species and fallow periods. Additionally, it can be considered as a cropping system model because it accounts for a wide range of dynamic interactions between the different modelled compartments: crop, soil, climate and agricultural management techniques and functions in continuous by simulating the management of crops and fallow periods over long periods of time.

The output variables describe crop yield in terms of quantity and quality (with criteria associated with C and N) as well as environmental impacts linked to soil-C changes and CO₂ emissions, water drainage, nitrate N leaching and gaseous N emissions. The elementary simulated object is a local cropping situation for which a physical medium (soil and weather) and a crop management schedule are set through simulation input parameters. The main simulated processes are crop development, growth and yield production, as well as carbon, water, nitrogen and energy balances, and soil functioning.

From a conceptual point of view, STICS includes many original features compared with other well-known crop models, such as simulation of crop temperature, a snow module, simulation of various techniques and management options, bi-specific inter-cropping, and many others. While most of the basic features are based on classical formalisms or have been adapted from existing models. Nevertheless, several strong points of the STICS model should be noted (Brisson *et al.*, 2003; Brisson *et al.*, 1998b):

- Crop genericity: adaptability to various type of crops covering a wide range of botanical families (wheat, maize, soybean, sorghum, flax, grassland, tomato, sugar beet, sunflower, vineyard, pea, rapeseed, banana, sugarcane, carrot and lettuce, among others)

– Robustness: ability to simulate various soil-climate conditions without a large margin of error in the outputs (Nadine Brisson *et al.*, 2002) and easy availability of its soil and technical parameters. However, this robustness can jeopardise accuracy on a local scale.

– Conceptual modularity: the possibility of adding new modules or complementing the system description (e.g.: ammonia volatilisation, symbiotic nitrogen fixation, plant and residues mulch, stony soils, many organic residues, etc.). The purpose of such modularity is to facilitate subsequent development in order to include a wide range of crops and management options, as a true and complete cropping system model.

STICS simulates, at a daily time-step, the soil-crop system behaviour of a single field context (1-D model), over one or several successive crop cycles (long-term simulation). This approach is considered as a dynamical modelling of an agronomic system or an agroecosystem (Figure 1.3)

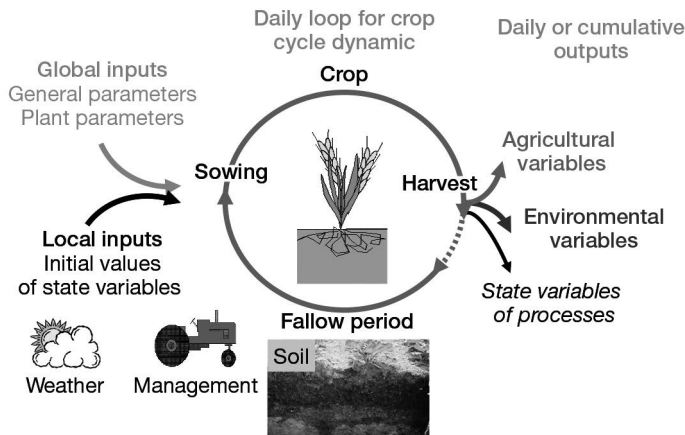


Figure 1.3. Simulation design.

STICS can simulate annual and perennial crops as well as bi-specific intercropping systems (§ 2.2.3).

►► 1.3 The STICS open book

STICS can be considered as a synthesis of the French agronomic and bioclimatology knowledge of cropping systems. It is a reference model used in the framework of agronomy, soil and crop sciences to help researchers, professionals and students in the partitioning and understanding of the cropping systems complexity. These reasons served as the motivation to update the original book on STICS (Brisson *et al.*, 2009). This new edition presents the formalisations found in version 10.0 of the STICS model (December 2022).

The book is arranged according to the way the model simulates the crop-soil system functioning. Each chapter is devoted to one main function such as development initiation, growth, yield onset, water uptake, C and N transformation of organic matter, etc. The option choices and parameterisation available to users regarding cropping system and long term simulations are also presented.

1.3.1 The functional links between thematic chapters

The STICS conceptual framework is fully described in § 2. The formalisms of main processes and modules of the soil-crop system are detailed in the chapters 3 to 13, each chapter including a section devoted to stress effects. The links between the chapters are presented in Figure 1.4. The last three chapters first aim to illustrate the STICS use cases (14), then to help users of the model (15), and finally to provide methods for how to integrate new plants or as well as new formalisms (16).

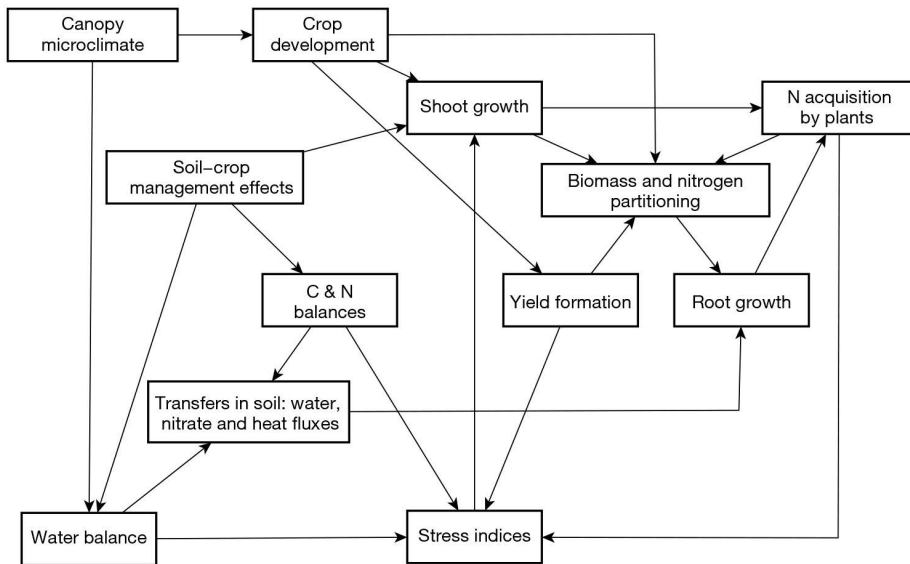


Figure 1.4. Main functional links between thematic chapters (3 to 13)

An additional chapter showing contributions to the model development (principles, governance, tools and rules) will be added in a future numerical version of this book.

1.3.2 The chapters related to the soil

The soil is described in chapter 10 concerning the properties of transfer of water, solutes (§ 10.1.1) and temperatures (§ 10.2), in chapter 11 concerning the evaporation properties (§ 11.2) and the physical soil surfaces conditions (§ 11.4) for effect of mulch, run-off, in chapter 12 concerning the C and N transformation in terms of decomposition of humified organic matter (§ 12.2.1), nitrification (§ 12.3) and denitrification (§ 12.4). The Carbon and nitrogen balance of the soil are finally presented in § 12.7. The soil structure can be change by the technical operations like soil tillage (§ 13.3.1). The parameterisation of the soil and the recommends' method to assign these parameters are described in § 15.4.2.

1.3.3 The chapters related to the mortality and recycling of crop residues

Mortality is described in each chapter relating to the growth of each organ: for the leaf (§ 4.1.2.2), for the roots (§ 5.5.4 and 5.4). The residues that remain on the ground decompose according to mechanisms described in § 12.2 and 7.8. The existence of this recycling depends on the cultivation techniques is described in § 13.5.3.

1.3.4 The chapters related to the intercropping

A general presentation of the bi-specific intercropping system is described in § 2.2.3 with a representation of the system simulated in STICS. Other chapters deal with the specificities of the intercropping: the density competition for the shoot growth (§ 4.1.1.1), the roots (§ 5.5.3), the radiation interception in crop cover (§ 9.2.2), the energy budget simulated in the both intercropped crops (§ 9.3.4).

▶▶ 1.4 Human-machine interfaces

1.4.1 Overview of the files

As Figure 1.5 illustrates, STICS relies on parameters describing the simulated soil-crop system: plant/crop, soil, crop management, soil-crop initial states (and possibly snow conditions), and forcing weather (climatic) variables. These inputs are organised in different files structured by major formalisms that include options. These options guarantee the genericity of STICS (§ 2.4). The local parameters are associated with a unit of simulation (USM). A USM describes a cropping situation combining a plant/crop, soil type and weather conditions. The files associated to a USM are found in the user's working directories. The files of general and plant parameters are not attached to the local context of the USM. These parameters are generic and come with the model, but they can be adapted by users as necessary. As a result of STICS specifications, the local model inputs (i.e. time and space related input variables) must be determined by each user while the global parameters (i.e. the constant values between usm), are defined by the STICS team modellers (§ 1.5.2).

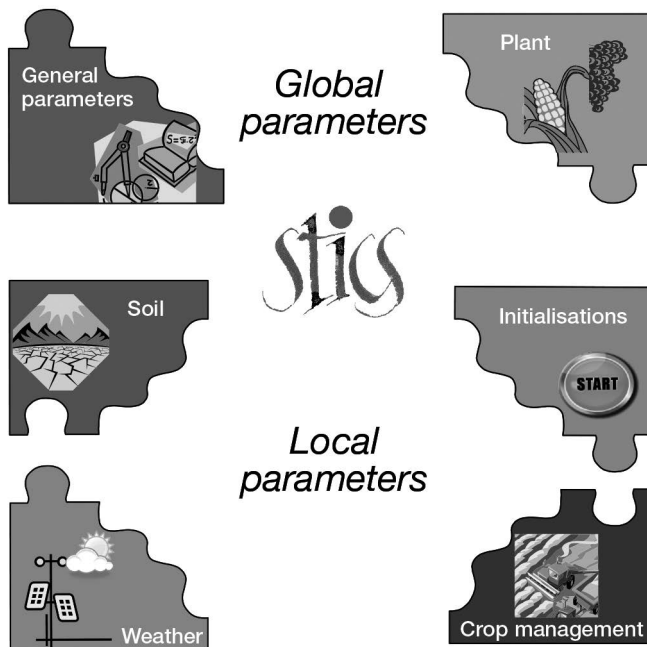


Figure 1.5. STICS input files.

All the parameters that are involved in simulated processes and attached to a USM are described in the following chapters. A full list is also included in the appendix section (§ 17.1). The simulation output variables of a simulation describe the different simulated processes on a daily time step, such as crop variables (phenological stages, yield, biomass, etc.) and soil and environmental variables (water, N, C balances, etc.). These variables are also listed in the appendix section (§ 17.2).

1.4.2 JavaStics interface

JavaSTICS is the software associated with STICS to facilitate its stand-alone use. It is a user-friendly interface that helps users understand and use the model features for various actions, such as i) creating or modifying USM and parameter files needed for simulations, ii) managing the input data, iii) running the model in different ways, iv) visualising a selection of output variables (possibly gathered with observed data), and v) optimising parameters using observed data.

JavaSTICS helps users prepare and launch multi-simulations such as long-term simulations, rotations and intercropping. In addition, the STICS executable (.exe) can be managed by using the JavaSTICS command line interface to facilitate complex experiment plan management involving multiple simulations to be run using various software languages (such as R language) and platforms.

Both JavaSTICS and the STICS model can be downloaded free of charge from the STICS website¹, where users will also find software documentation.

1.4.3 Platforms and tools using STICS

Since the early 2000s, STICS has also been available on different modelling platforms and integrated in workflows. For example, it has been encapsulated in the INRAE Record platform² since 2012 (Bergez *et al.*, 2014).

The principles and typology of coupling, along with several outstanding examples, are illustrated in § 14.4.2. Various technical aspects regarding the chosen methodology are presented in § 16.4.

STICS is also available in the AgGlob Workflow to use agronomic models at a global scale. AgGlob is a framework, based on a workflow developed on a Galaxy platform instance³ and designed to run massive simulations with some consistency checks integrated to help the users.

Moreover STICS has been used in many projects and scientific public expertise assessments coordinated by INRAE: evaluation of ecosystem services (EFESE project, Therond *et al.*, 2017), use of cover crops to reduce nitrate leaching (Cover crops as a pillar of agroecology in arable cropping systems project, Justes *et al.*, 2013).

1. http://www6.paca.inrae.fr/stics_eng

2. https://www6.inrae.fr/record_eng/

3. <https://galaxyproject.org>

►► 1.5 Tools for STICS users

1.5.1 Background on modelling performance

Model development is a continuous process that starts from building a conceptual model composed of information (input data, parameters and equations) that describing the bio-physical system or processes of interest. This conceptual model is then implemented in a computer program that is used to run simulations based on environmental factors. But both, the conceptual and the computer models, are prone to errors related to incomplete knowledge about the bio-physical system to be simulated, imperfect measurements and possible model programming errors or technical issues.

In practice, the development of a model is essentially an iterative process that includes model evaluation to assess i) the model's functioning, accuracy and limits, ii) how the model adapts to new conditions (e.g. new crops or varieties, new climatic conditions), and iii) the implementation of new processes (Figure 1.6). This book was written based on version 10 of STICS and describes the way the model has developed since its inception.

Modelling performances must be determined by evaluations which “include any action in which the quality of a model is established” using statistical criteria and graphs (Bellocchi *et al.*, 2010) and then indicate the level of relevance and accuracy of the model in reproducing the actual system (Coucheney *et al.*, 2015). It is a crucial step in the model improvement process. Performance evaluation depends on methods establishment, tools development, experimental database building and human dynamics to analyse, understand and assess the accuracy and reliability of the model outputs (Buis *et al.*, 2011).

A first complete evaluation of the accuracy, robustness and behaviour of the STICS model (v8.2.2) for a wide range of agro-environmental conditions in France was published in 2015 (Coucheney *et al.*, 2015). Using a database of experiments and software tools, the STICS project team (STICS-ProTeam) continuously carries out evaluations on a regular basis, and especially before releasing a new model version.

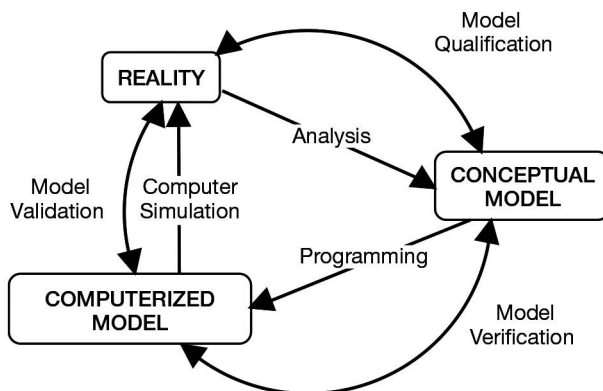


Figure 1.6. Phases of modelling steps in the model design and validation process. Adapted from Schlesinger and Bellocchi (Bellocchi *et al.*, 2011)

While the aim of this book is not to discuss model performance in great detail, the tools and the methods used in the evaluation process are described in § 16. Performance is addressed briefly for illustrative purposes in § 14.5.5.1.

1.5.2 Standard and research STICS version management

As previously mentioned, model development is a continuous process of implementation, adaptation and evaluation. As part of a collaborative development, these phases cannot be completed without an important set of guidelines for conception and implementation, as well as computing and mathematical tools.

One important basic collaborative tool for managing code evolutions is a version control system (Subversion⁴), which allows to create and merge development code sets derived from the main code known as ‘trunk’.

The STICS-ProTeam has also designed protocols for guiding developers through processes to improve model functioning or include new features in it. The protocols make it possible to produce and distribute an accurate standard version and include creativity through research development branches derived from the main version (Figure 1.7).

The STICS-ProTeam maintains the standard version of the model and regularly generates new stable versions to distribute them to end users.

Apart from this, research branches are created and modified by the team, but they may also be handled by contributors who want to improve existing processes or to adapt the model to new crops species or varieties. Every new branch creation is approved by the STICS governance team after an evaluation of the goals of the work.

Before merging back changes from branches into the standard version, they must pass through an integration process according to a specific evaluation protocol.

This way of managing the model allows the STICS-ProTeam to keep the lead on all model changes, while users can truly contribute to its development. Innovative research on processes or adaptations can then be integrated, and contributors have access to the collaborative tools for developing and evaluating model performances.

Some branches are now under construction or in progress, and will reintegrate the trunk as standard versions in the near future.

For example, in upcoming versions, the STICS-ProTeam plans to include changes related to:

- Phosphorus (P) cycle modelling: this is a priority in order to go beyond the current field of application and address questions linked, for instance, to crop P stress and the impacts of P on water eutrophication;
- Intercropping bi-specific systems: already in progress to improve the formalism of crop height kinetics and their consequence on the intercrop functioning for simulation competition for light, and other abiotic resources (water and nitrogen) between the two crops intercropped;
- Yield components driving factors: to improve the formalisms involved in carbohydrate and nitrogen remobilisations during the grain filling;

4. <https://subversion.apache.org>

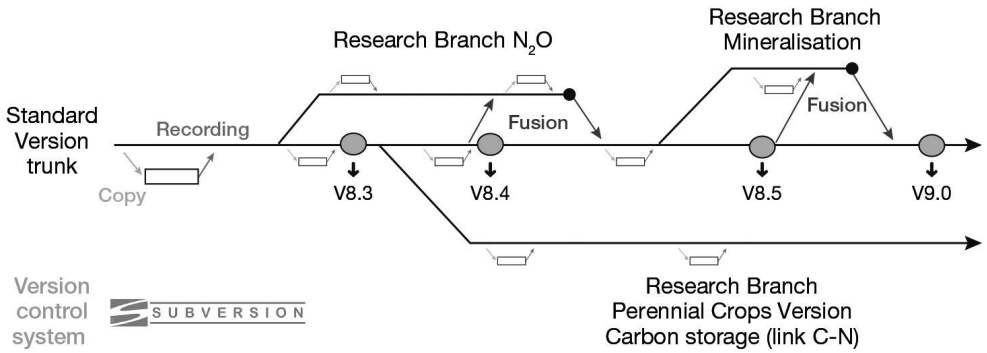


Figure 1.7. Model development versioning process

- Ozone absorption and its effects on plant growth that could induce stress and reduce biomass and yield production;
- Cryptogamic diseases interactions with plants: using a generic module to be coupled to STICS. The implemented formalism has been already published (Caubel *et al.*, 2017; Caubel *et al.*, 2014, 2012).

Other branches are also planned to improve the model robustness and accuracy for specific situations, such as:

- Cumulative effects of organic amendments on soil C-N storage (Levvasseur *et al.*, 2021);
- Perennial crops functioning (Strullu *et al.*, 2020; Strullu *et al.*, 2015), regarding diversity of grassland types and managements techniques (including animal returns at grazing) and their ability to store C in soil (Graux *et al.*, 2020).

These efforts illustrate that STICS stands for a past, present and also future soil-crop and cropping system model that is engaged in a dynamic process of continuous improvement.

1.5.3 Companion software and datasets

Several tools included in R packages (SticsRPacks) are available to STICS users and developers, to assess the quality of code development, evaluate the model performances and perform regression checking on a new version (Figure 1.8).

Client software (as for example TortoiseSVN, Raptidsvn) interfacing with a dedicated Subversion server is used for collaborative development and traceability of the STICS source code.

A continuous integration platform (Jenkins⁵) allows developers to execute automatically base and performance tests each time the model source code is modified on the versioning system. These actions are performed using a dedicated dataset (specifically IDE-STICS) and specific R packages functions to manage STICS simulations, evaluations, parameterisations and data extractions.

5. <https://www.jenkins.io>

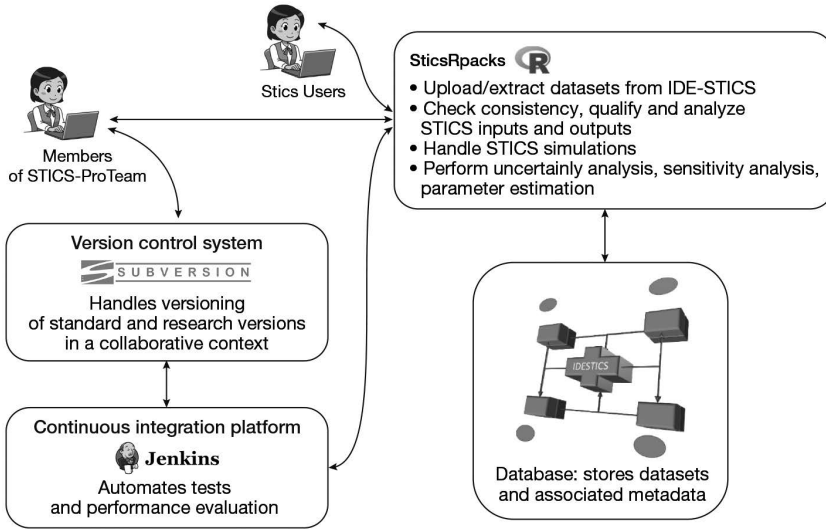


Figure 1.8. Diagram of the test bench of the model mobilising IDE-STICS.

1.5.3.1 SticsR Packs

The SticsR Packs suite project was initiated at the end of 2018 to develop tools for driving the STICS model using R language⁶. This collaborative project (INRAE/ CIRAD) is open source and hosted on the GitHub platform⁷.

The purpose of these tools is to:

- perform operations that are not provided in JavaSTICS, such as generate/modify parameters files, produce various graphs, handle statistical processing, etc.;
- automate these operations using scripts;
- reduce computation time to perform simulations.

More information about these tools is given in § 15.5.2.

1.5.3.2 The database associated with STICS evaluation: IDE-STICS

IDE-STICS is a private database managed by the STICS-ProTeam, which is used to develop and validate new versions of the model. The three reasons for improving and extending the IDE-STICS database are the followings: i) to include tropical and agro-ecological systems, ii) to test performance of new variables of interest not included in the current STICS database (i.e. N_2O emissions, soil C stocks) and iii) to improve and standardise the local input parameterisation between all the datasets. IDE-STICS integrates metadata that can be used to standardise soil parameterisation, to upgrade model inputs for a new version and finally to feed other models.

There are several main tasks attached to the IDE-STICS dataset:

- maintaining it as a reference dataset, using it in model evaluations;
- managing its access and use (taking into account intellectual property rights);

6. <https://www.r-project.org>

7. <https://github.com/SticsR Packs>

- defining and implementing functionalities for data requests for a given test;
- allowing scalability of model skills between STICS versions or several soil-crop models, thanks to a formalised thesaurus (following Porter *et al.* (2014) and the European AnaEE project).

Integrating data into IDE-STICS will require time, agronomic skills and reciprocal interest between modellers and agronomists. A prototype of data integration process has been already implemented and tested by experimental agronomists but is not yet available for users.

1.5.4 STICS model governance

Since its creation, STICS has been a common tool for a mixed collective of modellers, agronomists (in the broad sense), and users: the STICS User Network (SUN). About every two years, a meeting was held to bring together people from the network.

The dramatic increase in application requests led to code instability around 2004–2006. The SUN then reaffirmed the robustness priority of STICS and created the STICS-ProTeam to handle governance activities. The STICS-ProTeam decided to i) dissociate the standard version, which is only distributed and maintained, from research versions, and ii) to publish a reference document on the scientific and technical basis of STICS (Brisson *et al.*, 2009).

This freely accessible version of the book in different media formats (ePub, HTML and hard copy) is the result an open science project (OpenSTICS). This project will allow users and modellers to follow virtually in real time any changes to the standard version, whether every year or when a new STICS version is released.

The STICS-ProTeam is currently composed of 24 volunteers (the number varies), organised in two complementary groups – one for scientific activities and one for computing activities. These groups work closely together to manage the iterative building of the model and to guarantee the performance and robustness of the standard version of STICS (Beaudoin *et al.*, 2019).

The STICS-ProTeam has various functions, including:

- ensuring the model development by collaborating in the construction of ‘research’ versions;
- representing the model team at national and international level;
- coordinating the users’ community; and
- disseminating information on the STICS model and providing training for advanced use.

This project, like a boat, stays afloat thanks to two crucial elements: i) the SUN, a growing community recognised as an INRAE and CIRAD scientific network, and ii) the INRAE AgroEcoSystem division, whose support through honest and regular discussions is essential. The members of the STICS-ProTeam change regularly and can be found on the STICS web site⁸.

The STICS team also includes several emeritus members who have played a role at one time or another on the team: Nadine Brisson, of course, the original creator of the STICS model, Martine Guérif and Jean-Claude Poupa. There are also recently retired

8. https://www6.paca.inrae.fr/stics_eng/About-us/Project-Stics-Team

colleagues, such as Bruno Mary, who co-created the STICS model with Nadine; Nicolas Beaudoin, coordinator of the STICS-ProTeam when Nadine left us; and Françoise Ruget and Patrick Bertuzzi, who recently joined the contingent of emeritus members. We are ever grateful to all our retired colleagues who have helped make STICS what it is today!

1.5.5 STICS user services

Users from the scientific community can access information about STICS and reach out to the STICS project team in a variety of ways:

- STICS website: https://www6.paca.inrae.fr/stics_eng/
- STICS Twitter account: @STICS_CropModel
- STICS forum: https://w3.avignon.inra.fr/forge/projects/stics_main_projecu/boards (§ 15.5.3).

One or two training courses are held each year in France, and additional courses are regularly held outside France (e.g. in Asia).

The new generation of STICS training has opened up to the outside world because it is provided in Webinars (two in 2021). They are organized in 2 sessions of 2 days interspersed with work at home.

Chapter 2

Overall description of the modelled system

*NICOLAS BEAUDOIN, DOMINIQUE RIPOCHE-WACHTER,
MARIE LAUNAY, ERIC JUSTES AND NADINE BRISSON*

REVIEWED BY: FRANÇOISE RUGET

► 2.1 Conceptual framework

2.1.1 Introduction

STICS specifications were set out precisely in 1996 (§ 1). In short, they were designed to create a single model for different crops that would be general, robust, simple, operational and flexible, and which could describe the main interactions within the soil-crop-atmosphere and be upscaled in time and space. This chapter explains the STICS conceptual framework and how it translates in terms of programming design.

2.1.2 Simulated processes

The STICS modellers built a deterministic functional process-based soil-crop model to describe the energy, water, C and N dynamical balances across the crop cycle and during fallow periods. The aim was to allow users to predict a large range of agronomical and environmental variables of interest. As a result, STICS simulates the processes (using 1D description) occurring in a cropping system at daily step over the soil profile and the whole plant cycle. The upper boundary of the simulated system is delimited by the low layer of the atmosphere (2 m height). This boundary is commonly characterised by standard weather variables (radiation, minimum and maximum temperatures, rainfall, reference evapotranspiration and possibly wind and humidity). The lower boundary corresponds to the soil/sub-soil interface where water and nutrients are leached (out of the crop rooting system). Figure 2.1 illustrate the conceptual framework of crop modelling which is based on the classic functional approach.

Phenology, which refers to the plant development, governs the crop cycle time period. Crop growth is driven by energy interception and results in plant carbon accumulation (de Wit, 1978). Solar radiation absorbed by the foliage is transformed into aboveground biomass (energy conversion concept) whose a part is remobilised to the harvested organs when they become sinks. The crop nitrogen content depends on carbon accumulation in crop and mineral nitrogen availability in the soil

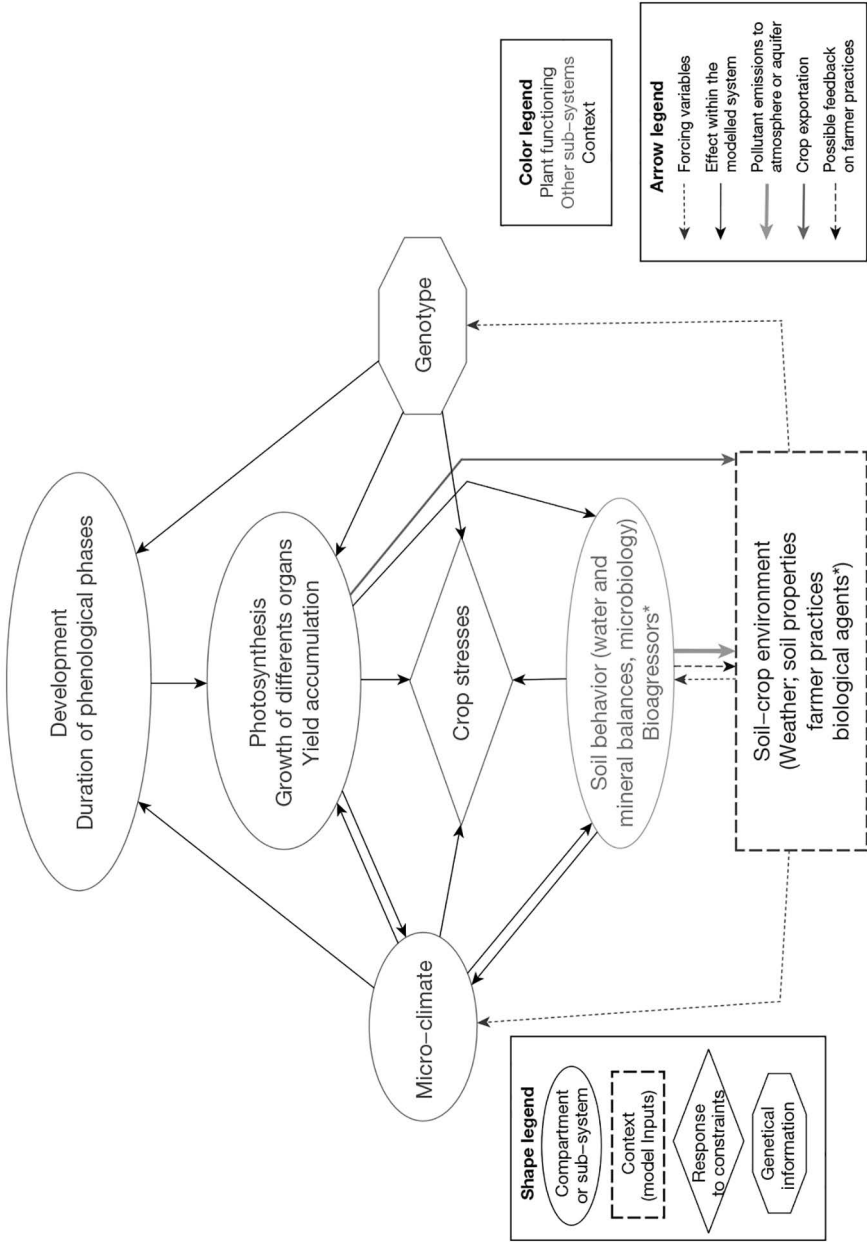


Figure 2.1. Schematic representation of a crop model, adapted from Bonhomme and Ruget (1991).
 * Bioaggressors can be accounted for thanks to STICS coupling.

(and N_2 fixed from atmosphere for legumes). Depending on plant type, crop development is driven either by i) a thermal index (degree-days), ii) a photo-thermal index which also takes photoperiod into account or iii) a vernalo-photo-thermal index which also takes vernalisation into account. The development module drives the kinetics of the leaf area index (lai) and the roots, which capture abiotic resources, and defines the harvested organ filling phase. Any water or nitrogen stresses will reduce leaf growth and biomass accumulation, and the degree of reduced growth is based on stress indices calculated by water and nitrogen balance modules. Other abiotic stresses, such as thermal (frost or high temperatures), trophic or waterlogging stresses are also taken into account, as limiting factors of growth and yield formation. The response function to environmental constraints can also integrate enzymatic activities, such as nitrate uptake.

Crop organs are defined as plant compartments to which generic ecological functions are assigned. Here, the distinction between the structural and temporary pool of carbohydrates is a key point. Only the structural aspect is assigned to the leaves, stems, fruit, perennial reserves and roots. Conversely, the temporary reserves are not located into the crop organs, in order to support the model genericity for all crops, including annual cereals and perennial forage crops. The storage organs and harvested organs can be grains, fruits, tubers or even stems. The new STICS version 10 now considers the C and N fluxes to and from temporary and perennial storage organs.

The model simulates the water and nitrogen elements balances in soil, to assess plant availability and environmental losses (§ 2.1.3). Their descriptions are based on the classic compartmental approach, which defines different pools in the system, their evolution and their relationships (input and output functions; see for instance Figure 12.5 from (Nicolardot *et al.*, 2001). The functions encompass physical, physico-chemical and bio-chemical processes. The compartment size depends on the process and ranges from centimetric (elementary layer) for solute content and transfers to decimetric (pedologic layer) for defining soil properties.

The processes are described in a way which can be qualified of functional and process-based or analogic, which aims to favour a simple integration of all the processes interacting in the soil-crop system, at the crop cycle scale as well as the crop rotation scale. The most emblematic illustrations of this conceptual choice are:

- The interception efficiency of the total solar radiation uses Beer's law, as an exponential response of the shadowing effect to leaf area index (lai), in the case of a homogeneous canopy.
- The conversion of photo synthetically active radiation (PAR) in aerial biomass is based on the concept of radiation use efficiency (RUE), assuming a specific potential linear response of biomass accumulation, at a stable radiation level when there is no carbohydrate remobilisation (Monteith, 1972); the simulated RUE depends on radiation level, water stress and N stress, CO_2 concentration and the crop stage.
- The nitrogen uptake and accumulation in the plant is based on the concept of N dilution curve in the aerial biomass of the canopy, in the case of vegetative growth, for either an isolated plant or dense canopy (Lemaire and Gastal, 1997). This allows the user to calculate the crucial concept of nitrogen nutrition index (NNI) which drives the N status of the crop in the vegetative phase.
- Fruit filling includes the concept of dynamic harvest index, as proposed by Spaeth and Sinclair (1985), for crop species with determinate development.

- The downward soil water storage, when daily rainfall exceeds the actual evapotranspiration amount, uses the tipping bucket concept, at the elementary layer infiltration scale, based on the hypothesis of infinite hydric conductivity.
- Nitrate leaching is simulated using a mixing cell model, with similar results to those of the resolution of the convective-dispersive equations (Darcy's law and Richard's law), except for soils with low hydric conductivity, with easier soil parameterisation and a much lower time of calculation (Van Der Ploeg *et al.*, 1995).
- Soil C and N mineralisation are simulated using a compartmental approach, with only three pools of organic matter, which resembles the AMG model (Clivot *et al.*, 2019); this compartmental approach allows an independent parameterisation linked to a residue typology (Nicolardot *et al.*, 2001). This approach is based on the crucial concept of C/N ratio of residues which drives their decomposition and humification rates, and determines the C and N mineralisation rate of the residues.

These processes are implemented by default in the standard STICS version; if their basic hypothesis is not met, an alternative process, involving a more complex conceptual approach, is described and workable. For instance, for a heterogeneous canopy (e.g. row crops or intercropping systems), the simple 'big leaf' model associated with the Beer's law can be replaced by a more complex energy balance based on crop architecture and a resistive approach. This alternative process allows determine the sunlit and shaded leaf layers of the bispecific intercrop and then the light capture differentiation between these two layers and furthermore, using a spatial discretisation along the crop inter-row (§ 9.3).

The effect of crop management on the dynamics of the soil-crop-microclimate systems is also given particular attention (§ 13). The reason is that crop specificities influence both ecophysiology and crop management (e.g. accounting for the various forms of forage cutting, fertilizer composition, plastic or crop residue mulching, etc.).

Finally, STICS model is either functional or process-based at daily scale; it is mechanistic at the crop cycle scale, since it deals with the main interactions between the system components. It can design the emergent properties at the crop cycle and crop rotation scales.

2.1.3 Simulated cycles

Crop development and crop growth are considered as a combination of responses to potential fluxes of energy or chemical elements (Figure 2.1). They are limited by environmental constraints which depend on physical, chemical and biological cycles.

With regard to physical cycles, the model first integrates the physical driving factors related to the climatic cycles of temperature and solar radiation (which have an annual period). The model then simulates the effective temperature, energy balance and water storage cycles in the soil and crop. Peculiarly, the model mobilises time discretisation at hourly scale for precise purposes: the daily cycle of the solar azimuth when using the resistive approach option for row crops (§ 9.2.1.2.1), the hourly climate state variables when using the Shuttleworth-Wallace submodel (§ 9.4), the water-filled pore space of elementary layers when simulating either nitrification or denitrification of soil nitrate (§ 12.3.5) and the soil surface ammonia concentration when simulation NH_3 volatilisation (§ 12.6).

The biological cycles include those pertaining to the crop(s), which may cover one or more cycles a year, and those related to the soil microbial biomass which depends on the decomposing residues and soil organic matter. In established perennial crops, a new crop cycle resumes according to either the imposed or calculated date of crop regrowth. In consequence, the simulated RUE encompasses both aerial biomass and perennial reserves building as opposed fine root system.

The biogeochemical cycles correspond to those for carbon and nitrogen. Each part of their cycles occurring in the soil-crop-atmosphere system is modelled based on several kinetic principles driven by the system forcing variables and according to the law of conservation of mass. The simulated C balance at the soil-crop level is almost as complete as compared to their description in literature (Hyvönen *et al.*, 2007): all net C fluxes are simulated except for CH₄ emission and dissolved organic or inorganic C in water drainage; however, only the difference between the gross primary production and its respective gross respiration is simulated. The N fluxes are complete, allowing to simulate positive or negative net N balance in function of the cropping system management and pedoclimatic conditions (Autret *et al.*, 2020).

2.1.4 Additional specifications about code and output availability.

STICS has evolved to deal with a larger range of issues that require new skills (Beaudoin *et al.*, 2019). The latter required the following supplementary specifications:

- Code modularity (§ 2.3)
- The options to force certain intermediate variables such as lai, potential evapotranspiration (PET), phenological stages (e.g. emergence, harvest), etc.
- The availability of all state and intermediate variables of agronomical, ecophysiological or biogeochemical interest; note that crop yield refers to the biological yield, not farm yield (no mechanical losses simulated); these variables can now be used to calculate the greenhouse gas (GHG) balance due to C-N cycles (except in grazed grasslands or flooded rice field, since CH₄ emissions are not yet simulated).

► 2.2 STICS validity domain

2.2.1 General case

The modelled system is the cycle of a crop (or bi-specific intercrop) growing either homogeneously or in row, in a given homogeneous soil under given homogeneous techniques and climatic conditions (§ 1.2). The STICS validity domain can be considered as either potential or actual.

From a theoretical point of view, the potential validity domain is the intersection of the validity domains of all the algorithms used; it depends on the simulated processes and the options activated by the user. For instance, if the canopy is heterogeneous, the radiative transfer model must be used instead of Beer's law relevant only for homogeneous stands; if hydric conductivity is weak, simulation of water status in the macroporosity compartment is also required. Users can activate these more complex options to expand the validity domain, but they must show more caution when parameterising the model and, where possible, with evaluating the model's performance.

From a practical point of view, the actual validity domain covers all the situations for which the model has been shown to produce acceptable results. This empirical concept is based on the model-use bibliometric (§ 14). Soil-crop model performance depends on how realistic the representations are as well as the reliability of the code, and the quality of the parameters (Loague and Green, 1991). Users who feed in the data and choose the simulation options and some parameters, can have a significant impact on the validity domain (Confalonieri *et al.*, 2016; Wallach *et al.*, 2021).

The STICS application domain can also be extended in space and time, thanks to the model's intrinsic ability for either successive simulations or bi-specific intercropping systems (see the next two sections) or by coupling the model with GIS (§ 14.3).

2.2.2 Case of the crop rotation

The STICS soil-crop model can simulate functioning of cropping systems, at the crop rotation scale as well as over the long term, by linking successive elementary simulations and taking crop and fallow periods into consideration, either with or without re-initialization after each USM (continuous mode). In continuous mode, the state variables required as initial values are transferred from the previous simulation (Figure 2.2). The variables that are transferred between successive simulation relate to the crops (stage, temperature, lai, biomass and N content of shoots, root length, biomass and N content of roots, biomass and N content of storage organs), non-decomposed residues (biomass and C-N contents of either mulch or buried residues and dead roots) and the soil (water, NO₃ and NH₄ content, organic C-N content in topsoil). In addition, residue predictions from the previous simulation become inputs for the following simulation. The list of transferred variables between simulations is slightly longer than the list of initial variables for the first simulation, because some of them are not available, namely the microbial biomass and the residue-sphere (mulch and dead roots). Thus, chaining simulations in a continuous mode provides supplementary information about the system state. However, the risk of model drift over along time needs caution (Beaudoin *et al.*, 2008).

Chaining simulations can show long-term trends and impacts in the cropping system. Some state variables such as soil carbon content or soil mineral content, are also variables that are important from an agro-environmental point of view. These variables can be used evaluate the long-term impact of agricultural practices, such as sowing a cover crop versus leaving bare soil in autumn; then the user can simulate the fate of NO₃ trapped by the cover crop instead of what would have been leached (Constantin *et al.*, 2012). Moreover, the fluxes simulated like N leaching, N₂O emission, and C sequestration can be cumulated, externally to the model, to assess the cropping system performances, especially the GHG emissions (Autret *et al.*, 2020). Other illustrations of considering the cropping system are provided in § 14.

2.2.3 Case of intercropping: simulation of bi-specific intercrops in STICS

2.2.3.1 Background, challenges and choice of formalism type

Intercropping consists in growing multiple crops (annual or perennial) simultaneously, with each crop developing and growing at its own rate as a result of interspecific interactions and resource partitioning. This practice is traditional in the tropics and is beginning

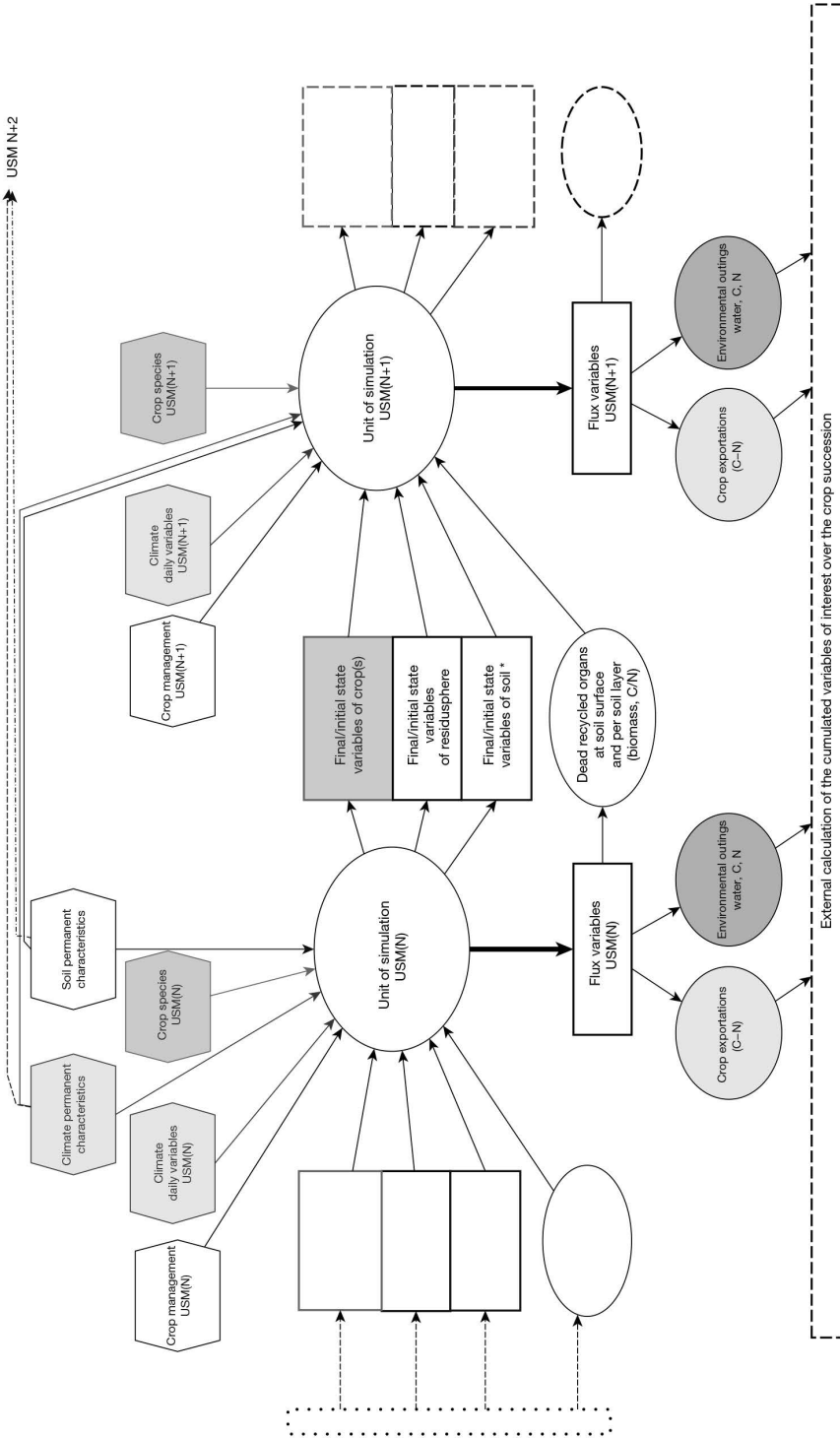


Figure 2.2. Simplified representation of the transferred variables between two successive units of simulation (USM); (*) organic C&N contents are simulated outputs while their initial values belong to the soil characterisation.

to be used, in either organic farming or conservation agriculture, in temperate climates to support the agroecological transition and mitigating the use of chemical inputs. Intercropping can be implemented with various spatial and genotype arrangements: mixed-on the row intercrops, strip intercrops, alley crops, mixed intercrops or even windbreaks, all of which exhibit differing levels of spatial heterogeneity. Given the complexity of intercropping system, agronomic models can be especially helpful for performing comprehensive intercropping analyses (Caldwell, 1995). The intercrop modelling framework can be summarised using three approaches. The first of these, consistent with the initial principles of (de Wit, 1978; de Wit *et al.*, 1970), is an extension of sole crop modelling. This principle consider that the system comprises two species instead of one and is simply organised within a kind of elementary pixel intended to represent the whole spatial design. In fact, this approach is the most operational (Caldwell and Hansen, 1993; Kiniry *et al.*, 1992), and focuses more on system dynamics than spatial heterogeneity. The second approach is based on a description of the intercropping system as a series of discrete crop-based or tree-based points with a flow of mass or energy between each. This spatially discretised approach can account for large spatial variations, with each point generally being simulated under the above-mentioned crop modelling principle, and the field response results from a spatially integrated calculation (Huth *et al.*, 2002). The last approach derives from architecture modelling and emphasises a realistic description of the 3D structure of the complex two-species canopy, which leads to fine-scale descriptions of processes (Sonohat *et al.*, 2002) at the organ level or the plant level. In this third approach, functional structural plant model (FSPM) were developed; however, accounting for system dynamics is more difficult because of the complexity of the interaction of organ dynamics and the whole plant behaviour.

The STICS crop model was adapted according to the first approach (Brisson *et al.*, 2004), with the aim of producing an operational model to support intercrop managements, while attempting to overcome the problems of unwarranted over-simplification. The STICS model considers only bispecific intercrops (parameters sets for two crops or two genotypes) intercrops. The adaptation of STICS's conceptual basis and formalisations to intercropping relies first depends on a simplified definition of the complex agronomic system of intercropping. Users must then adapt the modules calculating resource capture (light, water and nitrogen) between the two associated crops. Users can also simulate niche complementarity for N resources in cereal-legume intercrops since the rate of N₂ fixation by legumes can be favoured by the quickest cereal N uptake in the soil.

2.2.3.2 Representation of the intercropping system

Because the intercropping system is complex, the STICS model adopts some simplifying hypotheses. The soil-plant-atmosphere system is divided into three sub-systems (D, SU and LU) at the canopy level (Figure 2.3): the dominant crop (D) and the understorey crop (U) are divided into two parts: a shaded part (SU) and a sunlit part (LU), each defined by a light microclimate. These light microclimates, estimated from a radiation interception (§ 9.3), drive the different behaviours of the sub-systems in terms of growth (lai, dry matter accumulation) and water and nitrogen budgets (transpiration, nitrogen uptake, stress index) at daily time step. Estimating the water requirements for both associated crops depends on light partitioning coupled to a resistive scheme. The phasic development is considered the same for both parts of the understorey crop.

The soil environment is also assumed to be the same for both crops (i.e. the horizontal differentiation within the soil profile is disregarded in favour of the vertical differentiation). The assumption is made that the interactions between the two root systems result from the influence of the soil on each crop root profile, based on its penetrability and water dynamics.

This theory is applied within the STICS code via multiple calls to the elementary subroutines and re-calculation of the state variables as a function of the considered sub-system. Specific modules or options were added to account for the ecophysiological features of these complex systems. These modules cover radiation interception and the energy budget that drives water requirements and microclimate, and root system dynamics which are influenced by soil status over the various layers of the whole soil profile. Shoot growth was slightly modified to account for the understorey shaded crop growing under limiting radiation. Those modules and options are described in the relevant thematic chapters of this book. Reciprocally, the involved formalism options can be applied for sole crop simulations, like the energy budget for row crops.

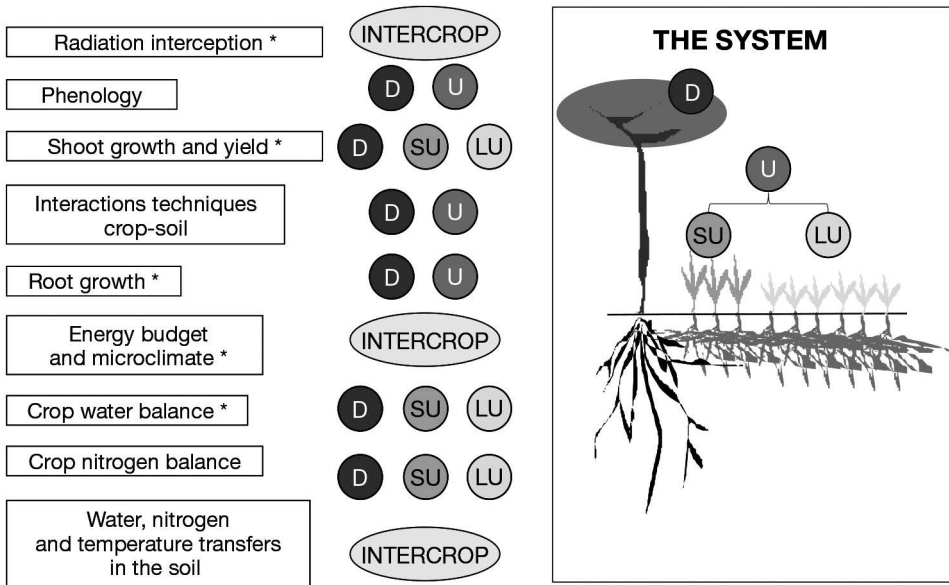


Figure 2.3. Simplified diagram of the model: on the right the system with its three sub-systems (D: dominant canopy; U: understorey canopy divided into a shaded part (SU) and a sunlit part (LU)); in the centre, the number of calls to each module devoted to a particular part of the system; on the left, the modules (grouped according to the way they are named in the code). * Corresponds to the modules modified for the adaptation to intercropping (from Brisson *et al.*, 2004).

►► 2.3 Relationship and priority between processes

2.3.1 Description of the main modules

STICS is a deterministic process-based model whose code is organised into modules, with each module composed of sub-modules dealing with specific processes/mechanisms.

A first set of three modules deals with the ecophysiology of above-ground plant parts (phenology, shoot growth, root growth, yield formation). A second set of four modules deals with how the soil responds in interaction with underground plant parts (root growth, water balance, nitrogen balance, soil transfers). The crop management module deals with the interactions between the applied techniques and the soil-crop system. The microclimate module simulates the combined effects of climate and water balance on the temperature and air humidity within the canopy.

Within each module, there are options that can be used to extend the scope of STICS application to various soil-crop systems. These options relate aspects of ecophysiology and crop management, such as:

- competition between vegetative organs and storage organs for assimilates (hereafter referred to as trophic competition);
- the canopy geometry when simulating radiation interception;
- description of the root density profile;
- use of a resistive approach to estimate the evaporative demand by plants;
- mowing of forage crops;
- plant residues or plastic mulching under vegetation.

Another of the model's strong point is its conceptual modularity: sub-programs are identified for each group of ecophysiological processes, such as N or water balance, crop growth, changes in soil C-N stocks, etc.

2.3.2 Priorities within the daily loop

All the processes are simulated at a daily scale, in interaction with agricultural techniques implemented at the crop cycle scale. The STICS source code is built as a sequential program where the instructions are executed one after the other and always in the same order. This order requires hypotheses about the priorities between the processes. Figure 2.4 summarises the calculation steps within the daily loop.

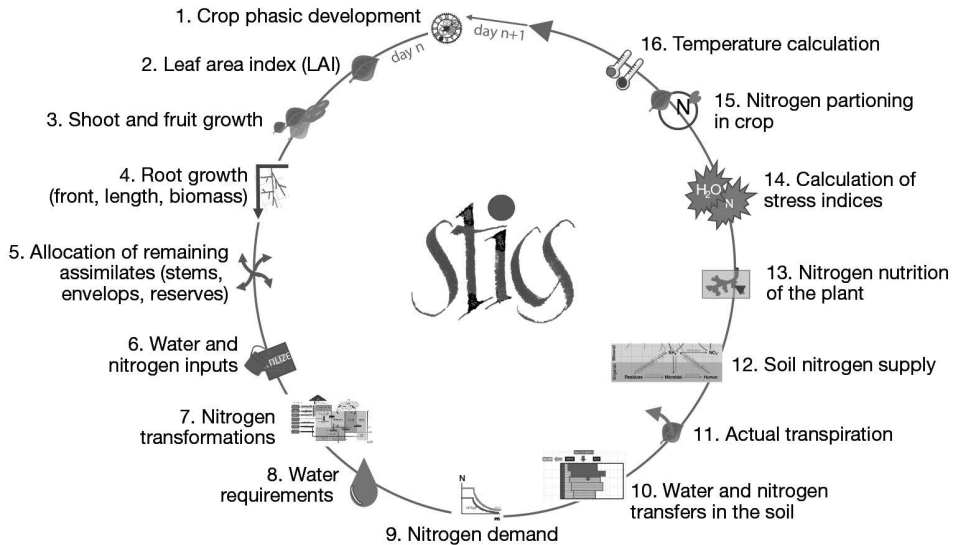


Figure 2.4. Simplified diagram of the order in STICS between processes within the daily loop.

At each step, another order between the elementary functions is defined. Users will find it is well worth their time to specify the order of priority of these elementary functions, especially within the following items:

- Crop growth: shoot growth, leaf senescence, yield elaboration, C and N assimilate allocation;
- C and N transformation: fertiliser, volatilisation, mineralisation, nitrification, denitrification;
- Water requirements: soil evaporation, crop transpiration;
- N nutrition of the crop(s): symbiotic fixation for legumes, N uptake (minimum of N demand and N supply);
- Stress indices calculation: water, nitrogen and abiotic factors (frost, anoxia);
- N partitioning in the crop(s): to the grain; between leaves, stems and reserves.

► 2.4 Model genericity

2.4.1 Means of model genericity

The aim of model genericity is to cover a wide range of crops over time (i.e. to simulate crop rotation) and under various soil and weather conditions. This can be achieved through:

- Parameter values: the value of a given parameter can be set according the observed system; note the distinction between global parameters (e.g. plant species); and local parameters (e.g. soil properties);
- Process options: Some options can be activated to deal with variability in crops, soils and practices;
- The conceptual framework: the functional or process-based description of processes are used to find a common description between general processes in the plant kingdom (e.g. temperature threshold, RUE for dry matter accumulation...);
- The STICS code modularisation: it allows for coupling within software platforms;

Of course, genericity does come with some trade-offs:

- Many parameters are equivalent when compared to those for mechanistic models, implemented in 3D and at an hourly scale;
- Some parameters are devoid of biophysical significance and must be mathematically calibrated;
- The actual validity domain depends on the quality and the range of situations covered by the calibration and validation databases.

Note that the activation and parameterisation of certain options depends on the input availability. For example, the use of a resistive model is based on the availability of additional climatic variables allowing the calculation of PET by the model, which requires data of wind and air humidity (§ 15.1).

2.4.2 Typology of the options driving the whole soil-crop-atmosphere system

The model genericity relies on existence of options which can be distinguished according to: i) their purpose and ii) the level of the modelled system they impact. These criteria can be cross-referenced, like in the examples provided in Table 15.1. There are two possible purposes and three levels for all the options.

Table 2.1. Examples of options according to their typology.

Level in the system	Model formalism	Model use
Global*	Intercropping, Perennial crop, Forage production, Climate change, Shelter microclimate.	Link of successive USM, Crop water stress, Crop nitrogen stress.
Function	Monocotyledon/dicotyledon, Indetermined/determined, Snow module, Soil macroporosity, Crop planting in rows...	lai forcing, Phenological stage forcing...
Process	ET calculation, Dormancy end, Crop driving temperature, Denitrification potential...	PET forcing, Crop N efficiency forcing, Harvest decision criterium...

* The list is exhaustive at this level.

Acronyms: USM=unit of simulation; lai=leaf area index; ET=evapotranspiration, PET=potential evapotranspiration

2.4.2.1 Distinguishing between options according to their purpose

First, a formalism option can be activated to take into account specific characteristics of the cropping system or to investigate various ways of representing the system behaviour. Formalism options automatically lead to new algorithms and parameters introduced. The option algorithms will be presented in detail in the chapters on formalisms (chapters 3 to 12).

Second, a STICS use option aims to modify the model's conditions of application without modifying formalisms or parameters. For instance, user can activate/deactivate the effects of water and/or nitrogen stress on crop growth to be able to simulate potential or actual growing conditions. The input variables can change, for instance with the option of forcing the lai against a dataset. The use options at global level can be called strategical options while all the others can be called driving options (§ 15.1).

2.4.2.2 Distinguishing between options according to the level of impact on the modelled system

2.4.2.2.1 Global level

Several compartments of the soil-crop-atmosphere system are directly impacted:

First, there are five global formalism options, which varying implementation:

- Intercropping code activation allows the user to simulate two intercrops that impact the whole cropping system;
- The perennial/annual choice impacts both the crop perennial reserve and crop management;
- The grasslands can be simulated using the code 'fou' which triggers the possibility of successive cuts of a forage crop and the existence of a residual lai after harvest;
- Climate change is a simulation option which calls for a single additional climatic variable (e.g. CO₂ concentration) and requires the user to activate several formalism options;
- Climate shelter forcing also affects the whole crop microclimate.

Secondly, there are three global use options (strategical):

- the choice between independent or linked successive USMs which affects the USM's initial soil and crop variables, except those of the first one;
- The water stress deactivation option affects lai expansion, crop growth and soil moisture;
- The nitrogen stress deactivation option affects lai expansion, crop growth, N uptake and soil N mineral content.

2.4.2.2.2 Function level

The formalism options at this level are numerous (see chapters 3 to 12); they can have three aims:

- to add either a compartment or a function, that strongly interacts with the other system components; for instance the snow option, in the climate module affects water, temperature and N loss emissions, as well as the macroporosity option in the soil module.
- to integrate the variability of crop traits. For instance, the option of indeterminate versus determinate species drives fruit filling. Notice that STICS does not directly integrate the C3-C4 plant trait, but takes it into account through the RUE value and the N dilution curve parameters.
- to compare several theoretical representations of the function. For instance, the representation of the root system can be addressed in true density expansion versus the profile type, with or without trophic links with shoot growth.

There are few use options at this scale; they include, for instance, options to force either the lai or crop stages according to measured values.

2.4.2.2.3 Process level

The process level concerns the design of the formalism simulating a given process (see chapters 3 to 12). They can be linked to the processes such as the end of seed dormancy or the harvest decision criteria.

Distinguishing between formalism and application options is not critical at this scale; the possibility of forcing the fertiliser nitrogen efficiency can be considered as STICS option use. The various options allow the STICS users to adapt a specific pathway of activated options for each crop or cropping system.

2.4.3 Examples of scenario of parameterisation

STICS allows for crop species genericity through the design of a 'parameterisation strategy' which combines activation of some formalisation options based on ecophysiological knowledge of the involved plant species. For example, the action of the photoperiod and the vernalisation requirements are activated, or not, in the module dedicated to plant development. There are formalism options of for each module which permit the model to take into account the specific ecophysiology of various crops, as shown in Figure 2.5. In wheat, for example, leaf surface growth is independent from trophic aspects, while in sugar beet, it depends on competition with storage organs. With intercropping, both plant files must include the options for radiative transfer, true density and resistive approach to simulate this system.

The same principle applies for crop management, as illustrated in Figure 2.6. Indeed, many different technical options may be activated or not, according to the crop onset, fertilisation type, irrigation management, canopy control or harvest decision rule. For intercropping, some techniques must be identical for both crops, according to site specific practical considerations, such as tillage or harvest criteria decision.

With less modalities, similar illustrations could be applied to soil or climate station. Finally, from a practical point of view, there is an asymmetry between the plant file, for which the parameterisation is already set by STICS team for some crops and other input files, which characterise the management, soil, climate and initial conditions. Filling these input files requires a minimal data collection and expertise by the user (chapter 16).

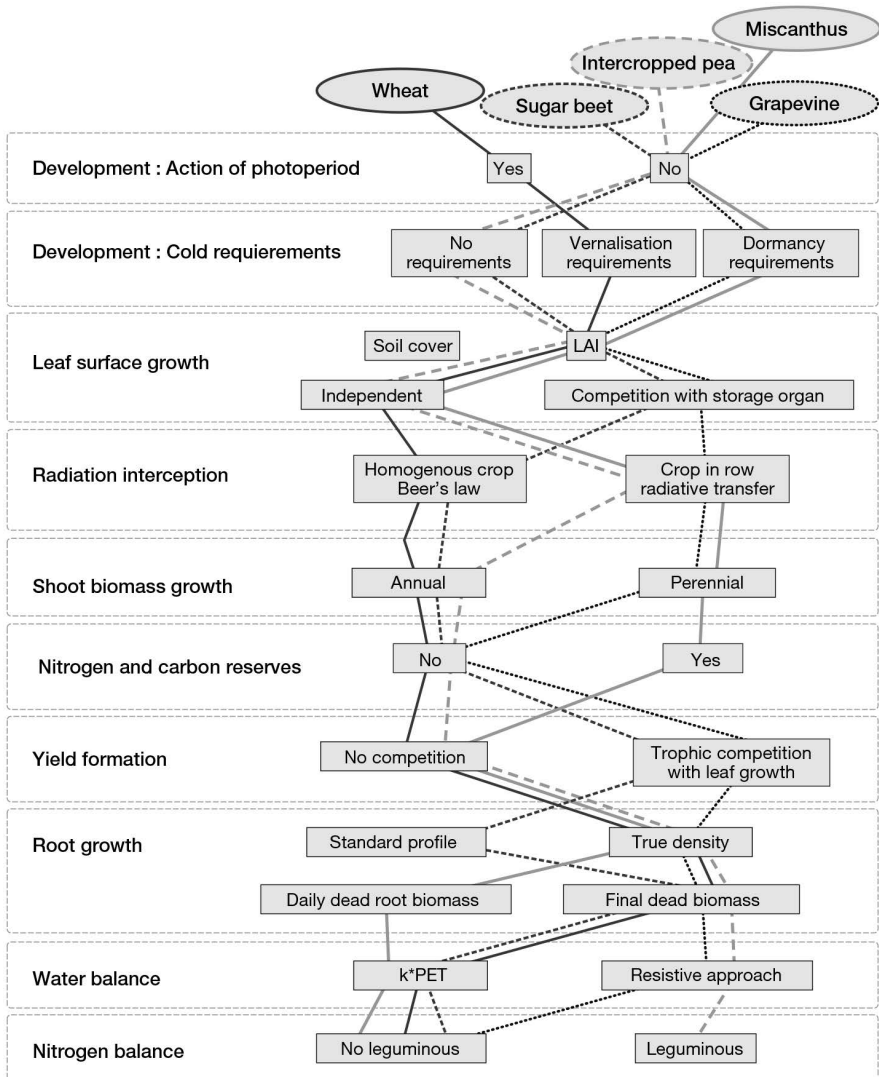


Figure 2.5. Examples of parameterisation strategies as the result of activating a set options in each specific plante file. Acronym: PET = potential evapotranspiration.

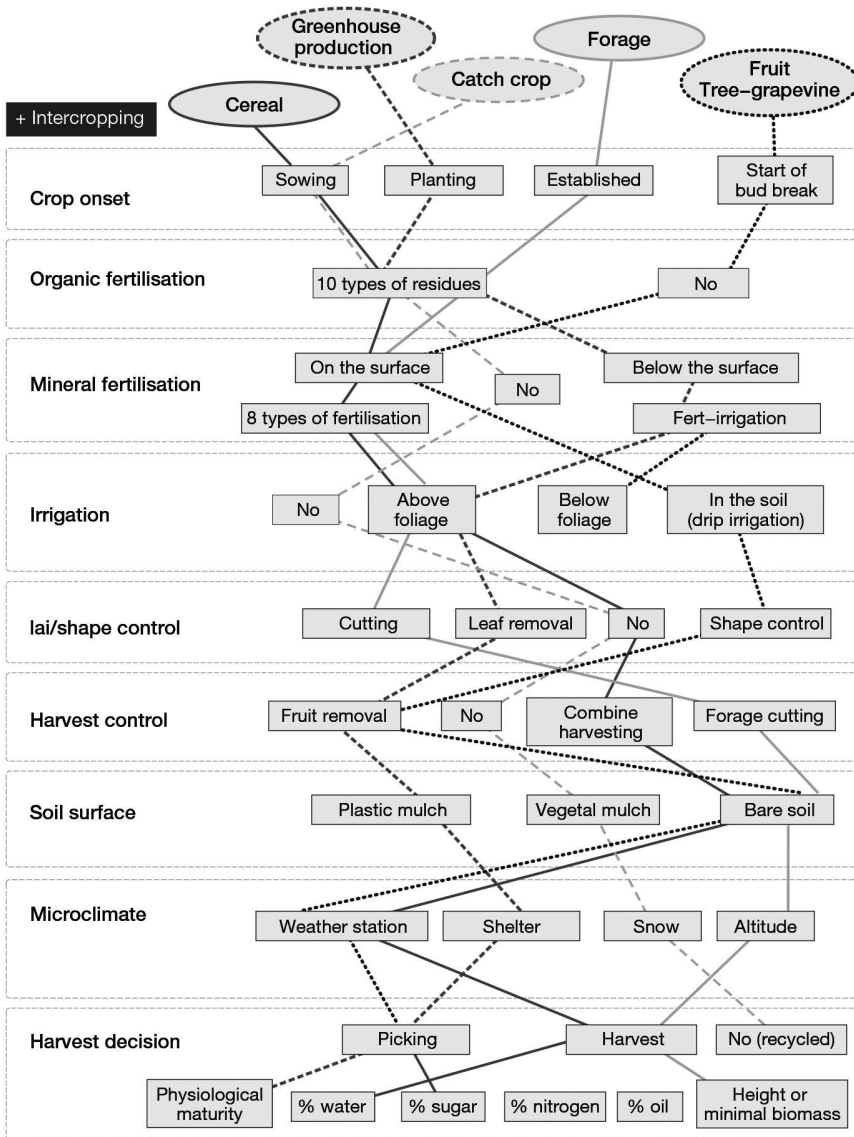


Figure 2.6. Examples activated option pathways to parameterise the crop management. Acronym: lai = leaf area index.

➤ 2.5 Parameterised crop species

2.5.1 Definitions

This explanation concerns the availability of plant species, for which three levels of quality of crop parameterisation can be defined:

- Finalised parameterisation means the plant file is currently being used and tested against a large dataset. The set of parameters was calibrated based on literature review

as well as a specific calibration database, before being tested against an independent database. Each new STICS version is documented and tested against a standard protocol (§ 16.3).

– Prototype parameterisation refers to a set of parameters whose performance quality is uncertain. Calibration was performed using either an overly limited dataset or an old STICS version. In the first case, prototype parameterisation can run with the current version, but users should exercise caution when doing so. In the second case, the parameterisation became incomplete and needs to be updated. In both cases, users running a prototype parameterisation are welcome to test it and, if possible, improve it and then share the performances within the STICS community, following the aforementioned protocol.

– Ongoing parameterisation refers to crop species at various stages of finalisation or awaiting for publication or for documentation of the validation database as regard the standard version. Users looking for more information about these species can contact the STICS team or post questions to the STICS community by using the forum.

2.5.2 List of parameterised crops

The current list of finalised and prototypes crop species is available on the STICS website, when the model is loaded. Figure 2.7 shows several kinds of plant files that are considered in STICS. Note that some species, such as turmeric and strawberry crops, which are perennial in botanical terms, can be parameterised as annuals using STICS, based on how farmers manage them. Additionnaly, the parameterisation of canola, finger-millet and marigold is ongoing while the parameterisation of triticale, white-clover, pigeon pea and winter fababean are waiting for documentation.

Perennial crops	Herbaceous Gramineous	Herbaceous leguminous	Market Gardening	Fruit trees
	fescue grass miscanthus timothy sugarcane	alfalfa	strawberry	grapevine banana
Annual crops	Cereals	Leguminous	Vegetables	Oilseeds
	spring_barley winter_barley spring_barley_IC corn winter_wheat durum_wheat sorghum Rice	soybean spring_pea spring_pea_IC	lettuce tomato Sugar beet potato Turmeric	flax winter_rapeseed sunflower
Catch crops	italianRyegrass_CC bristleOat_CC	vetch_CC crimsonClover_CC		mustard_CC
	Bare soil			

Figure 2.7. List of parameterised plant species as of 2021. The species given in bold have been fully parameterised while those in regular font are at the prototype one.

Chapter 3

Development

NADINE BRISSON, IÑAKI GARCÍA DE CORTÁZAR ATAURI, MARIE LAUNAY AND DOMINIQUE RIPOCHE-WACHTER

REVIEWED BY: NICOLAS BEAUDOIN AND BRUNO MARY

► 3.1 The importance of phenology on crop development

Phenology is the study of the seasonal rhythms of living organisms determined by the seasonal variations of climate (Schwartz, 2013). Phenology describes the different stages of development of a species and to provide information about its climatic feasibility in a given place. In a general way, phenology provides information about:

- the time step of the evolution of a crop: when it is seeded, when it can be harvested, when its flowering or budbreak takes place, etc.;
- the viability of the use of certain species or varieties in very different climatic contexts (Chuine, 2010): a late variety will have difficulty completing its cycle in a cold climate, while an early variety may finish its cycle too quickly (and thus affect its yield) or in an unfavourable period (for example, in the middle of summer when it is too hot);
- the optimal time to perform certain cultural practices (tillage, harvesting, cutting, pruning, etc.).

Moreover, phenology interacts with many other processes (especially growth and yield formation) by determining and prioritising the distribution of resources. For example, the parallel growth of vegetative and reproductive organs (both being managed by independent developmental cycles) will compete for the same resources but at different levels of intensity depending on the development cycle. The same is true for the initial crop phases in which the processes of reserve remobilisation can be highly dependent on the period and the development speed of the species. Finally, phenology will also have a direct or indirect impact on the effect of different biotic stresses (presence or absence of the organ being affected by a disease) and abiotic stresses (effect of the environmental conditions on a key crop process, such as very high temperatures on flowering or harvest).

The different formalisms and hypotheses used in the STICS crop model are described in the different subsections below. Examples of crop cycles (as described in the model) are provided at the end of this chapter. This chapter is related to other chapters in the book, such as those on leaf, root and fruit development.

►► 3.2 Simulated events

3.2.1 General phenology framework in STICS

In the STICS crop model, phenology is represented by different stages that describe the development of the independent dynamics of the two main group of organs simulated by the model: the vegetative organs (leaves and roots) and the harvested/reproductive organs (grains, fruits or tuber). The representation of each cycle depends on different options:

- the effect of environmental variables on the development of the simulated phases of each species. This concerns the various effects of temperature (hot or cold), photo-period, as well as abiotic stresses that can have a direct effect on the development;
- the way of starting the cycle: sowing, planting or if we consider that the crop was already established (a perennial crop).

The model will allow users to describe the different levels of precocity for each phenological stage at the intraspecies level using a set of variety parameters.

3.2.2 Phenological stages

The phenological stages (Table 3.1) are used as steps for simulating vegetative dynamics (leaf area index and roots) and harvested organ filling (grain, fruit, tuber). The two phenological scales are independent of each other: for example, the onset of filling of the harvested organs *IDRP* (named *idrps* in the sections that follow for the sake of convenience, because this variable represents the date when the stage is reached) can occur before or after the ‘maximal leaf area index’ stage *ILAX* (named *ilaxs* in the sections that follow).

Table 3.1. List of the phenological stages in STICS.

Vegetative stages / Leaf area stages	Harvested organs stages
IPLT: sowing or planting (annuals)	ILAT: beginning of the critical phase for grain number onset (determinate crops)
IMB: beginning of seed moistening	IFLO: flowering (start of fruit sensitivity to frost)
ILET: plantlet stage	IDRP: onset of filling of harvested organs
IGER: germination (sown crops)	INO: end of setting (indeterminate crops)
IDEBDORM: beginning of dormancy (perennial crops)	IDEBDES: onset of water dynamics in fruits
IFINDORM: end of dormancy (perennial crops)	IMAT: physiological maturity
ILEV: emergence or budding	IREC: harvest
ILET: end of the plantlet frost sensitive stage	
IAMF: maximum acceleration of leaf growth, end of juvenile phase	
ILAX: maximum leaf area index, end of leaf growth	

As in most crop models, the development stages simulated by STICS can differ from the stages defined in classical agronomic scales. The development stages in STICS are growth stages rather than organogenetic stages (Brisson and Delécolle, 1992). The stages actually correspond to changes in the trophic or morphological strategy of the crop that influence the evolution of leaf area index or grain filling (see examples in Figure 3.1).

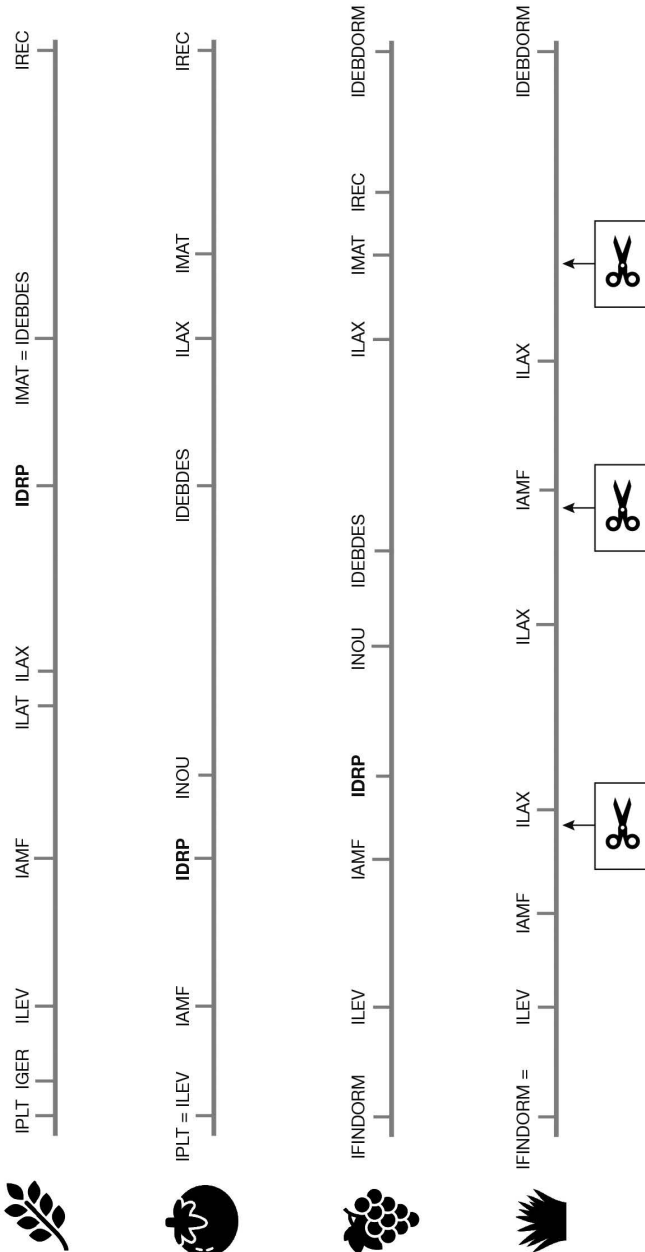


Figure 3.1. Illustration of the stages of interest for various types of crops such as wheat (annual determinate), tomato (annual indeterminate), grapevine (perennial indeterminate) and forage crop (perennial determinate interrupted by cuts symbolised by scissors). The flowering stage IFLO is mostly confounded with the **IDR** stage (in bold).

Using generic terms to name the various stages means that different species can be simulated, exhibiting either determinate growth (vegetative and reproductive growth occur successively) or indeterminate growth (vegetative and reproductive growth occur simultaneously, at least partly). The *IAMF* stage (named *iamfs* below) equates to the beginning of stem elongation and is generally not far from the end of leaf initiation: it is the '1 cm ear' stage for wheat and graminaceous forage crops, just slightly later than the double-ridge stage for most varieties, whereas it is the floral induction for corn. For indeterminate crops like tomato and grapevine, it is more difficult to find an equivalent in organogenesis, so this stage is instead regarded as the stage when the plant reaches a specific number of leaves (3, 4 or 5). The stage *ILAX* must be regarded as a growth stage since it is the end of leaf onset, which can occur before or after the *IDRP* stage. Nevertheless, some stages can also provide information about other developmental stages for some crops. This is the case, for example, with the *ILAX* stage, which is a proxy of the veraison stage (beginning of ripening) for grapevine. Moreover, the beginning of grain filling (*IDRP*) is always preceded by a key stage for the onset of the number of harvested organs (grains or fruits) which can be *ILAT* for determinate crops and *INOUE* (named *inouis* below) for indeterminate crops. At physiological maturity (*IMAT*) (named *imats* below) the harvested organs stop growing in dry matter terms and the *IMAT-IREC* period depends on the required quality for the final product.

►► 3.3 Main development processes

3.3.1 Time scale

The periods separating successive stages are specific to the species and variety. These periods are evaluated in development units, reproducing the phenological time of the plant.

Based on the long-accepted concept of growing degree days (Bonhomme *et al.*, 1994; Durand, 1967), temperature is always used in crop models as the driving variable of the phenological time. Yet authors like Ong (1983) and Pararajasingham and Hunt (1991) showed that it is better not to use the air temperature but rather a temperature closer to the plant (soil or organ) to explain the phasic chronology. In particular, this can explain the acceleration of the cycle in case of drought (Casals, 1996; Desclaux and Roumet, 1996; Seghieri *et al.*, 1995). Indeed, soil drying at the surface as well as at depth causes temperature increases at the plant level (Cellier *et al.*, 1993; Friend, 1991), which affect the progress of the cycle. Consequently, as in the model by Jamieson *et al.* (1995), we adopted the idea of Idso *et al.* (1978), who suggested linking phenological time to the crop temperature rather than to the air temperature. The other factors affecting the rate of development are modeled as brakes or accelerators on that rate per unit thermal time (Brisson and Delécolle, 1992). These factors generally include the photoperiod and vernalisation (e.g. CERES as described by Ritchie and Otter (1985) or ARCWHEAT by Weir *et al.* (1984)) and sometimes water deficit (e.g. CROPGRO by Jones *et al.* (2003)). Through the use of crop temperature, the effect of the water deficit on development is linked directly to the thermal units and not to a reducing factor. Of course, what is simulated by the use of crop temperature is an acceleration of the cycle, while some authors speak of delay in the case of early stress acting upon floral

induction (Blum, 1996; Seghieri *et al.*, 1995). Nitrogen nutrition conditions can also have an effect on the progress of the cycle (Girard, 1997), as well as light conditions through plant density (cryptochrome).

In STICS, crop temperature ($udev_{cult}$) drives development. It may be slowed by sub-optimal photoperiod conditions ($rf_{pi} < 1$), by non-compliance with vernalisation requirements ($rf_{vi} < 1$) or by the effect of water or nitrogen stress ($\mathbf{stressdev}_p > 0$ and $turf_{ac} < 1$ or $innlai < 1$). Thus, each day, the phasic course of the crop ($upvt$) is given according to the Eq. (3.1):

$$upvt(t) = udev_{cult}(t) \cdot rf_{pi}(t) \cdot rf_{vi}(t) \cdot [\mathbf{stressdev}_p \cdot \min(turf_{ac}(t), innlai(t)) + 1 - \mathbf{stressdev}_p] \quad (3.1)$$

As far as the emergence period is concerned, a specific calculation is made using the conditions prevailing in the soil (see § 3.4) as for the root lifespan ($\mathbf{debsenrac}_p$). Leaf lifespan is expressed in exponential type time (also called Q10 time) for reasons explained in § 4.1.2.

Most phasic courses between two successive stages are regarded as variety-specific (Table 3.2), as are the parameters indicating the sensitivity to the photoperiod and vernalisation requirements.

Table 3.2. Table summarising the various parameters of developmental duration and the driving variables used to calculate those durations. The $tcult$ variable is the crop temperature and $tsol$ is the soil temperature at the root front level.

Parameter of developmental duration	Positive thermal response							1
	$tcult$	$2tcult/10$	$tsol$	Cold requirement ¹	Action of photoperiod ¹	Slowing water stress effect ¹	Slowing nitrogen stress effect ¹	
$stpltger_p$			x			x		
$stdordebour_v$	x				x	x	x	
$stlevamf_v$	x			x	x	x	x	
$stlevdrp_v$	x			x	x	x	x	
$stdrpmat_v$	x			x	x	x	x	
$stdrpnou_v$	x							
$stdrpdsv$	x							
$stflodrp_v$	x				x	x	x	
$dureefruit_v$	x							
$durvief_v$		x						
$phyllotherme_p$	x							
$debsenrac_p$			x					

¹ If appropriate, this option is activated according to the plant sensitivity to the relevant factor.

3.3.2 Positive effect of temperature

In STICS, temperature positively affects plant phasic development from the emergence stage for annuals (ilevs) or from dormancy break for woody plants (ifindorms) until physiological maturity (imats). For herbaceous perennials, there is always a positive effect of temperature despite a rest period during winter. Crop temperature is calculated from the crop energy balance (see § 9.3.2). As has been shown in the article by Nadine Brisson *et al.* (2002), use of the crop temperature may modify the standard values used routinely with the air temperature. Consequently, multiplicative plant-dependent coefficients (**coeflevamf_p**, **coefamflax_p**, etc.) make it possible to modify ‘air temperature’ standards so that the crop temperature can be used, which has the advantage of representing shortenings in the cycle induced by drought.

The effect of temperature (Eq. (3.2)), achieved at a daily time step, increases linearly between the **tdmin_p** and **tdmax_p** thresholds, and decreases linearly between the **tdmax_p** and **tcxstop_p** thresholds, as illustrated in the Figure 3.2. Affecting the parameters **tdmax_p** and **tcxstop_p** is not easy because they correspond to occasional thermal conditions. Nevertheless, including this decrease in developmental and leaf growth (see § 4.1), in line with experiments in hot conditions, is worthwhile to be able to use the model in future climate conditions.

$$\begin{aligned}
 & \text{if } tcult(t) \leq \mathbf{tdmin}_p, \quad udevcult(t) = 0 \\
 & \text{if } \mathbf{tdmin}_p < tcult(t) < \mathbf{tdmax}_p, \quad udevcult = tcult(t) - \mathbf{tdmin}_p \\
 & \text{if } \mathbf{tdmax}_p \leq tcult(t) < \mathbf{tcxstop}_p \\
 & \quad udevcult(t) = \frac{\mathbf{tdmax}_p - \mathbf{tdmin}_p}{\mathbf{tdmax}_p - \mathbf{tcxstop}_p} \cdot (tcult(t) - \mathbf{tcxstop}_p) \\
 & \text{if } (tcult(t) \geq \mathbf{tcxstop}_p), \quad udevcult(t) = 0 \quad (3.2)
 \end{aligned}$$

The base temperature (**tdmin_p**) is assumed to be constant throughout the crop cycle (from ilevs to imats). However, it has been shown that this threshold could vary (Angus *et al.*, 1981) because the relationship between phasic development rates and temperature is not linear (Brisson *et al.*, 2006). For example, in the model ARCWHEAT (Weir *et al.*, 1984) or in Hunt and Pararajasingham (1995), various temperature thresholds are used according to the stages. However, since there is a correlation between the duration and the temperature threshold, these parameters are difficult to calibrate.

3.3.3 Effect of photoperiod

For photoperiodic plants, the photoperiodic slowing effect, **rfpi**, applies between the threshold photoperiods **phobase_p** and **phosat_p** (Eq. (3.3)). In the case of wheat, **phobase_p** is lower than **phosat_p**: wheat is a long-day plant. In the case of soybean, **phobase_p** is higher than **phosat_p**: soybean is a short-day plant (Figure 3.3 b). The current photoperiod (**phoi**) is calculated on the basis of calendar days and latitude (Figure 3.4) using classic astronomical functions (Sellers, 1965). The photoperiod is calculated by assuming that light is perceptible until the sun is at 6° below the horizon, which corresponds to a duration 50 to 70 minutes longer than the strictly defined daylength.

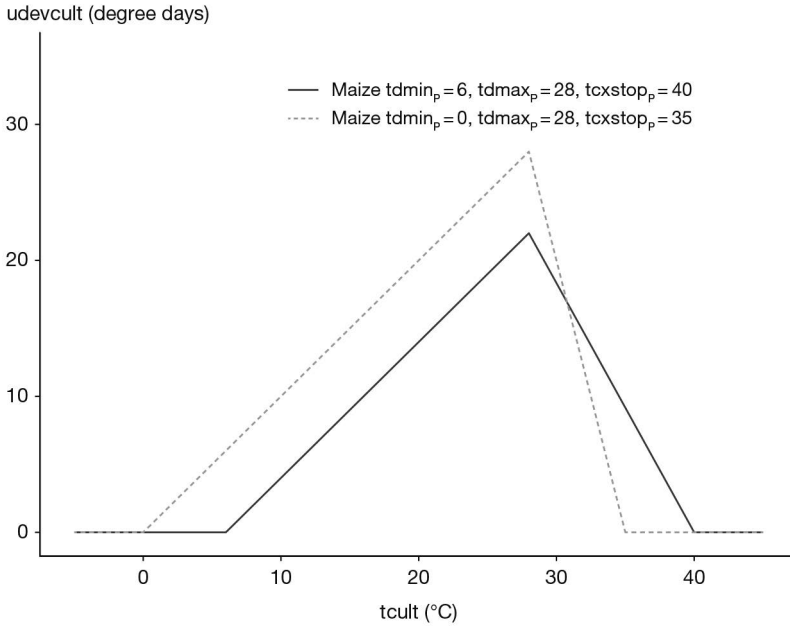


Figure 3.2. Development response to crop temperature.

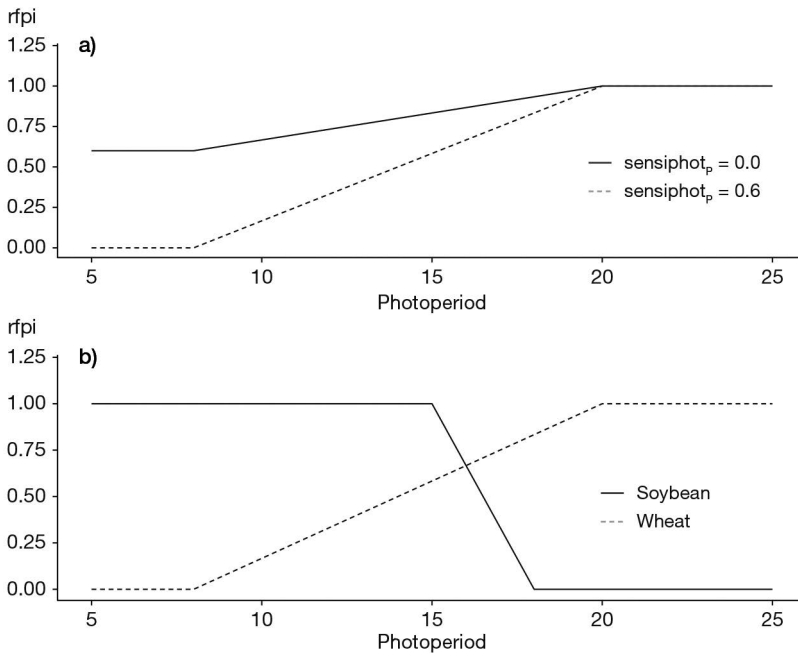


Figure 3.3. Photoperiodic limiting factor for phasic development ($rfpi$) when varying the sensitivity to photoperiod a) with response type of wheat or the photoperiodic response type b) with $sensiphot_p = 0.0$ for both species, for wheat ($[phobase_p, phosat_p] = [8.20]$) and for soybean ($[phobase_p, phosat_p] = [18.15]$).

The amplitude of sensitivity to the photoperiod is given by the **sensiphot_p** parameter: a value of 0 equals maximum sensitivity and a value of 1 cancels out this sensitivity (Figure 3.3a). The effect of the photoperiod is exerted between the ilevs (herbaceous) or ifindorms (ligneous) stages and idrps. This formalisation allows the sensitivity to photoperiod of different varieties to be characterised.

$$rfpi(t) = \left(1 - \text{sensiphot}_p\right) \cdot \frac{(\text{phoi}(t) - \text{phosat}_p)}{\text{phosat}_p - \text{phobase}_p} + 1$$

and $\text{sensiphot}_p \leq rfpi(t) \leq 1$ (3.3)

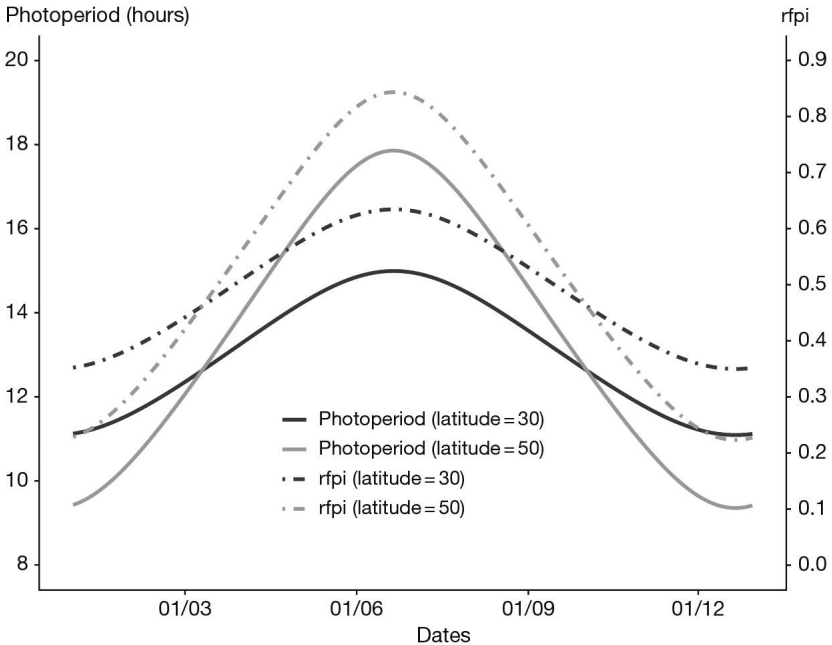


Figure 3.4. Annual variation of the photoperiod for two northern latitudes and the consequence on the corresponding limiting factor for phasic development (*rfpi*) calculated for wheat crop.

3.3.4 Cold requirements

Winter crops and perennial crops in temperate climate zones have vernalisation or chilling requirements. The formalisations classically applied and used in STICS differ for herbaceous plants (vernalisation) and woody plants (dormancy). For herbaceous plants, the resting state is considered not to be total, and the ‘vernalisation’ formalisation which applies to herbaceous plants allows a partial accumulation of development units during winter rest. For woody plants the ‘dormancy’ formalisations are much more severe, and development units are only active when all chilling requirements have been met. Consequently, noncompliance with vernalisation requirements slows ($rfvi > 1$ for herbaceous plants) or stops ($rfvi = 0$ for ligneous plants) crop development. For woody plants, the post-dormancy period is characterised by the phasic course between dormancy break (ifindorms) and budding (ilevs), i.e. **stdordebour_p**.

3.3.4.1 Vernalisation

Vernalisation requirements are defined by the genotype-dependent number of vernalising days (\mathbf{jvc}_p), and the vernalising value of a given day (jvi) depends on crop temperature (Figure 3.5). Vernalising days are counted from germination ($igers$) for annual crops, because an active metabolism is required to initiate the process, or from the $\mathbf{julvernal}_p$ day for perennial crops. A minimum number of vernalising days, $\mathbf{jvcmini}_p$ is required (Eq. (3.4)). The progress in crop vernalisation, $rfvi$, gradually increases until it reaches the value of 1.

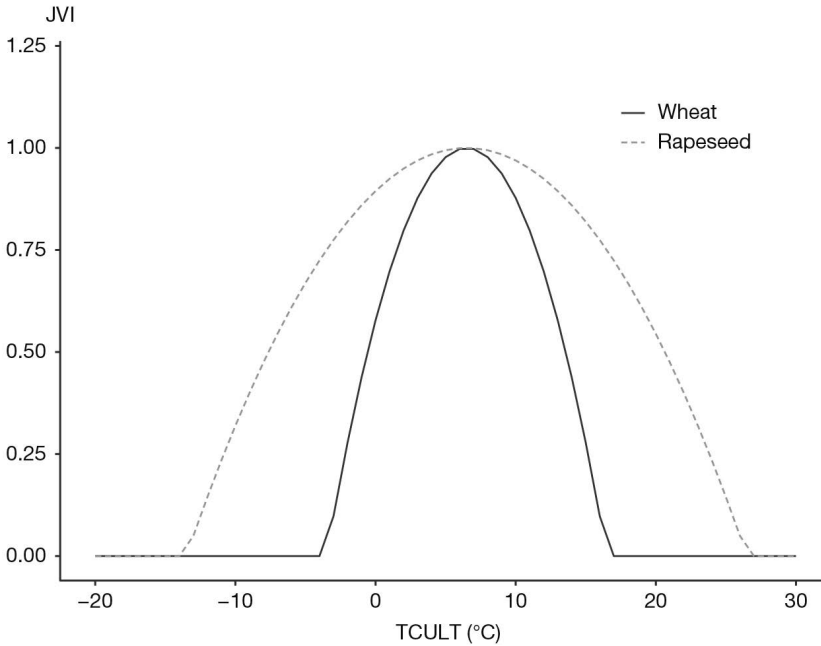


Figure 3.5. Vernalising value of a given day (jvi) as a function of the mean crop temperature ($tcult$) for wheat ($[\mathbf{tfroid}_p, \mathbf{ampfroid}_p] = [6.5, 10]$) and for rapeseed ($[\mathbf{tfroid}_p, \mathbf{ampfroid}_p] = [6.5, 20]$).

$$jvi(t) = \max\left(1 - \left(\frac{\mathbf{tfroid}_p - tcult(t)}{\mathbf{ampfroid}_p}\right)^2; 0.0\right)$$

$$rfvi(t) = \frac{\sum_{t=igers \text{ or } \mathbf{julvernal}_p}^t (jvi(t) - \mathbf{jvcmini}_p)}{\mathbf{jvc}_p - \mathbf{jvcmini}_p} \quad (3.4)$$

where \mathbf{tfroid}_p (optimum vernalisation temperature) and $\mathbf{ampfroid}_p$ (thermal semiamplitude of the vernalising effect) are parameters which provide the range of vernalising activity of temperatures (Figure 3.5). The $\mathbf{ampfroid}_p$ parameter indicates the sensitivity of the species to vernalisation: if it is low, the range of vernalising temperatures is narrow and a long period will be necessary to meet the requirements; if it is high, the temperature range is broader and results in more rapid vernalisation. Figure 3.6 illustrates the sensitivity of the model to this parameter and its effects on leaf growth dynamics (details of calculation in § 4.1.1).

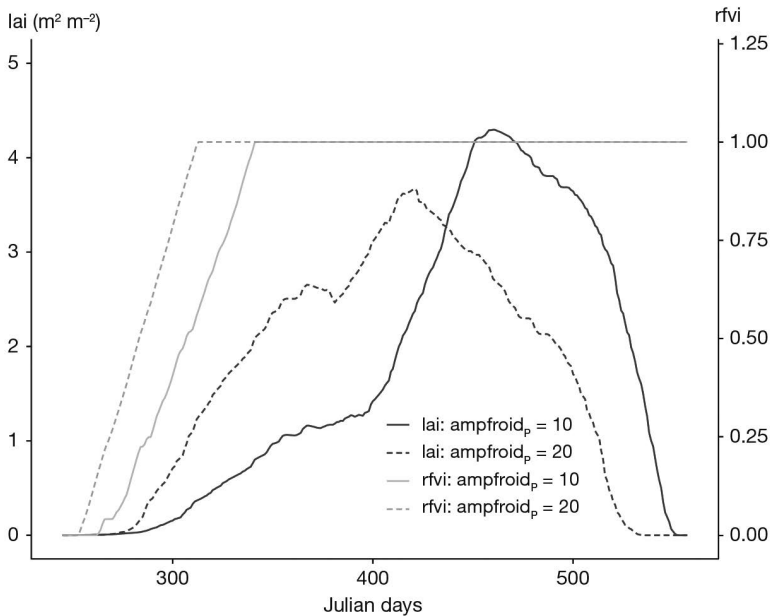


Figure 3.6. Sensitivity to the **ampfruid_p** parameter (assumptions of 10°C and 20°C) on the calculation of the period of vernalisation (*rfvi*) and its consequences on leaf growth (*lai*) for a ryegrass catch crop sown in late summer.

3.3.4.2 Dormancy

This section deals with the perennial dormancy and not with the dormancy break of seeds of annual crop grains such as wheat, barley or pea that can lead to germination of the grain on the plants before harvest which are described in § 3.4.1.

The aim is to calculate the day of dormancy break, which makes it possible to change the *rfvi* variable from 0 to 1, bearing in mind that it is always possible to impose this date and ignore the following dormancy calculations (using the parameter **ifindorm_p**).

For perennial plants, the active onset of vegetative development generally occurs after a period of winter rest (if this is not the case, chilling requirements are set to 0). The dormancy duration is calculated by meeting the chilling requirements. If the simulation is initialised at the **idor_j** stage, the model then assumes that this is the onset of dormancy (**idebdorms**) and that the chilling requirements are not met.

In 1965 Bidabe proposed a formula to calculate dormancy and post-dormancy durations for apple trees, based on the Q10 notion which corresponds to exponential-type responses to temperature. This is a well-known formula used for fruit trees for both vegetative or reproductive buds. In STICS, we only use that which concerns the dormancy period, since the post-dormancy period (i.e. from **ifindorms**). The daily responses are accumulated (*cu*, Eq. (3.5)) until the current day (*I*) from a starting date (**idebdorm_p**), generally taken to be during the autumn or the summer (García de Cortázar Atauri, 2006), which shows that the initial date has a little effect on the calculation (August 1st for grapevine). The genetic-dependent parameter for the amount of chilling requirement is **jvc_p**.

$$\begin{aligned}
 cu(t) &= \sum_{j=idbdorm}^t \left(q10_p \cdot \frac{-tmax(t)}{10} + q10_p \cdot \frac{-tmin(t)}{10} \right) \\
 \text{and } if \text{ } cu < jvc_p, \text{ } rfv(t) &= 0.0 \\
 if \text{ } cu \geq jvc_p, \text{ } rfv(t) &= 1.0 \quad (3.5)
 \end{aligned}$$

The Bidabe's formula (Bidabe, 1965) provides good results for grapevine (García de Cortázar Atauri *et al.*, 2009a).

3.3.5 Effect of stress

Early stresses can generate delays in the development of some crops. This effect counteracts the 'acceleration' effect induced by using the crop temperature. The effect is active up to the idrps stage, and can be modulated using a plant-dependent sensitivity parameter (**stressdev_p** = 0: crop insensitive to stress), as described in § 3.3.1. The lower of the two values of water stress (turfac) and nitrogen stress (innlai) is applied. For instance, this effect causes a five to eight day delay between a fertilised and an unfertilised situation in the Parisian basin for wheat (**stressdev_p** = 0.2). This effect is also accounted for in the calculation of leaf life span (see § 4.1.2, Eq. (4.11)).

► 3.4 Emergence and initiation of crop development and growth

This section concerns i) the emergence of sown annual crops, ii) the onset of crop development after planting for transplanted annual crops and iii) the onset of crop development after winter rest for perennial crops (bud growth of trees and the beginning of herbaceous growth).

3.4.1 Emergence of sown crops

In the first generation of crop models, such as in the models CERES, ARCWHEAT, and SUCROS models, the sowing-emergence phase was approached in a general way and related only to air temperature. Later on, the effect of the soil water status on the duration of emergence was also taken into account (Rao Kanneganti and Fick, 1991). Recent work on germination and the beginning of shoot growth (Dürr *et al.*, 2001; Hucl, 1993; Itabari *et al.*, 1993; Weaich *et al.*, 1996) now distinguishes two phases in emergence, e.g. in the model SHOOTGRO by McMaster *et al.* (1991), and its derivatives (MODWTH3 by Rickman *et al.* (1996)). Such an approach allows the simulated duration of emergence to vary with three main factors: temperature, soil water status, and sowing depth. The effect of soil water status has been shown to be particularly important (Alm *et al.*, 1993; Bouaziz and Bruckler, 1989; Bradford, 2002). These papers link the simulation of emergence to the good simulation of soil water status in the surface soil layers, especially when sowing is shallow. Generally, crop models do not account for soil structure (size, amount and distribution of soil aggregates), although models specifically dedicated to crop establishment do take it into consideration (Dürr *et al.*, 2001). In addition, the effects of waterlogging, through its physiological impact of anoxia on the embryo or through rooting effects, are not directly introduced.

In STICS, the emergence phase is broken down into three sub-phases: seed imbibition (moistening), followed by germination, and lastly, shoot elongation. The physical soil conditions influence not only the duration of emergence but also the number of emerged plants, especially in dry conditions or when there is a surface crust.

3.4.1.1 Moistening

Seed moistening can be regarded as a passive process starting at a species-dependent water potential prevailing in the seedbed (**potgermi_p** in MPa). The relationship from Clapp and Hornberger (1978), parameterised by the characteristic soil water contents of field capacity and wilting point, was used to convert **potgermi_p** into water content (see § 10.1.4). Once the seed is moistened, it has a limited number of days (**nbjgrauto**) during which it uses endosperm reserves for plantlet growth (Eq. (3.6)). This number has a species-dependent component (**nbjgerlim_p**) but also a thermal one, since it is thought that at low temperature (i.e. the average soil temperature in the seedbed, SB, from the beginning of moistening, IMB), respiration processes and the consumption of reserves are slower (the minimum at high temperature is **propjgermin_p** × **nbjgerlim_p**). When the temperature is lower than the germination base temperature, **tgmin_p**, then the day number is maximal (**nbjgerlim_p**). Above **tdmax_p**, the seed uses up its reserves in the least time, parameterised by default to 20% of the maximum (**propjgermin_p**=0.2).

$$nbjgrauto(t) = -\frac{1-propjgermin_p}{tdmax_p-tgmin_p} \cdot \left(\frac{\sum_{j=IMB}^t (tsol(SB,t))}{t-IMB+1} - tgmin_p \right) + 1$$

$$and \ propjgermin_p \cdot nbjgerlim_p \leq nbjgrauto \leq nbjgerlim_p \quad (3.6)$$

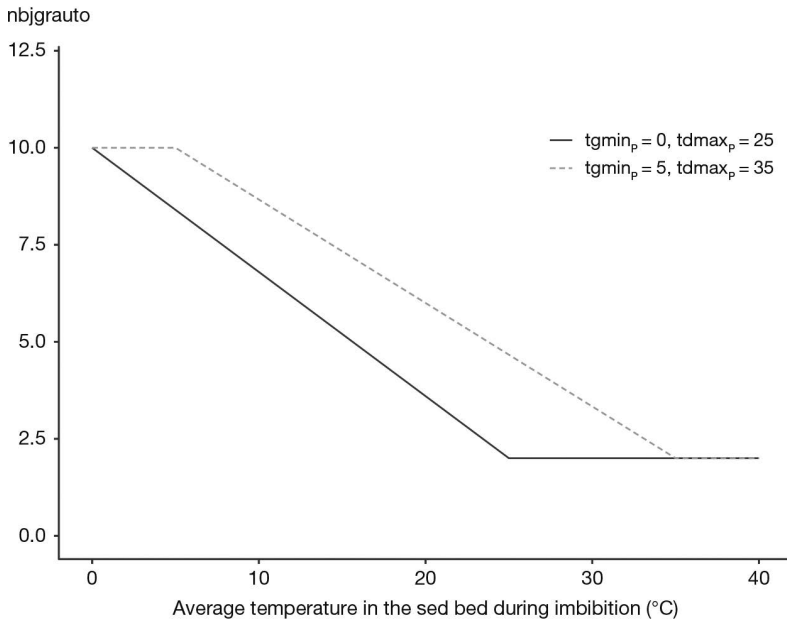


Figure 3.7. Evolution of the number of days of autotrophy as a function of temperature for two sets of cardinal temperatures.

3.4.1.2 Germination

Germination is achieved when the growing degree-days from planting in the seedbed (somger) reaches a given threshold (**stpltger_p**), with a condition as to the dryness of the soil (Eq. (3.7)).

$$I = igers \text{ if } somger(t) = \sum_{j=iplts}^t \left((tsol(SB, j) - tgmin_p) \cdot humirac(SB, j) \right) = stpltger_p$$

$$\text{and } SB = profsem_T \quad (3.7)$$

$tsol$ is the soil temperature and $tgmin_p$ is the base temperature for germination. Soil moisture in the seedbed ($SB = \text{depth of sowing} \pm 1 \text{ cm}$) influences germination through the $humirac$ variable (Eq. (3.8)).

if $humsol(SB, t) > hn$

$$\text{then } humirac(SB, t) = sensrsec_p + (1 - sensrsec_p) \cdot \frac{humsol(SB, t) - hn}{hx - hn}$$

if $humsol(SB, t) \leq hn$

$$\text{then } humirac(SB, t) = \frac{sensrsec_p}{hn} \cdot humsol(SB, t) \quad (3.8)$$

where $humsol$, hn and hx are the actual water content, the wilting point and the field capacity in the seedbed, respectively, and $sensrsec_p$ is a plant parameter which can be given a value between 0 and 1. If $sensrsec_p = 1$, the effect of soil dryness on all the functions of root growth is only effective for water contents below the wilting point (Figure 3.8); conversely, if $sensrsec_p = 0$, this effect is the highest.

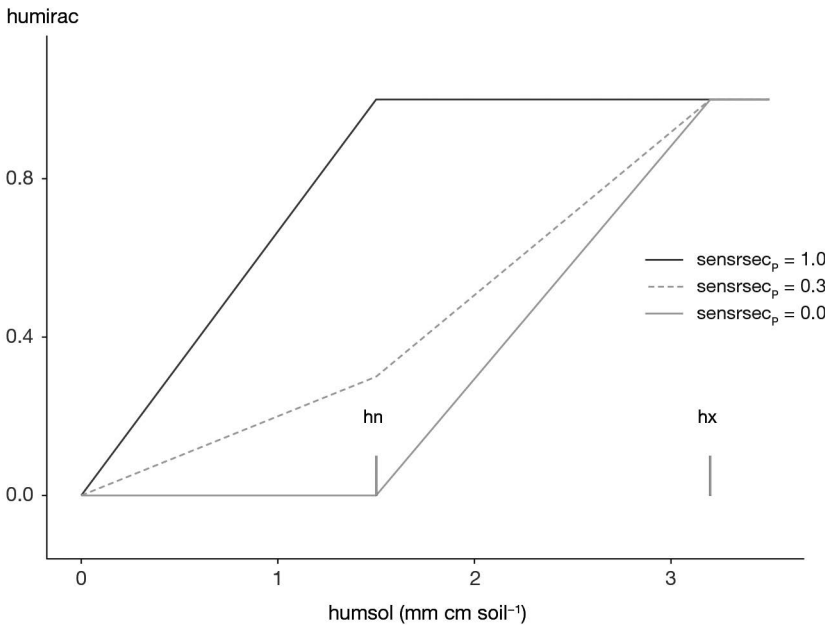


Figure 3.8. Evolution of the variable $humirac$ as a function of the parameter $sensrsec_p$ and the values of seedbed water contents at field capacity (hx) and at wilting point (hn).

If the seedbed dries out, it may delay germination significantly. This does not impair grain viability as long as the grain has not already imbibed water. If, however, the soil water content has been high enough to allow grain moistening, grain viability is reduced. To account for this effect, we relied on work by Bradford (2002, 1990) showing that too long a time for germination after moistening reduces the germination rate if the number of days of moistening ($nbjhumec$) is higher than a plant- and temperature-dependent threshold duration ($nbjgrauto$, Eq. (3.6)). It is assumed that germination occurs ($igers$ being the germination day) but at a reduced plant density (ratio between density of germinated plants, $densite(igers)$, to sowing density, $densitesem_T$) proportional to the thermal time deficit (Eq. (3.9)). An illustration of the chronology of germination in various soil conditions is given in Figure 3.9.

$$\begin{aligned}
 & \text{if } nbjhumec(t) > nbjgrauto(t) \\
 & \qquad \qquad \qquad \text{densite}(igers) = \text{densitesem}_T \cdot \frac{\text{somger}(t)}{\text{stpltger}_p} \\
 & \text{if } nbjhumec(t) \leq nbjgrauto(t) \\
 & \qquad \qquad \qquad \text{then } \text{densite}(igers) = \text{densitesem}_T \quad (3.9)
 \end{aligned}$$

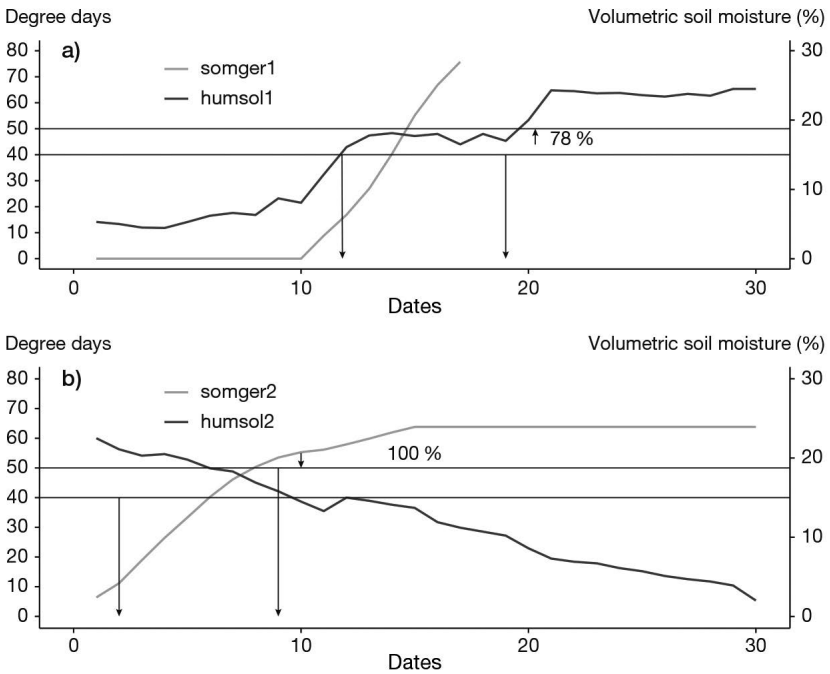


Figure 3.9. Chronology of germination represented for two different soil conditions: a) soil wetting and b) soil drying. The first arrow indicates the moistening date (soil above $potgermi_p$) and the second arrow the germination date. In the first case the required thermal time for germination ($stpltger_p = 50$ degree days) is not reached by six days ($nbjgerlim_p$) of moistening, which causes a decrease in density (78%).

3.4.1.3 Subsoil plantlet growth

Germination initiates the growth of the root and then of the shoot (see chapters 4 and 5). The growth rate of the shoot is assumed to be a logistic function (Eq. (3.10)) of soil degree-days that may slow down with unsuitable soil moisture (humirac).

$$\text{elong}(t) = \text{elmax}_p \cdot (1 - \exp(-(\text{belong}_p \cdot \sum_{j=\text{igers}}^t (\text{humirac}(\text{HB}, t) \cdot \text{crust}(t) \cdot (\text{tsol}(\text{HB}, t) - \text{tgmin}_p))^{\text{celong}_p}))) \quad (3.10)$$

The parameterisation of Eq. (3.10) can be significantly different in actual soil conditions when compared to laboratory conditions (finely sieved soil) because the presence of clods or compacted earth slows down the shoot's vertical upward growth. Emergence occurs when elongation (elong) is greater than sowing depth (**profsem_T**) as shown in Figure 3.10.

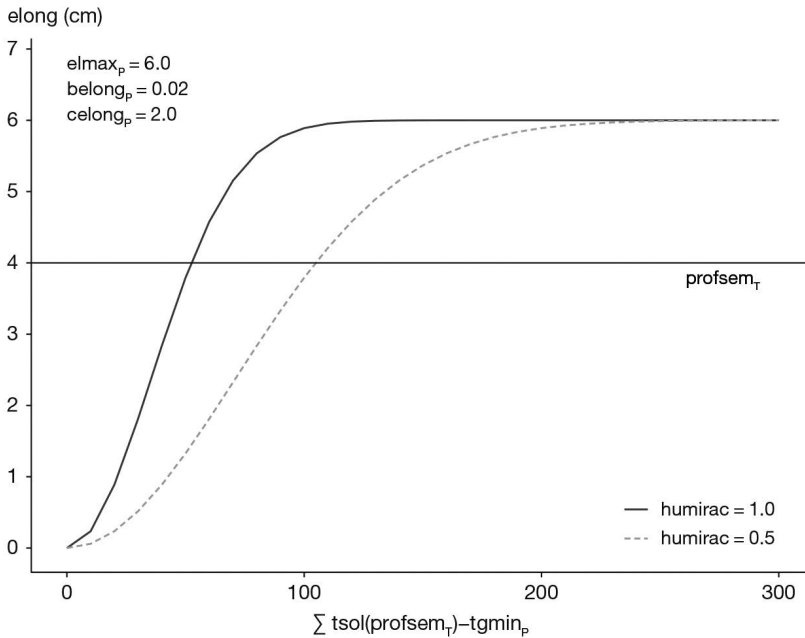


Figure 3.10. Elongation of the coleoptile (elong) as a function of soil temperature (tsol) and water status (humirac) and occurrence of emergence when $\text{elong} > \text{profsem}_T$.

Water status (humirac) is calculated as described in Eq. (3.8) by using the average soil moistures between the seedbed and the root front z_{rac} (layer denoted HB). The variable crust stands for soil crusting conditions and will be explained in the following section. In Eq. (3.10), **elmax_p**, **belong_p** and **celong_p** are species-dependent parameters.

As for germination, if the duration between germination (igers) and emergence (ilevs) is too long (**nlevlim_{1p}** and **nlevlim_{2p}** parameters in Figure 3.11), there may be emergence deficiencies represented by the variable coeflev (i.e. the ratio of the emerged to the germinated density (Eq. (3.11))).

$$\begin{aligned}
 & \text{if } ilevs - igers < \mathbf{nlevlim1}_p \text{ then } densite(ilevs) = densite(igers) \\
 & \text{if } \mathbf{nlevlim1}_p \leq ilevs - igers \leq \mathbf{nlevlim2}_p \\
 & \quad \text{then } densite(ilevs) = densite(igers) \cdot \text{coeflev}(ilevs) \\
 & \text{if } ilevs - igers > \mathbf{nlevlim2}_p \text{ then } densite(ilevs) = 0.0 \quad (3.11)
 \end{aligned}$$

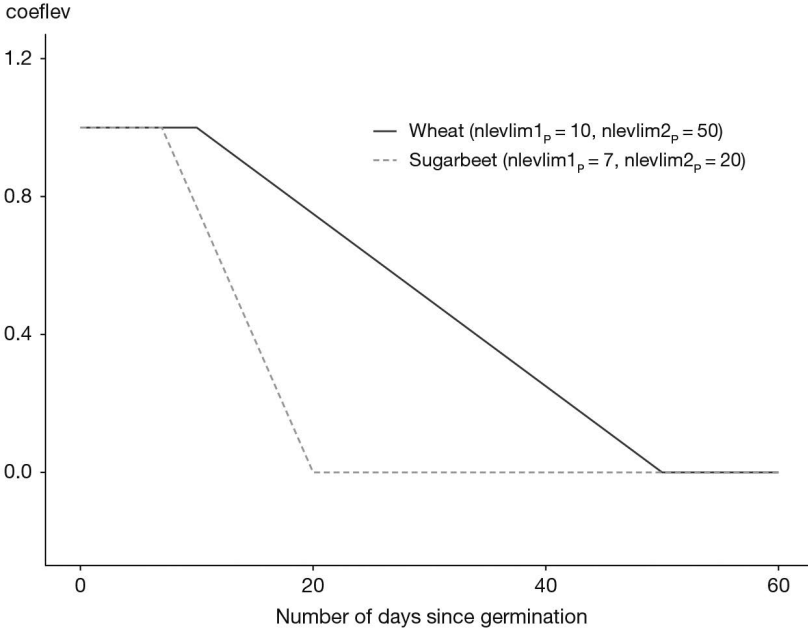


Figure 3.11. Simulation of emergence density proportion, $\text{coeflev}(ilevs)$, according to the length of the germination-emergence period ($ilevs_igers$).

The effect of frost on young plantlets can be simulated and causes an additional reduction in population density. The plantlet stage ($ilets$) is assumed to end at a defined number of leaves ($\mathbf{nbf gelle}_p$), calculated from the plastochrone ($\mathbf{phyllotherme}_p$). The frost damage function for emergence (fgelle) is calculated in the same way as other frost functions (§ 4.4.4.1) with thresholds of specific sensitivity for the plantlet stage ($\mathbf{tgelle}10_p$ and $\mathbf{tgelle}90_p$) and reduces the plant density in a multiplicative way (Eq. (3.12)).

$$densite(t) = densite(ilevs) \cdot \text{fgelle} \text{ where } ilevs < t < ilets \quad (3.12)$$

It may be necessary to modify the threshold values according to differential genetic tolerances and forms of frost occurrence (thermal amplitude, frost and thaw cycles).

3.4.1.4 Influence of soil crusting on emergence

In the particular case of loamy soils, a crust may occur after sowing, creating a physical obstacle to emergence (Duval and Boiffin, 1990). In addition to the textural characteristics of the surface soil layer, the development of such a crust depends on soil fragmentation following seedbed preparation and on the weather at the time. Indeed,

post-sowing rainfall may destroy soil fragments, and then drought renders this layer almost impenetrable for the plantlets, since the resistance to emergence depends on the weather through its evaporative demand and on the force exerted by the plantlet.

The formalisation of these processes in STICS relies partly on the work of Dürr *et al.* (2001). Surface crusting is assumed to occur only after sowing once a certain amount of rainfall (soil-dependent parameter **pluiebat_s**) has occurred. The crust is assumed to be dry when the natural mulch depth (xmulch: variable calculated from the soil evaporation formulations: see § 11.2.3)) is greater than the threshold parameter **mulchbat_s**, in which case xmulch is considered as the thickness of the crusted layer.

The subsequent delay in emergence can, just like the water deficit in the seedbed, reduce plant density. Yet not all the plantlets will be affected because of the heterogeneity of the crust and the differences in individual plantlet vigour. In STICS it is assumed that the ease of crust penetration is accounted for by a plant-dependent parameter (**vigueurbat_p**). The delay in emergence is formalised by stopping the accumulation of thermal time in Eq. (3.10) when the shoot reaches the base of the crust (crust=0.0 calculated in Eq. (3.13)).

$$\begin{aligned}
 & \text{if } \sum_{j=iplts}^t (trr(t)) \geq \text{pluiebat}_s \text{ then} \\
 & \text{if } xmulch(t) \geq \text{mulchbat}_s \text{ and } elong \geq \text{profsem}_r - xmulch(t) \\
 & \quad \text{then crust}(t) = 0.0 \\
 & \text{if } xmulch(t) < \text{mulchbat}_s \text{ and } elong < \text{profsem}_r - xmulch(t) \\
 & \quad \text{then crust}(t) = 1.0 \quad (3.13)
 \end{aligned}$$

The density reduction law is specific to the crusting phenomenon (coeflevb) but analogous to the other constraint law (coeflev depicted in Figure 3.12), with a minimum threshold corresponding to the **vigueurbat_p** parameter: if **vigueurbat_p** is greater than 0, which means that when the soil is crusted a proportion of plants succeed in emerging, the COEFEVB function is less effective than the water content and temperature-dependent coeflev function. The combination of both relationships is made dynamically by calculating the daily derivatives of both laws: if crust=0, which means a crust obstacle occurs the current day, the density reduction is calculated according to the coeflevb law; otherwise it is the COEFLEVB law that prevails (Figure 3.12).

Thus, as soon as significant rainfall occurs, the shoot continues to growth normally. Table 3.3 shows the sensitivity of the formalisations described above to the effect of soil crusting by varying the three required parameters.

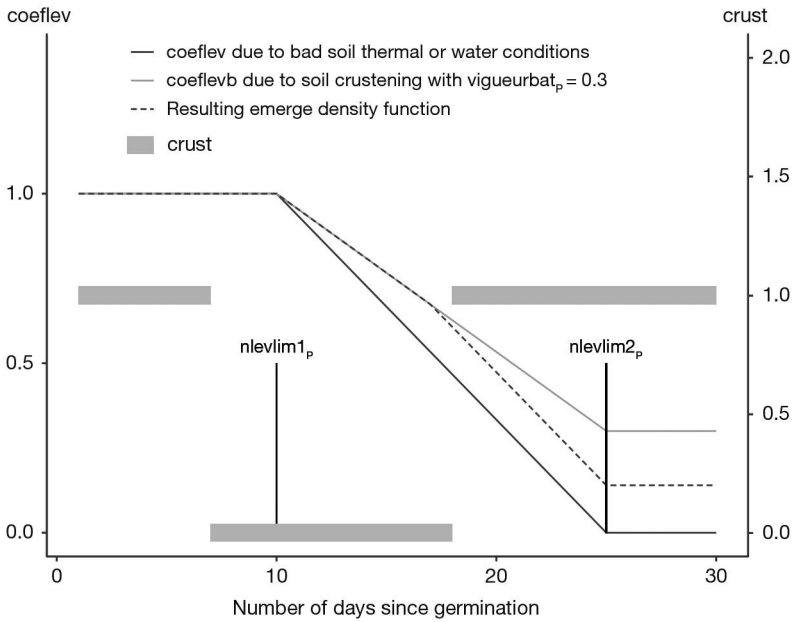


Figure 3.12. Combination of the two laws ($coeflev$ depending on non-optimal water content and temperature conditions and $coeflevb$ depending on the crust layer) affecting the emerged density as a function of the occurrence of the soil crust factor $crust=0.0$, which means a crust obstacle occurs, and the plantlet vigour ($vigueurbat_p$). The parameters $nlevlim1_p$ and $nlevlim2_p$ are defined in Eq. (3.11).

Table 3.3. Sensitivity analysis of the soil crusting parameters on the emergence variables (example of a maize crop in western France).

Sensitivity to crusting (SC)	No SC	High SC	Low SC	High SC
Plantlet vigour (PV)	–	High PV	Low PV	Low PV
pluiebat _s (mm)	50	3	9	3
mulchbat _s (cm)	0.5	0.5	1.5	0.5
vigueurbat _p	–	0.8	0.15	0.15
Sowing - emergence duration (days)	12	27	24	27
Emerged density relative to sown density (%)	77	64	31	19

Note: pluiebat and mulchbat are soil parameters, vigueurbat is a plant parameter.

3.4.2 Onset of crop development and growth after planting

For transplanted crops, a latency phase between planting and the onset of crop development can be simulated in the same way as the germination phase, based on accumulated growing degree-days. In this case, the simulated date of actual onset is the date corresponding to planting, to which is added the interval corresponding to the **stpltger_p** parameter, calculated from soil temperatures at the depth of planting and taking into account the effect of soil dryness, as in Eq. (3.7). The leaf area index (lai) of the plantlet (**laiplantule_p**) serves to initialise the dynamics of the leaf area index. If the 'coverage rate' option is selected rather than the 'LAI' option (see § 4.1.4), the **laiplantule_p** parameter must be given in terms of percentage of soil cover; otherwise, it is expressed in *lai* units (i.e. m² m⁻²). It is also possible to specify the number of leaves per plant (**nbfeuillplant_p**), which enables initialisation of the calculation of the number of leaves. In a similar way, biomass and rooting depth are initialised using the plant parameters **masecplantule_p** and **zracplantule_p**. The plantlet nitrogen content is calculated assuming the nitrogen use is only metabolic, i.e. as responding to the critical nitrogen curve for a low biomass canopy (see § 6.1.2.1) involving **adil_p** and the initial biomass (**masecplantule_p**) according to Eq. (3.14).

$$QNplantule(ipIts) = 10 \cdot \text{adil}_p \cdot \text{masecplantule}_p \quad (3.14)$$

3.4.3 Onset of crop development and growth in perennial plants

For perennial plants (e.g. grapevine), once the chilling requirements are met, the post-dormancy period (after dormancy break, *ifindorms*) is calculated using the sum of hourly temperatures (growing degree hours — GDH) obtained by the method of Richardson (Richardson *et al.*, 1975; 1974). To calculate GDH, the hourly temperature of day *t*, $T(h, t)$ is estimated very simply by linear interpolation between $Tn_x(t)$ and $Tn_x(t+1)$ by assuming a daylength of 12 h (example in García de Cortázar Atauri *et al.* (2009a), Eq. (3.15) and (3.16)).

$$\begin{aligned} T(h, t) &= Tn(t) + h \cdot ((Tx(t) - Tn(t))/12), \text{ if } h \leq 12 \\ T(h, t) &= Tx(t) - (h - 12) \cdot ((Tx(t) - Tn(t+1))/12), \text{ if } h > 12 \end{aligned} \quad (3.15)$$

Two cardinal temperatures limit the function of the linear response: T_{mindeb} and T_{maxdeb} .

$$\begin{aligned} Stdordebour &= \sum_{j=idebdorm}^t (T(h, t)) \\ &\text{with} \\ T(h, t) &= 0, \text{ if } T(h, t) < T_{mindeb} \\ T(h, t) &= T(h, t) - T_{mindeb}, \text{ if } T_{mindeb} < T(h, t) \leq T_{maxdeb} \\ T(h, t) &= T_{maxdeb} - T_{mindeb}, \text{ if } T_{maxdeb} > T(h, t) \end{aligned} \quad (3.16)$$

Finally, if the model is initialised at the **ilev_T** stage, the model assumes that the chilling requirements are met (note that this does not apply to annual crops). When the model is run for several years, the phasic and trophic status of the plant is saved from one year to the next (see § 14.2).

Chapter 4

Shoot growth

*LOÏC STRULLU, ALAIN MOLLIER, JEAN-LOUIS DURAND
AND NADINE BRISSON*

REVIEWED BY: NICOLAS BEAUDOIN AND BRUNO MARY

As all crop models do, STICS characterises the plant subsystem by its shoot biomass and leaf area index. Once calculated, the shoot biomass is partitioned into the various organs and feedback occurs between this partitioning and shoot growth for indeterminate plants. In STICS, indeterminate denotes species for which there is significant trophic competition between vegetative and harvested organs. This definition differs from the botanical one, and species like rapeseed or pea are considered as determinate in STICS. This is because the assumption of independence between vegetative and reproductive growth is acceptable, though these two developmental scales can overlap. Meanwhile, species like sugarbeet are regarded as indeterminate because the growing tuber greatly influences shoot growth. The harvested organs (grains, fruits or tuber) are the only ones characterized in terms of number (see § 8). The present chapter touches on various interrelated processes that are covered in other chapters. See figure 4.1 to see how the paragraphs of this chapter relate to other chapters.

►► 4.1 Leaf dynamics

4.1.1 Leaf area expansion

In most models, temperature is the main variable explaining potential leaf growth according to the crop's development stage (Abiven *et al.*, 2005; Amir and Sinclair, 1991; Hansen *et al.*, 1990; Weir *et al.*, 1984; Williams *et al.*, 1984). Yet in some models, the increase in the leaf surface area is derived from the increase in mass by means of the specific leaf area (van Keulen and Seligman, 1987). However, the specific leaf area is not a constant. It depends on the ratio between structural and non-structural mass (Thornley, 1996), which varies according to leaf age, temperature (Gary *et al.*, 1993), and the stresses experienced. As a result, this kind of formalism is not generally very robust (Tardieu *et al.*, 1999).

Many models have a marked preference for leaf-to-leaf simulation (Amir and Sinclair, 1991; Ritchie and Otter, 1985), using classic notions such as the phyllotherm and duration of leaf life (Muchow and Carberry, 1990). However Milroy and Goynes (1995)

cited several studies that showed that simulating leaf area index directly on a canopy scale produces results that are just as good as a leaf-to-leaf model. Baret (1986), Milroy and Goynes (1995), and Chapman *et al.* (1993) worked on a canopy scale and suggested dividing the evolution of leaf area index into two curves. The first curve represents growth (always a logistic curve) and the other senescence (logistic or exponential).

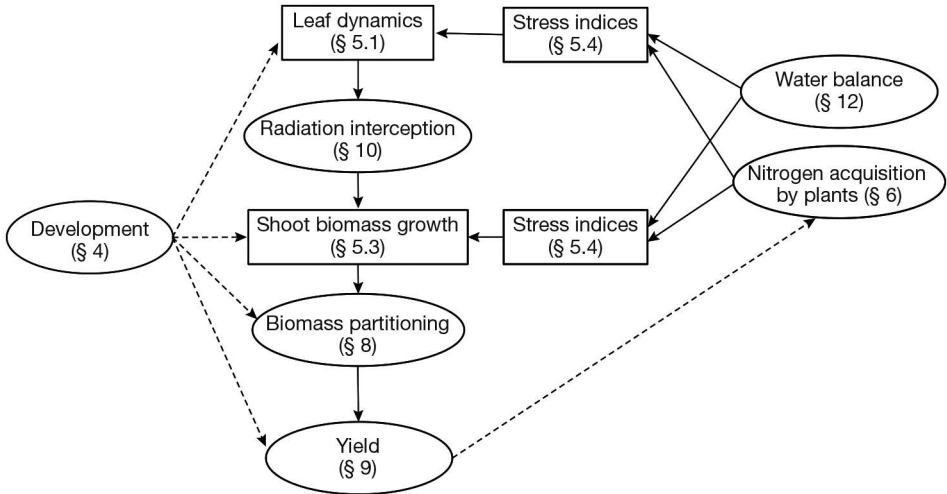


Figure 4.1. Main functional links between the paragraphs of this chapter and other chapters.

Several authors have proposed to make a direct link between the evolution of leaf area index and crop development (Dale *et al.*, 1980; Dwyer and Stewart, 1986; Hammer and Muchow, 1994; Nelder, 1961; Teittinen *et al.*, 1994). Jamieson *et al.* (1995) designed their model with four stages of evolution for leaf area index.

In STICS, leaf area growth is driven by phasic development, temperature and stresses. An empirical plant density-dependent function represents interplant competition. For indeterminate plants, trophic competition is taken into account through a trophic stress index, while for determinate plants a maximal expansion rate threshold is calculated to avoid unrealistic leaf expansion. In the first version of STICS (Brisson *et al.*, 1998b), net leaf growth was directly simulated, without splitting the evolution of the *lai* into gross growth and senescence, leading to a crude representation of leaf area index. However, when thinking in terms of efficiency of radiation interception, it appears that there is a plateau and the impact on radiation interceptions of high *lai* values is negligible (Allen and Richardson, 1968; Cowan, 1968; Otegui *et al.*, 1995; Varlet-Grancher and Bonhomme, 1979). However, simulation of senescence is necessary to have a good representations of C and N fluxes linked to leaf fall. Both options of simulations are always available in the model.

4.1.1.1 Valid calculations for all crop types

The leaf growth rate (Δlai in $m^2 m^{-2} d^{-1}$) is calculated as the product of four terms (4.1):

$$\Delta lai(t) = \Delta lai_{dev}(t) \cdot \Delta lai_T(t) \cdot \Delta lai_{dens}(t) \cdot \Delta lai_{stress}(t) \quad (4.1)$$

A first term (deltai_dev in $\text{m}^2 \text{ plant}^{-1} \text{ degree-day}^{-1}$) which represents the lai growth rate per plant follows a logistic curve, related to the $ilevs$, $iamfs$ and $ilaxs$ phenological stages. The other terms represent the effective crop temperature (deltai_T in degree-days), the plant density factor (deltai_dens) which represent the interplant competition and is specific of the variety, and the water and nitrogen stress index (deltai_stress).

The phasic development function (Eq. (4.2)) is comparable to that of the PUTU model (Singels and de Jager, 1991), i.e. a logistic function with dlaimaxbrut_p as the asymptote and pentlaimax_p as the slope at the inflexion point. This function is driven by a normalised leaf development unit ($ulai$) equal to 1 at stage $ilevs$ and 3 at stage $ilaxs$. At the end of the juvenile stage (stage $iamfs$), it is equal to vlaimax_p at the inflexion point. Between the stages $ilevs$, $iamfs$ and $ilaxs$, the model performs linear interpolation based on development units ($upvt$), which include all the environmental effects on phasic development (see § 3.3). As the $ilaxs$ stage approaches, a gradual decline in growth rate can be introduced using the udlaimax_p parameter corresponding to the $ulai$ value beyond which there is a decline in the leaf growth rate. If udlaimax_p is equal to 3, it has no effect and the leaf stops growing when the $ilaxs$ stage is reached (Figure 4.2).

$$\text{deltai_dev}(t) = \frac{\text{dlaimaxbrut}_p}{1 + \exp(\text{pentlaimax}_p \cdot (\text{vlaimax}_p - \text{ulai}(t)))} \text{ if } (\text{ulai}(t) < \text{udlaimax}_p)$$

$$\text{deltai_dev}(t) = \text{vlaimax}_p \cdot \left(1 - \frac{\text{ulai}(t) - \text{udlaimax}_p}{3 - \text{udlaimax}_p}\right)^2 \text{ if } (\text{ulai}(t) \geq \text{udlaimax}_p) \quad (4.2)$$

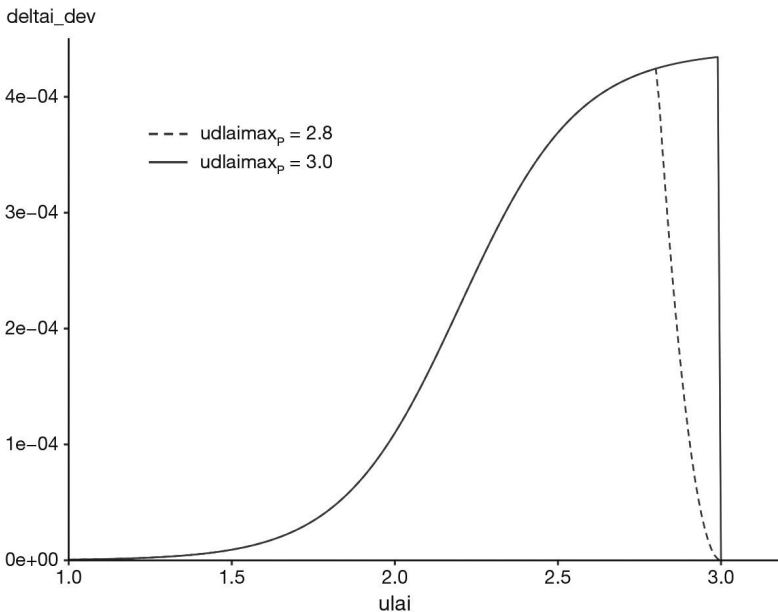


Figure 4.2. Leaf growth rate as a function of phasic development with the parameterisation corresponding to a wheat crop as given in Singels and de Jager (1991) ($\text{pentlaimax}_p = 5.5$, $\text{vlaimax}_p = 2.2$ and $\text{dlaimaxbrut}_p = 4.410^{-4}$) for two values of the parameter udlaimax_p .

The thermal function relies on crop temperature and cardinal temperatures (\mathbf{tcmin}_p and \mathbf{tcmax}_p), which differ from the temperatures used for the phasic development. The extreme threshold $\mathbf{tcxstop}_p$ is the same as for development.

$$\begin{aligned}
 \text{if } tcult(t) \leq \mathbf{tcmin}_p & \quad \text{deltai}_T(t) = 0 \\
 \text{if } \mathbf{tcmin}_p < tcult(t) < \mathbf{tcmax}_p & \quad \text{deltai}_T(t) = tcult(t) - \mathbf{tcmin}_p \\
 \text{if } \mathbf{tcmax}_p \leq tcult(t) < \mathbf{tcxstop}_p & \quad \text{deltai}_T(t) = \frac{\mathbf{tcmax}_p - \mathbf{tcmin}_p}{\mathbf{tcmax}_p - \mathbf{tcxstop}_p} \cdot (tcult(t) - \mathbf{tcxstop}_p) \\
 \text{if } tcult(t) \geq \mathbf{tcxstop}_p & \quad \text{deltai}_T(t) = 0 \quad (4.3)
 \end{aligned}$$

The density function (deltai_{dens}), is active when the leaf area index threshold ($\mathbf{laicomp}_p$) is reached and if the plant density (in plant m^{-2} calculated as explained in § 3.4 and possibly decreased by early frost, see § 4.4.4) is greater than the \mathbf{bdens}_p threshold, below which the plant leaf area is assumed independent of density (Eq. (4.4)). Beyond this threshold, leaf area per plant decreases exponentially. The \mathbf{adens}_p parameter represents the ability of a plant to withstand increasing densities. It depends on plant species and may depend on the variety (Figure 4.3).

For branching or tillering plants, \mathbf{adens}_p represents the plant branching or tillering ability (e.g. for wheat or pea). For single-stem plants, \mathbf{adens}_p represents competition between plant leaves within a given stand (e.g. for maize or sunflower).

$$\begin{aligned}
 \text{deltai}_{dens}(t) &= \text{densite}(t) \cdot \left(\frac{\text{densite}(t)}{\mathbf{bdens}_p} \right)^{\mathbf{adens}_p} \\
 \text{deltai}_{dens}(t) &= \text{densite}(t) \text{ if } lai(t) < \mathbf{laicomp}_p \text{ or } \text{densite}(t) < \mathbf{bdens}_p \quad (4.4)
 \end{aligned}$$

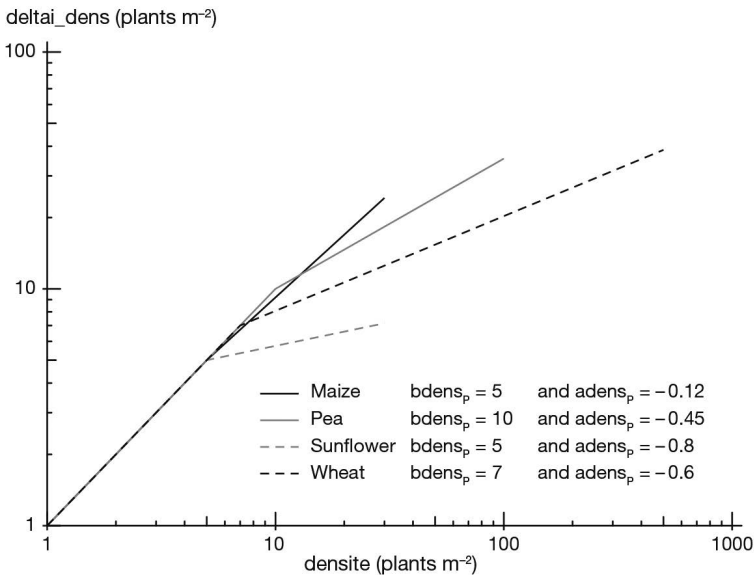


Figure 4.3. Density function deltai_{dens} versus plant density for various species (wheat, maize, pea and sunflower).

In the case of intercropping, the model calculates an equivalent plant density for the understorey crop ($densite_{equiv}$), which accounts for the presence of the dominant crop. If $densite_d$ and $densite_u$ are the planting densities of the dominant and the understorey crops respectively and $bdensd_p$ and $bdensu_p$ are the threshold densities for inter-plant competition, the equivalent density is calculated as in Eq. (4.5):

$$densite_{equiv}(t) = densite_u(t) + densite_d(t) \cdot \frac{bdensu_p}{bdensd_p} \quad (4.5)$$

This empirical relationship enables to simulate an increase in inter-plant competition compared to single crop (Figure 4.4)

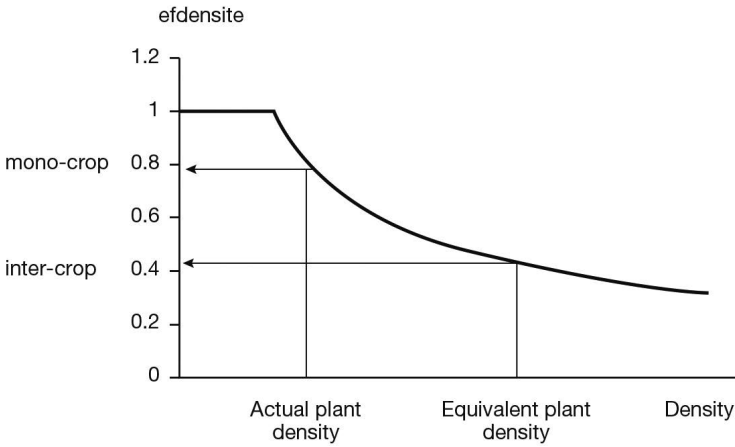


Figure 4.4. Illustration of the calculation of the equivalent plant density for the understorey crop.

Water and nitrogen can be limiting factors for growth, with stress indexes whose values vary between 0 and 1 (see § 4.4). Water ($turfac$) and nitrogen indexes ($innlai$) are assumed to interact, thereby justifying the use of the most severe of the two stresses. Meanwhile at the whole plant level, in the rare occasions where water deficit and water logging ($exolai$) occur in different horizons of the root zone, the water-logging stress index is assumed to act independently (Eq. (4.6)).

$$\delta_{tai_stress}(t) = \min(turfac, innlai(t) \cdot exolai(t)) \quad (4.6)$$

4.1.1.2 Determinate crops features

Failure to account for trophic aspects when calculating leaf growth may cause problems when the crop intercepts insufficient radiation to ensure leaf expansion (e.g. for crops under a tree stage or crops growing in winter). A trophic effect can be simulated from the $iamfs$ to calculate the growth rate (δ_{tai}) by considering a maximum threshold for leaf expansion (δ_{taimax} in $m^2m^{-2}d^{-1}$) using the notion of the maximum leaf expansion allowed per unit of biomass accumulated in the plant ($sbvmax$ in $cm^2 g^{-1}$) and the daily biomass accumulation ($dltams$ in $t.ha^{-1}day^{-1}$, possibly complemented by remobilised reserves $remobilj$ and $dltaremobil$). The $sbvmax$ variable is calculated using the $slamax_p$ and $tigefeuil_p$ parameters (Eq. (4.7)).

$$sbvmax = \frac{slamax_p}{1+tigefeuil_p}$$

$$and \text{deltai}_{max}(t) = (dltams(t-1) + dltaremobil(t-1) + remobilj(t-1)) \cdot sbvmax \cdot 10^{-2}$$

if $\text{deltai}_1(t) < \text{deltai}_{max}(t)$ or $t < iamf$

$$\text{deltai}_2(t) = \text{deltai}_1(t)$$

if $\text{deltai}_1(t) \geq \text{deltai}_{max}(t)$ or $t \geq iamf$

$$\text{deltai}_2(t) = \text{deltai}_{max}(t) \tag{4.7}$$

Figure 4.5 illustrates the evolution of the *lai* growth rate of a wheat crop receiving reduced radiation (20% of incoming radiations), which can happen under a tree canopy compared to a crop in the open field.

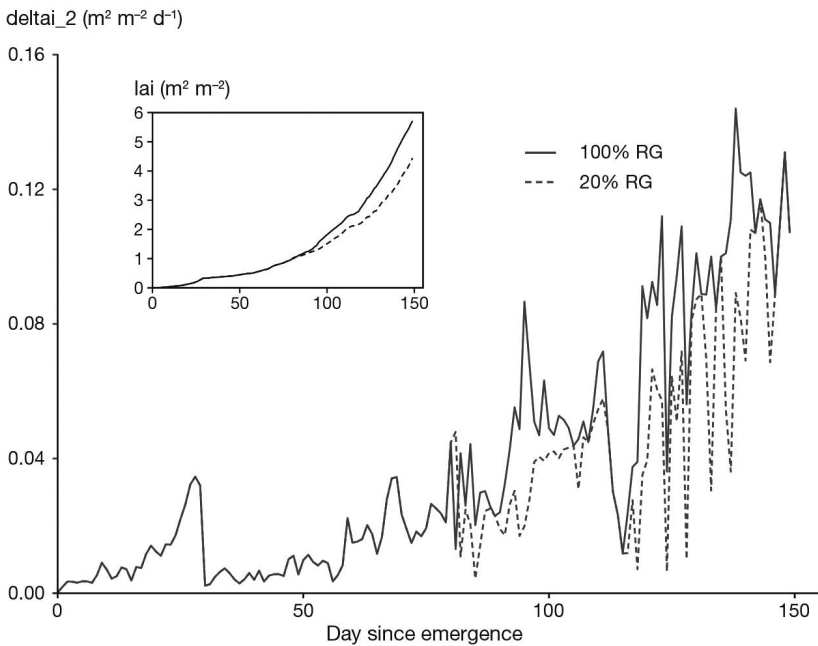


Figure 4.5. *lai* growth rate dynamics (deltai_2) of a durum wheat crop in southern France with 100 % and 20 % of the incoming radiation (RG) without any stress and the evolution of *lai* values during the growing phase.

4.1.1.3 Indeterminate crops features

The robustness of the formalism described above has been tested on a variety of crops, including those for which the vegetative and reproductive phases overlap (e.g. soybean and flax). The formalism is unsuitable when trophic competition between leaves and fruits is a driving force for crop production and management (e.g. tomato or sugar-beet). In this case, a second calculation is made (deltai_-) in order to account for trophic constraints in indeterminate crops (Eq. (4.8)), by introducing a trophic stress index ($splai$, explained in § 4.4.3).

$$\text{deltai}_2(t) = \text{deltai}_1(t) \cdot \text{splai}(t) \quad (4.8)$$

As a consequence, the leaf area index can decrease markedly during the growth phase if the crop experiences severe stresses during the harvested organ filling phase, as shown in Figure 4.6 for sugarbeet.

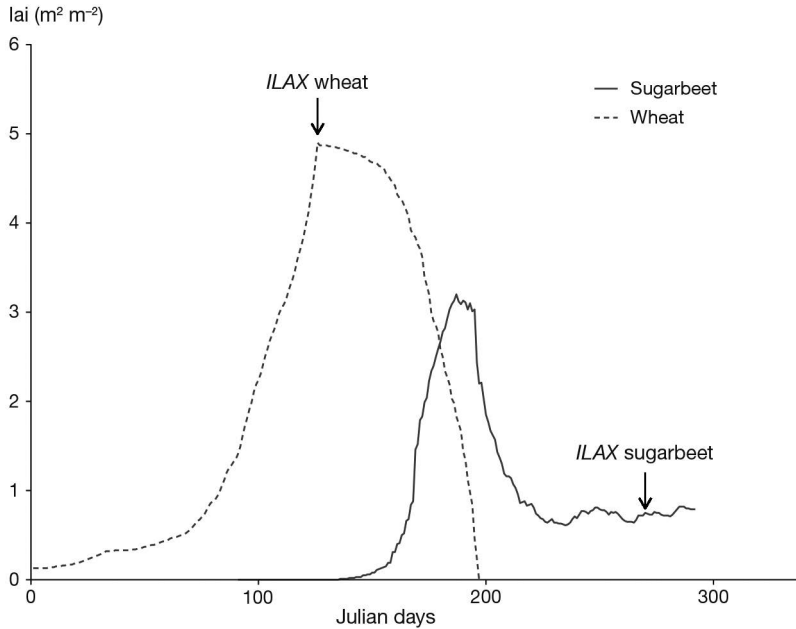


Figure 4.6. Comparison of determinate (wheat) and indeterminate (sugarbeet) *lai* dynamics. The ILAX stage indicates the end of leaf onset.

4.1.2 Senescence

In STICS, shoot senescence only concerns leaf dry matter and leaf area index. For crops that are harvested more than once (e.g. temporary or artificial grasslands), shoot senescence also affects the aerial biomass remaining after harvest. While senescence was implicit in the first versions of the model (Brisson *et al.*, 1998b), it is now explicit, with a clear distinction between natural senescence due to ageing of leaves, and senescence accelerated by stresses (water, nitrogen, frost). The concept of leaf lifespan, used for example by Maas (1993), is applied to the green leaf area and biomass produced. The leaf area and a fraction of the leaf biomass produced on a given day (see § 7) is therefore lost through senescence once the lifespan has elapsed (Duru *et al.*, 1995). This fraction corresponds to the **ratiosen_p** parameter (0-1), and its complement to 1 represents the fraction remobilised by the plant during senescence.

4.1.2.1 Calculating lifespan

The maximum leaf lifespan (*durage*) is determined by two values: the lifespan of early leaves (*durviel*) and the lifespan of the last leaves emitted **durvieF_p** genotype-dependent. *durviel* is calculated as the product of **durvieF_p** and the parameter **ratiodurvie_p**.

Until the iamfs stage, the maximum lifespan, calculated for the day when the leaves are emitted (t_0) is $durviel$; from iamfs to ilaxs, the maximal lifespan increases between $durviel$ and $durvieF_p$ as a function of the leaf development variable $ulai$:

$$durvieI = durvieF_p \cdot ratiodurvie_p$$

$$durage(t_0) = durvieI + \frac{ulai(t_0) - v_{laimax_p}}{3 \cdot v_{laimax_p}} \cdot (durvieF_p - durvieI) \quad (4.9)$$

Water or nitrogen stress may shorten the current lifespan if the stress on day t is more intense than the previous stresses encountered since time t_0 (Eq. (4.10)). Two specific stress indices for senescence are introduced: $senfac$ and $innsenes$ (see § 4.4). Frost ($fstressgel$, which can be either $fgeljuv$ or $fgelveg$; see § 4.4.4) may also reduce or even cancel lifespan. In case of high availability of nitrogen ($inn > 1$), the foliage lifespan is increased from the iamfs stage up to a maximum given by the $durviesupmax_p$ parameter:

$$senstress(t) = \min(senfac(t), innsenes(t), fstressgel(t))$$

$$durvie(t) = durviesup(t) + durage(t_0) \cdot \min[senstress(t)]$$

$$durviesup(t) = durvieF_p \cdot \min(durviesupmax_p, (inn(t) - 1)) \quad \text{if } inn(t) > 1$$

$$durviesup(t) = 0 \quad \text{if } inn(t) \leq 1 \quad (4.10)$$

Leaf lifespan is not expressed in degree days (like phasic development), because doing so has the disadvantage of stopping any progression as soon as the temperature drops below the base temperature ($tdmin_p$). To remedy this problem, the senescence course

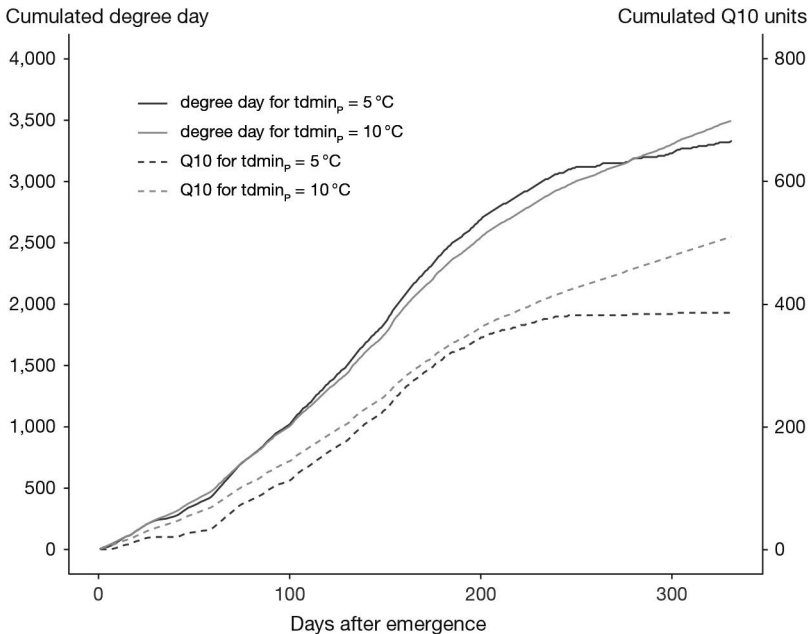


Figure 4.7. Comparison between phasic development courses expressed in degree days and in Q10 units for two $tdmin_p$ values.

between t_0 and t (somsen) is expressed by cumulative Q10 units (with $Q10=2$), i.e. an exponential-type function:

$$\text{somsen}(t) = \sum_{t=t_0}^t 2^{\frac{\text{udevcult}(t) \cdot (\text{stressdev}_p \cdot \min(\text{turfac}, \text{imlai}) + 1 - \text{stressdev}_p)}{10}} \quad (4.11)$$

The senescence course is affected by the same cardinal temperatures as phasic development and can be slowed down by stresses (see § 3.3.1. The leaf lifespan parameter (durvieF_p) expressed in Q10 units represents about 20% of the same lifespan expressed in degree days (Figure 4.7).

4.1.2.2 Calculating senescence

Material produced on day t_0 disappears via senescence after a period corresponding to $\text{durvie}(t_0)$. Depending on the evolution of temperature and lifespan as a function of phenology and stresses, senescence can vary from one day to another and affect several days of production ($J=t_0, t_0+1, \dots$) or may not occur if $\text{somsen} < \text{durvie}(t_0)$ (Eq. (4.12)). This principle is applied to the senescent leaf area (dltaisen) and the senescent biomass (dltamsen).

$$\begin{aligned} \text{if } \text{somsen}(t) &\geq \sum_{t=t_0}^t \text{durvie}(t) \\ \text{dltaisen}(t) &= \sum_{t=t_0}^t \text{deltai}(t) \\ \text{dltamsen}(t) &= \sum_{t=t_0}^t \text{dltams}(t) \cdot \text{ratiosen}_p \cdot \text{pfeuilverte}(t) \end{aligned} \quad (4.12)$$

where pfeuilverte is the proportion of leaf mass to total biomass produced on the current day, and the parameter ratiosen_p represents the fraction of leaf biomass which becomes senescent since part of the dead leaf biomass is remobilised and does not completely disappear.

The cumulative senescent foliage area is laisen . In forage crops (e.g. grasslands or alfalfa) with residual dry matter from the previous regrowth cycle (msresiduel_T), the senescence of residual dry matter (deltamsresen) starts from cutting. The senescent rate is calculated as follows:

$$\text{deltamsresen}(t) = \text{msresiduel}_T \cdot \text{ratiosen}_p \cdot \left(\frac{\text{tdevelop}(t)}{\text{durvieI}} \right) \quad (4.13)$$

Leaves falling onto the soil during crop growth are another source of organic residue. The falling rate is calculated with the parameter abscission_p which is the proportion of senescent leaves falling down. This phenomenon can be significant for some crops, such as rapeseed in winter after frost events. The decomposition of the fallen leaves at soil surface is simulated by the decomposition module (category 2, young plant residues). The C/N ratio of leaves when they fall off (CsurNresid) is calculated based on the nitrogen nutrition index of the whole crop using the plant parameter parazofmorte_p , as proposed by Dorsainvil (2002):

$$\text{CsurNresid}(t) = \frac{\text{parazofmorte}_p}{\text{inn}(t)} \quad (4.14)$$

Decomposition of organic residues is presented in § 12.

4.1.3 Photosynthetic function of storage organs

As storage organs mature, the chlorophyll function of the organs or their envelopes may induce significant biomass accumulation. Such processes have been demonstrated for wheat ears (Abbad *et al.*, 2004; Araus *et al.*, 1993; Casals, 1996) and also exist in rapeseed siliquae, pea pods or grapes during their green period. To account for this effect, we have introduced a parameter, \mathbf{sea}_p ($\text{cm}^2 \text{g}^{-1}$) which converts the biomass of these membranes ($\mathbf{maenfruit}$ defined in § 7.5 into their equivalent leaf surface area (\mathbf{eai}):

$$\mathbf{eai}(t) = \mathbf{maenfruit}(t) \cdot \frac{\mathbf{sea}_p}{100} \quad (4.15)$$

The assumption is that the photosynthetic function of storage organs lasts from the beginning of grain/fruit filling (\mathbf{idrps}) to the beginning of dehydration ($\mathbf{idebdess}$) stages.

4.1.4 Using ground cover instead of the leaf area index

Given the complexity and the numerous parameters required to calculate the leaf area index, De Tourdonnet (1999) proposed a simple alternative by directly calculating ground cover, which can be used as a status variable in calculations for radiation interception and water requirements. This can be particularly useful for plants with a complex foliage structure such as lettuce, or for a first modelling approach. This method is programmed in STICS as an alternative option to all previous calculations. It is of particular interest when leaves have a complex spatial arrangement or when the individual plant foliage is abundant.

To calculate ground cover ($\mathbf{tauxcouv}$), a temporal scale similar to that of \mathbf{lai} is used and called \mathbf{ulai} ; this scale varies from 0 to 2, depending on the phenological time. The competitive effect linked to population growth ($\mathbf{efdensite}$) is simulated similarly to that for the leaf area index and uses the same parameters, \mathbf{adens}_v , \mathbf{bdens}_p and $\mathbf{laicomp}_p$ (expressed as ground cover). The variable $\mathbf{tauxcouv}$ is calculated using a logistic curve:

$$\mathbf{efdensite} = 1 \text{ if } \mathbf{tauxcouv}(t-1) < \mathbf{laicomp}_p$$

$$\mathbf{efdensite} = \exp\left(\mathbf{adens}_p \cdot \left(\log\left(\frac{\mathbf{densite}(t)}{\mathbf{bdens}_p}\right)\right)\right)$$

$$\mathbf{efdensite} = 1 \text{ if } \mathbf{efdensite} > 1$$

$$\mathbf{tauxcouv}(t) = \mathbf{laiplantule}_p + \mathbf{efdensite} \cdot \mathbf{densite}(t) \cdot \left(\frac{\mathbf{tauxrecouvmax}_p}{1 + \exp(\mathbf{pentrecouv}_p(\mathbf{infrecouv}_p - \mathbf{ulai}(t)))}\right)$$

$$\mathbf{tauxcouv}(t) = 1 \text{ if } \mathbf{tauxcouv}(t) > 1 \quad (4.16)$$

where $\mathbf{tauxrecouvmax}_p$ is the asymptote, which represents the proportion of the soil covered by an isolated plant, $\mathbf{infrecouv}_p$ is the abscissa of the inflexion point, and $\mathbf{pentrecouv}_p$ is the slope at the inflexion point. At the \mathbf{iampfs} stage, \mathbf{ulai} is equal to $\mathbf{infrecouv}_p$.

The parameter $la_{plantule_p}$ is the plant ground cover at planting if the crop is transplanted rather than sown. Figure 4.8 shows the simulated evolution of ground cover for a lettuce crop with two planting densities.

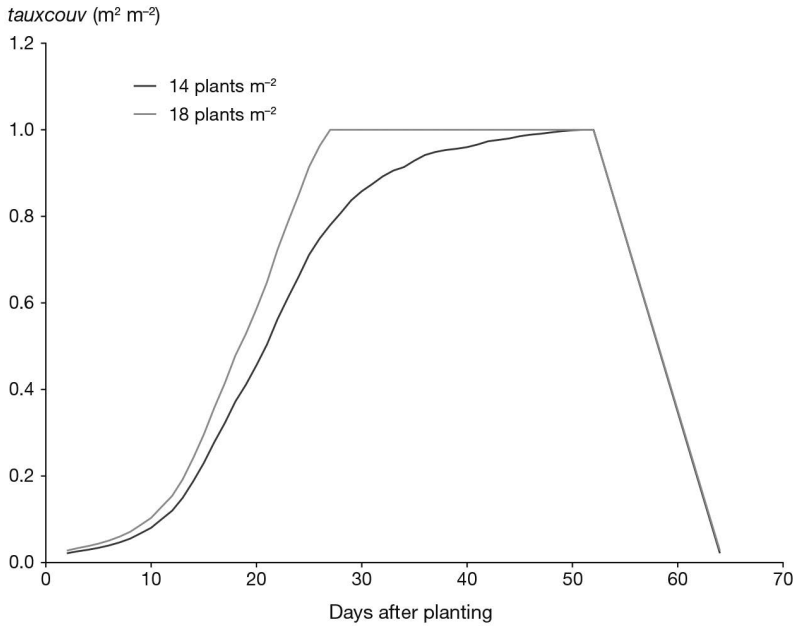


Figure 4.8. Ground cover dynamics for a lettuce crop comparing two plant densities. Parameters: $trecou_{max_p} = 0.072$, $infrecou_p = 0.85$, $pentrecou_p = 4.5$, $adens_v = -0.4$, $bdens_p = 5$, $la_{comp_p} = 0.14$.

Water and nitrogen shortage and waterlogging stresses are applied to the rate of ground cover growth, calculated as the derivation of Eq. (4.16). The method of combining stresses is the same as for the leaf area index: δai_{stress} described in Eq. (4.6).

4.1.5 Number of leaves

The calculation of the number of leaves ($nbfeuille$) is mainly indicative. Its only active role is to define the duration of the plantlet phase when calculating frost risks (see § 4.4.4). Indeed the plantlet stage is calculated as a leaf-number stage (2 or 3). The $nbfeuille$ variable is calculated up to the $ilaxs$ stage from the phyllotherm (the thermal period separating the emission of two successive visible leaves, $phyllotherme_p$ expressed in crop degree days as with phasic development).

4.1.6 Green leaf specific area

Although STICS does not use the specific leaf area (sla) as a driving variable to directly calculate leaf area from the carbon balance, it is useful for certain tests and can at least be valuable as an output Eq. (4.17).

$$sla(t) = \min(tursla(t), slamax_p, slamin_p) \quad (4.17)$$

The variable $tursla$ is the mean water stress turfacc experienced since emergence, and $slamax_p$ and $slamin_p$ are two parameters which define the limits of variation in specific leaf area sla between a satisfactory water level and a state of extreme stress.

►► 4.2 Radiation interception

Radiation interception can be calculated in different ways in the STICS model. These calculations are described in § 9.

►► 4.3 Biomass production

The linear relationship between accumulated biomass in the plant and radiation intercepted by foliage, as demonstrated by Monteith (1972), defines the radiation use efficiency (RUE) as the slope of this relationship. The total cumulated intercepted visible radiation is calculated following the procedure described in § 9. It is supposed to stay constant during relatively long periods of developments, where it takes the value of the ratio between cumulated above-ground biomass and cumulated absorbed or intercepted radiation. RUE is widely employed in crop models (Bonhomme *et al.*, 1982; Jeuffroy and Recous, 1999; Ritchie and Otter, 1985), because it synthesizes the processes of photosynthesis and respiration and therefore is very conservative in terms of the number of parameters. The value of this parameter also depends on the carbon allocation coefficient between aboveground and belowground parts of the plant, for the development period considered. Obviously, because of underlying physiological processes that ratio also varies with stresses, temperature and phenology (Muchow *et al.*, 1990; Sinclair *et al.*, 1993; Trapani *et al.*, 1992). To account for these effects, Sinclair (1986) proposed that RUE should be considered as a physiological function, to which stress indices should be applied. In other models (Boote *et al.*, 2018; Weir *et al.*, 1984) the photosynthesis and respiration processes are calculated separately and a specific allocation to roots is assumed. In view of the increasing atmospheric CO_2 concentration, crop models now need to take this factor into account Toreti *et al.* (2020).

The daily production of shoot biomass ($dltams$; Eq. (4.18)) is calculated using the RUE concept taking into account four factors known to influence the gross photosynthesis and respiration, defined in § 4.4 (f_{temp} , $swfac$, $inns$ and $exobiom$):

$$\begin{aligned} dltams(t) = & (ebmax(t) \cdot raint(t) - \mathbf{coefb}_G \cdot raint(t)^2) \cdot \\ & ftemp(t) \cdot swfac(t-1) \cdot inns(t-1) \cdot exobiom(t-1) \cdot fco2(t) \\ & + dltaremobil(t) \quad (4.18) \end{aligned}$$

where $ebmax$ is the maximum radiation use efficiency, $raint$ is the intercepted PAR (photosynthetically active radiation) and the parameter \mathbf{coefb}_G corresponds to the radiation saturating effect. This effect is the result, even buffered, of the saturation occurring within a short time step on the individual leaf scale and is easily observed when daily calculations are made with instantaneous formulae of canopy photosynthesis (Boote and Jones, 1987); such calculations lead to a value of 0.0815. Note that some variables are relative to previous day because of the consecutive nature of the calculations and modules. Summing up the variable $dltams$ throughout time gives the biomass of non-perennial organs for annual crops or both perennial and non-perennial organs for perennial crops, depending on simulation options (see § 7).

4.3.1 Influence of radiation and phasic development

Shoot biomass accumulation depends on the intercepted radiation ($raint$) (Varlet-Grancher *et al.*, 1981), and is almost linear but slightly asymptotic at high intercepted light values. It is simulated in STICS by a parabolic function involving a maximum radiation use efficiency specific to each species, $ebmax$ (Eq. (4.19)). Efficiency $ebmax$ may differ during the juvenile (ilevs-iamfs), vegetative (iamfs-idrps) and reproductive (idrps-imats) phases (corresponding to the parameters $efcroijuv_p$, $efcroiveg_p$ and $efcroirepro_p$, respectively):

$$\begin{aligned}
 ebmax &= \frac{efcroijuv_p}{100} \quad \text{if } namf = 0 \\
 ndrps = 0 \text{ then } ebmax &= \frac{efcroiveg_p}{100} \quad \text{if } namf > 0 \\
 ebmax &= \frac{efcroirepro_p}{100} \quad \text{if } ndrps > 0 \quad (4.19)
 \end{aligned}$$

Classically, the value of $efcroijuv_p$ equal to half of $efcroiveg_p$ is used to account for the preferential migration of assimilates towards the roots at the beginning of the growth cycle. The difference between $efcroiveg_p$ and $efcroirepro_p$ arises from the biochemical composition of storage organs: for example, for oil or protein crops, $efcroirepro_p$ is less than $efcroiveg_p$ because the respiratory cost to make oil and protein is higher than for starch or saccharose (Figure 4.9).

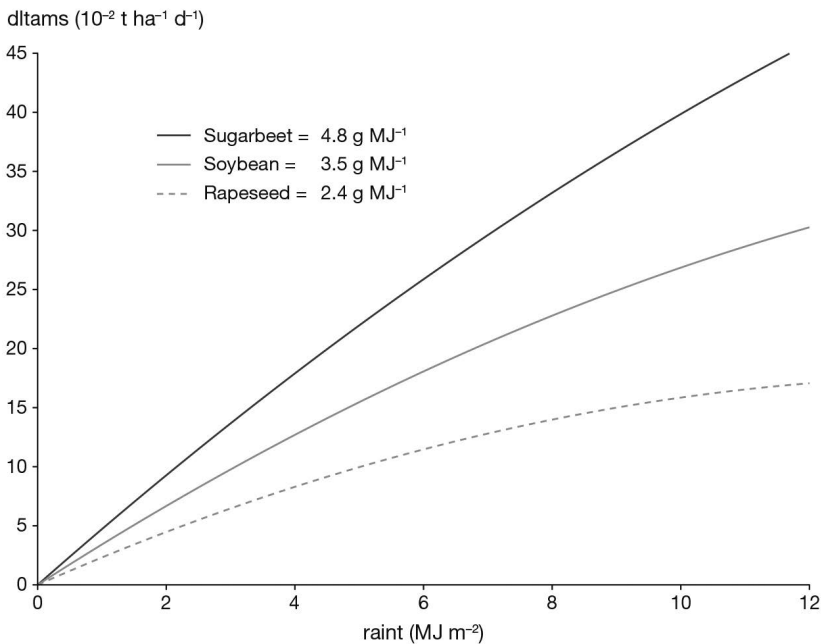


Figure 4.9. Potential daily biomass accumulation ($dltams$) versus intercepted radiation ($raint$) for three species during their filling stage. The parameter $efcroirepro_p$ is set at 4.8, 3.5 and 2.4 g MJ⁻¹ for sugarbeet, soybean and rapeseed respectively.

4.3.2 Effect of atmospheric CO₂ concentration

The CO₂ variable corresponds to the atmospheric CO₂ concentration, which can be higher than the reference value, assumed to be 350 ppm. The formalism chosen in STICS was adapted from Stockle *et al.* (1992): the effect of CO₂ on the relative radiation use efficiency (Eq. (4.20)) is simulated by an exponential relationship:

$$f_{co2}(t) = 2 - \exp\left(\log\left(2 - \mathbf{alphaCO2}_p\right) \cdot \frac{CO2(t) - 350}{600 - 350}\right) \quad (4.20)$$

where the parameter $\mathbf{alphaCO2}_p$ represents the sensitivity of the crop growth to the CO₂ concentration. It is calculated so that the curve passes through the point (600, $\mathbf{alphaCO2}_p$). It mainly varies with the plant metabolism (C3/C4), being around 1.1 for C4 crops and 1.2 for C3 crops (Peart *et al.*, 1989; Ruget *et al.*, 1996; Stockle *et al.*, 1992). The effect of CO₂ on stomatal resistance will be covered in the paragraph on water requirements (see § 9.3).

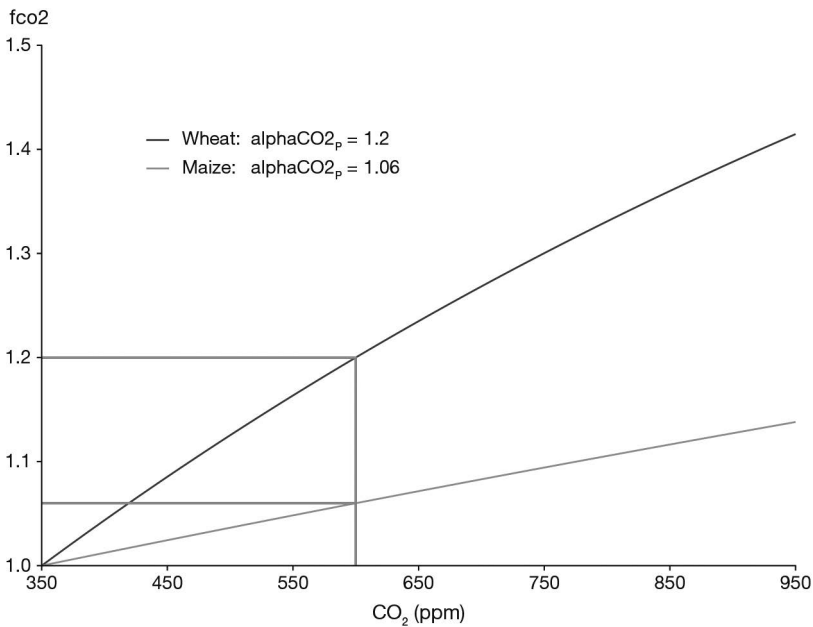


Figure 4.10. Relative radiation use efficiency versus atmospheric CO₂ concentration for two crop species. The parameter $\mathbf{alphaCO2}_p$ is 1.20 for wheat and 1.06 for maize.

4.3.3 Height-biomass conversion

For forage crops, it may be necessary to estimate an initial biomass value after each cutting on the basis of canopy height. The relationship between the two variables is:

$$\mathbf{msresiduel}_T = \mathbf{coefmshaut}_p \cdot (\mathbf{hautcoupe}_T - \mathbf{hautbase}_p) \quad (4.21)$$

The proportionality coefficient $\mathbf{coefmshaut}_p$ depends on plant type; it is set at 25 t ha⁻¹ m⁻¹ for grass.

►► 4.4 Stress indices

Stresses accounted for in most crop models are only of abiotic nature. They are represented by functions, varying between 0 and 1, that reduce process rates depending on stress variables such as fraction of transpirable soil water, nitrogen nutrition index, fraction of root system in waterlogged conditions etc. These stress variables must therefore also be calculated.

The reduction functions are empirical relationships based on the limiting factor principle. An overview of the concept was given by Gary *et al.* (1995). Nonetheless, they are based on our knowledge about the effects of stresses on plant growth and development. For example, water stress acts via a hormonal or hydraulic signal on stomatal conductance, which causes a reduction in photosynthesis and hence in radiation use efficiency. The empirical function links the reduction in radiation use efficiency directly to water stress. Similarly, water stress slows down cell expansion and division, phenomena which cause a reduction in leaf appearance and expansion and hence in the rate of increase of leaf area index. The empirical function then directly links the reduction in leaf area index increase to water stress. Yet as demonstrated by Boyer (1970) and reviewed in Bradford and Hsiao (1982) for water stress, the sensitivity of the various physiological functions can vary, thus requiring the calculation of several stress indices for the same stress status variable.

The regulation involved in interactions between stresses is poorly understood on the whole plant scale, and is therefore modelled very simply by using either the product or the minimum of the reduction factors. Improved physiological approaches (e.g. Farquhar *et al.*, 1980) could lead to more realistic models for photosynthetic processes, but raise the problem of parameterisation.

Most of the relationships in STICS are simple bilinear functions, i.e. equal to a constant until a critical level of the stress status variable is reached, when it then decreases linearly. The relationships are more complex for frost and waterlogging. The soil water content in the rooting zone is the water deficit stress variable, the nitrogen nutrition index is the nitrogen stress variable, the source/sink ratio is the trophic stress variable, the minimal crop temperature is the frost stress variable and the proportion of roots flooded is the water logging stress variable. The sensitivity to the various stresses can be represented by appropriate parameterisations of the stress functions or by a sensitivity parameter (e.g. for waterlogging or for roots sensitivity to water deficiency).

4.4.1 Water deficit

The stress variable is the available water content, i.e. the water content above the wilting point in the root zone (called *teta*). The stress indices are *swfac*, *turfac* and *senfac*; they depend on *teta* according to bilinear laws:

$$\begin{aligned}
 turfac(t) &= \max\left(\text{swfacmin}_p, \frac{\text{teta}(t)}{\text{teturg}(t)}\right) \text{ if } \text{teta}(t) < \text{teturg}(t) \\
 turfac(t) &= 1 \text{ if } \text{teta}(t) \geq \text{teturg}(t) \\
 swfac(t) &= \max\left(\text{swfacmin}_p, \frac{\text{teta}(t)}{\text{tetstomate}(t)}\right) \text{ if } \text{teta}(t) < \text{tetstomate}(t) \\
 swfac(t) &= 1 \text{ if } \text{teta}(t) \geq \text{tetstomate}(t) \\
 senfac(t) &= \max\left(\text{swfacmin}_p, \frac{\text{teta}(t)}{\text{tetsen}(t)}\right) \text{ if } \text{teta}(t) < \text{tetsen}(t) \\
 senfac(t) &= 1 \text{ if } \text{teta}(t) \geq \text{tetsen}(t)
 \end{aligned} \tag{4.22}$$

Each stress index has its specific threshold (*tetstomate*, *teturg* and *tetsen*) and a comon parameter (**swfacmin_p**) (Figure 4.11).

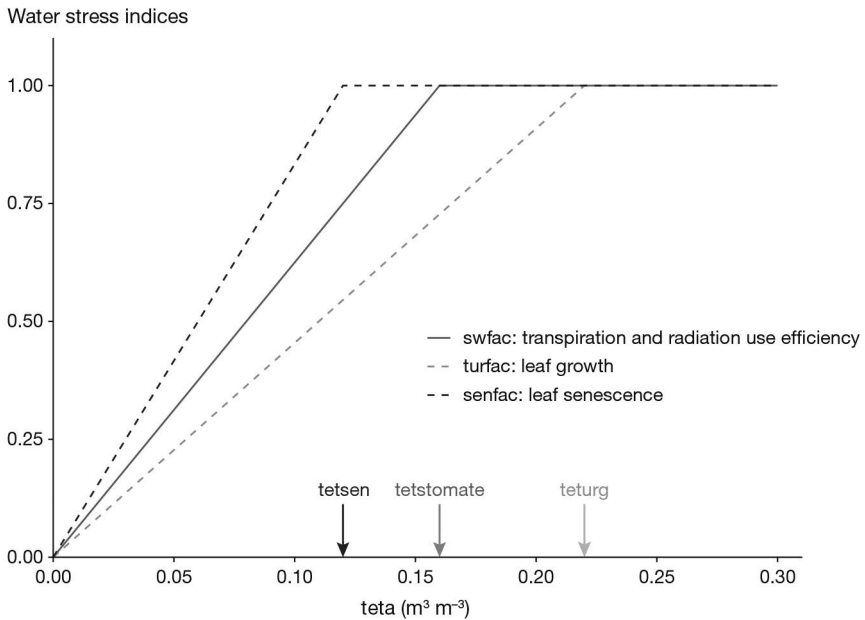


Figure 4.11. Water stress indices (*turfac*, *swfac*, *senfac*) as a function of the available water content in the root zone (*teta*).

The calculation of the *tetstomate* and *teturg* thresholds is explained in the chapter on transpiration (see § 11). *tetsen* is proportional to *teturg* thanks to the **rapsenturg_p** parameter (Eq. (4.23)).

$$\text{tetsen}(t) = \text{rapsenturg}_p \cdot \text{teturg}(t) \tag{4.23}$$

The hierarchy between the three stress indices is generally that which is indicated in Figure 4.11, with $\text{rapsesturg}_p > 1$. The functions of these three stress indices are summarised in Table 4.1. The germination and epicotyl growth phases can also be affected by water shortage in response to soil moisture in the seed bed (humirac_G index).

Table 4.1. Impact of water stress on physiological functions through the various water stress indices.

Physiological function	Water stress index
Emergence (delay)	humirac
Root growth in depth (slowing)	humirac
Development (delay)	turfac
Leaf growth (slowing)	turfac
Leaf senescence (acceleration)	senfac
Radiation use efficiency (decrease)	swfac
Transpiration (decrease)	swfac

4.4.2 Nitrogen deficiency

The nitrogen status of a crop can be characterized using the concept of critical nitrogen concentration (NC), which varies throughout time during the growth cycle (see § 6.1.2.1). STICS integrates the approach by Greenwood *et al.* (1991) and Lemaire *et al.* (1984), which relates the nitrogen concentration in plant shoots to the dry matter accumulated in them. In line with this approach, the NC at any stage of crop growth is defined as the minimum nitrogen content in the shoots enabling the maximum growth rate. The NC depends on the standing biomass according to a dilution curve and must be used to make a diagnosis of nitrogen nutrition (Justes *et al.*, 1994; Lemaire and Gastal, 1997): whenever the observed nitrogen content is below that curve, the crop is under nitrogen deficiency. When the actual nitrogen content is higher than the NC, the crop is not limited by nitrogen availability. The NC is thus the basis for defining a nitrogen nutrition index (*inn*) (Eq. (4.24)), which is the ratio of the actual nitrogen content ($\text{CN}_{\text{plante}}$, in % of dry matter) to the critical nitrogen content (NC) corresponding to the same biomass (masecabso) (Figure 4.12). In dense canopy, when the standing biomass is less than 1 t ha^{-1} , NC is constant and when the standing biomass is higher than 1 t ha^{-1} it follows a simple power function of the biomass with a constant negative power. In STICS both the value of NC when masecabso is 1 t ha^{-1} and the exponent are species dependent.

There is, however, an important limitation in the approach described above when calculating the *inn*, such as in the case of the nitrogen reserve which is available in perennial organs but which also belong to the standing biomass (e.g. grapevine, illustrated in Figure 4.13). An alternative stress variable corresponds to the nitrogen input flux relative to the critical input flux as proposed by Devienne-Barret *et al.* (2000). It is a kind of instantaneous INN named *inni* (Eq. (4.24)) relying on the daily accumulation of nitrogen (vabsN) and nitrogen dependent biomass (deltabso) (see § 6.1).

When the option of daily partitioning is chosen, perennial and non-perennial organs are distinguished as their N demand (see § 7 and § 6.1), and the *inn* is calculated only for non-perennial organs.

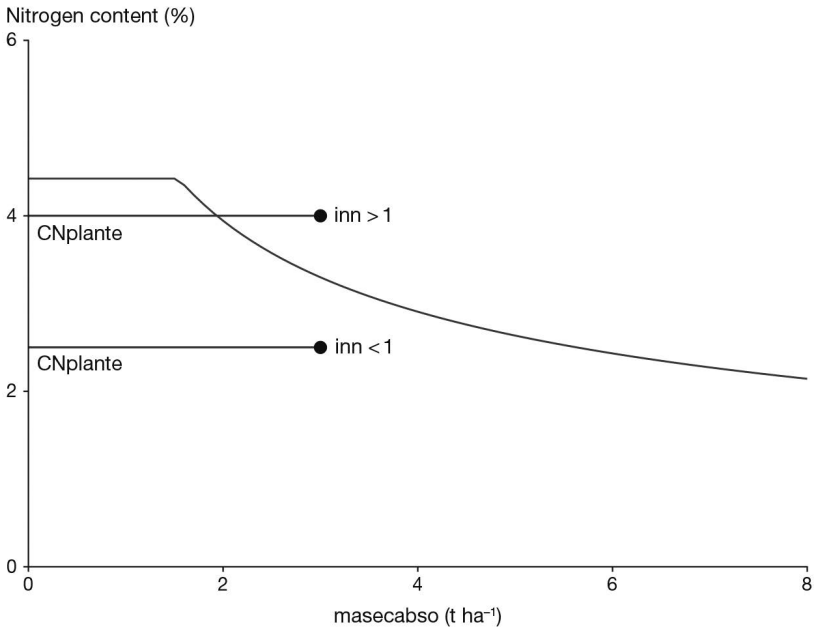


Figure 4.12. Critical nitrogen dilution curve (NC) and *inn* calculation as the ratio between *CNplante* and NC.

$$inn(t) = \frac{CNplante(t)}{NC(t)}$$

$$inn(t) = \frac{vabsN(t)}{deltabsot(t) \left(\frac{dNC}{dmasecabso} \right) (t)}$$

$$vabsN(t) = absotot(t) - absorad(t) \text{ if } \mathbf{code_acti_reserve}_p \text{ is not activated}$$

$$vabsN(t) = absoaer(t) + dltaremobilN(t) \text{ if } \mathbf{code_acti_reserve}_p \text{ is activated} \quad (4.24)$$

All nitrogen stress indices accept **INNmin_p** or **INNimin_p** as the floor value for the *inn* and the *inni* options, respectively. By definition, the *inns* index corresponds to the *inn* between **INNmin_p** and 1. The *innlai* and *innsenes* indices (Figure 4.14) are defined by point [1, 1] and by points **INNmin_p**, **innturgmin_p** and **INNmin_p**, **innsen_p**, respectively.

Setting the parameters in this way means the effect of nitrogen deficiency on photosynthesis can be differentiated from that for leaf expansion. In practice, it seems that these two functions react very similarly and **innturgmin_p** is similar to **INNmin_p**, while **innsen_p** is greater, indicating that the plants accelerate their senescence later than their growth decrease, just as for water stress. A commonly accepted value for **INNmin_p** is 0.3 and **INNimin_p** is 0.0. The functions of these three stress indices are summarised in Table 4.2.

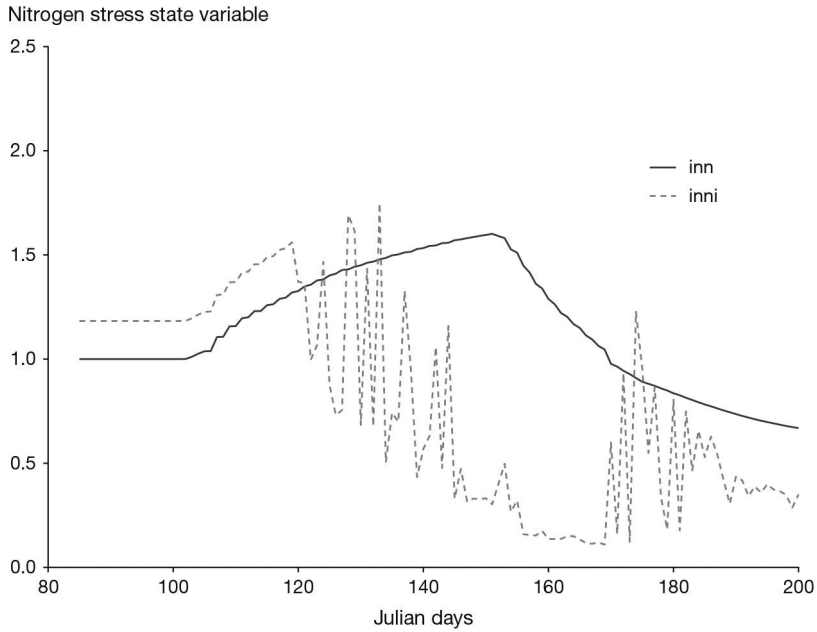


Figure 4.13. Comparison between *inn* and *inni* for a grapevine crop with nitrogen reserve at the beginning of the cycle.

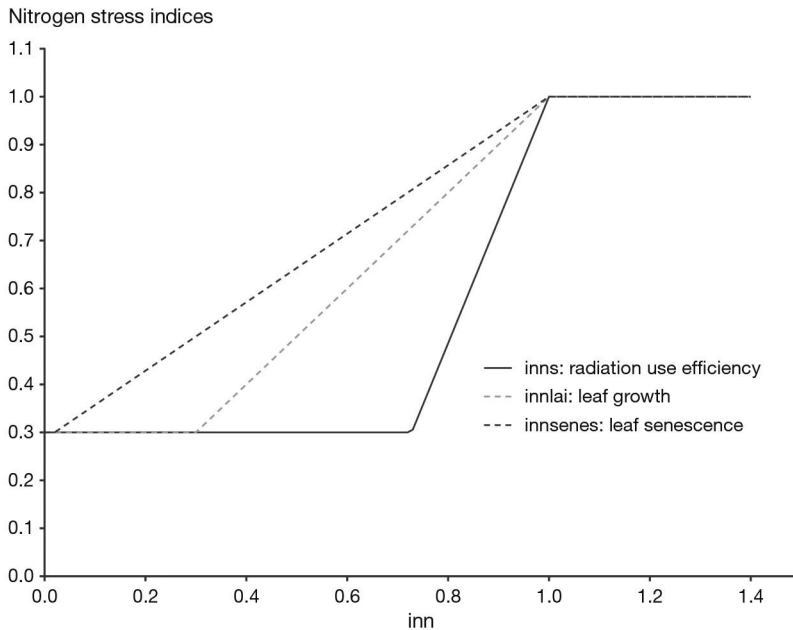


Figure 4.14. Nitrogen stress indices (*inns*, *innlai*, *innsenes*) as a function of the nitrogen nutrition index (NNI). Parameters: $INNmin_p = 0.3$, $innturgmin_p = -0.8$, $innsen_p = 0.5$

Table 4.2. Impact of nitrogen stress on physiological functions through the various nitrogen stress indices.

Physiological function	Nitrogen stress index
Development (delay)	innlai
Leaf growth (slowing)	innlai
Leaf senescence (acceleration)	innsenes
Radiation use efficiency (decrease)	inns

4.4.3 Trophic stress

The trophic stress indices only concern crops simulated as indeterminate. The functions of the three trophic stress indices are summarised in Table 4.3.

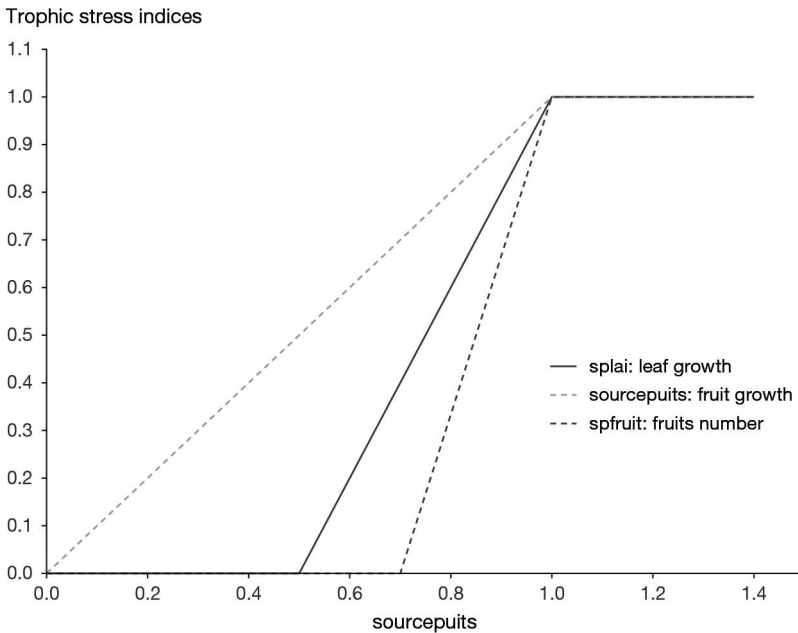


Figure 4.15. Trophic stress indices (*sourcepuits*, *splai*, *spfruit*) as a function of the source/sink ratio (*sourcepuits*). Parameters $splaimin_p = 0.5$, $splaimax_p = 1$, $spfrmin_p = 0.7$ and $spfrmax_p = 1$.

The stress variable *splai* is the ratio of the trophic sources to the sinks, *sourcepuits* (see § 7 for an explanation on how to calculate it). The *splai* and *spfruit* options are defined by the ***splaimin_p***, ***splaimax_p***, ***spfrmin_p*** and ***spfrmax_p*** parameters (Figure 4.15). The various trophic stress indices cannot be considered as equivalent to biomass allocation coefficients because they are not all applied to biomass. Accordingly, the relative position of the functions *sourcepuits* and *splai* does not indicate any priority between fruit and leaves: the priority needs to be calculated in terms of biomass and depends largely on the relative sink strengths of the organs.

Table 4.3. Physiological functions and associated trophic stress indices.

Physiological function	Trophic stress index
Fruit growth (decrease)	sourcepuits
Leaf growth (slowing)	splai
Fruit number (decrease)	spfruit

4.4.4 Temperature stresses

4.4.4.1 Frost

The stress variable is the minimum crop temperature, $tcultmin$ (see § 9). The frost stress indices correspond to frost damage (1 for no frost and 0 for lethal frost). The response to frost as well as the damage varies as a function of the developmental stage (Table 4.4).

Table 4.4. Impact of frost on physiological functions through the frost stress indices.

Physiological function	Frost stress index
Plant density	fgellev
Leaf senescence before AMF (acceleration)	fgeljuv
Leaf senescence after AMF (acceleration)	fgelveg
Fruit number	fgelflo

Each response is defined by four parameters (Figure 4.16). Two of them are independent of the developmental stage: $tdebgel_p$ (temperature at the beginning of frost action) and $tletale_p$ (lethal temperature); the two others are relative to frost damage: temperature inducing 10% or 90% frost damage. For the plantlet phase, the parameters are $tgellev10_p$ and $tgellev90_p$ which act on plant density through the index $fgellev$; for the juvenile phase (up to $iamfs$ stage), the parameters $tgeljuv10_p$ and $tgeljuv90_p$ act on foliage (acceleration of senescence) through the index $fgeljuv$. After the $iamfs$ stage, the parameters $tgelveg10_p$ and $tgelveg90_p$ are also active on foliage through the index $fgelveg$. For frost affecting flowers and fruits, the parameters $tgelflo10_p$ and $tgelflo90_p$ define the dynamics of the $fgelflo$ index.

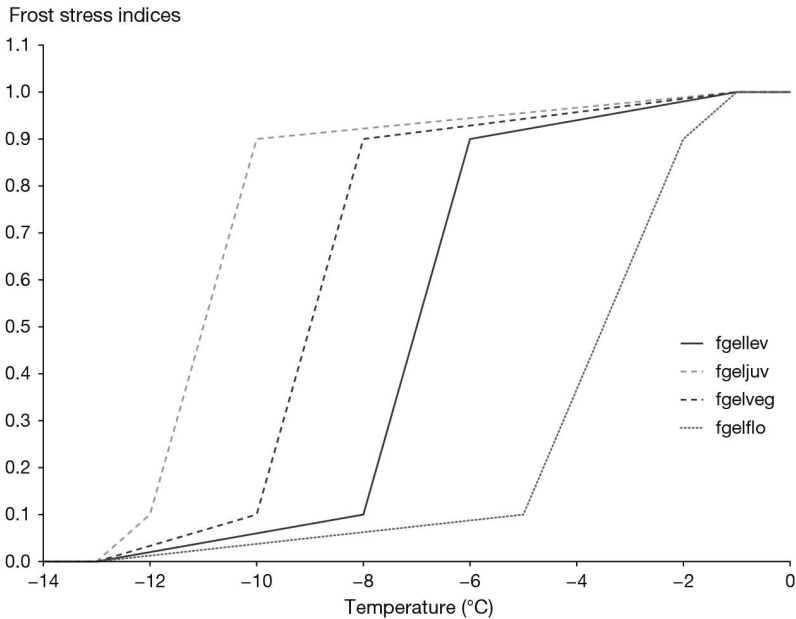


Figure 4.16. Frost stress indices (*fgellev*, *fgeljuv*, *fgelveg*, *fgelflo*) as a function of minimal crop temperature ($T_{cultmin}$). Parameters: $t_{deb} = -1$; $t_{gellev10} = -6$; $t_{gellev90} = -8$; $t_{geljuv10} = -10$, $t_{geljuv90} = -12$, $t_{gelveg10} = -8$, $t_{gelveg90} = -10$, $t_{gelflo10} = -2$, $t_{gelflo90} = -5$, $t_{lethal} = -13$.

4.4.4.2 Suboptimal temperatures

Stresses linked to temperatures which are too high or too low (without attaining frost thresholds) are included in the temperature effect functions. Temperature usually plays a driving role on development, growth and senescence of leaves, growth and senescence of roots and the functions concerned include thermal thresholds (minimum and maximum for functioning). Temperature may also reduce activity and be used as a stress factor. The thermal stresses considered vary according to the processes affected and the option chosen (average or extreme temperatures, crop, air or soil), as follows:

Table 4.5. Temperature stress factor or driver for each physiological function.

Physiological function	Temperature	Role	Function and thermal stress index
Emergence	Daily average soil temperature	pilot	
Aboveground development	Daily average crop temperature	pilot	
Vernalisation and dormancy	Daily average crop temperature	stress	
Leaf growth and senescence	Daily average crop temperature	pilot	
Root growth and senescence	Daily average crop or soil temperature	pilot	

Physiological function	Temperature	Role	Function and thermal stress index
Radiation use efficiency (decrease)	Daily average crop temperature	stress	ftemp
Filling at low temperatures (stop)	Minimum crop temperature	stress	ftemprem
Filling at high temperatures (stop)	Maximum crop temperature	stress	ftemprem

The temperature stress factor acting on the radiation use efficiency (RUE), f_{temp} , is calculated as:

$$\begin{aligned}
 \text{if } tcult(t) < \mathbf{Teopt}_p \quad f_{temp}(t) &= 1 - \left(\frac{tcult(t) - \mathbf{Teopt}_p}{\mathbf{Temin}_p - \mathbf{Teopt}_p} \right)^2 \\
 \text{if } \mathbf{Teopt}_p \leq tcult(t) \leq \mathbf{Teoptbis}_p \quad f_{temp}(t) &= 1 \\
 \text{if } tcult(t) > \mathbf{Teopt}_p \quad f_{temp}(t) &= 1 - \left(\frac{tcult(t) - \mathbf{Teoptbis}_p}{\mathbf{Temin}_p - \mathbf{Teoptbis}_p} \right)^2 \quad (4.25)
 \end{aligned}$$

The smooth shape of the RUE versus crop temperature (Figure 4.17) is quite classical (Ritchie and Otter, 1985) and comes from the combined responses of photosynthesis and respiration to temperature. Yet the cardinal temperature values are highly dependent on the time step used: in our case this is daily average crop temperatures. As far as fruit filling is concerned, the response in the model is yes/no.

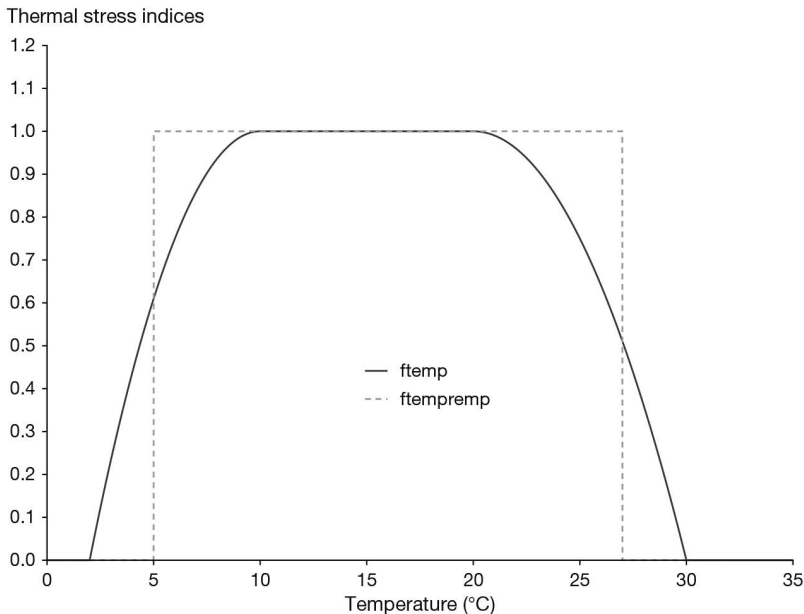


Figure 4.17. Thermal stress indices (f_{temp} and $f_{temprem}$) as a function of temperature using cardinal temperatures ($\mathbf{Temin}_p = 2$; $\mathbf{Teopt}_p = 10$; $\mathbf{Teoptbis}_p = 20$; $\mathbf{Temax}_p = 30$; $\mathbf{Tminrem}_p = 5$; $\mathbf{Tmaxrem}_p = 27$).

4.4.5 Waterlogging

Under waterlogged conditions, the model calculates the variable *exofac* (Eq. (4.26)) which represents the proportion of root length which is under anoxic conditions, in saturated layers:

$$exofac(t) = \frac{\sum_{profsem}^{zrac} lracz(z, t) \cdot anox(z, t)}{cumlracz(t)} \quad (4.26)$$

The variable (*anox*) is equal to 1 if the layer *z* is anoxic and 0 in the opposite case. Three anoxic stress indices are calculated (Eq. (4.27)): *izrac*, *exolai* and *exobiom*. They are relative to root growth, *lai* growth and RUE, respectively. They are based on the experimental work by Rebière (1996), reviewed by N. Brisson *et al.* (2002).

$$\begin{aligned} izrac(t) &= 1.6 \cdot \exp(-27 \cdot exofac(t)) - 0.6 \\ exolai(t) &= 1 - (1 - \exp(-5.5 \cdot exofac(t))) \cdot sensanox_p \\ exobiom(t) &= 1 - \frac{sensanox_p}{1 + \exp(3.95 - 14 \cdot exofac(t))} \end{aligned} \quad (4.27)$$

The root stress index *izrac* limits root growth at an efficient depth and density (see § 5). These relationships, applied to a wheat crop which is assumed to have a high sensitivity to water logging, are illustrated in figure 4.18.

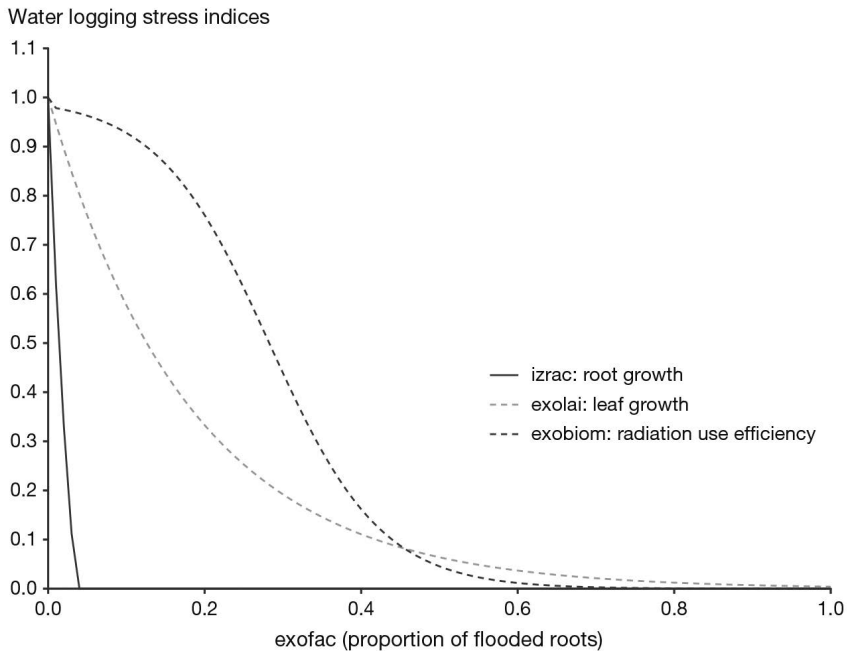


Figure 4.18. Waterlogging stress indices (*izrac*, *exolai* and *exobiom*) as a function of the proportion of flooded roots (*exofac*) for a wheat crop assumed to have a high sensitivity to anoxia (*sensanox_p*=1).

If the species (or variety) has developed adaptive mechanisms such as aerenchyma, the effects of excess water will be less pronounced and this is simulated by reducing the parameter **sensanox_p**. If **sensanox_p** = 1, the sensitivity is maximal, if **sensanox_p** = 0, the plant is indifferent to excess water (for example, rice).

Table 4.6. Effect of waterlogging on plant functions and stress indices.

Physiological function	Water logging stress
Root growth	izrac
Leaf growth (slowing)	exolai
RUE (decrease)	exobiom
Transpiration (decrease)	exobiom

4.4.6 Stresses directly linked to the soil structure

At the soil surface, the formation of a crust in some soils and weather conditions creates a resistance to plant emergence. It can provoke both a delay in emergence dates and a decrease in plant densities (see § 3).

The soil structure can be either loose or compact and can limit root soil colonisation during the growing period. The only soil parameter available to describe soil structure is the bulk density (**da_G**). It can be used as a stress variable together with the parameters **daseuilbas_G**, **daseuilhaut_G** and **contrdamax_p** to calculate a soil structure stress index (see § 5.2.3).

4.4.7 Interactions between stresses

The weakest point of the ‘limiting factor’ approach is most likely figuring out how to make the various stresses interact (Gonzalez-Dugo *et al.*, 2010). In STICS we adopted the principle that stresses are multiplied when their modes of action are thought to be independent. When their modes of action interact with each other, the resulting active stress is the most severe, i.e. the one with the lowest value (see table 4.7). For instance, water deficiency acts on radiation use efficiency at the stomatal level while nitrogen deficiency acts on the photosynthesis enzymes: these stresses are assumed to be independent of each other. However, both nitrogen and water stresses limit leaf growth by decreasing cell expansion and division and are thus assumed to be mutually dependent. For crop establishment the interactions are more complex, based on the idea of converting a stress-induced delay in emergence into plant mortality.

Trophic stress has a particular status because it does not originate from an environmental resource external to the crop, such as water or nitrogen, but results from the internal crop carbon imbalance. As such, it already integrates the trophic effects of the primary abiotic stresses, which makes unrealistic the hypothesis of stress independence, and can lead to overestimate the stress severity.

Table 4.7. How stresses are combined in the model for each physiological function.

Physiological function	Combination of stresses (*only for indeterminate crops)
Emergence duration	Water deficiency x Crusting
Plant density establishment	(Water deficiency x Crusting) x Frost
Development	min(Water deficiency, Nitrogen deficiency)
Leaf growth	min(Water deficiency, Nitrogen deficiency) x Water logging x Trophic*
Senescence	min(Water deficiency, Nitrogen deficiency, Frost)
Root growth	Water deficiency x Nitrogen deficiency x Frost
Radiation use efficiency	Water deficiency x Nitrogen deficiency x Temperature x Water logging
Number of fruits	Nitrogen deficiency x Frost x Trophic*
Fruit growth	Temperature x Trophic*
Transpiration	MIN(Water deficiency, Water logging)

To address the problems of oversimplifying a complex reality, the function parameters must be fit using contrasting data sets.

Chapter 5

Root growth

NADINE BRISSON, NICOLAS BEAUDOIN, ALAIN MOLLIER,
FLORENT CHLEBOWSKI, MARIE LAUNAY AND LOÏC STRULLU

REVIEWED BY: GAETAN LOUARN AND BRUNO MARY

» 5.1 Introduction

Apart from anchoring plants in soil, the root system is responsible for specific functions, such as the uptake of water and mineral elements (N, P, K...), N₂ symbiotic fixation (in legumes), rhizodeposition and possible generic functions like carbohydrate or N storage, which crop models may or not take into account and in different ways. The development of N-fixing nodules and their activity are less dependent on the root system (which plays a supporting role) than on the shoot dynamics and the physicochemical conditions of the surrounding soil (Burger, 2001).

The plant's ability to trap mineral elements relies on root system efficiency. Efficiency is not just related to the actual root length profile or root biomass – it is highly dependent on the mobility of the element of interest within the soil. For water and nitrate ions, the minimum root length density for unrestricted uptake is 0.5 cm cm⁻³ according to Bonachela (1996), equating to an average soil-root distance of 0.8 cm, which falls within the range of 0.5 cm to 1.0 cm proposed by Aura (1996). According to other authors (Kage and Ehlers, 1996; Robertson *et al.*, 1993) the minimum root length density can be lower. This means that the efficient root profile is different from the actual root system, especially in the subsurface layer where roots can more than adequately handle nitrate and water uptake, although they are needed for the uptake of less mobile ions. This efficiency must be dynamically estimated in order to correctly evaluate the supply/demand ratio. The effect of the soil (constraints to penetration, sensitivity to anoxia, etc.) on the shape of the root system (Nicoullaud *et al.*, 1994) must also be accounted for. While all these elements are taken into account in architectural root growth modelling approaches (Drouet and Pagès, 2003), this is seldom the case in crop models, where roots are not individualised but simply layered in the soil. In crop models, because the soil is considered in only one dimension, growth in depth must be treated separately from growth in density. The progression rate of the root front is generally based on degree-days (Giauffret and Derieux, 1991; Hunt and Pararajasingham, 1995) and the root density assumption mostly relies on an exponential decrease of roots with depth (de Willigen *et al.*, 2002; Gerwitz and Page, 1974; Heinen *et al.*, 2003). Although we can

rely on existing modelling patterns of root/shoot ratio in terms of biomass (Wilson, 1988), the extrapolation to root length is complicated, since the specific root length (length per unit weight) can vary depending on the phenological stage and experienced stresses in addition to well-known genetic factors (Bingham, 1995).

The conceptual framework to simulate the rooting system in STICS has always been dynamical and one-dimensional, but it has evolved considerably. When STICS was first developed, the root system was considered only as a set of exchange surfaces of water and nitrogen, growing in depth and length independently of shoot growth. This framework has been enhanced with the addition of several formalism options. The part of the root system which acts as a reserve organ can be regarded as either a harvested organ (e.g. tubers § 8) or part of the ‘non-located’ reserves (§ 7.2). Rhizodeposition is accounted for the recycling of the dead roots within the fresh soil organic matter (as a plant residue).

Given current efforts to mitigate global climate change, users need STICS to assess soil C sequestration. To do this, a STICS specification was designed to perform simulations for root biomass, root decay and soil humus mineralisation together. In STICS, soil C-N storage is addressed only through root biomass decay, while root exudation is not modelled. Root decay is directly derived from root length behaviour. By default, STICS only calculates the amount of recycled C-N at the end of the crop cycle, which allows a certain prediction robustness of C-N storage for annual crops but jeopardises STICS relevance for perennial crops. One STICS option allows users to dynamically simulate root biomass in direct relationship with root length expansion. Another STICS option can be used to simulate two kinds of roots, with the root turn-over rate linked to their sizes, according to the concepts of the ARCHISimple model (Pagès *et al.*, 2014). However, getting the true balance between N mineralisation and N organisation due to C root rhizodeposition is challenging for a daily dynamical model (Yin *et al.*, 2020). So, preventing the risk of drift of soil mineral nitrogen prediction requires accurate root module parameterisation.

Several optional calculations of root growth are proposed in STICS. In the model, roots first act as water and mineral nitrogen absorbers, and are described based on their front depth and density profile. Root growth begins with germination (for sown plants) or at planting; it combines the growth of the root front (four formalism options) and the expansion and spatial distribution of root length density (four formalism options, including a root mortality option). Second, root biomass production and rhizodeposition depend on the range of the previous active options and on another option permitting either daily root decay or delayed root recycling at harvest. Root expansion can be considered as either independent from or dependent on shoot biomass, according to the crop parameterisation strategy combining various options. If root expansion is considered dependent, the nutritional functions of the root system can be calculated from supply and demand principles, where demand originates from shoot metabolism while supply results from the combination of soil nutrients and the root system’s ability to capture those elements.

►► 5.2 Vertical root growth

5.2.1 Vertical root growth overview

Figure 5.1 shows the options governing the vertical growth of the root front. At first, the root growth onset depends on four plant options (**codehypo_p**, **codegermin_p**,

codedisrac_p and **codemonocot_p**), which can interact with the technical option **codeinstal**, to describe either seedling or established crop behaviour. The daily increment of root front, **deltaz**, is then determined only using parameters driving **deltaz** response to physical soil conditions, and the specific **croirac_p** parameter. Finally, the **deltaz** stop is specifically determined by the combination of a soil parameter (**obstarac_s**), a specific crop parameter (**stoprac_p**), which can be either **ilax_T**, **iflo_T** or **imat_T**, and two options (**code_acti_reserve_p**, **codeperenne_p**).

5.2.2 Root front growth

The first calculation gives the root front depth (**zrac**), beginning at the sowing depth (**profsem_T**) for sown crops and at an initial value for transplanted crops (**profsem_T** + **zracplantule_p**) or perennial crops (**zrac0_i**). In addition, when the **codedisrac_p** option is activated and the **codemonocot_p** is set to 1, vertical growth can occur from 1 cm in depth to either sowing depth or planting depth. This option better simulates the root activity in the topsoil, especially in fertilised cereals under dry conditions. The root front growth stops when it reaches the soil depth or an obstacle, which can be physical or chemical (the obstacle depth is defined by the parameter **obstarac_s**), or when the phenological stopping stage has been reached. For indeterminate crops, when trophic competition prevents vegetative growth, the root front growth is stopped (except before the **iamf_T** stage, when root growth is prioritised). The calculation of root front growth rate (**deltaz**) is broken down in Eq. (5.1), as the product of the genetic response of root growth to temperature (**deltaz_T**) and the soil physical stress index (**deltaz_{stress}**).

$$deltaz(t) = deltaz_T(t) \cdot deltaz_stress(t) \quad (5.1)$$

A first calculation of the front growth rate (**deltaz_T**) is proportional to temperature with a coefficient depending on the variety (**croirac_p**). The thermal function relies on either crop temperature Eq. (5.2) or soil temperature Eq. (5.3), according to the root growth dependence on the collar or apex temperature: i) if the driving temperature is that of the crop, the cardinal temperatures (**tcmin_p** and **tcmax_p**) are the same as those used for the thermal function of the leaf growth rate Eq. (4.3); ii) if the driving temperature is that of the soil at level **zrac** (± 1 cm), the minimum temperature is the base temperature for germination (**tgmin_p**), but the maximum temperature remains **tcmax_p**. Note that the value of the specific parameter **croirac_p** depends on the choice of driving temperature.

$$\begin{aligned}
 &tcult(t) \leq tcmin_p && deltaz_T(t) = 0. \\
 &tcmin_p < tcult(t) < tcmax_p && deltaz_T(t) = (tcult(t) - tcmin_p) \cdot croirac_p \\
 &tcult(t) \geq tcmax_p && deltaz_T(t) = (tcmax_p - tcmin_p) \cdot croirac_p \quad (5.2) \\
 &tso(ap(t), t) \leq tgmin_p && deltaz_T(t) = 0. \\
 &tgmin_p < tso(ap(t), t) < tcmax_p && deltaz_T(t) = (tso(ap(t), t) - tgmin_p) \cdot croirac_p \\
 &tso(ap(t), t) \geq tcmax_p && deltaz_T(t) = (tcmax_p - tgmin_p) \cdot croirac_p \\
 &with \quad ap(t) = zrac(t) \pm 1 \text{ cm} && (5.3)
 \end{aligned}$$

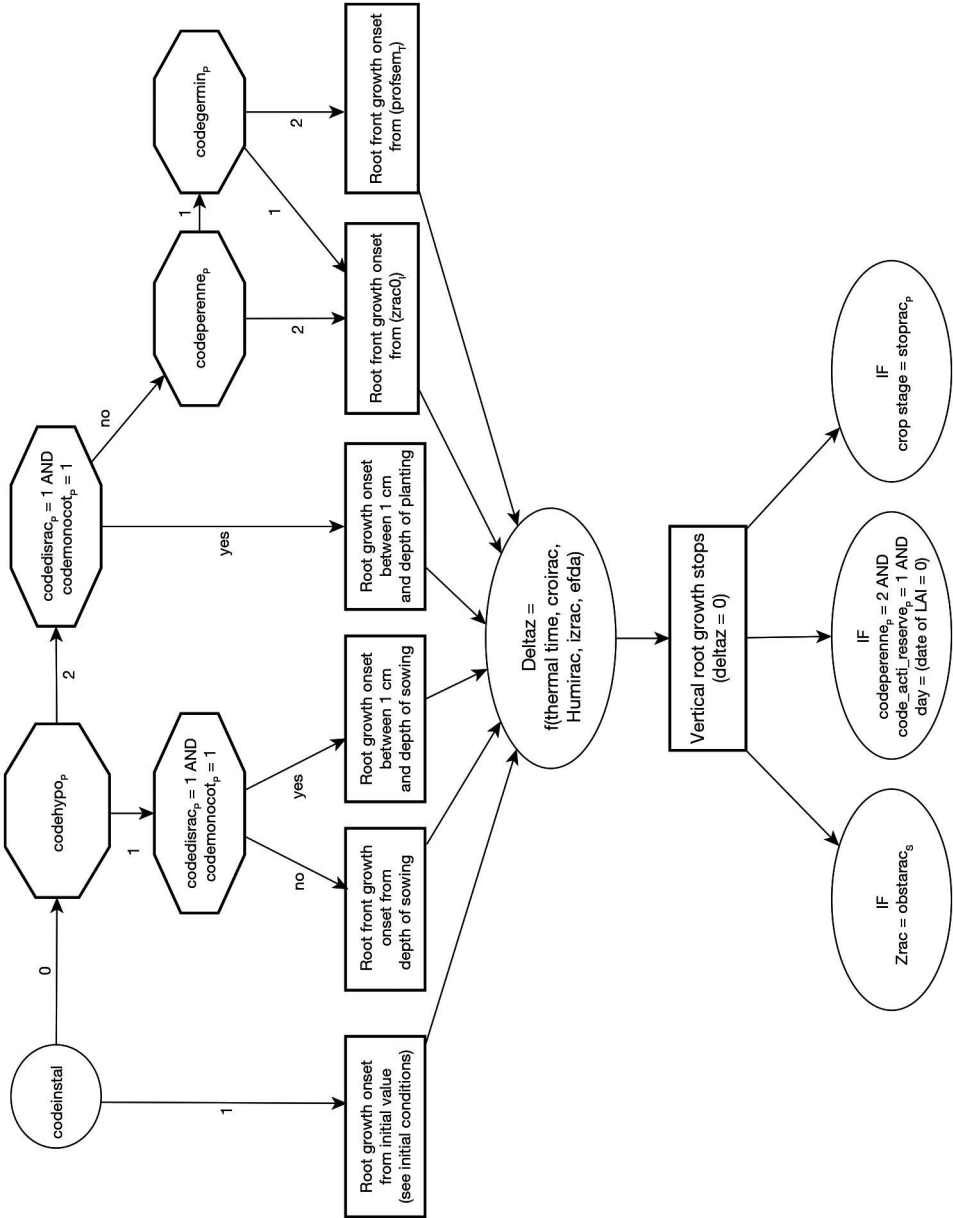


Figure 5.1. Flowchart of options controlling vertical root growth, leaving aside the options for thermal time calculation.

5.2.3 Physical soil conditions

The water and bulk density stress index (deltaz_stress) is calculated as the product of three variables (Eq. (5.4)), depending on soil dryness (humirac , Eq. (3.8) and Figure 3.8), water-logging (izrac , Eq. (4.26) and Figure 4.18), and bulk density (efda).

$$\text{deltaz_stress}(t) = \text{humirac}(AP(t), t) \cdot \text{izrac}(t) \cdot \text{efda}(zrac(t)) \quad (5.4)$$

The humirac variable, which reflects the influence of water content on germination and root growth calculated in Eq. (3.8) during emergence, becomes a bilinear variable after emergence Eq. (5.5). This variable depends on two parameters, i.e. root sensitivity to drought (sensrsec_p), and the wilting point (hn):

$$\begin{aligned} \text{humsol}(ap(t), t) > hn_s & \quad \text{humirac}(ap(t), t) = 1 \\ \text{humsol}(ap(t), t) \leq hn_s & \quad \text{humirac}(ap(t), t) = \frac{\text{sensrsec}_p}{hn_s} \cdot \text{humsol}(ap(t), t) \end{aligned} \quad (5.5)$$

Under waterlogged conditions, the proportion of root length which is under anoxic conditions, in saturated layers is exofac (Eq. (4.26)). The izrac root stress index limits root growth at an efficient depth and density (Eq. (4.27) and Figure 4.18).

The efda variable constitutes a constraint to penetration in compacted soils, or in rare cases a slowing of root penetration linked to a lack of soil cohesiveness. The formalisation proposed by Jones *et al.* (1991) and validated by Rebière (1996), was adapted for STICS (Figure 5.2). Root penetration is not constrained between the bulk density thresholds dacohe_G and daseuilbas_G . Above a bulk density threshold daseuilhaut_G the effect of bulk density (da) on root penetration is equal to the parameter contrdamax_p . The parameter contrdamax_p is assumed constant and corresponds to the plant's sensitivity to the penetration constraint. The daseuilbas_G and daseuilhaut_G values are 1.4 and 2.0 respectively. The dacohe_G value is poorly understood, and we have only

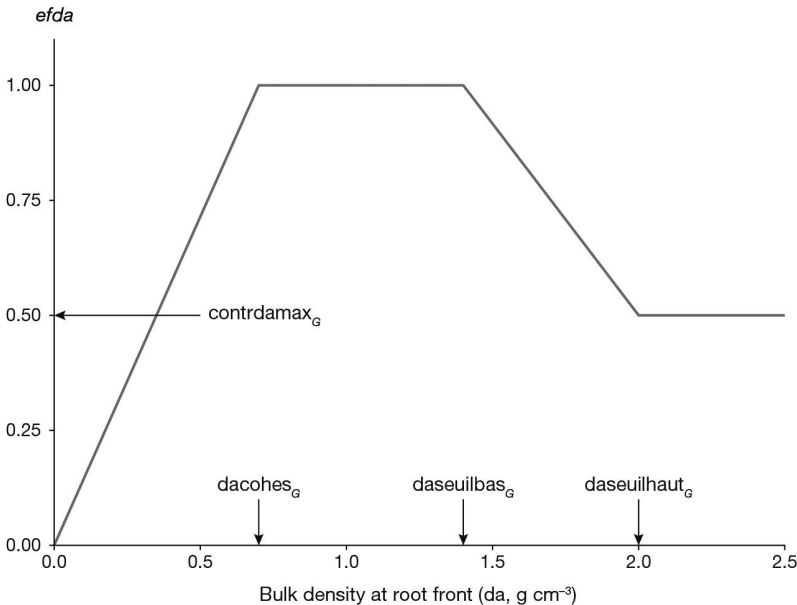


Figure 5.2. Root penetration constraint ($efda$) as a function of bulk density (da).

provided an order of magnitude. The bulk density d_a is the effective value, and takes into account fine earth and pebbles. Applying this formalism in presence of pebbles needs caution because their role on root penetration can be dual.

► 5.3 Root length density production and root distribution

5.3.1 Introduction

STICS first predicts the root length density distributed over the soil profile up to the root front, which is simply called 'root density profile.' The root density profile is calculated according to two possible options (Figure 5.3). The 'standard profile' and 'true density' options deal differently with the determinism of the root expansion. The standard profile and one default parameterisation of true density consider root growth independently of shoot growth. Conversely, the true density option allows users to account for a direct link between shoot and root growing rates.

The standard profile option can be used to calculate the root profile that is efficient with respect to absorption thanks to a naturalist approach of the observable profile of living roots.

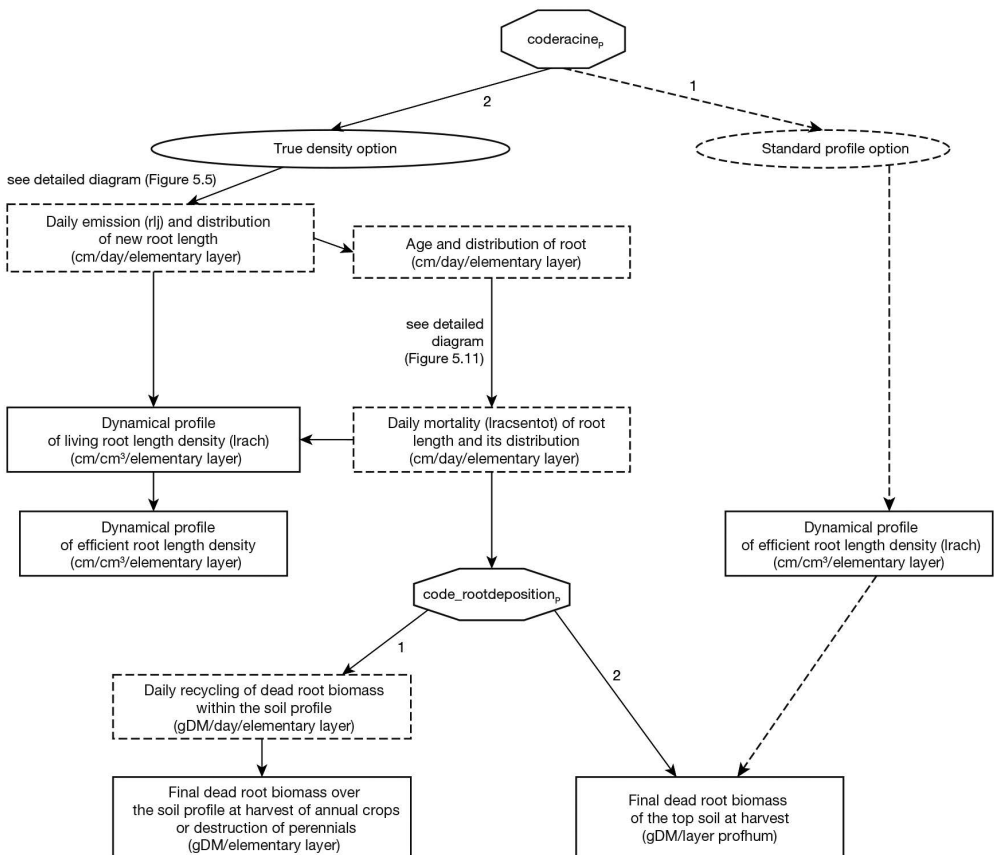


Figure 5.3. Flow chart of options controlling root length production and root biomass recycling.

Users can choose the true density option to simulate both root emission and root senescence versus time and depth. This approach is more relevant for simulating intercrops or low-density crops, for which root density is never optimal. This approach can also take into consideration the effects of constraints imposed by the soil on root distribution. The true density option contains itself six formalism options pertaining to root length density expansion and spatial distribution, which are each presented in separate diagrams.

Secondly, dead root biomass at harvest can always be estimated, as shown in Figure 5.3. The profiles of living roots and dead root biomass can be obtained dynamically.

5.3.2 Standard profile

The standard profile option is used to calculate the root profile that is efficient in terms of absorption. The standard profile is defined by the maximum current depth, z_{rac} , and the efficient root density profile, l_{racz} . This standard profile is calculated dynamically as a function of z_{rac} and takes a sigmoidal shape depending on the z_{labour_p} , z_{prlim_p} and z_{pente_p} parameters (Eq. (5.6)).

$$l_{racz}(z, t) = \frac{l_{vopt_G}}{1 + e^{-S(z - z_{demi}(z, t))}} \quad \text{with } S = \frac{4.6}{z_{labour_p} - z_{pente_p}}$$

and

$$z_{demi}(z, t) = \max\left(z_{rac}(z, t) - z_{prlim_p} + z_{pente_p} \frac{1.4}{S}\right) \quad (5.6)$$

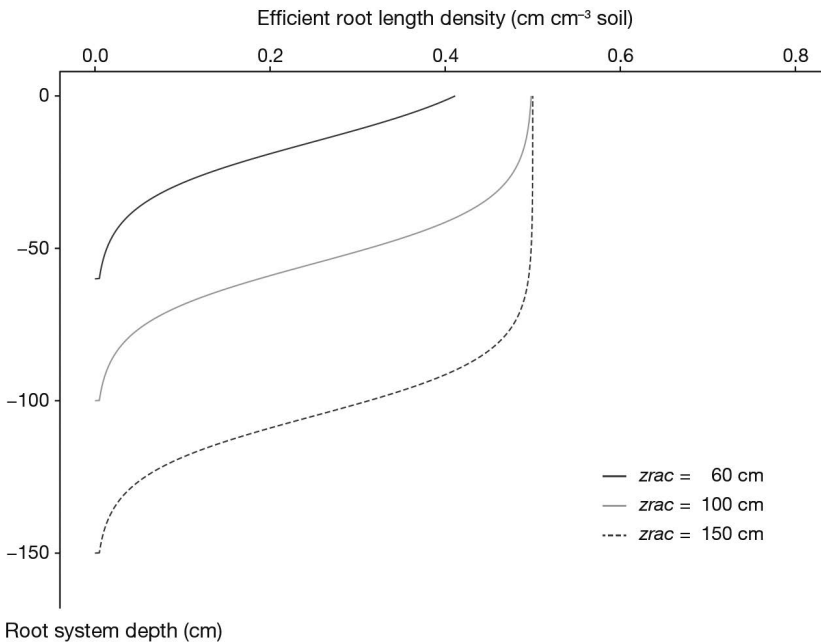


Figure 5.4. Reference root length density profile for rapeseed described by the efficient root density l_{racz} as a function of the root system depth z and according to the root front depth z_{rac} .

The $z_{demi} = 1.4/S$ threshold ensures at minimum an extraction of 20% of the water available near the soil surface. Roots located in dry layers of soil, with a water content equal to or below the wilting point, are considered as inefficient with respect to water uptake (see § 11.5.3). The total and efficient root length throughout the soil profile is called *cumlracz*.

These parameters define the shape of the reference root profile and are of considerable importance in terms of their interrelationships, but they do not define the final shape of the root system. In this respect, it is the differences between z_{pente_p} and z_{labour_p} , and particularly between z_{prlim_p} and z_{pente_p} which are determinant. The z_{labour_p} parameter corresponds to the depth of the tilled layer, where it is assumed that root proliferation is not limited with respect to water and mineral absorption: root density is optimum at this level ($lvopt_G$). The z_{pente_p} parameter is the depth at which root uptake efficiency is reduced by half, and the z_{prlim_p} parameter is the depth of the root front to which this reference profile can be attributed.

Using this method of calculation, any decrease in the root front depth causes reduced root length density. If the soil contains an obstacle to rooting (calculated as the lesser of the soil depth or an obstacle depth defined by the parameter $obstarac_s$), a fictitious root front (z_{nonli}) is calculated until the phenological stage of physiological stoppage of root front growth, $stoprac_p$. With this calculation, the course of root proliferation above the obstacle can be simulated. If the problem is anoxia (which slows but does not necessarily stop growth), in order to simulate root proliferation only above the saturated zone, the z_{prlim_p} parameter continues to grow at a rate reduced by 80% when compared with the rate without water-logging. This 80% value has been adjusted to obtain comparable results between the two root density approaches.

The main benefits of this formalism are simplicity and robustness. However, the hypotheses underlying the standard profile formalism may lead to some limits: i) in the tilled zone, root density is not always optimal with respect to water and nitrogen absorption (for woody species in widely-spaced rows, maximum root length density of about 0.2 cm cm^{-3} are measured, which is lower than the optimum density of 0.5 cm cm^{-3} (Ozier-Lafontaine *et al.*, 1999) and ii) the influence of soil constraints on the root distribution in the profile may be far from negligible. Limitations of the standard profile formalism could also occur if root system functions other than water and nitrogen absorption are considered (e.g. absorption of P and K, addition of organic matter).

5.3.3 True density

5.3.3.1 Principles and options

The true density option distinguished gross root expansion and root senescence according to thermal time. Several pathways can be chosen from the options presented in Figures 5.3 and 5.5. These options are used to calculate a root density profile that is comparable with measurements.

With the true density option, growth in root length expansion is first calculated, and then distributed to each soil profile layer. For sown crops, this calculation begins at

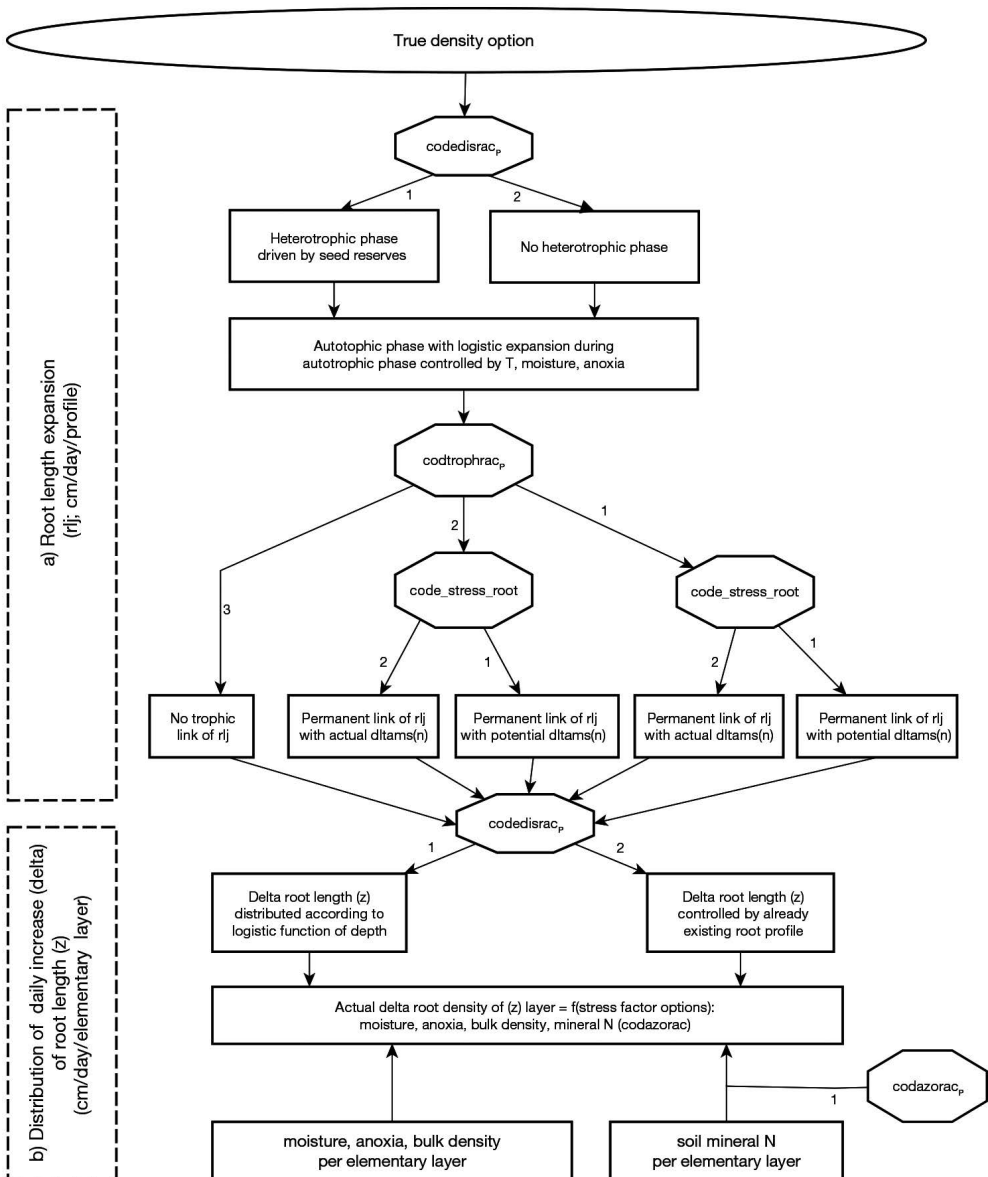


Figure 5.5. Flow chart of options controlling root length expansion and vertical distribution with True density option selected.

germination if the **codedisrac_p** is activated (§ 5.3.3.2.3) or by default, at emergence, which means that between germination and emergence, only the root front grows. For transplanted or implanted perennial crops, the calculation is initiated with an existing root density profile. After the crop completes its characteristic life cycle, the roots senesce (§ 5.3.3.4) and become crop residues either at each day or at the end of the crop cycle (§ 5.4). Root density above 0.5 cm cm⁻³ is not taken into account for water and nitrogen absorption.

5.3.3.2 Root length expansion and its possible shoot growth dependency

Two options are available to calculate root length expansion. In the ‘self-governing root length expansion’ option, to ensure the robustness of the model predictions of water and N balances, we chose to simulate the root length growth directly, without passing dealing with root biomass. The root biomass to shoot biomass ratio varies depending on the stresses suffered by the plant (Brisson *et al.*, 1998b).

Conversely, with the ‘trophic-link root length expansion’ option, root length expansion is driven by shoot growth, so that a reliable C soil-crop balance can also be predicted (although more parameters are required).

5.3.3.2.1 Self-governing root length expansion

The self-governing root length expansion option is the default option. It relies on the independence of root length expansion with regards to shoot biomass accumulation, but can sometimes result in an overestimation of root length. The self-governing root length expansion option occurs when **codtrophrac_p** is 3, root length expansion is then calculated using a logistic function that is analogous to that for leaves: the calculation of the root length growth rate (rlj in $m\ d^{-1}$) is broken down in Eq. (5.7). A first calculation of the root length growth rate (rlj_dev in $m\ plant^{-1}\ degree\text{-}day^{-1}$) describes a logistic curve. This value is then multiplied by the effective crop temperature (rlj_T in degree-days), the plant density combined with an inter-plant competition factor that is characteristic of the variety (rlj_dens in $plant\ m^{-2}$), and the water-logging stress index (rlj_stress). A second term is then added, corresponding to the growth at the root front ($rljfront$), depending on the front growth rate ($deltaz$).

$$rlj(t) = rlj_dev(t) \cdot rlj_T(t) \cdot rlj_dens(t) \cdot rlj_stress(t) + rljfront(t) \quad (5.7)$$

The logistic curve describing the root length expansion rate rlj_dev (Eq. (5.8)) depends on the maximum root growth parameter **draclong_p** and the normalised root development unit $urac$, ranging from 1 to 3 (such as $ulai$, the calculation of which is described in § 4.1.1). The logistic curve is thermally driven, even when the plant has vernalisation or photoperiod requirements. The plant parameters **pentlaimax_p** and **vlaimax_p** are already used to calculate leaf growth rate (Eq. (4.2)).

$$rlj_dev(t) = \frac{draclong_p}{1 + e^{(pentlaimax_p \cdot (vlaimax_p - urac(t)))}} \quad (5.8)$$

The thermal function rlj_T relies on crop temperature and cardinal temperatures (**tcmin_p** and **tcmax_p**) which are the same values as for leaf area growth calculation (Eq. (4.3)). The inter-plant competition function rlj_dens is the same as that calculated for leaf area growth $deltai_dens$ (Eq. (4.4)).

With this formalism, unlike this designed for the leaf area index, water and nitrogen deficiencies in the plant do not play any role in root length, which promotes root growth relative to aboveground growth in the event of stress. In contrast, anoxia acts via the waterlogging stress index rlj_stress , derived from the $izrac$ indicator, which is calculated in Eq. (4.27) and used in Eq. (5.9). In view of the difference which may exist between true density and efficient root density (as much as tenfold), the raw application

of *izrac* could have no effect on efficient root density, which would contradict experimental results (Rebière, 1996). So when *izrac* is less than 1 (i.e. under waterlogging stress conditions), it is multiplied by the ratio between efficient *cumlrac_z* to total *rltot* root length before it is applied to the *rlj* variable (Eq. (5.9)).

$$rlj_stress(t) = 1 - \mathbf{sensanox}_p + (\mathbf{izrac}(t) + \mathbf{sensanox}_p - 1) \cdot \frac{\mathbf{cumlrac}_z(t)}{rltot(t)} \quad (5.9)$$

At the root front, the root density is imposed and estimated using the parameter **lvfront_p**, and the growth in root length depends directly on the root front growth rate *deltaz* (Eq. (5.10)).

$$rljfront(t) = \mathbf{lvfront}_p \cdot 10^4 \cdot \mathbf{deltaz}(t) \quad (5.10)$$

5.3.3.2.2 Trophic-linked root length expansion

When **codtrophrac_p** is 1 or 2, root length growth relies on the daily production of shoot biomass (*dltams*) and on a dynamic underground/total biomass partitioning coefficient (*reprac* (Eq. (5.11) and Figure 5.6). The parameter **longsperac_p** is the specific root length to root mass ratio. The plant density effect is not taken into account because it is already integrated in the shoot biomass production. This value can replace calculation using Eq. (5.11) or act as a threshold if the chosen option is 2.

$$rlj(t) = \frac{\mathbf{reprac}(t)}{1 - \mathbf{reprac}(t)} \cdot \mathbf{dltams}(t) \cdot \mathbf{longsperac}_p \cdot 10^{-2} \quad (5.11)$$

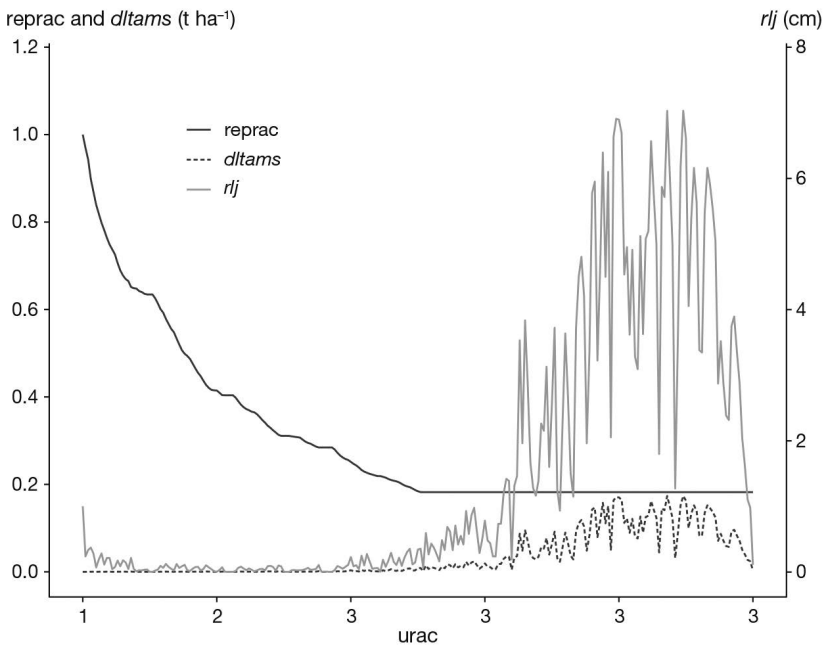


Figure 5.6. Example of the root length growth *rlj* as a function of the root development unit *urac* compared to the underground/total biomass partitioning coefficient *reprac* and the daily production of shoot biomass *dltams*; *reprac* is the daily aboveground/underground ratio of biomass partitioning; *dltams* is the daily growth of plant biomass.

The dynamic of the underground/total biomass partition coefficient (reprac) depends on root development through the normalised root development unit urac (Baret *et al.*, 1992), and on the specific parameters repracpermin_p , repracpermax_p and krepracperm_p (Eq. (5.12) and Figure 5.7).

$$\text{reprac}(t) = \left(\text{repracpermax}_p - \text{repracpermin}_p \right) \cdot e^{-\text{krepracperm}_p(\text{urac}(t)-1)} + \text{repracpermin}_p \quad (5.12)$$

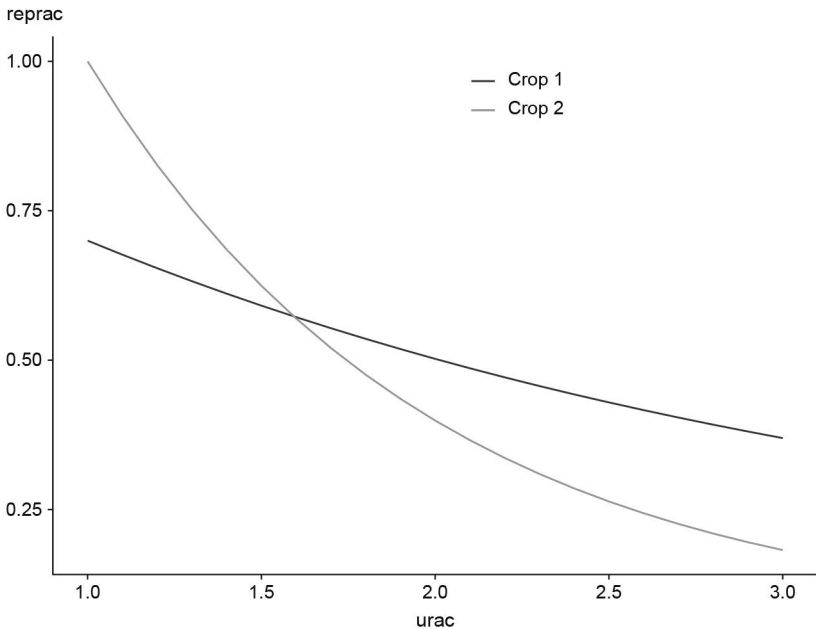


Figure 5.7. Aboveground/underground partition coefficient reprac as a function of the root development unit urac , in the case of two different crops. $\text{repracpermin}_p = 0.10$, $\text{repracpermax}_p = 0.7$ and $\text{krepracperm}_p = 0.40$ for crop 1. $\text{repracpermin}_p = 0.06$, $\text{repracpermax}_p = 1.0$ and $\text{krepracperm}_p = 1.02$ for crop 2.

Finally, the trophic effect can be combined with the effects of soil water and NO_3 limitation. The **code_INN_root_G** is designed to ignore the effect of stress on root growth. It allows users to simulate a preferential allocation of biomass to the roots in case of soil water or nitrogen stress.

5.3.3.2.3 Optional heterotrophic root length expansion in the seedbed

Setting the option **codedisrac_p** at 1 allows users to integrate a heterotrophic phase (Figure 5.5a) along a number of days nhet .

$$\text{nhet} = 2 \cdot (\text{nlev} - \text{nger}) + 1 \quad (5.13)$$

The number of days of heterotrophy is therefore equal to twice the duration of the germination phase (Deleens *et al.*, 1984). This calculation is used to allocate half of the seed's

reserves on the day of emergence, and the remainder until a period equivalent to the time of germination. This quantity of daily biomass from the seeds is calculated as follows:

$$newrac(t) = \frac{pgrainmaxi_p \cdot densite \cdot longspereac_p \cdot 10^{-2}}{nhet} \cdot alloperirac_p \quad (5.14)$$

We therefore assign over $nhet$ days from germination, a root length from seeds having emerged ($densite$) and their specific weight $pgrainmaxi_p$ converted into length $longspereac_p$. The new variable resulting from part of the seed reserves ($alloperirac_p$) thus makes it possible to define the root length allowed by the heterotrophy phase on a daily basis. The default value can be selected for this new parameter $alloperirac_p$, which is equal to 0.25 since 50% of the seed reserves are used for respiration and 50% of the remaining share are allocated to coleoptile growth. The variable $newrac$ is therefore added to rlj during $nhet$ days from germination. The $codedisrac_p$ option can thus be activated to simulate the root activity in early stages.

5.3.3.2.4 Examples of the impact of options driving root length expansion in the true density option

The model is very sensitive to $codtrophrac_p$ option activation. A simple example is given in Figure 5.8 for wheat crop grown in a conventional system, in northern France (Guérif *et al.*, 2001). Deactivating the $codtrophrac_p$ option caused higher rlj during the vegetative phase and lower rlj during the reproductive phase. As a side note, rlj appeared to not be very sensitive when the $codedisrac_p$ option was deactivated, when it mainly drives the root distribution (this phenomenon is explained in the following section). In addition to options, parameter such as $stoprac_p$ plays a strong role in determining the end of the crop cycle. In another study, activating the $codtrophrac_p$ option appeared to be relevant in the case of applying STICS to organic systems where mineral nitrogen can be scarce and limit accumulation of aerial dry matter (Autret *et al.*, 2020).

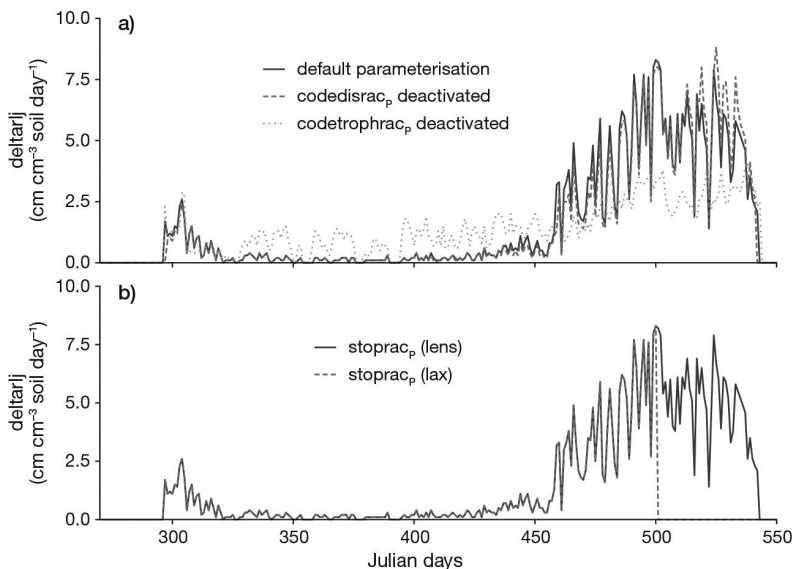


Figure 5.8. Example of the daily root growth rlj of winter wheat according to a) scenario options; b) $stoprac_p$ parameter value.

5.3.3.3 Root length distribution of grown roots in the soil profile

5.3.3.3.1 Biological drivers of root length density

The vertical distribution of the root length density is driven dramatically by the **codedisrac_p** option, which is presented in Figure 5.9. The default option (**codedisrac_p**=2 meaning deactivated) is applied to some crop species for which parameterisation has not yet been updated.

5.3.3.3.1.1 Root sink for root length controlled by initial root length

When **codedisrac_p** option is set to the default option of 2, the new root length is distributed in each layer of the soil profile in proportion to the roots present and as a function of the soil constraints. A ‘root sink strength’ is defined by the proportion of roots in the layer. This does not concern length expansion at the root front, for which growth in density is defined by **lvfront_p** (Eq. (5.10)).

This formalism, which has long been integrated in the model, has several limits, due to the priority given to the root front activity and the indirect role of root senescence parameters on the remaining root profile:

- since nil allocation to root happens before the emergence stage, there will be no roots in the soil layers higher than the depth reached on the day of seed emergence;
- if **rlj** is less than **rljfront**, no root will be allocated to the first horizons; they will only be allocated to the root front; if **rlj** is zero and the front grows in depth, the new zone created on **deltaz** today will not receive any roots;
- along with the previous point, if **rlj** is zero in a given 1 cm layer following a strong root mortality, there will also be no more roots in this area thereafter;

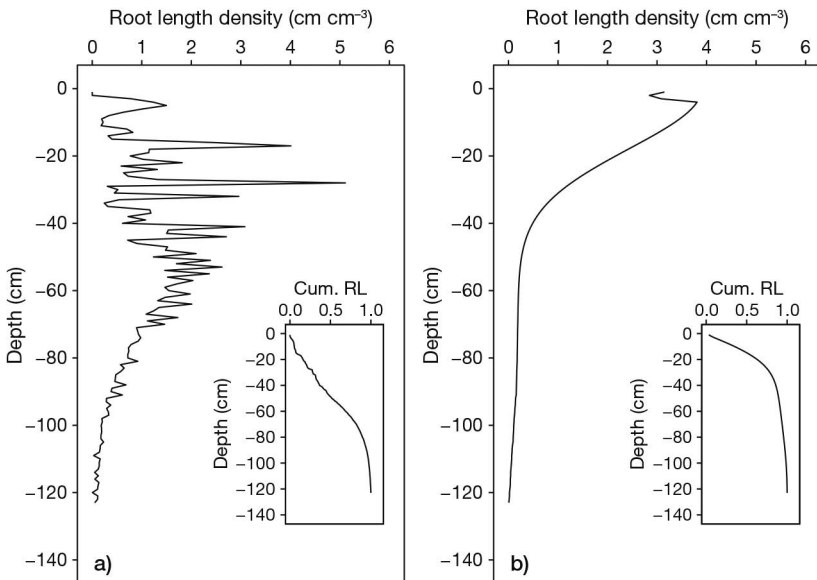


Figure 5.9. Simulated root length density profile and cumulated proportion of root length density (Cum.RL inset plot); a) **codedisrac**=2 i.e. driven by initial root length and b) **codedisrac**=1 i.e. driven by vertical distribution parameters.

– finally, it is possible to end up with a root profile where most of the roots are in the deep horizons, which contradicts the distribution of roots observed in many species (Fan *et al.*, 2016).

5.3.3.3.1.2 Dynamical distribution of increment of length versus depth according to vertical distribution parameters

When **codedisrac_p** option is set to the option of 1, the background of the STICS standard profile formalism is directly applied to the new root generation, as an exponential function of the depth. The function **dis** drives the root distribution function, involving the **lvfront_p** parameter and a new **kdisrac_p** parameter, as follows:

$$\text{dis}(z) = \text{lvfront}_p + (1 - \text{lvfront}_p) \cdot e^{-\text{kdisrac}_p(z)^2} \quad (5.15)$$

We therefore have a decreasing function of the depth z , (in cm), whose shape is determined by **kdisrac_p** and whose asymptote is equal to the parameter **lvfront_p**. A default value of **kdisrac_p** can be taken equal to 0.00158; this is the optimised value in order to obtain a root profile variability similar to those obtained from the meta-analysis by Fan *et al.* (2016).

If the crop is a monocotyledon, root length distribution starts from the surface and not from **profsem_T**.

5.3.3.3.2 Possible roles of physical and chemical factors

This potential ‘root sink strength’ is then reduced by the soil constraints in each layer. Each constraint is defined at the layer level, as an index between 0 and 1, and assumed to be independent of the others. The resulting **poussracmoy** index is the product of elementary indices:

$$\begin{aligned} \text{poussracmoy}(z, t) = & \text{humirac}(z, t) \cdot \text{efda}(z, t) \cdot \\ & (1 - \text{anoxmoy}(z, t) \cdot \text{sensanox}_p) \cdot \\ & \text{efNrac_mean}(z, t) \quad (5.16) \end{aligned}$$

where **humirac** (Eq. (3.8)) defines the effect of soil dryness and, accounts for the plant’s sensitivity to this effect. The variable **efda** defines the effect of soil compaction through bulk density (§ 5.2.2 and Figure 5.2). The anoxia index of each soil layer **anoxmoy** is assigned the value of 1 if the horizon has reached saturation; it is associated with the sensitivity of the plant to waterlogging **sensanox_p**.

The variable **efNrac_mean** defines the effect of mineral nitrogen, which contributes to root distribution in the layers with high mineral nitrogen content. The variable depends on the specific parameters **minazorac_p**, **maxazorac_p** and **minefnra_p**, which characterise the sensitivity of plant root growth to the mineral nitrogen content in the soil (Eq. (5.17); Figure 5.10). This last constraint is optional and can be deactivated in the model.

$$\begin{aligned}
 &AZ(z, t) \leq \text{minazorac}_p \text{ then} \\
 &efNrac_mean(z, t) = \text{minefnra}_p \\
 &\text{minazorac}_p < AZ(z, t) < \text{maxefnra}_p \text{ then} \\
 &efNrac_mean(z, t) = \text{minefnra}_p + \\
 &\frac{(1-\text{minefnra}_p)}{(\text{maxefnra}_p-\text{minefnra}_p)} \cdot (AZ(z, t) - \text{minefnra}_p) \\
 &AZ(z, t) \geq \text{maxefnra}_p \text{ then} \\
 &efNrac_mean(z, t) = 1 \quad (5.17)
 \end{aligned}$$

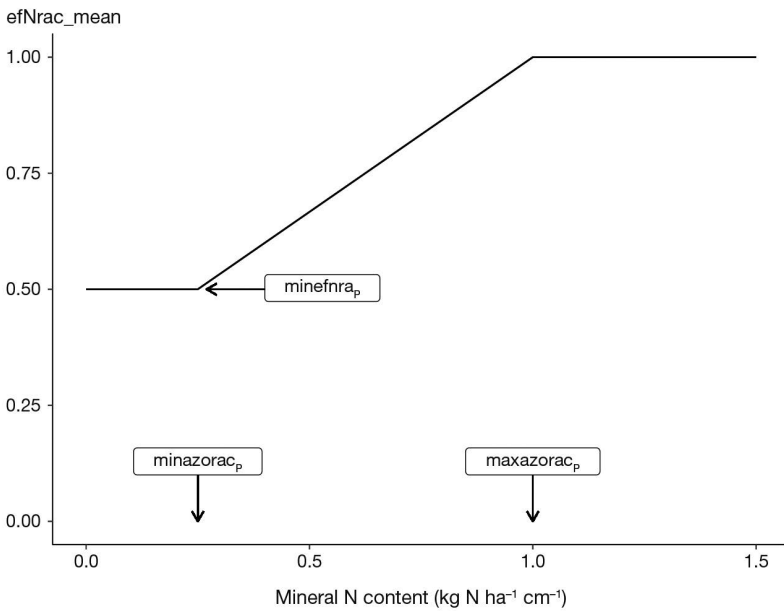


Figure 5.10. Constraint to root distribution $efNrac_mean$ as a function of the mineral nitrogen content in the soil $AZ(z, t)$, the sum of $AZamm(z, t)$ and $AZnit(z, t)$.

5.3.3.4 Senescence

5.3.3.4.1 Introduction

The concept of senescence is only present in the true density option. The root senescence formalism plays a direct role with regard to the actual root profile, and possibly an indirect role regarding root distribution, when the **codedisrac_p** option is deactivated (§ 5.3.3.3). It also directly drives root biomass turn over (see following § 5.4). The main option which drives senescence is **code_diff_root_p**, which allows users to choose between two types of roots (setting 1) or a single mean root type (setting 2)(Figure 5.11). If **code_diff_root_p** equals 1, the role of the root diameter on root lifespan follows the background of the ArchiSimple model (Pagès *et al.*, 2014). Modalities of **code_diff_root_p** can interact with options concerning either forage crops or perennial grasses.

A thermal duration in degree-days (*stdebsenrac_p*) defines root lifespan. Thus, the history of root production per layer is memorised in order to make the portion of roots (*stdebsenrac_p*) set earlier disappear through senescence. The dead root profile is *lracsenz*, while the corresponding total amount is *lracsentot*.

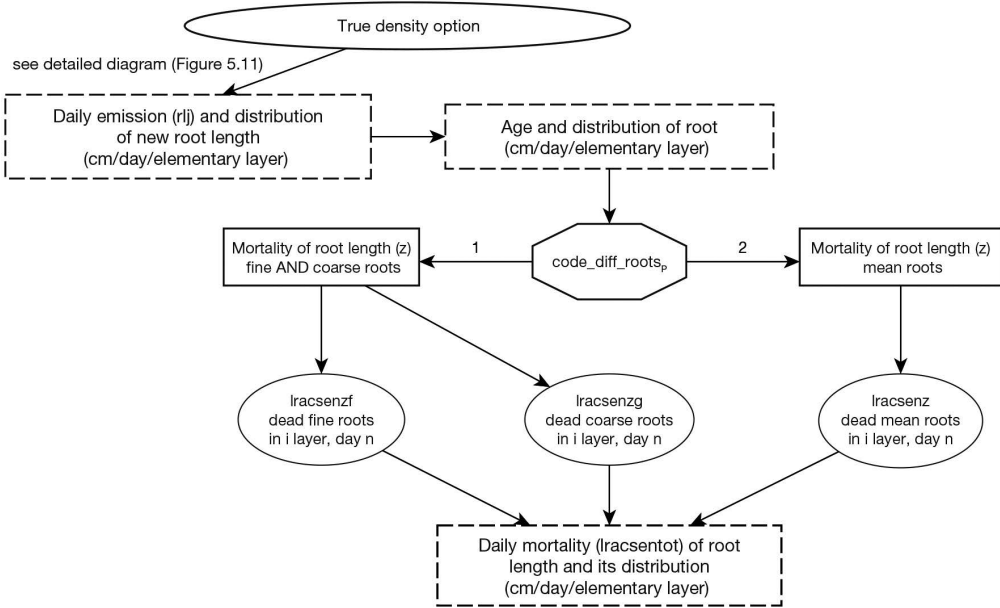


Figure 5.11. Flow chart of options controlling root mortality with true density option selected.

5.3.3.4.2 Calculation with two kinds of root

To be able to correctly simulate root density and root biomass as well as root turnover per soil horizon, roots can be divided into two types: ‘fine’ roots and ‘coarse’ roots with an arbitrary separation. The two types are characterised by the ratio between the diameters of coarse to fine roots (*rapdia_p*) and their respective lifespan (*debsenracf* and *debsenracg*). Their respective proportion is driven by the *propracfmax_p* parameter, which is the maximal share of fine roots. The *parazorac_p* parameter is the C/N ratio of roots when the nitrogen nutrition index (NNI) is 1.

$$\text{dracmoy} = \sqrt{\frac{4}{\pi \cdot \text{RTD}_p \cdot \text{longsperac}_p}}$$

$$\text{dracf} = \frac{\text{dracmoy}}{(1 - \text{propracfmax}_p) \cdot \text{rapdia}_p + \text{propracfmax}_p}$$

$$\text{dracg} = \text{rapdia}_p \cdot \text{dracf} \quad (5.18)$$

The specific root length is calculated for fine (*longsperacf*) and coarse roots (*longsperacg*):

$$\text{longsperacf} = \frac{4}{\pi \cdot \text{dracf}^2 \cdot \text{RTD}_p}$$

$$\text{longsperacg} = \frac{4}{\pi \cdot \text{dracg}^2 \cdot \text{RTD}_p} \quad (5.19)$$

The daily root length emission per elementary layer (drliz) is divided between fine and coarse roots in a proportion close to the initial value:

$$\mathbf{debsenracf} = \frac{\mathbf{debsenrac}_p}{\sqrt{\mathbf{rapdia}_p}}$$

$$\mathbf{debsenracg} = \mathbf{debsenrac}_p \cdot \sqrt{\mathbf{rapdia}_p} \quad (5.20)$$

The living biomass can be calculated for each type of root. These calculations are performed for each soil layer.

$$\mathbf{propracfiz}(z, t) = \frac{\mathbf{rlf}(z, t-1)}{\mathbf{rlf}(z, t-1) + \mathbf{rlg}(z, t-1)}$$

if ($\mathbf{propracfiz}(z, t) < \mathbf{propracmax}_p$) *then*

$$\mathbf{drlizf}(z, t) = \mathbf{drliz}(z, t)$$

$$\mathbf{drlizg}(z, t) = 0$$

else

$$\mathbf{drlizf}(z, t) = \mathbf{drliz}(z, t) \cdot \mathbf{propracmax}_p$$

$$\mathbf{drlizg}(z, t) = \mathbf{drliz}(z, t) \cdot (1 - \mathbf{propracmax}_p)$$

$$\Delta \mathbf{rltotf} = \Delta \mathbf{rltotf} + \mathbf{drlizf}(z, t)$$

$$\Delta \mathbf{rltotg} = \Delta \mathbf{rltotg} + \mathbf{drlizg}(z, t) \quad (5.21)$$

5.3.3.4.3 Calculation with a single kind of root

In this case, it is not necessary to define the parameters cited in the above section. Conversely, the specific root length (**longsperac_p**) becomes a parameter.

5.3.3.4.4 Illustrations of influences of parametrisation scenarios with the true density option

The example illustrated in Figure 5.12A originates from the aforementioned wheat crop case study in northern France. It demonstrates the sensitivity of the **rltot** and **lracsentot** variables to options and one parameter. The variable **rltot** exhibits a dynamical pattern close to patterns of the **lai** for annual crops. The default parameterisation of winter wheat entails activating of **codedisrac_p** and **codtrophrac_p** options as opposed to **code_diff_root_p** option. The **stoprac_p** parameter is equal to 'SEN'. A strong influence of **codtrophrac_p** appears in early stages, and either the **code_diff_root_p** option or **stoprac_p** parameter during the end of the cycle, when **codedisrac_p** option deactivation has a low influence.

Furthermore, two maps of the root system of the winter wheat crop were created in March and June, and provided a proxy of the root length (data not shown). The simulations were satisfactory with the default parameterisation in March and better in June when the **stoprac_p** parameter was changed from the 'SEN' to the 'LAX' stage, indicating the role of the root senescence parametrisation on the residual living roots.

The variable **lracsentot** presents a monotone increase versus time for the same example, shown in Figure 5.12B. Deactivating **codtrophrac_p** slows down root mortality in early stages. Activating **code_diff_root_p** triggers early mortality due to

the existence of fine roots; the final higher value with this option is influenced by the additional root parameters which it needed. Conversely, choosing the LAX stage for **stoprac_p** reduces the final value. The **codedisrac_p** option has low influence on mortality, as expected.

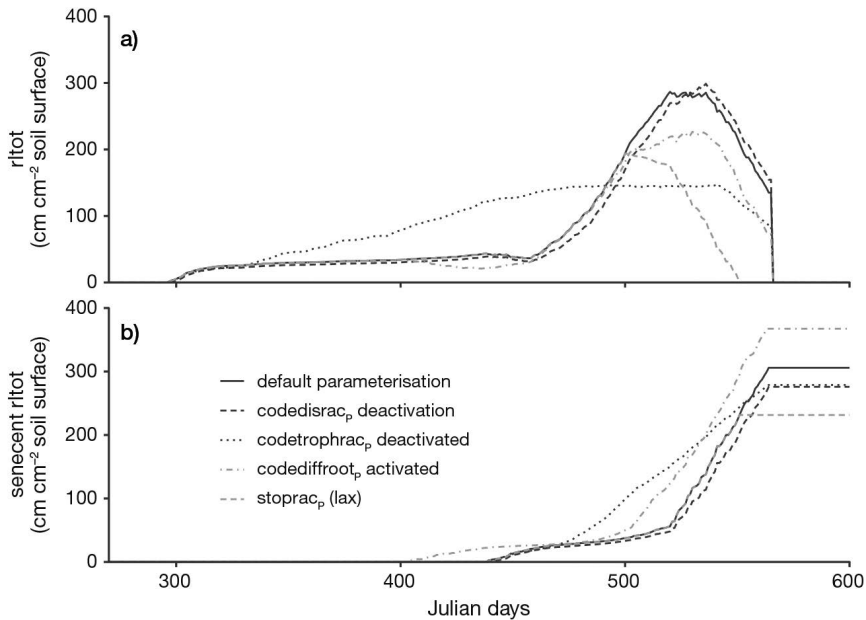


Figure 5.12. Example of the root length kinetics (cm root/cm² soil surface) versus time according to either **scenario options** or **stoprac_p** parameter value: a) length density of living *ritot*; b) length density of senescent roots *lracsentot*.

►► 5.4 Turnover of root biomass and N content allocation

5.4.1 Introduction

Root biomass turnover is by default acted at annual scale, regardless of whether the standard profile or true density option is selected (Figure 5.3). Both options can be used to calculate the dead root biomass at harvest. However, the true density option allows users to perform a dynamical simulation of the biomass decay when the **code_rootdeposition_p** is activated. This choice permits the daily simulation of N immobilisation due to root decomposition along a crop cycle. Accounting for this dynamical process appears to be mandatory to correctly simulate the soil mineral content in a perennial crop such as *Miscanthus x giganteus* (Strullu *et al.*, 2014). However, reliably predicting N immobilisation requires an accurate root parameterisation (Yin *et al.*, 2020).

5.4.2 Daily root biomass decay

Daily root senescence dltamsracmort is daily calculated in the case of **code_rootdeposition_p** activation.

If the **code_diff_root_p** option is not activated, there is no distinction between coarse and fine roots and the biomass of dead roots is calculated as follow:

$$\text{dltamsracmort}(z, t) = 100 \cdot \left[\frac{\text{drlsen}(z, t)}{\text{longsperac}} \right] \quad (5.22)$$

If the **code_diff_rootP** option is activated, then:

$$\text{dltamsracmort}(z, t) = 100 \cdot \left[\frac{\text{drlsenf}(z, t)}{\text{longsperacf}} + \frac{\text{drlseng}(z, t)}{\text{longsperacg}} \right] \quad (5.23)$$

When annual crops are harvested or when perennial crops are destroyed, the death of the whole living root system results in additional root residues. The biomass of the dead roots (**msracmort**) at soil depth z on day t is also calculated using either the mean root length when a single kind of root is simulated ((5.24)), or the root length of fine and coarse roots if the **code_diff_root_p** option is activated (**rlf** and **rlg**, respectively): Eq (5.25).

$$\text{msracmort}(z, t) = 100 \cdot \left[\frac{\text{rlf}(z, t)}{\text{longsperacf}} \right] \quad (5.24)$$

$$\text{msracmort}(z, t) = 100 \cdot \left[\frac{\text{rlf}(z, t)}{\text{longsperacf}} + \frac{\text{rlg}(z, t)}{\text{longsperacg}} \right] \quad (5.25)$$

The daily inputs of C due to dying roots (**dltacracmort**) are the product of **dltamsracmort** and the root C content (assumed to be equal to 380 g C kg⁻¹). The daily inputs of N due to dying roots (**dltacnracmort**) are the ratio of **dltacracmort** and the mean C/N ratio of the roots (**CsurNrac**) depending on the amount of N in the living root (**QNrac**). The cumulative C and N inputs over the whole root profile are then calculated as indicated previously:

$$QCracmort(t) = 380 \cdot \sum_1^{zrac} \text{msracmort}(z, t) \quad (5.26)$$

$$QNracmort(t) = 380 \cdot \sum_1^{zrac} \text{msracmort}(z, t) \cdot \frac{QNrac}{QCrac} \quad (5.27)$$

Part of these C and N inputs occur in the biologically active layer and thus undergo decomposition. The remaining fraction enters the deep soil layer (below **profhum_s**) and is summed up in the variables **Crprof** and **Nrprof**. This organic matter accumulates because this deep layer has no simulated biological activity.

The Figure 5.13 illustrates the daily prediction of root length and root biomass is given for two types of roots in a winter wheat crop (from the aforementioned example in northern France). The respective contribution of fine and coarse roots strongly varies in terms of length and biomass; obviously, this contribution depends on the values of their respective parameters.

5.4.3 Root biomass decay only at the crop growth scale

Dead root biomass is calculated by default either at the day of harvest of annual crops or of the forage cut. The root length can be converted into root biomass using the specific parameter **longsperac_p**. Note that a critical appraisal of the predicted root residue is welcome, in order to avoid overestimating N immobilisation due to root decay.

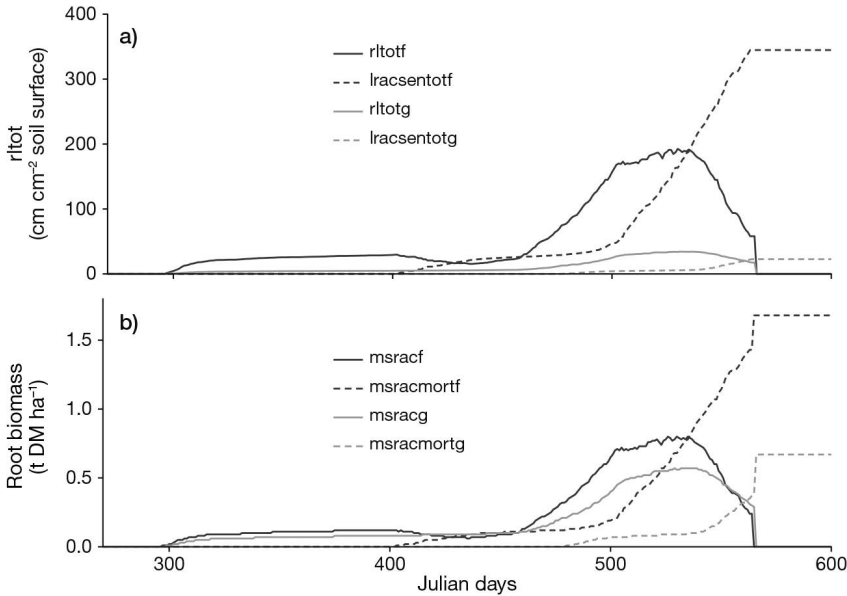


Figure 5.13. Illustration of root growth and root senescence versus time with different types of roots (`diff_rootp` activated; suffixes on root types: f = fine; g = coarse): a) in total root length $rltot$ and cumulative length of senescent roots $lracsentot$; b) in living root biomass $msracf$ and dead root biomass $msracmort$.

– When the *standard profile* option is selected ($coderracine_p = 1$), roots are assumed to accumulate in soil until plant death (usually at harvest). The biomass of dead roots ($msracmort$) is assumed to be a linear function of the aboveground biomass at harvest ($masecnp$):

$$msracmort = masecnp \cdot \mathbf{proprac}_G + \mathbf{y0msrac}_G \quad (5.28)$$

where $\mathbf{proprac}_G$ is a allocation coefficient between below- and above- ground organs (0.20) and $\mathbf{y0msrac}_G$ is the minimum root production when aboveground growth is very limited (0.7 t ha^{-1}). The two coefficients are assumed to be similar for all plants.

– When the *true density* option is selected ($coderracine_p = 2$), root growth and senescence are simulated continuously, while the biomass of died root is recycled back into soil only at harvest if the option `code_rootdepositionp` is not activated, as already shown in Eq (5.23).

For both options, *standard profile* or *true density*, the amount of carbon in the dead root material ($QCracmort$) is the product of the dead root biomass and its mean C content which is assumed to be 380 g C kg^{-1} .

As there is no absorption of N by roots when the option `code_rootdepositionp` is not activated, we assumed that the N content in roots is equal to the N content in the vegetative organs of the crop. The amount of nitrogen in the dead root material ($QNracmort$) is equal to the product of the dead root biomass and N content of vegetative organs. These inputs are assumed to be homogeneously distributed in the biologically active layer [0, $\mathbf{profhum}_s$]. Please note that in this case, the N balance does not loop.

► 5.5 Calculation of root density for water and nitrogen absorption

5.5.1 Root density profiles

The living root density profile is rl , as a variable of time and depth, while its integration at a given time (t) is rl_{tot} , as show in Eq. (5.29):

$$rl_{tot} = \sum_{z=0}^{z=z_{rac}} (rl(z, t))$$

$$rl(z, t) = rl(z, t - 1) + drliz - drlsen(z, t) \quad (5.29)$$

For water and nitrogen absorption, an efficient root length density l_{racz} is calculated by applying the threshold lv_{opt_G} to the total root length density, rl . By default, the value used for the optimum root density threshold lv_{opt_G} is 0.5 cm cm^{-3} soil (Brisson *et al.*, 1998b). In this way, it is possible to represent a root system for various species exhibiting fasciculate or pivotal type root systems (see Figure 5.14).

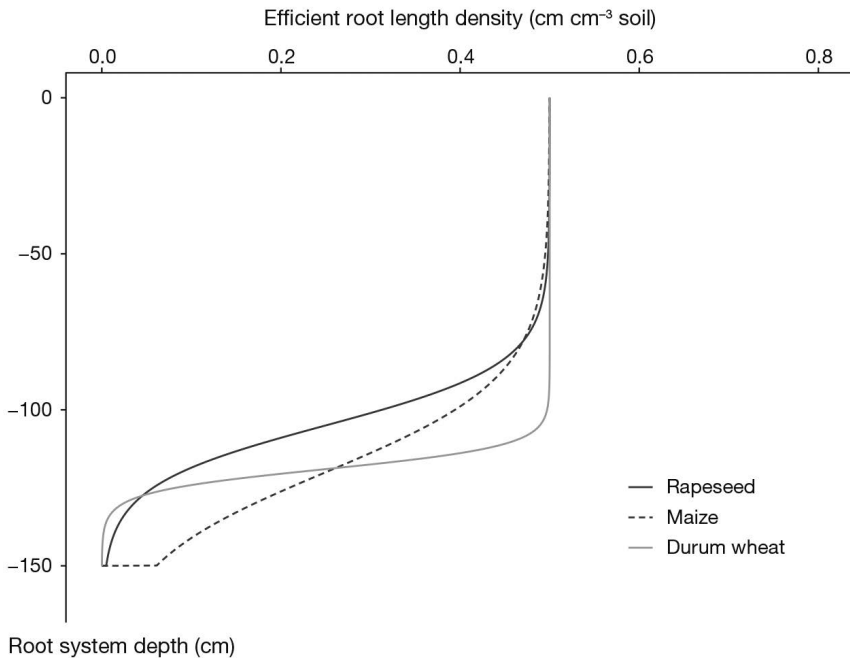


Figure 5.14. Root length density profile, with the standard profile option, for a root front depth of 150 cm, described by the efficient root density l_{racz} as a function of depth z , for rapeseed, maize and durum wheat.

5.5.2 Comparison of the two kinds of density profiles

The differences between the two options in root profile simulation can be significant (Figure 5.15), but the effect on the simulated water and nitrogen uptakes may not be significant because of the functional root density threshold of 0.5 cm cm^{-3} .

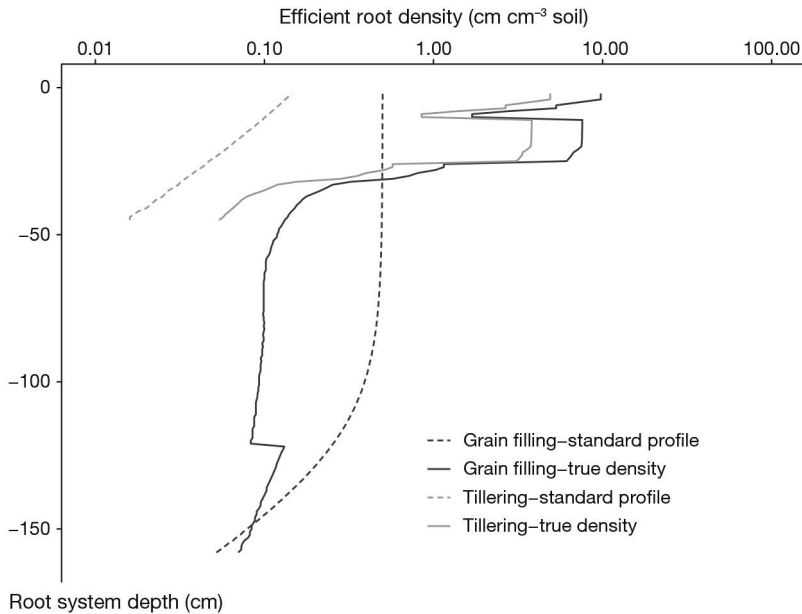


Figure 5.15. Root length density profile as a function of the root depth z , at tillering and at grain filling stages, simulated with the standard profile option (`codedisracp` option deactivated) and the true density option.

5.5.3 Comparison of root profiles in intercrops

STICS is able to simulate the effects of interaction between the shoots and roots of intercrops using the true density option for each crop (§ 5.3.3). STICS deals with intercropping using only the effect of the equivalent plant density on the root length density of each crop and the simulation of the micro-climate conditions (Eq. (4.5)).

The water and N competition between intercrops are accounted for by simulating their availability in soil. The soil volume occupied by each crop is different in sole crops and intercrops. Adiku *et al.* (2001) showed that root systems of component plants in a mixture may intermingle considerably in well-watered situations whereas under water-stressed conditions the root systems may show a tendency to cluster within their ‘own’ zones. This behaviour does not fit the notion of a standard root profile (§ 5.3.2), but it does fit with true density profiles. In our model, we considered neither allelopathy nor other direct effects of a crop species against the other (such as mechanical support), but we assumed that for intercrops, the influence of the crop root systems on each other results from the influence of the soil status on the root distribution. There is no adaptation of the threshold \mathbf{lvopt}_G , which is 0.5 by default for each species.

The Figure 5.16 illustrates the simulation of root profile dynamics in a case study of pea (*Pisum sativum*) and barley (*Hordeum vulgare*) sole crops and a pea-barley intercrop. This example shows the ability of the STICS model to describe the interaction between root systems due to intercropping. This interaction originates from two different phenomena: i) nitrogen and water stress conditions are modified in the intercrops;

ii) to a lesser extent, the thermal time differs because of the crop temperatures if the growth of the root front is calculated with the crop temperature option. This interaction mainly depends on the N supply (Corre-Hellou *et al.*, 2007).

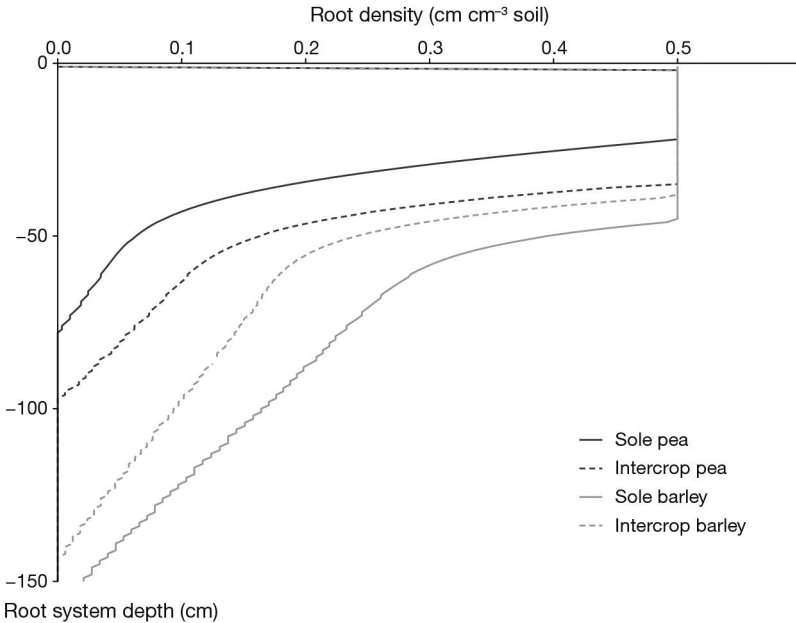


Figure 5.16. Comparison of root profiles in sole crop and intercrops at *stoprac* = LAX stage (23 June).

5.5.4 Root system evolution between successive cycles of perennials

The current version of STICS (10.0) allows users to simulate root system kinetics of perennial crops according the influences of both winter conditions and crop cut. Figure 5.17 provides an example where the dynamics of *rltotf* and *rltotg* are compared to those of LAI in a deep loamy soil in an organic system (Strullu *et al.*, 2020).

During winter, the fine root length decreases considerably while the coarse root length remains stable, due to the longer lifespan of coarse roots when LAI is nil. During spring and summer, both root lengths increase in concomitance with those of LAI and slightly decrease after a forage cut.

The simulated rhizodeposition then allows for reliable simulations of soil mineral nitrogen during and after crop destruction. The distribution of *rltotf* within the soil provides the variable root length density for each soil layer, i.e. from LRACH(1) to LRACH(5). In the Figure 5.18, the roots successively colonised the different layers according to their depth and then decayed.

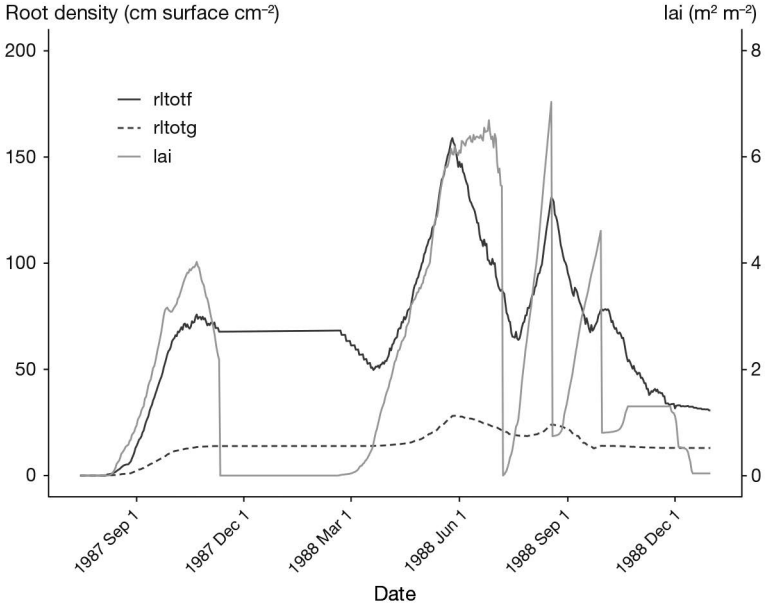


Figure 5.17. Dynamics of total root length for fine and coarse roots (*rltotf* and *rltotg*, respectively) compared to those of *lai* in a deep loamy soil in organic system for *Medicago sativa* L. with the STICS model v10.

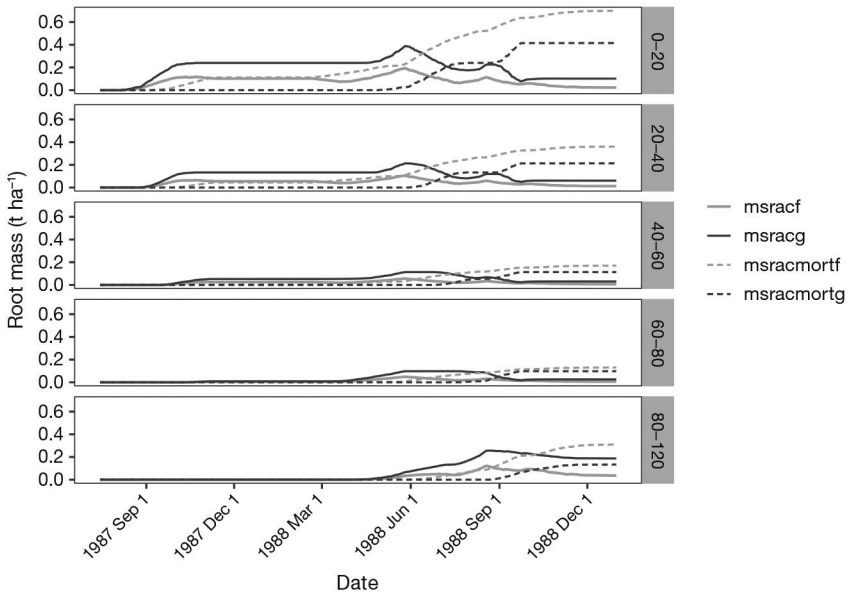


Figure 5.18. Dynamics of fine and coarse root mass in different soil layers for living root biomass (*msrac*) and dead root biomass (*msracmort*) for fine and coarse roots (suffixes *f* and *g* respectively) for *Medicago sativa* L. with the STICS model v10.

Chapter 6

Nitrogen acquisition by plants

*BRUNO MARY, FABIEN FERCHAUD, LOIČ STRULLU
AND NADINE BRISSON*

REVIEWED BY: NICOLAS BEAUDOIN

» 6.1 Nitrogen uptake by plants

6.1.1 Introduction

Nitrogen uptake by the crop is simulated using the concepts of soil supply and crop demand. Uptake is assumed to be equal to the smallest of these two terms, which is therefore the limiting factor of N uptake. The model calculates and compares these two terms daily.

The crop demand in STICS is defined by considering the concept of “nitrogen dilution curves”. Lemaire and Gastal (1997) have shown that the nitrogen concentration in plant shoots (expressed in g N kg^{-1} dry matter) inevitably decreases over time and along with shoot dry matter. This “dilution” is due to the increasing proportion of structural tissues and the increased shading of lower leaves throughout crop growth. It is possible to define a nitrogen concentration in shoots below which the crop growth rate is reduced: this concentration is called the “critical N content”. Its value decreases with time and with crop biomass. It is also possible to define maximal and minimal dilution curves by considering the upper and lower envelope curves representing data from all experiments. The maximal dilution curve allows to calculate the crop demand. The rate of decrease of these dilution curves varies throughout the crop lifecycle and depends on three factors:

- the plant metabolism, which requires less nitrogen in C4 than in C3 plants;
- the plant ability to store N in the form of reserves (protein, amino acids, etc.) which is greater, for example, in legumes than in cereals;
- inter-plant competition which affects senescence and thus the plant C/N ratio, requiring to consider differently isolated plants and plants within a dense canopy.

These three factors are not always given the same attention. If we consider isolated plants, N concentrations of the maximal and critical curves always decrease with time, whereas they remain constant during a very early crop phase under dense canopies. In practice only the critical curve can be determined rigorously (Justes *et al.*, 1994), whereas the maximum level is difficult to define accurately.

Finally, during the reproductive phase, the N demand of the storage organs has to be taken into account.

6.1.2 Nitrogen demand of the crop

If N_{max} is the maximum crop N concentration (in g N kg⁻¹) and W the crop biomass (sum of $masecnp$ and the harvested fruit biomass in case of fruit picking, in t ha⁻¹), the daily N demand ($demande$, in kg N ha⁻¹ day⁻¹) is the product of the crop growth rate ($dltams$, in t ha⁻¹ day⁻¹) and the derivative of N_{max} relative to W :

$$demande(t) = \frac{\Delta N_{max}(t)}{\Delta t} = \frac{\Delta N_{max}(W)}{\Delta W} \cdot dltams(t) \quad (6.1)$$

N_{max} depends on two factors: the density of the canopy and the presence of storage organs; the first factor defines the parameters of the curves $N_{max} = f(W)$ (according to Lemaire and Gastal (1997) or Justes *et al.* (1997)) and the second one defines W .

6.1.2.1 Nitrogen dilution curves in aboveground organs

According to the type of crop, plants can either interact within a dense canopy or be isolated plants. In the first case (dense canopy, **codeplisole** $N_p = 1$) the critical dilution curve (N_c) is defined by the classical power function:

$$N_c(t) = \mathbf{adil}_p \cdot W(t)^{-\mathbf{bdil}_p} \quad (6.2)$$

$$\text{with } W(t) = \max[masecnp, masecN_{max_p}] \quad (6.3)$$

and the maximum dilution curve (N_{max}) is defined by the function:

$$N_{max}(t) = \mathbf{adilmax}_p \cdot W(t)^{-\mathbf{bdilmax}_p} \quad (6.4)$$

In the case of isolated plants (**codeplisole** $N_p = 2$), the critical dilution curve (N_i) is described by two successive power functions:

$$N_i(t) = \mathbf{adili} \cdot W(t)^{-\mathbf{bdili}} \quad \text{if } masecnp \leq masecN_{max_p}$$

$$N_i(t) = \mathbf{adil}_p \cdot W(t)^{-\mathbf{bdil}_p} \quad \text{if } masecnp \geq masecN_{max_p} \quad (6.5)$$

$$\text{with } W(t) = \max[masecnp, masecmeta_p] \quad (6.6)$$

and the maximum dilution curve (N_{maxi}) is defined by the function:

$$N_{maxi}(t) = \mathbf{adilmaxi}_p \cdot W(t)^{-\mathbf{bdilmaxi}_p} \quad \text{if } masecnp \leq masecN_{max_p}$$

$$N_{maxi}(t) = \mathbf{adilmax}_p \cdot W(t)^{-\mathbf{bdil}_p} \quad \text{if } masecnp \geq masecN_{max_p} \quad (6.7)$$

The parameters **adil**_{*p*} and **bdil**_{*p*} are common to both options. The additional parameters used for the isolated plant option (**adili** and **bdili**) are obtained using the following assumptions:

- the N contained in young plantlets is only used for N metabolism, not in structures. The concentration of this metabolic-N (**Nmeta**_{*p*}) is a function of species metabolism: 6.47% for C3 crops (e.g. wheat) and 4.80% for C4 crops (e.g. maize) (Justes *et al.*, 1997; Lemaire and Gastal, 1997);
- N dilution starts when the plantlet biomass exceeds a biomass threshold called **masecmeta**_{*p*} (0.04 t ha⁻¹; Justes *et al.* (1997));

- the difference between the maximum and the critical N concentrations, when biomass is equal to $\mathbf{masecNmax}_p$, is $\mathbf{Nreserve}_p$;
- in dense canopy, when biomass is greater than $\mathbf{masecNmax}_p$, the curvature of the maximal curve is the same than that of the critical curve: $\mathbf{bdilmax}_p = \mathbf{bdil}_p$.

Using these assumptions, the missing parameters of Eq. (6.4) and (6.5) can be calculated as follows:

$$bdil_i = \frac{bdil_p \log(\mathbf{masecNmax}_p) - \log(\mathbf{adil}_p) + \log(\mathbf{Nmeta}_p)}{\log(\mathbf{masecNmax}_p) - \log(\mathbf{masecmeta}_p)} \quad (6.8)$$

$$adil_i = \frac{\mathbf{Nmeta}_p}{\mathbf{masecmeta}_p^{-bdil_i}} \quad (6.9)$$

$$\mathbf{adilmax}_p = \mathbf{adil}_p + \frac{\mathbf{Nreserve}_p}{\mathbf{masecNmax}_p^{-bdil_p}} \quad (6.10)$$

$$bdilmax_i = - \frac{\log(\mathbf{adilmax}_p \mathbf{masecNmax}_p^{-bdil_p}) - \log(\mathbf{Nmeta}_p)}{\log(\mathbf{masecNmax}_p) - \log(\mathbf{masecmeta}_p)} \quad (6.11)$$

$$adilmax_i = \frac{\mathbf{Nmeta}_p}{\mathbf{masecmeta}_p^{-bdilmax_i}} \quad (6.12)$$

An example of these dilution curves is given in Figure 6.1.

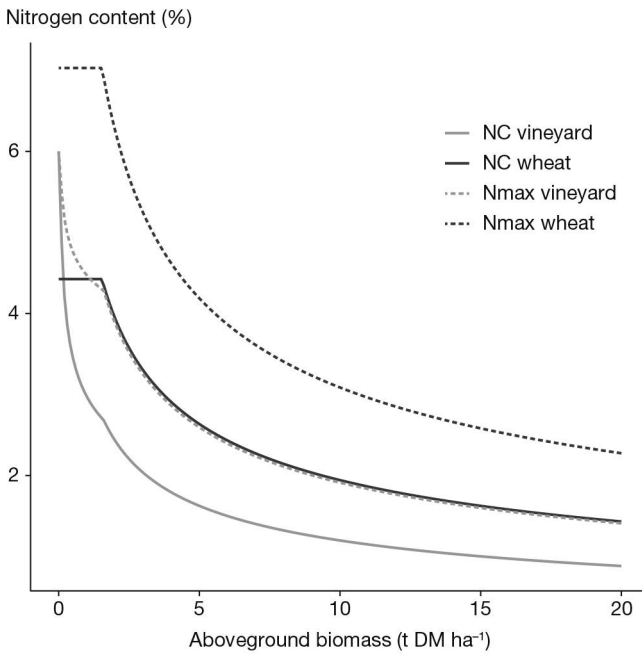


Figure 6.1. Maximal (Nmax) and critical (NC) dilution curves for wheat (dense canopy) and vineyard (isolated plants).

6.1.2.2 Nitrogen dilution during filling of storage organs

The N demand due to vegetative organs is assumed to follow the maximal dilution curve, whereas the demand associated with the “fruit” (either grains or storage organs) depends on the nitrogen status of the crop through the variable \mathbf{absdrp} . The biomass

(W) used to calculate the N demand from the maximal dilution curve depends on the vegetative biomass (*masecveg*), the daily increase of grain biomass (*dltags*) and the crop N status (*absodrp*):

$$W(t) = masecveg(t) + absodrp(t) \cdot dltags(t) \quad (6.13)$$

absodrp is defined using the parameters **inngrain1_p** and **inngrain2_p**:

$$absodrp(t) = \frac{inns(t) - inngrain2_p}{inngrain1_p - inngrain2_p}$$

$$absodrp(t) = 1 \quad \text{if } inns(t) \leq inngrain1_p$$

$$absodrp(t) = 0 \quad \text{if } inns(t) \geq inngrain2_p \quad (6.14)$$

The relationship between *inns* and *absodrp* is shown in Figure 6.2 for winter wheat (**inngrain1_p** = 0.26 and **inngrain2_p** = 1.60).

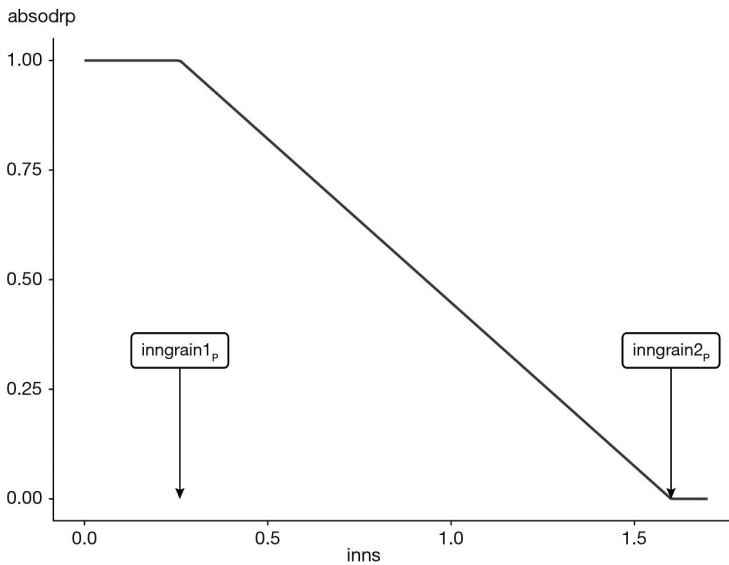


Figure 6.2. *absodrp* versus nitrogen stress index (*inns*).

6.1.2.3 Nitrogen demand of the structural part of non-perennial organs

The N demand of the structural part of green leaves and stems is used to determine the N allocation to leaves, stems and reserves (§ 7). It is calculated with the C/N ratio of these organs using the parameters **parazofmorte_p** and **parazotmorte_p** which represent the C/N ratio of the structural part of dead leaves or stems respectively, when the nitrogen nutrition index (*inn*) is equal to 1. The N demand of the two organs (*demandfv* and *demandet*, respectively) depends on the nitrogen nutrition index of the crop (*inn*) and the amount of biomass allocated daily to these organs (*dltafv* and *dltat*, respectively):

$$demandfv(t) = Cshoot \cdot \frac{dltafv(t)}{parazofmorte_p} \cdot inn \quad (6.15)$$

$$demandet(t) = Cshoot \cdot \frac{dltat(t)}{parazotmorte_p} \cdot inn \quad (6.16)$$

The structural N demand ($demand_{struc}$) is limited by the amount of N allocated to the aerial organs ($absoaer + dltaremobilN$):

$$demand_{struc}(t) = \min[demand_{efv}(t) + demand_t(t), absoaer(t) + dltaremobilN(t)] \quad (6.17)$$

6.1.2.4 Nitrogen demand of roots and perennial organs

The C/N ratio of roots ($CsurNrac$) and perennial organs ($CsurNper$) depends on the nitrogen nutrition index (inn) and the parameters **parazorac_p** and **Parazoper_p**:

$$CsurNrac = \frac{parazorac_p}{inn} \quad (6.18)$$

$$CsurNper = \frac{Parazoper_p}{inn} \quad (6.19)$$

The N demand of roots ($demand_{rac}$) and perennial organs ($demand_{per}$) is calculated using the C/N ratio of these organs (**parazorac_p** and **Parazoper_p**, respectively) which vary according to the inn and the amount of biomass allocated to these organs ($dltamsrac$ and $dltarestemp$, respectively) (Eq. (6.20) and (6.21)).

$$demand_{rac} = dltamsrac \cdot \frac{CCrac}{CsurNrac} \quad (6.20)$$

$$demand_{per} = dltarestemp \cdot \frac{CCper}{CsurNper} \quad (6.21)$$

where $CCrac$ and $CCper$ represent the carbon concentration in root and perennial organs (380 and 440 g C kg⁻¹, respectively).

6.1.3 Soil nitrogen supply

The soil nitrogen supply is the maximum amount of mineral N that the soil can deliver to the root surface, for a given status of soil and plant root system. It is calculated for each elementary layer (1 cm thick) from the surface to the maximum rooting depth ($zrac$, in cm). It does not account for possible nitrate upflow by capillary rise (this would require knowledge of the nitrate concentration in the subsoil below the maximum soil depth).

The soil N supply in each soil layer ($fluxso$, in kg N ha⁻¹ day⁻¹) is determined by the transport of mineral N from a given soil location to the nearest root by convection and diffusion:

$$fluxso(z, t) = conv(z, t) + diff(z, t) \quad (6.22)$$

The convection flow in each elementary soil layer ($conv$, in kg N ha⁻¹ day⁻¹) is the product of the water flow (i.e. the transpiration flow epz , in mm day⁻¹, see § 11.5.3) and the mean NO₃ concentration ($concN$, in kg N ha⁻¹ mm⁻¹ water). The exchangeable NH₄ is not included, since it is assumed to be immobile. There is no nitrate transport by convection if the transpiration is nil (due to absence of roots or severe water stress):

$$conv(z, t) = epz(z, t) \cdot concN(z, t) \quad (6.23)$$

The diffusion flow in each elementary soil layer ($diff$, in kg N ha⁻¹ day⁻¹) is the product of the effective diffusion coefficient of mineral N ($difNe$, in cm² day⁻¹) and the horizontal gradient of mineral N concentration in the soil (in kg N ha⁻¹ mm⁻¹ water cm⁻¹ soil).

This gradient is calculated from the effective root density profile ($lracz$), assuming that roots are vertical and equidistant and that mineral N concentration decreases linearly from the middle of two adjacent roots up to root surface (mineral N concentration is nil at the root surface). These assumptions lead to:

$$diff f(z, t) = 4\sqrt{\pi} \cdot difNe(z, t) \cdot (nit(z, t) + amm(z, t)) \cdot lrac(z, t) \quad (6.24)$$

The effective diffusion coefficient is a function of soil water content and bulk density (Cockborne *et al.*, 1988). Only the moisture effect (which is the main effect) is considered in STICS.

$$difNe(z, t) = \max\left[0, difN_G \cdot \frac{hur(z, t) - humin(z)}{hucc(z) - humin(z)}\right] \quad (6.25)$$

The uniform root distribution hypothesis maximises the diffusive flow. In fact, roots are heterogeneously distributed so that the diffusive flow is lower. In order to account for this effect, the diffusion coefficient at field capacity ($difN_G$) used in STICS ($0.018 \text{ cm}^2 \text{ day}^{-1}$) is lower than the measured values reported in the literature ($0.10\text{-}0.25 \text{ cm}^2 \text{ day}^{-1}$) (Barber and Silberbush, 2015; Cockborne *et al.*, 1988; Kersebaum and Richter, 1991).

6.1.4 Nitrogen uptake capacity of the crop

The N uptake by the root system is an active physiological process which depends on the intrinsic absorption capacity of the plant, its root density and the nitrate concentration in the soil. The specific absorption capacity $Vabs$ (per unit of root area, in $\mu\text{mol N h}^{-1} \text{ cm}^{-1} \text{ root}$) increases with the mineral N concentration according to

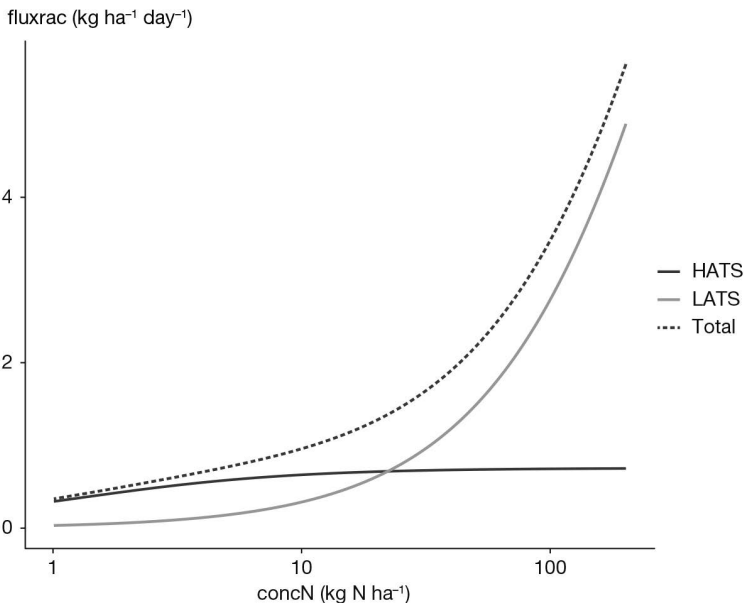


Figure 6.3. N uptake capacity of each system (HATS and LATS) versus nitrate content in soil (logarithmic scale). Parameter values: $Vmax1_p = 0.0018$; $Kmabs1_p = 50$; $Vmax2_p = 0.050$; $Kmabs2_p = 25000$; $lracz = 0.20$; $zrac = 60$; $hur = 0.20$, $DAF_s = 1.50$.

double Michaelis-Menten kinetics (Devienne-Barret *et al.*, 2000) (Eq. (6.26)). These kinetics correspond to two types of transport systems: a high affinity transport system “HATS” (with low $\mathbf{Vmax1}_p$ and $\mathbf{Kmabs1}_p$) and a low affinity transport system “LATS” (with high $\mathbf{Vmax2}_p$ and $\mathbf{Kmabs2}_p$).

$$V_{abs}(z, t) = \frac{\mathbf{Vmax1}_p \cdot concN(z, t)}{\mathbf{Kmabs1}_p + concN(z, t)} + \frac{\mathbf{Vmax2}_p \cdot concN(z, t)}{\mathbf{Kmabs2}_p + concN(z, t)} \quad (6.26)$$

In Eq. (6.26), $concN$ is the molar concentration of mineral nitrogen ($\mu\text{mol l}^{-1}$) and the parameters $\mathbf{Vmax1}_p$ and $\mathbf{Vmax2}_p$ are expressed in $\mu\text{mol cm}^{-1} \text{h}^{-1}$. Mineral N is considered as a whole ($\text{NH}_4 + \text{NO}_3$), so that any selectivity between ammonium and nitrate absorption is not accounted for.

The potential uptake rate in each soil layer is $fluxrac$ ($\text{kg N ha}^{-1} \text{day}^{-1}$). It is proportional to the effective root density (Eq. (6.27)) which is limited by the threshold \mathbf{lvopt}_G , above which uptake is no longer limited by root density:

$$fluxrac(z, t) = 33.6 \cdot V_{abs}(z, t) \cdot lrac(z, t) \quad (6.27)$$

The coefficient 33.6 is the ratio of $\mu\text{mol cm}^{-2} \text{h}^{-1}$ to $\text{kg ha}^{-1} \text{day}^{-1}$. Figure 6.3 shows the dynamics of $fluxrac$ versus the nitrate content in soil and the contribution of both transport systems to the uptake capacity.

6.1.5 Actual N uptake

The mineral N available for root uptake in each layer ($offrN$) is equal to the smallest of the three terms: soil supply, uptake capacity and available mineral N:

$$offrN(z, t) = \min(fluxsol(z, t), fluxrac(z, t), nit(z, t) + amm(z, t)) \quad (6.28)$$

The integration of $offrN$ over the whole profile yields $cumoffrN$. In each layer, the N supply can be compared to the crop demand through the ratio $demsup$:

$$demsup(t) = \min\left[1, \frac{demand_{tot}(t)}{cumoffrN(t)}\right] \quad (6.29)$$

If $demsup = 1$, the soil N supply is the factor limiting N uptake. In this case the N uptake in each layer is equal to the N supply $offrN$. Conversely, the demand is the factor limiting N uptake if $demsup < 1$; in this case, the actual N uptake in each layer is smaller than and proportional to the N supply.

In both cases, the actual N uptake in each soil layer ($absz$) and the total uptake over the root profile ($abso$) can be written as a function of the $demsup$ variable:

$$absz(z, t) = offrN(z, t) \cdot demsup(t) \quad (6.30)$$

$$abso(t) = cumoffrN(t) \cdot demsup(t) \quad (6.31)$$

►► 6.2 Nitrogen fixation by legumes

Many authors have demonstrated experimentally the influence of crop growth and phenology on the activity of biologic nitrogen fixation (BNF) as well as the influence of environmental factors, and especially of soil nitrate availability (Voisin *et al.*, 2002).

First, BNF intensity is known to vary during crop growth. It increases until the early stages of reproductive development and then plateaus before declining until the end of crop life (Bethlenfalvay *et al.*, 1978; Bethlenfalvay and Phillips, 1977; Lawrie and Wheeler, 1974). These variations are thought to be the result of competition for carbon between nodules and seeds (Jeuffroy and Warembourg, 1991), and differ according to species and sometimes cultivars (Cousin, 1997).

Second, BNF has been shown to be closely linked to crop photosynthetic activity through experiments using labelled CO₂ (Gordon *et al.*, 1985; Kouchi and Nakaji, 1985; Voisin, 2003; Warembourg, 1983), and thus correlated to crop growth rate (Finn and Brun, 1982; Jensen, 1987; Voisin *et al.*, 2002).

Finally, several abiotic factors have been mentioned to explain BNF inhibition, and especially soil nitrate availability. The negative effect of nitrate on BNF has been reported by several authors (MacDuff *et al.*, 1996; Waterer and Vessey, 1993), with soil nitrate availability inhibiting both nodule formation and nitrogenase activity (Sprent *et al.*, 1988). BNF is also limited by soil water deficiency (Peña-Cabriales and Castellanos, 1993), but this effect may be reversible (Guérin *et al.*, 1991). Waterlogging may prevent BNF by limiting O₂ availability for bacteria (Jayasundara *et al.*, 1997). Low temperatures reduce nodule activity (Rennie and Kemp, 1981) and high temperatures affect both bacterial lifespan in the soil (Hungria and Vargas, 2000) and nitrogenase activity.

In STICS, three criteria are considered to simulate symbiotic N₂ fixation by legumes. The first criterion is the presence of nodules, depending on their own phenology and lifespan as well as the inhibiting effect of excessive nitrate in the soil. The second is the capacity of the plant to feed these supplementary symbiotic organs depending on plant growth rate, and the third is the soil-dependent physicochemical conditions allowing optimal nodule activity, i.e. soil nitrate level, water deficit, anoxia and temperature (Debaeke *et al.*, 2001; Voisin, 2003). The first two criteria define the potential N₂ fixation while the third defines the actual N₂ fixation.

6.2.1 Potential N₂ fixation

The potential N₂ fixation (*fixpot*, in kg N ha⁻¹ day⁻¹) is calculated as the product of a phenology-dependent coefficient *propfixpot* (between 0 and 1) and the maximum fixation capacity of the crop (*fixmaxvar*, in kg N ha⁻¹ day⁻¹):

$$\mathit{fixpot}(t) = \mathit{propfixpot}(t) \cdot \mathit{fixmaxvar} \quad (6.32)$$

The *propfixpot* coefficient varies according to growing degree-days (Eq. (6.33)) and is calculated the same way as for root growth (see § 5.2.2). The fixation process begins at the *idno* stage (defined by the thermal duration **stlevdno_p**) and stops at the *ifno* stage (defined by the thermal duration **stdnofno_p**). The potential curve then decreases until the death of nodules, corresponding to the *ifvino* stage, during the **stfnofvino_p** thermal duration. The establishment rate of nodules between the *idno* and *ifno* stages depends on the potential rate **vitno_p** and on growing degree-days (Figure 6.4).

It may be inhibited by high mineral nitrogen levels, under the control of $nodn$ which is nil when the soil mineral nitrate concentration exceeds the threshold $concNnodseuil_p$ (in $kg\ N\ ha^{-1}\ mm^{-1}$ water), and otherwise is equal to 1.

$$propfixpot(t) = 0 \quad \text{if } t \leq idno \text{ or } t > ifvino$$

$$propfixpot(t) = propfixpot(t-1) + vitno_p \cdot nodn(t) \cdot \max[0, (tcult(t) - tcmin_p)] \\ \text{if } idno < t \leq ifno$$

$$propfixpot(t) = propfixpot(t-1) - \frac{propfixpot(t-1)}{stfnofvino_p} \cdot \max[0, (tcult(t) - tcmin_p)] \\ \text{if } ifno < t \leq ifvino$$

$$propfixpot(t) \leq 1 \quad (6.33)$$

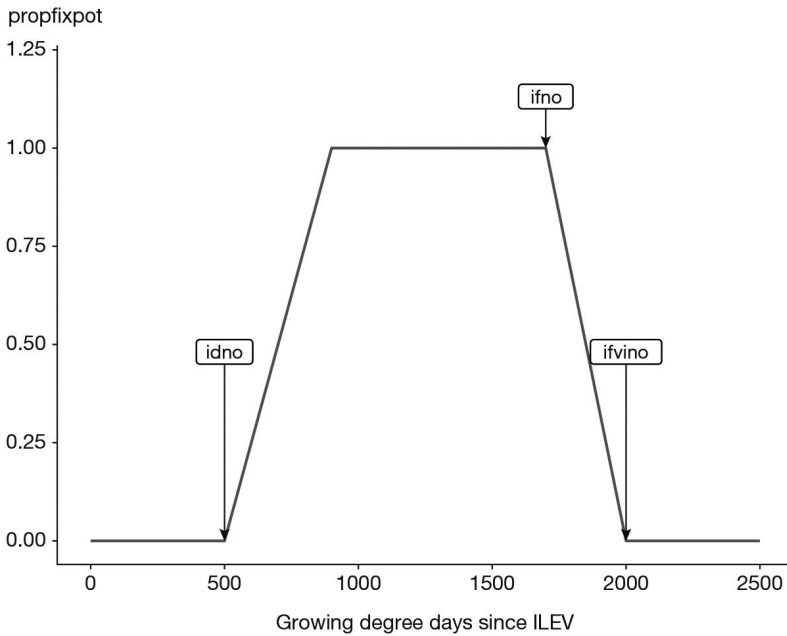


Figure 6.4. Evolution of Propfixpot versus thermal time, for a low level of soil nitrate content ($nodn = 1$). Parameter values: $stlevdno_p = 500$, $stdnofno_p = 1200$, $stfnofvino_p = 300$, $vitno_p = 0.0025$.

The maximum fixation capacity of the crop ($fixmaxvar$) can be either constant (equal to $fixmax_p$) if $codefixpot_p$ is equal to 1, or variable depending on vegetative and reproductive growth if $codefixpot_p$ is equal to 2. In the latter case, it is calculated as:

$$fixmaxvar = fixmaxveg_p \cdot (dltams(t) - dltagst(t)) + fixmaxgr_p \cdot dltagst(t) \quad (6.34)$$

where $dltams$ is the daily biomass increase and $dltagst$ is the daily increase of grain biomass. The parameter $fixmaxveg_p$ is the maximum amount of N fixed per ton of vegetative biomass and $fixmaxgr_p$ is the maximum amount of N fixed per ton of grain biomass.

6.2.2 Actual N₂ fixation

To calculate the actual N₂ fixation (*fixreel*, in kg N ha⁻¹ day⁻¹), the potential N₂ fixation *fixpot* is multiplied by indices (varying between 0 and 1) corresponding to constraints due to anoxia (*fxa*), temperature (*fxt*), water content (*fxw*) and soil mineral nitrogen (*fxn*):

$$fixreel(t) = fixpot(t) \cdot fxt(t) \cdot fxa(t) \cdot \min(fxw(t), fxn(t)) \quad (6.35)$$

The impact of temperature on fixation (*fxt*) is described by using soil temperature in the nodulation zone. It is a trapezoidal function defined by four cardinal temperatures (**tempnod1_p** to **tempnod4_p**) (Figure 6.5):

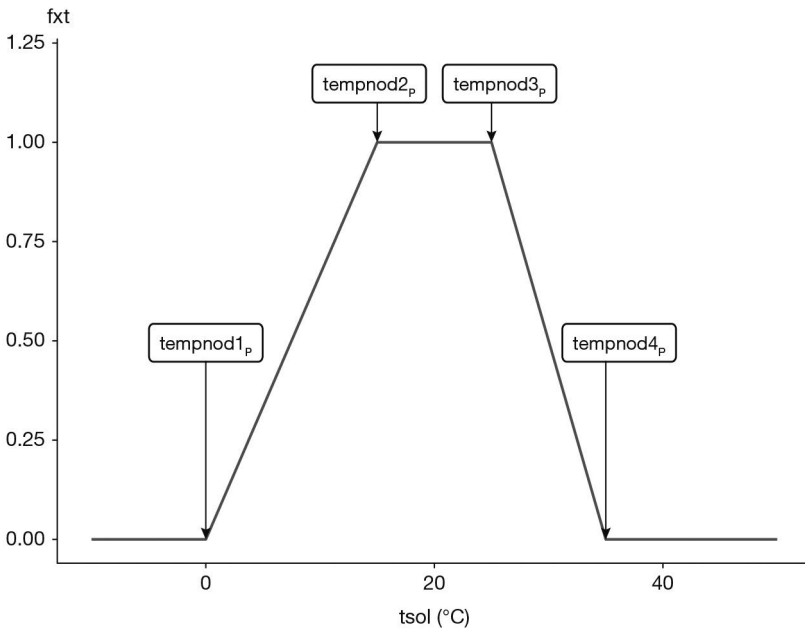


Figure 6.5. Effect of soil temperature on N₂ fixation. Parameter values are **tempnod1_p** = 0, **tempnod2_p** = 15, **tempnod3_p** = 25, **tempnod4_p** = 35.

The water stress factor (*fxw*) is equal to the proportion of elementary soil layers in the nodulation area which have a water content *hur* equal or greater than the permanent wilting point:

$$fxw(t) = \frac{1}{\mathbf{profnod}_p - \mathbf{profsem}_t + 1} \sum_{z=\mathbf{profsem}_t}^{\mathbf{profnod}_p} H(t, z)$$

with

$$H(t, z) = 1 \quad \text{if } hur(t, z) > humin(z)$$

$$H(t, z) = 0 \quad \text{if } hur(t, z) \leq humin(z) \quad (6.36)$$

Limitation by anoxia (*fxa*) is calculated according to the same principle (it is equal to the proportion of elementary soil layers which are in anaerobic conditions) using the anox variable (see § 5.3.3.3).

$$fxa(t) = 1 - \frac{1}{\mathbf{profnod}_p - \mathbf{profsem}_T + 1} \sum_{z=\mathbf{profsem}_T}^{\mathbf{profnod}_p} \mathbf{anox}(z, t) \quad (6.37)$$

Finally, fixation can be partially inhibited either by soil mineral nitrogen amount (if $\mathbf{codefxn}_G = 2$) or by mineral N concentration (if $\mathbf{codefxn}_G = 3$). There is no inhibition if $\mathbf{codefxn}_G = 1$. In the case where $\mathbf{codefxn}_G = 2$, N fixation is partly inhibited ($fxn < 1$) when the mean amount of mineral nitrogen in the rooting zone ($\mathbf{azorac}/\mathbf{zrac}$, in $\text{kg N ha}^{-1} \text{ cm}^{-1}$ soil) exceeds the threshold $\mathbf{concNrac100}_p$, and is fully inhibited ($fxn = 0$) when the amount exceeds the threshold $\mathbf{concNrac0}_p$ (Figure 6.6).

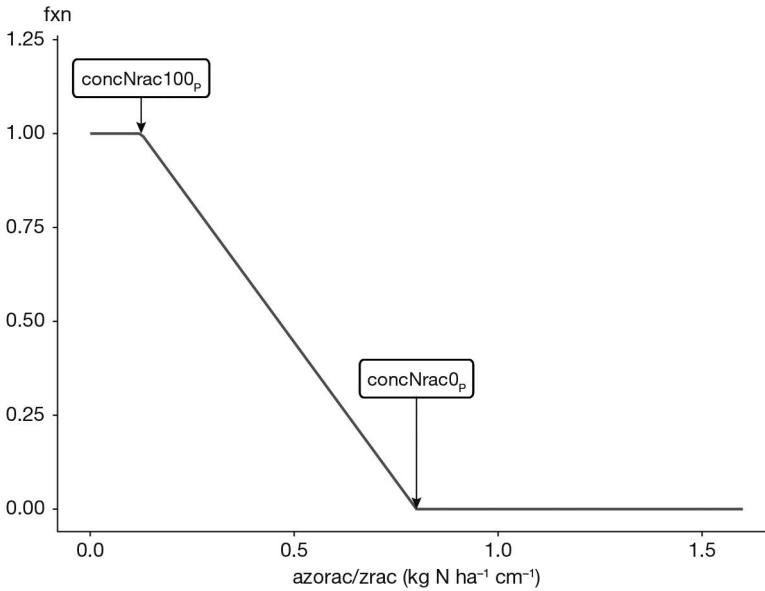


Figure 6.6. Effect of soil mineral N content on N_2 fixation ($\mathbf{codefxn}_p = 2$). Parameter values are $\mathbf{concNrac0}_p = 0.80$ and $\mathbf{concNrac100}_p = 0.125$.

Chapter 7

Biomass and nitrogen partitioning

*LOÏC STRULLU, JEAN-LOUIS DURAND, BRUNO MARY,
NICOLAS BEAUDOIN AND NADINE BRISSON*

►► 7.1 Introduction

Allocation of assimilates is critical to the operation of some models (such as SUCROS, described by Van Ittersum *et al.*, 2003). The STICS module for allocation of assimilates between organs was added at a late stage, mainly to help dimension the N and C reserve pools. For annual plants with determinate growth, the partitioning calculations allow users to dimension envelopes of harvested organs which may play a trophic role and ensure information input for the senescence module. For perennial plants or those with indeterminate growth, these calculations allow users to dimension a reserve compartment. We will refer to this concept as “cumulative partitioning” (**code_acti_reserve_p** = 2). It is suitable for annual simulations but not for long-term simulations of perennial plants. With the increasing interest among researchers in studying perennial crops as a means for biofuels production, C and N sequestration in soils or the effects of climate change on cropping systems, cumulative partitioning has shown its limits. These limits are due to:

1. The lack of location of reserve compartments in the plant and the absence of parallelism between biomass and nitrogen pools simulated by the model. This means the model cannot accurately simulate biomass or nitrogen dynamics in perennial or non-perennial organs.
2. The model’s incapacity to simulate biomass and nitrogen remobilisation from non-perennial to perennial organs, and thus to simulate long-term perennial crops functioning.
3. The absence of simulation of C and N fluxes from the plant to the soil due to perennial organ or root death leading to bias in long-term simulations of cropping systems with perennial crops.

We substantially modified the module for allocation of C and N assimilates in the plant to be able to simulate cropping systems with perennial crops over the long term (Strullu *et al.*, 2020, 2014; Strullu *et al.*, 2015). We will refer to this concept as “daily partitioning” (**code_acti_reserve_p** = 1) and will describe it in further detail in this chapter. The current STICS model includes both the cumulative and daily partitioning concepts because all crops have not yet been parameterised for the new daily partitioning concept.

►► 7.2 Identified organs and compartments

7.2.1 Cumulative partitioning

With this option (**code_acti_reserve_p** = 2), the reasons for identifying an organ or a compartment (Table 7.1) are to determine its internal trophic role within the plant or its external role in the carbon or nitrogen balance of the system (such as falling leaves and root recycling). The reserve compartment is not located in a specific organ: it represents a certain amount of carbon and nitrogen available for plant growth.

Table 7.1. Various organs identified in STICS for cumulative biomass partitioning.

		leaves	Green leaves	mafeuilverte
Un-harvested biomass	masecveg	mafeuil	Yellow leaves remaining attached to the plant	mafeuiljaune
			Structural part of stems	matigestruc
			Reserve as non-localised compartment	restemp
Yellow leaves falling to the soil	mafeuiltombe			
Harvested organs		Envelops		maenfruit
Roots	msrac	Fruits		mafruit

7.2.2 Daily partitioning

Currently, these new formalisms can only be applied to perennial crops. With this option (**code_acti_reserve_p** = 1), nitrogen partitioning mirrors biomass partitioning (Figures 7.1 and 7.2 adapted from Strullu *et al.*, 2020). Perennial organs (maperenne, QNperenne) are now distinguished from non-perennial organs (masecnp, QNplantenp). This allows the model to better describe and consider reserves dynamics within the crops. The fluxes between these compartments are due biomass remobilisation (no biomass is directly allocated to perennial organs) or nitrogen remobilisation and absorption for nitrogen. The biomass of non-perennial organs masecnp is divided into four compartments during the vegetative growth phase: the structural part of stems (matigestruc), the structural part of green leaves (mafeuilverte), the structural part of yellow leaves (mafeuiljaune) and the temporary reserves (restemp) contained in the stems and green leaves. The nitrogen content of non perennial organs (QNplantenp) is divided into three compartments during the vegetative growth phase: the structural part of stems (QNTige), the structural part of leaves (green or yellow leaves still on the crop) (QNfeuil), and the temporary reserves (QNrestemp) contained mainly in green leaves (RuBisCo).

The biomass of perennial organs maperenne is divided into two compartments: the structural part of perennial organs (resperennestruc) and the perennial reserves (resperenne). The nitrogen content of perennial organs QNperenne is divided into two compartments: the structural part of perennial organs (QNresperennestruc) and the perennial reserves (QNresperenne).

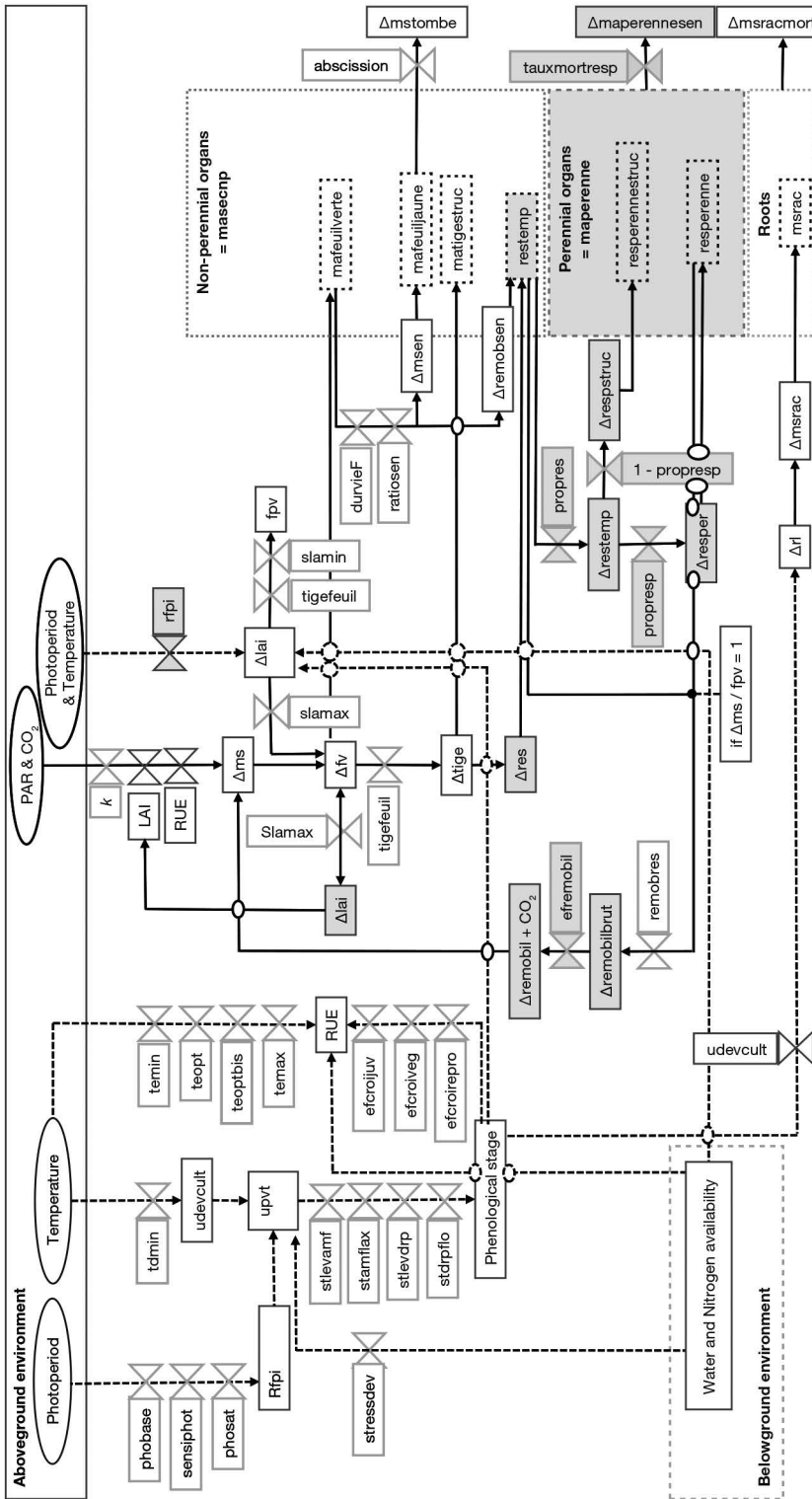


Figure 7.1a. Schematic representation of biomass partitioning. Black squares correspond to rate variables; black ovals correspond to input variables; grey squares correspond to parameters; dashed black squares correspond to cumulative variables. Grey shaded areas represent new fluxes and pools simulated by the model. Solid arrows indicate flows of energy or biomass and dashed arrows indicate relationship between components (adapted from Strullu *et al.*, 2020).

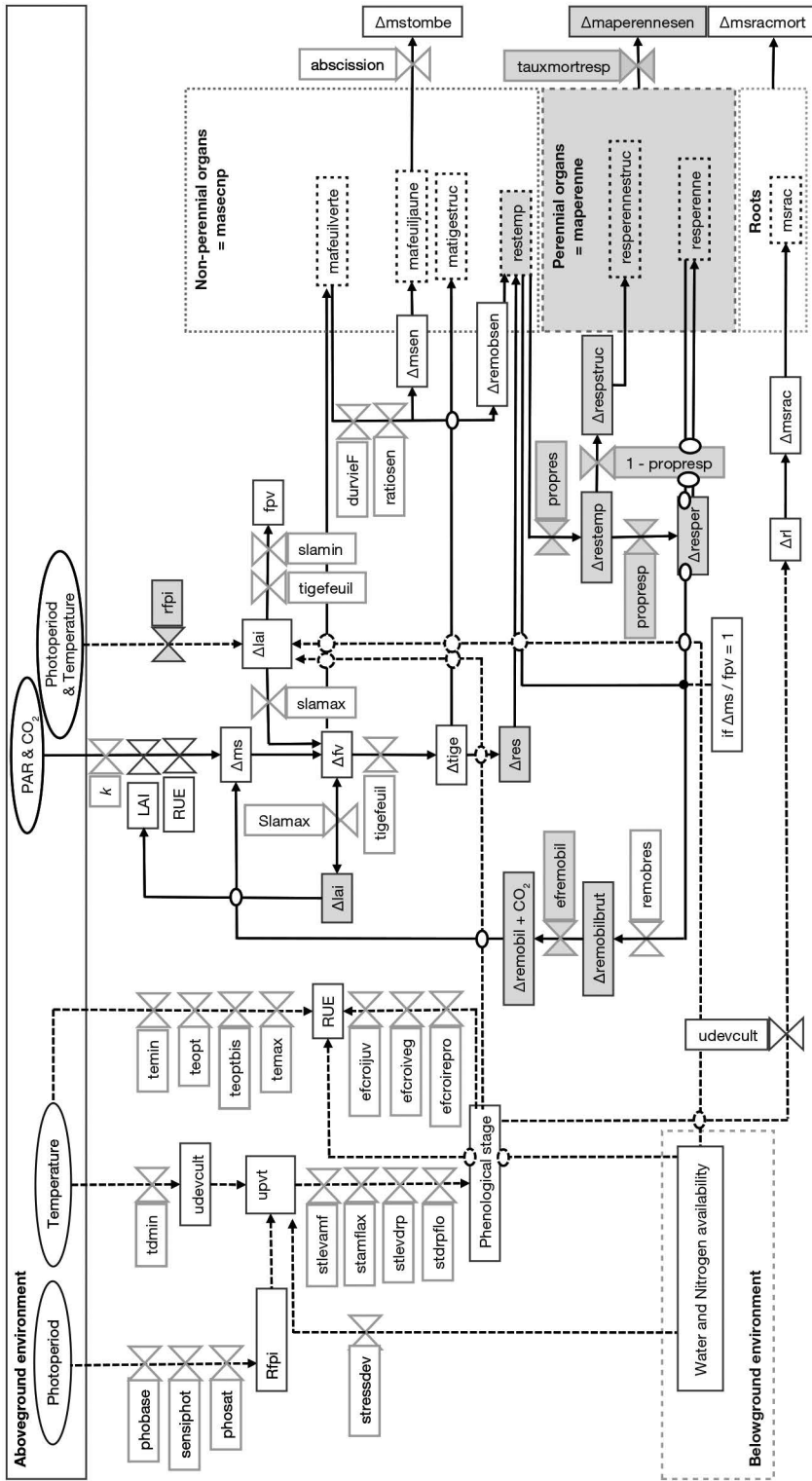


Figure 7.1b. Schematic representation of nitrogen partitioning. Black squares correspond to rate variables; black ovals correspond to input variables; grey squares correspond to parameters; dashed black squares correspond to cumulative variables. Grey shaded areas represent new fluxes and pools simulated by the model. Solid arrows indicate flows of energy or biomass and dashed arrows indicate relationship between components (adapted from Strullu *et al.*, 2020).

►► 7.3 Vegetative organs

7.3.1 Cumulative partitioning

7.3.1.1 Biomass

7.3.1.1.1 Stem and leaves

The biomass of green leaves is calculated without accounting for potential reserves that may be stored in the leaves and later remobilised. Instead, these are accounted for in the restemp non-located reserve pool. The mafeuilverte variable is deducted from the lai, based on the maximum specific leaf area parameter **slamax_p** (Eq. (7.1)). We assume that the difference between the actual sla and **slamax_p** corresponds to remobilised leaf carbon.

$$mafeuilverte(t) = \frac{lai(t)}{\mathbf{slamax}_p} \cdot 100 \quad (7.1)$$

The biomass of yellow leaves mafeuiljaune is calculated in the senescence module. The proportion of leaves in the senescent biomass on a given day (dltamsen) is determined using the pfeuilverte ratio (proportion of green leaves in the non-senescent biomass) on the day of production of this senescent biomass (Eq. (7.2)).

$$mafeuiljaune(t) = \sum_{ilev}^t dltamsen(t) \quad (7.2)$$

Some of these yellow leaves may fall to the ground depending on the **abscission_p** parameter (between 0 and 1). The daily falling quantity dltamstombe is recycled in the carbon and nitrogen balance; its cumulative value is mafeuiltombe (Eq. (7.3)).

$$dltamstombe(t) = \mathbf{abscission}_p \cdot dltamsen(t)$$

$$mafeuiltombe(t) = \sum_{i=ilev}^t dltamstombe(t) \quad (7.3)$$

The structural component of stems, matigestruc variable, is calculated as a constant proportion (**tigfeuille_p**) of the total mass of foliage (Eq. (7.4)).

$$matigestruc(t) = \mathbf{tigfeuille}_p \cdot (mafeuilverte(t) + mafeuiljaune(t)) \quad (7.4)$$

The non-structural component, if significant, can be included in the reserve compartment (e.g. for cereals) or in the harvested part (sugar cane). For monocotyledonous plants, the stem is secondary and the matigestruc variable is only incremented from the time when accumulated biomass allows it. It is thus assumed that the first organs to emerge are the leaves. For dicotyledonous plants, it is assumed that the **tigfeuille_p** proportionality is always respected. Consequently, if the accumulated biomass and the foliage biomass (calculated from the leaf area index and sla) are incompatible with this proportionality, then the sla (or leaf area index if the sla arises from fixed limits) is recalculated. The matigestruc variable cannot decrease, except in the case of cutting fodder crops.

7.3.1.1.2 Reserves

Reserves (restemp) are calculated as the difference between the total biomass and the accumulated biomass of leaves, stems and harvested organs (Eq. (7.5)).

$$\begin{aligned} restemp(t) = & masec(t) - mafeuil(t) - matigestruc(t) \\ & - maenfruit(t) - mafruit(t) \quad (7.5) \end{aligned}$$

For perennial plants, at the beginning of the cropping season, the reserves (carbon) can be initialised at a non-zero value ($restemp_0$), to represent the role played by reserves at growth resumption. The reserve pool is not located in the crop and the variable *restemp* represents the non-structural biomass that can be mobilised. The use of reserves applies to perennial or indeterminate plants. For determinate annuals, the use of reserves for grain filling is not simulated as such, but taken into account overall when calculating the *ircarb* variable (index of progressive harvest). The harvested organs (grains, fruits or tuber) are the only ones characterised in terms of number and biomass (see § 8).

Yet it is assumed that a limit exists regarding the reserve compartment size, which is called $resplmax_p$. If this limit is reached, a “sink / source” effect is simulated (Eq. (7.6)).

$$if \left(restemp(t) > 10 \cdot resplmax_p \cdot densite(t) \right) \quad dltams(t) = 0 \quad (7.6)$$

The results of the above calculations are illustrated in the case of wheat and grapevine in Figure (7.2):

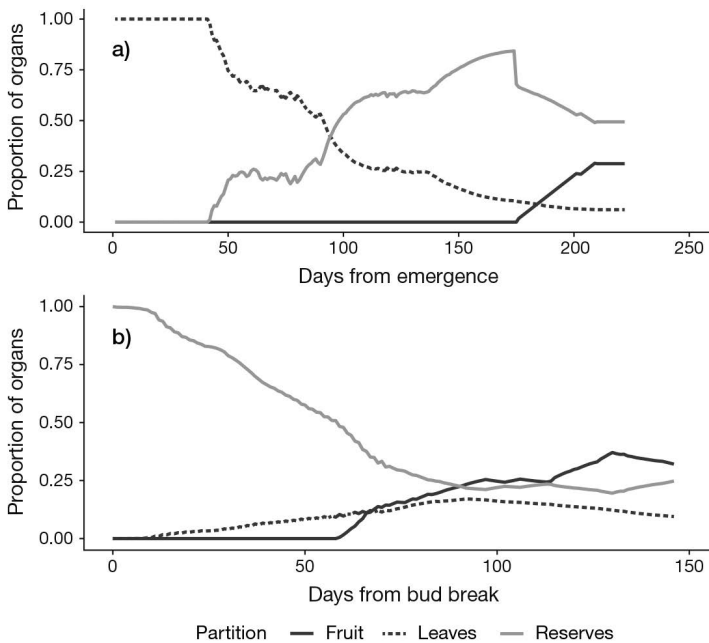


Figure 7.2. Proportion of the shoot biomass allocated to leaves, fruits or grains and to the virtual component of reserves for two different crops: a) wheat, b) grapevine.

7.3.1.2 Nitrogen

Nitrogen uptake and accumulation in the plant is a function of daily nitrogen uptake and nitrogen fixation by the crop (see § 6). Nitrogen is not found in one specific location

in the plant and can be defined as reserves or structural nitrogen. The only organs for which nitrogen partitioning is simulated are harvested organs (grains, fruits, tuber). For perennial plants, at the beginning of the cropping season, the N reserves can be initialised at a non-zero value ($\mathbf{QNplante0}_i$).

7.3.2 Daily partitioning

7.3.2.1 Non perennial organs

7.3.2.1.1 Biomass

When crop growth starts, the aerial biomass is initialised from an initial leaf area index, \mathbf{inilai}_p :

$$\begin{aligned} lai(t) &= \mathbf{inilai}_p \\ mafeuilverte(t) &= \frac{lai(t)}{\mathbf{slamax}_p} \cdot 100 \\ matigestruc(t) &= \mathbf{tigefeuille}_p \cdot mafeuilverte(t) \\ masecnp(t) &= mafeuilverte(t) + matigestruc(t) \quad (7.7) \end{aligned}$$

The daily biomass available for plant growth (\mathbf{dltams} and the remobilised biomass $\mathbf{dltaremobil} + \mathbf{remobilj}$) is shared between the different organs following the principles of i) priority of biomass allocation between the different organs, and ii) confrontation between supply and demand. It is important to note here that potential leaf and stem growth can be decrease due to a negative effect of the photoperiod on cell elongation and division (Eq. (7.8)). For this example, we used the reduction factor photoperiod index (\mathbf{rfpi}) calculated for crop development (see § 3). The negative effect of the photoperiod on potential leaf area index growth occurred when the photoperiod decreases. If the photoperiod is lower than the base photoperiod of the crop ($\mathbf{phobase}_p$), then growth of stems and leaves is null ($\mathbf{rfpi} = 0$).

$$\begin{aligned} & \text{if } (\mathbf{phoi}(t) < \mathbf{phoi}(t-1)) \\ & \mathbf{deltai}(t) = \mathbf{deltai}(t) \cdot \mathbf{rfpi} \\ & \mathbf{ratioTF} = \mathbf{tigefeuille}_p \\ & \text{if } (\mathbf{phoi}(t) < \mathbf{phobase}_p) \\ & \mathbf{rfpi} = 0 \\ & \mathbf{deltai}(t) = \mathbf{deltai}(t) \cdot \mathbf{rfpi} \\ & \mathbf{ratioTF} = \mathbf{tigefeuille}_p \cdot \mathbf{rfpi} \quad (7.8) \end{aligned}$$

We put forward the hypothesis that biomass is first used where it is produced and so the priority for biomass allocation is given to the structural part of green leaves (\mathbf{dltafv}). If the daily biomass production (\mathbf{dltams}) is insufficient to support the potential growth of $\mathbf{lai}(t)$, then the latter is limited (Eq. (7.9)) to respect the maximum specific leaf area (\mathbf{slamax}_p) of the green leaves.

$$\begin{aligned}
 dltafv(t) &= \frac{\text{delta}(t)}{\text{slamax}_p} \cdot 100 \\
 \text{if } (dltafv(t) > dltams(t)) \quad dltafv(t) &= dltams(t) \\
 \text{if } \left(\frac{\text{delta}(t)}{dltafv(t)} \cdot 100 > \text{slamax}_p \right) \quad \text{delta}(t) &= \text{slamax}_p \cdot \frac{dltafv(t)}{100} \\
 mafeuilverte(t) &= mafeuilverte(t-1) + dltafv(t) \\
 mafeuil(t) &= mafeuilverte(t) + mafeuiljaune(t) \quad (7.9)
 \end{aligned}$$

If there is still biomass available after leaf growth, then the growth of the structural part of stem (dltat) is calculated (Eq. (7.10)).

$$\begin{aligned}
 \text{if } (dltafv(t) < dltams(t)) \\
 dltat(t) &= \max(\text{ratioTF} \cdot (mafeuil(t) - mafeuil(t-1)), 0) \\
 \text{if } (dltat(t) > (dltams(t) - dltafv(t))) \\
 dltat(t) &= dltams(t) - dltafv(t) \\
 matigestruc(t) &= matigestruc(t-1) + dltat(t) \quad (7.10)
 \end{aligned}$$

Finally, after calculating the biomass actually allocated to the structural parts of the green leaves (dltafv) and stems (dltat), the biomass surplus is allocated to temporary reserves (dltares) (Eq. (7.11)).

$$\begin{aligned}
 dltares(t) &= dltams(t) - dltafv(t) - dltat(t) \\
 restemp(t) &= restemp(t-1) + dltares(t) \quad (7.11)
 \end{aligned}$$

During leaf senescence (Eq. (7.12)), some of the biomass can be remobilised (dltaremobsen) to feed the plant's temporary reserves pool (restemp).

$$\begin{aligned}
 dltaremobsen(t) &= \sum_{t_0}^t (dltams(t) \cdot (1 - \text{ratiosen}_p) \cdot pfeuilverte(t)) \\
 restemp(t) &= restemp(t-1) + dltaremobsen(t) \quad (7.12)
 \end{aligned}$$

Temporary reserves are limited and are accumulated during a growing cycle in living non-perennial vegetative organs, although they are not precisely partitioned between stems and leaves (Eq. (7.13)). The plant can remobilise these reserves (§ 7.4).

$$\begin{aligned}
 masecveg(t) &= masecnp(t) - magrain(t-1) \\
 restempmax(t) &= \text{propres}_p \cdot \frac{mafeuilverte(t)}{mafeuil(t)} \cdot masecveg(t) \quad (7.13)
 \end{aligned}$$

Figure 7.3 shows an example of biomass partitioning in non-perennial organs (stems and leaves) for *Medicago sativa* L.

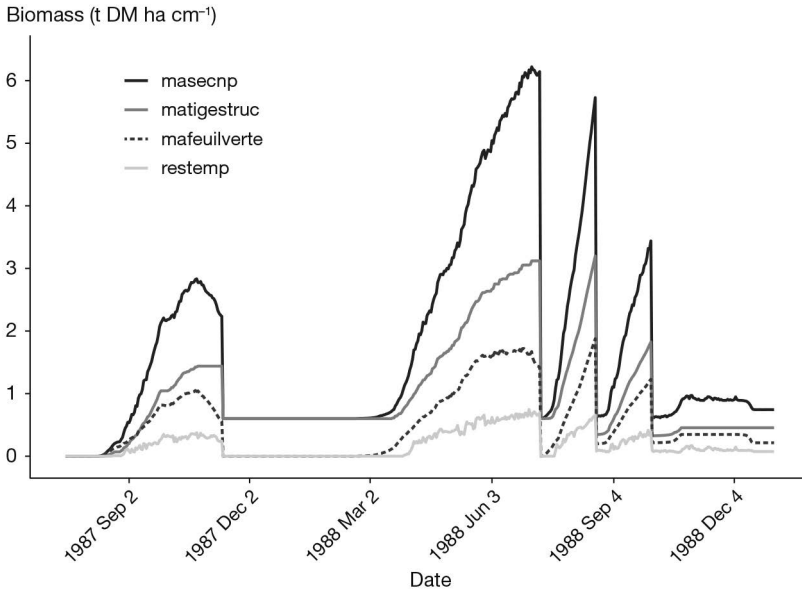


Figure 7.3. Simulation of biomass partitioning in non-perennial organs of *Medicago sativa* L.

7.3.2.1.2 Nitrogen

Nitrogen is allocated to the aerial non-perennial organs (*absoaer*) as a function of their nitrogen demand (see § 6), once the nitrogen demand of perennial organs (see § 7.3.2.2.2) and roots (see § 7.6.2) is met (Eq. (7.14)).

$$\begin{aligned}
 & \text{if } (absotot(t) - absoper(t) - absorac(t)) > 0 \\
 & \quad absoaer(t) = demande(t) \\
 & \text{if } (absoaer(t) > (absotot(t) - absoper(t) - absorac(t))) \\
 & \quad absoaer(t) = absotot(t) - absoper(t) - absorac(t) \quad (7.14)
 \end{aligned}$$

Prioritising nitrogen allocation between organs allows users to simulate the effect of root and perennial organs growth on nitrogen availability for the growth of aerial non-perennial organs. N is allocated to roots and non-perennial organs first, because N demand of perennial organs is nil at the beginning of a growing cycle (Figure 7.4).

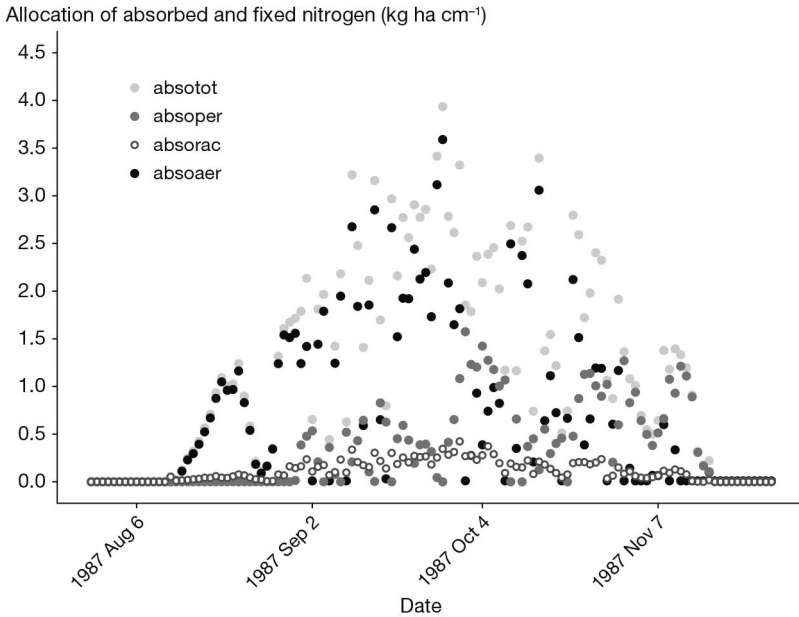


Figure 7.4. Simulation of nitrogen allocation in non-perennial organs, perennial organs and roots of *Medicago sativa* L. with the STICS model v10.

Nitrogen allocated to aerial non-perennial organs is shared among green leaves ($d\lambda_{QN\text{feuille}}$), stems ($d\lambda_{QN\text{tige}}$) and temporary reserves ($d\lambda_{QN\text{restemp}}$) following the same allocation priorities as biomass as a function of their nitrogen demand (see § 6) (Eq. (7.15)).

$$\begin{aligned}
 & \text{if } (demand_{fv}(t)) < (demand_{struc}(t)) \\
 & \quad d\lambda_{QN\text{feuille}}(t) = demand_{fv}(t) \\
 & \quad d\lambda_{QN\text{tige}}(t) = demand_{struc}(t) - demand_{fv}(t) \\
 & \quad d\lambda_{QN\text{restemp}}(t) = demand_{struc}(t) - (d\lambda_{QN\text{feuille}}(t) + d\lambda_{QN\text{tige}}(t)) \\
 & \text{if } (demand_{fv}(t)) > (demand_{struc}(t)) \\
 & \quad d\lambda_{QN\text{feuille}}(t) = demand_{struc}(t) \\
 & \quad d\lambda_{QN\text{tige}}(t) = 0 \\
 & \quad d\lambda_{QN\text{restemp}}(t) = 0 \quad (7.15)
 \end{aligned}$$

The Figure 7.5 shows an example of N partitioning in non-perennial organs (stems and leaves) for *Medicago sativa* L.

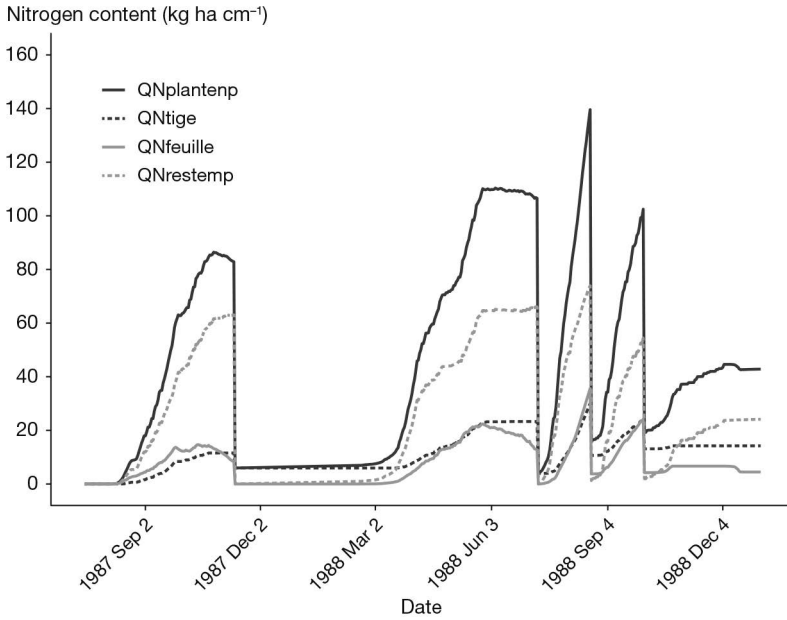


Figure 7.5. Simulation of nitrogen partitioning in non-perennial organs of *Medicago sativa* L. with the STICS model v10.

7.3.2.2 Perennial organs

7.3.2.2.1 Biomass

Biomass is allocated between reserves (*resperenne*) or structural parts of the perennial organs using an allocation coefficient (*alloresp*) (Eq. (7.16)). The underlying assumption is that the reserves are first stored in the pre-existing organs and then, when the perennial organs reach their reserve storage limit, the structural part of the perennial organs increases and receives new reserves. When developing the model, we considered that the perennial organs do not operate as sink organs for the biomass produced (unlike vegetative aerial organs or reproductive organs), but only as passive receptacles for the biomass surplus produced by the plant.

$$resperennemax(t) = \mathbf{propresp}_p \cdot maperenne(t)$$

$$resperenne(t) = resperenne(t) + dltarestemp$$

$$if (resperenne(t) > resperennemax(t))$$

$$alloresp = \mathbf{propresp}_p$$

$$dltaresper = alloresp \cdot dltarestemp$$

$$resperenne(t) = resperenne(t) - dltarestemp + dltaresper \quad (7.16)$$

7.3.2.2 Nitrogen

Nitrogen absorbed or fixed by the plant ($absotot$) is allocated first to the perennial organs ($absoper$; Eq. (7.17)) as a function of their nitrogen demand (see § 6).

$$\begin{aligned} absoper(t) &= demand_p(t) \\ \text{if } (absoper(t) > absotot(t)) \\ absoper(t) &= absotot(t) \\ absotot(t) &= absotot(t) - absoper(t) \quad (7.17) \end{aligned}$$

The nitrogen allocated to the perennial organs is shared between the structure and reserves ($dltaresperN$) according to the carbohydrate allocation and the parameter **proprespn_p** (Eq. (7.18)).

$$\begin{aligned} \text{if } (dltarespstruc(t) > 0) \quad dltaresperN(t) &= absoper(t) \cdot \mathbf{proprespn}_p \\ \text{if } (dltarespstruc(t) = 0) \quad dltaresperN(t) &= absoper(t) \quad (7.18) \end{aligned}$$

► 7.4 Remobilisation of reserves

7.4.1 Source/sink ratio

The source/sink ratio corresponds to a comparison between the daily biomass produced by the crop $dltams$ and the biomass demand by the vegetative or reproductive organs (Eq. (7.19)). Biomass remobilisation occurs if the source/sink ratio is lower than 1.

$$sourcepuits_1(t) = \frac{dltams(t)}{fpv(t) + fpft(t)} \quad (7.19)$$

The sink strength of vegetative organs fpv is a function of the daily real leaf area index growth rate $deltai$ and the potential growth rate of vegetative organs depending on the minimal specific leaf area parameter (**slamin_p**) and the ratio between stems and leaves (**ratioTF**) (Eq. (7.20)).

$$fpv(t) = \frac{deltai(t) \cdot 10^4}{\frac{slamin_p}{1+ratioTF}} \quad (7.20)$$

The sink strength of reproductive organs $fpft$ is calculated only for indeterminate crops and is described in § 8. It is important to note here that $fpft$ and fpv are not exactly the same: $fpft$ refers to potential growth while fpv corresponds to real growth. By design, this difference puts a priority on fruits and can generate a day-to-day instability of the variable $sourcepuits$ by the feedback of $sourcepuits$ on fpv via the stress index $splai$ (see § 4). A second source/sink ratio value ($sourcepuits$) is calculated to account for possible reserve remobilisation (Eq. (7.21)). This variable drives trophic stresses, useful for simulating indeterminate crop competition between vegetative and reproductive sinks.

$$sourcepuits(t) = \frac{dltams(t) + dltaremobil(t) + remobilj(t)}{f_{pv}(t) + f_{pf}(t)} \quad (7.21)$$

7.4.2 Calculation of reserves remobilisation for cumulative biomass partitioning

7.4.2.1 Biomass

The daily flux of remobilised biomass $dltaremobil$ is obtained by the remobilisation of reserves in perennial plants. Each day the maximal proportion of the reserves that can be remobilised is $remob$, until perennial stocks are exhausted (Eq. (7.22)). $restemp_{0_i}$ only represents carbon reserves, and nitrogen reserves can only be added through initiation of the $QNplante_{0_i}$ parameter. These remobilisations contribute to increasing the source/sink ratio the following day because they are counted in the variable $dltams$.

$$if (sourcepuits(t) < 1) \text{ and } (cumdltaremobil(t) \leq restemp_{0_i})$$

$$remob(t) = \frac{(f_{pv} + f_{pf}t)}{100} - dltams$$

$$if (remob(t) \leq \mathbf{remobres}_p \cdot restemp(t))$$

$$dltaremobil(t) = remob(t)$$

$$if (remob(t) > \mathbf{remobres}_p \cdot restemp(t))$$

$$dltaremobil(t) = \mathbf{remobres}_p \cdot restemp(t)$$

$$cumdltaremobil(t) = cumdltaremobil(t-1) + dltaremobil(t) \quad (7.22)$$

Reserves built up during the vegetative cycle ($restemp$) and reused later contribute to the the source/sink ratio estimation for indeterminate crops. The maximum quantity which can be remobilised per day ($remobilj$) is calculated similarly to $dltaremobil$ (Eq. (7.22)). If the plant is both perennial and indeterminate, the reserves originating from the previous cycle are first used ($dltaremobil$), and when they are exhausted, the current cycle's reserves ($remobilj$) can be used.

7.4.2.2 Nitrogen

The remobilisation rate of initial nitrogen perennial reserves $QNplante_{0_i}$ is assumed to be equal to the crop nitrogen demand, see § 6. The remobilisation stops when initial reserves are exhausted.

7.4.3 Calculation of reserves remobilisation for daily biomass partitioning

7.4.3.1 Biomass

Each day, the flux of remobilised raw carbohydrates ($dltaremobilbrut$) is obtained by remobilising perennial reserves (Eq. (7.23)), with temporary reserves given priority for remobilisation.

$$\begin{aligned}
 & \text{if } (\text{sourcepuits}_1(t) < 1) \text{ and } (\text{resperenne}(t) > 0) \\
 & \text{remob}(t) = \frac{(f_{pv} + f_{pf}t)}{100} - \text{dltams} \\
 & \text{if } (\text{remob}(t) \leq \mathbf{remobres}_p \cdot \text{resperenne}(t)) \text{ dltaremobilbrut}(t) = \text{remob}(t) \\
 & \text{if } (\text{remob}(t) > \mathbf{remobres}_p \cdot \text{resperenne}(t)) \\
 & \text{dltaremobilbrut}(t) = \mathbf{remobres}_p \cdot \text{resperenne}(t) \\
 & \text{if } (\text{dltaremobilbrut}(t) > \text{resperenne}(t)) \text{ dltaremobilbrut}(t) = \text{resperenne}(t) \\
 & \text{resperenne}(t) = \text{resperenne}(t) - \text{dltaremobilbrut}(t) \quad (7.23)
 \end{aligned}$$

Some of the carbohydrate reserves are burned through respiration of the perennial organs during the remobilisation phase ($\text{dltCO}_2\text{resperenne}$) (Avice *et al.*, 1996). Although respiration is taken into account in the model for the production of newly synthesised biomass via the radiation use efficiency (RUE), the respiration associated with the remobilisation of C and N reserves stored in perennial organs is not. This prevents an asymmetry when considering of respiration between the remobilisation of carbohydrate reserves in spring (for which respiration needs to be modelled) and carbohydrate storage (for which respiration is integrated into the RUE). The parameter $\mathbf{efremobil}_p$ corresponds to the remobilisation efficiency of carbohydrate reserves and is used to calculate the net flow of remobilised carbohydrate reserves as well as carbon losses in the form of CO_2 (Eq. (7.24)).

$$\begin{aligned}
 \text{dltaremobil}(t) &= \mathbf{efremobil}_p \cdot \text{dltaremobilbrut}(t) \\
 \text{dltCO}_2\text{resperenne} &= 0.40(1 - \mathbf{efremobil}_p) \cdot \text{dltaremobilbrut}(t) \quad (7.24)
 \end{aligned}$$

If the remobilisation of the perennial reserves is not sufficient to meet the demand of the growing vegetative or reproductive organs, the temporary reserves built up during the vegetative cycle (restemp) can in turn be remobilised (remobilj) (Eq. (7.25)).

$$\begin{aligned}
 \text{sourcepuits}_2(t) &= \frac{(\text{dltams}(t) + \text{dltaremobil}(t)) \cdot 100}{f_{pv}(t) + f_{pf}t} \\
 & \text{if } (\text{sourcepuits}_2(t) < 1) \text{ and } (\text{restemp}(t) > 0) \\
 & \text{remob}(t) = \frac{(f_{pv} + f_{pf}t)}{100} - \text{dltams}(t) + \text{dltaremobil}(t) \\
 & \text{if } (\text{remob}(t) \leq \mathbf{remobres}_p \cdot \text{restemp}(t)) \text{ remobilj}(t) = \text{remob}(t) \\
 & \text{if } (\text{remob}(t) > \mathbf{remobres}_p \cdot \text{restemp}(t)) \\
 & \text{remobilj}(t) = \mathbf{remobres}_p \cdot \text{restemp}(t) \\
 & \text{if } (\text{remobilj}(t) > \text{restemp}(t)) \text{ remobilj}(t) = \text{restemp}(t) \\
 & \text{restemp}(t) = \text{restemp}(t) - \text{remobilj}(t) \quad (7.25)
 \end{aligned}$$

In perennial plants, the storage of biomass in perennial organs ($dltarestemp$) (Eq. (7.26)) is calculated if:

1. The limit for storage of temporary reserves in aerial organs is reached: the biomass surplus is then allocated to perennial organs;
2. There is senescence of the aerial non-perennial organs: temporary reserves are allocated to perennial organs.

$$\begin{aligned} & \text{if } (restemp(t) > restempmax(t)) \\ & dltarestemp = restemp(t) - restempmax(t) \\ & restemp(t) = restempmax(t) \end{aligned} \quad (7.26)$$

7.4.3.2 Nitrogen

The amount of remobilised N ($dltaremobilN$) is a function of the amount of remobilised carbohydrates ($dltaremobilbrut$) and the N concentration of source organs ($CNresperenne$) (Eq. (7.27)). Nitrogen remobilisation cannot exceed the nitrogen demand of non perennial organs (see § 6).

$$CNresperenne(t) = \frac{QNresperenne(t)}{resperenne(t)}$$

$$dltaremobilN(t) = dltaremobilbrut(t) \cdot CNresperenne(t)$$

$$\text{if } (dltaremobilN(t) > demandeae(t)) \quad dltaremobilN(t) = demandeae(t) \quad (7.27)$$

During senescence of vegetative organs and when the emission of new leaves is nil ($ilax_T$ stage reached), temporary N reserves in the non-perennial organs are remobilised ($dltarestempN$) to the perennial organs. The $ilax_T$ stage can be reached for two reasons:

- The degree days required to reach the stage have been accumulated;
- The photoperiod is shorter than the photoperiod triggering senescence and the photoperiod is decreasing (when the option ‘effect of photoperiod on senescence’ is activated).

The amount of remobilised N is a function of the amount of remobilised carbohydrates ($dltarestemp$) and N concentration in temporary reserves ($CNrestemp$) (Eq. (7.28)).

$$\text{if } (nIax > 0 \text{ and } restemp(t) > 0) \quad CNrestemp(t) = \frac{QNrestemp(t)}{restemp(t)}$$

$$dltarestempN(t) = dltarestemp(t) \cdot CNrestemp(t)$$

$$\text{if } (dltarestempN(t) > QNrestemp(t)) \quad dltarestempN(t) = QNrestemp(t) \quad (7.28)$$

The partition of the N allocated to the perennial organs between reserves and structure is a function of remobilised carbohydrate allocation (Eq. (7.29)).

$$\begin{aligned}
 & \text{if } (dltarespstruc(t) > 0) \\
 & \quad dltaresperN(t) = dltarestempN(t) \cdot \mathbf{proprespn}_p \\
 & \text{if } (dltarespstruc(t) = 0) \\
 & \quad dltaresperN(t) = dltarestempN(t) \quad (7.29)
 \end{aligned}$$

►► 7.5 Harvested organs

7.5.1 Biomass

The calculation of the number and mass of fruits (indeterminate plants) or grains (determinate plants) is described in the § 8. The mass corresponding to the envelope is assumed to depend solely upon the number of organs. Regardless, it cannot exceed the residual biomass (masecveg-mafeuilverte-mafeuiljaune-matigestruc). The **envfruit**_p parameter corresponds to the proportion of pericarp related to the maximum weight of the fruit (Eq. (7.30)).

$$maenfruit(t) = nbfruit(t) \cdot \mathbf{envfruit}_p \cdot \mathbf{pgrainmaxi}_p \cdot 10^{-2} \quad (7.30)$$

If the **sea**_p parameter is not zero, then this biomass is transformed into an equivalent leaf surface area, photosynthetically active from the idrp stage to the idebdes stage.

7.5.2 Nitrogen

The amount of nitrogen in harvested organs QNgrain, is an increasing proportion of the amount of nitrogen in the biomass (see § 8).

►► 7.6 Roots

7.6.1 Biomass

The model features two methods of root biomass calculation, depending on the chosen simulation options. If the user choose the profile type option, the root biomass is calculated at harvest. It is a proportion (**proprac**_p) of the above ground biomass produced by the crop (masecnp). The parameter **y0msrac**_p corresponds to the minimal amount of root biomass which returns to the soil if above ground biomass is nil (Eq. (7.31)).

$$msrac(t) = masecnp(t) \cdot \mathbf{proprac}_p + \mathbf{y0msrac}_p \quad (7.31)$$

If the user chooses the true density option, the root biomass is calculated daily as a function of total length of fine and coarse roots (rltotf and rltotg respectively) and their specific root length (longsperacf and longsperacg respectively) (see § 5 for more detail concerning root system simulation) (Eq. (7.32)).

$$\begin{aligned}
 msracf(t) &= \frac{rltotf(t)}{longsperacf} \cdot 100 \\
 msracg(t) &= \frac{rltotg(t)}{longsperacg} \cdot 100 \\
 msrac(t) &= msracf(t) + msracg(t) \quad (7.32)
 \end{aligned}$$

7.6.2 Nitrogen

Consequently, the model has two methods to calculate root nitrogen content, depending on the chosen simulation options. If the user chooses the profile type or true density option, the root nitrogen content is calculated at harvest in function of root biomass and nitrogen concentration in the vegetative organs (Eq. (7.33)).

$$QNrac(t) = msrac(t) \cdot CNveget(t) \quad (7.33)$$

Daily nitrogen allocation to roots is calculated by the model if and only if the true density and root deposition options are activated. In that case, if there is still nitrogen available after nitrogen allocation to perennial organs, remaining nitrogen is allocated to the roots (*absorac*) as a function of their nitrogen demand (see § 6) (Eq. (7.34)).

$$if (absotot(t) - absoper(t)) > 0 \quad absorac(t) = demanderac(t)$$

$$if (absorac(t) > (absotot(t) - absoper(t))) \\ absorac(t) = absotot(t) - absoper(t) \quad (7.34)$$

►► 7.7 Biomass and nitrogen partitioning after cut of forages

7.7.1 A priori calculation or parameterisation of residual biomass, nitrogen content and LAI after cutting as a function of cutting height

If the option for the dynamic calculation of residual biomass and leaf area index is not activated, the model can either calculate both these variables from cutting height or read them in the technical file. Calculation of the residual biomass (*msres*) from cutting height (**hautcoupe_p**) is performed using the parameter **coefmshaut_p** to convert height into biomass, and the parameter **hautbase_p**, which corresponds to the basal height of the crop (Eq. (7.35)).

$$msres(t) = coefmshaut_p \cdot (\text{hautcoupe}_p - \text{hautbase}_p) \quad (7.35)$$

The residual leaf area index is calculated with the parameter **khaut_p** to convert crop height into leaf area, the previously defined parameter **hautbase_p** and the parameter **hautmax_p**, which corresponds to the maximum height of the crop (Eq. (7.36)).

$$lai(t) = \frac{-1}{\text{khaut}_p \cdot \log\left(1 - \left(\frac{\text{hautcoupe}_p - \text{hautbase}_p}{\text{hautmax}_p}\right)\right)} \quad (7.36)$$

The nitrogen content remaining in the residual biomass after harvest depends on the residual biomass and parameters of the nitrogen dilution curve (Eq. (7.37)).

$$if (msres(t) < \text{masecNmax}_p)$$

$$QNplantenp(t) = (\text{adil}_p \cdot \text{masecNmax}_p^{(-\text{bdil}_p)}) \cdot inn \cdot msres(t)$$

$$if (msres(t) \geq \text{masecNmax}_p)$$

$$QNplantenp(t) = (\text{adil}_p \cdot msres(t)^{(-\text{bdil}_p)}) \cdot inn \cdot msres(t) \quad (7.37)$$

7.7.2 A posteriori dynamic calculation of residual biomass, nitrogen content and LAI after cutting as a function of cutting height

The model dynamically simulates the biomass and the amount of nitrogen in perennial organs that will be available for regrowth. For the aerial part, the residual aerial biomass is determined from the cutting height (*hautcoupe*) (Eq. (7.35)). The model calculates the residual green leaf biomass (*mafeuilverte*) by removing the biomass of fallen leaves (*mafeuiltombefauche*), the biomass of dead leaves (*mafeuiljaune*) and the biomass remobilised during their senescence (*cumdltaremobsen*) between two cuts to the theoretical green leaf biomass remaining after harvest (Eq. (7.38)).

$$\begin{aligned} \text{mafeuilverte}(t) = & \text{msres}(t) \left(\frac{\text{mafeuilverte}(t-1)}{\text{masecnp}(t-1)} \right) \\ & - (\text{mafeuiltombefauche}(t) + \text{cumdltaremobsen}(t) + \text{mafeuiljaune}(t)) \end{aligned} \quad (7.38)$$

Finally, the residual *lai(t)* is calculated by multiplying the residual green leaf biomass by the maximum specific leaf area of leaves (**slamax_p**) (Eq. (7.39)).

$$\text{lai}(t) = \frac{\text{slamax}_p \cdot \text{mafeuilverte}(t)}{100} \quad (7.39)$$

The amount of nitrogen in the aerial part (*QNplantenp*) is determined using the amount of residual biomass after cutting (*msres*) and the N content of the plant prior to cutting (*CNplante*) (Eq. (7.40)).

$$\text{QNplantenp}(t) = \text{msres}(t) \cdot \text{CNplante}(t) \quad (7.40)$$

►► 7.8 N and C inputs to the soil from perennial crops

The turnover of storage organs (rhizomes, taproots, etc.) in perennial crops such as miscanthus, switchgrass or alfalfa leads to C and N inputs to the soil (**code_acti_reserve_p** = 1). The model assumes that these storage organs have a constant daily mortality rate (**tauxmortesp_p**), except when the plant is in its winter dormancy stage. In this case (i.e. when the leaf area index is nil), there is no more mortality of perennial organs. Decomposition of organic residues is presented in § 12.

The daily inputs of dead biomass are:

$$\text{dltamaperennesen}(t) = \text{tauxmortp} \cdot \text{maperenne}(t) \quad (7.41)$$

The cumulative C inputs related to storage organs mortality (*QCperennemort*) are calculated assuming a C content of 440 g kg⁻¹ in these organs:

$$\text{QCperennemort}(t) = 440 \cdot \sum_{nlev}^t \text{dltamaperennesen}(t) \quad (7.42)$$

The cumulative N inputs related to storage organs mortality (*QNperennemort*) are calculated using the C/N ratio of these organs (*CsurNper*):

$$\begin{aligned} \text{CsurNper}(t) &= \frac{\text{QNperenne}(t)}{\text{maperenne}(t)} \\ \text{QNperennemort}(t) &= \sum_{nlev}^t \text{dltamaperennesen}(t) \cdot \text{CsurNper}(t) \end{aligned} \quad (7.43)$$

These C and N inputs are assumed to be homogeneously distributed within the biologically active soil layer (**profhum_p**).

Chapter 8

Yield formation

*NADINE BRISSON, IÑAKI GARCÍA DE CORTÁZAR ATAURI,
FRANÇOISE RUGET AND BENJAMIN DUMONT*

REVIEWED BY: NICOLAS BEAUDOIN

Yield prediction is a goal of most crop models. Let's note that this chapter refers to the 'biological yield', as opposed to the 'farmer's yield', the latter being generally affected by losses of the combine harvester. By definition, yield is the weight and quality of the harvested organs. These organs can be reproductive organs – either grains (dehydrated) or fruits (hydrated) – or vegetative storage organs – either stems (sugarcane) or roots (tubers). Forage crops, where the total aboveground biomass (leaves, stems and sometimes grains) is harvested in its entirety, is also considered in the following sections. The determinate or indeterminate character (as defined within the STICS model¹) does not indicate the type of harvested organs. However, by convention, we will call the harvested organs of determinate species 'grains' and the harvested organs of indeterminate species 'fruit'.

Warren-Wilson (1972) suggested that the plant should be considered as a set of compartments playing the role of sources and/or sinks for assimilates. This concept can be applied to carbon, water, nitrogen or any metabolite of interest. However, hereafter we will use it only for carbon, though it is also thoroughly documented for nitrogen (Barbottin *et al.*, 2005; Jeuffroy *et al.*, 2000; Sinclair and de Wit, 1976). The source and sink compartments usually represent organs (e.g. roots, leaves, grains, etc.), which can change their function during a cycle: 'source then sink' for roots and trunks in perennial plants, or 'sink then source' for leaves. Application of this concept to crop models generates self-regulation of the system between the growth of different types of organs. It is particularly well-suited to crops with an indeterminate growth habit and to perennial crops, in which trophic competition exists between growing and storage organs (Jeuffroy and Warembourg, 1991; Munier-Jolain *et al.*, 1998). Source capacity includes both newly-formed assimilates and remobilised resources translocated from vegetative organs. Carbon sink strength, i.e. potential growth rate, is usually represented by a continuous or discrete function of the physiological age of the organ. The problems with this approach lie in determining the size of the source capacity and

1. Within STICS, 'indeterminate' denotes species for which there is significant trophic competition between vegetative organs and harvested organs.

remobilised resources, which is difficult to estimate experimentally. Furthermore, it is often necessary to introduce prioritisation between organs, thus reproducing the species strategy, and this may be speculative. One alternative is to impose a constant distribution of assimilates by phenological stage, which is frequently applied in determinate crops (Weir *et al.*, 1984). The source-sink approach is used, for example, by Ritchie and Otter (1985) or Jones *et al.* (2003).

A second alternative, proposed by Spaeth and Sinclair (1985), is to extend the notion of the final harvest index (ratio of grain biomass to total shoot biomass) to the dynamic accumulation of biomass in grains, understanding that a linear variation of the harvest index as a function of time could be assumed. This approach has the advantage of pooling the two sources of assimilates, and it is economical in terms of parameters. However, it is important to impose a threshold on this harvest index dynamic, in order to avoid simulating unrealistic remobilisation levels or exceeding the maximum filling allowed by the number of organs and the maximum weight of an organ. Apart from cereals, this approach can be used for very different species, such as pea (Lecoeur and Sinclair, 2001) or grapevine (Bindi *et al.*, 1999).

Both these approaches are implemented in the STICS model: the source/sink approach for indeterminate crops and the dynamic harvest index for determinate crops. The number of organs harvested is rarely simulated in crop models and, if so, is often calculated independently from yield simulation. In the STICS model, the number of harvested reproductive organs (grains or fruits) is explicitly calculated before the allocation of biomass to these reproductive organs and will act as a genetic limitation to yield.

►► 8.1 Quantitative yield

8.1.1 For determinate growth plants

In the case of plants with determinate growth, the hypothesis is made that the number and filling of organs for harvest do not depend on the other organs' growth requirements.

The number of grains is fixed during a phase of variable duration (**nbjgrain_p** in days), which precedes the onset of filling (**idrp_T**). This number depends on the mean growth rate of the canopy during this period (*vitmoy* in $g\ m^{-2}\ d^{-1}$), which in turns depends on dynamics specific to the particular species (Eq. (8.1)).

$$vitmoy(idrp_T) = \sum_{j=idrp_T-nbjgrain_p+1}^{idrp_T} \frac{dtams(j)}{nbjgrain_p} \quad (8.1)$$

The number of grains per m^2 (**nbgrains**) is defined at the **idrp_T** stage (Eq. (8.2)). It depends on i) the growth variable (*vitmoy* in $g\ m^{-2}$) that integrates the effect of the prevailing stresses during the period preceding the **idrp_T** stage, ii) three species-dependent parameters **cgrainv0_p** (unitless), **cgrain_p** (in $g^{-1}\ m^2$) and **nbrmin_p** (in $grains\ m^{-2}$) and iii) a genetic-dependent parameter **nbgrmax_p** (in $grains\ m^{-2}$). The last two parameters define the limits of variation of **nbgrains**.

$$\text{nbgrains}(\text{idrp}_T) = [\text{cgrainv0}_p + \text{cgrain}_p \cdot \text{vitmoy}(\text{idrp}_T)] \cdot \text{nbgrmax}_p$$

$$\begin{cases} \text{nbgrains}(\text{idrp}_T) = \text{nbgrmax}_p & \text{if } \text{nbgrains}(\text{idrp}_T) > \text{nbgrmax}_p \\ \text{nbgrains}(\text{idrp}_T) = \text{nbgrmin}_p & \text{if } \text{nbgrains}(\text{idrp}_T) < \text{nbgrmin}_p \end{cases} \quad (8.2)$$

According to Eq. (8.2), the normalised value $\frac{\text{nbgrains}}{\text{nbgrmax}_p}$ varies between $\frac{\text{nbgrmin}_p}{\text{nbgrmax}_p}$ and 1 and its variability among species expresses the sensitivity of grain onset to growth conditions (Figure 8.1).

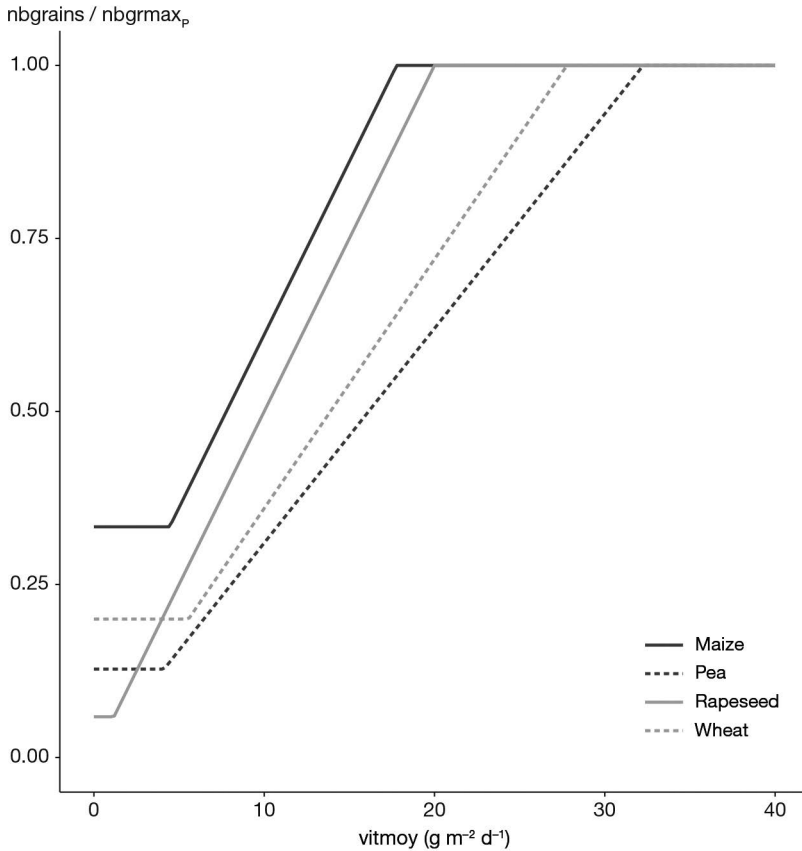


Figure 8.1. Proportion of grain number, for the maximum allowed by the variety ($\frac{\text{nbgrains}}{\text{nbgrmax}_p}$), as a function of growth during the pre-grain filling period. Examples are provided for maize (solid black line: $\text{cgrainv0}_p=0.111$, $\text{cgrain}_p=0.050$, $\text{nbgrmin}_p=1500$, $\text{nbgrmax}_p=4500$), pea (dash-dotted black line: $\text{cgrainv0}_p=0.000$, $\text{cgrain}_p=0.031$, $\text{nbgrmin}_p=447$, $\text{nbgrmax}_p=3500$), rapeseed (solid grey line: $\text{cgrainv0}_p=0.000$, $\text{cgrain}_p=0.050$, $\text{nbgrmin}_p=50000$, $\text{nbgrmax}_p=850000$) and wheat (dash-dotted grey line: $\text{cgrainv0}_p=0.000$, $\text{cgrain}_p=0.036$, $\text{nbgrmin}_p=6000$, $\text{nbgrmax}_p=30000$).

After the idrp_T stage, the grain number can be reduced in the event of frost (Eq. (8.3) and § 4.4.4) and the daily proportion of grains affected is $(1-\text{fgelflo})$, whatever their state of growth. The corresponding weight (pgraingel in $g\ m^{-2}$) is deducted from the

grain weight (Eq. (8.6)), using the elementary current grain weight (p_{grain} in g) defined in Eq. (8.7).

$$\text{for } t > \mathbf{idrp}_T \begin{cases} \mathbf{nbgraingel}(t) = \mathbf{nbgrains}(t-1) \cdot (1 - f_{gelflo}(t)) \\ \mathbf{nbgrains}(t) = \mathbf{nbgrains}(\mathbf{idrp}_T) - \sum_{j=\mathbf{idrp}_T+1}^t \mathbf{nbgraingel}(j) \end{cases}$$

$$p_{graingel}(t) = \sum_{j=\mathbf{idrp}_T+1}^t p_{grain}(j-1) \cdot \mathbf{nbgraingel}(j) \quad (8.3)$$

The quantity of dry matter accumulated in grains is calculated by applying a progressive ‘harvest index’ to the dry weight of the plant. This \mathbf{ircarb} index (defined in Eq. (8.4)) increases linearly with time ($\mathbf{vitircarb}_p$ in $g_{grain} g_{biomass}^{-1} d^{-1}$), from the \mathbf{idrp}_T day to the \mathbf{imat}_T day and the final harvest index is restricted to the \mathbf{imax}_p parameter. The dynamics of \mathbf{ircarb} for various species are depicted in Figure 8.2.

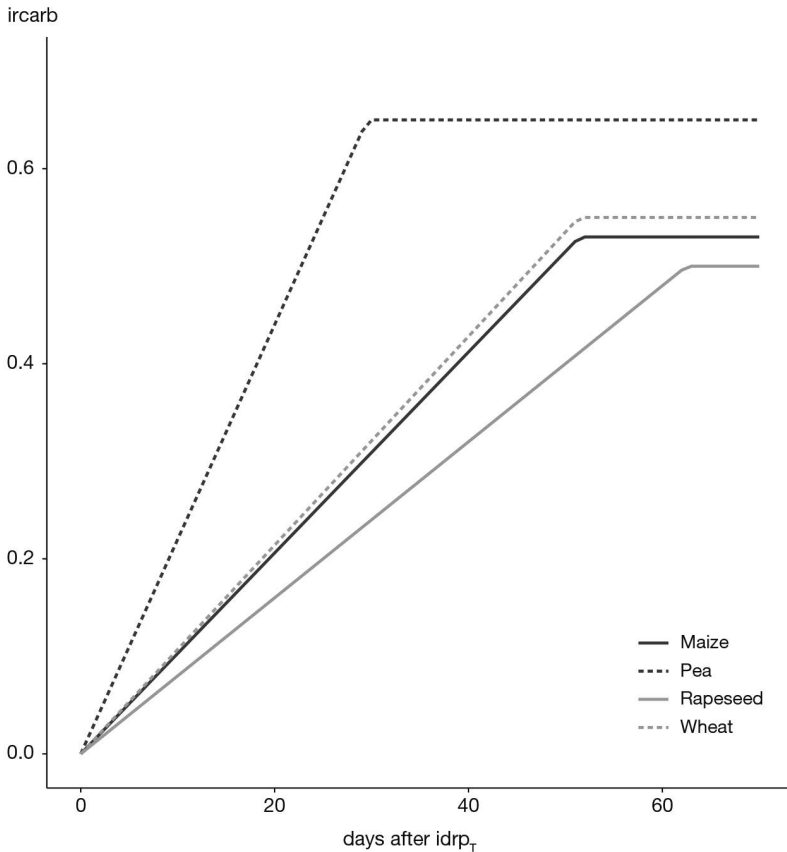


Figure 8.2. Dynamics of the grain to shoot biomass ratio (\mathbf{ircarb}), as a function of time since the stage \mathbf{idrp}_T . Examples are provided for maize (solid black line: $\mathbf{vitircarb}_p=0.0103$ and $\mathbf{imax}_p=0.53$), pea (dash-dotted black line: $\mathbf{vitircarb}_p=0.022$ and $\mathbf{imax}_p=0.65$), rapeseed (solid grey line: $\mathbf{vitircarb}_p=0.008$ and $\mathbf{imax}_p=0.50$) and wheat (dash-dotted grey line: $\mathbf{vitircarb}_p=0.0107$ and $\mathbf{imax}_p=0.55$).

$$\begin{aligned} \text{ircarb}(t) &= \text{vitircarb}_p \cdot (t - \text{idrp}_T + 1) \\ \text{ircarb}(t) &= \text{imax}_p, \text{ if } \text{ircarb}(t) > \text{imax}_p \end{aligned} \quad (8.4)$$

A transposition of the formalism has also been developed to account for thermal time. Under this formalisation, Eq. (8.4) is adapted: ircarb is computed by taking vitircarb_T as the input parameter, and the thermal time accumulation between idrp_T and imat_T as the dynamic variable of time.

Yet these dynamics may not be the actual grain filling dynamics since threshold translocation temperatures defining the thermal stress ftemprem_p (tminrem_p and tmaxrem_p , see § 4.4.4) may stop the carbon filling of harvested organs. Consequently, grain filling (dltags in $t\text{ ha}^{-1}$) is calculated at a daily time step, in order to account for the effect of a potential thermal stress (as defined by Eq. (8.5)).

$$\begin{aligned} \text{dltags}(t+1) &= [\text{ircarb}(t+1) \cdot \text{masec}(t+1) \\ &\quad - \text{ircarb}(t) \cdot \text{masec}(t)] \cdot \text{ftemprem}(t) \end{aligned} \quad (8.5)$$

The daily grain filling is then accumulated within the mafruit (in $t\text{ ha}^{-1}$) variable, as defined in Eq. (8.6). The mass of each grain is finally calculated as the ratio of the mass to the number of grains, although this cannot exceed the genetic pgrainmax_p limit, as defined in Eq. (8.7).

$$\begin{aligned} \text{mafruit}(t) &= \sum_{j=\text{idrp}_T}^t \text{dltags}(j) - \frac{\text{pgraingel}(t)}{100} \\ \text{mafruit}(t) &= \text{pgrainmax}_p \cdot \text{nbgrains}(t), \\ \text{if } \text{mafruit}(t) &> \text{pgrainmax}_p \cdot \text{nbgrains}(t) \end{aligned} \quad (8.6)$$

$$\begin{aligned} \text{pgrain}(t) &= \frac{\text{mafruit}(t)}{\text{nbgrains}(t)} \cdot 100 \\ \text{pgrain}(t) &= \text{pgrainmax}_p, \text{ if } \text{pgrain}(t) > \text{pgrainmax}_p \end{aligned} \quad (8.7)$$

8.1.2 For indeterminate growth plants

These species go on growing leaves while producing and growing harvested organs (fruits) during a period of time. The STICS model thus accounts for a trophic interaction between the growth of various groups of organs and among successive cohorts of harvested organs via the source/sink approach, using the notion of trophic stress defined in § 4.4.3). Both processes of organ setting and filling are concerned, assuming that abortion cannot occur during the filling phase.

The simulation technique adopted in the STICS model was inspired from the ‘boxcar-train’ technique (Goudriaan *et al.*, 1986) that is used in the TOMGRO model (Jones *et al.*, 1991). During growth, the fruits go through nboite_p compartments corresponding to increasing physiological ages. The time fruits spend in a compartment depends on temperature. In each compartment, fruit growth is equal to the product of a ‘sink-strength’ function and the source-sink ratio. The fruit sink strength is the derivative of a logistic function that takes the genetic growth potential of a fruit into consideration (Bertin and Gary, 1993).

8.1.2.1 Fruit setting

Fruits are set between the idrps stage and the inous stage (end of setting), defined by the **stdrpnou_p** phasic course. If this setting period lasts a long time, then the number of simultaneous compartments (i.e. fruits of different ages) is high, which indicates that there must be agreement between the values of **stdrpnou_p** and **nboite_p**.

During this setting period, on each day, the number of set fruits (*nfruitnou*) (Eq. (8.8)) depends on **afruitpot_p**, a varietal parameter expressed as the potential number of set fruits per inflorescence and per degree-day; the daily development rate (*upvt*); the number of inflorescences per plant (**nbinflo_p**); the plant density (*densite*); the trophic stress index (*spfruit*); and the frost stress index acting on fruits from flowering (*fgelflo*). Introducing the concept of inflorescence (group of fruits) into the model is only useful when technical or trophic regulation occurs at the inflorescence level (e.g. in grapevine). Furthermore, the number of fruit/flowers can also be modified (reduced) by human interventions (see § 13.2.3.2).

$$nfruitnou(t) = \mathbf{afruitpot}_p \cdot upvt(t) \cdot \mathbf{nbinflo}_p(t) \cdot densite(t) \cdot spfruit(t) \cdot fgelflo(t) \quad (8.8)$$

If the number of inflorescences is more than 1 (e.g. in the case of grapevine, inflorescences=bunches), it can either be prescribed (**nbinflo_p**), or calculated (*nbinflo_recal*) as a function of the trophic status of the plant at an early stage (we have chosen *iamfs*). In the latter case, *nbinflo_recal* is calculated using the **pentinflores_p** and **inflomax_p** parameters (see Eq. (8.9)).

$$nbinflo_recal(iamfs) = \frac{\mathbf{pentinflores}_p}{densite(iamfs)} \cdot [masec(iamfs) + resperenne0(iamfs)] \quad (8.9)$$

$$nbinflo_recal(iamfs) = \mathbf{inflomax}_p, \text{ if } nbinflo_recal(iamfs) > \mathbf{inflomax}_p$$

where *resperenne* (§ 7.3.1.1.2) is the amount of carbon reserves for perennial species coming from the previous cycle. Pruning is not accounted for in this calculation.

8.1.2.2 Fruit filling

The time spent by each fruit in a given compartment is $\frac{\mathbf{dureefruit}_p}{\mathbf{nboite}_p}$, where **dureefruit_p** is the total duration of fruit growth expressed in developmental units. In the last box (or age class), the fruits no longer grow and the final dry mass of the fruit has been reached: the fruit is assumed to have reached physiological maturity. A concrete example is shown in Figure 8.3.

Each day, in each growth compartment (K), the fruit growth (*croifruit*) depends on the number of fruits in the Kth compartment (e.g. in the first compartment: *nfruit*(t,1)) multiplied by the growth of each fruit, i.e. the elementary fruit sink strength (*fpft*), the trophic stress index (*sourcepuits*) and the thermal stress index (*ftemprem*) as given in Eq. (8.10).

$$croifruit(t, K) = nfruit(t, K) \cdot fpft(K) \cdot sourcepuits(t) \cdot ftemprem(t) \quad (8.10)$$

The fruit sink strength function is the derivative of the potential growth of a fruit (*potcroifruit*) plotted against the fruit development stage (*dfr*). There are two successive phases in fruit growth; the first corresponds to a cell division phase while the

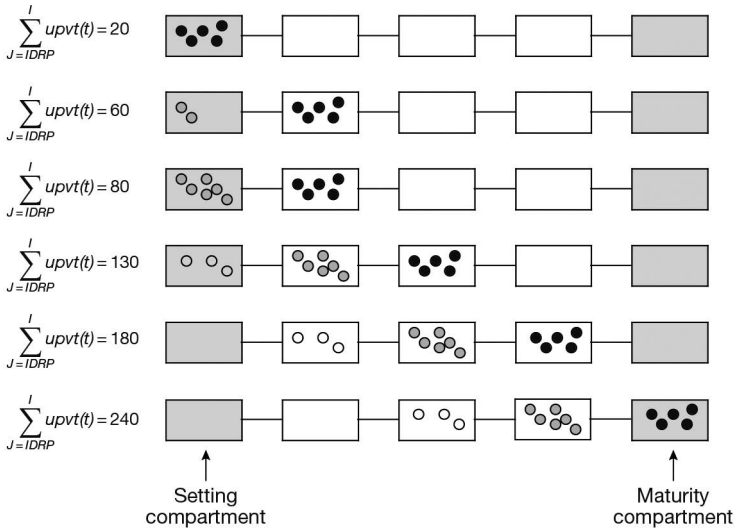


Figure 8.3. Illustration of the dynamics of fruit cohorts using the boxcartrain simulation technique. In this example $\text{stdrpnou}_p = 130$, $\text{nboite}_p = 5$, $\text{dureefruit}_p = 300$.

second is devoted to expansion of the cells already set. In order to account for this double dynamic, the fruit potential cumulative growth is defined as the sum of two functions, as specified in Eq. (8.11) and illustrated in Figure 8.4:

- an exponential-type function describing the cell division phase (using the parameters cfpf_p and dfpf_p)
- a logistic-type function describing the cell elongation phase (using the parameters afpf_p and bfpf_p)

$$\frac{\text{potcroifruit}(\text{dfr}(K))}{\text{pgrainmaxi}_p} = \text{dfpf}_p \cdot \left(1 - \exp\left(-\text{cfpf}_p \cdot \text{dfr}(K)\right)\right) + \frac{\alpha}{1 + \exp\left(-\text{bfpf}_p \left(\text{dfr}(K) - \text{afpf}_p\right)\right)} - \beta \quad (8.11)$$

In Eq. (8.11), α and β are calculated so that the following conditions are respected (Eq. (8.12)):

$$\begin{cases} \text{potcroifruit}(0) = 0 \\ \text{potcroifruit}(1) = \text{pgrainmaxi}_p \end{cases} \quad (8.12)$$

where pgrainmaxi_p is the genetic-dependent maximal weight of the fruit and dfr stands for the fruit development stage of each age class, varying between 0 and 1; this value is calculated for each age class (K) in a discrete way (Eq. (8.13)).

$$\text{dfr}(K) = \frac{K}{\text{nboite}_p} \quad (8.13)$$

This double dynamic is particularly interesting for grapevine (García de Cortázar Atauri *et al.*, 2009b; 2006). In many other cases (tomato, sugar beet, sugarcane), the cell division phase is so fast that the logistic function is enough to describe fruit growth (in this case, one of the parameters cfpf_p or dfpf_p must be zero).

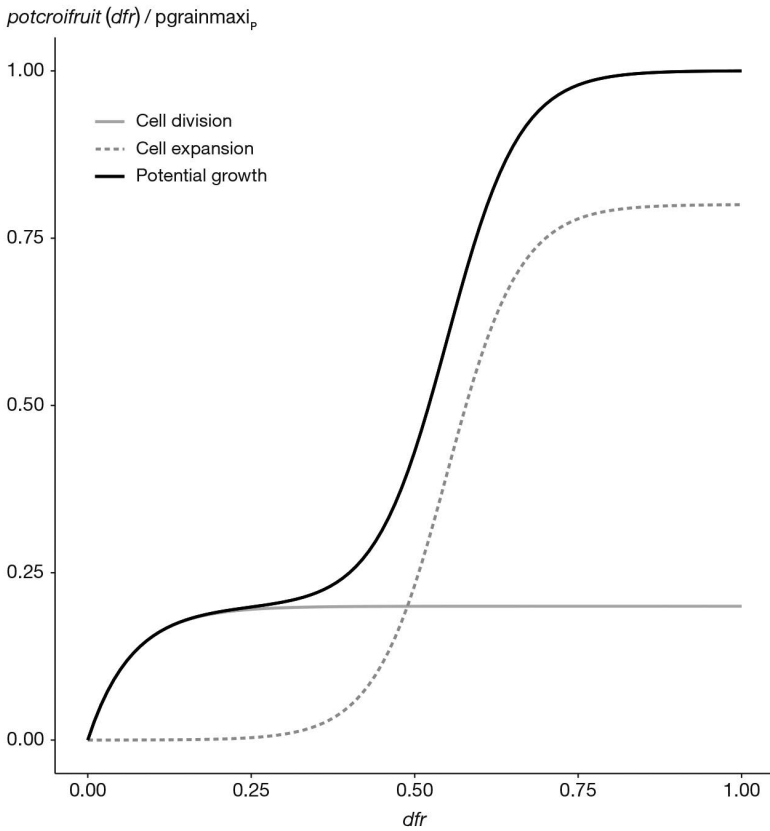


Figure 8.4. Normalised potential fruit growth ($\frac{\text{potcroifruit}}{\text{pgrainmaxi}_p}$) versus fruit development status (dfr) with its two components: the exponential dynamic representing cell division and the logistic-type dynamic representing cell expansion. In this example, we used grapevine values: $\mathbf{afpf}_p = 0.55$, $\mathbf{bfpf}_p = 18$, $\mathbf{cfpf}_p = 15$ and $\mathbf{dfpf}_p = 0.20$.

If the potential fruit growth is represented by a simple logistic curve, Figure 8.5 shows that when varying the parameters \mathbf{afpf}_p and \mathbf{bfpf}_p , various dynamics, including linear dynamic, can be represented.

The daily fruit sink strength function ($fpft$) is then calculated for each age class, according to Eq. (8.14), accounting for the duration of fruit growth from setting to maturity, expressed in developmental units ($\mathbf{dureefruit}_p$).

The sensitivity of the model for subdividing fruit growth into discrete units (\mathbf{nboite}_p parameter) also depends on the potcroifruit dynamics, as shown in Figure 8.6. Consequently, three elements must be taken into account to give a value to the parameter \mathbf{nboite}_p : the fruit setting duration, the fruit growth dynamics and the location of the idbbedss stage allowing the fruit water dynamics to be initiated.

$$f_{pft}(t, K) = \text{pgrainmaxi}_p \cdot \text{devjour}(t) \left[\text{dfpf}_p \cdot \text{cfpf}_p \cdot \exp(-\text{cfpf}_p \cdot \text{dfr}(K)) + \frac{\text{bfpf}_p \alpha Y}{(1+Y)^2} \right]$$

$$\text{with } \begin{cases} Y = \exp(-\text{bfpf}_p \cdot (\text{dfr}(K) - \text{afpf}_p)) \\ \text{devjour}(t) = \frac{t_{cul}(t) - t_{dmin}_p}{\text{dureefruit}_p} \end{cases} \quad (8.14)$$

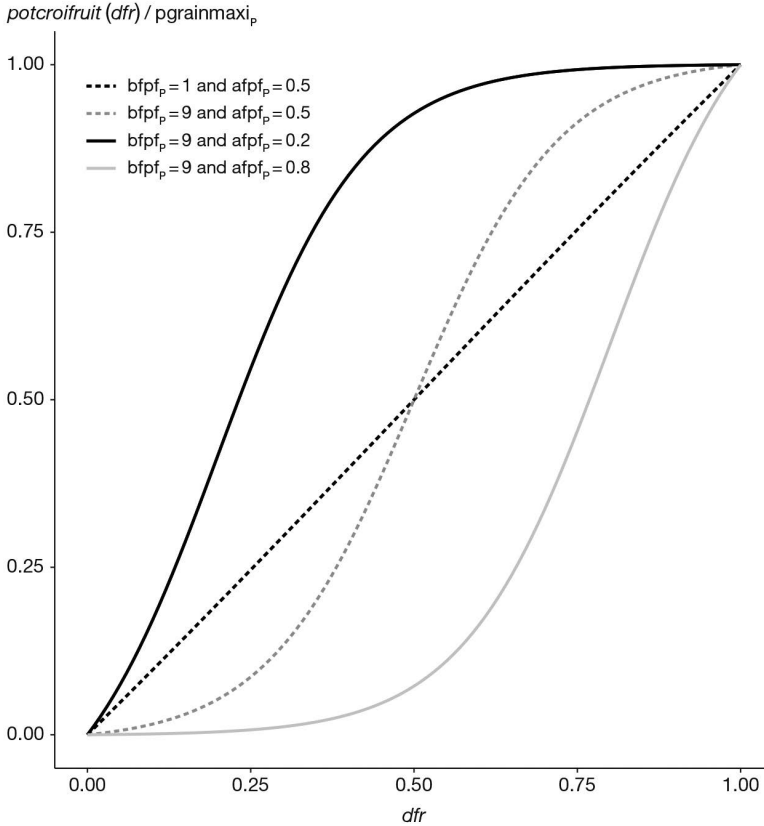


Figure 8.5. Normalised potential logistic fruit growth ($\frac{\text{potcroifruit}}{\text{pgrainmaxi}_p}$) versus fruit development status (dfr) with various parameterisations corresponding to afpf_p and bfpf_p values.

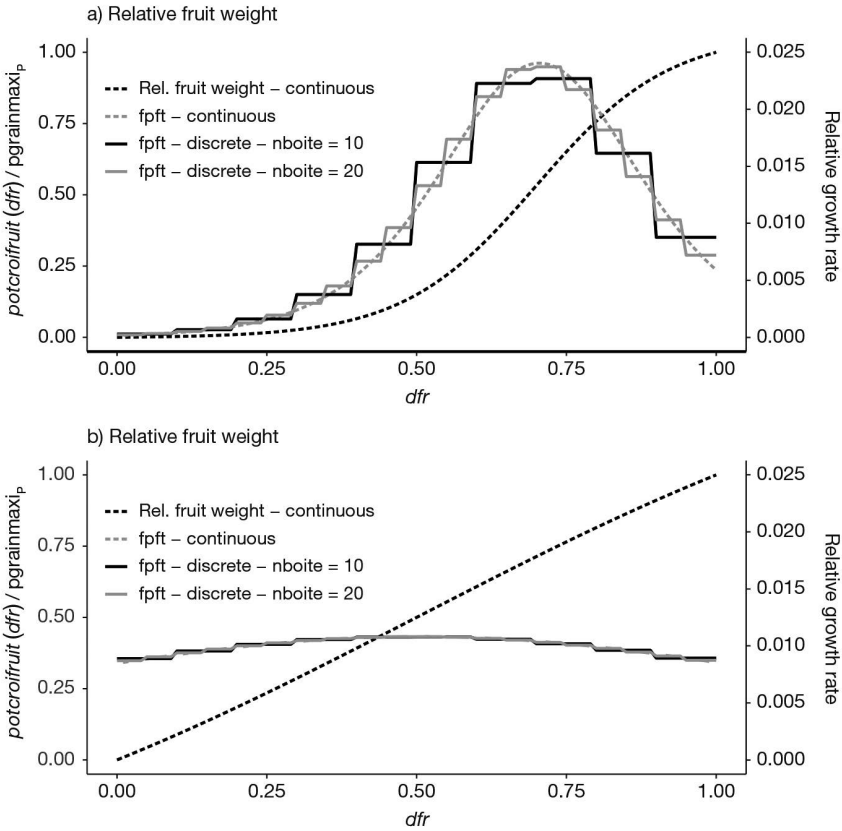


Figure 8.6. Influence of the discretisation of fruit growth through the number of boxes ($nboite_p$) in relation to the form of the dynamics: “S” shape in panel a): ($afpf_p = 0.7$ and $bpf_p = 9$) or nearly linear in panel b): ($afpf_p = 0.5$ and $bpf_p = 2$).

If allocation to fruits ($allocfruit$ variable calculated in Eq. (8.15)) exceeds the $allocfrm_{max_p}$ threshold, the $sourcepuits$ variable is reduced in proportion to the $\frac{allocfruit}{allocfrm_{max_p}}$ ratio. In the last box, the fruits are ripe and stop growing. The number of fruits on the plant, known as fruit load, is represented by $chargefruit$ variable. If the $codefrmur_G$ is set to 1, then $chargefruit$ will take into account the fruits in the last box (ripe); if not, it will only take into account the $(N - 1)$ first boxes.

$$allocfruit(t) = \frac{\sum_{K=1}^{nboite_p-1} croifruit(t, K)}{dltams(t)} \quad (8.15)$$

8.1.3 The special case of forage crop

8.1.3.1 General considerations

Like all crops, grasslands/pastures establish aerial and underground organs, whether they are natural and already established or newly sown, and whether they are monoculture or multi-specific and composed of grasses or legumes.

Unlike annual crops, where harvest means the death of the plant, grasslands/pastures are perennial crops. This means that after harvest of the exploitable yield, the plant will grow back. Accordingly, there are some specificities regarding the crop (re-)growth (§ 4) and yield elaboration (discussed in this section).

'Exploited grasslands' (agronomically speaking), also called mown grasslands, can be defined as perennial crops partially harvested by 'cutting' operations. Cutting can be achieved through machinery – here, we mean the actual operation of mowing using human-made tools – or via animals – i.e. grazing.

It will therefore be necessary to determine what is exported during a cut (i.e. the harvested part) and what remains in place, which is referred to as the remaining dry matter or the residual dry matter (see § 7.7).

In its current version, the STICS model is distributed with species of the functional type B, namely tall fescue (*Lolium arundinaceum*), orchard grass (*Dactylis glomerata*) or permanent pasture. The functional type B is defined by Duru, Tallowin and Cruz (2005) as a group of species with a capture strategy, rather than conservation, and with a slow organ recycling rate (Cruz *et al.*, 2002). In a broader context, according to their 'habitat preference and use-value', type B species are defined as 'species of fertile environments, that are fairly large in size, have a medium-to-early phenological development, are suitable to achieve a fairly early and good quality forage' (Cruz *et al.*, 2010).

The results presented in the following section are based on the standard parameter set distributed with the STICS soil-crop model and described in Ruget *et al.* (2006), which is itself based on considerations proposed by Diaz and Cabido (1997) to account for the functional type B species. Other functional types of grassland species could, of course, be re-parameterised to run the model. Finally, the STICS model has recently been successfully used to simulate C and N dynamics in alfalfa (*Medicago sativa* in Strullu *et al.*, 2020).

The following sections will describe how the decision to cut is taken (§ 8.1.3.2) and how the biomass is pooled into the different organs to constitute the harvestable/harvested organs and the residual dry matter (§ 8.1.3.3)

8.1.3.2 Decision to initiate cutting

A cut might be attempted when at least a given date has been reached. However, it is only undertaken if the dual conditions of minimal quantities to be left on the field and to be harvested are met.

Regarding the cutting date, two possibilities are offered, depending upon the nature of the work envisioned:

- If the calendar cutting dates are known, the 'calendar in days' option should be used. Each cutting date is then entered in the model immediately as a day of the year (**julfauche_T**);
- If the user wishes to perform cuts at similar grassland development under variable pedoclimatic contexts, the cutting dates should be defined at specific phenological stages (**tempfauche_T**), i.e. according to thresholds of cumulated upvt (§ 3.3), which must be initialised at sowing or reinitialised after the last cut (Duru *et al.*, 1993; Theau *et al.*, 1998).

A synthesis of the user-defined options related to forage cutting management is summarized at § 13.2.4.1. This section also describes a third option to perform cuts, using an automatic computation option.

Furthermore, the user must define what remains on the ground. This information can be entered in the model in two ways:

- From the height of the crop that has to remain on the field after cutting, i.e. the user-defined cutting height **hautcoupe_T** ;
- Alternatively, from the values of leaf area index (LAI) and biomass that the user would want to leave on the field after the cutting. These parameters are known respectively as the residual LAI - variable **lairesiduel_T** - and the residual biomass - variable **msresiduel_T**.

If the user enters the height, the residual LAI and biomass will not be read as input parameters even though they would have been defined. When height is stipulated, **lairesiduel_T** and **msresiduel_T** are calculated according to Eq. (8.16) and Eq. (8.17), that specify the relationships and changes in dry matter and LAI as a function of height (Brougham, 1956; see also § 7.7).

$$\mathbf{lairesiduel}_T = \frac{-1}{\mathbf{khaut}_p} \cdot \log\left(1 - \frac{\mathbf{hautcoupe}_T - \mathbf{hautbase}_p}{\mathbf{hautmax}_p}\right) \quad (8.16)$$

$$\mathbf{msresiduel}_T = \mathbf{coefmshaut}_p \cdot (\mathbf{hautcoupe}_T - \mathbf{hautbase}_p) \quad (8.17)$$

In these equations, **khaut_p** is the extinction coefficient, assumed to be plant-independent, connecting LAI to crop height (see § 9.2.1.1), **hautbase_p** and **hautmax_p** are plant-dependent parameters defining the lower and upper limits of foliage growth and **coefmshaut_p** accounts for the relationship between crop biomass and crop height.

Finally, additional conditions have to be met to ensure the cut can actually be performed:

- The LAI state reached by the crop must be higher than the LAI the user wants to leave on the field (i.e. **lairesiduel_T**);
- Similarly, the actual biomass state reached by the crop must be higher than the biomass the user wants to leave on the field (i.e. **msresiduel_T**);
- Finally, the harvestable fractions, called **msrec_fou** (§ 8.1.3.3), must be greater than a minimum amount that the user is willing to accept to harvest (**mscoupemini_T**).

In the actual model version, **mscoupemini_T** is defined by a unique parameter value that is specified for all cuts referring to a given management itinerary. Contrarily, the parameters **lairesiduel_T** and **msresiduel_T** are defined individually at each cut.

By modulating these criteria, cutting can be postponed until all three criteria (**lairesiduel_T**, **msresiduel_T** and **mscoupemini_T**) are met. These options were designed to allow adaptation of the management according to seasons or farmers' decisions, in order to match the harvest with needs.

8.1.3.3 Biomass pools, harvestable and harvested organs

The three biomass pools of interest in this section are the total crop biomass (**masec**) the biomass considered as potentially harvestable (**mafruit**) and the biomass that will actually be harvested (**msrec_fou**).

The variable *masec* represents the total aboveground biomass that exists on a given day. This biomass is the result of different sources (Eq. (8.18)):

- the residual biomass from the previous cut (**msresiduel_T**) that is still photosynthetically active;
- the newly produced biomass since the previous cut that is still photosynthetically active (*masecneo*).
- a dead fallen pool, which refers to a fraction of the biomass that might experience senescence and undergo abscission (*mafeuiltombe*, see § 7.3.1.1.1).

$$\begin{aligned} masec(t) &= [\mathbf{msresiduel}_T(nc) + masecneo] - mafeuiltombe \\ &= [\mathbf{msresiduel}_T(nc) + \sum_{i=nc_{day}+1}^n dltams(t)] - mafeuiltombe \end{aligned} \quad (8.18)$$

where *nc* is the number that corresponds to the last cut and *masecneo* is the sum of the daily increase in biomass (*dltams*) since the day following the last cut (**nc_{day}**) till day *n*.

In the case of forage, the non-senescent potentially harvestable biomass (*mafruit*, Eq. (8.19)) will be constituted by the non-senescent aboveground biomass which offers a use-value, i.e. which is photosynthetically active. The senescent tissues are considered as having no-value – they serve no purpose and/or will likely be lost during harvest. They must be removed from the aboveground biomass. In line with the two fractions comprising *masec*, the senescent tissues are pooled as follows:

- Senescent or dead pool coming from the residual biomass (*msresjaune*)
- The (non-fallen) senescent fraction of the newly formed biomass (*msneojaune*). It should be noted that *msneojaune* is assimilated to *mafeuiljaune* (§ 7.3.1.1.1).

$$mafruit = masec(t) - [\mathbf{msresjaune} + \mathbf{msneojaune}] \quad (8.19)$$

Finally, the harvested fraction *msrec_fou* (Eq. (8.20)) will be constituted by the non-senescent potentially harvestable biomass (*mafruit*) from which the fraction that will remain on the field/pasture after the next cut (**msresiduel_T**) must be removed.

$$msrec_fou = mafruit - \mathbf{msresiduel}_T \quad (8.20)$$

An additional variable integrating the whole forage produced is also outputted from the model (*masectot*). It accounts for all the biomass that has been produced (non-dead or senescent) and harvested along the cropping season.

Figure 8.7 shows the evolution over a cropping season of the variables related to forage production, including four cutting events, illustrating the differences between total aboveground biomass, harvestable and harvested biomass – namely *masec*, *mafruit* and *msrec_fou* – and showing the year-to-date production (*masectot*). Figure 8.7 illustrates how the harvested dry matter (*msrec_fou*) increases every day, and might, due to its mathematical construction, become negative when what is harvestable (*mafruit*) is lower than what should remain on the ground at the next cut (**msresiduel_T**). This usually occurs in periods of low productivity when senescence is active, i.e. mainly during dry summer.

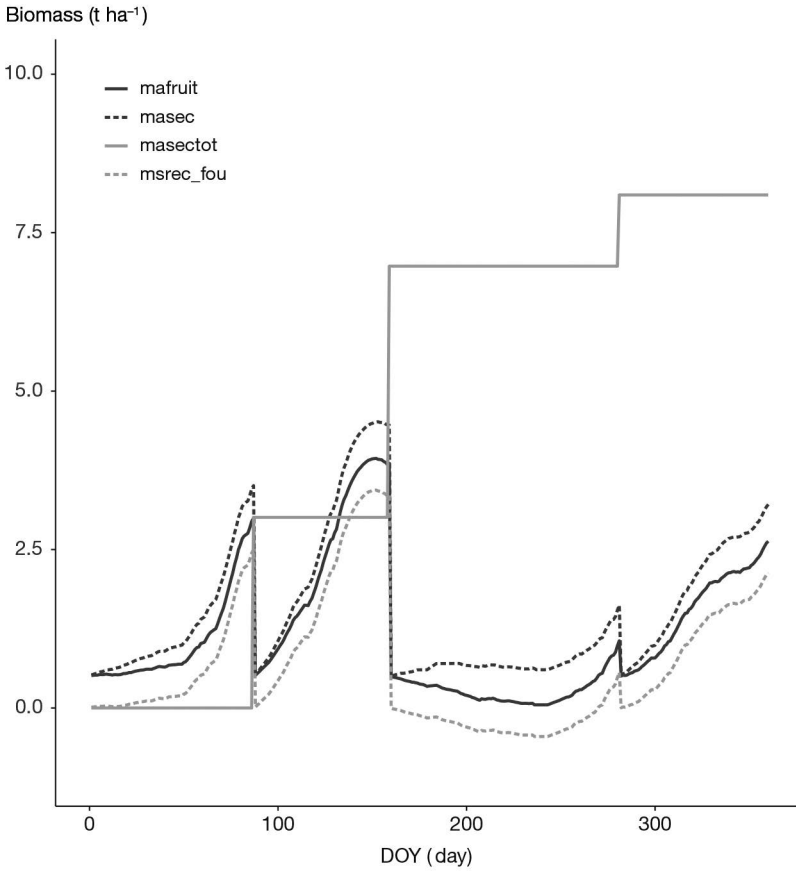


Figure 8.7. Evolution of biomass pools along a cropping season (Lusignan, France, 1991). In this example, three cuts are performed.

►► 8.2 Yield quality

8.2.1 Water content of organs

For non-harvested organs, the water contents are assumed to be constant. The corresponding parameters are called $h2ofeuilverte_p$, $h2ofeuiljaune_p$, $h2otigestruc_p$ and $h2oreserve_p$ for green leaves, dead leaves, stems and reserves, respectively: they are expressed in terms of fresh weight (hereafter referred to as ‘FM’), i.e. in $g_{water} \cdot g_{FM}^{-1}$. They are used to calculate the fresh weight of each organ: mafraisfeuille (for all green and yellow leaves), mafraistige (stems) and mafraisres (reserves).

For harvested organs, it is assumed that the water content is constant ($h2ofrvvert_p$) up to the stage *idebdes* (§ 3). This stage may occur before physiological maturity. For indeterminate plants, it does not occur at the same time for all fruit cohorts but it corresponds to one of the age classes. We shall call this stage ‘onset of fruit water dynamics’, which can be hydration or dehydration and which results from the concomitant water and dry matter influx into the fruit or grain. From this stage, we assume

that there is a 'programmed' time course in the water content of fruits, and so this is expressed using the **deshybase_p** parameter (in $g_{water} g_{FM}^{-1} d^{-1}$), which will modify the fruit water content (teaugrain) day after day from its initial value **h2ofrvert_p**. For dehydration, **deshybase_p** is positive; if the programme evolution tends towards hydration, **deshybase_p** is negative. Dehydration may be accelerated (or provoked) by water stress, which is characterised by the difference between the crop and air temperatures. The proportionality coefficient is called **tempdeshyd_p** (in $g_{water} g_{FM}^{-1} °C^{-1}$). In summary, the water content (teaugrain) is the result of Eq. (8.21) where the index K (for the box number) is of no use for determinate plants. An example is provided for grapevine in Figure 8.8.

$$\text{teaugrain}(t, K) = \text{h2ofrvert}_p - \text{deshybase}_p \cdot (t - \text{idebdess}(K) + 1) - \sum_{j=\text{idebdess}(K)}^t \left(\text{tempdeshyd}_p \cdot (tcult(j) - \text{tair}(j)) \right) \quad (8.21)$$

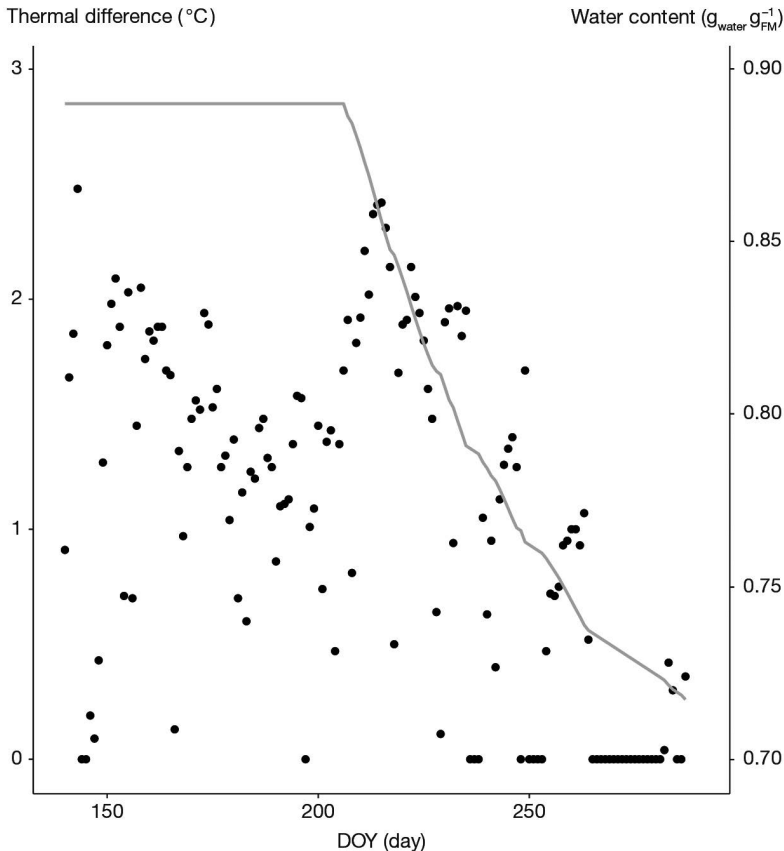


Figure 8.8. Evolution of the thermal difference ($tcult - tair$, black points) and the grape water content (solid grey line) for the 2003 season in Montpellier, France, influenced by the phenological course (the dynamic started on 26 July).

8.2.2 Biochemical composition

The quantity of nitrogen in harvested organs, both for determinate and indeterminate species (QN_{grain}), is an increasing proportion ($irazo$ computed in Eq. (8.22)) of the quantity of nitrogen in the biomass (QN_{plante}): the concept of the harvest index is extended to nitrogen (Lecoeur and Sinclair, 2001), using the parameter **vitirazo_p** (see also § 6.1.2.2). Obviously, as for carbon, the grain/fruit nitrogen filling can be affected by thermal stress which requires a daily calculation ($dltazo$ computed in Eq. (8.23)). The temperature effect on nitrogen grain filling is assumed to be the same as for carbon. The nitrogen harvest index is assumed to be limited to a parameter **irazomax_p**, as explained in Eq. (8.22).

$$\begin{aligned}
 irazo(t) &= \mathbf{vitirazo}_p \cdot (t - \mathbf{idrp}_T + 1) \\
 irazo(t) &= \mathbf{irazomax}_p, \text{ if } irazo(t) > \mathbf{irazomax}_p
 \end{aligned}
 \tag{8.22}$$

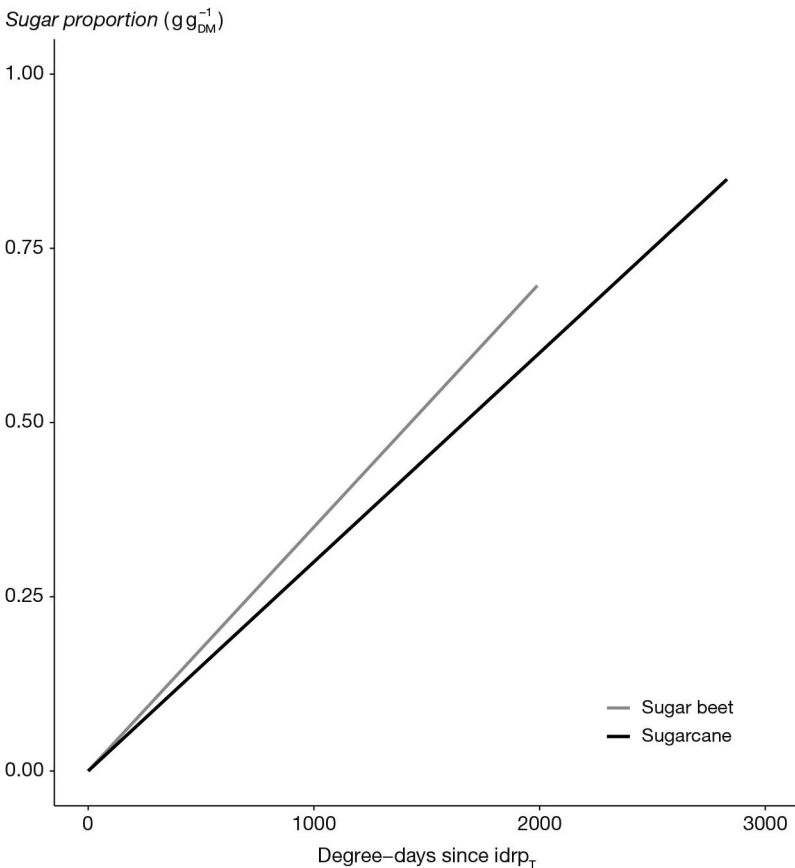


Figure 8.9. Evolution of sugar content in relation to fruit development for sugarcane ($\mathbf{vitpropsucre}_p = 0.00030$) and sugar beet ($\mathbf{vitpropsucre}_p = 0.00035$).

$$\begin{aligned} d\text{tazo}(t+1) = & [\text{irazo}(t+1) \cdot QN\text{plante}(t+1) \\ & - \text{irazo}(t) \cdot QN\text{plante}(t)] \cdot f\text{temprep}(t) \end{aligned} \quad (8.23)$$

To complete the quality components of simulated harvested organs, we propose a very simple estimate of the sugar and oil contents. From the beginning of fruit/grain filling until physiological maturity, we assume that there is a gradual increase in the proportions of these two types of components in the fruit dry matter. This increase is determined using the **vitprosucre_p** (Figure 8.9) and **vitprohuile_p** parameters expressed in $g\ g_{DM}^{-1}\ \text{degreeday}^{-1}$. The combination of this evolution and the evolution in the water content in fruits produces contents based on fresh matter, which depends on the development of each crop.

For indeterminate crops, the calculation is made for each age class separately, and then combined for all age classes. Finally, for the special case of grapevine, it should be noted that a new formalism was developed to compute and predict the sugar content, which will influence the alcohol content, based on the evolution of water content (García de Cortázar Atauri *et al.*, 2009b).

Chapter 9

Canopy microclimate

NADINE BRISSON, MARIE LAUNAY AND GAETAN LOUARN

REVIEWED BY: NICOLAS BEAUDOIN AND DIDIER COMBES

►► 9.1 Introduction

9.1.1 Context and importance of the microclimate

Biological processes in the crop-soil system directly depend on several physical variables such as light, temperature and humidity. The physical properties of biological entities within this system and the way they function also affect the environmental variables at their immediate boundary. The climate to which the plants and soil are exposed (i.e. the microclimate) can thus differ substantially from the standard plant climate as defined for weather forecast (local climate). These changes result from an exchange of force, momentum, energy, and mass within the boundary layer (Jones, 2013). These exchanges imply two important kinds of coupling: radiative coupling, where energy is transferred through electromagnetic vibration, and diffusive coupling, where heat, water vapor, are exchanged.

This chapter examines the modelling principle related to the plant microclimate in STICS. The relevant variables (i.e. crop temperature, light interception and air humidity), drive many processes that take place within the plant canopy such as phasic development, photosynthesis and evapotranspiration. Moreover, they provide the boundary conditions for the calculation of soil microclimate (see § 10) and thus influence processes occurring within the soil, such as organic matter mineralisation (see § 12), and plant germination (see § 3). Microclimate also alters water balance (see § 11).

Most crop models do not go into detail about microclimate calculation and use the standard measured weather variables as the driving variables for the model (Brisson *et al.*, 2006). The calculation of the temperature and air humidity within the canopy from a daily energy balance is among the original components of STICS, and it allows users to account for the combined effects of weather and water balance.

The energy balance calculations with a daily time step, although questionable in terms of physics, have already been carried out as part of an operational estimation of crop water requirements (Smith *et al.*, 1998). The daily crop temperature is assumed to be the

arithmetic mean of the maximum and minimum crop temperatures. Two calculation methods are proposed (depending on the availability of wind and air humidity input data): one uses an empirical relationship from Seguin and Itier (1983) and the other solves the energy balance. Both methods rely on the calculations of the daily sum of evaporative fluxes and net radiation.

Table 9.1. Available formalism options for calculating microclimate in STICS.

Main process	Output variable	Key variable	Option
A=Radiation interception	Intercepted radiation (%)		A.1 Beer's law
			A.2 Radiation transfers
B=Energy budget	a. Net radiation	Longwave radiation	B.a.1 Brunt's formula
			B.a.2 Brutsaert's formula
	b. Crop temperature	Daily minimum and maximum crop temperature	B.b.1 Empirical approach
			B.b.2 Energy balance
C=Evaporative fluxes	Crop transpiration, soil and crop surface evaporations	Potential evapotranspiration	C.1 Crop coefficient
		Soil evaporation, maximum plant transpiration, direct evaporation of water intercepted by the foliage or by the mulch, surface resistances	C.2 Resistance approach (Shuttleworth-Wallace)
		Plant surface evaporation	C.3 Water persistence on foliage

9.1.2 Formalism options in STICS

STICS has several options to calculate the microclimate variables. Some of them are alternatives to be chosen, some are mandatory for given purposes, and others are options that may be activated or not according to the targeted availability of the inputs. Table 9.1 summarises the available options.

Hypothesis	When is it mandatory	Comment
Homogeneous crop	Canopies in row; intercropping; when the leaf status variable is the ground cover instead of the leaf area	Options A.1 and A.2 are alternatives (one or the other must be activated)
Simplest option: depends on the crop temperature, the insolation fraction and the vapour pressure		Options B.a.1 and B.a.2 are alternatives
More precise: illustrates clearly the soil and atmospheric components		
Daily minimum crop temperature = daily minimum air temperature Daily maximum crop temperature = linear function (net radiation, daily maximum air temperature, daily evapotranspiration, canopy height and surface rugosity)	When neither wind speed nor air humidity data are available	Options B.b.1 and B.b.2 are alternatives
Daily maximum and minimum temperatures are calculated from two instantaneous energy balances assuming that all fluxes are maximal and minimal at the same time: (i) maximum values of crop temperature, air temperature, net radiation, soil heat, evapotranspiration and aerodynamic resistance occur at midday, while (ii) minimum values of the same variables occur at the end of the night		Brutsaert's formula is used to calculate the long wave radiation component of the two energy balances; the Shuttleworth-Wallace approach is used to calculate the aerodynamic resistance between the cover and the reference level
Homogenous canopy with leaves being randomly distributed	(i) Canopies in rows; heterogenous crop (such as intercrop); (ii) Climate change studies (this option allows users to illustrate the CO ₂ concentration effect on the stomatal conductance)	Options C.1 and C.2 are alternatives; Option C.3 is additive (may be activated or not)
	When evaporation of intercepted water (rainfall, irrigation) mostly offsets (even exactly) for the decrease in evaporative demand	

STICS has two options with regard to radiation interception: a simple Beer's law, recommended for homogenous crops, and a more complex calculation for radiation transfers within the canopy, recommended for crops in rows. If the leaf status variable is the ground cover and not the leaf area index (LAI), then only the Beer's law option is permitted. The longwave radiation component of the net radiation may be calculated according to the Brunt's formula or the Brutsaert's formula; the latter formula clearly illustrates the soil and atmospheric components of the longwave radiation. Two calculation methods are proposed for crop temperature, depending on weather data availability: users may choose either an empirical approach or the energy balance. Finally, evaporative fluxes can be assessed using the simple crop coefficient approach, the potential evapotranspiration as the driving variable to calculate the plant water requirement, or the resistance approach using empirical resistance parameters to estimate the energy budget of canopies.

9.1.3 Linking with other modules

The upstream microclimate module provides key variables for other modules in the model. The intercepted radiation, the canopy temperature and moisture, the evaporative fluxes and the stomatal conductance are calculated here, allowing users to simulate both crop development and growth as well as the water balance. The intercepted radiation determines the photosynthesis outcome and thus the crop growth (see § 4). As soon as the canopy temperature is activated as a driver (instead of the air or soil temperature), it drives leaf and root growth (see § 4 and 5), while becoming a limiting factor when reaching extreme values, especially for the filling of grain, fruit or other storage organs (see § 8). When the resistance approach is activated, the evaporative fluxes (soil evaporation, direct evaporation of water intercepted by the foliage or mulch, and maximum plant transpiration) and the stomatal conductance control the water balance (see § 11). Finally, when coupling STICS with models running at an hourly time scale, crop temperature and canopy moisture may be provided at the same time step, thanks to the microclimate module skills.

►► 9.2 Radiation interception

9.2.1 Sole crop

Since most crop models are designed for industrial crops, the canopy is assumed to be a homogenous environment with leaves being randomly distributed over the area. A consequence of this random, homogeneous representation is that an optical analogy (Beer's law) can be used to estimate the interception of photosynthetically active radiation. This law, having only one parameter (the extinction coefficient), has been thoroughly studied for many crops (Varlet-Grancher *et al.*, 1989): the more erect the plant leaves, the smaller the extinction coefficient.

This approach produces very good results for homogenous crops, but is poorly suited to canopies in rows or during the first stages of an annual crop because the homogeneity hypothesis cannot apply. Consequently, the STICS model, like CROPGRO (Boote and Pickering, 1994) can simulate canopies in rows, with prediction of light interception dependent not only on LAI, but also on plant height and width, row spacing, plant spacing, and direct and diffuse light absorption (radiative transfer approach). Such capabilities are also required to simulate intercropping (see 9.3.4).

9.2.1.1 Beer's law and calculation of height

The radiation intercepted by the crop r_{aint} (Eq. (9.1)) is expressed according to a Beer's law function of lai . The extin_p parameter is a daily extinction coefficient and parsurr_G is a climatic parameter corresponding to the ratio (in radiative energy) of photosynthetically active radiation to the global radiation tr_g (around 0.48, Varlet-Grancher *et al.*, 1982). The ratio r_{aint} to tr_g for different homogeneous crops is plotted in Figure 9.1.

Using explicit lai :

$$r_{\text{aint}}(t) = 0.95 \cdot \text{parsurr}_G \cdot \text{tr}_g(t) \cdot (1 - \exp(-\text{extin}_p \cdot (\text{lai}(t) + \text{eai}(t))))$$

Using ground cover $\text{tauxcouv}(t)$:

$$r_{\text{aint}}(t) = 0.95 \cdot \text{parsurr}_G \cdot \text{tr}_g(t) \cdot \text{tauxcouv}(t) \quad (9.1)$$

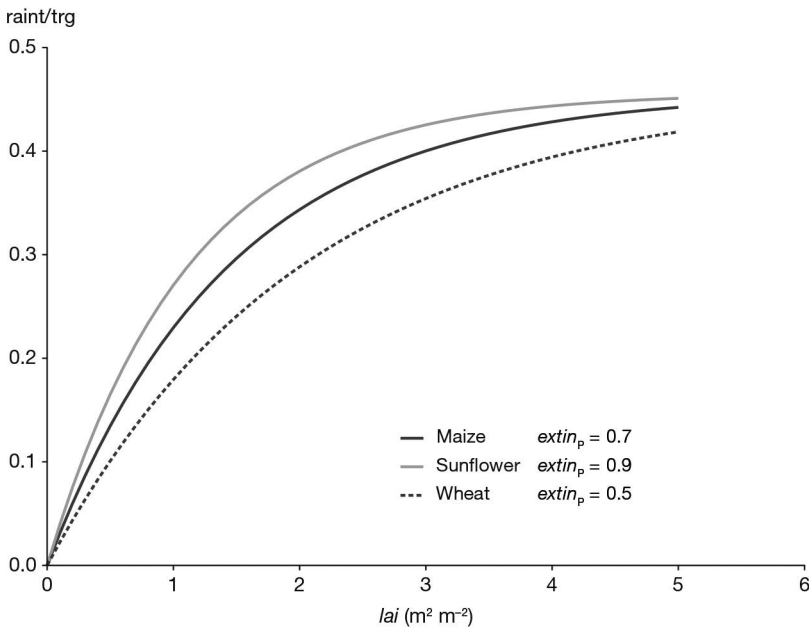


Figure 9.1. Proportion of global radiation ($r_{\text{aint}}/\text{tr}_g$) intercepted for maize, sunflower and wheat (extin_p values of 0.7, 0.9 and 0.5, respectively).

The height of homogeneous crops is deduced from the leaf area index or the ground cover (Eq. (9.2)). It is used especially in the calculation module for water requirements via the resistive option. The khaut_G parameter is assumed to be plant independent (a general value of 0.7 is proposed), while the potential height of foliage growth (hauteur) is mostly plant dependent and defined by the two limits hautbase_p and hautmax_p .

Using explicit lai :

$$\text{hauteur}(t) = \text{hautmax}_p \cdot (1 - \exp(-\text{khaut}_G \cdot (\text{lai}(t) + \text{laisen}(t)))) + \text{hautbase}_p$$

Using ground cover $\text{tauxcouv}(t)$:

$$\text{hauteur}(t) = \text{hautmax}_p \cdot \text{tauxcouv}(t) + \text{hautbase}_p \quad (9.2)$$

9.2.1.2 Radiative transfers and plant shape

Calculating the radiation transfer enables users to estimate the radiation intercepted by a crop in rows, and a simple approach takes the crop's geometry into account. The objective is to estimate, on a daily time step, the fraction of radiation intercepted by the crop and the fraction transmitted to the layer below, which can be either the soil or another crop (e.g. in intercropping). To calculate these two fractions, the soil surface is divided into a shaded part and a sunlit part. By convention, the shaded part corresponds to the vertical projection of the crop foliage onto the soil surface. The available daily variables are the leaf area index (lai), calculated independently, and the global radiation (trg).

9.2.1.2.1 Radiation transfers

The simplest method of calculating the radiation received at a given point X (located on the soil in the inter-row, see Figure 9.2) is to calculate angles H1 and H2, which correspond to the critical angles between which point X receives direct radiation. At angles below H1 and above H2, point X receives an amount of radiation that is less than the radiation value due to absorption by the crop. Within those angle windows, Beer's law is used to estimate the fraction of transmitted radiation.

It is assumed that a canopy can be represented by a simple geometric shape (rectangle or triangle) and that it is isotropically infinite. We can therefore describe the daily radiation received at point X as the sum of the radiation not intercepted by the crop (rdroit) (sun at an angle between H1 and H2) and the radiation transmitted (rtransmis). The 'infinite canopy' hypothesis allows us to assume that when the sun is at an angle below H1 and H2, all the radiation passes through the crop.

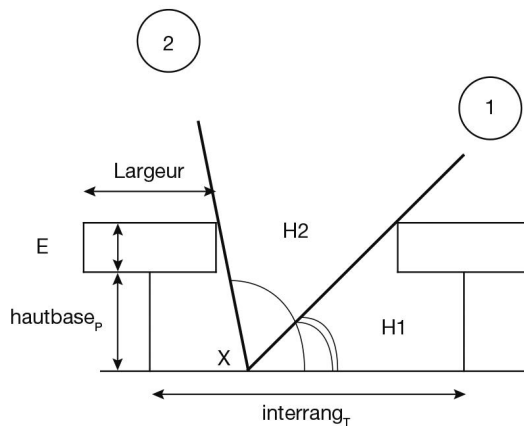


Figure 9.2. Simplified representation of the plant canopy and the principles used to calculate daily radiation received by the inter-row ($interrang_p$): $hautbase_p$ is the base height of the canopy, E its thickness, $largeur$ its width, X is any point located in the inter-row and $H1$ and $H2$ are the two sun height angles corresponding to the daily positions 1 and 2 of the sun between which X is directly illuminated (adapted from Brisson *et al.*, 2004).

Each part of the radiation received at X includes a direct component and a diffuse component. Let us assume that, for the transmitted part, the same extinction coefficient ($ktrou_p$) applies to both fractions (which is generally accepted to be the case when the

general Beer's law is used with a daily time scale). In Eq. (9.3), the parameter \mathbf{ktrou}_p corresponds to a gap fraction (Baret *et al.*, 1993).

$$\mathbf{rtransmis}(t, X) = (1 - \mathbf{rdroit}(t, X)) \cdot \exp(-\mathbf{ktrou}_p \cdot (\mathbf{lai}(t) + \mathbf{eai}(t))) \quad (9.3)$$

In contrast, for \mathbf{rdroit} (Eq. (9.4)), direct and diffuse components should be separated because of the directional nature of the direct component, which requires the calculation of separate proportions of radiation reaching the soil ($\mathbf{kgdiffus}$ and $\mathbf{kgdirect}$ are the proportions of diffuse radiation, $\mathbf{rdiffus}$, and direct radiation, $\mathbf{rdirect}$, respectively, that reach the soil):

$$\mathbf{rdroit}(t, X) = \mathbf{kgdiffus}(t, X) \cdot \mathbf{rdiffus}(t) + \mathbf{kgdirect}(t, X) \cdot \mathbf{rdirect}(t) \quad (9.4)$$

– The case of direct components

If θ_1 and θ_2 are the hourly angles (the actual angles that are zero at 12h TSV) corresponding to H1 and H2, and assuming sinusoidal variation in the direct radiation during the day, we can write (Eq. (9.5)):

$$\mathbf{kgdirect}(t, X) = 0.5 \left(\cos\left(\frac{\pi}{2} + \theta_1(t, X)\right) + \cos\left(\frac{\pi}{2} + \theta_2(t, X)\right) \right) \quad (9.5)$$

In order to calculate the θ angles, we must solve the following set of equations (Eq. (9.6)):

$$\sin(\mathbf{H}) = \sin(\mathbf{latitude}_C) \cdot \sin(\mathbf{DEC}) + \cos(\mathbf{latitude}_C) \cdot \cos(\mathbf{DEC}) \cdot \cos(\theta)$$

$$\cos(\mathbf{A}) = \frac{(-\cos(\mathbf{latitude}_C) \sin(\mathbf{DEC}) + \sin(\mathbf{latitude}_C) \cos(\mathbf{DEC}) \cos(\theta))}{\cos(\mathbf{H})}$$

$$\tan(\mathbf{H}) = G \cdot \sin\left(\mathbf{A} + \mathbf{orientrang}_r\right) \quad (9.6)$$

where \mathbf{H} is the height of the sun, \mathbf{A} its azimuth, $\mathbf{latitude}_C$ is the latitude of the location, \mathbf{DEC} the declination angle which depends on the day (Varlet-Grancher *et al.*, 1993), and $\mathbf{orientrang}_r$ is the azimuth angle of the rows. \mathbf{G} , the apparent tangent of \mathbf{H} in Figure 9.2, depends on canopy geometry ($\mathbf{largeur}$, \mathbf{E} and $\mathbf{hautbase}_p$ defined in Figure 9.2) and the position of the given point within the inter-row (\mathbf{X}).

For example, assuming $\mathbf{X} > \frac{\mathbf{largeur}}{2}$ and the angle \mathbf{H}_2 , $G = \frac{\mathbf{hautbase}_p + \mathbf{E}}{\mathbf{X} - \frac{\mathbf{largeur}}{2}}$

The borderline between sun ($\mathbf{surf(as)}$) and shade ($\mathbf{surf(ao)}$) is arbitrarily considered as $\mathbf{largeur}/2$. The above set of equations cannot be solved using analytical methods, and must therefore be solved numerically (loop over θ with a basic variation of 3 degrees followed by linear interpolation).

– The case of diffuse components

We take 46 directions (azimuth, height) and their corresponding percentage of diffuse radiation (SOC standard). For each direction, point \mathbf{X} is checked to see if it is directly illuminated, depending on canopy geometry. The variable $\mathbf{kgdiffus}$ corresponds to the cumulative proportion of radiation received at point \mathbf{X} for the 46 directions.

The diffuse to total radiation ratio (\mathbf{rdif} ; Eq. (9.7)) is calculated according to Spitters *et al.* (1986) on the basis of the total to extraterrestrial radiation ratio (\mathbf{RsRso}), with the extraterrestrial radiation being calculated from the classical astronomical formula (Varlet-Grancher *et al.*, 1993) represented in Figure 9.3.

$$\begin{aligned}
 & \text{if } \text{RsRso}(t) < 0.07 \quad \text{rdif}(t) = 1 \\
 & \text{if } \text{RsRso}(t) \geq 0.07 \quad \text{rdif}(t) = 1 - 2.3 \cdot (\text{RsRso}(t) - 0.07)^2 \\
 & \text{if } \text{RsRso}(t) > 0.35 \quad \text{rdif}(t) = 1.33 - 1.46 \cdot \text{RsRso}(t) \\
 & \text{if } \text{RsRso}(t) > 0.75 \quad \text{rdif}(t) = 0.23 \quad (9.7)
 \end{aligned}$$

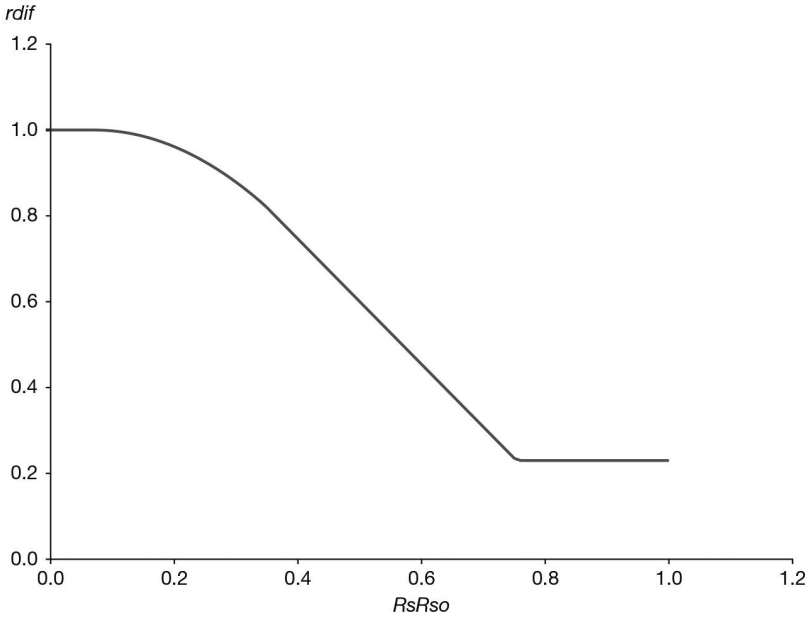


Figure 9.3. Relationship between the diffuse to total radiation ratio (*rdif*) and the total to extraterrestrial radiation ratio (*RsRso*).

The above equations are applied to points spread equally along the inter-row, and the transmitted radiation values are then averaged for the shaded fraction (*rombre*) and the sunlit fraction (*rsoleil*). The complementary part to the global radiation corresponds to the radiation intercepted by the crop (*raint*; Eq. (9.8)).

$$\begin{aligned}
 \text{raint}(t) = & \text{parsurr}_g \cdot \text{trg}(t) \cdot (1 - \text{rombre}(t) \cdot \text{surf}(\text{ao})(t) \\
 & - \text{rsoleil}(t) \cdot \text{surf}(\text{as})(t)) \quad (9.8)
 \end{aligned}$$

9.2.1.2.2 Crop geometry

The *largeur* and *E* values are calculated using the following assumptions:

- The volume of the crown (or the group of crop leaves) has a simple shape. We assume that its cross section is rectangular or triangular (parameter **forme_p** as a code).

This volume can be evaluated on the basis of *lai*, the inter-row value (**interrang_T**), the leaf density (*dfol*), and the **rapforme_p** ratio (thickness/width: *E/largeur*) of the shape. The *dfol* value is a ‘within the shape’ leaf density, which differs from the classical definition of leaf density as a ratio of leaf surface to 1 m³ of air. The *dfol* value can vary

between two limits ($\mathbf{dfolbas}_p$ and $\mathbf{dfolhaut}_p$). It depends on the foliage produced FP , which accounts for lai, eai, laisen and leaves suppressed by specific techniques such as topping ($lairognecum$) or leaf removal ($laieffeuil_T$) (Eq. (9.9); see § 13.2.3) and the slope \mathbf{adfol}_p . If we assume a constant foliage density, then $\mathbf{dfolbas}_p = \mathbf{dfolhaut}_p$.

$$\mathbf{FP}(t) = lai(t) + eai(t) + lairognecum(t) + laieffcum(t) + laisen(t)$$

$$\text{if } \mathbf{adfol}_p > 0 \quad dfol(t) = \mathbf{adfol}_p \cdot \mathbf{FP}(t)$$

$$\text{if } \mathbf{adfol}_p < 0 \quad dfol(t) = \mathbf{adfol}_p \cdot \mathbf{FP}(t) + \mathbf{dfolbas}_p + \mathbf{dfolhaut}_p$$

$$\text{if } dfol(t) \leq \mathbf{dfolbas}_p \quad dfol(t) = \mathbf{dfolbas}_p$$

$$\text{if } dfol(t) \geq \mathbf{dfolhaut}_p \quad dfol(t) = \mathbf{dfolhaut}_p \quad (9.9)$$

– This formalisation of leaf density makes it possible to represent both foliage getting denser while growing (e.g. grapevine) or conversely becoming less dense while growing (e.g. cereals, Figure 9.4).

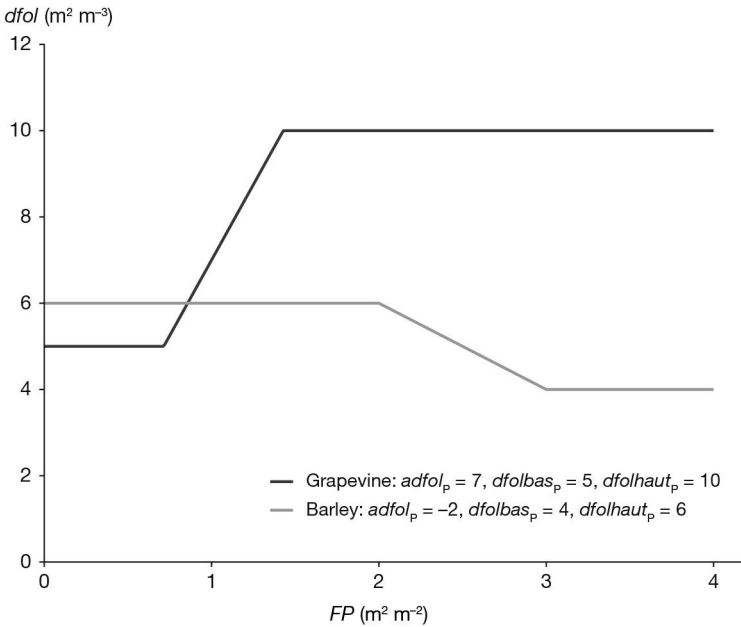


Figure 9.4. Leaf density ($dfol$) evolution for grapevine and barley according to the cumulative foliage produced (FP), as two opposite examples.

– The plant canopy width $largeur$ is calculated according to its rectangular or triangular shape (Eq. (9.10)).

$$largeur(t) = \sqrt{\frac{lai(t) \cdot \mathbf{interrang}_T}{dfol(t) \cdot \mathbf{rapforme}_p}} \quad \text{for the rectangle}$$

$$largeur(t) = \sqrt{2 \frac{lai(t) \cdot \mathbf{interrang}_T}{dfol(t) \cdot \mathbf{rapforme}_p}} \quad \text{and for the triangle} \quad (9.10)$$

– Two types of triangles can be chosen: ‘right way up’ or ‘upside down’. The more appropriate shape for radiative transfer is the ‘right way-up’ triangle (Brisson *et al.*, 2004) because this shape suggests that the low leaf density (in the classical sense of leaf area per m³) measured in the upper parts allows more radiation to be transmitted than in the lower parts where the leaf density is higher. With our simple model based on a constant leaf density within the shape, this can be accounted for only by a triangle. Thus the shape required as a parameter in the model is more closely linked to the leaf density profile than to the external shape of the plant foliage.

A maximum limit, **hautmax_p**, is imposed on the plant height value (**hautbase_p** + *E*). Thereby, in the first stage, the shape of the plant evolves isotropically. Once the **hautmax_p** value is reached, the only way in which the shape can evolve is in terms of width. Height and width can also be limited by topping.

9.2.2 Intercrop

In intercropping systems (see 2.2.3 for more information on the conceptual framework), the objective is to estimate, on a daily time step, the part of the radiation intercepted by the dominant crop and the part transmitted to both components of the understorey crop: the shaded (*rombre*) and the sunlit (*rsoleil*). To solve this problem, STICS uses the most complex method for radiation transfers within the canopy (see details in § 9.2.1.2). While the basic level of calculation for sole crops is the soil, for intercropping, it is the top of the understorey canopy. On a daily time step, the shaded part of the understorey canopy corresponds to the vertical projection of the dominant foliage at the soil surface. The elementary pixel for calculation consists of the *largeur*/2 part of the dominant crop (see § 9.2.1.2.2 and Figure 9.2), the shaded surface of the understorey crop (*surf(ao)*) and the sunlit surface of the understorey crop (*surf(as)*) (Figure 9.5).

9.2.2.1 Radiation intercepted by both crops

The radiation intercepted by the dominant crop and its complementary part transmitted to the understorey canopy must be calculated using the radiation transfer formalisms, using the series of equations and crop geometry given in § 9.2.1.2. Those equations lead to the simple calculations of *rombre* and *rsoleil*, assuming a discretisation of the inter-row distance of 20 points.

Thus, for 20 points spread equally along the inter-row, *XSH* points are on the shaded part of the understorey crop, and *rombre* (Eq. (9.11)) is the average value for those *XSH* points of the transmitted radiation (which is the sum of the radiation not intercepted by the dominant crop (*rdroit*), and the transmitted radiation through the dominant crop (*rtransmis*), while *rsoleil* is the complementary value for the 20 – *XSH* points (Eq. (9.11); see Eq. (9.4) and Eq. (9.3) for *rdroit* and *rtransmis* calculations).

$$\begin{aligned}
 \textit{rombre}(t) &= \frac{1}{XSH} \cdot \sum_{X=1}^{XSH} (\textit{rdroit}(t, X) + \textit{rtransmis}(t, X)) \\
 \textit{and} \\
 \textit{rsoleil}(t) &= \frac{1}{20-XSH} \sum_{X=1}^{20-XSH} (\textit{rdroit}(t, X) + \textit{rtransmis}(t, X)) \quad (9.11)
 \end{aligned}$$

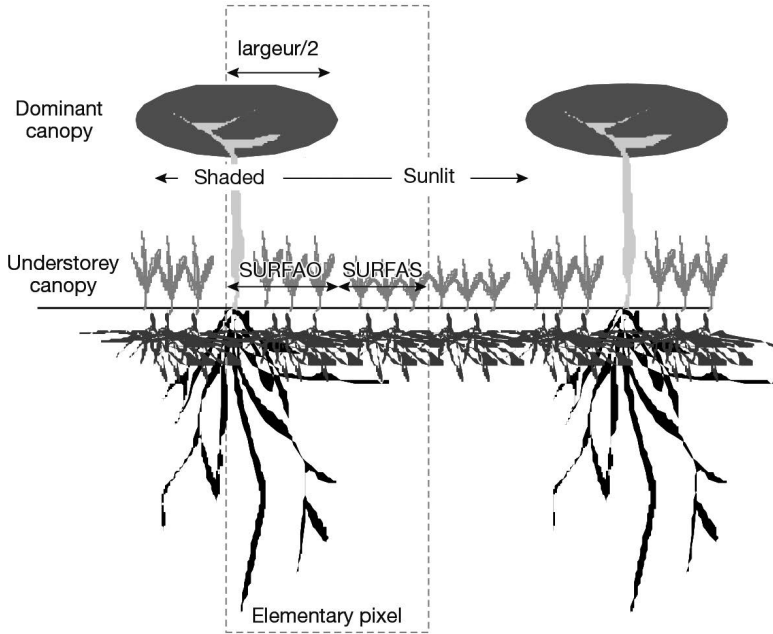


Figure 9.5. Simplified representation of an elementary pixel of the system. $largeur/2$ represents the half-width of the dominant crop part, SURFAO represents the shaded surface of the understorey crop part, and SURFAS represents the sunlit surface of the understorey crop part of this elementary pixel.

The proportion of income radiation intercepted by the dominant ($fapar_D$) and the understorey crop ($fapar_U$) can then be easily obtained from Eq. (9.11) coupled to Eq. (9.1) (Beer's law analogue applied to the understorey crop) (Eq. (9.12)).

$$fapar_D(t) = 1 - ombre(t) \cdot surf(ao)(t) + rsoleil(t) \cdot surf(as)(t)$$

and

$$fapar_U(t) = \frac{raint_U(t,AO) \cdot surf(ao)(t) + raint_U(t,AS) \cdot surf(as)(t)}{parsurg_c.trg(t)} \quad (9.12)$$

The $fapar$ of both crops greatly depends on their respective heights, which not only depend on the plant characteristics but also on the growth conditions as demonstrated in Figure 9.6.

9.2.2.2 (Inter)crop geometry

When both canopies (dominant and understorey) are vertically mixed, the sole upper part of the dominant crop, located above the understorey crop, is accounted for in the radiative transfer calculations. Accordingly, an efficient shape is defined for the dominant crop; in the case of the 'upside down' triangle, the efficient shape is trapezoidal but it is assumed to be rectangular to simplify the geometrical calculations.

To allow inversion of dominancy of both crops, the intercrop plant status (dominant or understorey) is based on the respective plant heights, which can change several times throughout the growing cycle as a function of growth rates of each crop.

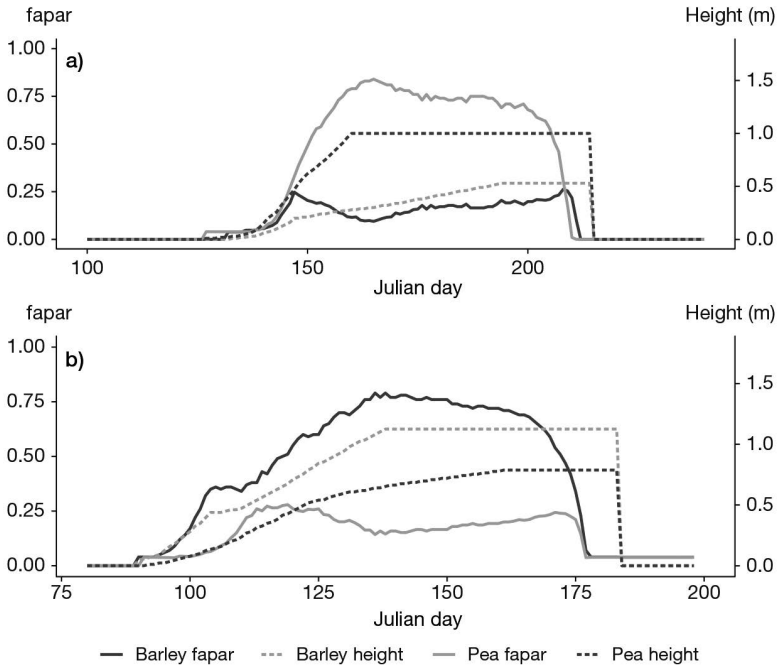


Figure 9.6. Comparison of pea-barley intercrops in Denmark a) and France b) in terms of respective crop heights (hauteur) and proportion of intercepted radiation (fapar).

►► 9.3 Energy budget and crop temperature

9.3.1 Calculation of net radiation

Net radiation (Eq. (9.13)) takes into account both the surface albedo (albedolai) applied to solar radiation (trg), and long wave radiation (Rglo).

$$rnet(t) = (1 - albedolai(t)) \cdot trg(t) + Rglo(t) \quad (9.13)$$

9.3.1.1 Albedo

The surface albedo (albedolai; Eq.(9.14)) varies between the soil value (albsol) and the vegetation value (**albveg_C**) which is equal to 0.23 (Ritchie, 1985).

$$albedolai(t) = \mathbf{albveg}_C - (\mathbf{albveg}_C - \mathbf{albsol}(t)) \cdot e^{(-0.75lai(t))} \quad (9.14)$$

The soil albedo (albsol) varies as a function of soil type (**albedo_S** of dry soil), moisture in the surface layer (Figure 9.7), and the presence of any plastic or plant cover (see § 11.4.7). It decreases linearly with the water content of the surface layer (hur (1)) according to a relationship established from experimental results obtained for different types of soil (hucc (1) and humin (1) being the water content at field capacity and wilting point, respectively). The albedo of the plastic or plant cover (**albedomulchplastique_T** and **albedomulchresidus_G**, respectively), is taken into account, as well as the proportion of soil cover (parameter **couvermulchplastique_T** for a plastic cover, and variable **couvermulch(t)** for a plant cover).

$$albsol(t) = albedo_s \cdot \left(1 - 0.517 \cdot \frac{hur(t,1) - humin(1)}{hucc(1) - humin(1)}\right) \cdot (1 - couvermulch(t)) + albedomulch \cdot couvermulch(t)$$

and

$$hur(t, 1) \geq humin(1) \longrightarrow hur(t, 1) = humin(1)$$

$$hur(t, 1) \leq hucc(1) \longrightarrow hur(t, 1) = hucc(1) \quad (9.15)$$

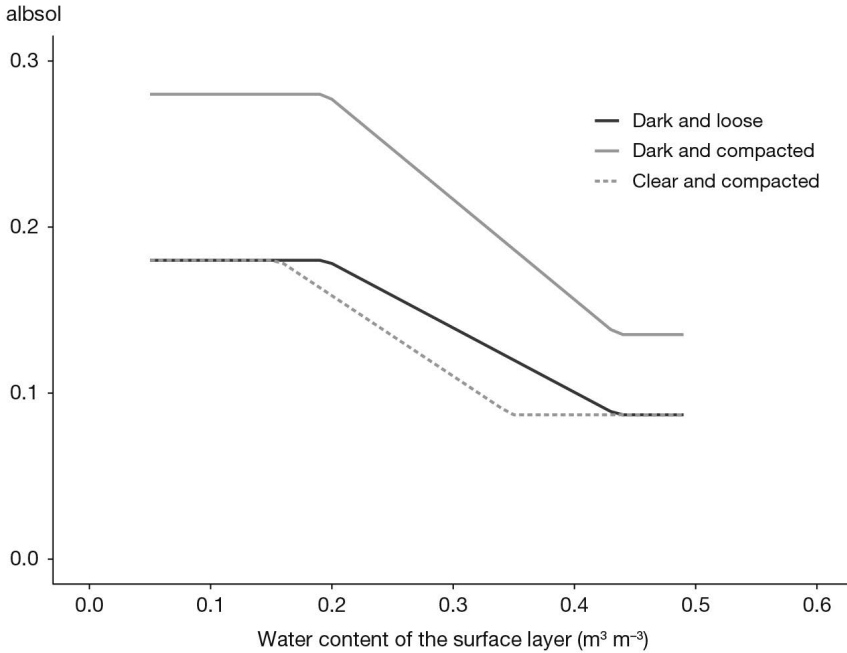


Figure 9.7. Variation in a loam-sandy soil albedo based on its surface characteristics: water content, colour (dry albedo of 0.18 for a dark soil or 0.28 for a light soil) and bulk density (1.2 for a loose soil or 1.5 for a compacted soil).

9.3.1.2 Long wave radiation

Two formulas are proposed to calculate long wave radiation (R_{glo} in MJ m^{-2}) based on crop temperature (t_{cult} in $^{\circ}\text{C}$), the insolation fraction ($fracinsol$) and the vapour pressure (tpm in mbars). Brunt's formula (Brunt, 2007), given in Eq. (9.16), is used in many applications such as in Penman's potential evapotranspiration formula (Penman, 1948), while Brutsaert's formula (Brutsaert, 1982), given in Eq. (9.17), is considered to be more precise (Guyot, 1997). The latter clearly illustrates the soil (R_{sol}) and atmospheric (R_{atm}) components of R_{glo} using the Stefan-Boltzman law and the emissivity of the atmosphere ($emissa$).

$$R_{gld}(t) = -4.9e^{-9} \cdot (t_{cult}(t) + 273.16)^4 \cdot (0.1 + 0.9 \cdot fracinsol(t)) \cdot (0.56 - 0.08 \cdot \sqrt{tpm(t)}) \quad (9.16)$$

$$\begin{aligned}
 Rglo(t) &= Ratm(t) - Rsol(t) = 5.67 \cdot 10^{-8} \cdot (tcult(t) + 273.15)^4 \\
 &\quad \cdot (1 - emissa(t)) \cdot 3600 \cdot 24 \cdot 10^{-6} \\
 &\quad \text{and} \\
 emissa(t) &= Eabrut(t) + (1 - fracinsol(t)) \\
 &\quad \cdot (1 - Eabrut(t)) \cdot \left(1 - 4 \cdot \frac{11}{tcult(t) + 273.15}\right) \\
 &\quad \text{and} \\
 Eabrut(t) &= 1.24 \cdot \left(\frac{tpm(t)}{tcult(t) + 273.15}\right)^{\frac{1}{7}} \quad (9.17)
 \end{aligned}$$

The insolation fraction is estimated using Angström's formula (Eq. (9.18)), the parameters of which are **aangst_C** = 0.18 and **bangst_C** = 0.62. Extraterrestrial radiation (RGEX) is calculated using standard astronomic formulae (Gebet, 1993). If the vapour pressure is not available, it is estimated as the saturated vapour pressure at the temperature TDEW = tmin - **corecTrosee_C**.

$$fracinsol(t) = \frac{\frac{trg(t)}{rgex(t)} - \mathbf{aangst}_C}{\mathbf{bangst}_C} \quad (9.18)$$

The saturated vapour pressure/temperature function (TVAR: Eq. (9.19)) is represented in Figure 9.8 (see also Figure 9.9). The order of magnitude of the parameter **corecTrosee_C** is of a few degrees, from 0 for the wettest locations to 3°C for the driest ones.

$$TVAR(TDEW) = 6.1070 \cdot \left(1 + \sqrt{2} \cdot \sin\left(\frac{0.017453293 \cdot TDEW}{3}\right)\right)^{8.827} \quad (9.19)$$

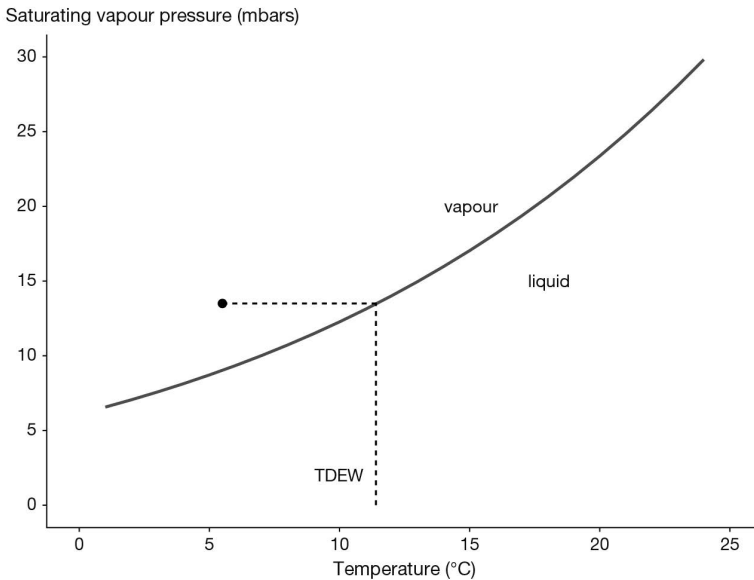


Figure 9.8. Variation in the saturated vapour pressure as a function of temperature according to Alt (1978) referred to by Guyot (1997). The water status in the air is vapour represented by the point and the temperature corresponding to the same pressure on the curve is the dew temperature (TDEW).

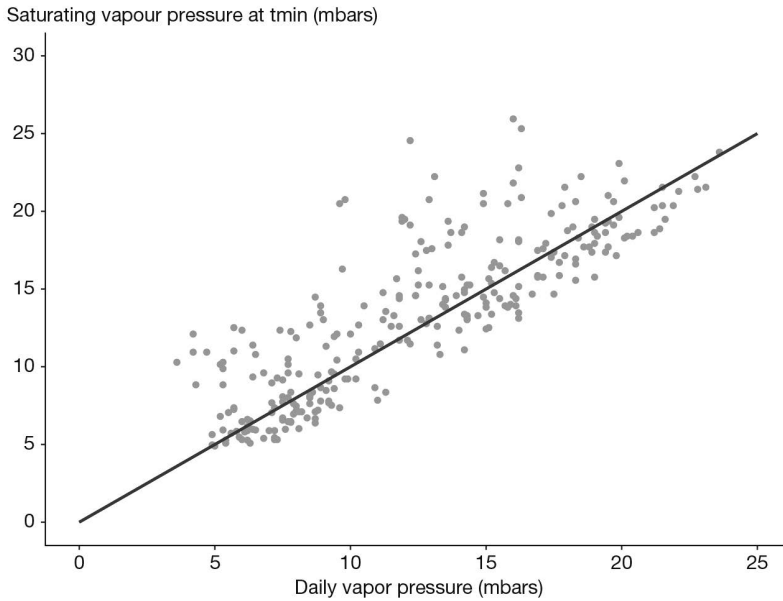


Figure 9.9. Visual evaluation of the estimate of the actual vapour pressure using the hypothesis $TDEW=t_{min}$ in Avignon, France.

In both calculations, which are compared in Figure 9.10, the crop temperature is subjected to an iterative convergence procedure (explained in § 9.3.2), meaning that these calculations need to be performed several times in succession.

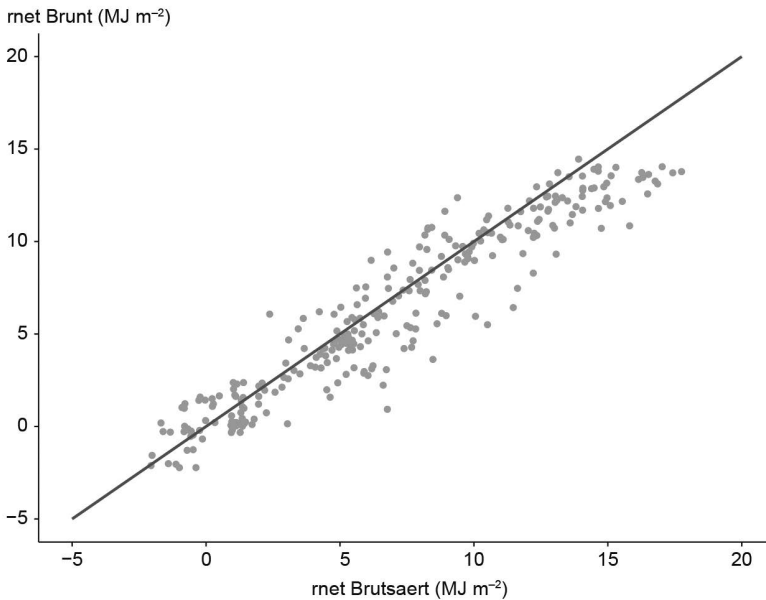


Figure 9.10. Comparison of Brunt's and Brutsaert's formulae for the calculation of net radiation in Avignon, France.

9.3.2 Calculation of crop temperature

The t_{cult} value is assumed to be the arithmetic mean of the maximum crop temperature ($t_{cultmax}$) and the minimum crop temperature ($t_{cultmin}$).

9.3.2.1 Empirical approach

This method must be used when neither wind speed nor air humidity data are available. It is based on a relationship between midday surface temperature and daily evaporation (Seguin and Itier, 1983), and allows users to calculate $t_{cultmax}$ (Eq. (9.20)) taking in account the parameterisation from Riou *et al.* (1988).

$$t_{cultmax}(t) = t_{max}(t) + \frac{\left(\frac{r_{net}(t)}{2.46} - et(t) - 1.27\right)}{\frac{1.68}{\ln\left(\frac{1}{z0(t)}\right)}}$$

$$z0(t) = 0.13 \cdot hauteur(t)$$

and

$$z0(t) \leq 0.01 \longrightarrow z0(t) = 0.01 \quad (9.20)$$

where r_{net} is the net daily radiation in $MJ\ m^{-2}$, et is the daily evapotranspiration in mm, and $hauteur$ is the canopy height (see § 9.2.1.1). The $t_{cultmax}$ value cannot be lower than t_{max} . In this approach, we assume that $t_{cultmin} = t_{min}$.

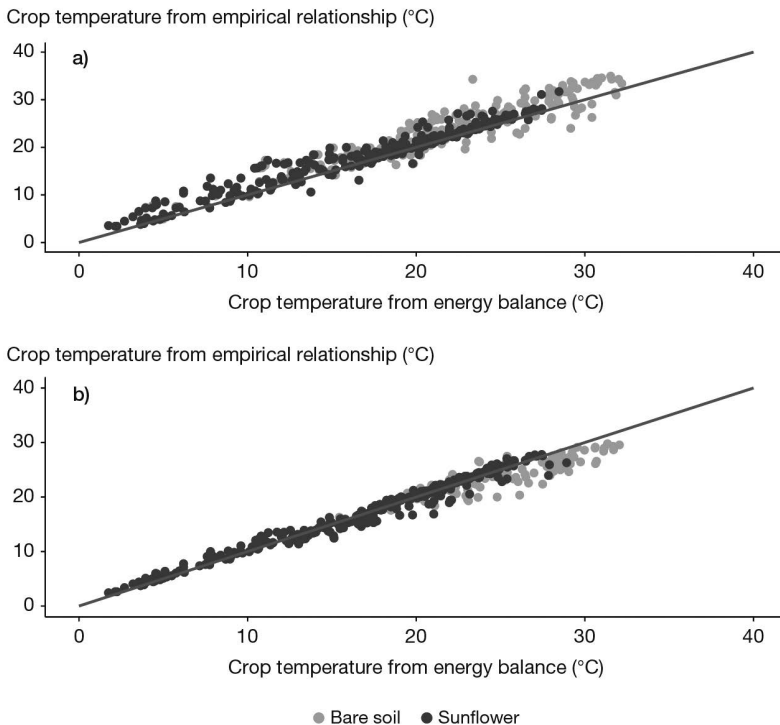


Figure 9.11. Comparison between the empirical relationship and the energy balance for the calculation of crop temperature for two different surfaces (bare soil and a sunflower crop) in Avignon, France, using two bare soil roughness factors $z0_{solnu_s}$: a) 1 mm and b) 5 mm).

9.3.2.2 Energy balance

Two instantaneous energy balances are calculated to estimate $t_{cultmax}$ and $t_{cultmin}$, which are assumed to occur at midday and at the end of the night, respectively.

$$\begin{aligned} t_{cultmax}(t) &= t_{max}(t) + \frac{r_{netmax}(t) - g_{max}(t) - et_{max}(t)}{1200} \cdot ra_{amax}(t) \\ t_{cultmin}(t) &= t_{min}(t) + \frac{r_{netmin}(t) - g_{min}(t) - et_{min}(t)}{1200} \cdot ra_{amin}(t) \end{aligned} \quad (9.21)$$

Eq. (9.21) shows the minimum and maximum values of the various fluxes: net radiation (r_{netmin} and r_{netmax}), soil heat (g_{min} and g_{max}) and evapotranspiration (ET_{MIN} and et_{max}), as well as the minimum and maximum values of the aerodynamic resistance (ra_{amin} and ra_{amax}).

To calculate long wave radiation, i) atmospheric radiation is assumed to remain constant throughout the day and is estimated using Brutsaert's formula (Eq. (9.17)), and ii) surface radiation is calculated using $t_{cultmax}$ and $t_{cultmin}$, requiring the iterative convergence procedure. At the end of the night, ET_{MIN} and rg_{min} are zero, while rg_{max} and et_{max} are estimated assuming sinusoidal changes during the day. The g_{min} value is calculated as an empirical function of the wind speed under the cover (Cellier *et al.*, 1996). The g_{max} value is assumed to be 25 % of the maximum net radiation below the cover. In addition to the canopy height (*hauteur*) and the bare soil roughness (z_{0solnu_s}), the calculation of ra_{amax} and ra_{amin} requires wind speed values (see § 11.3.2): the nighttime wind speed is assumed to be equal to 50 % of the daily mean wind speed, and the daytime wind speed is assumed to be 150 % of the daily mean wind speed.

Figure 9.11 shows the impact of surface type and soil roughness on the temperature calculation: the rougher the soil, the greater the soil evaporation. Meanwhile, Figure 9.12 shows that the energy balance method, for the minimum temperature, produces results which are identical to the driving hypothesis of the empirical method ($t_{cultmin} = t_{min}$).

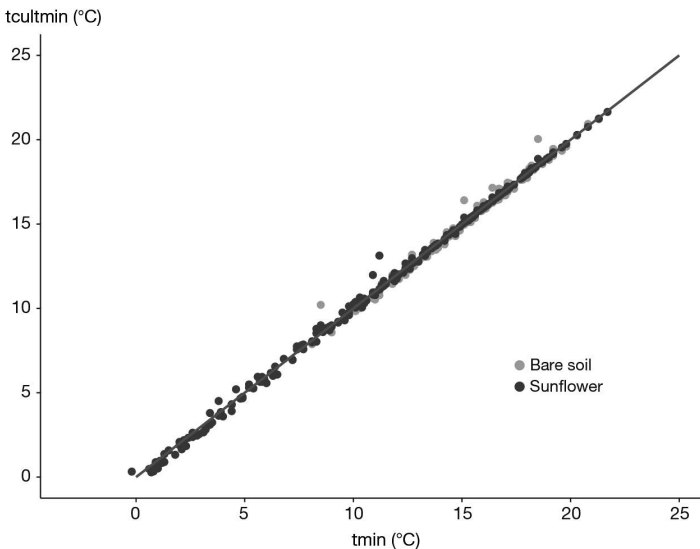


Figure 9.12. Evaluation of the assumption $t_{cultmin} = t_{min}$ by running the energy balance in Avignon, France.

9.3.2.3 Iterative calculation of $tcult$

We have seen that $tcult$ is involved in the calculation of net radiation, which in turn is used to calculate energy balances. We introduced an iterative calculation process based on a difference of 0.5°C between two iterations. In the option using the reference evapotranspiration as an input, the iterative process is only used to calculate net radiation, while in the option using Shuttleworth-Wallace the iteration also concerns estimates of water requirements (Figure 9.13).

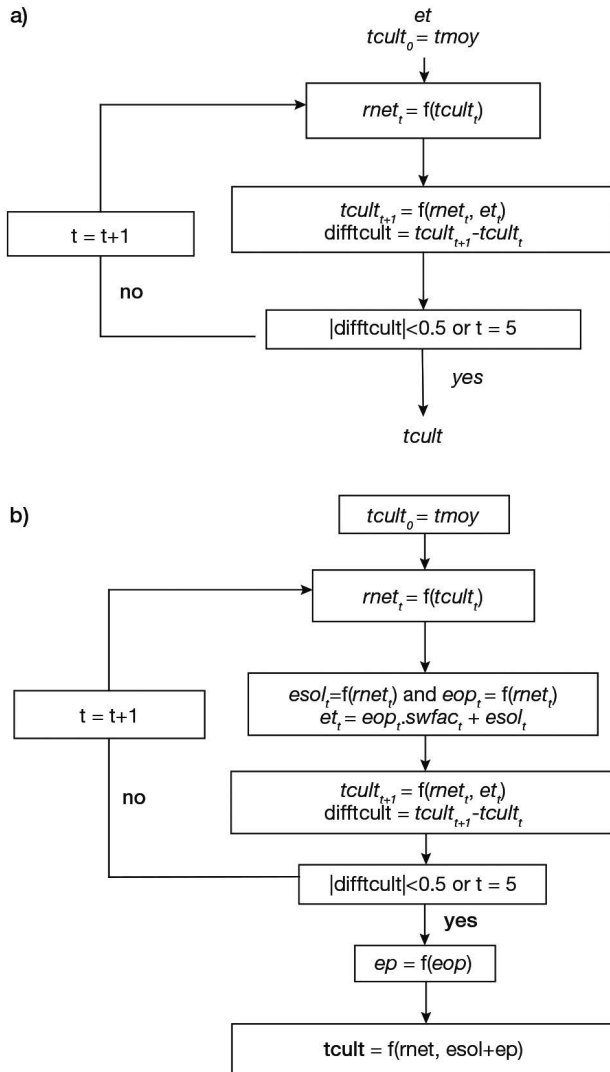


Figure 9.13. Diagrams representing the iteration loop of $tcult$ calculations implementing a test on the value of $diffcult$ for each option: a) reference evapotranspiration and b) Shuttleworth and Wallace. $diffcult$ is the variation of $tcult$ between two successive days, eop is the maximum plant transpiration, EP the actual plant transpiration, $SWFAC$ the EP/eop ratio from the previous day, and $esol$ the actual soil evaporation.

9.3.3 Calculating the energy budget using the resistance approach

The calculations are based on the resistance scheme shown in Figure 9.14 and involving four flows: i) soil evaporation (e_{sol}), ii) maximum plant transpiration (e_{op}), iii) direct evaporation of water intercepted by the foliage (E_{md}) or mulch (e_{mulch}), and iv) two types of resistance: resistance to diffusion between the canopy and soil (r_{as}) and the cover and reference level (r_{aa}), and the surface resistance of canopy (r_c) and canopy boundary layer (r_{ac}). All the fluxes are actual ones except the plant transpiration flux, which is the maximum one (whether or not it is actual).

Each flux is calculated using the same type of formula as for the potential soil evaporation (Eq. (11.3), see § 11.2.1), resulting in Eq. (9.22), (9.23) and (9.24).

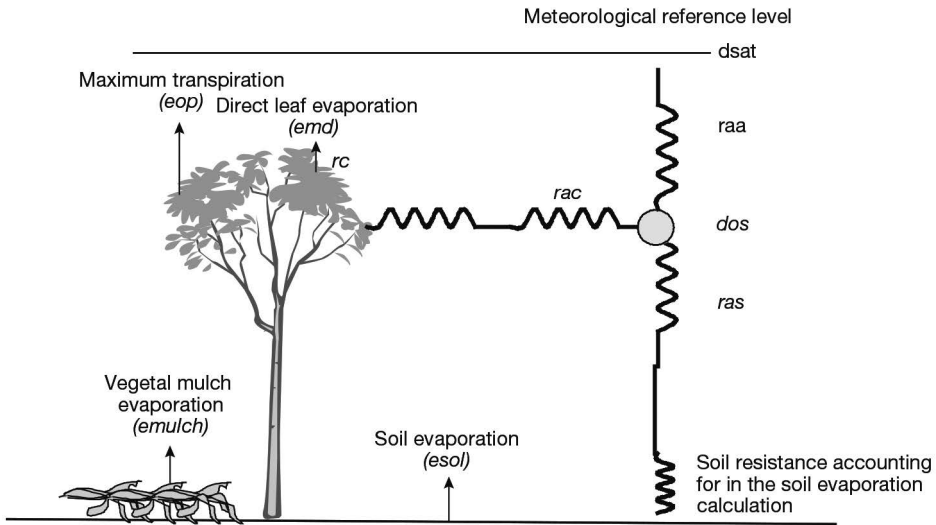


Figure 9.14. Drawing of the resistance scheme applied to the soil crop system (adapted from Brisson *et al.*, 2004).

– Limited by mouillmulch:

$$e_{mulch}(t) = \frac{\text{deltat}(t) \cdot r_{netS}(t) + 105.03 \cdot \frac{dos(t)}{ras(t)}}{L \cdot (\text{deltat}(t) + \text{gamma})} \cdot \text{couvermulch}(t) \quad (9.22)$$

– Limited by mouill:

$$E_{md}(t) = \frac{\text{deltat}(t) \cdot R_{NETP1}(t) + 105.03 \cdot \frac{dos(t)}{rac(t)}}{L \cdot (\text{deltat}(t) + \text{gamma})} \quad (9.23)$$

and:

$$e_{op}(t) = \frac{\text{deltat}(t) \cdot r_{netp2}(t) + 105.03 \cdot \frac{dos(t)}{rac(t)}}{L \cdot (\text{deltat}(t) + \text{gamma} \cdot \left[1 + \frac{rc(t)}{rac(t)}\right])} \quad (9.24)$$

The amount of energy required for the direct evaporation of water on leaves (Emd) is RNETP1 while this energy used for direct evaporation must be deducted to evaluate the resulting energy available for transpiration (RNETP2). Energy distribution between bare soil and the soil cover (mulch) depends on couvermulch (Eq. (9.22)), with mouill being the water retained on the foliage and mouillmulch the water retained by the vegetal mulch. The deltat value is the gradient of the relationship between saturation vapour pressure and temperature, rnetS is the net radiation at the soil surface, and γ is the psychrometric constant (mbar °C⁻¹). The dos variable is the saturation deficit within the vegetation and links all the fluxes. It is calculated (Eq. (9.25) using the method by Shuttleworth and Wallace (1985).

$$dos(t) = dsat(t) + (deltat(t) \cdot rnet(t) - (deltat(t) + \gamma) \cdot L(t) \cdot EVAPO(t)) \cdot \frac{raa(t)}{105.03} \quad \text{with}$$

$$EVAPO(t) = esol(t) + emulch(t) + Emd(t) + eop(t) \quad (9.25)$$

where dsat is the air saturation deficit (mbar); rnet (MJ m⁻²) is the net daily radiation; L is the latent heat of vaporisation (MJ kg⁻¹); raa is the aerodynamic resistance between the canopy and the reference height of weather measurements (z_{rC} generally 2 m) calculated from the canopy height and wind speed (see § 11.3); EVAPO is the total transpiration and evaporation; esol, emulch and emd are evaporation (in mm) from soil, mulch, and free water on leaves, respectively; and eop is the daily maximum plant transpiration flux (in mm).

Eq. (9.25) is very similar to Eq. (9.37) (see § 9.4.1), except that the evaporative term EVAPO implies a **potential** transpiration flux: EVAPO is the accumulation of transpiration fluxes eop and all the direct evaporation fluxes, i.e. esol, Emd and emulch. The value of this direct evaporation affects dos and can cause the evaporative demand of the plant to fluctuate. The three components of the direct evaporation are calculated from an intermediate value of the saturation deficit dos based on the hypothesis that, at complete saturation of the surfaces, the evaporation can be treated using a Priestley-Taylor type formalisation (Brisson *et al.*, 1998a).

To solve the above equations, several terms must be calculated: i) the distribution of the energy sources between the soil and the plants (rnetS, RNETP and RNETP), ii) the water retention on the foliage and in the mulch (Emd and emulch), iii) the resistances to diffusion (raa and ras), and iv) the surface resistances (rc and rac) (see § 9.3.3.3), and v) the soil evaporation (esol).

9.3.3.1 Available energy and its distribution

The calculation of the whole surface net radiation was described in § 9.3.1. To evaluate the distribution of this available energy between the soil and the plants, we use the fraction of PAR intercepted by the plants (fapar) calculated using the raint variable (Eq. (9.26)). Thornley (1996) inferred the net radiation extinction coefficient from the extinction coefficient of the total radiation by applying a coefficient of 0.83, which corresponds to the range of measurements under a soya bean canopy (Brisson *et al.*, 1998a).

$$\begin{aligned} \text{RNETP1} &= 0.83 \cdot f_{\text{apar}} \cdot r_{\text{net}}(t) \\ \text{and } f_{\text{apar}} &= \frac{r_{\text{ain}}(t)}{\text{parsurr}_{\text{g}_c \cdot \text{tr}_g(t)} \\ r_{\text{netS}} &= r_{\text{net}}(t) - \text{RNETP1} \\ \text{RNETP2} &= \text{RNETP1} - E_{\text{md}}(t) \quad (9.26) \end{aligned}$$

9.3.3.2 Calculation of resistances to diffusion

We have adopted the formalisations proposed by Shuttleworth and Wallace (1985), which are described in detail in Brisson *et al.* (1998a). The characteristic lengths, bare soil roughness ($z0_{\text{solnu}_s}$), crop roughness (z) and displacement height (dh) are usually estimated as a function of the canopy height (*hauteur*), when plants are present, and as a fixed value for bare soil (Eq. (9.27)).

$$\text{For a plant stand: } z0(t) = 0.10 \cdot \text{hauteur}(t)$$

$$\text{For a bare soil stand: } z0(t) = z0_{\text{solnu}_s} \quad \text{and} \quad dh(t) = 6.6 \cdot z0(t) \quad (9.27)$$

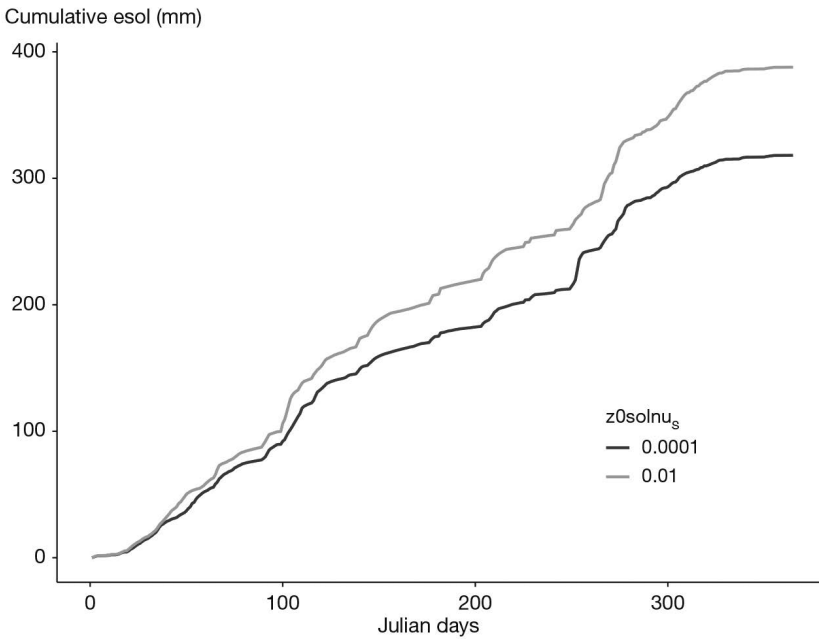


Figure 9.15. Influence of soil roughness ($z0_{\text{solnu}_s}$ in m) on the cumulative soil evaporation over one year in the region of Avignon, France.

The bare soil value of roughness can vary from 10^{-2} for very rough ploughing to 10^{-4} m for a very flat soil surface. Figure 9.15 shows the effect of this parameter on soil evaporation: the greater the roughness, the higher the soil evaporation in the given example, the annual difference between extreme values is about 70 mm. The reference height taken for meteorological data is 2 m. If the plant canopy height exceeds this threshold, a wind speed value is recalculated at a reference height of over 2 m (parameter zr_C) by

applying a logarithmic profile. The other meteorological values are not recalculated. The calculations of diffusive resistances are different for bare soil (Eq. (9.28)) and cover crops (Eq. (9.30) for $lai \geq 4$), while for non-cover crops ($0 < lai < 4$) an LAI-dependent linear combination of the two first values is used (Eq. (9.29)). They all depend on wind speed ($tvent$).

$$\begin{aligned}
 & \text{For } lai(t) = 0 \\
 & ras_0(t) = \frac{\ln\left(\frac{zr_c}{z0solnu_s}\right) \ln\left(\frac{z0(t)+dh(t)}{z0solnu_s}\right)}{0.41^2 \cdot tvent(t)} \\
 & raa_0(t) = \frac{\ln\left(\frac{zr_c}{z0solnu_s}\right)^2}{0.41^2 \cdot tvent(t)} - ras_0(t)
 \end{aligned}
 \tag{9.28}$$

$$\begin{aligned}
 & \text{For } 0 \leq lai(t) < 4 \\
 & ras(t) = \frac{1}{4}(lai(t) \cdot ras_\infty(t) + (4 - lai(t)) \cdot ras_0(t)) \\
 & raa(t) = \frac{1}{4}(lai(t) \cdot raa_\infty(t) + (4 - lai(t)) \cdot raa_0(t))
 \end{aligned}
 \tag{9.29}$$

$$\begin{aligned}
 & \text{For } lai(t) \geq 4 \\
 & ras_\infty(t) = \frac{\ln\left(\frac{zr_c-dh(t)}{z0(t)}\right)}{0.41^2 \cdot tvent(t)} - \frac{hauteur(t)}{2.5(hauteur(t)-dh(t))} \cdot \\
 & \left(12.18 - \exp\left(2.5 \cdot \left(1 - \frac{dh(t)+z0(t)}{hauteur(t)}\right)\right)\right) \\
 & raa_\infty(t) = \frac{\ln\left(\frac{zr_c-dh(t)}{z0(t)}\right)}{0.41^2 \cdot tvent(t)} \cdot \\
 & \left(\ln\left(\frac{zr_c-dh(t)}{hauteur(t)}\right) + \frac{hauteur(t)}{2.5(hauteur(t)-dh(t))} \cdot \right. \\
 & \left. \exp\left(2.5 \cdot \left(1 - \frac{dh(t)+z0(t)}{hauteur(t)}\right) - 1\right)\right) \tag{9.30}
 \end{aligned}$$

9.3.3.3 Calculation of surface resistances

To simplify calculations, the resistance of the canopy boundary layer (rac ; Eq. (9.31)) is solely a function of the leaf area index of the canopy:

$$rac(t) = \frac{50}{2 \cdot lai(t)} \quad \text{with a lower threshold at } rac(t) = 12.5 \text{ sm}^{-1} \tag{9.31}$$

The canopy resistance (rc ; Eq. (9.32)) is the product of four factors:

$$rc(t) = r\mathit{smi}n_p \cdot \frac{0.5 \cdot lai(t) + 1}{lai(t)} \cdot (0.039 \cdot dsat(t) + 0.45) \cdot \frac{28}{2.5 + trg(t)} \cdot fco2s \tag{9.32}$$

where $r\mathit{smi}n_p$ is the minimal stomatal resistance of leaves, $dsat$ (in mbars) is the saturation deficit, trg (in $\text{MJ m}^{-2} \text{ s}^{-1}$) is the global radiation and $fco2s$ is a CO_2 dependent variable.

Due to the daily time step, the parameter $rsmin_p$ cannot be inferred from the instantaneous values of measurements but must be obtained using a top-down approach (Brisson *et al.*, 1998a; Tolk *et al.*, 1996; Baldocchi *et al.*, 1991). Values of 250, 215 and 220 sm^{-1} were found for soybean, maize and sorghum respectively (Brisson *et al.*, 1998a; Brisson *et al.*, 2004). The sensitivity of ep to those variables are shown in Figures 9.16 and 9.17

The ‘saturation deficit’ and ‘radiation’ components are taken from research by Stockle and Kjelgaard (1996). With regard to the conditions for applying the proposed formulae, the saturation deficit is calculated at the meteorological scale and the radiation is the incident radiation above the crop.

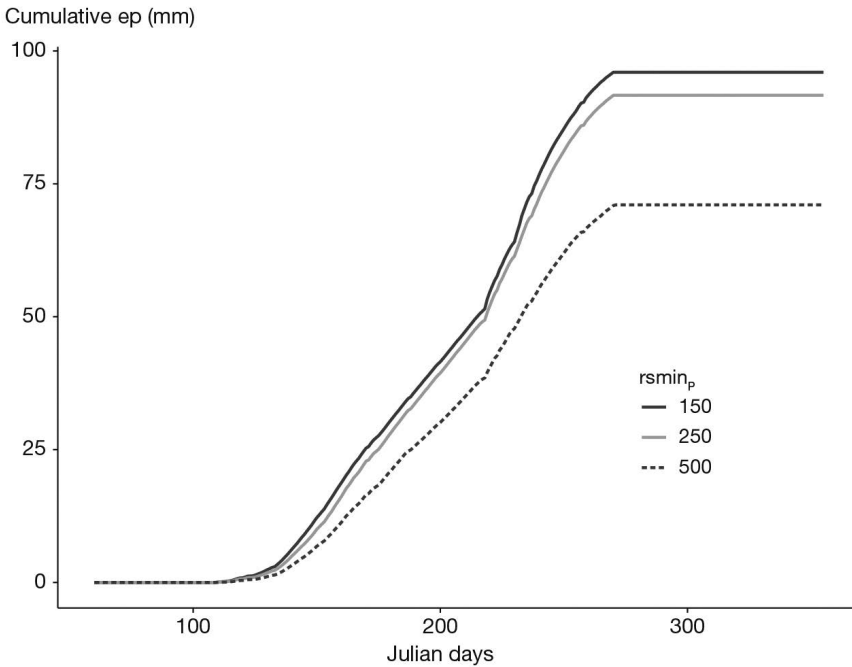


Figure 9.16. Influence of the minimal stomatal resistance ($rsmin_p$ in $m s^{-1}$) on the cumulative transpiration of a rainfed vineyard in Avignon, France.

If the atmospheric CO_2 is high, stomatal conductance falls. Idso (1991) demonstrated the existence of proportionality between the CO_2 effect on conversion efficiency and the CO_2 effect on stomatal conductance, at a ratio of 2.5 for the addition of 300 ppm in the nominal concentration. Furthermore, Stockle *et al.* (1992) proposed a species-dependent formalisation (Figure 9.18). We propose combining these two approaches to take into account the species and ensure a continual effect of CO_2 (Eq. (9.33)). The $fco2$ value is the species-dependent CO_2 effect on conversion efficiency (Eq. (4.20)), which affects the value of the species-dependent factor on stomatal closure ($fco2s$).

$$fco2s = \frac{1}{1 + 0.77 \left(1 - \frac{fco2}{2.5}\right) \cdot \left(1 - \frac{CO_2}{330}\right)} \quad (9.33)$$

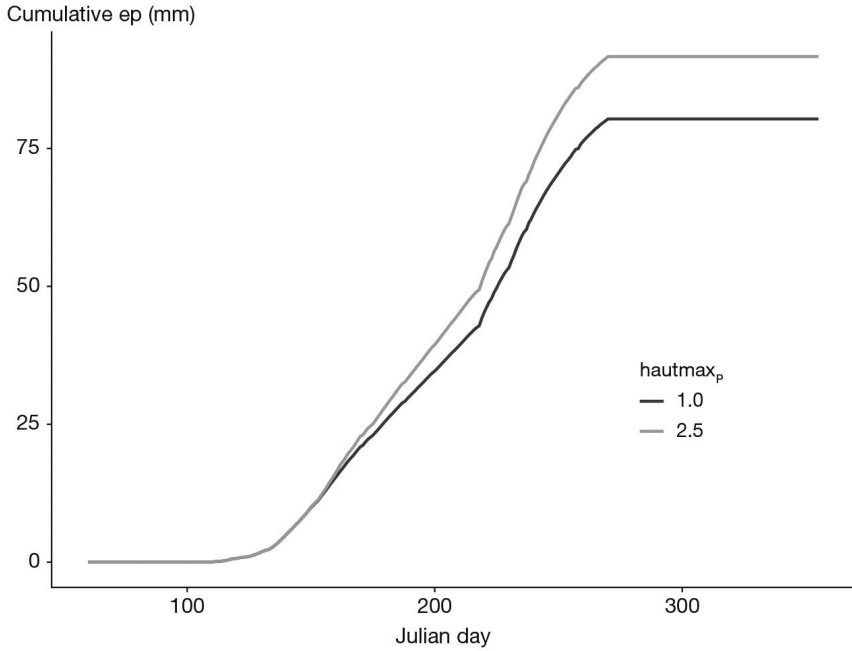


Figure 9.17. Influence of the plant maximum height ($hautmax_p$ in m) on the cumulative transpiration of a rainfed vineyard in Avignon, France.

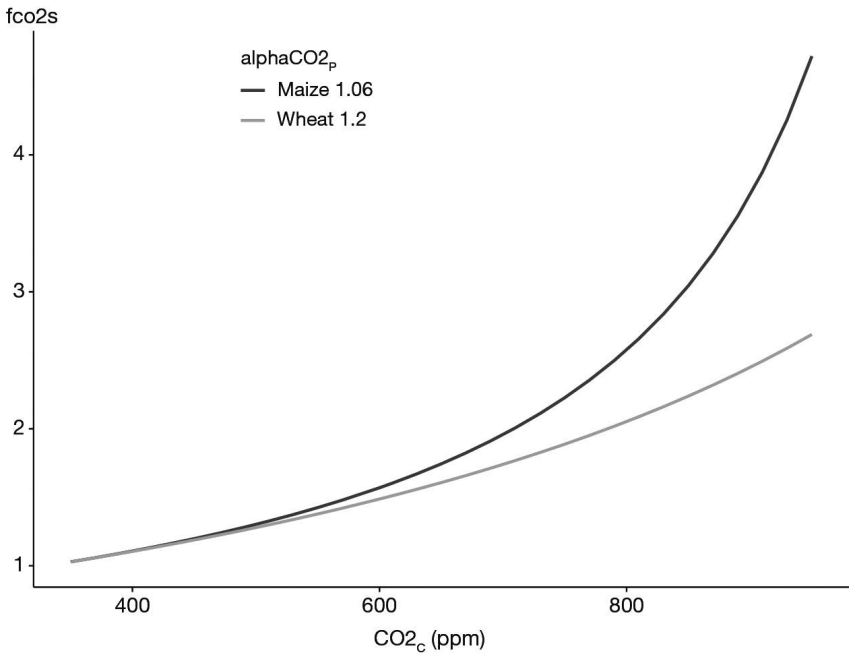


Figure 9.18. Influence of the species on the stomatal resistance CO_2 dependent effect.

9.3.4 Intercrop

To simulate intercropping, the later energy budget, calculated using the ‘resistance approach’ option is used to estimate the crop water requirement. This approach is particularly relevant for intercrops because it allows for microclimatic effects on water requirements: convection beneath the dominant canopy and a decrease in the vapour pressure deficit due to transpiration from the understorey plants. Actual soil evaporation and plant transpiration are then calculated independently by means of a soil water balance (see § 11.2 and 11.5). These fluxes are then re-introduced into the energy budget to calculate crop temperature, which is a driving variable for plant growth and development (see § 3, 4, and 5). The required adaptations for intercrops concern the first stage.

9.3.4.1 Theoretical basis

Following the relative position of the dominant and the understorey crops, the energy budget calculations rely on slightly different resistance networks (Figure 9.19). This simplification aims to limit the number of sites playing the role of water vapour sources to just two. The resistance scheme for a low understorey crop (Figure 9.19a) was extrapolated from the original model by Shuttleworth and Wallace (1985), and the resistance scheme for a high understorey crop (Figure 9.19b) was extrapolated from the model proposed by Wallace (1995) for intercrops. Those two schemes are applied at a daily time step relying on Monteith’s theory (Monteith, 1965) and its consequences (Allen *et al.*, 1994), as well as on a previous study (Brisson *et al.*, 1998a) in which full details of definitions and formulations are given.

The calculations involve five evaporative fluxes, three net radiation budgets, and three types of resistance. The five evaporative fluxes are i) soil evaporation (e_{sol}), ii) maximum plant transpiration for the dominant crop (e_{op_D}), iii) maximum plant transpiration for the understorey crop (e_{op_U}), iv) direct evaporation of the water intercepted by the “dominant” leaves (emd_D) and v) direct evaporation of the “understorey” leaves (emd_U). The three net radiation budgets are i) the net radiation for the soil r_{netS} , ii) the net radiation for the dominant crop r_{netP_D} and iii) the net radiation for the understorey crop r_{netP_U} . The three types of resistance are i) the eddy diffusion resistances r_{as} and r_{aa} , ii) the bulk boundary layer resistances of both crops R_{AC_D} and R_{AC_U} and iii) the surface resistances: soil resistance is accounted for in the soil evaporation calculation, r_{c_D} , and r_{c_U} . Each flux is calculated using a formula such as those given in Eq. (9.24) and (9.25) (Brisson *et al.*, 2004). Combining the three subsystems (soil and both crops) into two requires varying the bulk boundary layer resistance applied to the lower level: either ($R_{AC_U} + r_{as}$) for the low configuration or R_{AC_U} for the high configuration of the understorey crop.

9.3.4.2 Available energy and its distribution in intercropping systems

To evaluate the distribution of available energy between the soil and both crops, we have based our method on the hypothesis that we know the proportion of global radiation intercepted by the crops (f_{apar_D} and f_{apar_U} , see Eq. (9.12)). In the case of intercrops, the net radiation corresponding to plants (R_{NETP1} in Eq. (9.34)) consists of the net radiation of the dominant and understorey crops, r_{netP_D} and r_{netP_U} respectively (Eq. (9.34)).

$$\begin{aligned}
 RNETP1(t) &= rnetP_D(t) + rnetP_U(t) \\
 &= 0.83 \cdot fapar_D(t) \cdot rnet(t) + 0.83 \cdot fapar_U(t) \cdot rnet(t) \quad (9.34)
 \end{aligned}$$

But the energy actually available for crop transpiration must also account for possible direct water evaporation from the leaves.

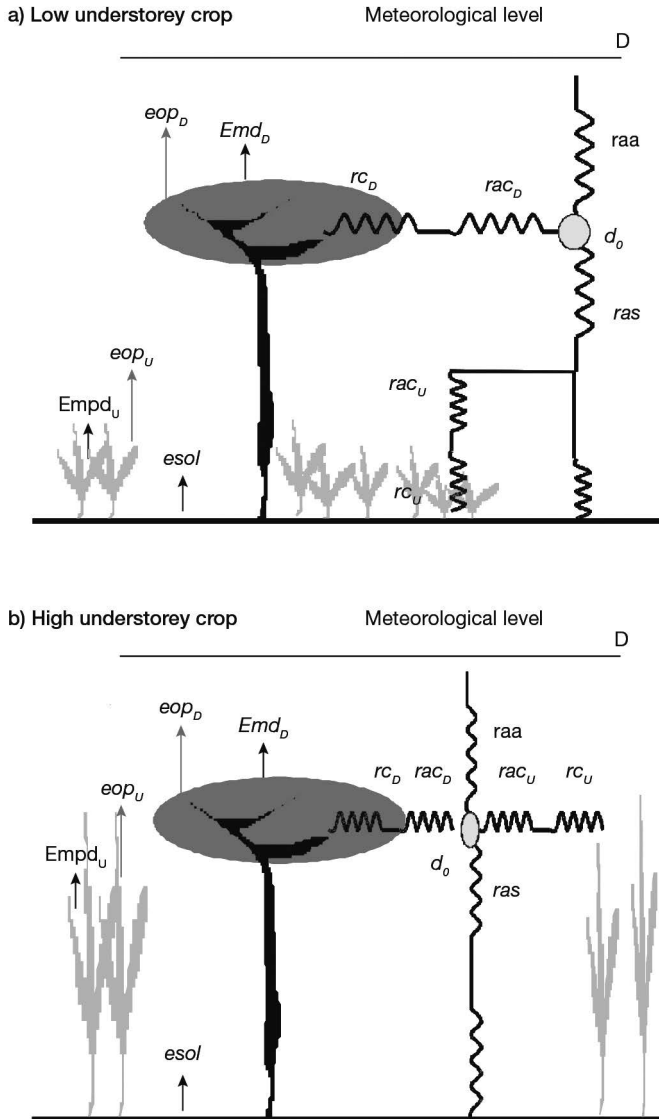


Figure 9.19. The two possible schemes of resistance networks used to estimate water requirements for intercropping (right-hand side of the schemes) and the fluxes (left-hand side of the schemes). a) The understorey crop is near the ground, b) the understorey crop is nearly as high as the dominant crop (adapted from Brisson *et al.*, 2004).

9.3.4.3 Water persistence on foliage

Most crop models do not usually include the simulation of rainfall interception, although it is an important process in forestry models (Bussière, 1995). A common idea is that evaporation of intercepted water offsets the decrease in evaporative demand exactly, especially for herbaceous canopies (McMillan and Burgy, 1960). With regard to intercrops, the processes are more complex and the abovementioned offsetting is not very likely; offsetting depends on rain events, evaporative demand and intercrop structure. It would seem worthwhile to include these processes in an intercrop model to correctly predict water use by canopies, especially in humid tropical climates (high evaporative demand combined with frequent rainfall). The objective of simulating stemflow and direct water evaporation from leaf surfaces is to correctly evaluate the amount of water that will reach the soil rather than to partition water between the two crops. Indeed, once the water is in the soil, it is assumed to be evenly available for both root systems, which overlooks the horizontal variability of soil water content.

To account for these processes, water persistence and direct evaporation from the dominant (emd_D) and understorey (emd_U) crop foliage as well as the stemflow along the dominant stems are simulated as described in § 13.4.2 and 11.3. Another value of net radiation is then obtained (RNETP2) using Eq. (9.34).

9.3.4.4 Specific considerations when calculating the eddy diffusion resistance (raa and ras)

Specific aspects that must be considered regarding the application to intercropping are the crop and soil roughness (z and zs) and the displacement height (DH), which are evaluated as follows:

For the low understorey crop (Eq. (9.35); see Figure 9.19a):

$$\begin{aligned} DH(t) &= 0.66 \cdot hauteur_D(t) \\ z0(t) &= 0.10 \cdot hauteur_D(t) \\ z0S(t) &= 0.10 \cdot hauteur_U(t) \end{aligned} \quad (9.35)$$

For the high understorey crop (Eq. (9.36); see Figure 9.19b):

$$\begin{aligned} DH(t) &= 0.66 \cdot \left(hauteur_U(t) + \frac{hauteur_D(t) - hauteur_U(t)}{2} \right) \\ z0(t) &= 0.10 \cdot \left(hauteur_U(t) + \frac{hauteur_D(t) - hauteur_U(t)}{2} \right) \\ z0S(t) &= z0solnu_s \end{aligned} \quad (9.36)$$

where $hauteur_D$ and $hauteur_U$ are the heights of the dominant and the understorey crops respectively. The threshold height for the low understorey crop is arbitrarily fixed at 0.2 m. The reference height taken from meteorological data is 2 m. If the plant canopy height exceeds this threshold, a wind speed value is recalculated at a reference height of over 2 m by applying a logarithmic profile. The other meteorological values are not recalculated.

9.3.4.5 Surface resistances

The resistances of the boundary layers are calculated for dominant and understorey crops as functions of the leaf area index of each crop, as described for a sole crop in Eq. (9.31). Concerning the canopy resistances (Eq. (9.32)), the saturation deficit is the same for both crops, corresponding to the **D0** level (Figure 9.19), while the incident radiations differ for each crop.

►► 9.4 Canopy moisture

9.4.1 Daily average

The saturation deficit within the canopy (*dos* in mbars, Eq. (9.37)) can be calculated using the Shuttleworth-Wallace formula (Shuttleworth and Wallace, 1985) and the sum of evaporation fluxes (evaporation from soil, mulch, free water on leaves and transpiration). If the resistance approach is not activated, a default value of the aerodynamic resistance is used, which is supposed to be constant and depends on the location of the weather station.

$$dos(t) = dsat(t) + (deltat(t) \cdot rnet(t) - (deltat(t) + \gamma(t)) \cdot L(t) \cdot EVAP(t)) \cdot \frac{raa(t)}{105.03}$$

with

$$\begin{aligned} dsat(t) &= TVAR(TAIR(t)) - tpm(t) \\ deltat(t) &= TVAR(TAIR(t) + 0.5) - TVAR(TAIR(t) - 0.5) \\ EVAP(t) &= esol(t) + emulch(t) + emd(t) + ep(t) \\ L(t) &= (2500840 - 2358.6 \cdot TAIR(t)) \cdot 10^{-6} \\ \gamma &= 0.65 \cdot \frac{PATM_c}{1000} \quad \text{and } PATM_c \text{ in mbars} \end{aligned} \quad (9.37)$$

where *deltat* is the gradient of the relationship between saturation vapour pressure and temperature; *tair* (°C) is the average daily temperature; *rnet* (MJ m⁻²) is the net daily radiation; *L* is the latent heat of vaporisation (MJ kg⁻¹); γ is the psychrometric constant (mbar °C⁻¹) depending on atmospheric pressure **patm_C**; *dsat* is the air saturation deficit (mbar); *TVAR* is the saturated vapour pressure based on the temperature (mbar) (see § 9.3.1.2); *raa* is the aerodynamic resistance between the canopy and the reference height of weather measurements (**zr_C** generally 2 m) calculated from the canopy height and wind speed (see § 11.3); *esol*, *emulch* and *emd* are evaporation (in mm) from soil, mulch, and free water on leaves, respectively; and *ep* is plant transpiration (in mm).

The average daily moisture (*humidite*) is then calculated based on the crop temperature (Eq. (9.38)):

$$humidite(t) = \frac{TVAR(tcult(t)) - dos(t)}{TVAR(tcult(t))} \quad (9.38)$$

If the wind speed weather variable is not available, a default value of *raa* is used (**ra_C**). If air humidity is not available the same assumption is made as before, using the parameter **corecTrosee_C** (see § 9.3.1.2). The moisture variable can thus be calculated if actual weather data is not available.

9.4.2 Reconstitution of hourly variables

To enable coupling with plant disease models, an hourly reconstitution of microclimate state variables (crop temperature and air moisture) is made according to the following principle:

- The maximum crop temperature is assumed to occur at 14:00 UTC and the minimum at sunrise. Between these two time points, linear interpolations make it possible to reconstitute hourly temperatures.
- The dew point temperature is calculated from $tcult$ and $humidite$ by reversing the TVAR function (Eq. (9.19)). An hourly reconstitution similar to that used for the crop temperature is made by applying recurrent hypotheses to the minimum value of the dewpoint temperature, until there is convergence at the level of average daily moisture levels (Figure 9.20):

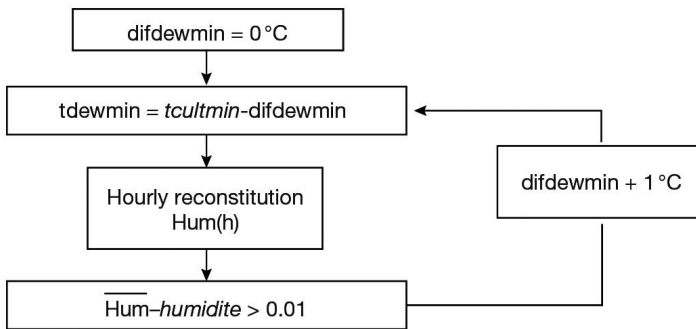


Figure 9.20. Diagrams representing the iteration loop of hourly humidity ($Hum(h)$) calculations based on the convergence between the average hourly values and the daily value, the fitted variable being the minimum dewpoint value.

Convergence is generally achieved in under five iterations, and the comparison between mean daily values and daily values for crop moisture and temperature is satisfactory (no bias and $r^2 > 0.99$; Figure 9.21). The dynamics over a few days are presented in Figure 9.22.

►► 9.5 Climate under shelter

The incoming radiation above the crop (trg) grown under a shelter is less than the outside radiation ($trgext$) and the proportionality coefficient between the two (Eq. (9.39)) is the transmission coefficient (**transplastic_T**), the value of which depends on the plastic used for the structure.

$$trg(t) = trgext(t) \cdot \mathbf{transplastic}_T \quad (9.39)$$

For an unheated ('cold') shelter, water requirements are estimated using the reference evapotranspiration approach. The potential evapotranspiration is easily estimated (Eq. (9.40)) using a multiplicative coefficient of radiation, **coefdevil_C** (De Villele, 1974).

$$tstp(t) = trg(t) \cdot \mathbf{coefdevil}_C \quad (9.40)$$

Rainfall is assumed to be zero and thus the crop must be watered by irrigation.

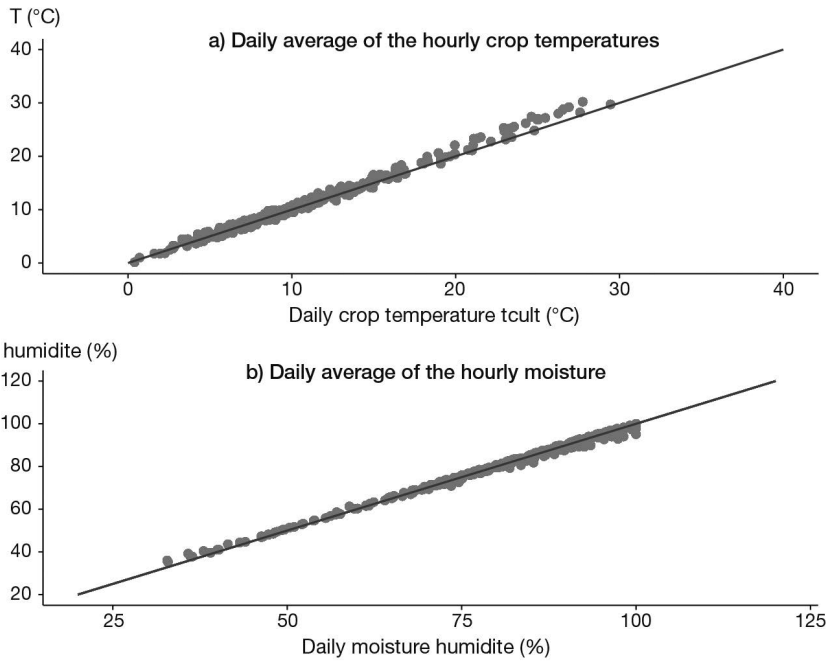


Figure 9.21. Comparisons between average hourly values and daily values of a) crop temperature and b) canopy humidity.

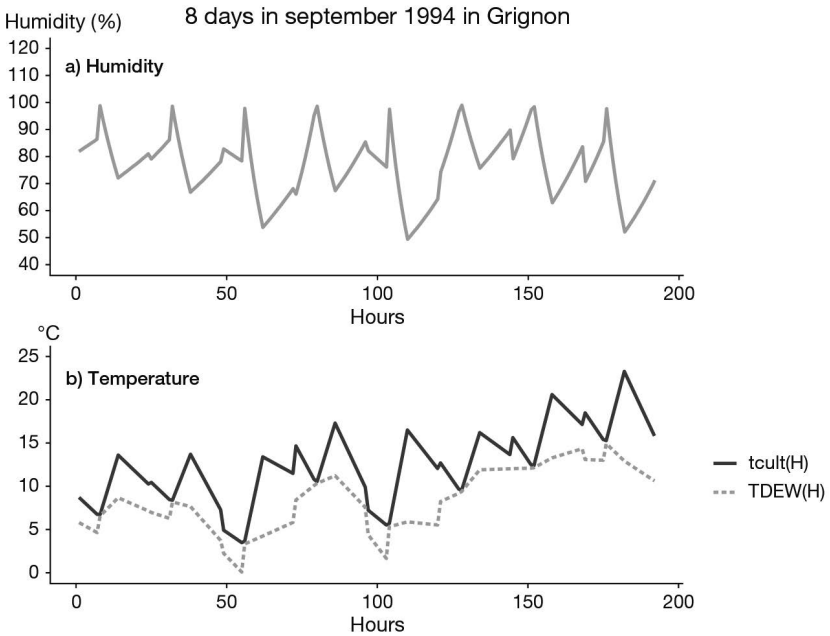


Figure 9.22. Hourly dynamics of the microclimatic variables over eight days: b) crop temperature, dew point and a) humidity.

Temperature variations under a cold shelter are estimated using an energy balance based on the work by Boulard and Wang (2000). On a daily time step, the heat flux in the soil is ignored, assuming that the losses and gains balance out. The difference in mean daily temperature inside and outside ($deltatemp$) is thus expressed in Eq. (9.41).

$$deltatemp(t) = \frac{1}{(kh(t)+ks(t))24 \cdot 3600 \cdot 10^{-6}} \cdot (coefrnet_C \cdot trgext(t) - L(t) \cdot estimet(t)) \quad (9.41)$$

where kh is the coefficient of heat transfer ($W \text{ m}^{-2} \text{ K}^{-1}$) of the shelter, ks is the coefficient of energy losses between the outside and inside of the shelter ($W \text{ m}^{-2} \text{ K}^{-1}$), $coefrnet_C$ is a synthetic coefficient which converts external global radiation into net interior radiation (with a standard value of 0.59), L is the latent heat of vaporisation and $estimet$ is the evapotranspiration estimated from the water balance for the previous day (et) and the evaporative demand for the day ($tetp$, Eq. (9.42)).

$$estimet(t) = \frac{et(t-1)}{tetp(t-1)} \cdot tetp(t) \quad (9.42)$$

where ks (Eq. (9.43)) increases with the external wind speed ($tvent$) using the parameters aks_C and bks_C , equal to 6.0 and 0.5 respectively. The kh variable (Eq. (9.43)) depends on the proportion of vents related to the total surface area of the greenhouse ($surfouvre_T$) and the wind speed. The values of the constants $cvent_C$ and $phiv0_C$ are 0.16 and $4 \cdot 10^{-3}$, respectively. The $surfouvre$ input can take three values during the growth cycle.

$$\begin{aligned} ks(t) &= aks_C + bks_C \cdot tvent(t) \\ kh(t) &= 1215.6 \cdot \left(\frac{surfouvre(t)}{2} \cdot cvent_C \cdot tvent(t) + phiv0_C \right) \end{aligned} \quad (9.43)$$

These calculations enable an estimation of the mean elevation of temperature under shelter ($tmoy$) by comparison with the mean external temperature ($tmoyext$). This difference is entirely allocated to the maximum temperature (Eq. (9.44)).

$$\begin{aligned} tmoy(t) &= tmoyext(t) + deltatemp(t) \\ tmin(t) &= tminext(t) \\ tmax(t) &= 2 \cdot tmoy(t) - tmin(t) \end{aligned} \quad (9.44)$$

►► 9.6 Correcting temperatures for high altitude climates

The model is driven by standard weather variables (radiation, minimum and maximum temperatures, rainfall, reference evapotranspiration and possibly wind speed and humidity) on a daily time step. These meteorological data are obtained from a weather station and entered in an input file. The difference in altitude between the weather station and the simulation site can be taken into account but only in terms of recalculation of temperatures, the other weather readings remain unchanged.

As a general rule, temperatures in mountain regions (see Figure 9.23) show a gradual fall with altitude, and a difference in temperature between the south-facing and north-facing slopes. In addition, the temperature inversion phenomenon, which affects minimum temperatures, must be accounted for. Different studies Seguin and

Antonioletti (1988) have conducted on temperatures in mountain regions, and the values used are thus taken from these studies. Differences in incident radiation also occur between south and north-facing slopes but the model does not account for them.

9.6.1 Parameterisation of the various phenomena

The **altisimul_C** and **altistation_C** parameters are the altitudes of the simulation site and the weather station, respectively, with the assumption that **altisimul_C** > **altistation_C**.

To account for the gradual fall in temperature with increasing altitude (adiabatic gradient), we have used the values provided by Douguedroit (1986), who proposed a reduction of 0.55°C (± 0.08°C) per 100 m at night and a reduction of 0.61°C (± 0.03°C) during the day. These mean values were assigned to the parameters **gradtx_C** and **gradtn_C**, which affect the calculation of the maximum and minimum temperatures, respectively.

For the differences between south- and north-facing slopes, the problem is more complex, and studies are lacking. According to Seguin and Antonioletti (1988), the difference between south- and north-facing slopes is mainly found to affect maximum temperatures. In the case of Mont Ventoux (south-eastern France), maximum temperatures exhibit an almost constant difference of about 1.4°C. The parameter **ombragetx_C** represents this constant difference, and is removed to the maximum temperature when the simulation site is on the north-facing slope (parameter **codadret_C** = 2, otherwise = 1).

The phenomenon of temperature inversion is due to the circulation of air masses during clear weather at night, which causes a flux of cold air into valleys. This leads to a rise in temperature as the altitude increases (approximately 1.3°C per 100 m up to an altitude of between 400 m and 900 m) (Antonioletti, 1986). This has been included in the model through the parameter **gradtninv_C** up to the threshold altitude **altinversion_C**. The notion of 'clear weather' has been taken into account by calculating the complement of cloud cover *fracinsol* (Eq. (9.18)), which must reach at least the value of the parameter **cielclair_C**.

9.6.2 Calculation of the maximum temperature

The maximum temperature at **altisimul_C** (*tmax*) depends on the reference maximum temperature measured by the weather station (*tmaxs(t)*) and the adiabatic gradient (**gradtx_C**) corrected by **ombragetx_C** (>0) for a north-facing slope (Eq. (9.45))

$$tmax(t) = tmaxs(t) + gradtx_C \cdot \frac{altisimul_C - altistation_C}{100} + (codadret_C - 1) \cdot ombragetx_C \quad (9.45)$$

9.6.3 Calculation of the minimum temperature

The relative position of the inversion altitude requires defining two functions, corresponding to the adiabatic (ADIA) and the inversion (INV) gradients (Eq. (9.46)).

$$ADIA(T, ALT1, ALT2) = T + gradtn_C \cdot \frac{ALT2 - ALT1}{100}$$

$$INV(T, ALT1, ALT2) = T + gradtninv_C \cdot \frac{ALT2 - ALT1}{100} \quad (9.46)$$

where T is the temperature, and $ALT1$ and $ALT2$ are two increasing altitudes ($ALT2 > ALT1$), $gradtn_C < 0$ and $gradtninv_C > 0$. Two cases must then be considered to calculate the resulting minimum temperature of the simulated site ($tmin$) based on the measured reference temperature ($tmins(t)$); Eq. (9.47):

$$\left\{ \begin{array}{l} 1. \text{altinversion}_C > \text{altistation}_C, \text{altisimul}_C \\ \quad tmin(t) = INV(tmins(t), \text{altisimul}_C, \text{altistation}_C) \\ 2. \text{altisimul}_C > \text{altinversion}_C > \text{altistation}_C \\ \quad tmin(t) = ADIA[INV(tmins(t), \text{altinversion}_C, \text{altistation}_C), \text{altisimul}_C, \text{altinversion}_C] \end{array} \right. \quad (9.47)$$

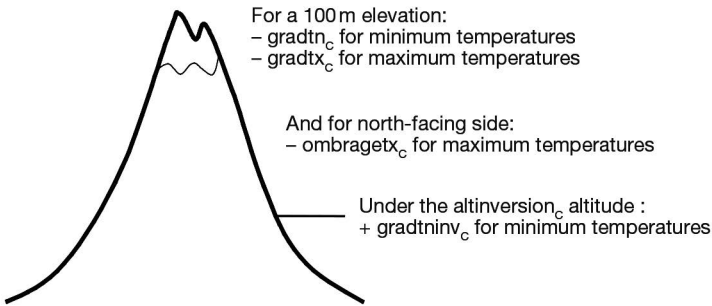


Figure 9.23. Temperature variations at high altitudes (northern hemisphere).

Chapter 10

Transfers in soil: water, nitrate and heat fluxes

JOËL LÉONARD, BRUNO MARY, GUILLAUME JEGO,
NICOLAS BEAUDOIN AND NADINE BRISSON

REVIEWED BY: PATRICE LECHARPENTIER

» 10.1 Water and nitrate fluxes

Two main approaches are commonly used to model the transfer of water and solutes in the soil (Addiscott and Wagenet, 1985): the functional reservoir-type model, which is simple and easy to parameterise, and the flux-gradient model which has a stronger physical basis. Most crop models perform successfully using the first approach. Several studies have shown that the transfer of nitrate can be accurately simulated with a reservoir-type model provided that the thickness of elementary soil layers used for calculation is proportional to the soil dispersivity length (Van Der Ploeg *et al.*, 1995; Vinten and Redman, 1990). The main limitations of the reservoir approach are related to the redistribution of water during evaporating phases and the capillary rise of water and nitrate, which are simulated empirically. These processes can be rigorously simulated with models based on Darcy's law and the convection-dispersion equation (Addiscott and Wagenet, 1985). Pedotransfer functions are increasingly available to estimate the hydrodynamic parameters of these models using soil properties. However, these parameters remain strongly variable in space and time and are difficult to assess locally with sufficient accuracy. Another limit of the reservoir approach is that it is difficult to predict rapid variations in soil water content in the superficial soil layers, especially near water saturation. This can hinder accurate prediction of processes taking place near soil surface, such as plant germination and emergence or denitrification. However, models based on Darcy's law and Richards' equation and using daily rainfall inputs only are also limited when it comes to such processes.

10.1.1 Soil layers and pore space compartments

In STICS, the soil is described through a maximum of five horizontal soil layers, each with its own specific physical properties. The layers can be defined either as soil horizons if they show strong discontinuities in soil properties or as standard layers when soil properties vary continuously. In the latter case, the layer thickness can be constant

(e.g. 30 cm) in order to compare with water or mineral N measurements that are made at the same depths. Each layer is characterised according to five basic physical properties:

- the gravimetric water content at field capacity (**hccf_s**, in %),
- the gravimetric water content at permanent wilting point (**hminf_s**, in %),
- the volumetric content of pebbles (**cailloux_s**, in %),
- the bulk density of the fine earth fraction (**DAF_s**, in g cm⁻³),
- the dispersion thickness (**epd_s**, in cm).

These properties must be defined in the soil input file. They are used to derive total soil porosity assuming a constant solid density (2.66 g cm⁻³). For computational purposes, the five layers are divided into “elementary layers” (1 cm thick) in order to simulate water, nitrate and heat transfers in soil as well as root functioning. However, model outputs are mostly available at the scale of each soil layer described in the soil input file. The soil pore space can involve up to five compartments: microporosity, macroporosity, cracks, pebbles and artificial drains:

- Microporosity is the main compartment and the only one which is mandatory because this is where the non-preferential flow of water and nitrate occurs. At the daily scale, water content in microporosity cannot exceed field capacity. It can exceed field capacity temporarily at an hourly scale when the hourly water filled pore space (WFPS) option is active (§ 12.3.5).
- Macroporosity allows water in excess over field capacity to accumulate at the bottom of any soil layer when its infiltration rate is limiting, i.e. lower than the downwards water flow. The volume occupied by the macroporosity, which is assumed to be nil by default, is calculated if **codemacropor_s** = 1, as follows:

$$\text{macroporosity} = 1 - \frac{\text{DAF}_s}{2.66} - \frac{\text{hccf}_s}{100} \cdot \text{DAF}_s \quad (10.1)$$

- Cracks are intended to simulate water flow in swelling clay soils and bypass flow in soils having a variable porosity. Cracks, which are not activated by default, are active if **codefente_s** = 1 and if the macroporosity option is also active.
- pebbles can be explicitly taken into account when they represent a large percentage of the soil volume because their properties strongly differ from those of the soil matrix. Pebbles, which are not activated by default, are active if **codecailloux_s** = 1.
- artificial drains are sometimes installed on poorly draining soils. Their effect is not simulated by default but is activated if **codrainage_s** = 1 and if the macroporosity option is also activated.

Among these five pore space compartments, which are summarised in Figure 10.1, only the first is compulsory. The four other optional compartments should be used in specific situations that cannot be handled by the standard soil description and associated transfer model, which is the only one that has been extensively tested. The optional compartments and their associated formalisms require additional parameters which are not easy to provide. It should be noted that the nitrification, denitrification and N₂O emissions routines incorporate a hourly WFPS option which allows users to take into account occurrence of soil water content values between field capacity and saturation near the soil surface on rainy days (§ 12.3.5). However, these water content values do not appear in daily outputs: it is assumed that they occur only within a 24 hour period and do not influence the return to field capacity the next day.

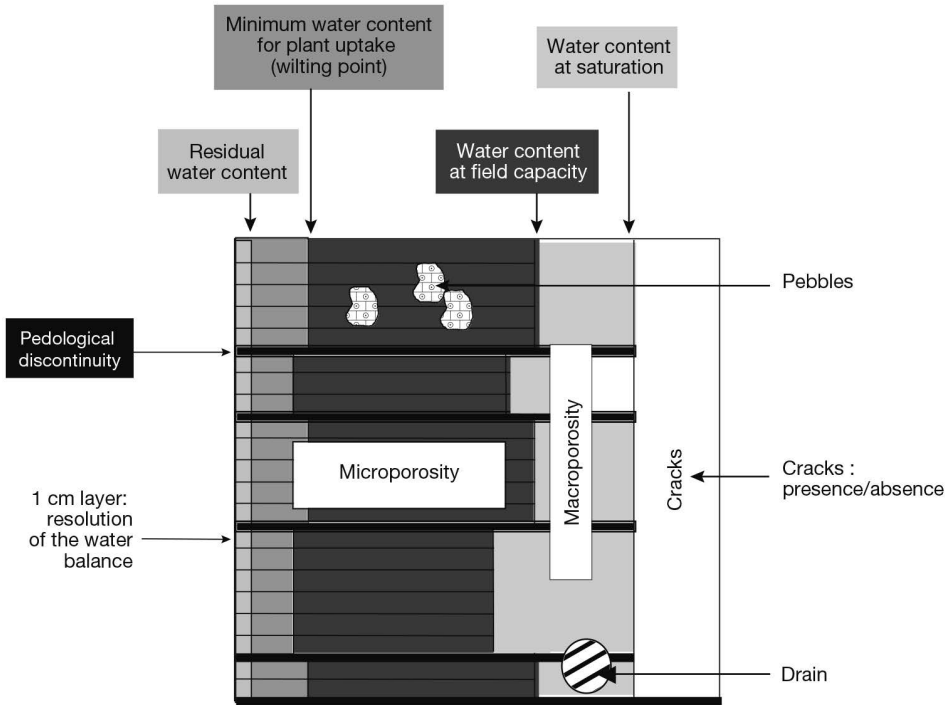


Figure 10.1. Diagram of soil pore space components.

10.1.2 Transfer of water and nitrate in freely draining soil

The standard model of water and nitrate transfer occurs in the soil microporosity. Soil water content is calculated in each elementary layer (1 cm) using a reservoir-type analogy. Water entering the soil fills the elementary layers from top to bottom, assuming that the maximum soil water content of each layer is its field capacity. The initial soil moisture, water contents at field capacity and permanent wilting point of each elementary layer are derived from the five soil layers described in the soil input file. When an elementary layer is filled, the excess water above field capacity infiltrates downwards (without any flow rate limitation) into the next layer and so on. Equilibrium occurs within a day. Soil water can only be removed from each elementary layer through evaporation and plant transpiration. Evaporation can occur down to a maximum depth (z_{esx_s} , in cm) and may deplete the water content of each elementary layer down to a minimum (the residual soil water content), which is itself estimated from clay content. Soil water removal by plant transpiration occurs over the soil depth colonised by roots but transpiration only cannot dry out a layer below soil water content at the permanent wilting point.

The transfer of nitrate is also described using this reservoir-type analogy, according to the “mixing cells” principle: any nitrate arriving by convection with water in an elementary layer mixes with the nitrate already present in this layer. Excess water then flows downward with the new concentration of the mixture. This description produces results which are close to those obtained with a convection-dispersion model if the thickness of the mixing cell is equal to double the dispersivity length (Mary *et al.*,

1999; Van Der Ploeg *et al.*, 1995). In the first STICS versions, the thickness of mixing cells was equal to that of elementary layers (1 cm) which often resulted in an under-estimation of nitrate dispersion in the soil profile. This is why the thickness of mixing cells is now considered independently from the thickness of elementary layers and provided in the soil input file as a specific dispersion parameter of each layer (**epd_s**). This parameter varies between 1 cm and 30 cm, depending on the type of soil porosity. The relationship between dispersivity and soil textural class, as shown for example in Perfect *et al.* (2002) can be used to estimate the mixing cell thickness. STICS does not simulate the upward nitrate movement.

When water or nitrate reaches a layer deeper than maximum root depth, it becomes unavailable for plants. It may be retrievable by a subsequent crop if it remains above the base of the soil profile. If not, it is definitively lost. The model allows users to define a minimum nitrate concentration level which cannot be leached or taken up by the crop. This threshold (**concseuil_s**, in kg ha⁻¹ mm⁻¹) allows users to simulate soils having an anionic exchange capacity. It is provided in the soil input file.

When they represent a significant percentage of the soil volume, pebbles can affect the properties of the soil microporosity and then water and nitrate flows. In STICS, the volumetric percentage of pebbles in each soil layer **cailloux_s** (%) can be provided, together with the type of pebble. Each type of pebble has a specific bulk density **masvolcx_G** (g cm⁻³) and moisture at field capacity **hccc_G** (%), while the minimal moisture content of pebbles is assumed to be equal to $\text{hminf}_s \frac{\text{hccc}_G}{\text{hccf}_s}$. Using this information, equivalent properties of the whole soil are calculated as the volume-weighted average of the fine earth fraction and pebble properties. When the percentage of pebbles is high, fluxes such as evaporation can be strongly affected (Figure 10.2).

10.1.3 Transfer of water and nitrate in restricted conditions

When at least one soil layer impedes the downward transfer of water, the macroporosity option may be used to simulate this process. When this option is activated, the water flow at the bottom of this layer cannot exceed a maximum infiltration rate (**infil_s**, in mm day⁻¹) given in the soil input file. When the deepest elementary layer included in this layer has reached field capacity, part of the excess water flows downward at a rate equal to the infiltrability while the rest of the excess water accumulates in the macroporosity. When the macroporosity of this elementary layer is filled, water begins to fill the macroporosity of the next elementary layer up. This means the considered soil layer will progressively fill from the bottom to the top. The macroporosity option has no effect if the rainfall intensity is lower than the infiltrability rate. When an elementary layer has reached saturation (macroporosity is filled), its anoxia index becomes equal to 1 and can restrict root growth. The macroporosity option may be useful for simulating the effect of soil flooding or a plough sole, as illustrated in Figure 10.3.

In addition to the macroporosity option itself, several suboptions are available to describe capillary rise, bypass flow through cracks or agricultural drainage. In all cases, the macroporosity option must be activated.

Capillary rise from the subsoil can be described, although crudely, by an alternative use of the macroporosity option. To do this, the infiltrability of the deepest soil layer should be equal to 0. Capillary rise occurs only if the deepest layer becomes drier

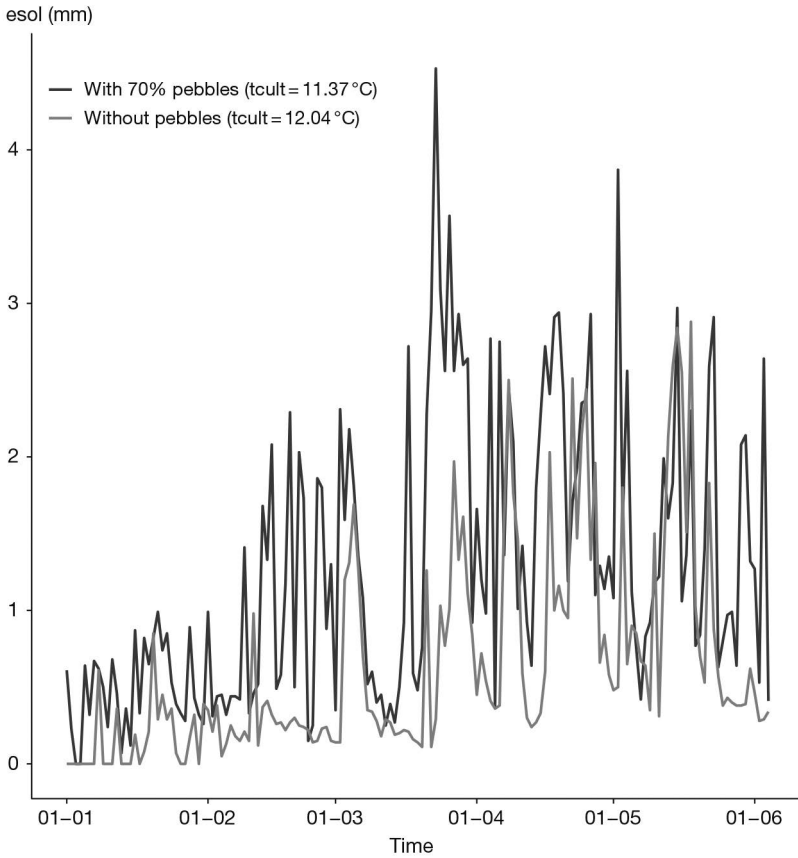


Figure 10.2. Effect of pebbles (70 % in volume) on soil evaporation and the consequences on mean spring crop temperature in a vineyard in south-eastern France.

than the water content threshold $\mathbf{humcapil}_s$ (%). Capillary rise occurs at a constant rate $\mathbf{capiljour}_s$ (mm day^{-1}) until the water content of the deepest layer reaches the $\mathbf{humcapil}_s$ threshold (in %).

Bypass flow can be considered in the case of swelling clay soils, where water flow can enter the soil through shrinkage cracks. In the model, cracks are represented in the form of a unique compartment, extending from the soil surface to the maximum soil depth, which replaces the macroporosity described above. The macroporosity volume (in mm cm^{-1} soil) is then redefined as a proportion (50%) of the available water:

$$\mathbf{macroporosity} = 0.05 \cdot (\mathbf{hccf}_s - \mathbf{hminf}_s) \cdot \mathbf{DAF}_s \quad (10.2)$$

Cracks can only be filled from the soil surface, due to overflow from the surface layer or runoff when present. Direct feeding by rainfall interception is not considered.

The impact of an artificial drainage system (e.g. mole drains) installed on poorly draining soils can be taken into account in the model. Although artificial drainage is better described in three dimensions rather than one and with shorter time steps than the day, it can be approximated by steady state drainage equations such as the

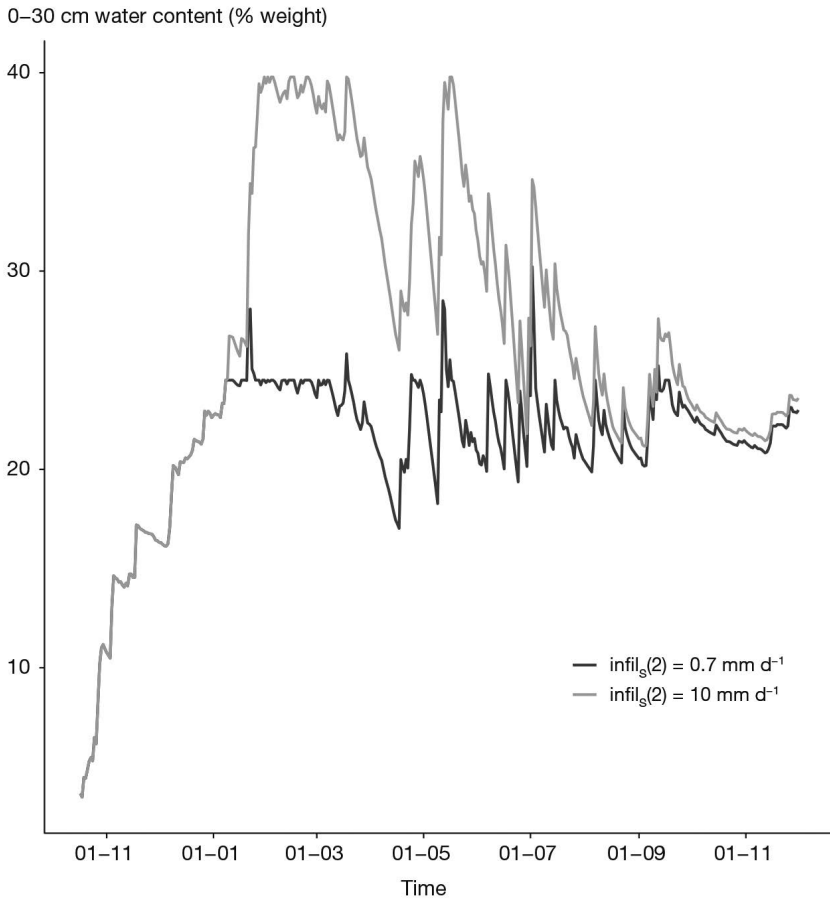


Figure 10.3. Effect of a strong decrease in infiltrability (infil_s) at the base of the second layer located at 30 cm on the soil water content over 0-30 cm.

Hooghoudt equation (Hooghoudt, 1940; Tournebize *et al.*, 2004), which assumes constant drain spacing and uses the property of symmetry that results from it. The drainage system is described in the soil input file of STICS with four parameters:

- the depth of the drains profdrain_s (cm),
- the spacing of drains ecartdrain_s (cm),
- the upper depth of the impermeable layer (from soil surface) profimper_s (cm),
- the hydraulic conductivity ksol_s (mm day^{-1}).

The daily water outflow from drains is obtained from a simplification of the original Hooghoudt’s equation. The hydraulic conductivity is assumed to be the same above and below the drains. The nitrate leached through the drains is calculated assuming that nitrate concentration in the drained water equals the soil nitrate concentration at the depth corresponding to the top of water table.

Figure 10.4 summarizes the different types of water and nitrate transfers available in STICS and above described.

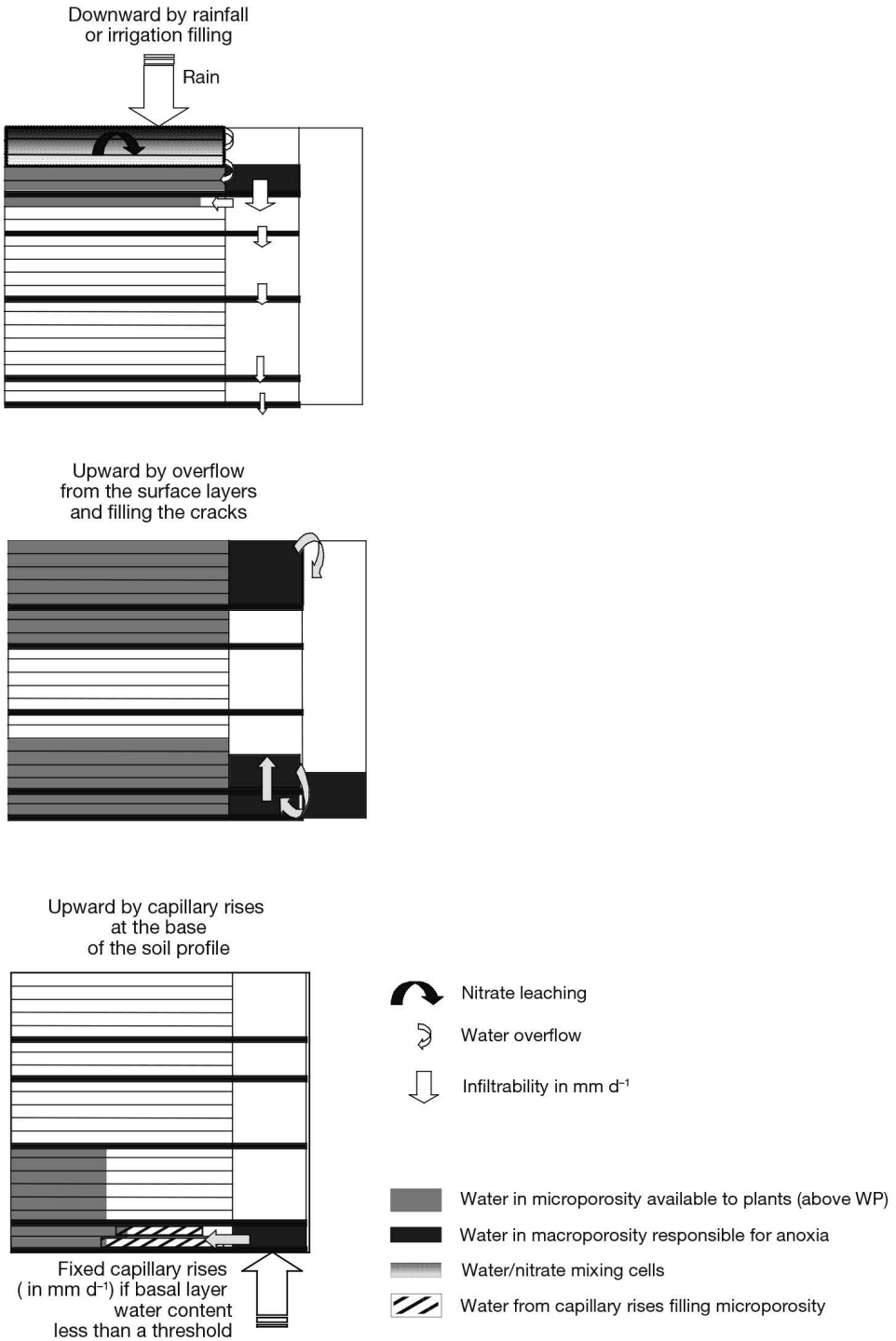


Figure 10.4. Water and nitrate flows in the soil: they are mainly downward but can be upward if cracks are present or if capillary rise occurs.

10.1.4 Predawn plant water potential

At dawn, plant water potential is assumed to be in equilibrium with the soil water. This measurement is then often used as a daily assessment of water stress and provides a relevant integrated measurement of soil behaviour. To be able to compare STICS outputs to this type of measurement, a simple calculation of predawn plant water potential is proposed, based on Brisson *et al.* (1993). Predawn plant potential is calculated as the arithmetic mean of soil water potential over depth, weighted by root density.

The soil potential psisol (Mpa) in each elementary layer is calculated according to the Clapp and Hornberger (1978) formula:

$$\text{psisol}(z, t) = \text{psisols} \cdot \left(\frac{\text{hur}(z, t) + \text{sat}(z, t)}{\text{wsat}(z)} \right)^{-\text{bpsisol}} \quad (10.3)$$

with wsat depending on whether the **codefente_s** option is active or not (§ 10.1.1 and 10.1.3).

The parameters bpsisol (unitless) and psisols (MPa) are calculated using the two points: (**hucc**, -0.03 MPa) and (**humin**, -1.5MPa).

The predawn leaf water potential (psibase) is calculated as:

$$\text{psibase}(t) = \frac{\sum_{z=\text{profsem}_r}^{\text{zrac}(t)} \text{racineps}(z, t) \text{psisol}(z, t)}{\sum_{z=\text{profsem}_r}^{\text{zrac}(t)} \text{racineps}(t)} \quad (10.4)$$

with

$$\begin{aligned} \text{racineps}(z, t) &= \text{lracz}(z, t) \quad \text{if } \text{psisol}(z, t) > -1.5 \\ \text{racineps}(z, t) &= 0 \quad \text{if } \text{psisol}(z, t) \leq -1.5 \end{aligned} \quad (10.5)$$

since the roots contributing to predawn water potential are only those located in moist layers, in which psisol is above -1.5 MPa.

The predawn leaf water potential depends on the rooting system and rainfall events as illustrated in Figure 10.5.

►► 10.2 Soil temperature

Temperature variation in soil depends both on the soil surface conditions which determine the daily thermal variation and on the thermal inertia related to the environment. This inertia is the cause of the attenuated daily average temperature variations in deep layers compared to those at the surface. The temperature at the upper limit used to calculate soil temperature is assumed to be tcult (°C). Crop temperature calculations are explained in § 9.3.2. The daily thermal amplitude amplsurf (°C) at the soil surface is then:

$$\text{amplsurf}(t) = \text{tcultmax}(t) - \text{tcultmin}(t) \quad (10.6)$$

The daily thermal amplitude amplz is calculated using a formalism suggested by McCann *et al.* (1991):

$$\text{amplz}(z, t) = \text{amplsurf}(t) \cdot \exp\left(-z \sqrt{\frac{7.272 \cdot 10^{-5}}{2 \text{diftherm}_G}}\right) \quad (10.7)$$

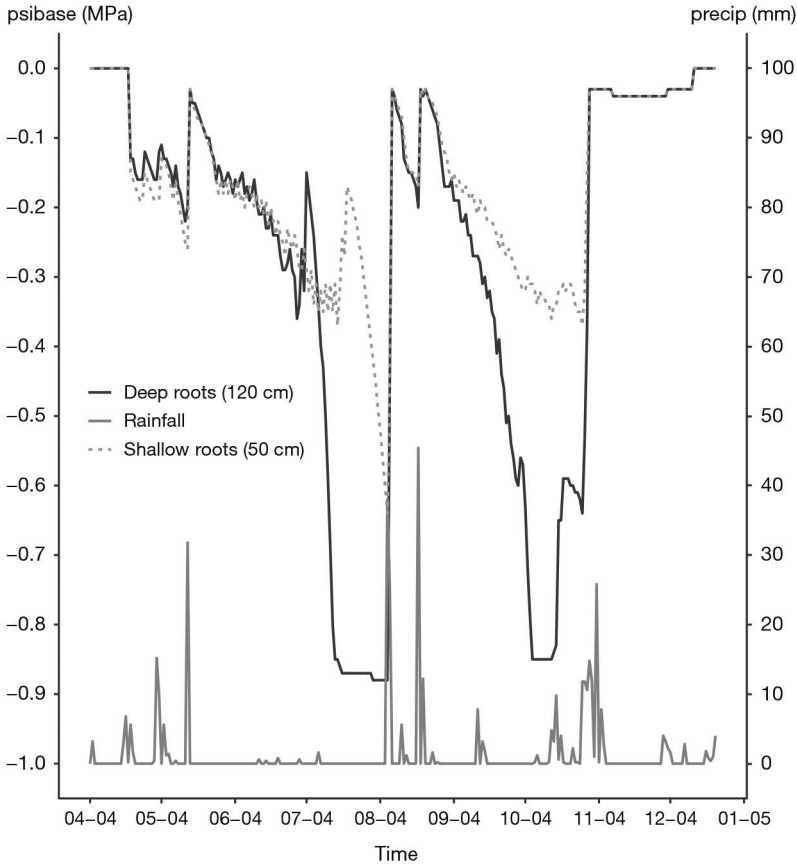


Figure 10.5. Influence of rooting depth and rainfall events on psibase. Example of a vineyard in the Rhône valley: the simulated production of the shallow rooted vineyard is half of that of the deeply rooted vineyard.

The thermal diffusivity diftherm_G ($\text{cm}^2 \text{s}^{-1}$) is assumed to be a constant whatever the soil or soil water content. A value of $5.37 \cdot 10^{-3} \text{cm}^2 \text{s}^{-1}$ is proposed, based on the work of McCann *et al.* (1991).

The soil temperature tso ($^\circ\text{C}$) at the soil depth z is calculated recurrently, using the temperature of the previous day:

$$\begin{aligned} \text{tso}(z, t) = & \text{tso}(z, t-1) - \frac{\text{amplz}(z,t)}{\text{amplsurf}(t)} (\text{tcult}(t-1) - \text{tcultmin}(t)) \\ & + 0.1(\text{tcult}(t-1) - \text{tso}(z, t-1)) + \frac{\text{amplz}(z,t)}{2} \quad (10.8) \end{aligned}$$

An example of soil temperature evolution in spring is given in the following figure:

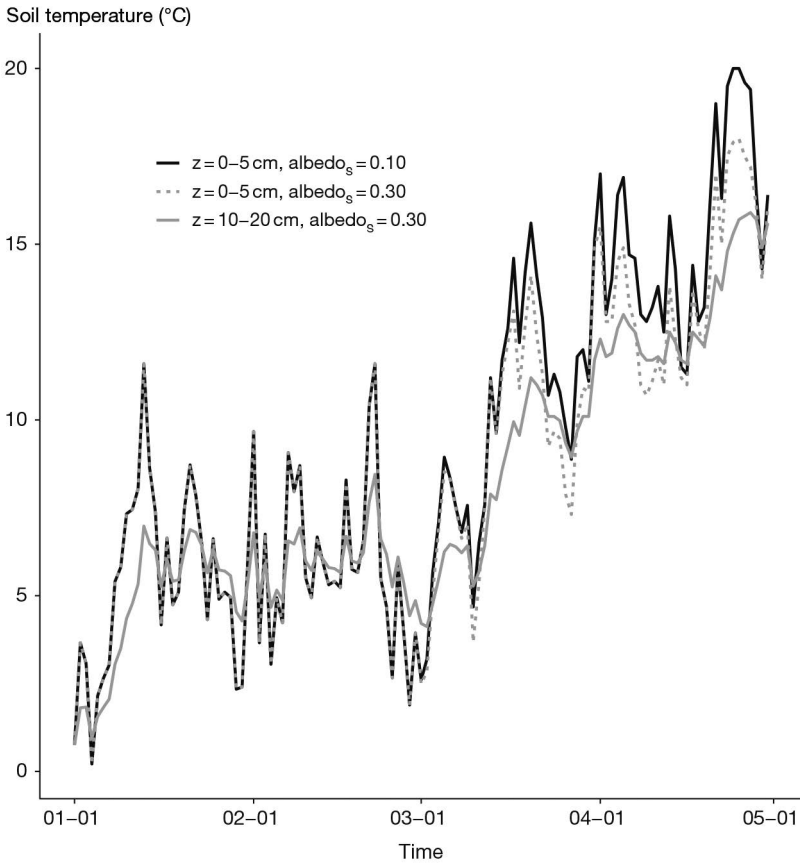


Figure 10.6. Simulated evolution of the soil temperature in two soil layers for two values of albedo at soil surface, in spring and northern France.

►► 10.3 Modifications of surface conditions that influence water and heat transfer

Generally, rainfall (or irrigation) and surface temperature directly control the transfer of water and heat in soil. However there are situations in which these control variables have to be corrected to reflect the real boundary conditions at the soil surface. This is the case for example when precipitation falls as snow, in which case it accumulates until snowmelt, thus delaying water flow into the soil. The snow cover also acts as an insulator, preventing the soil surface temperature to reach negative values. Another example is surface runoff, where only part of the rainfall infiltrates into the soil or is intercepted by vegetation or mulch.

To deal with snow precipitation and its consequences, STICS uses a method proposed by Trnka *et al.* (2010). A snow-cover model pre-processes the climate data to account for the influence of snow cover on the soil temperature and water budget (see § 10.3.1 below). Equations derived from the work of Bélanger *et al.* (2002) were used for the calculation of snow accumulation. For snow melt and snow

depth calculations, equations derived from Thorsen *et al.* (2010) were used. Model parameterisation and validation under Canadian climatic conditions are presented in Jégo *et al.* (2014).

Regarding runoff, STICS does not include a component dedicated to its prediction, such as depending on soil surface state or rainfall properties. However, STICS does integrate a linear relationship between runoff and daily rainfall that can be used to reproduce the water loss from runoff by providing adequate parameters (see § 11.4.3). The presence of vegetation cover or mulch modifies runoff behaviour by intercepting some of the rainfall.

10.3.1 Simulation of the snow cover and its consequences

Snow fall is estimated using a set of equations that had previously been validated for several sites across Canada (Jégo *et al.*, 2014). Unlike in the original snowMAUS model proposed by Trnka *et al.* (2010), these equations use the daily maximum temperature (t_{max}) to determine the partitioning between snowfall and rainfall. The fraction of snowfall in the precipitation (FS) depends on two threshold temperatures tr_{max_C} and ts_{max_C} (in °C). Between these two thresholds, the model assumes a mix of rain and snow:

$$\begin{aligned} FS &= \frac{tr_{max_C} - t_{max}(t)}{tr_{max_C} - ts_{max_C}} & \text{if } ts_{max_C} \leq t_{max}(t) \leq tr_{max_C} \\ FS &= 0 & \text{if } t_{max}(t) > tr_{max_C} \\ FS &= 1 & \text{if } t_{max}(t) < ts_{max_C} \end{aligned} \quad (10.9)$$

The snowfall accumulation on day t ($Snowaccu$, expressed in mm water) is the product of FS and the daily total precipitation (trr , in mm d⁻¹):

$$Snowaccu(t) = FS \cdot trr(t) \quad (10.10)$$

The snow cover is either affected by the process of refreezing or the process of melting. The amount of snow cover in the refreezing process (M_{rf} , in mm d⁻¹) depends on the average daily air temperature (t_{moy}) and the threshold temperature T_{mf_C} (in °C):

$$M_{rf} = \max[0, SW_{rf_C} \cdot (T_{mf_C} - t_{moy})] \quad (10.11)$$

The refreezing process is controlled by the parameter SW_{rf_C} (in mm °C⁻¹ d⁻¹). M_{rf} is nil if t_{moy} is higher than T_{mf_C} .

The amount of snow cover in the process of melting (M , in mm d⁻¹) also depends on t_{moy} and T_{mf_C} :

$$M = \max[0, K \cdot (t_{moy}(t) - T_{mf_C})] \quad (10.12)$$

where K (in mm °C⁻¹ d⁻¹) is the melting rate. Due to the seasonal variation in incoming solar radiation and albedo, K follows a sinusoidal function over a year period, with a minimum melting rate (K_{min_C} , in mm °C⁻¹ d⁻¹) reached on December 21, and a maximum amplitude (DK_{max_C} , in mm °C⁻¹ d⁻¹) reached on June 21:

$$K = K_{min_C} + \frac{DK_{max_C}}{2} \left(1 + \sin \pi \left(\frac{t}{183} - 0.46 \right) \right) \quad (10.13)$$

The snow cover which consists in a mixture of water in a solid state and liquid state is estimated according to the model proposed by Thorsen *et al.* (2010), using the daily precipitation. The amount of snow cover in a solid state (S_{dry} , in mm) is calculated as follows:

$$\begin{aligned} \text{Sdry}(t) &= \text{Sdry}(t-1) + \text{Fs} \cdot \text{trr}(t) + \text{Mrf} - \text{M} \\ &\quad \text{if } \text{M} \leq \text{Sdry}(t-1) \\ \text{Sdry}(t) &= 0 \quad \text{if } \text{M} > \text{Sdry}(t-1) \end{aligned} \quad (10.14)$$

The amount of snow cover in a liquid state (Swet, in mm) is calculated similarly, but cannot exceed 10% of the amount of solid snow:

$$\begin{aligned} \text{Swet}(t) &= \max[0.1 \text{Sdry}(t), \text{Swet}(t-1) + (1 - \text{Fs}) \cdot \text{trr}(t) - \text{Mrf} + \text{M}] \\ &\quad \text{if } \text{Mrf} \leq \text{Swet}(t-1) \\ \text{Swet}(t) &= 0 \quad \text{if } \text{Mrf} > \text{Swet}(t-1) \end{aligned} \quad (10.15)$$

The snow depth (Sdepth, in m) is calculated as the sum of three terms:

$$\text{Sdepth}(t) = (1 - \mathbf{E}_C) \cdot \text{Sdepth}(t-1) + \frac{\text{Snowacc}(t)}{100} - \frac{\text{M}}{\text{ps}} \quad (10.16)$$

The first term represents the remaining snow after sublimation and compaction of the accumulated snow. The empirical parameter \mathbf{E}_C (in $\text{mm mm}^{-1} \text{d}^{-1}$) is assumed to capture the combined effect of the metamorphosis of snow crystals and the densification of the lower snow layers. The second term corresponds to the addition of new snow, the density of which is assumed to be 100 kg m^{-3} , i.e. 10 times lower than water density. The third term stands for the snow melting on the current day. It is determined using the density of the snow cover (ps , in kg m^{-3}), itself calculated as follows:

$$\text{ps} = \frac{\text{Sdry}(t-1) + \text{Swet}(t-1)}{\text{Sdepth}(t-1)} \quad (10.17)$$

The snow cover behaves as a thermal insulator: it prevents the soil temperature to drop as low as the minimum air temperature (t_{\min}) and to get as high as the maximum air temperature (t_{\max}). In order to simulate this thermal effect, the climate input data are modified on days with a snow cover: the minimum and maximum air temperature data are replaced by re-calculated values (called $t_{\min\text{rec}}$ and $t_{\max\text{rec}}$) as indicated below, and the model run again with these new climatic data.

When the snow depth Sdepth (m) reaches or exceeds a user-defined threshold prof_C , the re-calculated minimum air temperature $t_{\min\text{rec}}$ reaches a threshold called $\mathbf{tminseuil}_C$ (in $^{\circ}\text{C}$), and the re-calculated maximum air temperature $t_{\max\text{rec}}$ reaches $\mathbf{tmaxseuil}_C$ (in $^{\circ}\text{C}$).

When the snow depth lies between 0 and prof_C , a linear function is used to calculate the new temperatures: $t_{\min\text{rec}}$ varies linearly between t_{\min} and $\mathbf{tminseuil}_C$; $t_{\max\text{rec}}$ varies linearly between t_{\max} and $\mathbf{tmaxseuil}_C$. If there is no snow cover, $t_{\min\text{rec}}$ and $t_{\max\text{rec}}$ are equal to t_{\min} and t_{\max} :

$$\begin{aligned} t_{\min\text{rec}}(t) &= \mathbf{tminseuil}_C - (t_{\min}(t) + \mathbf{tminseuil}_C) \left(1 - \frac{\text{Sdep}}{\text{prof}_C}\right) \\ &\quad \text{if } 0 < \text{Sdep} \leq \text{prof}_C \\ t_{\min\text{rec}}(t) &= \mathbf{tminseuil}_C \quad \text{if } \text{Sdep} > \text{prof}_C \text{ and } t_{\min}(t) < \mathbf{tminseuil}_C \\ t_{\min\text{rec}}(t) &= t_{\min}(t) \quad \text{if } \text{Sdep} > \text{prof}_C \text{ and } \mathbf{tminseuil}_C \leq t_{\min}(t) \leq \mathbf{tmaxseuil}_C \\ t_{\min\text{rec}}(t) &= \mathbf{tmaxseuil}_C \quad \text{if } \text{Sdep} > \text{prof}_C \text{ and } t_{\min}(t) > \mathbf{tmaxseuil}_C \\ t_{\min\text{rec}}(t) &= t_{\min}(t) \quad \text{if } \text{Sdep} = 0 \end{aligned} \quad (10.18)$$

$$\begin{aligned}
tmaxrec(t) &= tmaxseuil_c + tmax(t) \left(1 - \frac{Sdep}{prof_c}\right) \\
&\quad \text{if } 0 < Sdep \leq prof_c \text{ and } tmax(t) > 0 \\
tmaxrec(t) &= 0 \quad \text{if } 0 < Sdep \leq prof_c \text{ and } tmax(t) \leq 0 \\
tmaxrec(t) &= tminseuil_c \quad \text{if } Sdep > prof_c \text{ and } tmax(t) < tminseuil_c \\
tmaxrec(t) &= tmax(t) \quad \text{if } Sdep > prof_c \text{ and } tminseuil_c \leq tmax(t) \leq tmaxseuil_c \\
tmaxrec(t) &= tmaxseuil_c \quad \text{if } Sdep > prof_c \text{ and } tmax(t) > tmaxseuil_c \\
tmaxrec(t) &= tmax(t) \quad \text{if } Sdep = 0 \quad (10.19)
\end{aligned}$$

The snow cover also influences the soil water budget. If both rainfall and snowfall occur, only the liquid water fraction enters the soil and moves down in soil. The water equivalent of the snowfall is assumed to enter the soil profile only after melting.

The snow water equivalent (S_WE , in mm) is the sum of $Sdry$ and $Swet$:

$$S_WE(t) = Sdry(t) + Swet(t) \quad (10.20)$$

The variation in the snow cover depth ($\Delta Snowmelt(t)$, in mm water) is:

$$\Delta Snowmelt(t) = 100 (Sdepth(t-1) - Sdepth(t)) \quad (10.21)$$

The daily rainfall $preciprec$ (in $mm\ d^{-1}$) is re-calculated based on the total daily precipitation and the snow cover depth variation, as follows:

$$\begin{aligned}
preciprec(t) &= trr(t) - Snowaccu + \Delta Snowmelt(t) - Mrf \\
&\quad \text{if } S_WE(t) < S_WE(t-1) \\
preciprec(t) &= trr(t) - Snowaccu \quad \text{if } S_WE(t) \geq S_WE(t-1) \quad (10.22)
\end{aligned}$$

In order to simulate these effects on soil water, the climate input data are modified on days with a snow cover: the daily precipitation data are replaced by re-calculated values ($preciprec$) as indicated above for temperature data, and the model run again with these new climatic data.

Chapter 11

Water balance

*NADINE BRISSON, REMI VEZY, DOMINIQUE RIPOCHE-WACHTER
AND PATRICK BERTUZZI*

REVIEWED BY: NICOLAS BEAUDOIN AND JEAN-LOUIS DURAND

►► 11.1 Background and conceptual framework

The water balance in crop models (Brisson *et al.*, 2006) has a dual purpose: to estimate soil water content and fluxes (which drive nitrogen mineralisation and leaching in the soil, for example) and water stress indices (which drive plant behaviour). Being able to estimate water stress indices differentiates crop models from irrigation management models, and forces a distinct separation between evaporation and transpiration.

This separation is usually applied at the level of the potential crop demand, according to the partitioning into potential plant transpiration and potential soil evaporation using a calculation based on Beer's law. The potential crop demand comprises both crop and weather components. However, this variable differs from the classic maximum evapotranspiration variable, as defined for example by (Itier *et al.*, 1997) because it assumes that all surfaces (soil and foliage) are saturated with water.

As for the weather component, the local availability of meteorological data usually determines the calculation method. Yet when compared to standard, well-watered grass measurements, differences emerge. Allen *et al.* (1998) showed that the FAO24 Penman model predicted overly severe water deficits compared to the FAO56 Penman-Monteith model, while Sau *et al.* (2004) showed that the Priestley-Taylor function (Priestley and Taylor, 1972) tended to over-predict for cool regions, although it did produce good results for conditions of moderate evaporative demand.

The crop component is usually linked to the leaf area index at time t (lai). The lai not only represents the gas exchange surface area with the atmosphere but also the crop height and its roughness during growth (with reference to the standard grass evaporation). It also affects the degree of the convective component of evapotranspiration. Convection under the plant canopy, which affects maximum transpiration, may be poorly reproduced by this optical analogy, particularly for row crops; as such, applying an energy balance calculation (optional in STICS) may be justified.

To calculate the amount of water actually transpired by the crop, most models are based on a concept which includes the amount of water physically available in the soil and the

capacity of the plant to extract this water due to its root characteristics. This is the fraction of transpirable soil water (Lacape *et al.*, 1998; Pellegrino *et al.*, 2002; Sinclair, 1986), which also corresponds to the concept of maximum available water content (amount of water between field capacity and wilting point). This approach does not allow a precise estimation of the location of root absorption in the soil layer (on a daily time step, all models assume that transpiration equals absorption), but it does have the advantage of implicitly taking into account capillary rise within the root zone. However, the threshold of sensitivity may vary over time. This global estimate of transpiration is used in STICS, while in other models (e.g. CERES) the calculation of uptake is differentiated in terms of the soil layer, because of the need to simulate capillary rise. In that alternative approach, water uptake per unit root length is based on the equation for radial flow to roots.

►► 11.2 Soil evaporation

Soil evaporation is calculated in two steps: potential evaporation related to the energy available at the soil level and actual evaporation related to water availability. It is then distributed over the soil profile.

There are two options for calculating potential evaporation related to plant cover above the soil: i) using either LAI or fractional ground cover, and ii) the possible presence of an inert cover placed on the soil (Brisson *et al.*, 1998a). The first option corresponds to a Beer's law equivalent applied to the potential evaporation/reference evapotranspiration ratio (Penman) with a constant extinction coefficient. The second is an energy balance approach (§ 9.1.2).

The calculation of actual evaporation, described in detail in Brisson and Perrier (1991), is based on concepts that resemble those put forward by Ritchie (1972).

11.2.1 Potential evaporation

The two methods calculating soil evaporation (eos) involve the plant cover above the soil (lai or *tauxcouv*) and, if relevant, the presence of any mulch on the soil (*couvermulch*).

The first method, Eq. (11.1) illustrated in Figure 11.1, relies on a Beer's law equivalent and is linked to the 'crop coefficient approach' for the estimation of plant requirements (§ 11.3); it uses the reference potential evapotranspiration (*tetp*):

$$eos(t) = tetp(t) \cdot e^{-\delta lai(t)} \cdot (1 - couvermulch(t)) \text{ with } \delta = \mathbf{extin}_p - 0.2 \quad (11.1)$$

or, if the cover rate is used instead of the lai (§ 4.1.4; Eq. (11.2)):

$$eos(t) = tetp(t) \cdot (1 - \mathit{tauxcouv}(t)) \cdot (1 - \mathit{couvermulch}(t)) \quad (11.2)$$

When using the radiation transfer option, the values of \mathbf{extin}_p and $\mathbf{\delta}$ are dynamically recalculated as a function of the canopy geometry and the quality of radiation (direct/diffusive radiation). However, for row crops, which justify the use of the radiation transfer calculations, it is highly recommended to use the second method, known as the energy balance approach, which is explained as follows.

The energy balance method (Eq. (11.3)) is available only if the lai is explicitly calculated:

$$eos(t) = \frac{\delta lai(t) \cdot rnetS(t) + 105.03 \cdot \frac{dos(t)}{ras(t)}}{L \cdot (\delta lai(t) + \mathbf{\gamma})} \cdot (1 - \mathit{couvermulch}(t)) \quad (11.3)$$

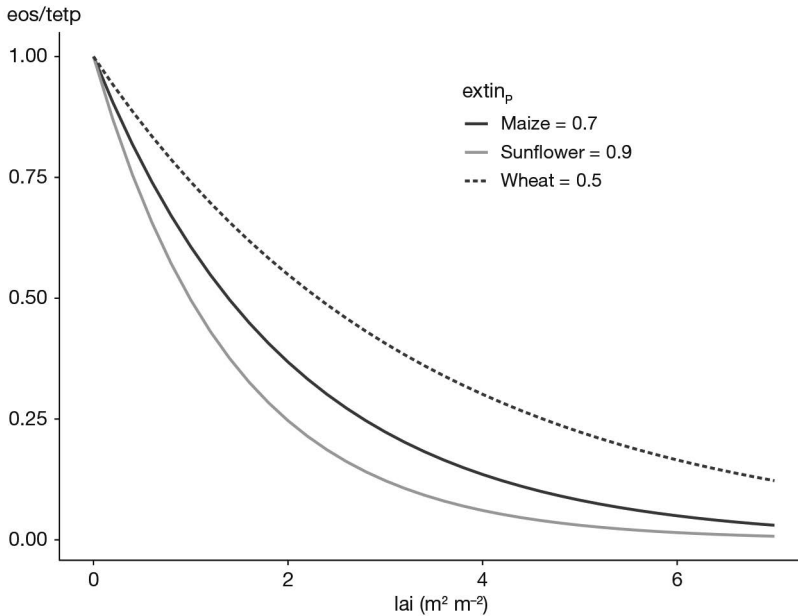


Figure 11.1. Relative potential evaporation as a function of LAI for three different crops.

where $rnetS$ is the net radiation at soil level (Eq. (9.26)), $deltat$ is the slope of the relationship between saturation vapour pressure and temperature (Eq. (11.4)) using the function TVAR explained in chapter 9 (Eq. (9.19)), L is the latent heat of vaporisation, γ is the psychrometric constant (Eq. (9.37)), ras is the aerodynamic resistance between the soil and the vegetation (Eq. (9.28), (9.29), (9.30)) and dos is the saturation deficit in the vegetation (Eq. (11.5)).

$$deltat(t) = TVAR(t_{air}(t) + 0.5) - TVAR(t_{moj}(t) - 0.5) \quad (11.4)$$

The dos variable is calculated assuming that, under soil conditions which are kept moist, total evapotranspiration (ePT: soil+canopy) can be written in the form of evaporation according to Priestley and Taylor (Brisson *et al.*, 1998a) as:

$$dos(t) = dsat(t) + [\gamma \cdot rnet(t) - (deltat(t) + \gamma) \cdot ePT(t)] \cdot \frac{raa(t)}{105.03} \quad \text{with}$$

$$ePT(t) = 1.32 \cdot rnetS \cdot \frac{deltat(t)}{deltat(t) + \gamma} \quad (11.5)$$

where raa is the aerodynamic resistance between the vegetation and the reference level (Eq. (9.28), (9.29), (9.30)), and $dsat$ is the air saturation deficit at the same level.

11.2.2 Actual soil evaporation

The calculation of actual soil evaporation relies on a semi-empirical model that is fully developed and justified in Brisson and Perrier (1991). Following a rain event, soil evaporation is assumed to follow two successive phases, as in Ritchie's approach (Ritchie, 1972), improved by Boesten and Stroosnijder (1986).

During the first phase, evaporation is potential until the daily evaporation accumulation reaches the $q0_s$ threshold. During the second phase, evaporation decreases; this decrease depends on the weather and soil type through the parameter $aevap$ (Eq. (11.6)):

$$\sum_{beginning\ 2^{nd}\ phase} esol(t) = \sqrt{\left(2 \cdot aevap \cdot \sum_{beginning\ 2^{nd}\ phase} eos(t) + aevap^2\right)} - aevap$$

with

$$aevap = \frac{1}{2} \cdot \mathbf{aclim}_C \cdot (0.63 - ha)^{\frac{5}{3}} \cdot (\mathbf{hucc}(1) - ha) \quad \text{and} \quad ha = \frac{\mathbf{argi}_s}{1500} \cdot \mathbf{DAF}(1)_s \quad (11.6)$$

where \mathbf{aclim}_C is a weather parameter which depends mainly on the average wind speed, \mathbf{hucc} is the water content at field capacity of the surface layer, \mathbf{DAF}_s is the bulk density of the surface layer and \mathbf{argi}_s is the clay content used here to estimate the residual moisture, ha . Nevertheless, the sensitivity of soil evaporation to these parameters (Figures 11.2 and 11.3) is rather low compared to the sensitivity to $q0_s$ (Figure 11.4). Although $q0_s$ depends on the soil texture and structure, it is difficult to infer it from soil particle size distribution or bulk density. It generally varies between 0 to 30 mm.

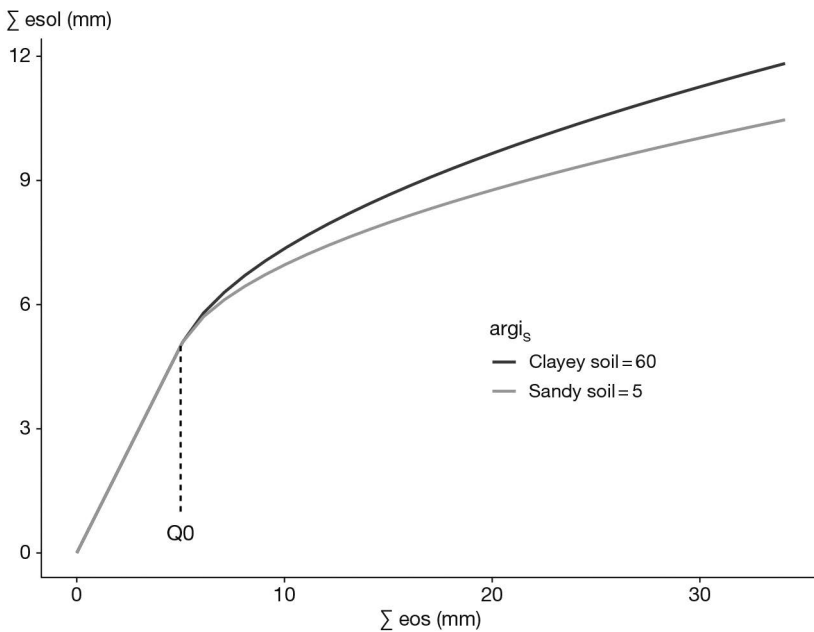


Figure 11.2. Sensitivity of cumulative soil evaporation (ces) as function of the cumulative evaporative demand (sum_eos) for two soil types (Clay soil: $\mathbf{argi}_s=60$ and $\mathbf{hucc}=0.4$, Sandy soil: $\mathbf{argi}_s=10$ and $\mathbf{hucc}=0.2$).

The formalisation (Eq. (11.6) and Eq. (11.7)) also provides an estimate of the thickness of the dry layer in the surface (or natural mulch: \mathbf{XMULCH}), which is accounted for in the water profile in the soil, since this layer is assumed to not participate in evaporation.

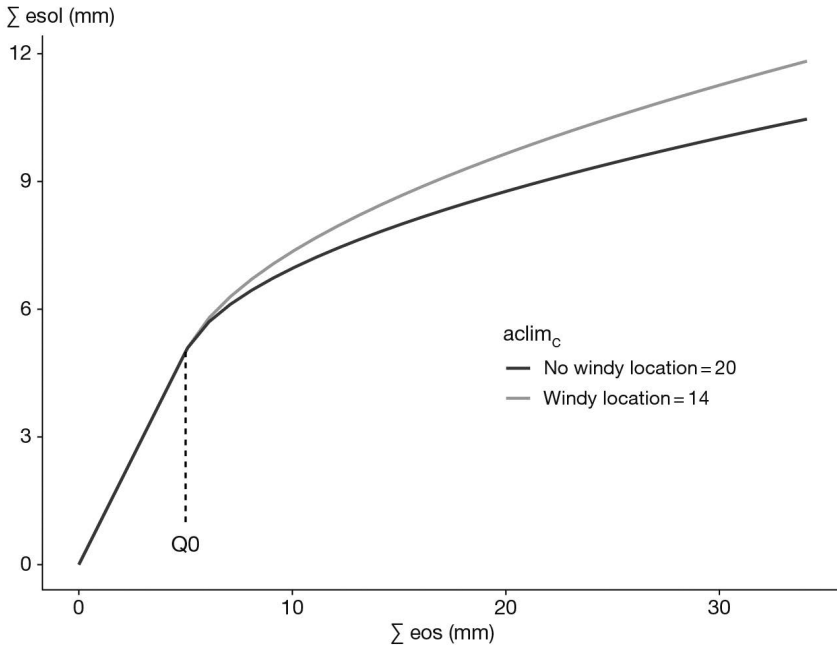


Figure 11.3. Sensitivity of cumulative soil evaporation (ces) as function of the cumulative evaporative demand (sum_eos) for two weather conditions (No windy location, for wind speed of 1 m s^{-1} , $\text{aclim}_C = 20$, Windy location, for wind speed of 2 m s^{-1} , $\text{aclim}_C = 14$).

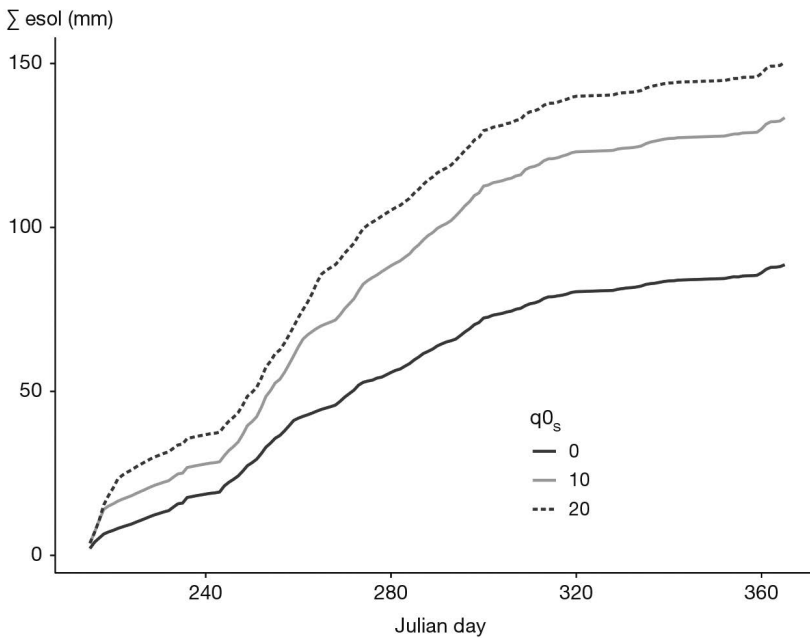


Figure 11.4. Cumulative soil evaporation from 1 August until 31 December in northern France for three values of $q0_s$.

11.2.3 Distribution of soil evaporation in the soil profile

The method of calculating the distribution of evaporation resembles that in the LIXIM model (Mary *et al.*, 1999). The daily evaporation value $esol$, calculated in equation (11.6), is assumed to affect the layers of soil up from the base of the natural mulch $XMULCH$ (if present) to a maximum depth of z_{esx_s} . Below this depth, there is no evaporation. The contribution of each basic soil layer to evaporation esz decreases with depth, according to the following function (Eq. (11.7)):

$$\begin{aligned}
 & \text{for } XMULCH < z \leq z_{esx_s} \\
 & \frac{esz(z,t)}{esol(t)} = \frac{\left(1 - \frac{z}{z_{esx_s}}\right)^{cfes_s} \cdot Wi(z,t)}{\sum \left(1 - \frac{z}{z_{esx_s}}\right)^{cfes_s} \cdot Wi(z,t)} \\
 & \qquad \qquad \qquad \text{with} \\
 & Wi(z, t) = \frac{hur(z,t) - ha}{hucc(z) - ha} \quad (11.7)
 \end{aligned}$$

where $cfes_s$ is a slope coefficient, and Wi is an ‘evaporative conductance’, hur is the actual volumetric soil water content, ha is the residual soil water content defined in Eq. (11.6). By varying parameters z_{esx_s} and $cfes_s$, it is possible to account for differences in hydraulic conductivity from one soil to another. A very high surface moisture gradient during soil drying is correctly represented by a high $cfes_s$ value. The sensitivity of the soil evaporation depth partitioning to the parameters $cfes_s$ and z_{esx_s} is represented in Figures 11.5 and 11.6. If nothing is known about the soil, the user can enter the standard proposed values: $cfes_s \approx 5$ and $z_{esx_s} \approx 60$ cm.

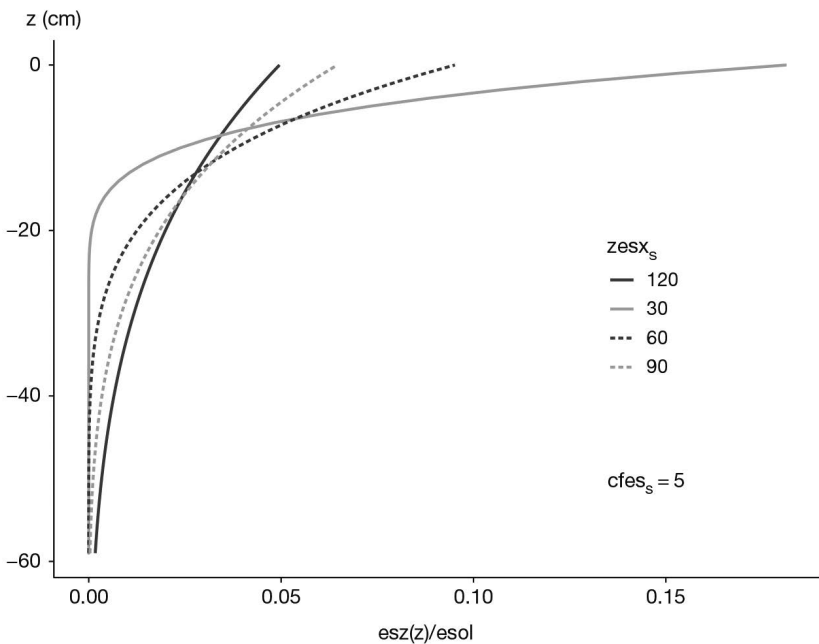


Figure 11.5. Partitioning of soil evaporation with depth as a function of the parameter z_{esx_s} and $cfes_s = 5$, assuming $Wi = 1$ and $XMULCH = 0$.

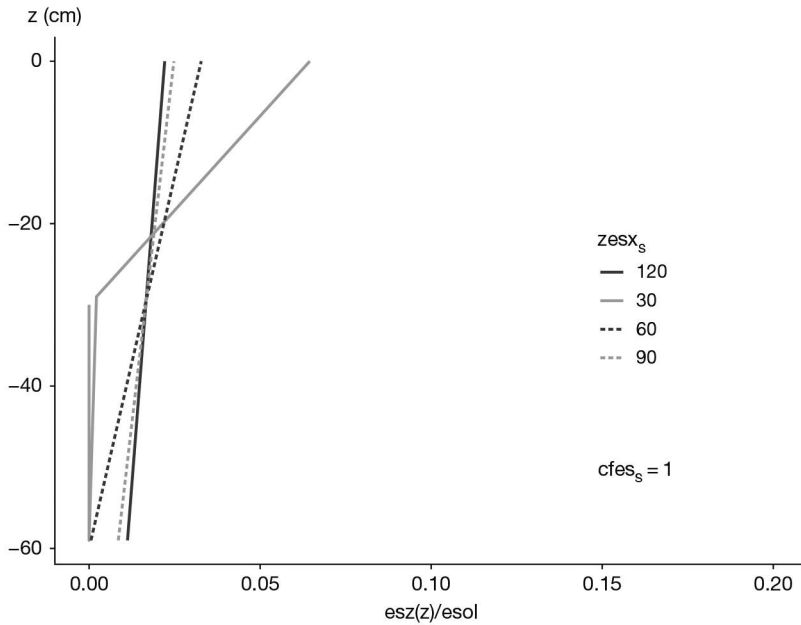


Figure 11.6. Partitioning of soil evaporation with depth as a function of the parameter $zesx_s$ and $cfes_s = 1$, assuming $Wi = 1$ and $XMULCH = 0$.

►► 11.3 Potential crop water requirements

The two approaches described for soil potential evaporation have their equivalent for plant water requirements (or maximum transpiration, eop).

11.3.1 The crop coefficient approach

In the crop coefficient approach, fully documented in Brisson *et al.* (1992), plant water requirements (maximum transpiration) are calculated in several steps using the potential evapotranspiration as the driving variable.

The first calculation pertains to what the crop evaporation value would be if none of the soil or plant surfaces had limited water (eo). This evaporation is a logistic function of the lai (or a linear function of the ground cover), which involves the $kmax_p$ parameter, the maximum crop coefficient of the crop (Eq. (11.8) and (11.9) and Figures 11.7 and 11.8). The $kmax_p$ value is attained when the lai is approximately 5 (or $tauxcouv$ equals $tauxrecouv kmax_p$, generally taken to 1) and depends on the reference evapotranspiration used (Penman, Penman-Monteith or Priestley-Taylor: Penman (1948), Monteith (1965), Priestley and Taylor (1972)).

$$eo(t) = tetp(t) \cdot \left[1 + \frac{kmax_p - 1}{1 + e^{-1.5lai(t)-3}} \right] \quad (11.8)$$

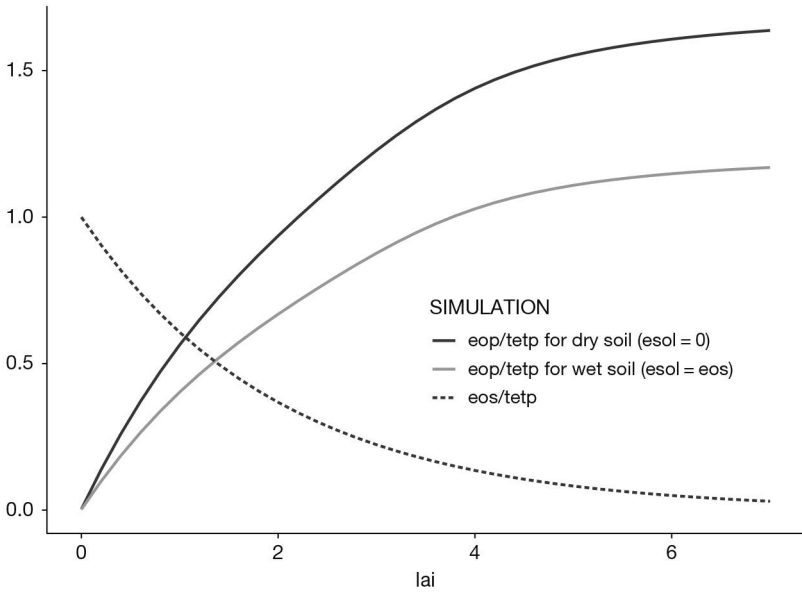


Figure 11.7. Relative evaporative demand applied to soil (eos/tetp) and crop (eop/tetp) accounting for the actual soil surface water state (esol=eos or esol=0) for canopy qualified in lai.

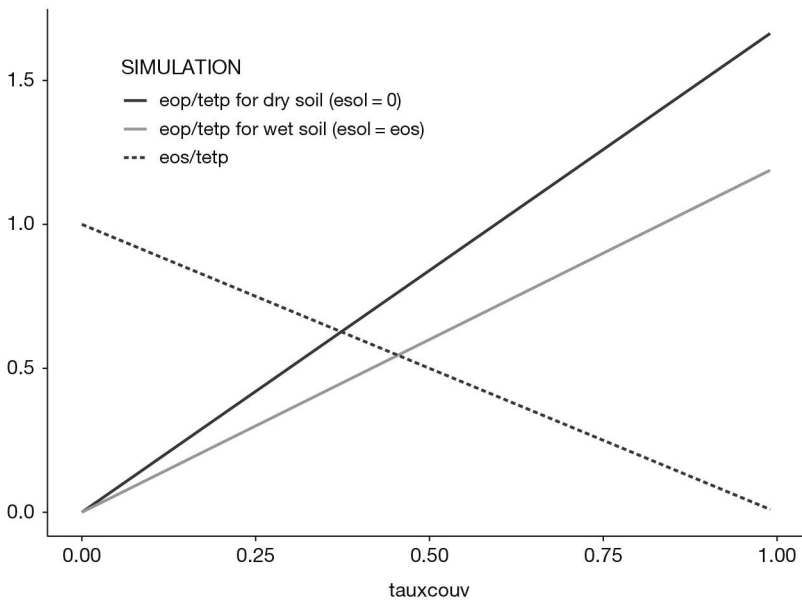


Figure 11.8. Relative evaporative demand applied to soil (eos/tetp) and crop eop/tetp) accounting for the actual soil surface water state (esol=eos or esol=0) for canopy qualified in ground cover (tauxcouv).

If ground cover is used instead of lai (§ 4.1.4):

$$\begin{aligned}
 eo(t) &= tetp(t) \cdot \left[\frac{tauxcouv(t)}{tauxrecouv\mathbf{kmax}_p} \cdot (\mathbf{kmax}_p) - 1 \right] + 1 \\
 &\quad \text{if } tauxcouv(t) < \mathbf{tauxrecouv\mathbf{kmax}_p} \\
 eo(t) &= \mathbf{kmax}_p \cdot tetp(t) \\
 &\quad \text{if } tauxcouv(t) \geq \mathbf{tauxrecouv\mathbf{kmax}_p} \quad (11.9)
 \end{aligned}$$

If the leaves ($mouill \neq 0$) or the plant mulch laid on the soil surface ($mouillmulch \neq 0$) have intercepted water (§ 9), this water will evaporate depending on the reference evaporative demand ($tetp$): E_{md} for leaves (Eq. (11.10) and (11.11)) and e_{mulch} for mulch (Eq. (9.22)). Naturally, the E_{md} threshold is set by the amount of water retained on the foliage ($mouill$), while the e_{mulch} threshold is set by the amount of water retained in the mulch ($mouillmulch$). The evaporated water contributes to reducing evaporative demand at the plant level.

$$E_{md}(t) = \min(mouill(t), eo(t) - tetp(t) \cdot e^{-DELTA\mathbf{la}(t)}) \quad (11.10)$$

Or, if ground cover is used instead of lai § 4.1.4:

$$E_{md}(t) = \min(mouill(t), eo(t) - tetp(t) \cdot (1 - tauxcouv(t))) \quad (11.11)$$

Maximum transpiration depends on the available energy in plants, estimated by subtracting e_{os} from e_o , but also on atmospheric conditions in the vegetation. To account for the increase in plant demand due to the dryness of the soil below the vegetation, we use the empirical relationship (Eq. (11.12)) based on the parameter $BETA_G$ deduced from work by Denmead (1973), Ritchie (1985) or Feddes and Hooghart (1987).

$$eop(t) = (eo(t) - E_{directM}(t)) \cdot \left[\mathbf{beta}_G - (\mathbf{beta}_G - 1) \cdot \frac{E_{direct}(t)}{E_{directM}(t)} \right] \quad (11.12)$$

considering that $E_{directM}$ corresponds to evaporation of water intercepted by soil, mulch and leaves together, and that E_{direct} corresponds to the actual evaporation of the three together. A value of 1.4 is taken for \mathbf{beta}_G . This value causes eop to increase by a maximum of 40% when the soil is completely dry.

11.3.2 The resistance approach

The crop coefficient approach can create problems in cases where it is not possible to apply Beer's law in a straightforward way (see § 4.2, or when the relationship between LAI and canopy height is not stable). Moreover, that approach is somewhat unreliable with regard to the soil evaporation variable and the microclimatic effect around the plant. We therefore implemented an alternative approach which consists in estimating plant water requirements and soil evaporation using the Shuttleworth-Wallace daily time-step model (Brisson *et al.*, 1998a). This has proved to be effective for explaining the canopy energy budget (Sene, 1994), provided that appropriate empirical resistance parameters are used (Fisher and Elliot, 1996) (see § 9.3.3 for a full description of theoretical bases and resistance calculations).

11.3.2.1 Calculating soil evaporation

Soil evaporation, which was described in § 11.2, is calculated using a potential evaporation value obtained from an intermediate value of the saturation deficit. This computation is based on the hypothesis that the evaporation can be estimated using a Priestley-Taylor-type formalisation when the soil is near complete saturation.

►► 11.4 Physical soil surface conditions

11.4.1 Impacts of mulch on soil water balance

This section is devoted to the characterisation of the soil surface conditions to predict their effects on the water and heat balances of the soil-crop system. These effects are integrated into the calculations of water requirements (§ 11.3) and water and heat transfers (§ 10). However, to make it easier to understand the formalisations used in these processes, we explain below the modifications that result from taking soil surface conditions into account.

Soil surface conditions are characterised by soil and technical parameters. One of them is the soil albedo under dry conditions (**albedo_S**). Another is the runoff coefficient (**ruisolnu_S**), which provides the proportion of rainfall subject to runoff that occurs when the soil is bare and when rainfall exceeds a given threshold (**pminruis_G**). These parameters summarise the effects of soil slope and roughness on surface runoff, which are assumed to be constant throughout the simulation.

The model also needs to know whether a plant or plastic mulch is present (§ 13.2.7).

Height processes are modelled, the first five of which are related to the impacts of plant mulching on soil water balance, which is the theme of this section. The last three processes – effect on crop temperature and crusting – are discussed in the cited chapters. The height processes are:

- Plant mulch dynamics and proportion of soil cover (§ 12.2.3);
- Surface runoff due to the presence of obstacles at the soil surface (§ 11.4.3);
- Water interception by the mulch (see § 11.4.4, in relation to the energy balance calculations in § 9.3);
- Direct evaporation by the mulch and the decrease in soil evaporation induced by the presence of mulch (§ 11.2);
- Effects of these modified fluxes on the plant's water requirements (§ 11.3);
- Modifications to crop temperature linked to changes in the fluxes and albedo of the soil surface (§ 9.3);
- Soil crusting during emergence (§ 3.4.1.4);
- Snow effect on water transfer and crop temperature (§ 10.3).

Figure 11.9 provides an example to illustrate the abovementioned effects of mulch on the water balance (transpiration, soil and mulch evaporation) on a winter wheat crop growing in the north of France. Note that this example is also treated on Figure 13.1 with other variables.

The link between the physical role of the plant mulch accounted for here and the biochemical role of carbon and nitrogen mineralisation is not programmed in STICS yet.

To account for this biochemical role, it is essential to also consider the mulch as a crop residue left on the soil surface, and to determine its chemical composition with appropriate parameters (§ 13.5.3).

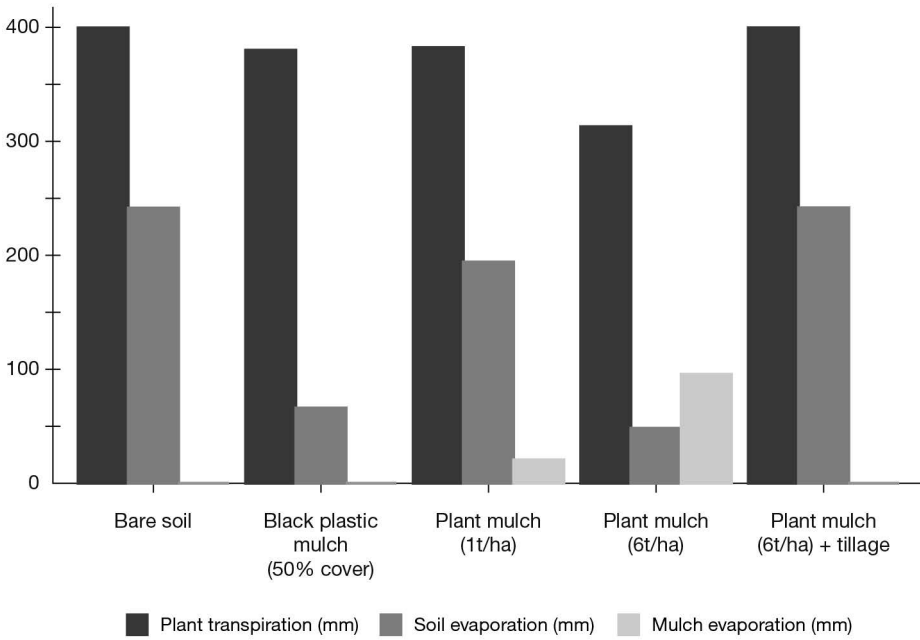


Figure 11.9. Simulated effects of a mulch on the various processes involved in the water and nitrogen balances, and their consequences on the water fluxes.

11.4.2 Evolution of soil cover

The processes of mulch decomposition and mulch quantity are presented in § 12.2.3.

The proportion of soil covered by mulch (**couvermulchplastique_T**) is also exponentially related to the quantity of mulch (q_{mulch} , in $t\ ha^{-1}$) using the parameter **kcouvmlch_G** (Eq. (11.13)). Scopel *et al.* (1998) gave **kcouvmlch_G** values ranging from 0.092 to 0.367 depending on the type of plant residue (entire plant, fresh or decomposed, stalks). This parameterisation indicates that the type of plant residue affects both the proportion of soil cover and the rate of decomposition (Figure 11.10). As for plastic mulching, **couvermulch** is constant and treated as a technical parameter.

For plant mulching:

$$couvermulch(t) = 1 - e^{-kcouvmlch_G q_{mulch}(t)} \quad (11.13)$$

For plastic mulching:

$$couvermulch(t) = \mathbf{couvermulchplastique}_T \quad (11.14)$$

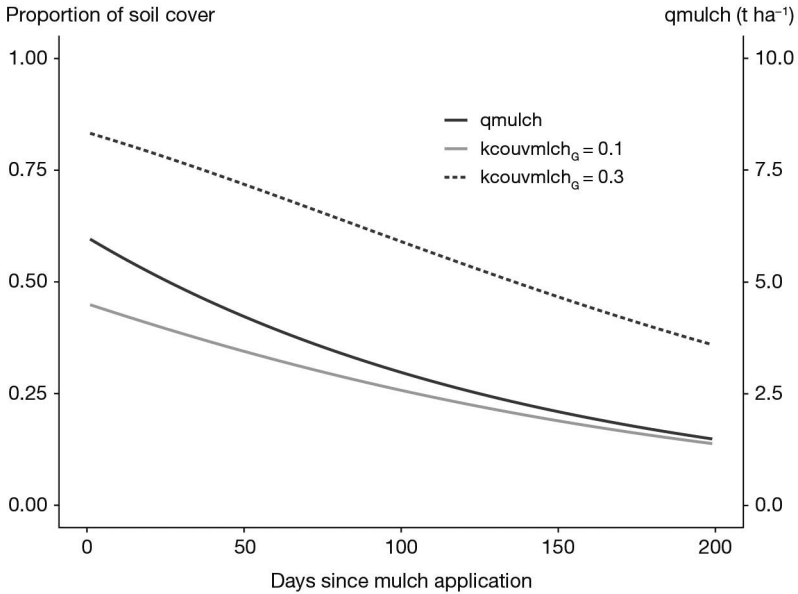


Figure 11.10. Variation in the proportion of the soil covered by a plant mulch, whose quantity (q_{mulch} in $t\ DM\ ha^{-1}$, initial mulch amount = $6\ t\ DM\ ha^{-1}$) decreases as a function of the type of the crop residue given by the parameter $kcouvmlch_G$ (a high value for entire fresh plants and a low value for cut stalks).

11.4.3 Surface runoff

We separate surface runoff associated with soil surface conditions ($ruisselsurf$) and runoff associated with a lack of soil infiltrability; the latter is simulated by the water and nitrogen transfer (§ 10.1). We calculate the surface runoff $fruis$ variable (Eq. (11.16)), which is the proportion of runoff water above the activation threshold ($pminruis_G$), as shown in Eq. (11.15).

$$\begin{aligned}
 ruisselsurf(t) &= fruis(t) \cdot (precip(t) - stemflow(t) - pminruis_G) \\
 &\quad \text{if } (precip(t) - stemflow(t)) > pminruis_G \\
 ruisselsurf(t) &= 0 \\
 &\quad \text{if } (precip(t) - stemflow(t)) \leq pminruis_G \quad (11.15)
 \end{aligned}$$

where $qmulchruis0_G$ is the mass of mulch above which runoff starts. For values between $qmulch = 0.1$ and $qmulch = qmulchruis0_G$, we use the relationship established by Scopel *et al.* (1998) to calculate FRUIS: above $qmulchruis0_G$, FRUIS is zero, and below 0.1 we take the value of $ruisolnu_S$ (Figure 11.11).

$$\begin{aligned}
 fruis(t) &= ruisolnu_S \quad \text{if } (qmulch(t) < 0.1) \\
 fruis(t) &= 0.33 \cdot (qmulchruis0_G - qmulch) \quad \text{if } 0.1 < qmulch(t) < qmulchruis0_G \\
 fruis(t) &= 0 \quad \text{if } qmulch(t) > qmulchruis0_G \quad (11.16)
 \end{aligned}$$

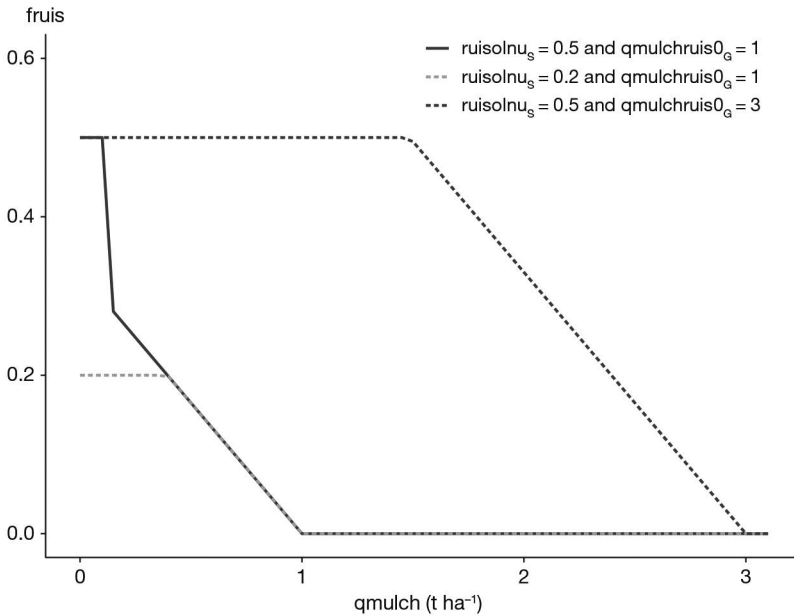


Figure 11.11. Proportion of runoff water as a function of the soil surface (**ruisolnu_s**) and the plant mulch (**qmulchruis0_G** and **qmulch**).

The effect of vegetation being present above the soil (*lai*) is accounted for via mechanisms for the flow of water along stems (stemflow) as the *fruis* proportion only applies to the amount of water not involved in stemflow (Eq. (11.17)).

$$\text{stemflow} = \text{stemflowmax}_p \cdot (\text{trr}(t) + \text{airg}(t)) \cdot [1 - \exp(-\text{kstemflow}_p \cdot \text{lai}(t))] \quad (11.17)$$

The **stemflowmax_p** parameter may vary from 0.2 to 0.5, depending on the species. The **kstemflow_p** parameter is less well known: it can initially be equal to the solar radiation extinction coefficient (**extin_p**).

11.4.4 Interception of water by mulch

The maximum water content of the plant mulch (**mouillmulch**), calculated using Eq. (11.18) is proportional to the mulch mass (**qmulch**), and its wettability (**mouillabilmulch_G**). The mulch wettability can vary between 0.22 and 0.38 mm t⁻¹ ha⁻¹ (Scopel *et al.*, 1998). The amount of water retained is limited by the incident rainfall minus the surface runoff.

$$\text{mouillmulch}(t) = \text{mouillabilmulch}_G \cdot \text{qmulch}(t) \quad (11.18)$$

The amount of water directly evaporated from the mulch (**emulch**) can be calculated in two ways, using either the reference evapotranspiration (Eq. (11.19)) given in the weather input file (**tetp** intended to be the Penman value) or the raw weather variables, which include wind speed and air humidity. The **emulch** value is limited by **mouillmulch**:

$$emulch(t) = tetp(t) \cdot couvermulch(t) \cdot \exp(-(\mathbf{extin}_p - 0.2) \cdot lai(t))$$

Or if cover rate is used instead of

$$emulch(t) = tetp(t) \cdot couvermulch(t) \cdot (1 - tauxcouv(t))$$

and $emulch(t) \leq mouillmulch$ (11.19)

With the first method, it is assumed that the water contained in mulch evaporates in the same way as from a grass canopy, according to a resistance/height compensation phenomenon. This phenomenon corresponds to the ‘extinction of energy at the soil level’ by the vegetation (as is the case for soil). If the \mathbf{extin}_p parameter is not active (because the radiation intercepted by the canopy is calculated with the radiation transfer model and not using the Beer’s law approach as explained in § 9.2.1.1), the value is recalculated and varies depending on the crop geometry and the quality of radiation.

With the second method, the Shuttleworth-Wallace formalisation is applied as explained in § 11.3.2, and $emulch$ evaporates in the same way as free water located at the soil level receiving energy. It takes into account the proportion of soil covered by the mulch ($couvermulch$).

In both cases $emulch$ is limited by the amount of water intercepted by the plant mulch, $mouillmulch$.

11.4.5 Modification to soil evaporation due to the presence of mulch

Incident energy at the soil level under the mulch is linearly related to the proportion of soil covered, which considerably reduces direct soil evaporation. In the option using the reference evapotranspiration as an input, the relationship is directly applied to the potential soil evaporation (eos) as given in Eq. (11.20), while it is applied to the radiation balance in the option using the Shuttleworth-Wallace formalisation (§ 11.2).

$$eos(t) = tetp(t) \cdot (1 - couvermulch) \cdot e^{-(\mathbf{extin}_p - 0.2)lai(t)} \quad (11.20)$$

11.4.6 Modification of crop requirements by the presence of mulch

If the Shuttleworth-Wallace formalisation is used, $emulch$ contributes to a reduction in the saturation deficit (dos) in the same way as direct soil evaporation and the evaporation of water intercepted by the foliage (§ 11.2 and § 9.3.4.3). If the reference potential evapotranspiration approach is adopted, $emulch$ also reduces the evaporative demand according to an empirical formula given in § 11.3.

11.4.7 Modification of crop and soil temperatures by the presence of mulch

First, the mulch influences the temperature regime by modifying the soil surface albedo as defined in Eq. (9.15), using the parameter $\mathbf{albedomulchresidus}_G$. Second, the total evapotranspiration from the soil-plant system (evaporation + transpiration), to which the energy balance is applied, accounts for evaporation from the mulch. Taken together, these two phenomena modify the crop temperature. When plastic mulch is used, the temperature is considerably modified.

►► 11.5 Plant transpiration and derived stresses

To calculate actual transpiration, we chose to use a relationship linking relative transpiration (ratio of actual to maximum transpiration) to soil water content. Such a simplified mathematical representation was proposed by van Bavel (1953) for the total evapotranspiration. He suggested a straight-line relationship allowing simple calculations of soil water balance. Subsequent studies have shown that the relationship was more likely to be curvilinear (Denmead and Shaw, 1962; Eagleman, 1971) or exponential (Baier, 1969). Nevertheless a bilinear function may provide a good representation of experimental data (Burch *et al.*, 1978; Meyer and Green, 1981; Robertson *et al.*, 1993; Rosenthal *et al.*, 1985) and was adopted as the driving equation of many simple water balance models (Leenhardt *et al.*, 1995). This relationship assumes that a crop is able to take up soil water at a maximal rate to meet atmospheric demand until the soil water content falls below some threshold value. Though in many models, this threshold is assumed to be a constant equal to 30%, 40% or 50% of the maximum available water content (Fisher and Elliot, 1996; Hunt and Pararajasingham, 1995; Mailhol *et al.*, 1996; Robertson *et al.*, 1993), it was shown to depend on atmospheric demand, species and time within the crop cycle (Burch *et al.*, 1978; Cordery and Graham, 1989; Doorenbos *et al.*, 1980; Gardner, 1991; Hallaire, 1964; Novak, 1989; Palacios and Quevedo, 1996; Texeira *et al.*, 1996). Based on work by Slabbers (1980), we proposed an operational formula to calculate this threshold using the soil water content, derived from basic laws governing water transfer in the soil-plant atmosphere continuum (Brisson *et al.*, 1998a).

11.5.1 Actual transpiration

On a daily time scale, root uptake can be considered to be equal to leaf transpiration. The overall calculation of root uptake is then distributed between the soil layers. Relative transpiration, *i.e.* the relationship between actual transpiration and maximum transpiration (ep/eop), is a bilinear function of the available water content in the root zone, $teta$ (*i.e.* the water content above the wilting point in cm^3 of water cm^{-3} of dry soil). The ep/eop ratio is considered as the stomatal water stress ($swfac$, Eq. (11.21)), which is represented in Figure 4.11.

$$swfac = \frac{ep(t)}{eop(t)} \quad (11.21)$$

The water content threshold separating the maximum transpiration stage and the reduced transpiration stage ($tetstomate$) depends on root density, the stomatal functioning of the plant, and the evaporative demand as expressed in Eq. (11.22), according to Brisson *et al.* (1998a), who showed that that this threshold does not depend on the soil type, for example via the maximal available soil water content.

$$tetstomate(t) = \frac{1}{80} \cdot \ln \left(\frac{eop(t)}{2\pi \cdot cumlrac z(t) \cdot psisto_p \cdot 10^{-4}} \cdot \ln \left(\frac{1}{\text{rayon}_p \cdot \sqrt{\frac{cumlrac z(t)}{zrac(t)}}} \right) \right) \quad (11.22)$$

where $cumlrac z$ is the sum over the whole rooting depth ($zrac$), of effective root length density $lrac z$ (in $cm \text{ cm}^{-3}$), $psisto_p$ (positive in bars) is the critical leaf water potential

of stomatal closure, and rayon_p is the mean root radius, which is assumed to be equal to 0.02 cm. When using this formula, we find that the tetstomate threshold tends to be stable beyond a certain root depth (Figure 11.12). Table 11.1 summarises the role played by the various factors influencing this value. It highlights the dominant effect of evaporative demand (EOP), and the parameter of stomatal closure, psisto_p .

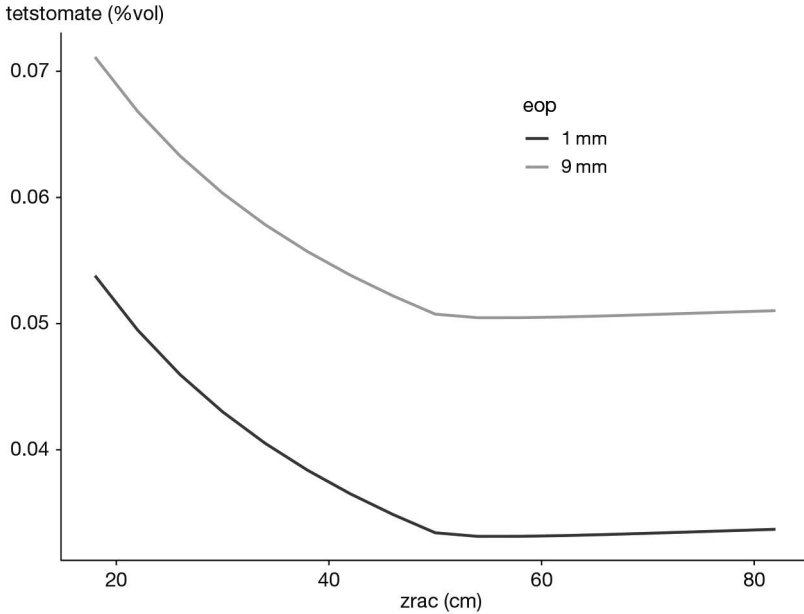


Figure 11.12. Influence of the rooting depth (zrac) and the maximum daily transpiration (eop) on the threshold of soil water content above wilting point (tetstomate) below which the transpiration is reduced.

Table 11.1. Sensitivity analysis of the threshold tetstomate (in cm^3 water cm^{-3} soil above the wilting point).

Parameters	Nominal value	tetstomate sensitivity	
Root profile (pivot, ramified)	In between	0.050	0.068
rayon ($5e-3$ to $7e-2$ cm)	0.02	0.052	0.060
psisto (5 to 25 bars)	15	0.050	0.070
eop (1 to 9 mm)	4	0.039	0.066

11.5.2 Extrapolation to the water stress turgor index

The ep/eop ratio is equal to the stomatal stress index, swfac . The stress turgor index turfac , which affects leaf growth, comes into play earlier. The method for calculating this index is similar to the method used for swfac and uses the critical potential of cell expansion psiturg_p in Eq. (11.22). Since psiturg_p is lower than psisto_p , we obtain a higher teturg threshold. In other words, leaf growth can be inhibited even when transpiration is still at its maximum level (Figure 4.11).

11.5.3 Distribution of root water extraction within the profile

Water absorption ep is distributed in the root zone (epz profile) 1 per 1 cm layer of soil, according to two factors, each having the same influence: the effective root density profile, $lracz$, and the available water content ($hur - humin$) (Eq. (11.23)). The roots are assumed to be effective whenever the soil layer water content is above wilting point. Moreover, it is assumed that the water located in the macroporosity does not contribute to transpiration. It is assumed that macroporosity fills up when microporosity is already filled.

$$epz(z, t) = ep(t) \cdot \frac{lracz(z)(hur(z) - humin(z))}{\sum_{z=1}^{z=soil\ depth} lracz(z)(hur(z) - humin(z))} \quad (11.23)$$

An iterative calculation distributes the transpiration within the soil profile, ensuring that the whole of ep is shared out according to both root and water availability.

►► 11.6 Water balance

The calculation of all the variables contributing to water fluxes in the soil-plant-atmosphere continuum contributes to the water balance (Table 11.2). These fluxes are used to compute the water balance of the daily soil water content.

Table 11.2. Components of the water balance in a STICS output.

Inputs	(mm)	Outputs	(mm)
Initial water content	300	Final water content	284
Rain	830	Evaporation	46
Irrigation	94	Transpiration	448
		Runoff	0
		Capillary rise	0
		Deep infiltration	364
		Mole drainage	0
		Leaf interception	0
		Mulch interception	82
		Ineffective irrigation	0
INITIAL TOTAL	1224	FINAL TOTAL	1224

Chapter 12

Carbon and nitrogen transformations in soil and balances

*BRUNO MARY, FABIEN FERCHAUD, HUGUES CLIVOT
AND JOËL LÉONARD*

REVIEWED BY: NICOLAS BEAUDOIN

►► 12.1 Organic and mineral C-N pools

The nitrogen balance in the soil-plant system depends on the main processes affecting the organic and/or mineral nitrogen pools in soil (mineralisation, immobilization, nitrification, volatilisation, denitrification, leaching) and the source/sink effect of the crop (symbiotic N fixation, absorption of mineral N). The various C and N pools considered in the STICS model, together with the corresponding C and N fluxes, are shown in Figure 12.1. They include:

- mulch residues, i.e. organic residues added and remaining at the soil surface, coming from aerial crop residues brought after harvest operations (QCressuite), leaves or stems falling to the soil during pruning or trimming operations (QCrogne), senescent leaves falling to the soil (QCplantetombe) and exogenous organic residues (QCresorg) such as manure, added as fertilisers or amendments;
- organic residues mixed in soil layers (Cr) down to the depth **profhum_s**;
- microbial biomass (Cb) involved in the decomposition of these organic residues ('zymogeneous biomass'), both in the mulch and the biologically active soil layers;
- 'humified' organic matter (Chumt), composed of an active pool (Chuma) and an inert pool (Chumi);
- mineral pools (CO₂ and mineral N) resulting from the decomposition of organic matter or N inputs through N fixation and mineral N fertilisers.

The net N mineralisation, *i.e.* the net production of mineral N by the soil, is the sum of two components:

'Humus' mineralisation, which results from the decomposition of the active soil organic matter pool. This is a permanent process which always leads to a release of mineral N, *i.e.* a positive net mineralisation, called 'basal' mineralisation.

Organic residues mineralisation, which is associated with the decomposition of crop residues (straw, roots, etc.) or organic wastes added to the soil. It is a process

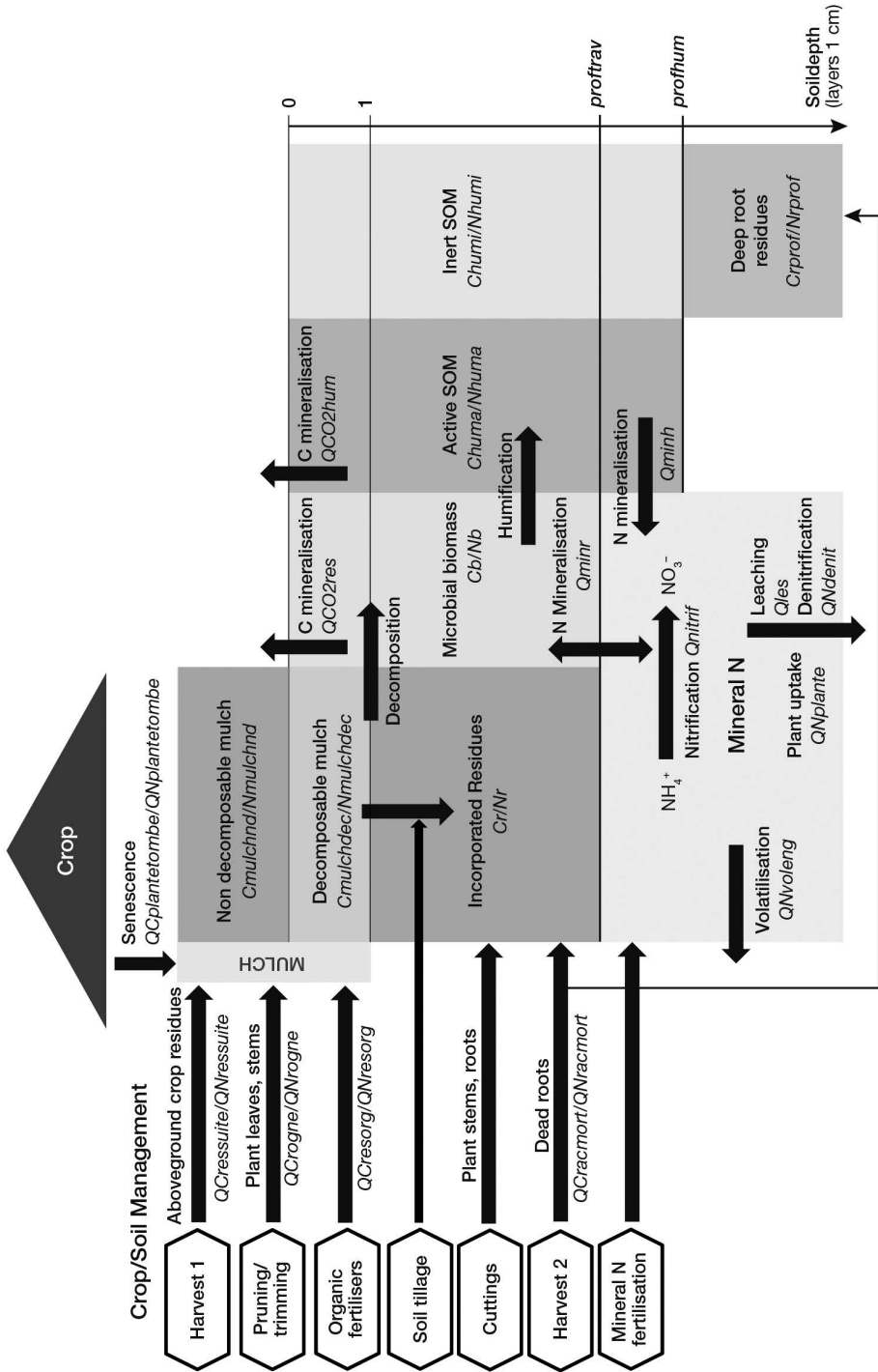


Figure 12.1.1. Soil C and N compartments and incoming and outgoing C and N fluxes in the STICS model (adapted from Autret *et al.*, 2020). STICS variable names are in italics.

which is highly variable over time. During a first phase after the addition of residues, the mineralisation can be positive or negative (immobilisation of soil mineral N). During the second phase, it is positive through the 're-mineralisation' process which releases N coming from either the residue or the microbial biomass which has broken it down.

The humified organic N in soil (N_{humt} , in kg ha^{-1}) is composed of two pools: an active pool (N_{huma}) and an inert pool (N_{humi}). The first pool is fed by the humification of fresh organic residues and contributes to mineralisation, whereas the second is assumed to be inert on the time scale of a century. Such an inert pool is included in most models simulating the long-term evolution of soil organic matter. However the models differ greatly in the size of this pool, which may vary from less than 10% in ROTHC (Coleman and Jenkinson, 1996) to 50% in CENTURY (Parton *et al.*, 1987), 40% to 80% in AMG (Clivot *et al.*, 2019) and even 60% to 80% (Ludwig *et al.*, 2007, 2003).

In STICS, the initial proportion of the inert pool (\mathbf{finert}_s , ratio of $Chumi$ to $Chumt$) is set to a default value of 0.65. This value appeared to be adequate to simulate the evolution of soil organic carbon in long-term arable experiments with the AMG model (Saffih-Hdadi and Mary, 2008), which includes a mineralisation function similar to STICS (Clivot *et al.*, 2019). However this value depends on the cropping history of the field. It should be smaller (down to 0.40) if the soil had a recent history of grassland or forest land use or if it received large amounts of organic amendments.

The decomposition and mineralisation processes are dependent on soil and environmental conditions, and may be affected differently by them, particularly soil temperature and water content. The effect of temperature on C or N mineralisation in soil is still a matter of controversy, as pointed out by Kirschbaum (2006). We attribute some of the disagreement between authors to the fact that the temperature response differs according to the type of organic matter decomposed. In STICS we use a different function for decomposition of humified soil organic matter (SOM) and fresh organic residues. The effect of soil moisture might also be different for the two processes, but little is known about this aspect. Therefore we use a single function to describe the effect of water content on decomposition and C and N mineralisation.

► 12.2 Decomposition and mineralisation of organic matter

12.2.1 Mineralisation of humified organic matter

Decomposition of humified SOM takes place mainly in the upper layer of soil. Although the soil below the tilled depth and the subsoil may contain important reserves of organic C and N, their decomposition rate appears to be slow compared to the upper soil layer (Fontaine *et al.*, 2007; Clivot *et al.*, 2017). In STICS, mineralisation is assumed to occur down to a maximum depth ($\mathbf{profhum}_s$, in cm) and be negligible below this depth. The N mineralisation rate (V_{minh} , in $\text{kg N ha}^{-1} \text{ day}^{-1}$) depends on the amount of active soil organic nitrogen (N_{huma} , in kg N ha^{-1}) over this depth and the actual mineralisation rate constant ($K2$, in day^{-1}):

$$V_{minh}(t) = K2(t) \cdot N_{huma}(t) \quad (12.1)$$

Nhuma varies throughout time. At the beginning of simulation, Nhuma is calculated as follows:

$$Nhuma = 1000 \sum_{z=1}^{\text{profhum}_s} \mathbf{Norg}_S \cdot (1 - \mathbf{finert}_G) \cdot \mathbf{DAF}_S(z) \cdot \left(1 - \frac{\mathbf{cailloux}_S(z)}{100}\right) \quad (12.2)$$

where $\mathbf{profhum}_s$ is the depth of the biologically active layer (in cm), \mathbf{Norg}_S is its organic N content (in %), \mathbf{finert}_s is the fraction of inert carbon in SOM, \mathbf{DAF}_s (in g cm^{-3}) is the bulk density of the fine earth and $\mathbf{cailloux}_s$ is the volumic percentage of pebbles in soil (proportion of material > 2 mm, in %).

The actual mineralisation rate constant K2 is calculated as:

$$K2(t) = K2hum \cdot \text{tnh} \quad (12.3)$$

with

$$\text{tnh} = \frac{\sum_{z=1}^{\text{profhum}_s} \text{fh}(t, z) \cdot \text{fth}(t, z)}{\mathbf{profhum}_s} \quad (12.4)$$

Khum is the potential mineralisation rate constant (day^{-1}), i.e. the mineralisation rate constant of a soil maintained at the reference temperature value ($\mathbf{trefh}_G = 15^\circ\text{C}$) and reference moisture content (field capacity). The tnh factor (unitless) is the normalised time for humus mineralisation, accounting for the effect of soil moisture and temperature compared to reference conditions.

The soil water content (hur) modifies the mineralisation rate according to a multi-linear function (Eq. (12.5)). Mineralisation is nil when the soil water content is below \mathbf{hminm}_G (Figure 12.2). It increases when the water content increases and then decreases. The maximum rate is reached when the soil water content (expressed as a proportion of field capacity) is between \mathbf{hoptm}_G and 1. It decreases and reaches the rate $\mathbf{fhminsat}_G$ when the soil is saturated. Values of these parameters can be different for temperate and tropical soils.

$$\begin{aligned} \text{fh}(z, t) &= \min \left[\frac{\frac{\text{hur}(z,t)}{\text{hucc}(z)} - \mathbf{hminm}_G}{\mathbf{hoptm}_G - \mathbf{hminm}_G}, 1 \right] \quad \text{if } \mathbf{hminm}_G < \frac{\text{hur}(z,t)}{\text{hucc}(z)} \leq 1 \\ \text{fh}(z, t) &= \frac{(1 - \mathbf{fhminsat}_G) \cdot \text{wfps} + \text{wfpscc} \cdot \mathbf{fhminsat}_G - 1}{\text{wfpscc} - 1} \quad \text{if } \frac{\text{hur}(z,t)}{\text{hucc}(z)} \geq 1 \\ \text{fh}(z, t) &= 0 \quad \text{if } \frac{\text{hur}(z,t)}{\text{hucc}(z)} < \mathbf{hminm}_G \end{aligned} \quad (12.5)$$

where wfps and wfpscc are the values of the water-filled pore space at actual water content and at field capacity, respectively.

The effect of soil temperature on basal mineralisation (fth) can be described either by an Arrhenius or a logistic function (Valé, 2006). We have chosen a logistic function which enables to simulate the slower increase in mineralisation rate at high temperatures when microbial activity slows down (Figure 12.3).

The proposed function is roughly exponential from 0°C to 25°C and increases more slowly above this temperature (Eq. (12.6)). It relies on three parameters including the

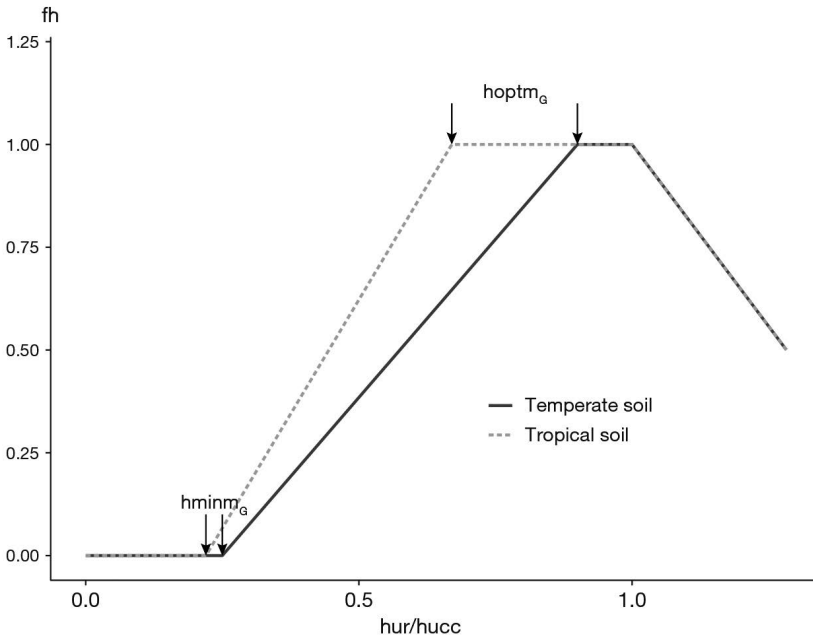


Figure 12.2. Influence of relative soil water content ($hur/hucc$) on decomposition rate of soil organic matter in two soils. Values of $hoptm_G$ and $hminm_G$ are 0.90 and 0.25 for the temperate soil (standard parameters, adapted from Rodrigo *et al.* (1997)) and 0.67 and 0.22 for the tropical soil (Sierra *et al.*, 2003). $fhminsat_G = 0.50$ and $DAF_S = 1.50$ in both soils.

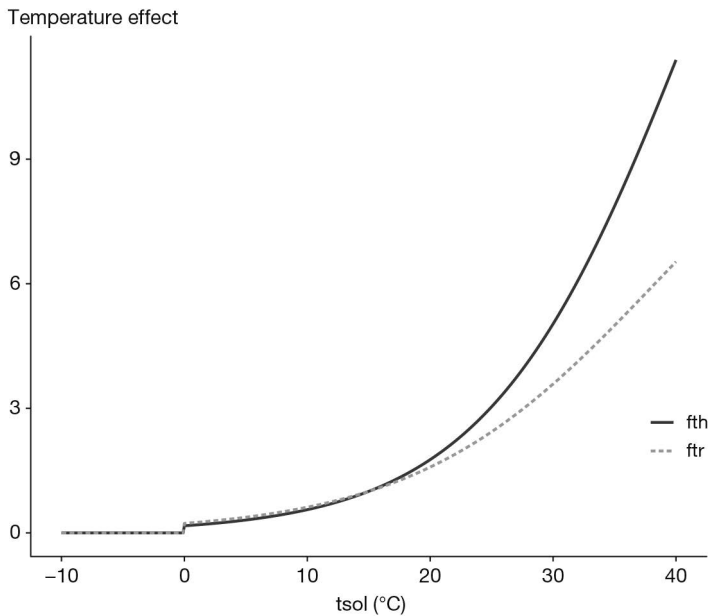


Figure 12.3. Influence of temperature on decomposition rates of organic matter: factor fth for humus and ftr for organic residues. Parameter: $tmin_mineralisation_G = 0$.

reference temperature (\mathbf{trefh}_G , set at 15°C). The parameter \mathbf{ftemha}_G corresponds to the asymptotic value of \mathbf{fth} and has been set to 25. Using these settings, the two parameters defining \mathbf{fth} are $\mathbf{ftemh}_G = 0.120 \text{ K}^{-1}$ and $\mathbf{ftemhb} = 145$.

$$\mathbf{fth}(z, t) = \frac{\mathbf{ftemha}_G}{1 + \mathbf{ftemhb} \cdot \exp(-\mathbf{ftemh}_G \cdot \mathbf{tsol}(z, t))}$$

$$\mathbf{fth}(z, t) = 0 \quad \text{if } \mathbf{tsol}(z, t) < \mathbf{tmin_mineralisation}_G \quad (12.6)$$

with

$$\mathbf{ftemhb} = (\mathbf{ftemha}_G - 1) \cdot \exp(\mathbf{ftemh}_G \cdot \mathbf{trefh}_G) \quad (12.7)$$

where $\mathbf{tmin_mineralisation}_G$ is the temperature below which mineralisation rate is nil. This logistic function allowed several authors to adequately simulate C or N mineralisation kinetics measured in controlled conditions in temperate or tropical soils (Balesdent and Recous, 1997; Nicolardot *et al.*, 2006; Valé, 2006). It is very close to an Arrhenius function with an activation energy $E_A = 78 \text{ kJ mol}^{-1} \text{ K}^{-1}$ between 0 and 35°C. It is also equivalent to a Van't Hoff function between 0°C and 25°C with a Q_{10} coefficient equal to 3.15.

The effect of soil tillage is not explicitly considered but is accounted for as follows. In a regularly ploughed soil, the nitrogen concentration is homogeneous in the ploughed layer and corresponds to \mathbf{Norg}_S . In this case $\mathbf{profhum}_S$ must be equal to or slightly greater than the ploughing depth in order to take into account the contribution of lower layers to the total mineralisation. However several studies (Valé, 2006; Oorts *et al.*, 2007; Clivot *et al.*, 2017) suggest that this contribution is small.

If the soil is no longer ploughed, the organic nitrogen distribution in the old plough layer becomes heterogeneous. The same calculation can be applied but $\mathbf{profhum}_S$ corresponds to the old depth of ploughing and \mathbf{Norg}_S represents the mean organic N concentration over this depth. If \mathbf{Norg}_S is measured over the new (and smaller) depth of soil tillage, $\mathbf{profhum}_S$ must correspond to that depth. In both cases, the possible change in bulk density (increase due to the reduction in soil tillage) must be taken into account.

According to Clivot *et al.* (2017), the potential mineralisation rate constant (\mathbf{Khum}) depends on the clay content measured after decarbonation (\mathbf{argi}_S in %), the CaCO_3 content (\mathbf{calc}_S in %), the soil pH measured in water (\mathbf{pH}_S) and the C/N ratio of the soil organic matter ($\mathbf{CsurNsol}$). \mathbf{Khum} is the product of four factors ($f1$ - $f4$) and involves seven parameters ($\mathbf{gmin1}_G$ - $\mathbf{gmin7}_G$):

$$\mathbf{K2hum} = \mathbf{gmin1}_G \cdot f1 \cdot f2 \cdot f3 \cdot f4 \quad (12.8)$$

with

$$f1 = \exp(-\mathbf{gmin2}_G \cdot \mathbf{argi}_S) \quad (12.9)$$

$$f2 = \frac{1}{(1 + \mathbf{gmin3}_G \cdot \mathbf{calc}_S)} \quad (12.10)$$

$$f3 = \exp(-\mathbf{gmin4}_G \cdot (\mathbf{pH}_S - \mathbf{gmin5}_G)^2) \quad (12.11)$$

$$f4 = 0.2 + 0.8 \cdot \exp(-\mathbf{gmin6}_G \cdot (\mathbf{CsurNsol} - \mathbf{gmin7}_G)^2) \quad (12.12)$$

The effects of clay content, CaCO_3 content, pH and C/N ratio on $\mathbf{K2hum}$ are illustrated in Figure 12.4.

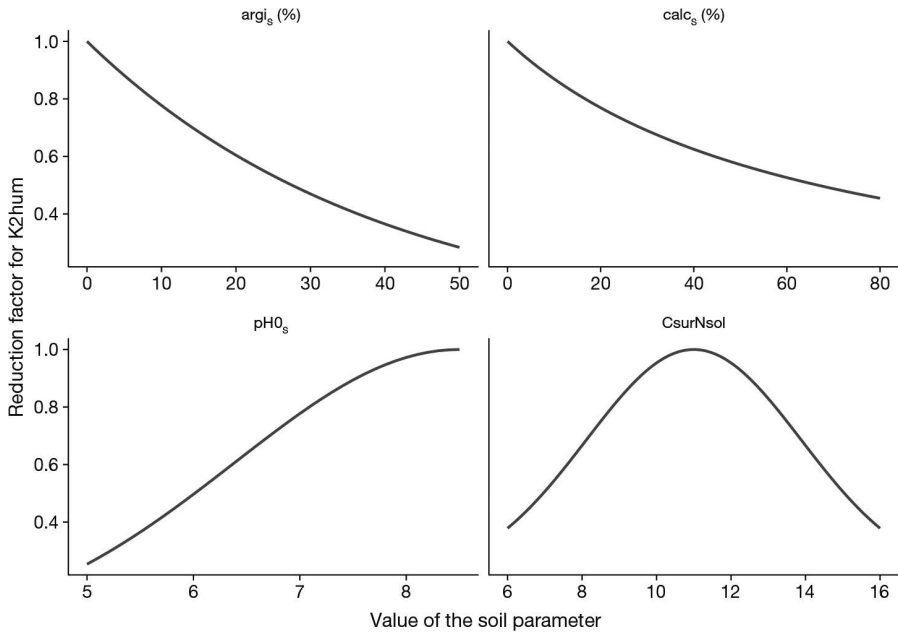


Figure 12.4. Influence of clay content (argi_s in %), CaCO_3 content (calc_s in %), pH (pH0_s) and C/N ratio (CsurNsol) on the potential decomposition rate of soil organic matter.

12.2.2 Decomposition of organic residues mixed in the soil

STICS simulates the decomposition of various organic residues and their humification due to microbial activity, as described by Nicolardot *et al.* (2001) and Justes *et al.* (2009) for crop residues. Nitrogen mineralisation depends on the decomposition rate of organic residues (i.e. carbon fluxes), their C/N ratio (CsurNres_T), the C/N ratio of the zymogeneous biomass (CNbio) and the C/N ratio of the newly formed humified matter (CNhum).

Ten categories (index r) of organic residues are considered in STICS:

- crop residues from mature crops (e.g. straw)
- crop residues from young plants (e.g. cover crops)
- animal manures
- green composts
- sewage sludges
- vinasses
- cattle horn
- vineyard prunings
- pig slurry
- rhizomes.

The fate of residues in each category (r) is followed separately. Figure 12.5 shows the carbon and nitrogen flows occurring during the decomposition of the organic residues.

The model is defined by six parameters, three of them being residue-dependent: two decomposition rate constants (k_{res} and kbio_G , in day^{-1}), two partition parameters

($yres_G$ and $hres$) and two C/N ratios (CN_{bio} and CN_{hum}). For a given category, the parameters are either constant ($kbio_G$, $yres_G$, and $CN_{hum}=1/Wh_G$) or dependent upon the C/N ratio of the organic residue ($CsurNres_T$), according to the following relationships:

$$kres(r) = akres_G(r) + \frac{bkres_G(r)}{CsurNres_T(r)} \quad (12.13)$$

$$CN_{bio}(r) = awb_G(r) + \frac{bwb_G(r)}{CsurNres_T(r)} \quad (12.14)$$

$$hres(r) = 1 - ahres_G(r) \cdot \frac{CsurNres_T(r)}{bhres_G(r) + CsurNres_T(r)} \quad (12.15)$$

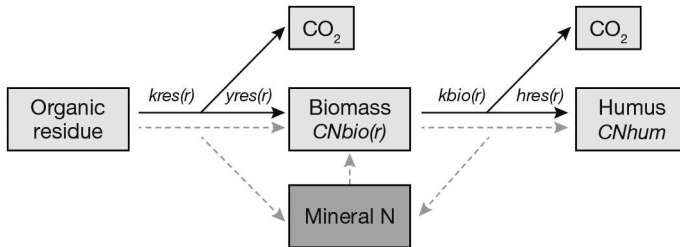


Figure 12.5. Flow diagram of the decomposition of organic residues in soil (Nicolardot *et al.*, 2001). The continuous lines indicate carbon flows and the dashed lines nitrogen flows.

The decomposition rate of organic residues ($\Delta Cres$, in $kg\ C\ ha^{-1}\ day^{-1}$) is assumed to follow first order kinetics versus the amount of decomposable carbon ($Cres$) and depends on their nature ($kres$), soil temperature (fth), water content (fh) and the soil mineral nitrogen in the layers containing the residues:

$$\Delta Cres(z, t, r) = -kres(r) \cdot Cres(z, t, r) \cdot ftr(z, t) \cdot fh(z, t) \cdot fredkN(z, t) \quad (12.16)$$

where $fredkN_G$ is a reduction factor of the decomposition rate of residues due to lack of nitrogen.

The change in the associated microbial biomass ($Cbio$) and the rate of humus formation ($\Delta Chum$), both in $kg\ C\ ha^{-1}\ day^{-1}$, are calculated as follows:

$$\Delta Cbio(z, t, r) = -yres_G(r) \cdot \Delta Cres(z, t, r) - kbio_G(r) \cdot Cbio(z, t, r) \cdot ftr(z, t) \cdot fh(z, t) \quad (12.17)$$

$$\Delta Chum(z, t, r) = kbio_G(r) \cdot hres(r) \cdot Cbio(z, t, r) \cdot ftr(z, t) \cdot fh(z, t) \quad (12.18)$$

The soil moisture content influences decomposition similarly to the decomposition of humified materials (Eq. (12.5)) whereas the soil temperature has a specific effect on the decomposition rate of organic residues. The thermal effect on residue mineralisation ftr is based on the data published by Balesdent and Recous (1997). It is similar to the logistic function defined for humus decomposition (Eq. (12.6)), but with different parameters. Using the same reference temperature ($trfr_G$), the parameters are: $ftrmr_G = 0.103\ K^{-1}$ and $ftrmra_G = 12$. The shape of the curve is shown in Figure 12.3.

The depth of residue incorporation in soil modifies their decomposition since water content and temperature vary with depth and their localisation determines the amount of mineral nitrogen available for the microbial biomass. Each tillage

operation is assumed to mix the residues uniformly with the soil over the depth defined by a minimal value (**profres_T**) and a maximal value (**proftrav_T**). The lower depth is a rather straightforward parameter to define. The upper depth has no true physical meaning (it should be 0) but is an equivalent depth defining the “residuesphere”, i.e. the volume of soil in close contact with the residues. It has been shown that decomposition and N immobilisation are markedly reduced when residues are stratified (i.e. located in a fraction of soil volume) compared to a situation where residues are homogeneously distributed throughout the soil (Magid *et al.*, 2006). Oorts *et al.* (2007) obtained a good simulation of C and N mineralisation under field conditions after addition of straw by considering that the residuesphere represented 10% of the total soil volume. Since STICS is a 1D model, it is not possible to simulate this effect explicitly: it must be done indirectly by considering the ratio **profres_T / proftrav_T** as the fraction of soil volume occupied by the residuesphere (see § 13.3.2).

The net N mineralisation rate (ΔN , in kg N ha⁻¹ day⁻¹, positive or negative) resulting from residue decomposition is calculated as the complement of the variation in the three organic pools:

$$\Delta N(z, t) = \sum_{r=1}^{10} -\Delta N_{res}(z, t, r) - \Delta N_{bio}(z, t, r) - \Delta N_{hum}(z, t, r) \quad (12.19)$$

A lack of mineral nitrogen modifies the decomposition and mineralisation rates through five domino effects:

- a reduction in the decomposition rate of residues (Giacomini *et al.*, 2007; Recous *et al.*, 1995) (factor **fredkN_G**);
- a shift in the C/N ratio of the zymogeneous biomass which reduces the N immobilisation rate (factor **fNCbio**);
- a reduction of the N humification rate (factor **fNChum**);
- a priming effect resulting in an increase of the decomposition rate of humified organic matter (factor **Priming**);
- a decrease in the microbial assimilation yield (factor **fCUE**).

The changes in the three N pools (residue, microbial biomass, humus) are calculated using the C/N ratio or N/C ratio of the three compartments, as follows:

$$\Delta N_{res}(z, t, r) = \frac{C_{res}(z, t, r)}{C_{surN_{res}}(r)} \quad (12.20)$$

$$\begin{aligned} \Delta N_{bio}(z, t, r) = & -\mathbf{yres}_G \cdot \Delta C_{res}(z, t, r) \cdot N_{Cbio}(r) \cdot \mathbf{fNCbio}(z, t) \\ & - \mathbf{kbio}_G \cdot N_{bio}(z, t) \cdot \mathbf{ftr}(z, t) \cdot \mathbf{fh}(z, t) \end{aligned} \quad (12.21)$$

$$\Delta N_{hum}(z, t, r) = \Delta C_{hum}(z, t, r) \cdot N_{Chum} \cdot \mathbf{fNChum} \quad (12.22)$$

Examples of C and N dynamics predicted by the model are given in Figure 12.6. The variation in organic pools may exceed the amount of N added by the residue when mineral N is immobilised.

The C and N mineralisation kinetics differ according to the type of organic residue (Figure 12.7). Decomposition results in net release of N for residues with a low C/N ratio (vinasse, C/N=8; catch crop C/N=15) and net immobilization with residues poor in N (rapeseed straw, C/N=45).

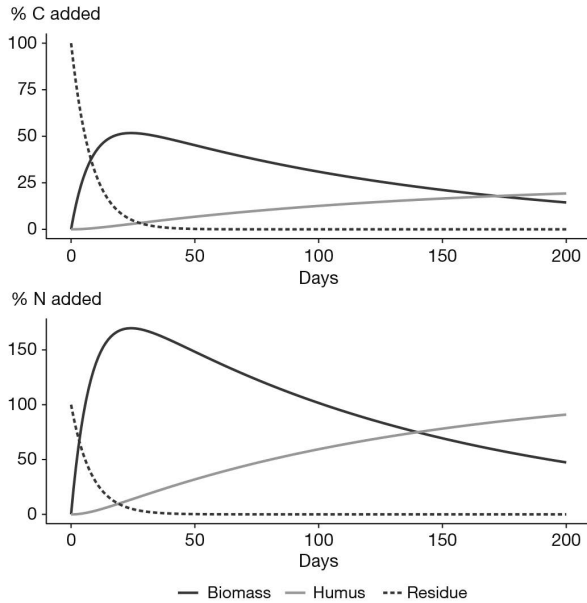


Figure 12.6. Evolution of C and N pools simulated during the decomposition of a crop residue (rapeseed straw) finely mixed in the soil, assuming no limitation by mineral N. The abscissa represents the normalised time (constant temperature and moisture). The ordinate is expressed in % of C or N added by the residue.

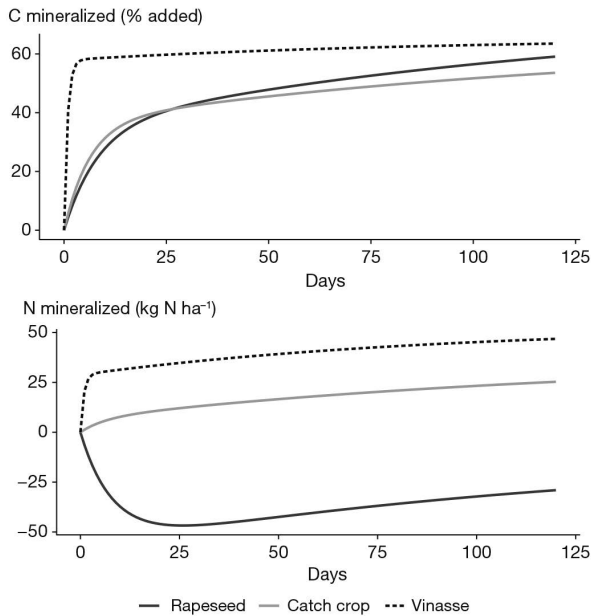


Figure 12.7. Evolution of C and N mineralised due to the decomposition of three types of organic residues (rapeseed straw, catch crop shoots and vinasse). The abscissa represents the normalised time (constant temperature and moisture, no limitation by mineral N). The ordinate is expressed in % of C added or kg N ha⁻¹.

12.2.3 Decomposition of organic residues at the soil surface

The decomposition of organic residues left as mulch at the soil surface is simulated similarly to mixed residues but with two main differences. First, the mulch is assumed to be composed of two layers: i) the upper layer, which is supposed to be above the soil and therefore cannot decompose; ii) the lower layer, in contact with the soil, which is decomposable. The partition between the two layers depends on the mulch amount. The lower layer corresponds to a mulch mass equal or lower than $q_{mulchdec_G}$. Every day, the part of the mulch which decomposes in the lower layer is replaced by an equivalent mass coming from the upper layer until complete depletion of this layer. Second, the decomposition parameters of organic residues decomposing in the mulch are modified compared to residues mixed in soil, and particularly the decomposition rates which are reduced. The calibration was also realized by fitting the model to incubation experiments, with or without soil mixing.

12.2.4 CO₂ emissions

STICS simulates the net CO₂ exchange between plant and atmosphere, but does not simulate the gross photosynthesis and the autotrophic respiration of the plant. It simulates the cumulative CO₂ emitted by the soil and distinguishes the origin of the emissions: coming from mineralisation of humus (QCO2hum), mineralisation of residues in the mulch (QCO2mul) and mineralisation of all residues including mulch and residues incorporated in the soil (QCO2res). The variable QCO2sol is the sum of QCO2res and QCO2hum; it corresponds to the heterotrophic respiration of soil.

►► 12.3 Nitrification

Nitrate production in soil results from two successive processes: mineralisation (or ammonification) and nitrification. Nitrification is often a rapid process in cultivated soils under temperate climates, which may justify avoiding describing nitrification and assimilating mineral N to nitrate-N. However in some soil and climatic conditions (e.g. acidic, hydromorphic or tropical soils), the nitrification process may be much slower and ammonium ions may persist in soil. Furthermore, the simulation of N₂O emissions due to nitrification requires a description of nitrification, as well as the simulation of ammonia volatilisation which is highly dependent on NH₄⁺ concentration. Accordingly, the present version of STICS can simulate nitrification and the two forms of mineral N separately.

Nitrification is calculated in the biologically active layer ($profhum_G$). If the nitrification option is not activated, the ammonium produced by the soil or added as fertilizer is instantly converted into nitrate. If the nitrification option is activated, the nitrification rate (v_{nit} , in mg N kg⁻¹ day⁻¹) is calculated as the product of the potential nitrification rate (v_{nitpot} , in mg N kg⁻¹ day⁻¹) and three factors depending on environmental conditions: soil pH ($fpHn$), temperature (fTn) and water content (fhn).

$$v_{nit} = v_{nitpot} \cdot fpHn \cdot fTn \cdot fhn \quad (12.23)$$

12.3.1 Potential nitrification rate

The potential nitrification rate is calculated as the product of a maximum nitrification rate (v_{nitmax} , in $\text{mg N kg}^{-1} \text{ day}^{-1}$) and a function depending on the ammonium concentration (f_{NH_4} , unitless):

$$v_{nitpot} = v_{nitmax} \cdot f_{NH_4} \quad (12.24)$$

v_{nitpot} can be calculated in two ways according to the option **code_vnit_G**.

With the first order option (**code_vnit_G** = 1), v_{nitmax} is proportional to the ammonium concentration:

$$v_{nitmax} = \mathbf{fnx}_G \cdot NH_4 \quad (12.25)$$

$$f_{NH_4} = 1 - \frac{NH_{4min}}{NH_4} \quad (12.26)$$

where \mathbf{fnx}_G is the maximum fraction of NH_4 which can be nitrified daily (day^{-1}) and NH_{4min} (mg kg^{-1}) is the minimal concentration of exchangeable NH_4 in soil.

With the second option (**code_vnit_G** = 2), v_{nitmax} is an input value (**vnitmax_G**). The effect of ammonium concentration is described by a Michaelis-Menten function:

$$f_{NH_4} = \frac{NH_4 - NH_{4min}}{NH_4 - NH_{4min} + w \cdot Kamm_G} \quad (12.27)$$

where w is the gravimetric soil water content (L kg^{-1}) and **Kamm_G** (mg N L^{-1}) is the affinity constant of nitrifiers for NH_4 .

Figure 12.8 shows v_{nitpot} when **code_vnit_G** = 1 and when **code_vnit_G** = 2 for two values of **Kamm_G** (24 and 202 mg N L^{-1}) and two values of w (0.15 and 0.24 g g^{-1}).

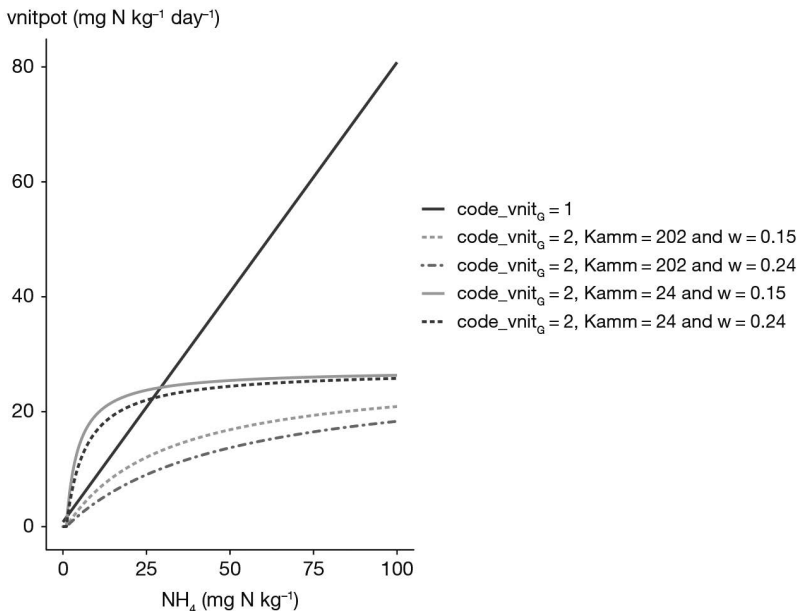


Figure 12.8. Influence of the soil NH_4 content on the potential nitrification rate. Parameters: $\mathbf{fnx}_G = 0.8$, $\mathbf{vnitmax}_G = 27.3$ and $NH_{4min} = 1$.

However, the second option has its drawbacks. Indeed, after a classical fertilisation at soil surface, the nitrogen supplied is located in the first elementary soil layer. Since the thickness of this layer is only 1 cm, ammonium concentration becomes very high and f_{NH_4} reaches 1. The nitrification rate is maximum in the first centimetre of soil and can be very low in the soil below 1 cm. Total nitrification may be greatly under-estimated. This effect can be corrected by placing the fertiliser over a greater depth, but this requires one more parameter to estimate. The linear approach avoids this difficulty thanks to the absence of a saturation of the nitrification rate that compensates for the small thickness of the soil layer concerned.

12.3.2 pH effect

The effect of pH on nitrification is linear between $\text{pH}_{\text{minnit}_G}$ where nitrification is zero and $\text{pH}_{\text{maxnit}_G}$ where nitrification is maximum. Figure 12.9 illustrates this relationship with the default values in STICS.

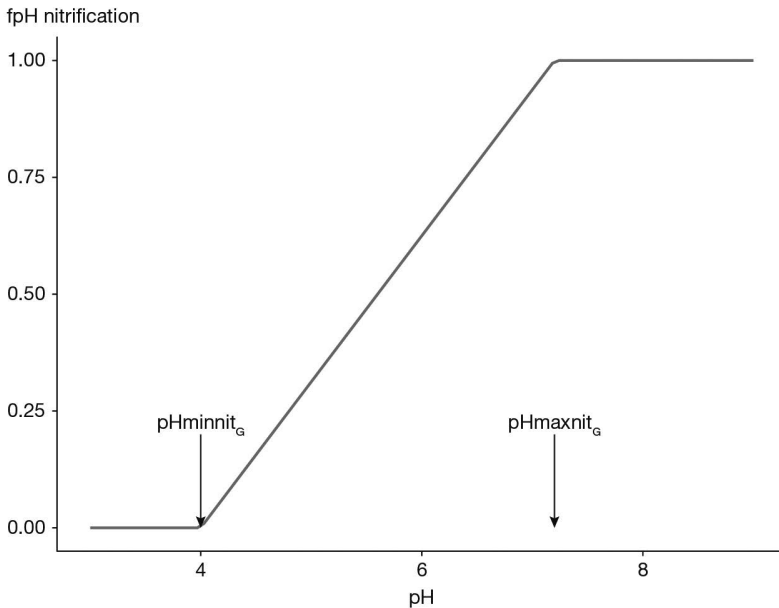


Figure 12.9. Influence of soil pH on the relative nitrification rate. Parameters: $\text{pH}_{\text{minnit}_G} = 4.0$, $\text{pH}_{\text{maxnit}_G} = 7.2$.

12.3.3 Temperature effect

The temperature effect is described either by a piecewise linear model ($\text{code_tnit}_G = 1$) or by a Gaussian function ($\text{code_tnit}_G = 2$). In the first case, nitrification rate is maximal when soil temperature lies between tnitopt_G and $\text{tnitopt}2_G$. In the second case, nitrification rate is maximal when soil temperature is equal to tnitopt_gauss_G and is defined as follows:

$$fTn = \exp\left(-\frac{(\text{tsol} - \text{tnitopt_gauss}_G)^2}{\text{scale_tnitopt}_G^2}\right) \quad (12.28)$$

It is easier to use the Gaussian function to manipulate the optimum temperature, such as when shifting it according to the average temperature. The two functions are illustrated in Figure 12.10.

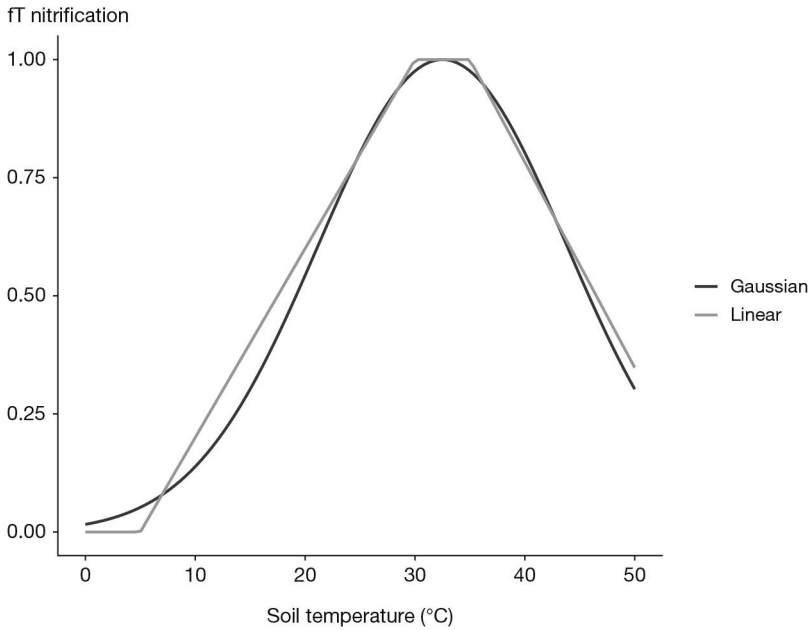


Figure 12.10. Influence of soil temperature on the relative nitrification rate. Parameters: $tnitopt_gauss_G = 32.5$, $scale_tnitopt_G = 16.0$.

12.3.4 Water content effect

Soil water content has a double effect on nitrification by simultaneously changing the soil water potential and the volume of water saturated soil. Therefore, nitrification rate increases when soil water content increases until a maximum and then decreases due to anoxia which stops nitrification. This effect is described by a piecewise linear function of the relative water content or water-filled pore space (Figure 12.11). The two soil moisture thresholds ($hminn_G$, $hoptn_G$) are expressed as a fraction of soil moisture at field capacity. Nitrification is zero below $hminn_G$ or when the soil is completely saturated with water. It is optimal between $hoptn_G$ and 1 (field capacity). It increases linearly between $hminn_G$ and $hoptn_G$, and decreases linearly between 1 (field capacity) and saturation.

$$\begin{aligned}
 fh_n &= \max\left[0, \frac{hur - hminn_G}{hoptn_G - hminn_G}\right] & \text{if } hur < hucc \cdot hoptn_G \\
 fh_n &= 1 & \text{if } hucc \cdot hoptn_G \leq hur \leq hucc \\
 fh_n &= \max\left[0, \frac{1 - wfps}{1 - wfpsc}\right] & \text{if } hur > hucc \quad (12.29)
 \end{aligned}$$

It must be noticed that the optimal water contents for nitrification ($hoptn_G$) and mineralisation ($hoptm_G$) can be different, which can lead to NH_4^+ accumulation in soil.

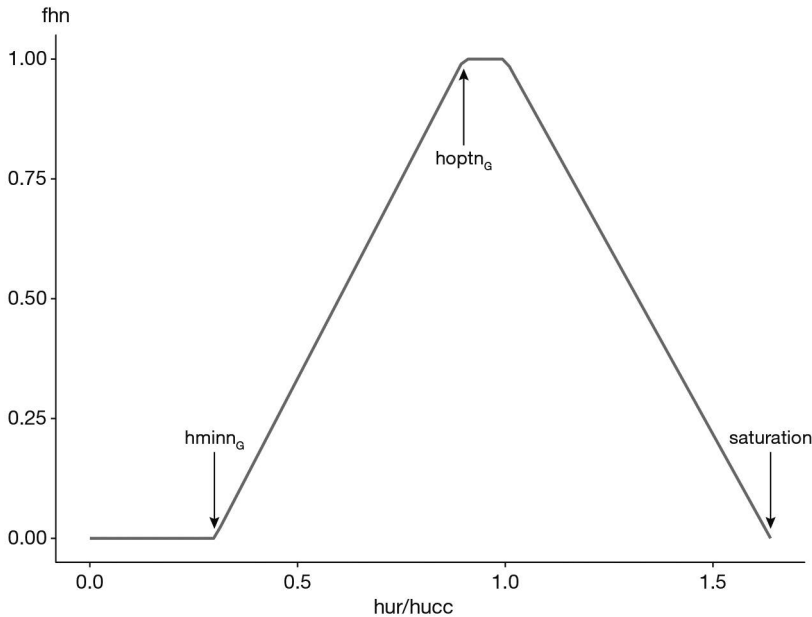


Figure 12.11. Influence of the relative water content ($hur/hucc$) on the relative nitrification rate. Parameters: $hminn_G = 0.30$, $hoptn_G = 0.90$. Bulk density = 1.30 g cm^{-3} , water content at field capacity = 0.24 g g^{-1} .

12.3.5 Daily or hourly simulations of water content at soil surface

Soil WFPS is a key variable for both nitrification, denitrification and associated N_2O emissions. However, the STICS model is a daily time step tipping-bucket model where drainage to the underlying soil layers occurs as soon (and only) as field capacity is reached. As a result, without any additional mechanism, the near-saturation soil water content that may temporarily exist near the ground surface during rainfall or in the hours that follow is not simulated. Moreover, since the soil water content is limited to field capacity which corresponds more or less to the soil water content at which anoxia begins to develop, all processes that are highly dependent on this anoxia (nitrification rate, proportion of N_2O emitted by nitrification, denitrification rate, reduction of N_2O to N_2) are underestimated.

An option is available for simulating soil water at the hourly scale. It is activated by default. Activating the hourly WFPS calculation options for nitrification (`code_hourly_wfps_nitG = 1`) and denitrification (`code_hourly_wfps_denitG = 1`) enables to simulate soil water content as temporarily higher than field capacity during days with rainfall, and its consequences on the nitrification, denitrification and N_2O emissions processes.

If $\text{precip} > 0$ (day with rain or irrigation), a wetting front depth is calculated by gradually rising the soil water content up to saturation. Each elementary layer from top to bottom becomes saturated until all of the precipitation has been stored. The water volume of each layer being filled is the difference between θ_{sat} and hur . Water is then redistributed by free drainage. The evolution of soil water content until the next day is

assumed to be driven by drainage, the rate of which is proportional to the water excess, $\theta_{\text{sat}} - \theta_{\text{hucc}}$. This results in an exponential evolution of soil water content over time (every hour), in which k_{desat_G} is the desaturation rate constant (day^{-1}):

$$\theta_{\text{huc}}(t) = \theta_{\text{hucc}} + (\theta_{\text{sat}} - \theta_{\text{hucc}}) \cdot \exp(-k_{\text{desat}_G} \cdot t) \quad (12.30)$$

Figure 12.12 illustrates the hourly evolution of the volumetric water content of a top soil layer after initial saturation by rainfall, using the default k_{desat_G} value = 3 day^{-1} .

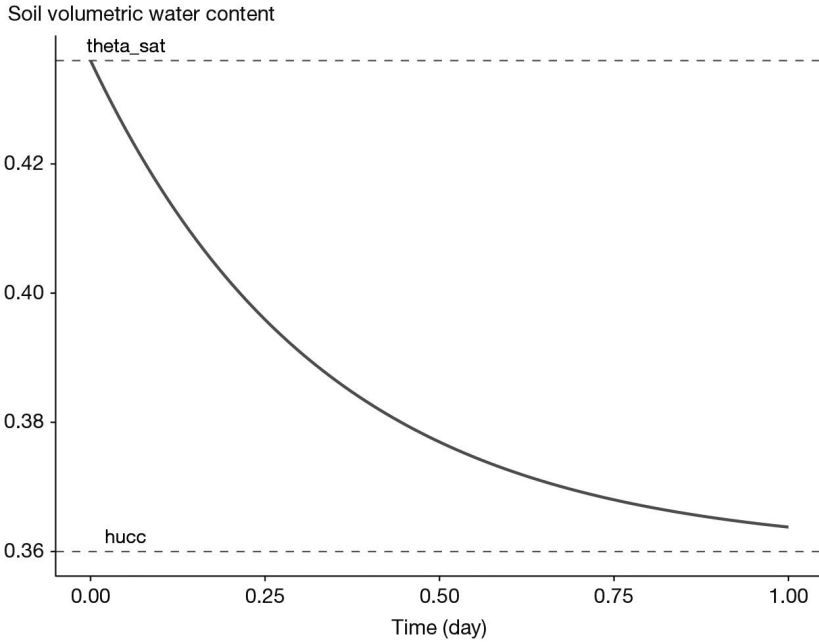


Figure 12.12. Evolution of the volumetric water content of a top soil layer during a day after initial saturation by rainfall ($\text{DAF}_S = 1.50 \text{ g cm}^{-3}$, $\theta_{\text{hucc}} = 0.36 \text{ cm}^3 \text{ cm}^{-3}$).

The default value of k_{desat_G} enables 95% of the water to be drained during one day and thus to reach at the end of the day a value which is very close to field capacity, in line with the daily soil water content calculated by the STICS water transfer submodel.

Each function of soil moisture or w_{fps} is then integrated from $t=0$ to $t=1$ instead of being applied to the daily soil moisture content, thus accounting soil water contents exceeding field capacity and simulating active denitrification.

►► 12.4 Denitrification

Denitrification is assumed to occur only in the top soil, over the depth defined by the parameter profdenit_S . The denitrification rate (v_{denit} , in $\text{kg N ha}^{-1} \text{ day}^{-1}$) is calculated as the product of a potential rate (v_{potdenit} , in $\text{kg N ha}^{-1} \text{ day}^{-1}$) and three control factors: the substrate availability (f_{NO_3}), the soil temperature (f_{Td}) and the water-filled pore space (f_{wfps}):

$$v_{\text{denit}} = v_{\text{potdenit}} \cdot f_{\text{NO}_3} \cdot f_{\text{Td}} \cdot f_{\text{wfps}} \quad (12.31)$$

There is no pH effect taken into account on the denitrification rate itself, although some studies suggest that the optimum pH may be soil dependent.

12.4.1 Potential denitrification

The potential denitrification rate can either be read from the file sols.xml (**vpotdenit_s**, if **code_pdenit_G** = 1 which is the default value) or calculated from soil organic carbon concentration (if **code_pdenit_G** = 2).

With the first option, the value read in the soil file (**vpotdenit_s**) represents the potential denitrification rate ($\text{kg N ha}^{-1} \text{ day}^{-1}$) over the depth **profdenit_s**. This value can be converted to $\text{mg kg}^{-1} \text{ day}^{-1}$ by dividing it by soil bulk density and **profdenit_s**.

With the second option, the potential denitrification rate (in $\text{mg N kg}^{-1} \text{ day}^{-1}$) is calculated as a function of the initial soil organic carbon concentration, using the variables **Norg_s** and **CsurNsol_s**. The calculation is based on a data compilation from the literature relating to the denitrification potential and the soil carbon content. However the diversity of methods and conditions used to characterise the denitrification potential makes this function uncertain. Furthermore soil carbon content may not be a good estimate of easily available carbon. This aspect needs further work and the proposed function should be used with care. The potential denitrification rate is minimal when the soil organic C concentration is lower than **cmin_pdenit_G** (in %) and maximal when the soil organic C concentration exceeds **cmax_pdenit_G** (in %). It increases linearly between these two values. The minimum value of the potential denitrification rate is equal to **min_pdenit_G** and its maximum value to **max_pdenit_G** (Figure 12.13).

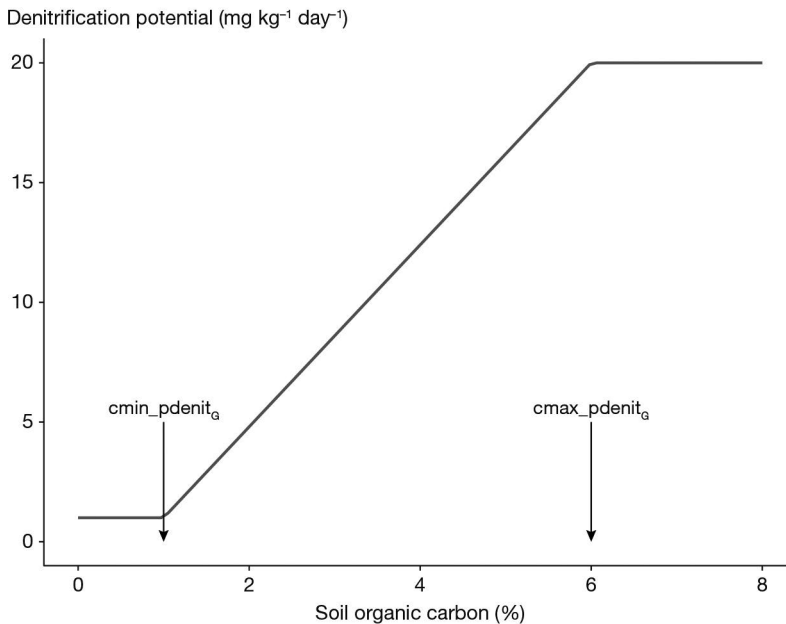


Figure 12.13. Influence of the soil organic carbon content (%) on the potential denitrification rate. Parameters: **cmin_pdenit_G** = 1, **cmax_pdenit_G** = 6, **min_pdenit_G** = 1, **max_pdenit_G** = 20.

The denitrification potential values refer to specific reference conditions. In STICS the reference conditions are a temperature of 20°C, a soil nitrate concentration of 200 mg N kg⁻¹, water saturation (wfps = 1) and no addition of carbon substrate. Under these reference conditions, the actual denitrification rate is equal to the potential denitrification rate.

12.4.2 Effect of nitrate concentration

Nitrate concentration modulates denitrification (f_{NO_3}) according to a Michaelis-Menten function:

$$f_{NO_3} = \frac{NO_3}{NO_3 + wKd_G} \quad (12.32)$$

where w is the gravimetric soil water content (L kg⁻¹), NO_3 is the nitrate content (mg N kg⁻¹ soil) and Kd_G (mg N L⁻¹) is the affinity constant of denitrifiers for nitrate (Figure 12.14).

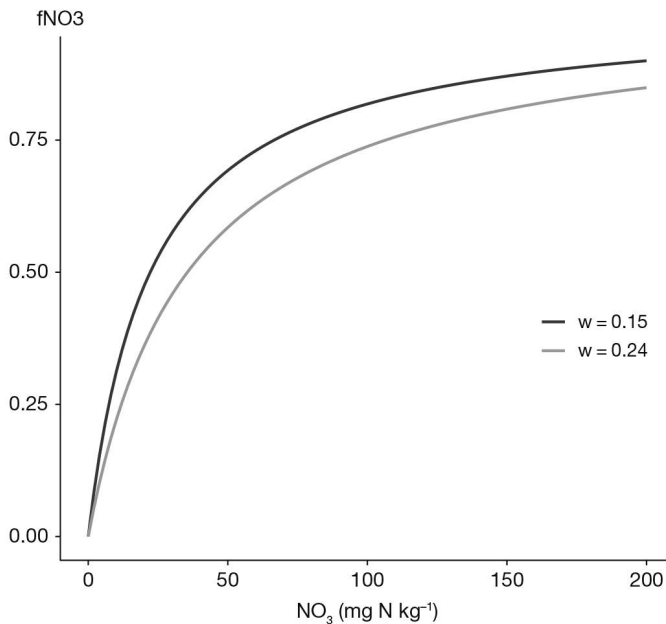


Figure 12.14. Influence of the soil nitrate concentration on the relative denitrification rate for two values of w (0.15 and 0.24 g g⁻¹). Parameter: $Kd_G = 148$.

12.4.3 Effect of temperature

The effect of temperature on denitrification is described by a Gaussian function (Figure 12.15):

$$fTd = \exp\left(-\frac{(t_{sol} - t_{denitopt_gauss_G})^2}{scale_t_{denitopt_G}^2}\right) \quad (12.33)$$

where $t_{denitopt_gauss_G}$ is the optimal temperature for denitrification:

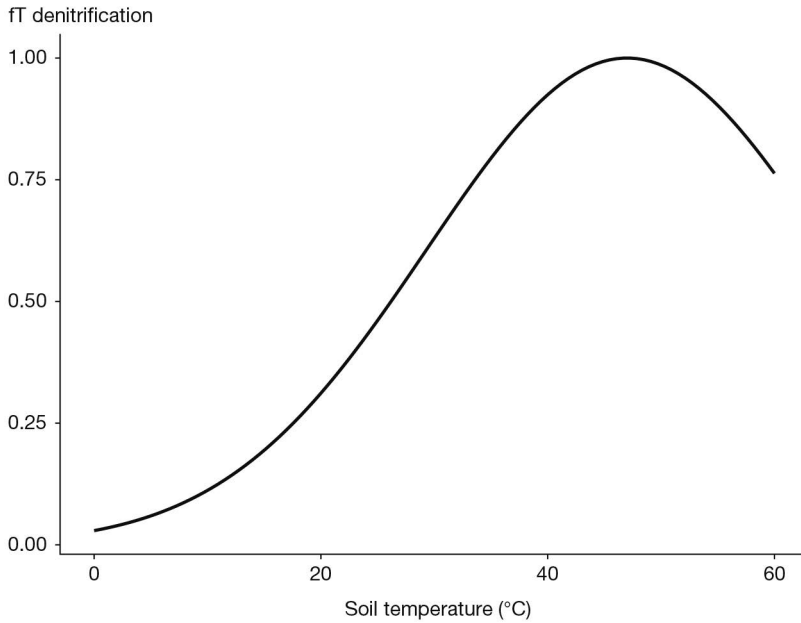


Figure 12.15. Influence of the soil temperature on the relative denitrification rate. Parameters: $\mathbf{tdenitopt_gauss}_G = 47$ and $\mathbf{scale_tdenitopt}_G = 25$.

12.4.4 Effect of water-filled pore space

Denitrification is an anaerobic process. Thus, the higher wfps, the less aerated the soil is and the more active the denitrification is. The intensity of denitrification is described as a function of wfps via a function combining a threshold above which denitrification is active (\mathbf{wfpsc}_G) and a rapid increase of the denitrification rate above this threshold (Figure 12.16):

$$f_{WFPS} = \max\left[0, \left(\frac{\mathbf{wfps} - \mathbf{wfpsc}_G}{1 - \mathbf{wfpsc}_G}\right)^{1.74}\right] \quad (12.34)$$

The \mathbf{wfpsc}_G threshold depends on soil texture. Some work suggests that it varies from about 0.50 for a coarse texture to 0.70 for a fine texture. However, there is currently no function linking this threshold to soil texture in STICS and the default value is $\mathbf{wfpsc}_G = 0.62$.

An option is available to simulate the soil water content and the wfps at an hourly time step. If it is activated ($\mathbf{code_hourly_wfps_denit}_G = 1$), water content and wfps are calculated every hour, assuming that each layer being saturated after a rainfall event then desaturates at an exponential rate ($\mathbf{kdesat}_G = 3 \text{ day}^{-1}$). The values of the hourly water content and water-filled pore space are calculated (see Eq. (12.30)) and integrated at the daily scale.

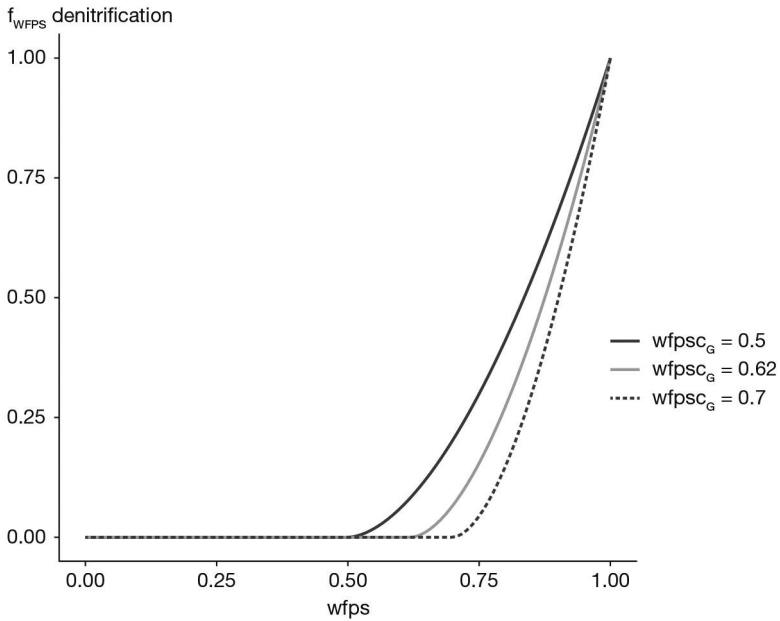


Figure 12.16. Influence of the water-filled pore space on the relative denitrification rate, with the default value of $\mathbf{wfpsc}_G = 0.62$ and two alternative values (0.50 and 0.70).

►► 12.5 N₂O emissions

The N₂O emissions associated with each of the two processes, nitrification and denitrification, are described as a fixed or variable proportion of the nitrification or denitrification rate, respectively:

$$N_2O_{nit} = z \cdot vnit \quad (12.35)$$

$$N_2O_{denit} = r \cdot vdenit \quad (12.36)$$

12.5.1 Emissions associated with nitrification

If $\mathbf{code_rationit}_G = 1$, the fraction z of the nitrified nitrogen emitted as N₂O is constant and is equal to $\mathbf{rationit}_G$, whose default value is 0.0016 (Khalil *et al.*, 2004).

If $\mathbf{code_rationit}_G = 2$ (default option), the z fraction varies with wfps:

$$z = \mathbf{rationit}_G \cdot \left(\frac{1.04 - 0.40 \cdot wfps}{1.04 - wfps} \right) \quad (12.37)$$

As wfps approaches 1, anoxia becomes dominant in soil and favours losses in the N₂O form (Figure 12.17). For low wfps values, the value of z is 0.16% (like the default constant value).

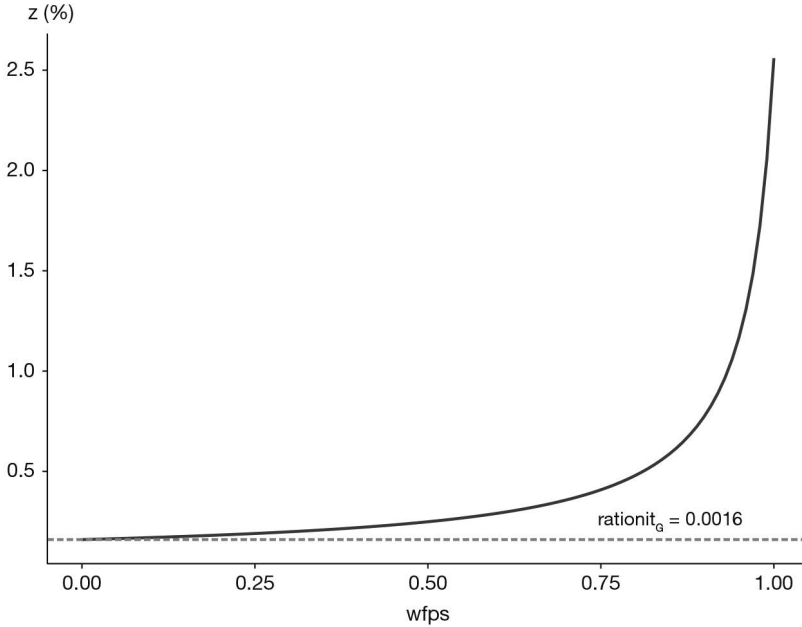


Figure 12.17. Influence of the water-filled pore space on the fraction of nitrified nitrogen emitted as N_2O . Parameter: $\text{rationit}_G = 0.0016$.

12.5.2 Emissions associated with denitrification

If $\text{code_ratiodenit}_G = 1$, the fraction r of denitrified nitrogen emitted as N_2O is constant and equal to ratiodenit_G , whose default value is set at 0.20.

If $\text{code_ratiodenit}_G = 2$ (default option), the fraction r varies with pH (factor G_{ph}), water-filled pore space (factor G_w) and nitrate concentration (factor G_n), in decreasing order of importance. It is calculated as:

$$r = \min[1, r_0 \cdot G_{ph} \cdot G_w \cdot G_n] \quad (12.38)$$

where the factor r_0 depends on the value of the wfps threshold for denitrification (wfpsc_G). With the standard value $\text{wfpsc}_G = 0.62$, r_0 is equal to 2.05.

12.5.2.1 pH effect (factor G_{ph})

Soil pH has a strong effect on the soil ability to reduce N_2O to N_2 . Reduction is usually very limited when pH is below 6 and close to its maximum when pH reaches 8. The fraction r of denitrified nitrogen emitted as N_2O is therefore highly pH dependent. The relationship (obtained from the compilation of data from different studies) between the observed values of r and soil pH is a piecewise linear function. The G_{ph} factor is equal to 1 (denitrification only produces N_2O) if the pH is less than pHminden_G ; it is zero (denitrification only produces N_2) if the pH is greater than pHmaxden_G and decreases linearly between these two thresholds (Figure 12.18):

$$G_{ph} = \min\left[1, \frac{\text{pHmaxden}_G - \text{pH}}{\text{pHmaxden}_G - \text{pHminden}_G}\right] \quad (12.39)$$

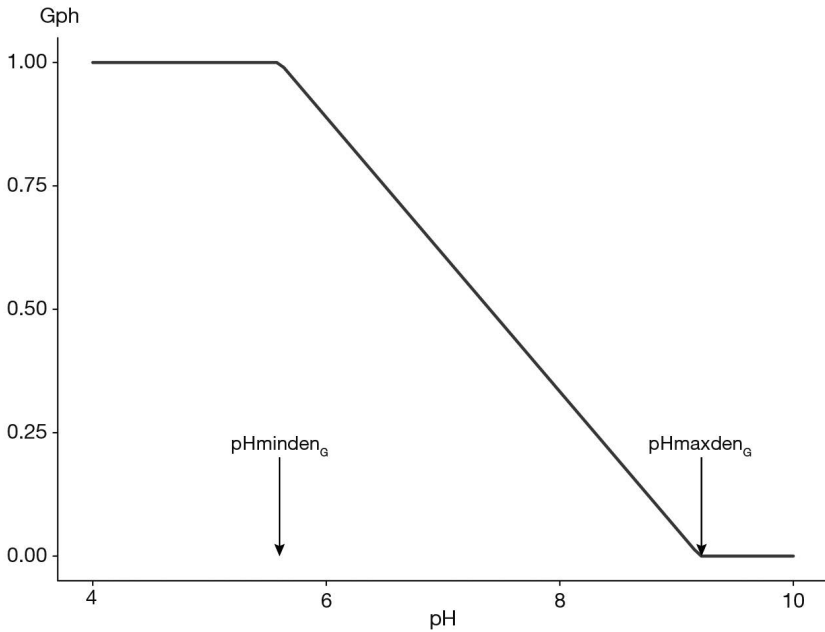


Figure 12.18. Effect of soil pH on the proportion of N₂O emitted by denitrification. Parameters: **pHminden_G** = 5.6, **pHmaxden_G** = 9.2.

12.5.2.2 Effect of water-filled pore space (factor Gw)

Water content and **wfps** influence the molar fraction *r* because high values of **wfps** result in low oxygen availability, promoting complete denitrification and reducing the proportion of denitrified nitrogen emitted as N₂O. When **wfps** is close to the threshold above which denitrification begins to start (**wfp_{sc}G**), the soil is still well aerated and the reduction of N₂O to N₂ is minimal, and *r* is maximum. On the contrary, when the soil is completely saturated with water, the reduction is maximum and *r* is minimum. The **wfps** effect (factor Gw) on *r* is assumed to decrease linearly with **wfps**, between **wfp_{sc}G** and 1 (Figure 12.19):

$$Gw = \min \left[1, \frac{1 - \text{wfps}}{1 - \text{wfp}_{sc}G} \right] \quad (12.40)$$

12.5.2.3 Effect of nitrate concentration (factor Gn)

The value of *r* is also influenced by nitrate concentration through an inhibition of the reduction of N₂O to N₂, which increases with nitrate concentration. This effect is represented in STICS by a Michaelis-Menten function (where nitrate concentration is expressed in mg kg⁻¹):

$$Gn = \frac{NO_3}{NO_3 + 1} \quad (12.41)$$

This function is shown in Figure 12.20. Inhibition is important as soon as nitrate concentration exceeds a few mg kg⁻¹. Thus, in most conditions where nitrate levels are significant, this effect is not noticeable because Gn is close to 1.

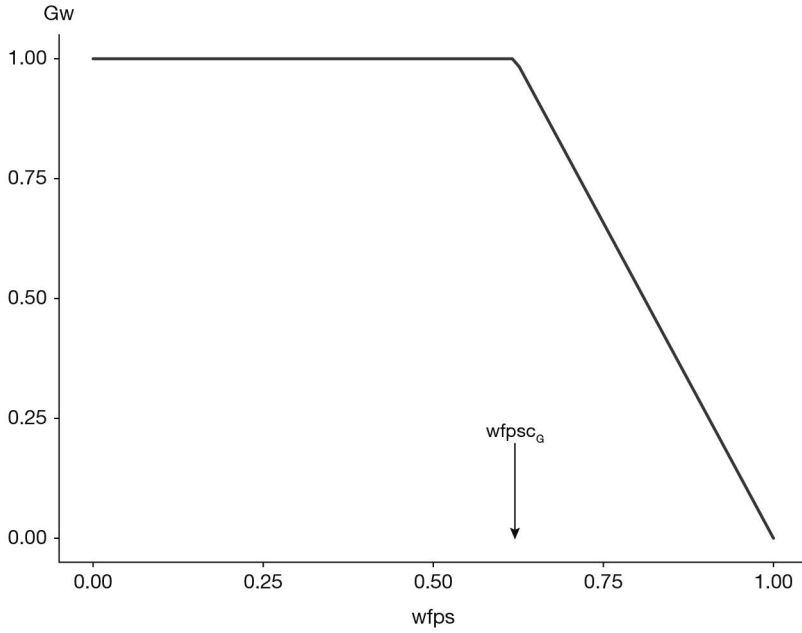


Figure 12.19. Effect of water-filled pore space on the proportion of N_2O emitted by denitrification. Parameter: $wfpsc_G = 0.62$.

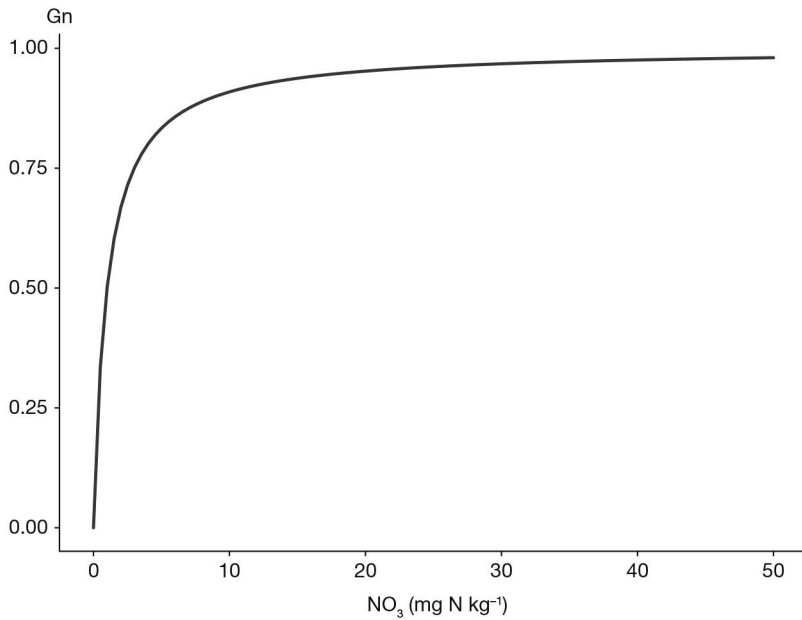


Figure 12.20. Effect of soil nitrate concentration on the proportion of N_2O emitted by denitrification.

The combined effects of pH, wfps and nitrate on the molar fraction r are illustrated in Figure 12.21.

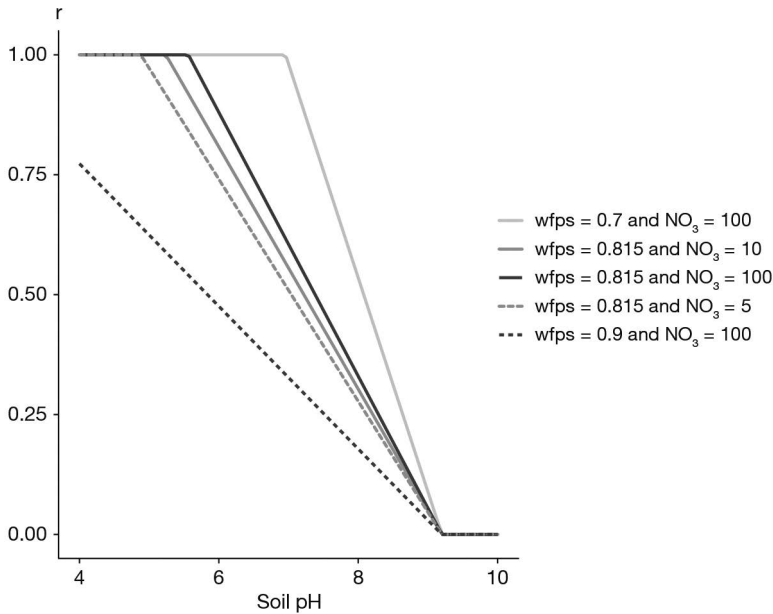


Figure 12.21. Influence of combined factors on the fraction of denitrified nitrogen emitted as N_2O .

►► 12.6 Ammonia volatilisation

Ammonia volatilisation is a purely chemical process which operates on the soil ammonium pool (NH_4^+) and converts it into gaseous ammonia (NH_3). It affects the ammonium derived from mineral fertilisers or from organic fertilisers which contain large amounts of ammonium (such as liquid manure) and/or which have rapid mineralising potentials (e.g. vinasses). The current STICS version explicitly simulates the volatilisation only in the case of an application of liquid organic manure (see § 13.5.2.1 for volatilisation from mineral fertilisers).

In order to simulate volatilisation, four forms of ammonia compounds which are in equilibrium (Génermont and Cellier, 1997) must be considered:

- NH_4s : ammonium ions (NH_4^+) adsorbed onto the mineral or organic soil fractions;
- NH_4l : ammonium ions in solution in the liquid soil phase;
- NH_3l : ammonia molecules (NH_3) in solution in the liquid soil phase;
- NH_3g : ammonia molecules in the gaseous soil phase.

All conditions which move these equilibria towards the last form (e.g. high pH and temperature) stimulate volatilisation. Volatilisation occurs at the soil surface and depends on the NH_4^+ concentration there: it is thus affected by fertiliser type, fertiliser rate, soil water content and NH_4^+ movement in soil. The equilibrium between NH_4s and NH_4l forms can be characterised by an adsorption isotherm which depends on soil CEC (cation exchange capacity, itself linked to clay and organic matter contents).

NH_4l and NH_3l are linked through a chemical equilibrium which is pH and temperature dependent. The solubility equilibrium between NH_3l and NH_3g forms mainly depends on temperature.

The first step consists in defining the volatilisable NH_4^+ immediately after the application. The exchangeable NH_4^+ (Nminres_T , in kg N ha^{-1}) is split into two pools: a pool which remains at the soil surface and which can be volatilised (Nvolatorg , in kg N ha^{-1}) and a pool which infiltrates and is not volatilisable. The volatilisable NH_4^+ at the time of application (t_0) is:

$$\text{Nvolatorg}(t_0) = \text{Nminres}_T \cdot \text{propvolat} \quad (12.42)$$

The proportion of the volatilisable fraction (propvolat) decreases with the water content of the manure (eaures_T), as follows in Figure 12.22.

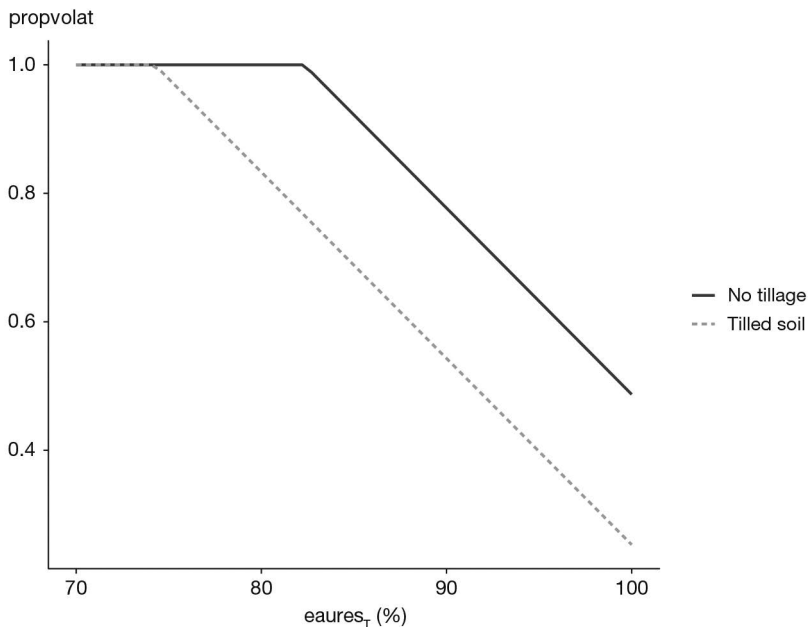


Figure 12.22. Effect of soil tillage and water content of slurry on its volatilisable fraction.

The proportion of the volatilisable fraction is also affected by soil tillage: it decreases if the soil has been tilled during the last 7 days before manure spreading ($\text{trsolvolat} = -1$) and increases otherwise ($\text{trsolvolat} = +1$) (Morvan, 1999). It is calculated as follows:

$$\text{propvolat} = 0.37 + 0.029 \cdot (100 - \text{eaures}_T) + 0.117 \cdot \text{trsolvolat} \quad (12.43)$$

Furthermore, the addition of manure (containing urea-type compounds and bicarbonates) is accompanied by a pH increase which is considered in the calculations. Immediately after the manure application, the soil pH at soil surface (pHvol) increases by a value dpHvol , which varies with the mineral N level as follows:

$$\begin{aligned} \text{dpHvol} &= \text{dpHvolm} && \text{if } \text{pH}_S < 7 \\ \text{dpHvol} &= \text{dpHvolm} \cdot \frac{\text{pHvols}_G - \text{pH}_S}{\text{pHvols}_G - 7} && \text{if } 7 \leq \text{pH}_S \leq \text{pHvols}_G \\ \text{dpHvol} &= 0 && \text{if } \text{pH}_S > \text{pHvols}_G \end{aligned} \quad (12.44)$$

with

$$\text{dpHvolm} = \min[\text{dpHvolmax}_G, \text{alphapH}_G \cdot \text{Nminres}_T] \quad (12.45)$$

Using the data given by Morvan and Leterme (2001) and Chantigny *et al.* (2004), we can propose the following parameter values: $\text{alphapH}_G = 0.005$, $\text{dpHvolmax}_G = 1.0$ and $\text{pHvols}_G = 8.6$. Based on these values, the soil pH variation immediately after manure application is shown below:

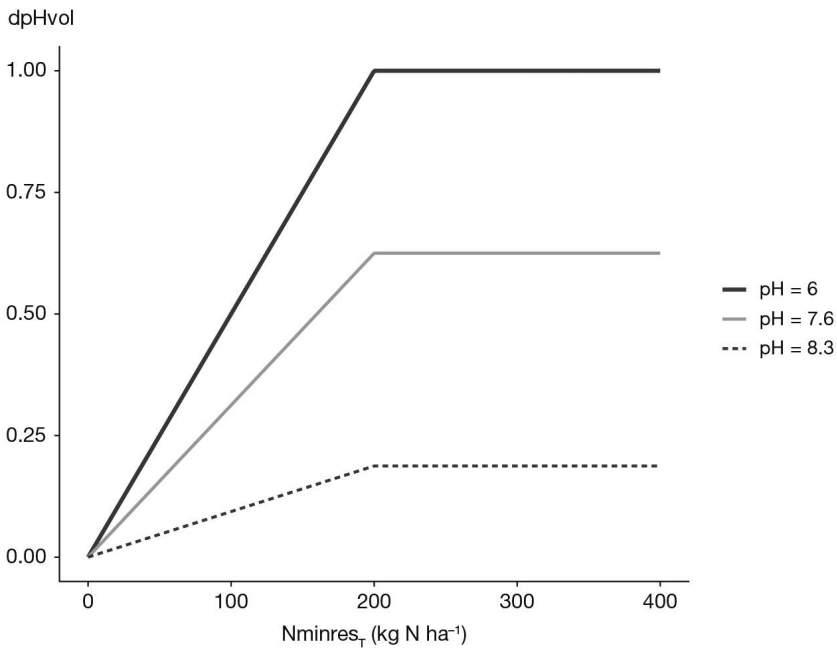


Figure 12.23. Effect of mineral N content of slurry and soil pH on the initial pH increase following slurry application.

During the following days, the pH at the soil surface (pHvol) returns to the soil pH value (pH_S), at a rate proportional to the decrease in the volatilisable pool:

$$\text{pHvol}(t) = \text{pH}_S + \text{dpHvol} \cdot \frac{\text{Nvolatorg}(t)}{\text{Nvolatorg}(t_0)} \quad (12.46)$$

The model then calculates the amounts of the four forms: NH_4s , NH_4l , NH_3l and NH_3g (in mol m^{-2}), using the acido-basic equilibria equations, the Henry solubility equation and the transfer equations of Beutier and Renon (1978). These amounts depend on soil temperature, water content, soil porosity, pH at soil surface and wind speed. The ammonia concentration at the soil surface (NH_3surf , in $\mu\text{g N m}^{-3}$) is:

$$\text{NH}_3\text{surf}(t) = 1.2 \cdot \text{NH}_3\text{g}(t) \cdot 10^9 \quad (12.47)$$

The potential ammonia volatilisation rate (F_{SNH} , in $\mu\text{g N m}^{-2} \text{s}^{-1}$) is:

$$F_{\text{SNH}}(t) = \frac{\text{NH3}_{\text{surf}}(t) - \text{NH3}_{\text{ref}_c}}{\text{ras}(t) + \text{raa}(t)} \quad (12.48)$$

where $\text{NH3}_{\text{ref}_c}$ is the atmospheric ammonia concentration, which is about $10 \mu\text{g m}^{-3}$ in cattle production areas and 0 elsewhere; ras and raa (in s m^{-1}) are the resistances calculated according to Shuttleworth and Wallace (1985) if the 'resistive' option is activated ($\text{codeetp}_C = 4$); otherwise raa is the default parameter ($\text{ra}_C = 50$) and $\text{ras} = 0$. The calculation of F_{SNH} is made hourly because volatilisation decreases rapidly, assuming constant weather data throughout the day.

The actual ammonia volatilisation rate (N_{volorg} , in $\text{kg N ha}^{-1} \text{day}^{-1}$) is proportional to F_{SNH} through a coefficient 0.864 which is a unit conversion factor ($\mu\text{g m}^{-2} \text{s}^{-1}$ into $\text{kg ha}^{-1} \text{day}^{-1}$). However it can exceed neither the amount of ammonium at the soil surface ($\text{amm}(1)$) nor the volatilisable pool (N_{volatorg}):

$$N_{\text{volorg}}(t) = \min[0.864 \cdot F_{\text{SNH}}(t), \text{amm}(1), N_{\text{volatorg}}(t)] \quad (12.49)$$

Finally, the volatilisable pool is updated daily:

$$N_{\text{volatorg}}(t) = N_{\text{volatorg}}(t) - N_{\text{volorg}}(t) \quad (12.50)$$

►► 12.7 Carbon and nitrogen balances

The C and N balances in soil are provided by the STICS output balance file (`mod_b'usm'sti`). They concern the soil mineral N pool and the soil organic C and N pools. They display the variations in the pools between the initial and final simulation dates, and the input and output fluxes occurring during the simulation period. The sum of initial pools and input fluxes is equal to the sum of final pools and output fluxes.

12.7.1 Soil mineral N balance

The mineral N pool is composed of NH_4 and NO_3 . The input fluxes include N contained in rainfall, irrigation and mineral fertilisers, and the net mineralisation derived from humus or organic residues. The output fluxes include plant N uptake, nitrate leaching through natural and artificial drainage, fertiliser immobilisation, NH_3 volatilisation derived from mineral or organic fertilisers and N losses as ($\text{N}_2 + \text{N}_2\text{O}$) derived from denitrification and nitrification.

12.7.2 Soil organic N balance

The whole soil organic N pool is composed of N contained in humified organic matter (active and inert), microbial biomass (zymogeneous), organic residues mixed in soil, organic residues in mulch at soil surface and deep root residues (present below the biologically active layer). The zymogeneous biomass-N and deep root residue-N are assumed to be nil when simulation starts. The input fluxes include the mineral fertiliser immobilisation and the addition of organic fertilisers, crop residues, fallen and trimmed leaves, dead roots and dead perennial organs. The output fluxes concern only net N mineralisation, including that produced by the priming effect (PE).

Table 12.1. Components of the soil mineral nitrogen balance (kg N ha⁻¹).

Initial pools		Final pools	
NH ₄ -N	3		4
NO ₃ -N	30		25
Total mineral N	33		29
Input fluxes		Output fluxes	
		Plant N uptake	273
Precipitation	17	Nitrate leaching	8
Irrigation	10	Leaching in mole drains	0
Fertiliser	110	Fertiliser immobilisation	32
		Fertiliser volatilisation	12
Humus mineralisation	187	Manure volatilisation	0
Residue mineralisation	10	(N ₂ +N ₂ O)-N losses	13
TOTAL INITIAL	367	TOTAL FINAL	367

Table 12.2. Components of the soil organic nitrogen balance (kg N ha⁻¹).

Initial pools		Final pools	
Active humified	1963		1751
Inert humified	3646		3646
Zymogeneous biomass	0		64
Organic residues	0		11
Deep root residues	0		4
Mulch residues	0		327
Total organic N pools	5609		5803
Input fluxes		Output fluxes	
Fertiliser immobilisation	0		
Organic fertiliser	3		
Crop residues	309		
Fallen leaves	67	priming (PE)	0
Trimmed leaves	0	mineralisation - PE	238
Dead roots	53		
Dead perennial organs	0		
TOTAL INITIAL	6041	TOTAL FINAL	6041

12.7.3 Soil organic C balance

The whole soil organic C pool comes from the same organic pools as those for nitrogen. The zymogeneous biomass-C and deep root residue-C are also assumed to be nil when simulation starts. The input and output C fluxes are similar to those relative to N fluxes.

Table 12.3. Components of the soil organic carbon balance (kg C ha⁻¹).

Initial pools		Final pools	
Active humified	27877		24870
Inert humified	51771		51771
Zymogeneous biomass	0		868
Organic residues	0		432
Deep root residues	0		152
Mulch residues	0		6762
Total organic C pools	79648		84855
Input fluxes		Output fluxes	
Fertiliser immobilisation	0		
Organic fertiliser	12		
Crop residues	6468		
Fallen leaves	1059	priming (PE)	0
Trimmed leaves	0	mineralisation - PE	4319
Dead roots	1987		
Dead perennial organs	0		
TOTAL INITIAL	89174	TOTAL FINAL	89174

12.7.4 Nitrogen surplus and losses

The mineral N surplus ($N_{\text{surplus_min}}$) is the difference between the inputs and outputs relative to the soil-plant system. The inputs include the atmospheric N supply (precipN), the irrigation N supply (irrigN), the mineral fertiliser-N (totapN) and the biological N fixation (Q_{fix}). The only output is the crop N exported (Q_{Nexport}):

$$N_{\text{surplus_min}} = \text{precipN} + \text{irrigN} + \text{totapN} + Q_{\text{fix}} - Q_{\text{Nexport}} \quad (12.51)$$

The total N surplus (N_{surplus}) is similar, but also includes the supply of organic fertiliser (Q_{Nresorg}):

$$N_{\text{surplus}} = N_{\text{surplus_min}} + Q_{\text{Nresorg}} \quad (12.52)$$

The gaseous N losses (Q_{Ngaz}) are the sum of N denitrified (Q_{Ndenit}), N volatilised by mineral fertilisers (Q_{Nvoleng}), N volatilised by organic fertilisers (Q_{Nvolorg}) and N emitted as N_2O by nitrification ($Q_{\text{em_N2Oit}}$):

$$Q_{\text{Ngaz}} = Q_{\text{Ndenit}} + Q_{\text{Nvoleng}} + Q_{\text{Nvolorg}} + Q_{\text{em_N2Oit}} \quad (12.53)$$

The total N surplus can also be written:

$$N_{\text{surplus}} = D_{\text{SON}} + D_{\text{SMN}} + D_{\text{QNtot2}} + Q_{\text{Ngaz}} + Q_{\text{les}} \quad (12.54)$$

where D_{SON} is the variation in soil organic N, D_{SMN} is the variation in soil mineral N, D_{QNtot2} is the variation in crop N content (one or two crops in the case of intercropping) and Q_{les} is the N leaching loss during the whole simulation period.

If we consider annual crops grown for several years, the terms DSMN and DQNtot2 are negligible. In that case, Eq. (12.54) can be simplified as:

$$N_{surplus} = DSON + QNgaz + Qles \quad (12.55)$$

This equation shows that: i) a negative N surplus implies that soil organic N is necessarily decreasing over time and ii) a positive N surplus indicates that N losses (NO_3 , NH_3 , N_2 , N_2O) occur and/or that N has been stored in soil organic matter.

12.7.5 Greenhouse gas budget

The greenhouse gas budget (GHG) is calculated as the contribution of two gases, CO_2 and N_2O , assuming that the emission of CH_4 is negligible. This assumption holds for all crops except flooded crops such as rice. The other assumption is that the amount of CO_2 evolved from the soil-plant system is equal to the variation in soil organic carbon (DSOC). This is valid for annual crops, but not for perennial crops which can store significant amounts of C in their biomass. The global warming potential GWP is assumed to be 1 for CO_2 and 298 for N_2O (IPCC, 2007). The GHG budget during the simulation is calculated in $\text{kg CO}_2\text{eq ha}^{-1}$ as follows:

$$GHG = -DSOC \cdot \frac{44}{12} + 298 \cdot Qem_{N2O} \cdot \frac{44}{28} \quad (12.56)$$

where DSOC is the variation in soil organic carbon and Qem_{N2O} is the amount of N emitted as N_2O during the simulation period. Other emissions due to fertiliser production and fuel consumption must be added to this value in order to have a complete GHG assessment (e.g. Autret *et al.*, 2020).

Chapter 13

Soil-crop management effects

*NADINE BRISSON, BRUNO MARY
AND DOMINIQUE RIPOCHE-WACHTER*

REVIEWED BY: NICOLAS BEAUDOIN

►► 13.1 Introduction

The very first crop models (de Wit, 1978; Weir *et al.*, 1984) sought to describe the ecophysiology of crops in detail, often for didactic purposes; however, they paid little attention to agronomic objectives. The next generation of models started to include farming practices in the inputs (Ritchie and Otter, 1985; Williams *et al.*, 1984), particularly those related to irrigation and fertilisation. Accounting for farming practices in the models requires an explicit and adequate simulation of the main state variable(s) that the practice is assumed to modify, such as soil water content for irrigation, organic residue dynamics for manure application or annual wood production for pruning. In STICS, emphasis has been placed on crop and soil management which is important for simulating industrial crops and essential for high value-added crops. However, some techniques are not yet accounted for in the model when the corresponding state variables are poorly described (e.g. those relating to soil structure) or not calculated at all (e.g. those relating to crop health status).

►► 13.2 Crop management

For industrial crops, the direct effects of crop management on the soil-plant system are at minimum induced by the two boundary operations of sowing and harvest. They also often include operations related to fertilisation and irrigation. For high-value crops such as vegetables or grapevine, farmers perform additional operations during the crop cycle to regulate yield. Finally, other operations such as soil tillage, organic fertilisation or pruning may occur outside the crop cycle period, impacting both the soil functioning and the growth of the following crop.

13.2.1 Plant establishment

For annual crops, there are two choices of plant establishment: by sowing seeds (wheat, rapeseed, sugarbeet, etc.) or transplanting plantlets (lettuce, tomato, strawberry, etc.). With the sowing option, the very first stages of plant growth occurring beneath the

soil (germination and underground shoot growth) are simulated (§ 3.4.1), depending on sowing depth. With the planting option, the model simply considers a lag time from transplanting to the start of actual plantlet growth (§ 3.4.2); this option requires the user to initialise the plant state in terms of leaf area index, biomass, nitrogen status, rooting depth and root density profile.

For STICS the uncertainty on sowing depth is assumed to be 2 cm, so that the prevailing soil conditions for emergence (humidity in the seed bed) are those found in the layer $[x-2, x+2]$, where x is the prescribed sowing depth. However, this variation in depth does not lead to variability in the emergence rate: all plants that emerge do so at the same time.

The model also requires information about the crop's geometrical pattern, which is very important for radiation interception. The pattern can either be homogeneous or in rows. In the latter case, the model requires geometrical parameters, such as the inter-row distance and row orientation (§ 9.2.1.2).

STICS can also simulate a companion crop such as grass in vineyards. In this case, the system is simulated as an intercropping system (§ 9.3.4).

13.2.2 Sowing

Users have the option to prescribe the sowing date (**iplt**_T) or calculate it (iplts) using rules relative to the weather and soil water status. To calculate the sowing date, a period when sowing is allowed and defined as the interval [**iplt**_j, **iplt**_j + **nbjmaxapressemis**_T]. Four criteria are taken into account to postpone sowing within this sowing window:

- the soil must be wet enough: the water content in the seedbed layer must be greater than the water content at wilting point. The depth of the seedbed is defined as **profsem**_T ± 2 cm;
- the soil must be warm enough: the air temperature (**tair**) must exceed **tadmin**_p for several days (**nbjseuiltempref**_T) to avoid germination delay or the stopping of plant emergence (§ 3.4.1);
- the risk of freezing must be low: the minimum air temperature (**tmin**) must be greater than **tdebgel**_p for at least **nbjseuiltempref**_T days (§ 3.4.1.3);
- the soil must be not too wet so as to avoid compaction risks: the soil water content is considered as damaging if it exceeds **prophumtassem**_G × **hccf**_s in the zone between the soil surface and the depth **profhumsemoir**_T (§ 13.3.1.1).

13.2.3 Regulation of canopy structure and yield

Yield regulation is generally used for high-value crops such as tomato or grapevine. It can be performed either by foliage regulation or by fruit removal.

13.2.3.1 Foliage regulation by topping or leaf removal

This option is activated using the code **codepalissage**_T in the .tec file.

If the plant exhibits indeterminate growth, a trellis system may be required to support plants. It can be simulated by imposing a maximum height and width: **hautmaxtec**_T and **largtec**_T.

Topping only concerns crops having a row structure and consists in restricting plant structure in terms of height (**hautrogne_T**) and/or width (**largrogne_T**). Two topping options are available. With automatic calculation, topping occurs as soon as the plant height exceeds **hautrogne_T+margerogne_T**. With the second option, topping is performed at an imposed date (**julrogne_T**). In this case, topping is carried out at the specified height (**hautrogne_T**) or width (**largrogne_T**). The topped LAI (**lairogne**) depends on these parameters and the foliage density.

The topped biomass (**biorogne**) is calculated as:

$$biorogne(t) = 100 \cdot \frac{lairogne(t)}{sbv(t)} \quad (13.1)$$

with

$$sbv(t) = \frac{sla(t)}{1+tigefeuil_p} \quad (13.2)$$

where **sla** is the specific leaf area and **tigefeuil_p** is the ratio of stem to leaf area. Topping is performed only if the topped biomass exceeds a specified threshold (**biorognem_T**). The topped biomass and the corresponding LAI are subtracted from the biomass and LAI of the plant. The topped biomass returns to the soil and is recycled in C and N soil pools.

Leaf removal is another technique which directly reduces the leaf area and does not depend on the canopy geometry like topping does. Two options are possible for leaf removal. With automatic calculation, a constant proportion (**effeuil_T**) of the new foliage generated each day (**deltai**) is removed as soon as the LAI reaches a threshold value (**laidebeff_T**). With the second option, leaf removal is performed only once on day **juleffeuil_T** and the specified leaf area **laieffeuil_T** is removed. The corresponding biomass is calculated from the specific leaf area (**sla**) and subtracted from the living plant biomass. The location of leaf removal may be either the top or the bottom of the canopy, which affects the radiation interception and water balance of crops in rows.

13.2.3.2 Fruit removal

This option is activated using the code **codeclaircie_T** in the .tec file.

Fruit removal occurs on day **juleclair_T** and the prescribed parameter is the number of fruits or inflorescences removed per plant (**nbinfloect_T**). For mono-inflorescence plants, only the younger fruits (taken from the first or younger “box”) are removed whereas for multi-inflorescence plants, the removed fruits are taken from all “boxes” (§ 8.1.2). This action interacts with the other determinisms of the number of fruits (§ 8.1.2.1).

13.2.4 Harvest management

There are two harvest methods: cutting (the entire plant is cut and removed or partly returned onto the soil) or picking (only the fruits are picked). There may be several cuts (e.g. forage crops) or several pickings (e.g. fruit crops with a spread of maturity).

13.2.4.1 Harvest of forage crops

This option is activated using the code **codefauche_T** in the .tec file.

Forage crops can be cut according to one of the following three methods:

- With automatic calculation, as soon as the crop reaches the stage defined by the parameter **stadecoupedf_T**, the forage crop is cut at the height corresponding to **hautcoupedefault_T**. The biomass of the cutting is calculated using the crop-specific conversion parameter **coefmshaut_p** (in $t\ ha^{-1}\ m^{-1}$).
- With imposed dates, a table providing all cutting dates is entered, linked to either a single parameter (the cutting height **hautcoupe_T**) or five other parameters: the residual LAI after cutting (**lairestiduel_T**), the residual biomass after cutting (**msresiduel_T**), the N fertilisation rate after cutting (**anitcoupe_T**), the minimum aerial biomass required for cutting (**mscoupemini_T**) and the fraction (0-1) of the cut which is exported (**tauxexportfauche_T**). This last parameter allows users to simulate leys with a partial or total return of the grass biomass. The default value for this parameter is 1 (the whole cut is exported). If the user does not supply these five parameters, they are calculated based on the cutting height using the parameter **coefmshaut_p** and the height/LAI ratio.
- With imposed crop stages, the procedure is similar but uses physiological dates instead of Julian days, with the cutting dates defined by cumulative development units.

Whatever the method chosen, the amount of biomass harvested equals the difference between the non-senescent living biomass and the biomass left on the ground. It must be greater than a minimum fixed by the user. Once the cutting date or stage has been reached, these conditions define the remaining and harvestable parts. Cutting occurs if three conditions are fulfilled:

- lai is greater than the minimum harvestable LAI (**lairestiduel_T**);
- the aerial biomass (masec) is greater than the minimum harvestable biomass (**msresiduel_T**);
- the harvestable biomass (msrec_fou) is greater than the minimum amount that we accept to harvest (**mscoupemini_T**).

These three criteria (residual LAI, residual biomass and harvestable biomass) are defined for each cut and allow cuts to be postponed. The third criterion makes it possible to change the threshold according to the season or the farmer's decisions, according to the harvest needs (e.g. small quantities if there is stress on herd feeding).

13.2.4.2 Protracted fruit picking

This option is activated using the code **codcueille_T** in the .tec file.

Protracted maturity occurs for indeterminate crops (e.g. tomato) after a long period of fruit setting (parameter **stdrpnou_p**) and leads to the harvest being spread out. The first harvest starts at physiological maturity of the first cohort of fruits (transferred into the last "box") (see § 8.1.2.1) and the summary outputs concern the last ripe fruits. The number of cuttings and the harvest duration depend on the picking rate (**cadencerec_T**) which represents the number of days between two successive pickings. If the rate is too fast with respect to the fruit growth rate, harvest is delayed until ripe fruits appear again (i.e. fill in the last "box" of the fruit growth-development period).

13.2.4.3 Harvest decision

This option is activated using the code **codrecolte_T** in the .tec file. The harvest date can either be imposed (fixed date) or calculated using a decision rule. In the latter case,

the decision to harvest is taken based on crop maturity status or depending on other criteria such as soil water status, crop health or even economic criteria. The harvest date is calculated according to one of the six following criteria:

- the physiological maturity (end of growth-development period) is reached,
- the maximum fruit water content is reached, as shown by the dehydration dynamics (**h2ograinmax_T**) after the stage idebdes,
- the minimum fruit water content is reached, as shown by the hydration dynamics (**h2ograinmin_T**) after the stage idebdes,
- the minimum fruit sugar content (**sucrerec_T**) is reached,
- the minimum fruit nitrogen content (**CNgrainrec_T**) is reached,
- the minimum fruit oil content (**huilerec_T**) is reached.

If the soil is too wet at this date, it is possible to postpone harvest to avoid soil compaction. In this case, a period (**nbjmaxapresrecolte_T**) following the calculated harvest date is defined during which the average soil water content is tested. The average soil water content in the zone between soil surface and the maximum depth affected by the harvesting equipment (**profhumrecolteuse_T**) is considered damaging if it is greater than **prophumtassrec_G** × **hccf_S**. However, harvest cannot occur after **irecbutoir_T** which is the latest date for harvesting. Several reasons lead to fix this deadline: the risk of crop health problems or yield losses or the need to free up the field for the following crop or due to economical constraints.

13.2.5 Pruning

This option is activated using the code **codetaille_T** in the .tec file.

Winter pruning is used for perennial woody crops like grapevine. On the prescribed day of winter pruning (**jultaille_T**), the biomass of stems and leaves remaining on the plant (mabois) is removed from the living plant and returned to soil so that the following cycle starts with the reserves only. The C and N concentrations in these organs are assumed to be 420 g C kg⁻¹ and 5 g N kg⁻¹ respectively, yielding a C/N ratio of 84.

In reality, pruning is also a technique to regulate yield through the number of remaining buds. However the model does not establish a relationship between pruning and the number of inflorescences (**nbinfo**) or the number of fruits removed (**nbinfoecl_T**), which are predicted independently.

13.2.6 Plant mulching

Plant mulch affects the physical conditions at soil surface (§ 11.4.1) and therefore the water balance and the C-N transformations (§ 12.2.3). If the mulch is a crop residue applied at the beginning of the simulation, the user must specify the amount of plant mulch supplied (**qres_T**), the day it was applied (**julres_T**) and the type of mulch (**coderes_T**) (Table 13.4). At harvest, crop residues are returned to the soil surface as mulch. The user only needs to indicate the fate of the residues (**ressuite_T**) (§ 13.5.3.2).

13.2.7 Plastic mulching

Plastic mulch also affects the soil moisture and temperature conditions (§ 11.4.1). These effects are simulated if the plastic mulch option is activated using the code

codepillage_T in the tec file. The user must specify two parameters: the albedo of the plastic cover, which is related to its colour (**albedomulchplastique_T**) and the proportion of soil cover (**couvermulchplastique_T**). Another option (**codeactimulch_G**) can also be activated. It re-enforces the simulation of the “natural” mulch effect, i.e. drying out at the soil surface.

Figure 13.1 simulates a winter wheat crop growing in the north of France, with a cover crop used as mulch residue to provide an example showing an order of magnitude related to the above mentioned mulch effects, which are described in further detail later (§ 11.4.1 and § 12.2.3). The parameter **albedomulchplastique_T** is 0.49 (Hidayat *et al.*, 2019) and the fraction of soil covered (**couvermulchplastique_T**) is 0.50. The increase in N mineralisation is simply due to the increase in soil temperature.

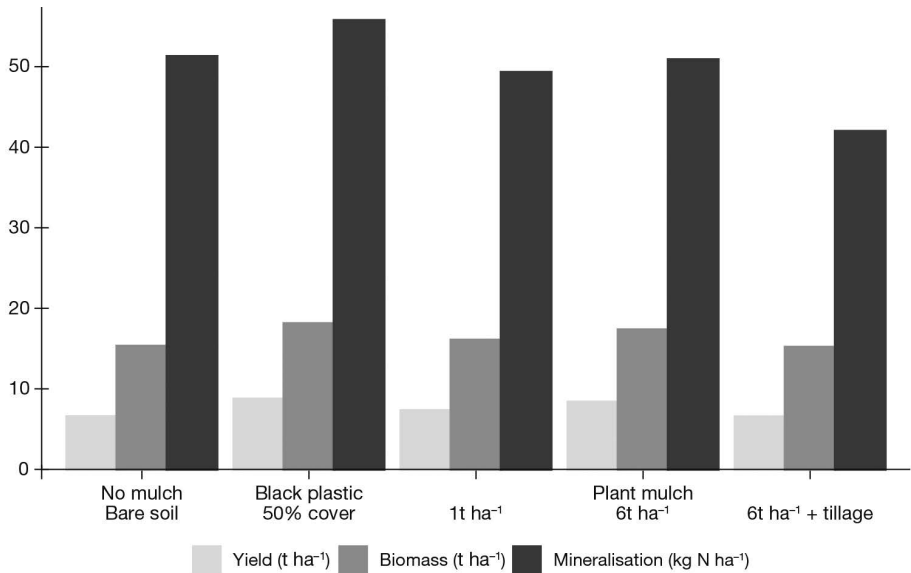


Figure 13.1. Simulated effects of various mulches on the crop yield, crop biomass and net N mineralisation

The simulated effects of the same mulches on the various processes involved in the water and their consequences on the water fluxes are presented in Figure 11.9.

13.2.8 Crop destruction

This option is activated by the code **codejourdes_T** in the tec file.

Crop destruction occurs automatically after harvest of annual crops, but can be forced on a given day for perennial crops. In both cases, crop destruction results in the death of above- and below-ground organs; they are returned to the soil as dead organic residues (§ 13.5.3.2). The amount of N returned to soil is equal to the amount of N present in the living plant on destruction day, whereas the amount of C returned to the soil (kg C ha⁻¹) is equal to the plant biomass (t ha⁻¹) multiplied by the C concentration of organs (g C kg⁻¹). C concentration in aerials, roots and perennial organs is assumed to be equal to 420, 380 and 440 g C kg⁻¹, respectively.

» 13.3 Crop operations and soil tillage

The aim of crop operations, particularly sowing and harvesting, and soil tillage operations is to support crop growth. However, they can also impact soil structure, physical soil conditions (water, temperature and aeration) and biological processes in soil (decomposition, denitrification).

13.3.1 Changes in soil structure

By default, STICS considers that the soil structure is a permanent characteristic that is invariable during the simulation. The primary variables used to describe the structure of each soil layer are the bulk density (\mathbf{DAF}_S in g cm^{-3}) and the infiltrability (\mathbf{infil}_S in mm day^{-1}) at the base of the layer (see Fig 15.22).

Knowledge of bulk density is used to calculate the total soil porosity, assuming that the solid density (density of the solid phase) is equal to 2.66 g cm^{-3} . Furthermore, the soil water content prediction allows the user to calculate the proportion of the porosity filled with water, called the water filled pore space (wfps). Porosity can be divided into two parts: textural porosity (or microporosity) which is filled with water at the field capacity (\mathbf{hccf}_S) and structural porosity (or macroporosity) which is its complement.

While the assumption of invariability of soil structure in deep layers is relevant, it may not hold for the upper layers, where the structure is affected by tillage and farming equipment operations in conjunction with the climate (Richard *et al.*, 2007). An alternative option is available for simulating a change in soil structure due to crop or soil operations ($\mathbf{codeDST}_T = 2$). However, this option has not been fully tested in all situations. The corresponding formalisms have been developed in the DST project to assess the risks of soil degradation linked to the soil compaction (http://temis.documentation.developpement-durable.gouv.fr/docs/Temis/0070/Temis-0070960/19514_Synthese.pdf) and a Ph.D. thesis (Lefebvre, 2010). Furthermore, this option does neither simulate the eventual de-compaction effects of climate, root activity and macrofauna, nor the protection effect of the soil structure thanks to the pebbles, due to a lack of knowledge about these effects.

Users can activate this option to simulate a change in soil compaction after farming operations: either an increase in bulk density and a decrease of soil infiltrability (\mathbf{infil}_S in g cm^{-3}) after sowing or harvesting or a decrease in bulk density (\mathbf{DAF}_S in mm day^{-1}) and an increase of soil infiltrability after tillage by ploughing or chiselling. With this option, STICS simulates a change in soil parameters driving soil evaporation: the soil depth affected by evaporation (\mathbf{zesx}_S in cm) and the cumulative soil evaporation above which the evaporation rate is decreased ($\mathbf{q0}_S$ in mm), as demonstrated in a loamy soil of the Paris Basin (Richard *et al.*, 2007; Table 13.1).

Table 13.1. Values of parameters linked to the bulk density of the ploughed soil layer in the Paris Basin, established from the data taken from (Mumen, 2006).

DAFS	infilS	zesxS	q0S
1.1	5.2	30.0	9.0
1.2	3.7	32.4	7.2
1.3	2.6	35.0	5.7
1.4	1.8	37.8	4.5
1.5	1.3	40.8	3.6
1.6	0.9	44.1	2.9

13.3.1.1 Compaction caused by sowing and harvesting operations

This option is activated using the code **codeDSTass_T** in the tec file.

It is assumed that the farming machinery that causes severe compaction is only that involved in sowing and harvesting operations. Six parameters are involved at sowing and harvest:

the relative soil water contents (fraction of water content at field capacity) above which compaction occurs (**prophumtasse_{mG}** at sowing and **prophumtasse_{recG}** at harvest);

– the soil depths affected by compaction (**profhumsemoir_T** at sowing and **profhumrecolteuse_T** at harvest);

– the bulk densities reached after compaction (**dasemis_T** at sowing and **darecolte_T** at harvest).

The relationships between these parameters and the nature of the soil machinery could be linked in the future as more mechanistic knowledge of soil mechanics is gained (Defossez *et al.*, 2003). Compaction is assumed to occur in the first two upper soil layers. It results in an increase in bulk density, a decrease in layer thickness, a decrease in layer infiltrability, an increase in the depth affected by evaporation (**zesx_G**) and an increase in **q0_S** (Table 13.1). The soil surface roughness (**z0solnu_G**) is assumed not to be affected.

The modification of the soil geometry affects the water and mineral N contents throughout the soil profile: soil mass conservation is assumed in the new layers with uniform partitioning within each layer.

13.3.1.2 Fragmentation caused by tillage operations

This option is activated using the code **codeDST_T** in the .tec file.

Soil tillage operations, whether they invert the soil or not, fragment the soil and decrease bulk density. Depending on the type of tool used, fragmentation occurs either in a superficial layer (e.g. surface tillage after harvest) or in the whole tilled layer if a mouldboard plough or subsoiler is used. Consequently, changes in the soil structure depend on soil tillage operations. For each tool, the resulting bulk density and roughness are defined as technical parameters. For instance bulk density reaches **dachisel_T** (1.10 g cm⁻³) after chiselling and **dalabour_T** (1.30 g cm⁻³) after ploughing. The soil roughness becomes **rugochisel_T** (0.001 m) and **rugolabour_T** (0.01 m) respectively.

The modification in bulk density affects infiltrability, water and nitrogen profiles, following the rules previously defined. So ploughing tends to increase soil evaporation by increasing the roughness of soil surface, but the water balance generally remains positive due to the increase in water storage as a consequence of greater infiltrability.

13.3.2 Impact of soil tillage on C and N cycles

The positioning of organic residues in soil and their subsequent decomposition are also affected by soil tillage operations. The effects of tillage are twofold: the operation i) mixes the newly added organic residues and remixes the previous residues that are decomposing; and ii) modifies the environmental conditions of decomposition: temperature, soil water content, aeration and mineral N availability which may exert a feedback effect on decomposition. Only three parameters are required to characterise the tillage operations: the date, the upper depth (**profres_T**) and the lower depth (**proftrav_T**) affected by tillage. The zone affected by tillage is the layer [1, **proftrav_T**] whereas the zone in which organic residues are mixed is the layer [**profres_T**, **proftrav_T**] (see § 12.2.2). The parameter **profres_T** can either be set by the user (see Beaudoin *et al.* (2008)) or calculated by the model (when **code_auto_profres_T** = 1). In that latter case, the default values for the parameters **resk_T** and **resz_T** are 0.14 and 5, respectively.

As soon as tillage occurs, the mulch at the soil surface disappears. Consequently, the decomposition parameters shift from those specific to the soil surface to those specific to mixed residues in soil, resulting in particular in an increase of the decomposition rate of crop residues.

Tillage is supposed to mix the residues and humified C-N pools, the water and the mineral N contents uniformly in the layer [**profres_T**, **proftrav_T**]. As a result, the environmental soil conditions (temperature, soil water content, aeration and mineral N) are modified either immediately after tillage or later on. The mulch disappearance also changes the albedo of the soil-plant system.

STICS can simulate no-till situations, although it does not involve a specific tillage coefficient for simulating an eventual reduction in mineralisation rate due to the reduction of physical disturbance. Such a coefficient (which appears in other models) may not be necessary to simulate the absence of soil tillage, as shown by Mary *et al.* (2020) in a 47-year experiment on soil tillage. Meta-analyses relative to long-term tillage (Luo *et al.*, 2010; Meurer *et al.*, 2018) have shown that the main effect of reduced or no tillage is a stratification of organic matter in the soil profile rather than a change in carbon storage over the whole soil profile. These findings confirm results obtained in temperate wet climates (Dimassi *et al.*, 2014, 2013).

» 13.4 Soil water management

Water reaching the soil is attributable to rain or irrigation, after eventual transit through vegetation and losses through surface runoff. The daily amount of water which infiltrates the soil is called precip.

13.4.1 Irrigation

Depending on the irrigation system used, water may be applied above the foliage (**codlocirrig_T** = 1), below the foliage (**codlocirrig_T** = 2) or in the soil (**codlocirrig_T** = 3)

at a given depth (**locirrig_T**) intended to mimic drip irrigation. For irrigation below the foliage, water supply is not subject to the mechanism of rainfall interception by the foliage. For underground irrigation, water supply is also withdrawn from the soil evaporation calculation. The parameter **effirr_T** stands for irrigation efficiency (0-1), which accounts for water losses during irrigation. It is applied as a multiplier to each irrigation amount.

The amounts of water applied can be entered from an irrigation calendar or calculated automatically by the model if the code **codecalirrig_T** is activated.

In automatic mode, a specified irrigation rate (**irrlev_G**) of about 20 mm is applied at the sowing date if rainfall on that day is smaller than this value, in order to ensure good germination. The model then calculates the water inputs needed over time to satisfy a fraction (**ratiol_T**) of crop water requirements: the model triggers irrigation when the stomatal stress index (swfac) becomes smaller than **ratiol_T**. The amount of irrigation applied (**airg**) allows to raise the soil water content between soil surface and rooting front up to field capacity. It cannot exceed a maximum daily irrigation rate dose authorised by the irrigation system (**dosimx_T**) and is nil if it is smaller than **doseirrigmin_T**:

$$\begin{aligned} \text{airg}(t) &= \min\left[\text{dosimx}_T, \sum_{z=1}^{z_{\text{rac}}(t)} (\text{hucc}_s(z) - \text{hur}(z, t))\right] & \text{if } \text{swfac}(t) < \text{ratiol}_T \\ \text{airg}(t) &= 0 & \text{if } \text{airg}(t) < \text{doseirrigmin}_T \end{aligned} \quad (13.3)$$

The irrigation schedule calculated by the model can be restricted to a specific time period. If the code **codedate_irrigauto_T** is activated, irrigation is initiated on day **datedeb_irrigauto_T** and ends on day **datefin_irrigauto_T**.

13.4.2 Interception of water by foliage

This option is activated using the code **codeintercept_p** in the .plt file.

The interception of water by foliage concerns rainfall (**trr**) and irrigation above foliage (**airg**). It does not concern the irrigation water provided by drip irrigation or micro-irrigation under the plant canopy. Water that persists on the foliage, which is directly subject to the evaporative demand of the surrounding atmosphere, may significantly reduce the saturation deficit within the canopy as the water evaporates, and thus affect the crop water requirements. In humid, tropical environments with a high frequency of rainfall combined with a high evaporative demand (mainly radiative), this phenomenon exerts a marked effect on the water balance (Brisson *et al.*, 1998a). Similar effects can occur in summer under irrigated crops in temperate and Mediterranean climates.

The importance of runoff down stems (stemflow) needs to be evaluated to avoid over-estimating the retention of water on foliage. Based on the work of Bussiere (1995), stemflow is considered as a priority. It is calculated based on incident rainfall (**trr** + **airg**) with a maximum given by **stemflowmax_p**, and increases with the LAI (see Eq. (11.17)).

Water that does not flow away via stemflow is partly retained on the foliage, up to a maximum value which is proportional to the LAI. The proportionality parameter, **mouillabil_p**, represents leaf wettability (mm m⁻²) and depends on leaf surface properties: shape, texture and pilosity. The value can be obtained by direct measurement or by solving the water balance equation (examples of values are given in Table 13.2). This water retained on the foliage then evaporates like free water (§ 11.3).

Table 13.2. Leaf wettability of several plants.

Plant	Forage grass	Maize	Sorghum	Gliricidia	Banana
Indirect estimate	0.27	0.27	0.28	0.23	0.68
Direct measurement	-	-	-	0.17	-

►► 13.5 Nitrogen and carbon inputs in soil

The inorganic N pool in soil can be replenished with the addition of synthetic fertilisers (called ‘mineral fertilisers’), organic fertilisers which contain significant amounts of mineral N (e.g. pig slurry or distillery vinasse), and mineral N contained in rainfall or irrigation water.

The N inputs coming from rain and irrigation are summed up in the variables `precipN` and `irrigN`, respectively. The N inputs derived from mineral fertilisers (NH_4^+ and NO_3^-) and from the inorganic fraction of organic fertilisers are summed up in the variable `totapN`.

13.5.1 N inputs from rain and irrigation

The daily N inputs from rainfall `precipjN` ($\text{kg N ha}^{-1} \text{ day}^{-1}$) are the product of the amount of rainfall (`trr`, in mm day^{-1}) and its mean N concentration `conccrrG` ($\text{kg N ha}^{-1} \text{ mm}^{-1}$). Let us remind that a mean concentration of 1 mg N L^{-1} corresponds to $0.01 \text{ kg N ha}^{-1} \text{ mm}^{-1}$. The N input from rainfall occurs at the soil surface and is assumed to consist of 50% NH_4^+ and 50% NO_3^- .

The N inputs from irrigation water `irrigjN` ($\text{kg N ha}^{-1} \text{ day}^{-1}$) are also the product of the amounts of irrigation water `airg` (mm day^{-1}) and its mean concentration (`concirrT` in $\text{kg N ha}^{-1} \text{ mm}^{-1}$), defined in the `.tec` file. The N input is located either at the soil surface or at the depth `locirrigT` if the option ‘localised irrigation’ is activated (`codlocirrigT = 3`). The mineral N in the irrigation water is assumed to be exclusively in the form of NO_3^- .

13.5.2 N inputs from mineral fertilisers

The N added as mineral fertiliser can be applied either at the soil surface or at a given depth (`locfertiT`) if the option ‘localised fertilisation’ is activated (`codlocfertiT = 2`).

The STICS model includes eight types of mineral fertilisers. As a simplification, urea is considered as an ammonium fertiliser since its hydrolysis into ammonium carbonate is a very fast process (Recous *et al.*, 1988). The main characteristics of these fertilisers are given in Table 13.3.

The fraction of ammonium (or ammonium formed from urea) contained in the fertiliser (`engammG`) is used when the option ‘nitrification’ is activated (`codenitrifS = 1`). In this case, the NH_4^+ and NO_3^- forms are distinct. The other variables are defined in the following paragraph. The type of mineral fertiliser added must be defined for each date of fertiliser application.

For forage crops, forage cuts and mineral fertilisation can be synchronised. The fertiliser rate associated with each cut is defined in the `.tec` file as `anitcoupeT`. Fertilisation is then triggered by the cutting calendar.

Table 13.3. List of available mineral fertilisers and corresponding parameters.

Code	1	2	3	4	5	6	7	8
Type	Ammonium nitrate	UAN solution	Urea	Anhydrous ammonia	Ammonium sulfate	Ammonium phosphate	Calcium nitrate	Fixed efficiency ¹
engammt	0.50	0.75	1.00	1.00	1.00	1.00	0.0	0.50
denengt	0.11	0.13	0.10	0.10	0.10	0.10	0.2	0.05
volengt	0.12	0.30	0.35	0.35	0.25	0.25	0.0	0.05
orgengt	30.00	33.80	37.70	37.70	37.70	37.70	25.0	0.20

¹ With this option the denengt volengt and orgengt values represent the proportion of fertiliser which is denitrified, volatilised and immobilised in soil, respectively.

13.5.2.1 Nitrogen use efficiency

The nitrogen use efficiency $effN$, i.e. the fraction of fertiliser N available for plant uptake (0-1), can either be imposed or calculated by the model. If $effN$ is fixed, the type 8 mineral fertiliser must be chosen and its nitrogen use efficiency must be defined in the general parameter file. Part of the fertiliser is considered to be unavailable to the plant because it will be immobilised in the soil by microbial activity, denitrified or volatilized. The efficiency $effN$ is the complement of these 'losses' to 1. It should be noted that nitrate leaching is not included in these losses since the nitrate transfer module operates directly on the soil mineral nitrogen amount.

The nitrogen use efficiency can be measured either by the difference in plant uptake between a fertilised and an unfertilised treatment, relative to the fertiliser rate, or by the ¹⁵N method which provides the recovery of a ¹⁵N-labelled fertiliser in the crop directly. The first method often results in higher values than the second option; the difference is mainly attributed to substitution effects occurring between the soil and the fertiliser. In STICS, the efficiency falls between the two methods because the model considers all sources of losses aside from fertiliser leaching.

The calculation of losses is based on the concept of competition between the soil and the crop. (Limaux *et al.*, 1999) have shown that the nitrogen use efficiency depends on the crop growth rate at the time of fertiliser application. The greater the crop growth rate, the higher the N use efficiency. Since nitrate leaching from fertiliser is usually negligible, the higher efficiency is attributed to smaller gaseous losses (denitrification and volatilization) from the fertiliser.

In STICS these losses are assumed to depend on the nitrogen uptake rate immediately before fertiliser application ($vabsmoy$, in $kg\ N\ ha^{-1}\ day^{-1}$). The parameters **deneng_G** and **voleng_G**, specific to each type of fertiliser, represent the maximum amounts of N losses by denitrification and volatilisation, respectively (Table 15.12). The potential gaseous losses are assumed to be proportional to the N fertiliser rate ($anit$, in $kg\ N\ ha^{-1}$). The actual losses depend on the nitrogen uptake rate recorded during the five days before fertiliser application ($vabsmoy$) through a hyperbolic relationship.

The daily N loss through denitrification (emitted as N_2+N_2O) is calculated as follows:

$$N_{denit}(t) = \mathbf{deneng}_G \cdot \frac{\mathbf{Vabs2}_G}{\mathbf{Vabs2}_G + \mathbf{vabsmoy}} \cdot \mathbf{anit}(t) \quad (13.4)$$

where the parameter $\mathbf{Vabs2}_G$ corresponds to the crop uptake rate ($\text{kg N ha}^{-1} \text{ day}^{-1}$) at which losses represent 50% of their maximum.

The daily N loss through NH_3 volatilization (N_{voleng}) is calculated in a similar way, but also depends on soil pH: it increases linearly when the soil pH increases from $\mathbf{pHminvol}_G$ to $\mathbf{pHmaxvol}_G$:

$$N_{voleng}(t) = \mathbf{voleng}_G \cdot \frac{\mathbf{Vabs2}_G}{\mathbf{Vabs2}_G + \mathbf{vabsmoy}} \cdot \mathbf{anit}(t) \cdot f_{pH} \quad (13.5)$$

with

$$f_{pH} = \frac{\mathbf{pH}_S - \mathbf{pHminvol}_G}{\mathbf{pHmaxvol}_G - \mathbf{pHminvol}_G} \quad \text{if } \mathbf{pHminvol}_G < \mathbf{pH}_S < \mathbf{pHmaxvol}_G$$

$$f_{pH} = 0 \quad \text{if } \mathbf{pH}_S \leq \mathbf{pHminvol}_G$$

$$f_{pH} = 1 \quad \text{if } \mathbf{pH}_S \geq \mathbf{pHmaxvol}_G \quad (13.6)$$

The Figure 13.2 is an example of N losses predicted by the model versus N uptake rate:

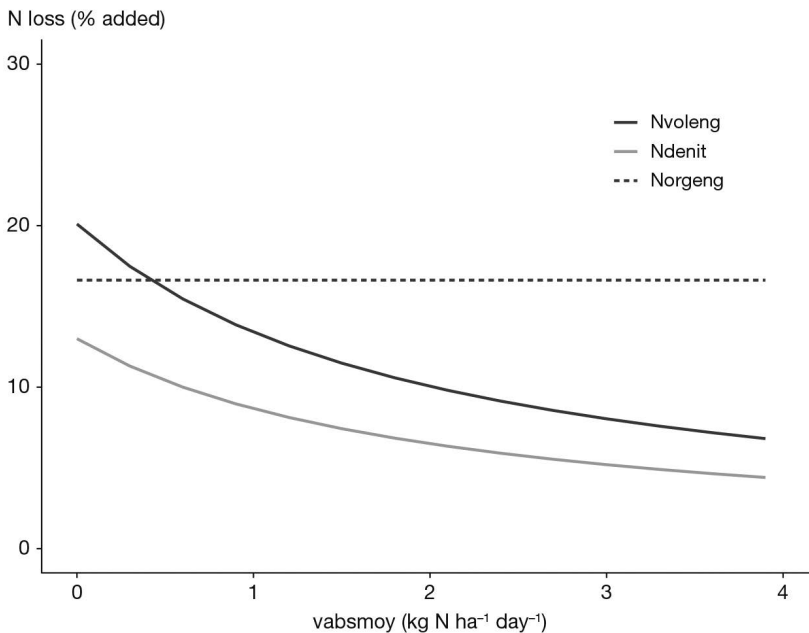


Figure 13.2. Predicted fertiliser-N losses versus crop N uptake rate at the time of fertiliser application. The example applies to UAN (urea and ammonium nitrate) fertiliser added at the rate of 100 kg N ha^{-1} in a soil with a pH of 7.5.

The N fertiliser losses through immobilisation and volatilisation are always calculated as indicated above. However the N losses through denitrification (coming from soil and fertiliser) can be calculated more mechanistically by activating the option `codedenits` (§ 12.4).

With regard to N immobilisation, studies conducted with ¹⁵N-labelled fertilisers have shown that the microbial immobilisation of N derived from fertiliser depends mainly on the N rate and the type of fertiliser (Bronson *et al.*, 1991; Limaux *et al.*, 1999; Powlson *et al.*, 1986; Recous *et al.*, 1992; Recous and Machet, 1999). Using these published data, we have derived a quadratic relationship between the amount of N immobilised (Norgeng, in kg N ha⁻¹) and the fertiliser N rate:

$$\begin{aligned}
 Norgeng(t) &= \mathbf{orgeng}_G \cdot \frac{anit(t)(2\mathbf{Xorgmax}_G - anit(t))}{\mathbf{Xorgmax}_G^2} \\
 &\quad \text{if } anit(t) < \mathbf{Xorgmax}_G \\
 Norgeng(t) &= \mathbf{orgeng}_G \quad \text{if } anit(t) \geq \mathbf{Xorgmax}_G \quad (13.7)
 \end{aligned}$$

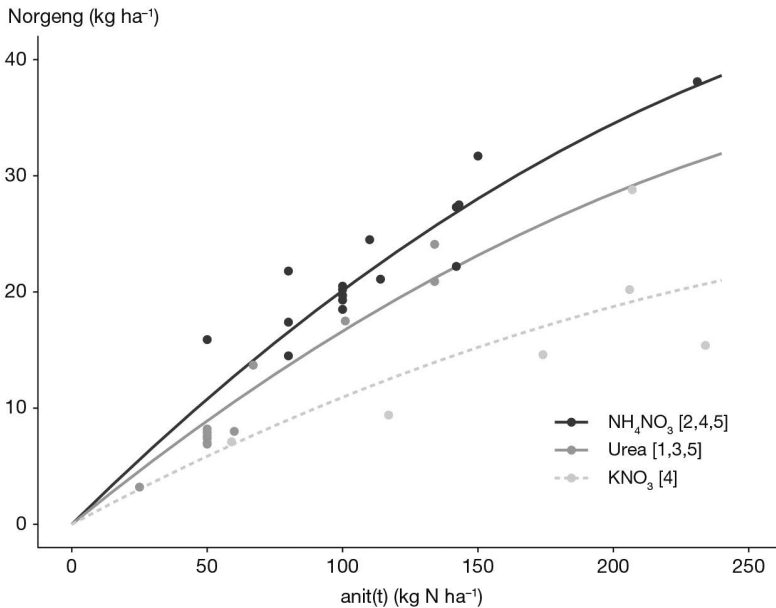


Figure 13.3. Relationship between fertiliser-N immobilised in soil and the amount of fertiliser, for three types of ¹⁵N-labelled mineral fertilisers. (Data from: [1] Recous and Machet, 1999; [2] Limaux *et al.*, 1999; [3] Bronson *et al.*, 1991; [4] Powlson *et al.*, 1992; [5] Recous *et al.*, 1992).

The parameter **orgeng**_G represents the maximum amount of microbial immobilised N from the fertiliser and **Xorgmax**_G is the N rate at which this maximum is reached. Only the **orgeng**_G parameter is specific to the type of fertiliser. Both parameters are expressed in kg N ha⁻¹.

It is also possible to impose a fixed efficiency by choosing a type 8 fertiliser. In this case, the microbial immobilisation, the volatilisation and denitrification are fixed and expressed as a fraction (0-1) of fertiliser-N. The efficiency is the complement of these values to 1.

Whatever the chosen option, the final N use efficiency (effN) is calculated as:

$$\text{effN}(t) = 1 - \frac{QNvoleng(t) + QNdenit(t) + QNorgeng(t)}{totapN(t)} \quad (13.8)$$

where $Q_{Nvoleng}$, Q_{Ndenit} and $Q_{Norgeng}$ represent the cumulative losses by denitrification, volatilisation and immobilisation.

13.5.2.2 Fertilisation calendar

The amounts of Fertiliser N applied can be entered from an fertiliser calendar or calculated as a proportion of a total amount if the code **codefracappN_T** is activated. The mineral fertiliser type must be known and documented for each date.

Similarly to water applications, fertiliser N applications can be either prescribed (option generally used) or calculated by the model. Conversely to water applications, it is a non sense to daily optimise fertiliser N applications. Optimal fertilisation is expected to cover all the crop cycle in order to anticipate the balance between the crop needs and the soil N supply (Berthommé, 2012). So this option should be used with great care.

13.5.3 N and C inputs from organic residues

13.5.3.1 Typology of residues

The N inputs from organic residues arrive onto the soil either under mineral form (mainly as NH_4^+) or under organic form. The mineral fraction enters the soil mineral pool and is submitted to NH_3 volatilization, nitrification, leaching and plant uptake. The organic fractions decompose at different rates and mineralise C and N according to the decomposition module (§ 12.2). The module is generic and can simulate most types of organic residues. Ten categories are considered:

Table 13.4. Types of organic residues.

Residue type	Residue number
Mature crop	1
Catch crop	2
Manure	3
Green compost	4
Sewage sludge	5
Vinasse	6
Horn meal	7
Grapevine shoots	8
Liquid manure	9
Rhizomes	10

Roots are also considered specifically.

The decomposition parameters (Table 13.5) are specific to each type of residue. The net mineralisation (positive or negative) associated with the decomposition of these residues depends on the type of residue and its C/N ratio. The characteristics of each type of organic residue are defined in the .tec file: category, depth of incorporation in soil, amount of fresh matter added, carbon content, C/N ratio, water content and mineral N content. Default values are proposed:

Table 13.5. List of organic residues and corresponding default parameters.

	Residue code	Average rate	Carbon content	C/N ratio	Mineral N content	Water content	Reference (pers. com.)
		t FM ha ⁻¹	%DM		%FM	%FM	
	coderes _t	qres _t	crepsc _t	csurnres _t	nminres _t	eaures _t	
MATURE CROP RESIDUES							
Cereals (straw)	1	9	42	90	0	7	
Sugarbeet (leaves and crowns)	1	40	42	22	0	90	J.-M. Machet
Grain maize (stalks)	1	12	43	60	0	25	
Soya bean (straw and roots)	1	5	44	75	0	10	
Proteaginous pea (foliage and roots)	1	4	42	28	0	10	B. Nicolardot
Rapeseed (roots, pods and straw)	1	6	44	45	0	10	E. Justes
CATCH CROP RESIDUES							
Wheat, rye (cereals)	2	8	42	15	0	80	
Mustard (cruciferous)	2	10	42	15	0	70	J.-M. Machet
Phacelia (cruciferous)	2	15	42	20	0	80	
Radish, oil seed (cruciferous)	2	10	42	16	0	80	E. Justes
Ryegrass (grass)	2	18	40	25	0	80	
MANURE							
Bovine manure	3	45	32	20	0	75	
Ovine manure	3	45	45	20	0	75	T. Morvan
Poultry manure	3		22			45	
COMPOST							
Rubbish compost	4	10	25	19	0.08	44	
Green waste compost	4	10	26	18	0.04	30	S. Houot
Compost of sewage sludge	4	10	37	19	0.04	50	
SEWAGE SLUDGE							
Non-processed sludge	5	60	30	8	0.12	90	

	Residue code	Average rate t FM ha ⁻¹	Carbon content %DM	C/N ratio	Mineral N content %FM	Water content %FM	Reference (pers. com.)
	coderes _t	qres _t	crespc _t	curnres _t	nminres _t	eaures _t	
Limed sludge	5	25	25	10	0.13	70	V. Parnaudeau
Physicochemical sludge	5	20	30	15	0.05	75	
CONCENTRATED VINASSE	6	3	40	8	0	50	J.-M. Machet
GROUND HORN	7		40	3.8	0	10	B. Nicolardot
Grapevine prunings (not yet known)	8						
LIQUID MANURE							
Porcine liquid manure	9	50	35	15	0.35	91	T. Morvan
Bovine liquid manure	9	50	25	18	0.1	94	
Rhizomes (not yet known)	10						

The coderes number refers to mineralisation dynamics as described in § 13.5.3.2.

13.5.3.2 N and C inputs from aboveground residues

Crop residues return to the soil either after harvest for annual crops or after destruction of the perennial crops at a prescribed date (julses). The calculation of crop residues returning to the soil, in terms of quantity (Qressuite) and quality (CsurNressuite), depends on the parameter **ressuite_T** which defines six possible management practices according to the harvest technique:

- roots (**ressuite_T** = "roots") when all the aboveground biomass is exported, e.g. with lettuce or textile flax;
- straw and roots (**ressuite_T** = "straws+roots") when all of the straw is returned to the soil, e.g. with cereals, sugarbeet or potato;
- stubble and roots (**ressuite_T** = "stubble+roots") when stubble (representing 35% of the straw) is returned to the soil, e.g. with cereals;
- stubble and roots (**ressuite_T** = "stubbleveg") when a variable fraction of aboveground biomass (**stubbleveg_G**) is returned to the soil, e.g. with silage maize or meadow cuts;
- whole crop (**ressuite_T** = "whole_crop") when all of the biomass is returned to the soil, e.g. with catch crops, cover crops or volunteers;
- prunings (**ressuite_T** = "prunings") corresponding to the return of wood prunings to the soil, e.g. in vineyards.

The C and N returned to soil at harvest as aboveground residues ($QC_{ressuite}$ and $QN_{ressuite}$) are calculated by assuming that the crop residues have a carbon content of 420 g kg^{-1} , as follows:

$$QC_{ressuite} = (masecnp - mafruit) \cdot 420$$

and

$$QN_{ressuite} = QN_{plantenp} - QN_{grain} \quad \text{if } \mathbf{ressuite}_T = \text{"straw+roots"}$$

$$QC_{ressuite} = 0.35 \cdot (masecnp - mafruit) \cdot 420$$

and

$$QN_{ressuite} = 0.35 \cdot (QN_{plantenp} - QN_{grain}) \quad \text{if } \mathbf{ressuite}_T = \text{"stubble+roots"}$$

$$QC_{ressuite} = \mathbf{Stubblevegratio}_G \cdot (masecnp - mafruit) \cdot 420$$

and

$$QN_{ressuite} = \mathbf{Stubblevegratio}_G \cdot (QN_{plantenp} - QN_{grain}) \quad \text{if } \mathbf{ressuite}_T = \text{"stubbleveg"}$$

$$QC_{ressuite} = masecnp \cdot 420$$

and

$$QN_{ressuite} = QN_{plantenp} \quad \text{if } \mathbf{ressuite}_T = \text{"whole_crop"}$$

$$QC_{ressuite} = mabois \cdot 420$$

and

$$QN_{ressuite} = mabois \cdot 5 \quad \text{if } \mathbf{ressuite}_T = \text{"prunings"} \quad (13.9)$$

Plant residues are assumed to remain at the soil surface until being buried by the next soil tillage, except for dead roots which remain at depth in the layer where they were produced.

For chained simulations, the model simulates the characteristics of the crop residues being returned to the soil and takes them into account automatically in the following simulation (§ 12.1).

Chapter 14

Ways of STICS use

*NICOLAS BEAUDOIN, JULIE CONSTANTIN, ANNE-ISABELLE GRAUX,
GATIEN FALCONNIER, FRANÇOIS AFFHOLDER,
FRANÇOISE RUGET AND LAURENT RUIZ*

This chapter will discuss the purposes of STICS uses along with scale variability and coupling possibilities.

Some 328 peer-reviewed papers involving the use of STICS were published from 1998 to 2020 (not counting numerous operational papers and reports) that showed that STICS specifications allowed for a large range of uses. The topics of these papers were analysed according to their abstracts, with a focus on the last decade (Figure 14.1). In 58% of them, STICS use dealt with agronomy and crop and environmental sciences, while statistics and modelling sciences, bioclimatology and soil science also represented a substantial share (32%). STICS applications in microbiology, ecology, animal science and rural economy were less frequent.

Since it was first developed in 1996, STICS has evolved to deal with an larger range of issues requiring new skills (Beaudoin *et al.*, 2021). STICS has been used in various decision-support systems and participatory approaches in several countries (e.g. France, Canada, Brazil, India) to: assess regional production potential, quantify crop water and nitrogen needs, identify opportunities to reduce nitrate leaching through innovative agricultural practices, support precision agriculture (including by assimilation of remote sensing data), forecast forage production, and adapt to climate change. In recent years, the focus has shifted to evaluating agronomic and environmental performances of agroecological cropping systems, intercrops, perennial crops for bioenergy. It has also focused more on greenhouse gas (GHG) emissions and long-term soil carbon sequestration. STICS is now one of the five most cited soil-crop models in academic literature (Keating and Thorburn, 2018). A majority of publications (58%) over the last decade deal with case studies outside France.

This chapter explains the many possible uses of STICS, while the chapters on ‘tools’ and ‘model extension’ provide more practical details. This chapter starts by defining the ‘unit of simulation (USM)’; a core concept in STICS, and then shows possible STICS applications for simulations on large temporal and spatial scales and on objects beyond soil-crop systems through model coupling. A typology of STICS uses for diagnosis, scenario exploration, support for decision-making and testing of scientific

hypotheses is then described, with examples from case studies. The chapter concludes with options for model improvements, including concepts and methods to integrate issues related to agroecology. Some paragraphs of this chapter come from the translation of the book chapter “Modélisation du fonctionnement des agro-écosystèmes: l’épopée STICS” (Beaudoin *et al.*, 2019), with the permission of QUAÉ Editions.

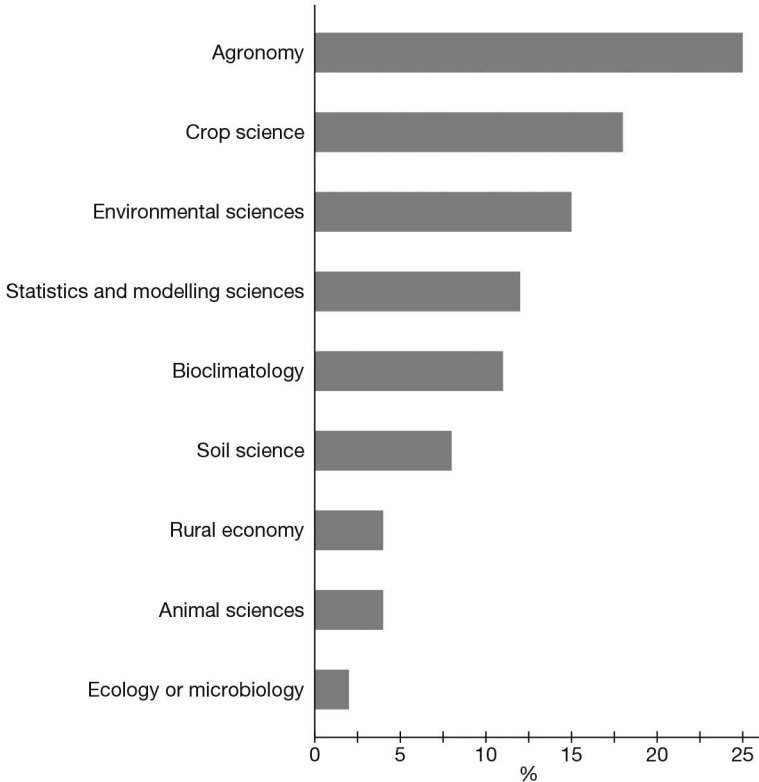


Figure 14.1. Discipline classification of papers involving STICS from 2010 to 2020 (n=231).

►► 14.1 Defining the unit of simulation (USM)

A unit of simulation (USM) corresponds to a cropping situation for which all the parameters determining the results of a simulation are assumed to be spatially constant. Thus, a USM is the combination of a soil type, a weather condition and a crop species with its management (§ 1.4.1). It is determined for a simulation period over the crop-growing season and can be preceded or followed by a bare soil period. A USM gathers the required information to run the simulation (Figure 14.2): daily weather data for the simulation period, soil characteristics, ecophysiological and agronomic characteristics of the crop species, and crop management (sowing date, density and depth, fertilisation and irrigation amounts and dates, etc.). Other important inputs are the initial soil water and nitrogen contents and, if necessary, the plant growth status when the simulation starts. Depending on the user’s objectives, STICS may simulate a single or successive USMs in order to simulate crop rotations in the same plot (§ 2.2.2).

Considering spatial scale, STICS is usually used to simulate plots. However, it can be used to simulate a few square meters and up to several square kilometers, depending on the realism of the assumption relative to the invariance of the parameters over the area considered.

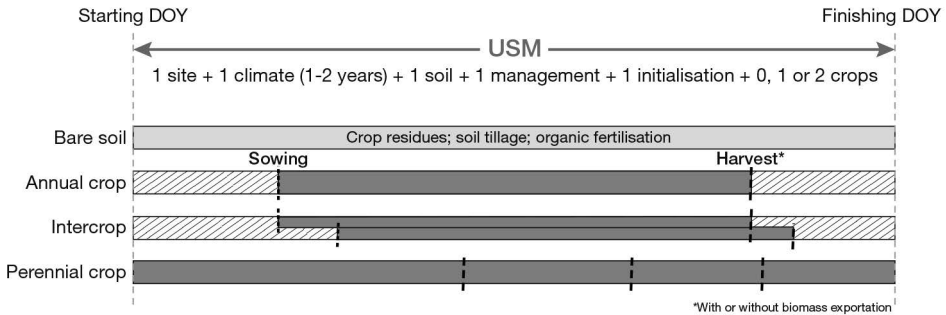


Figure 14.2. Different types of unit of simulation (USM) in STICS. Bare soil periods are in brown and crop growing periods in green. Hatches mean that simulating a bare soil period is optional, depending on the objectives of the simulation. DOY: day of the year.

14.1.1 Single crops

A USM generally corresponds to one crop but can be run with two crops or none at all. The simulation can start with or without an established crop (useful for perennial crops). If there is no crop at the start of the simulation, sowing can be simulated, and is characterised mainly by sowing date, density and depth. The model simulates harvest at a fixed date, or calculates the date according to physiological maturity or water, oil or sugar content of harvested organs. At harvest, the user must choose the share of biomass to export (between 0 and 1): only grains, or grains and straw for cash crops. In the case of perennial crops such as grass or grapevine, several cuts or harvests defined either at fixed dates or according to the sum of temperatures and decision rules (e.g. minimal biomass to be harvested) can be simulated. A period of bare soil can be simulated before and/or after the crop-growing period, within the same USM. This is optional as simulations can run from sowing to harvest or within a specific crop-growing period.

14.1.2 Bare soils

STICS can simulate bare soils (without any crops), if for example a user wants to analyse soil water and N dynamics during a bare fallow. All management options such as fertilisation, irrigation, organic input (manure, crop residues) and soil tillage actions can be simulated during bare soil periods. The model will simulate water, N and C balances for the bare soil, i.e. residue decomposition, C and N mineralisation, water drainage, nitrate leaching and gaseous emissions.

14.1.3 Intercrops

Intercropping consists of growing several crops (annual or perennial) simultaneously, each crop developing and growing at its own rate because of resource partitioning (§ 2.2.3). USMs are created to simulate intercropping using one unique soil type and

weather data, and agro-physiological and management properties specific to the two intercropped species. Although various spatial arrangements exist (strip intercrops, alley crops, mixed intercrops or even windbreaks), STICS is only able to simulate row intercropping.

The two management files of the USM and separated initialisation of the two crops allow users to simulate i) different crop statuses at the start of the simulation and ii) different sowing and harvest dates (Figure 14.2). N fertilisation, irrigation and soil tillage apply to both crops.

» 14.2 Rotations and long-term simulations

Our literature review showed the crop cycle scale represented in 57% of the publications involving STICS over the last decade under either actual or future climate when the daily scale was marginally investigated, mainly for sensitivity studies (Figure 14.3). Mid- or long-term studies together accounted for 38% of the publications, which means that STICS is useful for cropping system model simulation (Keating and Thorburn, 2018). Short-term (day to month) biological and physical processes such as soil anoxia, denitrification and crop freezing occur during the crop cycle. These short-term processes can have little impact in the long run (several years to a decade). Conversely processes affecting soil organic matter (SOM) mainly play a long-term role through their cumulative effects.

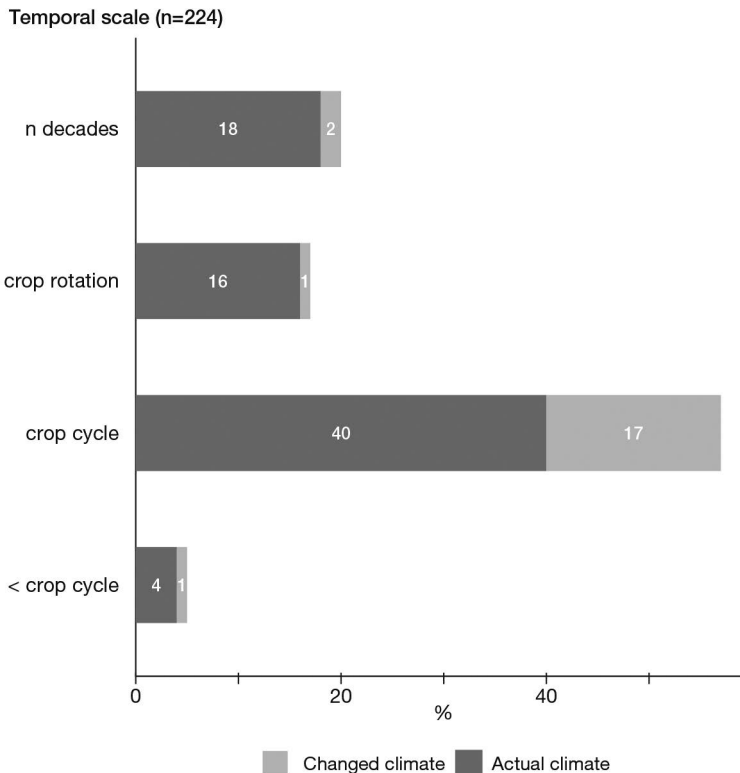


Figure 14.3. Temporal scale investigated in papers involving STICS from 2010 to 2020.

STICS can be used over the long term either i) with regular re-initialisation (reset) using in situ observations or ii) with continuous simulations, where the initial water and N content for only the first USM are provided. In the first case, reset runs allow a close fit of the model to the observations. This close fit allows the model to simulate accurately variables that are difficult to measure, such as N and C mineralisation, nitrate leaching, water drainage and N₂O emissions. In the second case, the model can simulate the impacts of alternative crop management, cropping systems and future plausible climates. The complementarity of these two possible uses has been well illustrated (Beaudoin *et al.*, 2008; Constantin *et al.*, 2012). A lack of observations on initial soil status for each USM shows the advantages of the continuous option over the reset option in long-term simulations (Kollas *et al.*, 2015); their respective interests are detailed in 14.2.2.

The comparison of soil carbon and nitrogen turnover simulations with a range of soil-crop models (CERES, NCSSOIL, SUNDIAL and STICS) highlighted a trade-off between short-term (day to year) prediction of N mineralisation and long-term (year to decade) SOM dynamics in arable cropping systems (Gabrielle *et al.*, 2002). STICS correctly simulated the SOM mineralisation rate when the amount of incorporated residues was known. Similarly, long-term predictions were sensitive to root biomass parameters (Yin *et al.*, 2020). This topic will be further discussed in § 14.2.4.

14.2.1 Defining USM for crop rotations or perennial crops

Using STICS to simulate rotations requires defining crop sequences, bare soil periods and their repetition over time. These rotations can correspond to monocrops, cereal rotations (including temporary grassland or not), cover crops and bare soil periods, and permanent cover such as permanent grassland or grapevines.

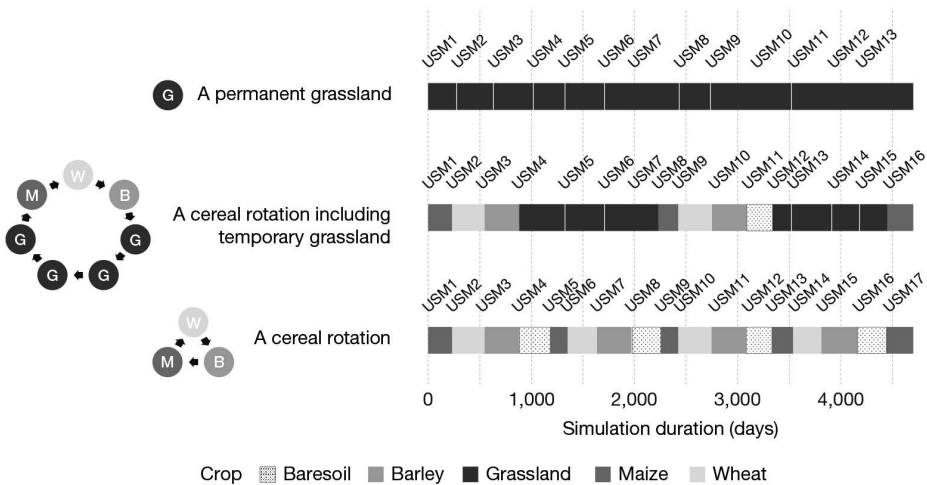


Figure 14.4. Example of three rotations defined to simulate the ORE-ACBB experiment (long term experimental observatory system for environmental research of biogeochemical cycle and biodiversity in agrosystems) over the period 2005-2017 (<https://www.soere-acbb.com>).

The user needs to define the schedule of each of the USMs involved in the rotation (Figure 14.4). The simulated period can be divided into USMs in several ways; the same rotation and its repetition over time can be defined differently depending on

the user. However, each USM must start the day after the previous USM ended. In the case of a sown annual crop, the USM can start a few days before sowing and end a few days after harvest. The user can also choose to define independent USMs for bare soil periods only, as discussed previously.

When chaining USMs, STICS automatically considers the final simulated values of SOM and recycled crop residues from the previous USM as initial conditions for the following USM (§ 2.2.2). A USM cannot exceed two years. Thus, for grassland, for example, the user must create several USMs. The first USM could start a few days before sowing of the grassland or January 1st in the case of established grasslands. The USM can end a few days after the final autumn or winter herbage removal of the first year. The following USMs may start the following day and end a few days after the final autumn or winter herbage removal of the second year, and so on, for the rest of the simulation period.

14.2.2 Long term simulations with USM re-initialisation or chaining

There are two ways to simulate long-term experiments:

- Run a single USM over a long-term climatic series, with a fixed management strategy, to represent monocropping (activation of ‘succession’ in the ‘climatic series’ option in the ‘param_gen.xml’ file).
- Run different USMs successively with specific crop management practices to represent crop rotation.

The successive runs can either be independent or linked with both options (Table 14.1).

- In ‘reset’ or ‘independent’ USM mode, initial conditions at the beginning of each USM are set by the user.
- In ‘continuous’ or ‘linked’ USM mode, initial conditions at the beginning of a given USM are provided by model outputs of the previous USM.

The ‘reset’ option can be used to:

- assess model sensitivity to cumulative effects by comparing outputs between reset and continuous options (Constantin *et al.*, 2012),
- provide a confident diagnosis of the impact of past agricultural practices when both crop management and initial values are well known (Beaudoin *et al.*, 2008; Ferchaud and Mary, 2016; Nicoullaud *et al.*, 2004). This approach requires observations of all state variables to define the initial conditions of each USM.

The ‘continuous’ option is recommended to:

- account for the absence of observations of the initial conditions of each USM, especially in lysimeters where coring is excluded (Yin *et al.*, 2020) or better account for the impact of SOM changes and residue decomposition on environmental outputs such as nitrate leaching (Constantin *et al.*, 2012).
- simulate perennial crops. For instance, the response of various French vineyards to global warming was evaluated by comparing STICS simulations for 1970–2000 and 2070–2099 (García de Cortázar Aauri, 2006).
- perform long-term predictive studies with climate change impact or cropping system change (Ducharne *et al.*, 2007; Tribouillois *et al.*, 2018a).

With the ‘continuous’ option, results do not depend on the segmentation of the simulated period into successive USMs but rely on STICS accuracy in simulating long-term dynamics of soil and plant variables. If observation of the initial conditions of the first

USM are missing, the model can be run for some years preceding the first year of interest to calculate reliable simulated initial values, such as initialization of multi-year STICS prediction in organic alfalfa systems (Strullu *et al.*, 2020).

Table 14.1. Summary of key differences between reset and continuous options in simulations.

	Option for long-term simulations	
	("climatic series" in the param_gen files or rotation with different USMs)	
	Reset	Continuous
Link between USMs	Independent, no link	Dependent on the previous one
Crop status	Values from the "*_ini.xml" file	Last values simulated in the previous USM
Soil water and N mineral content	Values from the "*_ini.xml" file	Last values simulated in the previous USM
Soil Organic N initialization	Value from 'norg' in the soil file	Last 'Nhumt' simulated in the previous USM
Other soil parameters	Values from the soil file	Values from the soil file except organic N (see above)
Crop residues at the start of the USM	Values provided in the "*_tec.xml" file	Last values simulated in the previous USM, according to ressuite parameter in the "*_tec.xml" file

In the following sections, we will illustrate how these two options can influence model outputs.

14.2.3 Illustration of the impact of “reset” and “continuous” options

14.2.3.1 Monocrops: simulation of grassland carbon reserves

Plant carbon reserves (resperenne) are supplied once the demands of all organs – i.e. leaves, stalks and possibly seeds or fruits – are satisfied (see § 7.3.1.1.2). They can also be consumed when photosynthesis is insufficient (see § 7.4). Reserve filling or emptying depends both on plant parameters (**slamax_p**, **tigefeuil_p**, **remobres_p**) and soil and weather conditions (Figure 14.5). The choice of a continuous or reset option largely affects the carbon reserve dynamic. With the reset option, the plant starts each year without any reserves. The continuous option allows the simulation of plurianual behavior of C reserves, which is more consistent with our knowledge of how grasslands function. Differences in carbon reserve simulation between the reset and continuous options are particularly important in winter when grassland reserves are used to initiate spring growth.

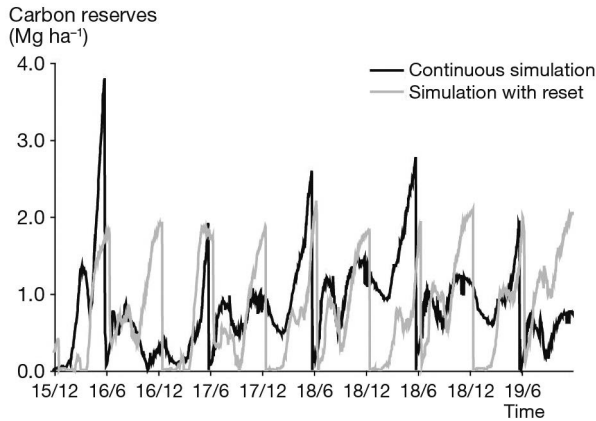


Figure 14.5. Carbon reserve (resperenne) dynamics for a temperate grass (*Festuca arundinacea*), with reset and continuous simulations from 1994 to 2003 (Ruget and Brisson, 2007).

14.2.3.2 Crop rotation and simulation of soil mineral content

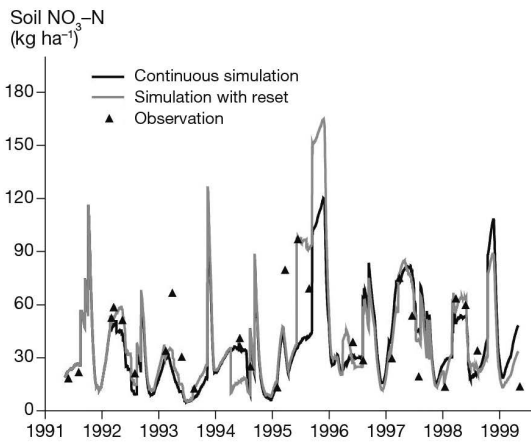
STICS was run on various soils of the small catchment of Bruyeres, in northern France, using either the reset or continuous options; the simulations were then compared. Simulated biomass and residue N content differed only marginally between the two options, but residue mineralisation was significantly greater with the continuous simulations (Table 14.2). With the continuous option, the amount of root residues from the previous crop was simulated; this was not the case with the reset simulations. The impact of the two options differed across soil types. In sandy soils, residue mineralisation was similar in reset and continuous simulations due to the high N content of root residues that did not induce significant N immobilisation in the next USM; conversely, residue mineralisation differed most between the two options in deep loamy soils.

Table 14.2. Comparison of STICS predictions of annual residue biomass, N content and mineralisation for reset and continuous simulations in the Bruyères catchment from 1991 to 1999. Measurements were taken from 36 sampling sites with various soil types (Beaudoin *et al.*, 2008).

Mean prediction		soil type			
		deep loam	shallow sandy loam on limestone	shallow loamy clay on marl and rock	shallow loamy sand on sand.
reset simulations					
Residue biomass	mg ha ⁻¹ y ⁻¹	8	7.3	5.6	5.7
Residue N content	%	0.8	0.9	0.8	1.3
Residue mineralization	kg ha ⁻¹ y ⁻¹	-5	-9	-5	-8
continuous simulations					
Residue biomass	mg ha ⁻¹ y ⁻¹	7.7	6.6	5.2	5.6
Residue N content	%	0.8	0.8	0.8	1.3
Residue mineralization	kg ha ⁻¹ y ⁻¹	-21	-22	-17	-6

Simulated and measured soil nitrate contents for continuous and reset simulations were compared for two contrasting soils within the same field (Figure 14.6): a) shallow sandy stony loam overlying limestone and b) deep loamy soil. In the reset simulations, soil nitrate values were reset twice a year against data and the model correctly mimicked the remaining part of observed data. Continuous simulations were less in agreement with measurements, especially in the case of the deep loamy soil. The largest discrepancies occurred for long fallow periods during dry winter conditions. Hence, using measurements to force the initial soil nitrate USM provides better results at the year scale. This study also showed that model sensitivity to soil parameters such as **profhum_s** (thickness of mineralisation layer) or **obstarac_s** (depth of obstacle to root system) greatly depends on both the simulation duration and the nature of the variable of interest.

a) Shallow sandy loam



b) Deep loam

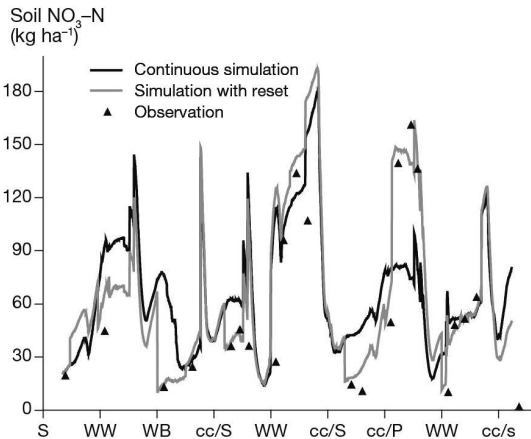


Figure 14.6. Observed and simulated soil nitrate contents during the 1991–1999 period for two use options (reset vs continuous) and two contrasting soils: a) shallow sandy loam overlying limestone and b) a deep loamy soil from the same field. The successive crops include sugarbeet, winter wheat, winter barley, catch crops, spring peas (Beaudoin *et al.*, 2008).

14.2.4 Carry-over effects in simulated soil organic matter

The incorporation or export of crop residues has a strong influence on the long-term change in SOM. Crop residues can include different plant parts (e.g. fine roots only, or the whole plant for green manure), in addition to stems and stubble (**ressuite_T**). The crop residues C/N ratio (**CsurNres_T**) and the amount of crop residues left on the soil (**qres_T**) are accounted for in the crop management file. The user can supply them when using the reset option, while the model calculates them in the continuous option. Residue incorporation is determined by tillage depth and the dates documented in the crop management file (for both options). If these operations occur at the end of the USM, crop residue decomposition carries over in the next USM in the continuous simulation. In this case, errors in the estimation of crop residue biomass, C/N ratio and incorporation depth can cause bias in the simulated changes in SOM and N mineralisation. The equations detailing the incorporation of crop residue according to the **ressuite_T** parameter and root simulation options are given in § 12.

As a result, parameters governing SOM dynamics are more influential in continuous simulation than in reset simulations, especially in low N input systems. Estimating these parameters requires specific attention for long-term simulation, but they have little influence over the short term (i.e. one year). The influence of model calibration, cropping systems, and crop management on net N mineralisation in continuous simulations is illustrated in Table 14.3. Blind model runs, i.e. without parameter calibration, slightly underestimated net N mineralisation, which resulted in underestimated N uptake and N leaching. The independent calibration of crop root parameters of sugar beet, peas and mustard coupled with optimisation of the soil parameters **profhum_S**, **obstarac_S** and **finert_S** (initially stable: total soil organic N ratio), against a quarter of the dataset, improved model performance, despite a slight remaining bias.

Table 14.3. Comparison of simulated (continuous simulations) and measured (lysimeter experimental data) net N mineralisation ($\text{kg N ha}^{-1} \text{ year}^{-1}$) over 1990-2012, for a bare soil and a crop rotation with and without cover crops. *Independent calibration of root parameters and optimization of three soil parameters against a part of the dataset (adapted from Yin *et al.*, 2020).

	Bare soil	Without cover crop	With cover crop
Mean observed	42	124	132
Simulated mean in blind test	33	89	90
Simulated mean after calibration*	41	111	120

14.2.5 Climate change scenarios

14.2.5.1 Background and challenges

At the end of the 1990s, assessing the impact of climate change on agricultural production became a key objective. In the 2000s, climate series became available at spatial scales compatible with impact models, including STICS. Modelling studies dealing

with climate change and STICS were scarce at first (Ducharne *et al.*, 2007; Perarnaud *et al.*, 2005) but that quickly changed: climate change became a major topic and was covered in 21% of the papers involving STICS published from 2010 to 2020. Crop models can be used to study the impact of climate change on crops through changes in temperature, radiation, CO₂ concentration and water availability, as well as alternative and more adapted cropping systems.

To estimate the possible contribution of agricultural systems to climate change mitigation, accurate simulations of greenhouse gas emissions (GHG), such as N₂O, is essential (Bessou *et al.*, 2010; Brilli *et al.*, 2017; Ehrhardt *et al.*, 2018; Peyrard *et al.*, 2017). Carbon storage simulation is also crucial to assess cropping system GHG balance (Pellerin *et al.*, 2020; Tribouillois *et al.*, 2018b). Accurate and meaningful simulations imply that the effect of climate change on C inputs and soil C mineralisation are accurately predicted.

STICS can take into account climate change-related issues in three ways by i) estimating the effects of climate change and increased atmospheric CO₂ concentrations on changes in agricultural productivity and environmental impacts; ii) designing and evaluating strategies to adapt management practices and cropping systems; and iii) proposing ways to mitigate GHG emissions from agriculture.

Using STICS in this changing climatic context has meant revisiting some of the model's formalisms to address extreme temperature phenomena, prolonged water stress, increased atmospheric CO₂ concentrations, and the way these phenomena interact. It has also led to coupling STICS with other models, especially when it comes to considering biotic factors. This section provides some examples.

14.2.5.2 Selected options

When simulating the impact of future climate on soil-crop systems, the user must first choose between reset or continuous simulations (§ 14.2.2). Independent simulations with annual re-initialisation of soil status can be useful to compare crop performance under current and future climate conditions while avoiding possible cumulative effects (Durand *et al.*, 2018; Jing *et al.*, 2017). Conversely, the continuous simulation option is appropriate for studies that aim to assess long-term dynamics (e.g. for soil organic carbon) where continuous soil water, C and N calculations are needed (Constantin *et al.*, 2012; Ducharne *et al.*, 2007). To simulate cropping system adaptation, the user can simulate different cropping systems by modifying the crop rotation (or 'USM chaining') and technical files accordingly.

To take into account the effect of CO₂ atmospheric concentration effect on photosynthesis and radiation use efficiency, the user must activate the 'climate change' option in the station file. Changes in atmospheric CO₂ concentration can also affect crop transpiration efficiency. To consider this effect, the user must choose the 'Shuttleworth and Wallace' equations (in the station file) to compute evapotranspiration (§ 9 and 15).

14.2.5.3 Examples of climate change studies using STICS

The ANR CLIMATOR project (2007–2010), coordinated by Nadine Brisson, is a major point of reference in France on the study of climate change impacts and the required adaptation of agriculture at the scale of France (Figure 14.7).

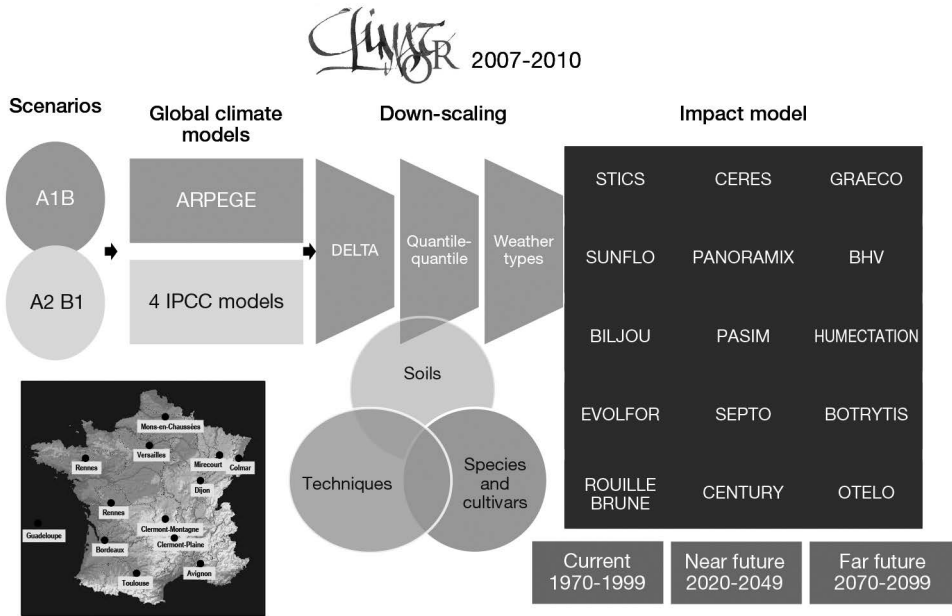


Figure 14.7. Approach of the ANR CLIMATOR project: multi-site implementation of a set of models and multi-criteria analysis of climate change impacts (Brisson and Levraut, 2010).

In the ANR CLIMATOR project, STICS highlighted the interaction between crop phenology shifts due to global warming, and the occurrence of increasing abiotic factors such as heat and drought. The model behaved differently between spring and winter crops in terms of their development and the consequences on flowering and maturity dates (Figure 14.8). The model also showed a shift and increase in total water requirements, which increased the need for irrigation at a time of the year when aquifers are vulnerable. This *in silico* experiment showed that sorghum was a relevant alternative to maize in southern cropping systems facing increasing droughts caused by climate change.

It also is crucial to properly anticipate the direct and indirect effects of climate change (via a host) on crop diseases. The impact of climate change on biotic factors (pests and diseases) often remains poorly understood, particularly in the case of fungal diseases, which are nowadays responsible for 16% of harvest losses and thus already threatening the food security (Flood, 2010; Savary *et al.*, 2012). Coupling STICS to integrate pest and disease pressure is therefore challenging when it comes to dealing with climate deregulation (see § 14.4.2 for the method). For instance, in the ANR CLIMATOR project, a dedicated disease module (MILA) was developed and coupled with STICS to reproduce fungal disease development and damage on crop development (Caubel *et al.*, 2014, 2012). In a recent study on the evolution of leaf rust of wheat in France, STICS-MILA showed a much earlier disease onset and an increase in final disease severity for the 2070–2100 period (Caubel *et al.*, 2017; Caubel *et al.*, 2012).

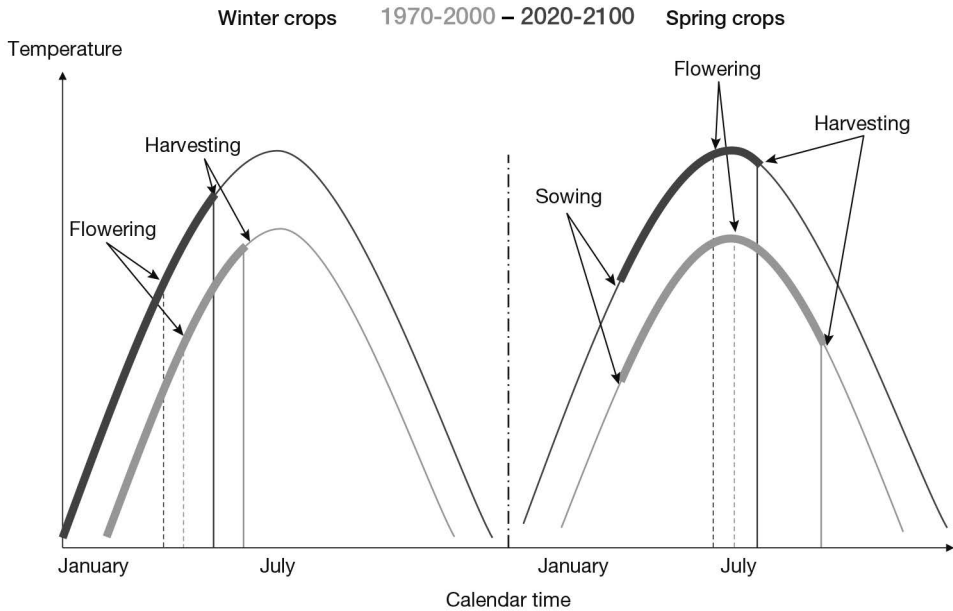


Figure 14.8. STICS simulations for the CLIMATOR ANR project: global warming impacts differently winter and spring crops, at a fixed sowing date (Brisson and Levrault, 2010).

14.2.5.4 Uncertainties and interest of model intercomparison

Exploring the impact of climate change on soil-crop systems with STICS comes with uncertainties that the user needs to deal with. Uncertainties can arise from two sources: i) crop model structure and parameterisation, and ii) the climate models and downscaling method used. The use of climate and crop model ensembles can help quantify the contribution of these different sources to the total variance of final outputs. A total of 33% of the 115 publications in our literature review (for the 2016–2020 period) that involved STICS used the intercomparison approach. As a general guideline, crop model structure was found to contribute most to the total variance of ensemble projections, followed by downscaled climate projections and crop parameters (Tao *et al.*, 2018). Below we describe in more detail how users can address uncertainty related to crop model structure and parameterisation.

By using STICS to explore the impact of climate change on crops, the user makes the implicit assumption that model structure and parameterisation is appropriate to reproduce the impact of elevated CO_2 concentration ($e\text{CO}_2$), extreme temperatures, drought and excess water on crops. But most crop models, including STICS, were not developed for this purpose (Rotter *et al.*, 2012). Recently, initiatives within the Agricultural Model Intercomparison and Improvement Project (AgMIP), among other initiatives, have started to compare crop model predictions with observations made in free-air CO_2 enrichment (FACE) experiments, with possible additional heat stress (e.g. heat shocks and continuous temperature increases) and water stress (e.g. rainfed versus supplemental irrigation). So far, models accuracy in reproducing the impact of $e\text{CO}_2$ has only been evaluated for wheat (Asseng *et al.*, 2019), $e\text{CO}_2$ combined with

temperature and/or water stress and maize (Durand *et al.*, 2018), eCO₂ combined with water stress. These studies showed that models generally captured the impact of eCO₂ and its interaction with heat and drought stress quite well, despite considerable variability across models. STICS has participated in these studies and benefited from the lessons drawn from these activities so users can get information about STICS prediction reliability of the impact of eCO₂, drought and heat on wheat and maize. To date, no systematic appraisal of model accuracy exists when dealing with eCO₂, temperature or water stress for crops other than wheat and maize. Initiatives are ongoing for crops including rice, soybean, potato and canola, and STICS is participating in some of these initiatives, but great caution is required when analysing the outcomes of a climate change impact study using STICS for crops other than wheat or maize.

Existing ensemble studies have mainly focused on temperate, high-input environments. Recently, the AgMIP ‘low-input smallholder systems’ study has given users the ability to assess the ability of a crop model to accurately predict maize yield (and other intermediary variables) in low-input environments in the tropics. STICS was ranked among the more accurate and consistent models (Figure 14.9). The study in question explored the potential impact of climate change (i.e. changes in CO₂, temperature and rainfall), but the simulated impacts of eCO₂, heat stress and water stress were not compared against experimental data.

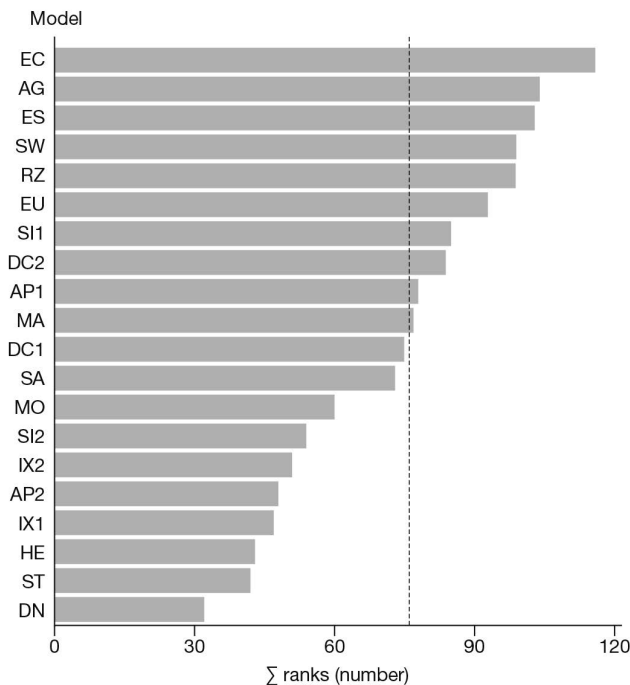


Figure 14.9. Sum of ranks (based on relative root mean squared error for maize grain yield, total aboveground plant biomass at maturity, maximum leaf area index, aboveground plant nitrogen at maturity, harvest index and in-season soil water content) for 20 fully calibrated models on ten experimental plots across sub-Saharan Africa (Falconnier *et al.*, 2020). The vertical dotted line indicates the median sum of ranks. ST=STICS model. The most consistent models have a low sum of rank (i.e. they are among the best models, for all simulated variables).

Climate change can also impact soil processes (e.g. the dynamics of soil organic matter mineralisation). Despite a review of the strengths and weaknesses of different crop models to simulate C and N fluxes (Brilli *et al.*, 2017), we are unaware of any study to date that has tested the accuracy of a simulated impact of eCO₂, heat stress and drought stress on soil processes against experimental data. However, the hypothesis of the effect of a probable microbial biomass adaptation to climate change was tested in tropical conditions (Sierra *et al.*, 2010; § 14.5.4).

►► 14.3 Simulation over large spatial scales

14.3.1 Principles of spatial application for STICS

Spatialising a crop model such as STICS over a large scale consists in simulating a large number of elementary spatial units. Elementary spatial unit size generally exceeds that of a field; accordingly, the soil, climate and management characteristics for these units are assumed to be homogeneous over an area larger than one field. Since the STICS model is often used for large-scale assessment (38% of publications from 2010–2020) some principles of large-scale application are given in this section.

Several approaches for large-scale application of a crop model, called ‘scaling-up’ methods, are presented in Ewert *et al.* (2011) and Faivre *et al.* (2004). There are several ways to apply STICS at large scale, namely:

- A-Sampling representative conditions to explore the range of variability encountered over the region by simulating only some specific points;
- B-Using a grid approach with full coverage, at high or low resolution depending on input data availability and the study objectives;
- C-Dividing the studied area into agro-ecological zones and simulating them as homogeneous areas.

In approach A, only a few ‘representative points’ are simulated. The user can spatially extrapolate the outputs of the model to obtain full coverage of the spatial area studied if necessary. A meta-model can be developed to extrapolate them as in Julie Constantin *et al.* (2015) or Graux *et al.* (2020).

In approaches B and C, inputs are spatialised before applying the model and cover the whole spatial area. These approaches generally involve more simulations, particularly when using a high-resolution grid (Hoffmann *et al.*, 2016a). Moreover, the limit of the system as well as the link between the different spatial units of simulation have to be defined. For instance, some water or matter fluxes can be simulated between near-by fields, due to runoff or erosion, particularly in watersheds with a sharp slope. These hypotheses can drive the framework since the spatial units behave independently (I) or dependently (D) when considering the modelled processes.

- Assumption (I) can be achieved by coupling STICS to a geographical information system (GIS), which includes soil mapping of the agroecosystem (Guérif *et al.*, 2007; Nicoullaud *et al.*, 2004).
- Assumption (D) can be achieved by coupling STICS to a spatially distributed hydrological model, which allows the user to describe lateral interactions occurring across the landscape (Beaujouan *et al.*, 2002; Ferrant *et al.*, 2014). These kinds of links are not necessarily considered in spatialised simulations, but they can be essential depending on the objectives of the model application.

The use of STICS at scales larger than a homogenous field requires expertise and information about soil and agricultural practices. A useful example is the case study of the Seine River basin (PIREN-Seine) (§ 14.3.2). In this study, pedotransfer functions were developed to infer STICS inputs (soil parameters such as field capacity and wilting point) from a soil map that included qualitative soil description (Le Bas, 2016; Lefebvre, 2010). Using data from remote sensing or digital soil mapping can also be useful to access, through model inversion, to: i) soil properties, since the climatic conditions allowed to exhibit these properties, e.g. water storage versus drought (Varella *et al.*, 2010a); ii) technical parameters that are not accurately available everywhere (Courault *et al.*, 2010).

Finally, STICS simulation accuracy is mainly evaluated at plot scale and there are limited possibilities to evaluate this accuracy at larger scales such as the region, watershed or country (Beaudoin *et al.*, 2018; Beblík and Kersebaum, 2001; Loague and Corwin, 1996). In this case, analysis of model output sensitivity to varying spatial resolution and accuracy of inputs can guide the parameterisation work and indicate the required improvement in input accuracy depending on the focus of the study.

14.3.2 Sensitivity of STICS output to input data

Some data such as crop/soil management, soil properties or even weather data are not available at high resolution for large-scale assessment. Nevertheless, the user must still find a way to enter the model parameters. The chosen scaling-up approach will influence STICS results. Since management data over large areas are scarce, the assumption of homogeneous, fixed management is often made. Alternatively, farmer decision rules can be defined to simulate crop/soil management according to climate and/or soil conditions.

The impact of input choices is also dependent on the temporal (daily, annual and/or multi-annual) and spatial (field, small watershed, region, country) level of analysis of the outputs. Some studies on scaling methods for crop models, within the MACSUR and AgMIP projects, have been conducted to quantify the impact of climate, soil and management resolutions on STICS outputs (crop yield, gross primary production, drainage and soil organic matter changes over time). These impacts were analysed depending on the output of interest and its level of aggregation in space or time. The detailed results are available in several publications (Constantin *et al.*, 2019; Grosz *et al.*, 2017; Hoffmann *et al.*, 2016b; Hoffmann *et al.*, 2015; Kuhnert *et al.*, 2017; Maharjan *et al.*, 2019; Zhao *et al.*, 2016, 2015). These studies showed that:

- The regional multi-annual average of model outputs was not sensitive to the resolution (from 1 × 1 km to 100 × 100 km) of the simulation grid or the variability in climate, soil and management.
- The impact of the resolution of climate, soil and management data varied per output; for example, soil organic matter dynamics through time were strongly impacted by the soil data resolution, but they were not very sensitive to climate.
- The regional annual average of model outputs was, in some cases, very sensitive to the input data resolution.
- Comparing soil and climate resolutions, the impact of soil resolution is higher than that for climate, which reflects the higher variability of soil than climate.
- The impact of the management data resolution can be substantial and should not be neglected at a large scale, despite the scarcity of observed data.

We believe that these outcomes can help users make relevant choice to represent climate, soil and cropping systems in accordance with the objectives of the large-scale assessment.

14.3.3 Examples of spatial application

– Case study of type A:

The long-term evaluation of impacts of application of recommended practices in cropping systems in the Bruyères small arable catchment relied on the survey of 36 permanent soil-sampling sites representing the soil-crop variability within a 145 ha area over 22 years (Beaudoin *et al.*, 2021). The STICS model was used to simulate infiltrated water and nitrate leached below the rooting zone at the year-sampling site scale. In order to improve prediction accuracy of N leached, the model was reset every year using soil mineral nitrogen (SMN) data measured at harvest. The predicted values were then extrapolated within the same field to the zone having the same parent material. It was assumed that running STICS at well characterised sample sites was more relevant than distributing the model over all the soil units without knowing their initial SMN. The assumption was supported by a previous comparison between the output of this type A approach and the outputs of the type C approach, applied with fine soil map resolutions (1:7500 and 1:25000), which showed the water and nitrogen fluxes were close on average at the basin scale (Beaudoin, 2006). Coupling STICS and the dataset provided a sufficiently robust prediction of the NO₃ concentration in drained water to be able to determine the efficacy of recommend practices to meet EU limits for drinking water.

– Case study of type B and C:

Three studies, commissioned by the French ministries of agriculture and ecology to assess the ecosystem services of agroecosystems, grasslands and the 4per1000 initiative (Graux *et al.*, 2020; Pellerin *et al.*, 2020; Therond *et al.*, 2017), used STICS for national-scale assessment on agricultural land. In these case studies, we used a high-resolution modelling approach to quantify various aspects of French agriculture linked with crop production, C storage and GHG balance, or water and N services provided by current and alternative crop rotations or permanent grasslands in France. The cropping systems (rotations and crop management) and the associated pedoclimatic conditions were described in as much detail as possible to run long-term STICS simulations. We considered that STICS had been thoroughly calibrated and evaluated for a wide range of cropping systems, soils and climates in France (Constantin *et al.*, 2012; Coucheney *et al.*, 2015; Graux *et al.*, 2020; Yin *et al.*, 2020) to simulate water, N and C balances at the field scale.

Soil mapping units of the 1:1,000,000 French soil map and 8 km × 8 km SAFRAN climate grids were spatially intersected to identify 30,966 pedoclimatic units (Figure 14.10). A total of 23,149 pedoclimatic units (PCUs) of agricultural area were selected according to the French Land Parcel Identification System, representing 97% of the agricultural area in mainland France (annual and perennial crops, grasslands, market gardens and fallow land). Since spatial distribution of soil types within each soil mapping unit was unknown, they were selected in decreasing order of percentage until they covered at least 70% of the area. Initial soil organic carbon (SOC) stock in the topsoil was estimated from soil data at a 90 m × 90 m resolution (Mulder *et al.*, 2016). The one to two

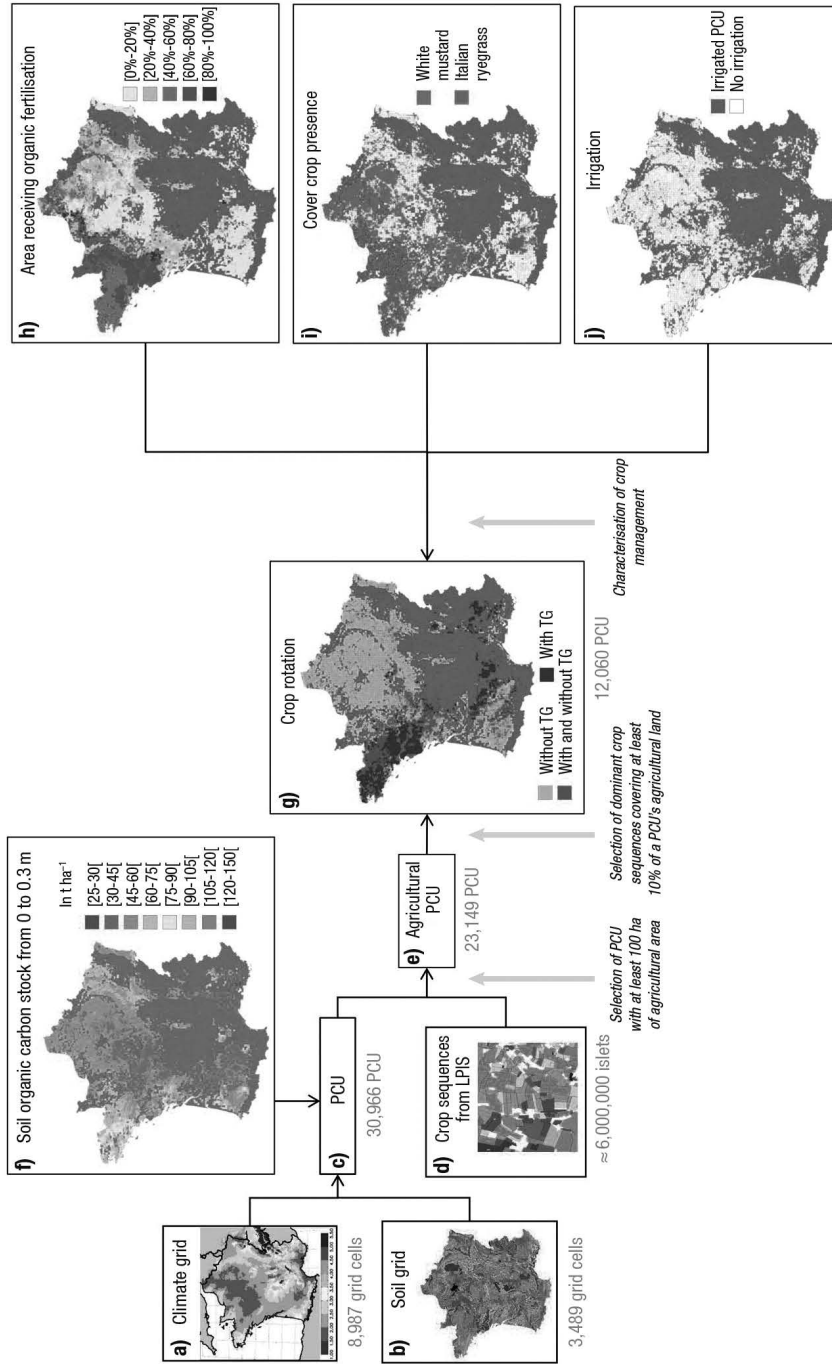


Figure 14.10. The workflow developed to represent current cropping systems in France. PCU: pedodimatic units, LPIS: Land Parcel Identification System, TG: temporary grasslands. Only the three main irrigated crops in France (maize, wheat and sunflower) were considered to be irrigated in the simulations (from Launay *et al.*, 2021).

most common crop rotations were chosen, including only crops that were calibrated in STICS. For maize, we adapted the crop cycle duration of cultivars to each PCU growing-degree days available between sowing and harvest. For the other crops, we chose the most common cultivar in France available in STICS.

We used the Agricultural Practices Survey conducted in 2006 and 2011 by the French Ministry of Agriculture, Agrifood and Forestry for around 14,000 fields throughout France to determine crop management. Since the data was available and considered representative at the administrative region level (NUTS II; Eurostat, 2018), we used the median of observations per arable crop and administrative region for sowing and harvest dates, mineral or organic fertiliser dose, dates of mineral N fertilisation, percentage of the crop with organic N fertilisation, type and frequency of organic N fertilisation, and frequency of tillage.

In accordance with the French application of the European Union Nitrates Directive (Council Directive 91/676/EEC), cover crops were included in rotations in PCUs located in Nitrate Vulnerable Zones in 2012. Nitrate Vulnerable Zones are “areas of land which drain into polluted waters or waters at risk of pollution and which contribute to nitrate pollution”. Cover crops were sown before spring crops, except when the previous crop was grain maize or sugar beet, after which the soil was left bare. Cover crop species (white mustard or Italian ryegrass) and dates of sowing and destruction by soil tillage were defined per region based on the Agricultural Practices Survey. Results were expressed at a spatial scale larger than the field by averaging results, weighted by their areas. Figure 14.11 shows one example of the results obtained from the 4per1000 initiative.

The first two years were used only to initialise soil mineral N and water contents according to agro-pedoclimatic conditions. Yearly outputs were then analysed for 1984–2013 and averaged over the 30 years at the PCU level.

– Case study of type C:

The Interdisciplinary Research Programme on water and the environment in the Seine basin (PIREN-Seine) started in 1989 to protect and manage the water resources of the Seine river and Normandy basins. Multiscale evaluations of the impact of either actual or improved cropping systems on yield and water resource quality aimed to prevent diffuse pollution from nitrate and pesticides affecting drinking water, which mainly comes from deep aquifers. A modelling chain was created to quantify the impacts of scenarios of farming practices (Ledoux *et al.*, 2007; Tavakoly *et al.*, 2019) on crop yield and water resource quality. STICS was calibrated and tested independently before being integrated into the modelling chain. The STICS inputs were provided by cross-referencing several datasets that integrated all the spatiotemporal variability at a given resolution (Figure 14.12).

The Figure 14.12 indicates the following:

- Upper line, information layers (from left to right):
- SAFRAN grid providing local meteorological data (Quintana Segui *et al.*, 2009);
- French soil geographical database at 10^{-6} scale (INRA, 1998) containing the soil mapping units (SMUs); each SMU can contain several soil type units (STUs);
- Agricultural database (Mignolet *et al.*, 2007; Mignolet *et al.*, 2004; Puech *et al.*, 2015; Schott *et al.*, 2010) containing both the 95 agricultural modelling units (AMUs)

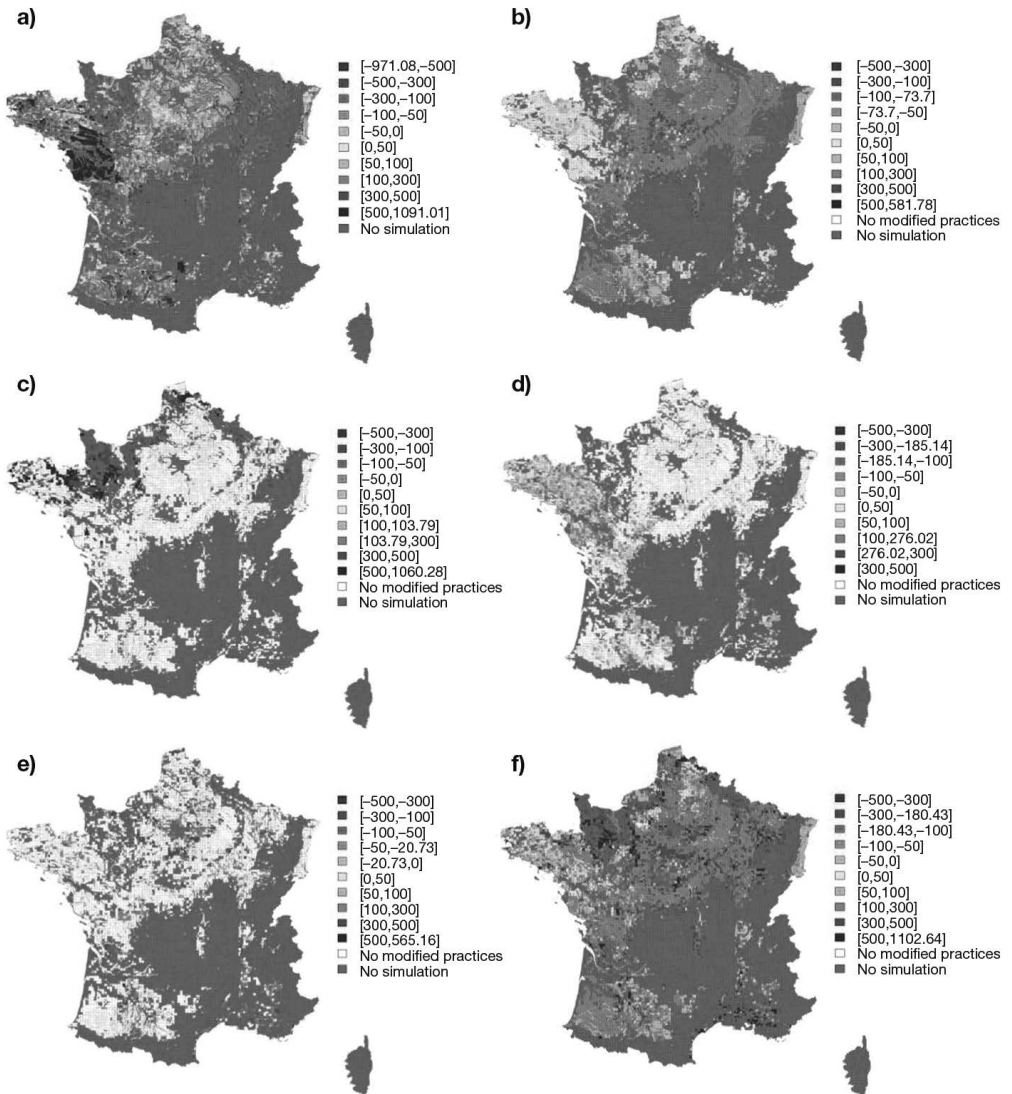


Figure 14.11. Maps of a) annual soil organic carbon (SOC) storage in the baseline scenario and b) to f) additional SOC storage in mitigation scenarios ($\text{kg C ha}^{-1} \text{ yr}^{-1}$) in the topsoil (0–0.3 m deep) in cropping systems simulated over 30 years with STICS. Additional SOC storage potential relative to the baseline scenario when implementing mitigation scenarios: b) cover crop insertion, c) insertion of temporary grasslands instead of silage maize, d) extension of temporary grassland duration, e) improved recycling of organic resources and f) consistent combination of these mitigation scenarios when possible at the cropping system scale (from Launay *et al.*, 2021).

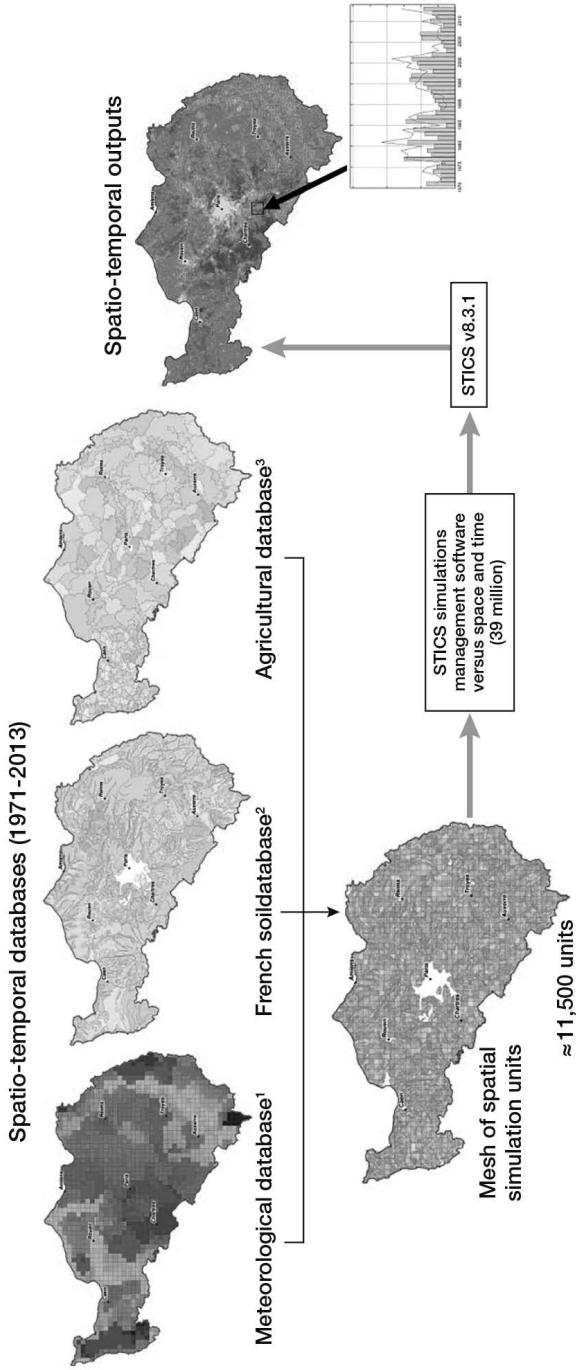


Figure 14.12. Method of distribution of the STICS agronomic model over the Seine-Normandie basin (from Beaudoin *et al.*, 2018).

and the seven agricultural districts, which originated from expert enquiries and crop succession modelling using the Markov chain.

– Lower line, distribution process of the model run in time and space.

Finally, a quality assurance protocol (Refsgaard *et al.*, 2005) was used to qualify the reliability of STICS outputs over the Seine-Normandie basin (Beaudoin *et al.*, 2018). The modelling chain predictions were tested and submitted for expert appraisal before being discussed with stakeholders (Figure 14.13). In this project, stakeholders needed to explore the consequences of innovative scenarios that would ensure food security while reducing the transfer of nitrates and pesticides to surface and deep water, and of gaseous pollutants to the atmosphere. These scenarios were simulated at the scale of local catchments (Seine tributary basin and Seine River Basin). They showed, for example: no change in fertilisation, a 20% reduction in N fertilisation, adoption of best management practices, and the generalisation of organic farming. Scenarios were developed with involvement from farmers' groups, agricultural extension services and water resource stakeholders. Using STICS required a rigorous calibration and evaluation of the model ability to reproduce the impact of various N management practices on N balance. Moreover, the ability of STICS to simulate GHG emissions and N balance of conventional or agroecosystems was improved both for experimental conditions (Autret *et al.*, 2020; Peyrard *et al.*, 2017) and "on farm" research (Benoit *et al.*, 2016; Rakotovololona, 2018). Scenarios highlighted strong differences in terms of N balance and N gaseous losses between systems.

►► 14.4 Simulation with coupled models

14.4.1 Principles and typology of coupling

Coupling two models involves the exchange of information between them. Models can be linked externally or internally (Table 14.4). There are four types of external links that deal with STICS inputs or outputs. A geographical link can connect model inputs or outputs of STICS to vectors of coordinates managed in a geographical information system (GIS) at the same spatiotemporal resolution as STICS. A statistical link uses an equation built with a numerical experiment on the response of the variable of interest to the variability of STICS inputs, at a more integrating time step than STICS. A dynamical link uses STICS outputs as inputs for the second model at STICS spatio-temporal resolution. STICS was mostly used to force another model downstream. The upstream forcing of STICS by another model is also possible.

The internal link implements a dialogue (involving a change in model codes) during model daily loops. It results in intermediate variable exchange between the coupled models. STICS then comes into play both upstream and downstream of the other model along the daily loop. The two models must have the same time step, but their spatial resolutions can differ. Similarities in model specifications (e.g. functional or generic) favour the coupling. This linkage can be implemented in stand-alone computer software or through a platform that frequently connects to a GIS.

With regard to the published papers involving STICS, the type of link appeared to be weakly influenced by the application domain of the study: a given link can occur in different application domains (Table 14.4). These different types of links are illustrated

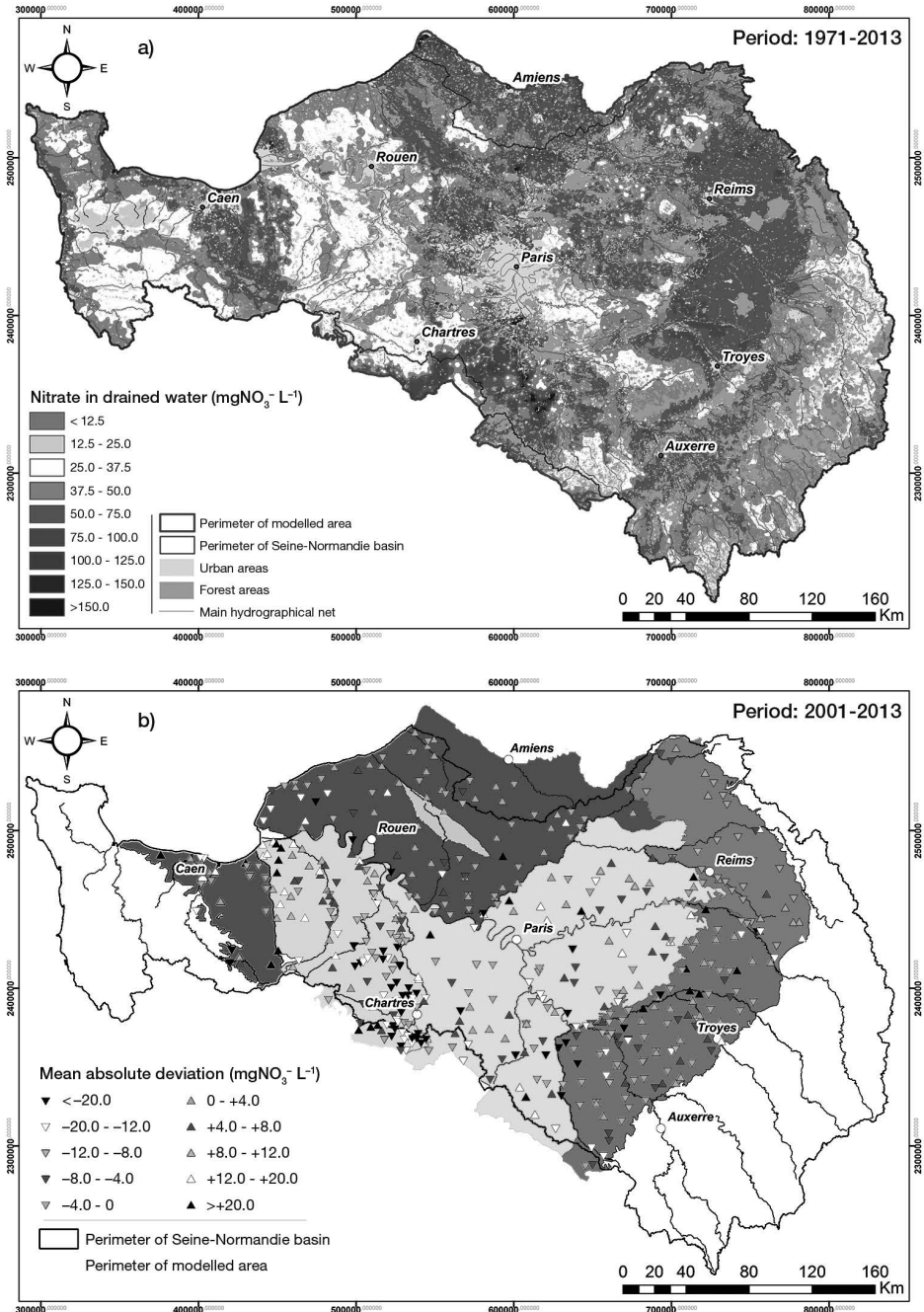


Figure 14.13. Maps of spatially mean outputs of the chain modelling (Beaudoin *et al.*, 2018): a) weighted mean nitrate concentration in drained water simulated in agricultural areas; b) mean difference (simulated value – observed value) in nitrate concentration at monitored outlet of the aquifers represented by different colors.

in the following paragraph. The use of the lone GIS seems limited to biological or biogeochemical studies. The use of the statistical response function appeared most frequently in socio-economic studies. However, these studies can also mobilise internal links. This short overview indicates that the coupling specifications must be driven by considerations of scale, operational skills and the expectations of the project partner rather than by standard rules. However, the scientific basis for linking models across disciplines and scales is still weak and requires specific attention in future research (Ewert *et al.*, 2009).

Table 14.4. Typology of the STICS coupling according to the publications involving STICS for the 2016-2020 period.

Nature of the link	Code link	Application domain				Total
		Geographical (GIS)	Biological and/or biochemical	Socio-economical	Agronomical and socio-economical	
1) Lone GIS	External	Yes	6	0	0	6
2) Statistical response fonction	External	Yes	0	0	7	7
		No	1	0	0	1
3) Dynamical upstream	External	Yes	0	1	0	1
		No	1	0	0	1
4) Dynamical downstream	External	Yes	5	0	0	5
		No	4	1	1	6
5) Dynamically interactive	Internal	Yes	7	0	2	9
		No	3	0	0	3
Total			27	2	10	39

14.4.2 Examples of STICS model coupling

STICS has been coupled in various forms and for various purposes. In this section, we provide illustrations of each type of link and then, one example that combines several types of link.

– *With GIS*

Coupling a crop model with a GIS has emerged as a promising opportunity since the 1990s in agro-environmental studies. Doing so has allowed users to deal with the spatial variability of land use, soil properties and crop management (Corwin and Wagenet, 1996; Wagenet and Hutson, 1996). Behind the apparent simplicity of the approach is a combination of naturalistic or mechanistic models (Nicoullaud *et al.*, 2004):

- spatial representations of the distribution of soil types and climate;
- databases of the values of parameters or functions, known as pedotransfer;
- a soil-crop model, generally one-dimensional;
- a panel of rules for forecasting initial conditions;
- a model for farmer decisions or a data-base of technical interventions.

A first type of application is the spatially distributed prediction of crop production, like in the EU's European BIOMA platform for forage production. Other examples show the reliability of STICS application for predicting crop production and nitrate leaching at small catchment scale (Schnebelen *et al.*, 2004; Tournebize *et al.*, 2004); the results of these studies can support STICS application at the larger basin scale (§ 14.3.2).

– Statistical response function

Numerical experiments using STICS produced statistical functions or surface responses for a range of variables (e.g. crop yield, crop water requirement, NO₃ losses, N₂O emissions) to the variability of inputs (e.g. nitrogen supply) for a given cropping system. These statistical models simplify the link with the economic model. One example of the whole process is the AROPAJ platform (Figure 14.14). This meta agro-economic model generator can optimise farm production systems. Several studies applied it to investigate the environmental responses of cropping systems to different policy scenarios (Humblot *et al.*, 2013; Jayet and Petsakos, 2013; Leclère *et al.*, 2013). Another example consists in using STICS to simulate the impacts on N₂O emission of scenarios of urban waste application and irrigation, using life cycle assessment (LCA) in African cities (Perrin *et al.*, 2017).

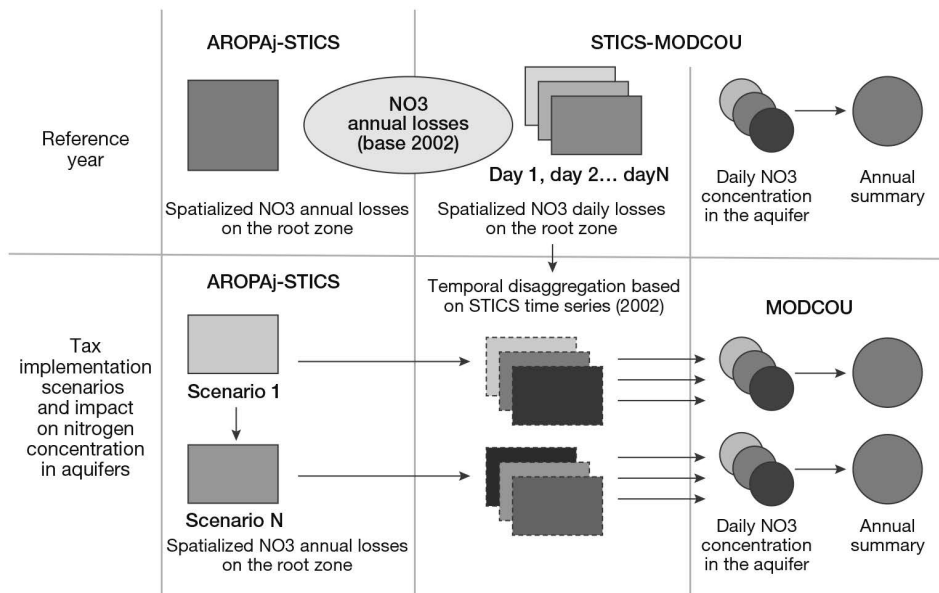


Figure 14.14. Diagram of the coupling of STICS and hydrologic (MODCOU) and economic (AROPAJ) models in the PIREN-Seine modelling platform (Beaudoin *et al.*, 2019).

– Dynamical upstream external link

This type of link is rarely used. One good example is the satellite data assimilation by STICS. Onboard remote sensing instruments provide high spatial resolution images of land cover and crop canopy. However, the raw data must be geolocalised and corrected for atmospheric effects using physical models. Multispectral pixel data can be used

to calculate vegetation indices and ultimately LAI using statistical relationships. The computed LAI can be forced into the model, or used to re-optimize unknown model inputs (e.g. field capacity). Such an approach has been implemented to estimate forage and annual crop production (Courault *et al.*, 2010; Jégo *et al.*, 2012a) and optimize soil parameters (Ferrant *et al.*, 2014; Varella *et al.*, 2010a).

– *Dynamical downstream external link*

This type of link was more frequent in published studies involving STICS. The exchange between models concerns their respective outputs and retroaction cannot be implemented. A good example is the STICS-MACRO chain, which aims to simulate pesticide transfer within the soil profile (Figure 14.15). It combines the strengths of each model: STICS can account for the effects of varying agricultural practices (fertilisation, waste, mulch or crop residue management) on soil organic C/N changes; MACRO integrates the roles of microporosity and macroporosity on the retention and transfer of pesticide molecules. The coupling implements a sequential transfer of data on the soil parameters of both models. STICS outputs (potential evapotranspiration, LAI, height, root depth) are then transferred to MACRO; some MACRO parameters are re-estimated. A MACRO run will eventually predict pesticide behaviour.

Another example of the downstream external link is the chaining of STICS with ecological and hydrological models, within a platform including a GIS. Here, the pixels cannot spatially interact and the outputs of the agronomical model become inputs for the hydrological one. For example, in the PIREN-Seine project, the platform simulates crop production and soil C and N balances in cropping systems as well as their long-term impacts on water resources (§ 14.3.2). Another example is the ORCHIDEE land surface model, which predicts water and C flows at the European scale (Wu *et al.*, 2016).

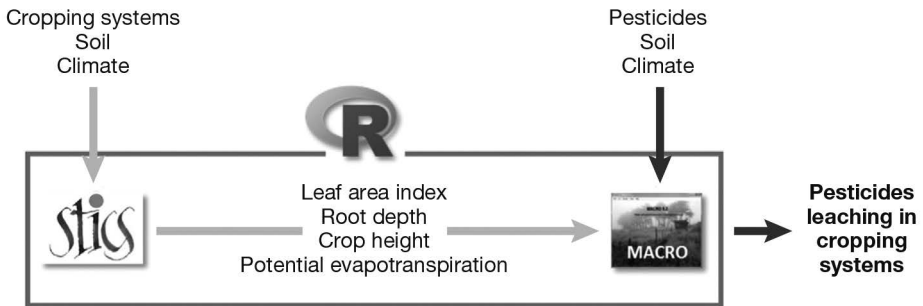


Figure 14.15. Sequential use of the STICS crop model and the MACRO pesticide fate model to simulate pesticide leaching in cropping systems (from Lammoglia *et al.*, 2017).

– *Internal link*

This type of link allows the retroactions between models by coupling the daily loops of the models. Examples of stand-alone STICS coupling cover a large range of topics: – MILA-STICS simulates in 1D, the development and impact of pathogenic fungi on LAI and crop growth. The crop-disease model MILA-STICS was able to simulate a range of airborne fungal diseases (Figure 14.16).

The climate change is an emblematic stake for this couple (§ 14.2.5.3).

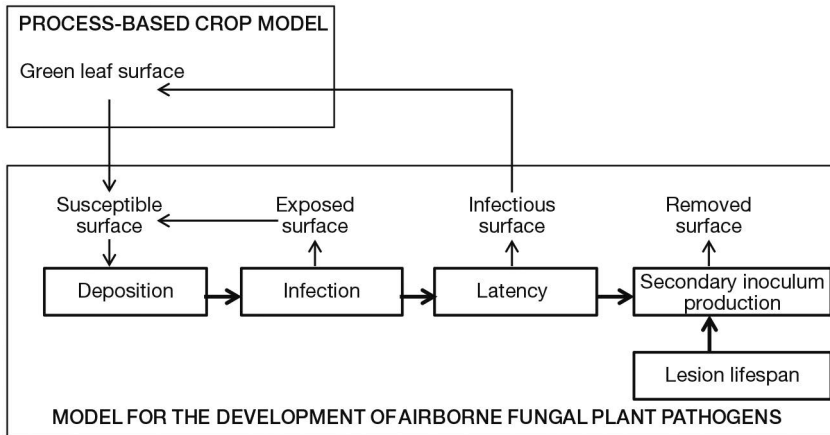


Figure 14.16. Calculation of the susceptible, exposed, infectious and removed surface areas in the conceptual design of and feedback to a process-based crop model (MILA-STICS coupling). The available surface is the green leaf surface minus the exposed surface. The infectious surface is deducted from the green surface (from Caubel *et al.*, 2012).

- PE-STICS simulates, in 1D, the retention and transfer of pesticides and nitrate within the daily loop (Queyrel *et al.*, 2016).
- FLORSYS predicts crop - weed interactions in 3D; seed stock, seed germination and seed stock growth are simulated at plant level, while STICS predicts soil temperature, moisture, nitrate availability and organic matter dynamic in 1D (Moreau *et al.*, 2021).
- Hi-sAFe simulates agroforestry system behaviour in 3D by coupling STICS with a tree model (sAFe-Tree) on a daily time step (Dupraz *et al.*, 2019).

Encapsulating STICS in the RECORD platform results in a turnkey simulator for cropping system functioning and management at varying spatiotemporal scales (Bergez *et al.*, 2013). Encapsulation relies on the modularity of the STICS code within its daily loop (§ 16). It addresses the following issues: (1) water resource management at farm and regional scales with MouSTICS (Bergez *et al.*, 2012); (2) ecosystem service assessment with the EFESE project (Therond *et al.*, 2017); (3) livestock farm studies with MELODIE (Moreau *et al.*, 2013); and (4) water and N cycles within the agrohrosphere at landscape scale, with the TNT model, which allows users to deal with interactions between pixels (Beaujouan *et al.*, 2002; Ferrant *et al.*, 2014).

– Combining multiple links

The case study of the Adaptation of Irrigated Agriculture to Climate Change (AICHA) and Accompanying The adaption of irrigated agriculture to climate CHAnge (ATCHA) projects, in India, is an emblematic example where multiple links were combined. The ‘groundwater revolution’ started three decades ago and allowed millions of small-holder farmers to access irrigation with individually owned bore wells. It increased crop production but resulted in a well-identified ‘groundwater crisis’ with tremendous impact on water resources and ecosystems. In such a highly dynamic system, a multi-link approach was necessary to account for the critical interactions and feedback between the variations of groundwater availability and crop prices, and farmer decisions for crop choice and irrigation scheduling. The STICS model is a component

of the integrated biophysical and economic model NAMASTE (Robert *et al.*, 2018) created to design and assess scenarios of farming system adaptation, with a participatory approach involving farmers and policymakers, in a network of experimental watersheds in southern India (Figure 14.17).

Using this soil-crop model to simulate the impact of management scenarios in the Indian context is a scientific and technical challenge due to the high diversity of crop species found in Indian farming systems. In addition to several intensively farmed cash crops (e.g. maize, sunflower) for which default calibration is available in STICS, there are many other crops (e.g. millet, pulses, spices such as turmeric) that need to be calibrated by drawing on a reliable database (see the chapter on ‘model extension’). Another challenge consists in checking the reliability of the water-C-N balance predictions in the tropical context of South India, characterised by the monsoon regime, and the impact of soil salinisation, which occurs in some places due to potash fertilisation (Buvaneshwari *et al.*, 2020). Accordingly, the salinity impact on crop growth was quantified (§ 14.5.1). STICS coupling with a groundwater model showed that groundwater irrigation plays an important role in the accumulation of saline solute in soil and groundwater, and threatens the sustainability of farming systems in the long term (Buvaneshwari *et al.*, 2018).

STICS was also used to estimate soil properties by model inversion using surface soil moisture and LAI data assimilation (Sreelash *et al.*, 2017, 2012). Finally, STICS application at field scale relies on the classic coupling with a GIS and the data assimilation from remote sensing to secure its predictions.

►► 14.5 Typology of STICS uses

STICS specifications associated with the STICS community dynamic allowed a large range of uses. With regard to issues on biophysical system behavior, crop models have two main types of uses: diagnosing an agronomic situation or a new part of the model, and creating a prognosis to estimate hard-to-measure variables. For issues dealing with agro-ecosystem management as well as the scientific protocol design of science building, diagnosis and prognosis are frequently combined in more complex approaches. Finally, this chapter briefly addresses model calibration and testing, which also contribute to the heuristic approaches (§ 16).

14.5.1 Diagnosis

Agronomic diagnosis mobilizes scientific knowledge to explain observations. For yield gap analysis, simulated potential yield (P) or water limited or only N limited yield, are compared to measured actual yield, namely farmer yield (F). STICS was used for yield gap analysis in tropical regions, at the scale of France (Brisson *et al.*, 2010) or at global scale (Kvakić *et al.*, 2018). STICS was also used to estimate yield losses due to water and N limitations in complex contexts, as following. In tropical smallholder farms, STICS was used to quantitatively determine the respective share of suboptimal stand density, water stress and nitrogen stress in deviations of actual yields to potential yield across a region, and helped determine the role of other biotic and abiotic stresses (Affholder *et al.*, 2003 and Figure 14.18). In temperate organic systems, STICS was used to predict the potential yield and the water and N stresses in the actual situation; so it was assumed the

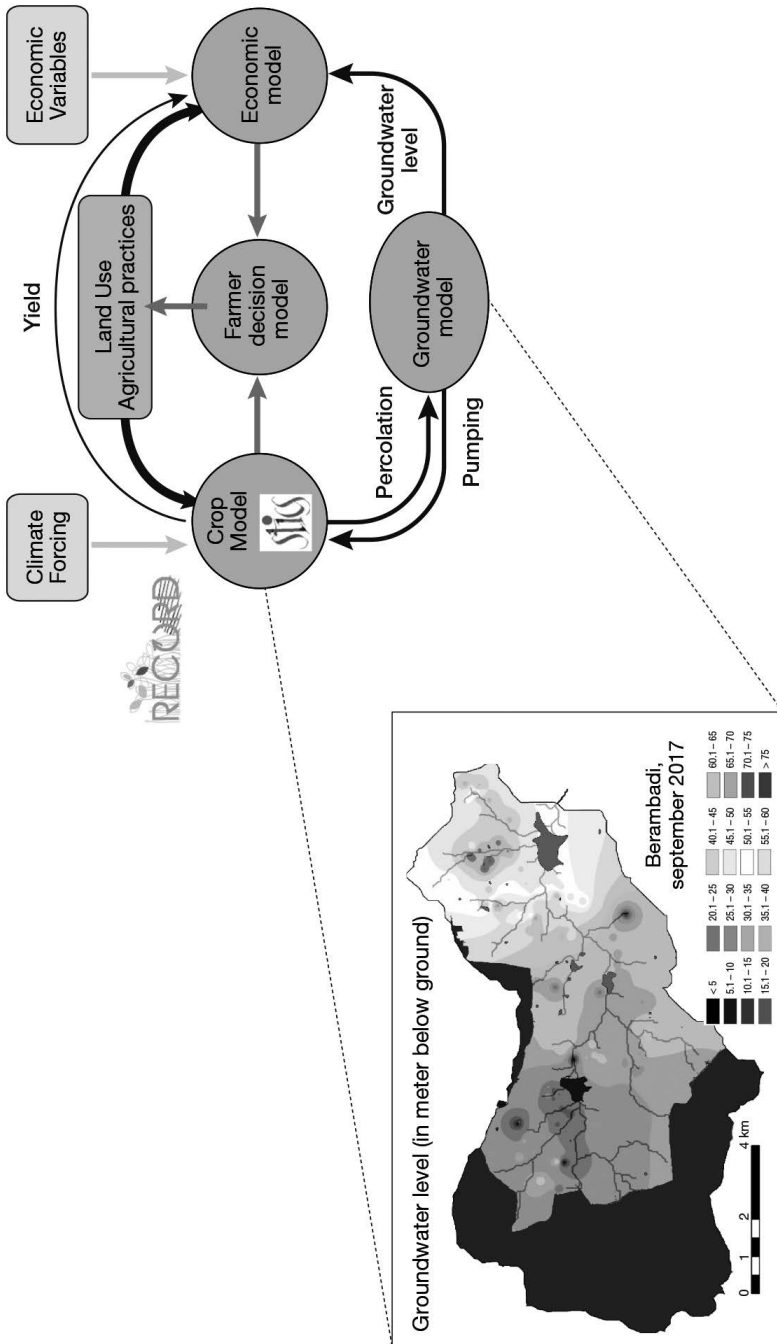


Figure 14.17. Diagram of the multidisciplinary approach in the ATCHA project (2016).

N availability to the crop was well predicted when the actual crop yield was affected by both abiotic and biotic stresses (Rakotovololona, 2018). In the aforementioned ATCHA project, the impact of groundwater salinisation on turmeric yield was quantified in a watershed in Karnataka using yield gap analysis (Figure 14.19).

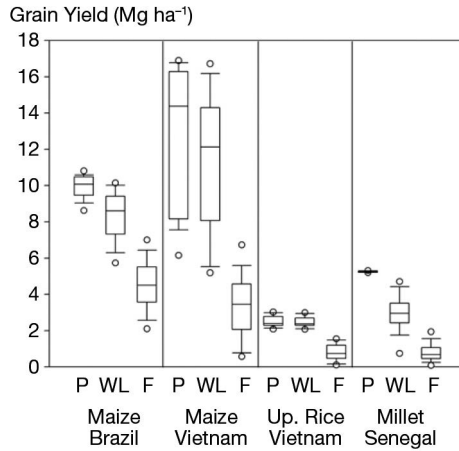


Figure 14.18. Boxplots of potential (P), water-limited (WL) and farmers' (F) grain yield. "Up. Rice": upland rice. Predictions were made using an ad-hoc model for potential yield estimation derived from STICS and SARRA models (Affholder *et al.*, 2013).

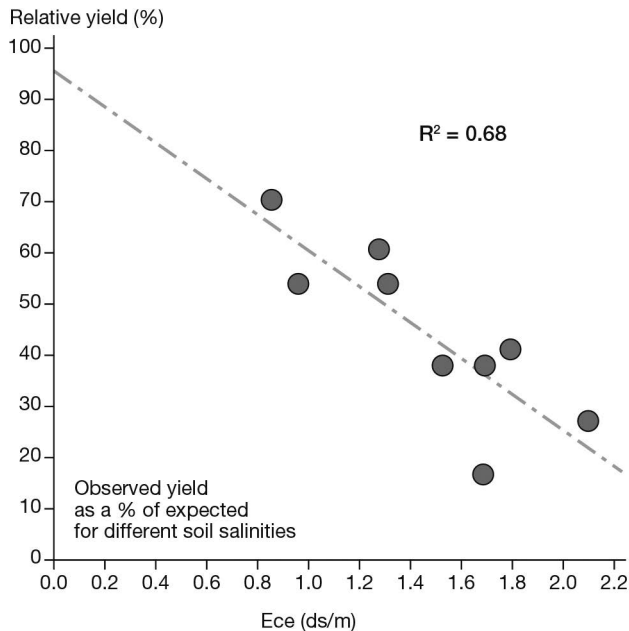


Figure 14.19. Effect of groundwater salinity on turmeric production. X axis = electrical conductivity (Ece, deciSiemens per metre) of irrigated water; y axis = observed yield to potential yield simulated by STICS ratio (Kizza *et al.*, 2016).

14.5.2 Prognosis

In prognosis, the model predicts the behaviour of a given system. Context and variables of interest can differ and include: i) crop yield response to sowing date, e.g. durum wheat, in water scarcity contexts (Debaeke and Aboudrare, 2004), ii) nitrogen leaching with current practices (Schnebelen *et al.*, 2004), iii) nitrate in drained water according to varying catch crops. This third situation provides the following emblematic example of STICS relevance for prognosis.

14.5.2.1 Stochastic prognosis of catch crop effectiveness.

The model was used in the INRA expertise report on the effectiveness of cover crops in reducing nitrate pollution establishment (Justes *et al.*, 2017). After calibration of cover crop species, a multi-site frequency study of the outputs of the numerical experiment focused on nitrate leaching and nitrogen uptake of the subsequent crop in response to different fallow period management methods (Figure 14.20). With meta-modelling, indicators for optimal management (reducing nitrate losses and maximising the 'green manure' effect) were defined in France (J. Constantin *et al.*, 2015a, 2015b) and, in Switzerland (Buchi *et al.*, 2016).

Assimilation of remote sensing data to increase model reliability at regional scale can be used for prognosis, such as to predict grassland or maize yields (Courault *et al.*, 2010; Jégo *et al.*, 2012a).

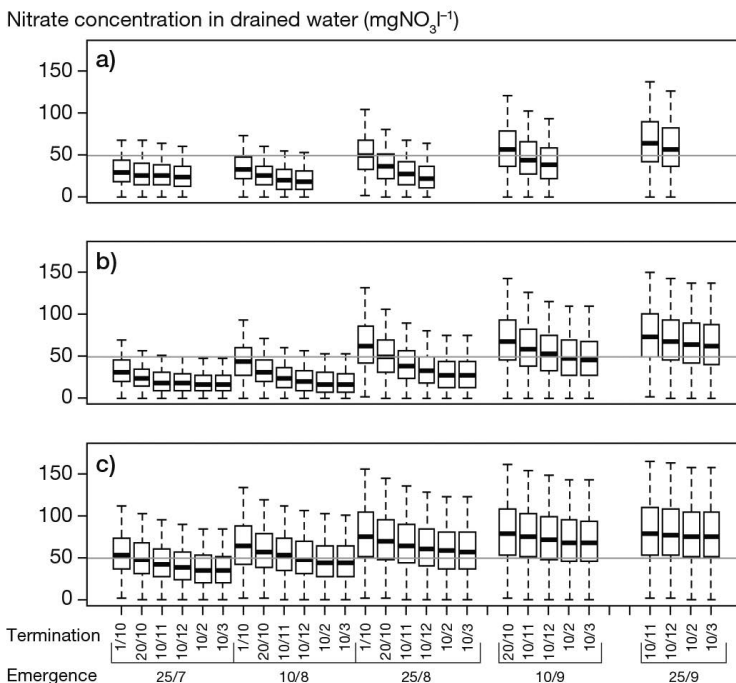


Figure 14.20. Simulated response of nitrate concentration in drained water to catch crop management versus emergence and termination dates and species: a) mustard, b) ryegrass, c) vetch. The line is the EU standard of water drinkability (Justes *et al.*, 2012).

14.5.2.2 Regional yield of grasslands

There were two main types of yield estimations: i) the present yield (in real time), and ii) the future achievable yield, taking into account the possible future climate. In order to estimate inter-annual variations in grassland production in approximately 200 regions in France, the input data are entered at various regional scales (Gateau *et al.*, 2006): information for climate in each forage area and several items for soil and management practices. The model was parameterised for each type of grassland (permanent, less than six years or pure legumes) and was interfaced with specially built national databases characterising climate, soil and technical conditions for the areas of France where sufficient surfaces of grasslands exist.

STICS was then used to estimate regional inter-annual yield variations. STICS contributed to the monitoring of the forage production response to water stress in mainland France (ISOP, Ruget *et al.*, 2006). This monitoring system has been used since 2000 by the French Ministry of Agriculture to financially compensate farmers in the event of production losses due to drought. A yield indicator for permanent grasslands – ‘ISOP’ – is regularly provided. It equals, at a given date, the ratio between the cumulative growth at this date since the beginning of the year and the cumulative growth at the same date calculated over the reference period 1989–2018 (Figure 14.21).

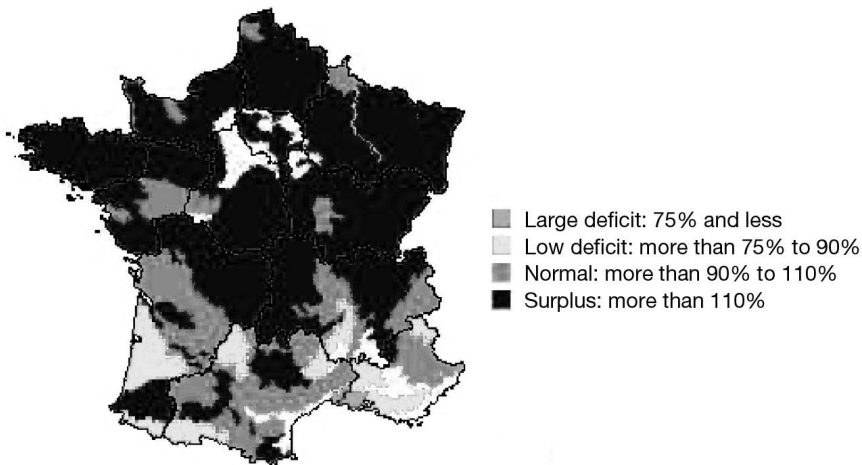


Figure 14.21. Permanent grassland yield indicator, by forage region, as of April 20, 2021. (Agreste Infos rapides, 2021)

Several other projects have explored the impacts of climate change on grassland production. Knowing the response of forage production to pedoclimatic variability is crucial for the feed security of livestock farms and for the dairy and meat industries. Studying the effect of global climate change relied on an accurate representation of the changed environmental conditions with regard to primary production and soil water consumption (Gonzalez-Camacho *et al.*, 2008; Ruget *et al.*, 2012). The model thus helped farmers adapt their livestock feeding strategies (Moreau *et al.*, 2012), which illustrates the following section: the model can be used to support decision making.

14.5.3 Decision-making support

– Example of public policy

Addressing global challenges requires model coupling within a modelling platform (§ 14.4.2). One particular platform can be highlighted here: The AROPAj platform linked a STICS meta-model with an economical model to study the response of farmer income and N leaching to scenarios of fertiliser tax policy (Jayet and Petsakos, 2013). Besides, the SVAT-ORCHIDEE platform was used to study the influence of cropland on the European carbon and water budgets (Gervois *et al.*, 2004). The TNT platform was used to evaluate scenarios of land occupation and management with regard to the risk of green tide (Moreau *et al.*, 2012).

– Examples of decision tools for farmers

Decision tools can support either tactical or strategical decision-making. Some of them have already been described in § 14.4.2 since they require coupling in a user-friendly interface. Tactical tools need STICS to be coupled with decision rules. Such tools have addressed either crop irrigation (e.g. MOUSTICS tool, Bergez *et al.*, 2012) or N fertilization for precision farming (Baret *et al.*, 2007; Mesbah *et al.*, 2017). Strategical decision-making tools require coupling with a farm-decision model. STICS has been used to prototype innovative cropping systems, e.g. in the MICMAC-Design project (Bergez *et al.*, 2014).

The EpiSTICS model combines a biophysical and a decisional model designed to generate irrigation and N fertilisation schedules in apple orchards (Nesme *et al.*, 2006). Irrigation and fertilisation are key management activities for fruit tree cropping systems. The simulation of crop water and N requirements was adapted for orchards. First, EpiSTICS simulated state variables (soil nitrate, water content) were positively compared with observations. Second, model-generated schedules were qualitatively evaluated based on interviews with farmers about their own practices. The model prediction generally aligned with actual farmer practices, but it showed a sharp difference at the beginning of the irrigation period (Figure 14.22). Model simulation would improve by taking into account irrigation rounds and the constraints imposed by specific practices to control scab and codling moth.

In a tropical context, STICS was used to determine optimal sowing dates, accounting for both agronomic and environmental indicators (Silva *et al.*, 2019). The case study was maize cultivation in the Brazilian Cerrado, in two locations with contrasting climates: Goiânia (1600 mm annual rain) and Barreiras (1160 mm). Three management options were evaluated – conventional tillage, no-tillage, and no-tillage with millet residue mulch – on shallow (**obstarac**_s = 90 cm) and deep (**obstarac**_s = 180 cm) soils. Optimal sowing windows were identified based on maximum yield, minimum yield variability, run-off and drainage. Cultivar-specific parameters for tropical maize and parameters for millet residue mulch were calibrated based on two field experiments in the study area. A series of historical weather data was used to run scenarios with the calibrated model. The simulation highlighted that no-tillage systems i) increased grain yield compared with conventional tillage systems, ii) decreased water run-off and the associated erosion risk, but iii) increased water drainage below the root zone and thus the associated risk of nutrient leaching (Figure 14.23).

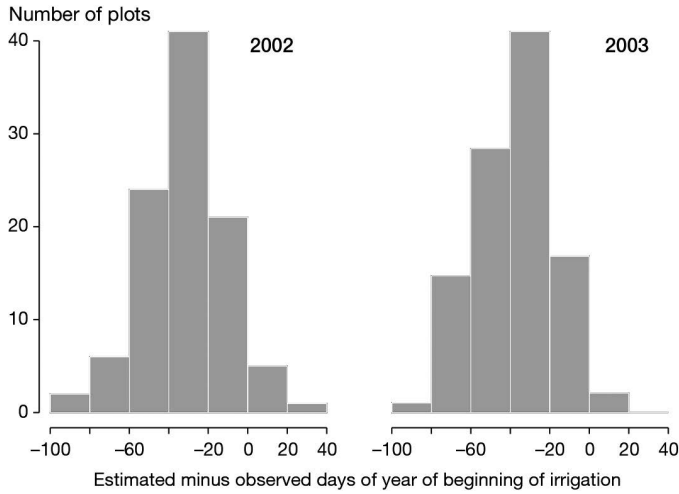


Figure 14.22. Difference in simulated minus observed days of year of beginning of irrigation in 2002 and 2003 (Nesme *et al.*, 2006).

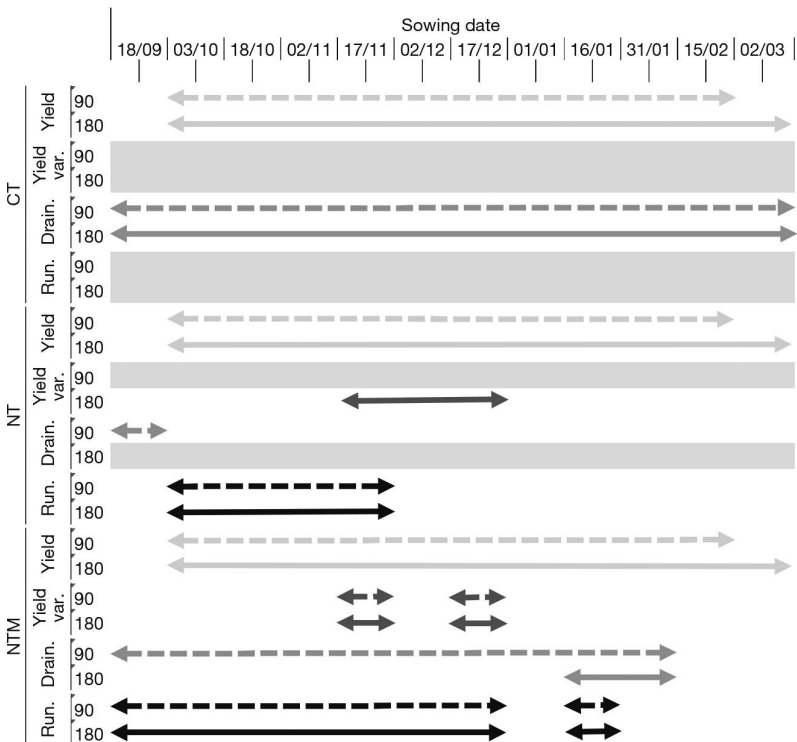


Figure 14.23. Optimal sowing windows calculated to comply with criteria on yield (Yield), yield variability (Yield var.), drainage (Drain.) and runoff (Run.) for the conventional tillage (CT), no-tillage (NT), no-tillage with millet residue mulch (NTM) cropping systems, for two maximum rooting depths (90 and 180 cm) at the Goiânia experimental site. Grey bars indicate that no sowing dates matched the criteria (from Silva *et al.*, 2019).

Maximising yield while minimising yield variability, water run-off and drainage could only be achieved for a narrow optimal sowing window. The approach developed in this study can form the basis of a comprehensive decision support system that accounts for soil characteristics, mulch effects, and the occurrence of dry spells during the rainy season.

14.5.4 Testing scientific hypotheses

STICS has also been used to test hypotheses on agro-ecological systems functioning. Three examples of different purposes are provided in this section: i) to simulate energy, water and nitrogen shares between intercrops, ii) to test the effect of climate change on microbial activity or iii) to test the role of perennial nitrogen reserves on the regrowth of multi-year species.

The first example, intercropping, illustrates how to represent a complex system in several functional units. Since the STICS model is 1D, adapting it to intercropping involves a simplified definition of the agronomic system (§ 2.2.3). This simplified representation determines the way the light intercepted by each crop according to its respective spatial structure throughout the day is calculated (Brisson *et al.*, 2004). Each day is divided into 24 parts to integrate the variation of the sun azimuth (§ 9.2.1.2.1). The part of the radiation intercepted by the dominant crop and the part transmitted to both components of the understorey crop are then simulated according to the geometry of each crop (§ 9.2.2). This conceptual framework was applied to spring pea-barley intercropping (Corre-Hellou *et al.*, 2009). It permitted a realistic prediction of the land equivalent ratio (LER) for aerial dry matter and N accumulation of each intercrop and their association (Figure 14.24).

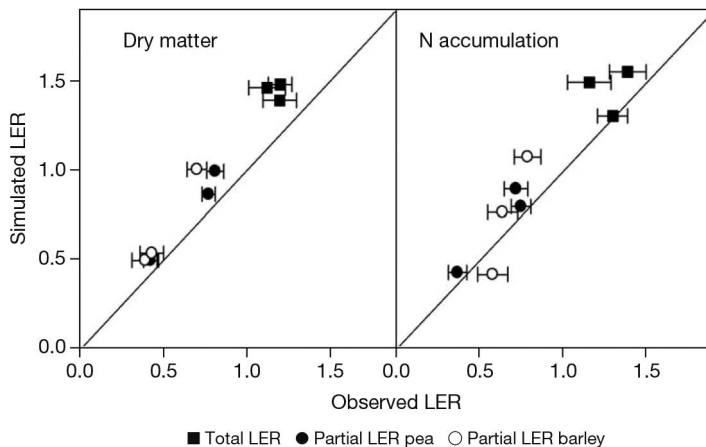


Figure 14.24. Comparison of simulated and observed total and partial land equivalent ratio (LER) values for dry matter and N accumulation, in pea-barley intercropping. Average values obtained in intercrops grown in 2002 and 2003 with N or without N fertilization. Error bars represent the standard error of observed values (from Corre-Hellou *et al.*, 2009).

A second example deals with the controversial effects of climate deregulation on SOM behaviour in the tropics (Sierra *et al.*, 2010). The impact of climate change on the

underlying mechanisms controlling SOM dynamics was analysed in ferralitic soil under two contrasting tropical crops (maize as C4 plant and banana as C3 plant) with the tropical humid conditions of Guadeloupe (French Antilles). The effect of microbial thermal adaptation on C mineralisation was modelled at crop system scale and was introduced in STICS. This adaptation was based on a reported theory for thermal acclimation of plant and soil respiration. The climatic generator (ARPEGE model with IPCC emission scenario A1B) predicted a 3.4°C increase in air temperature and 1100 mm yr⁻¹ for rainfall as a response to a 375 ppm increase in atmospheric carbon dioxide concentration in 2090–2099 compared with 1950–1959. STICS simulations indicated that crops affected SOM response to climate change by controlling the change in C input, soil temperature and soil moisture. SOM content varied little until 2020, and then decreased faster for maize than for banana. This decrease was weakened under the hypothesis of thermal adaptation, and this effect was greater for maize than for banana (Figure 14.25). The greater SOM loss in maize was mainly due to the negative effect of warming on maize growth that decreased C input from residues. Climate change had a small effect on banana growth, and SOM loss was linked to the climate change impact on C mineralisation. Thermal adaptation reduced the initial increase in mineralisation, but its effect was lower on the final decrease, which was mainly controlled by substrate limitation. No stabilisation in SOM status was attained at the end of the analysed period because C mineralisation was always greater than C input. Model predictions indicated that microbial thermal adaptation modifies the temporal pattern of SOM dynamics, without changing its trend.

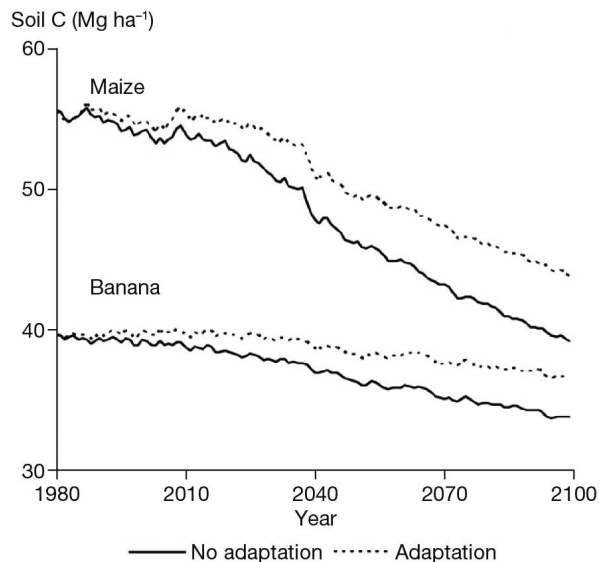


Figure 14.25. Impact of thermal adaptation of soil microorganisms and crop system on the dynamics of organic matter in a tropical soil under a climate change scenario (Sierra *et al.*, 2010).

For perennial crop behaviour, the hypothesis was double: i) the remobilisation of the perennial pool of N reserves represents the main N supply of the growing canopy, when senescence of the canopy permitted this pool to refill, and ii) the crop N status

is the main driver of canopy growth as opposed to crop ontology; thus, the nitrogen nutrition index (NNI) allows to mimic its behaviour, with a unique corpus of formalisms and parameters from sowing to destruction. This hypothesis was positively tested with the bioenergy crop *Miscanthus G.* and then for the perennial leguminous alfalfa (Strullu *et al.*, 2020, 2014). In unfertilised treatment of *Miscanthus G.*, the perennial reserve can reach 200 kg N ha^{-1} . Periodic depletion affects the perennial biomass pool, when aerial biomass is accumulating. The model was calibrated against treatment with late harvest and tested against the ones with early harvest. The periodic pattern was satisfactorily simulated by the model during four growing seasons (Figure 14.26).

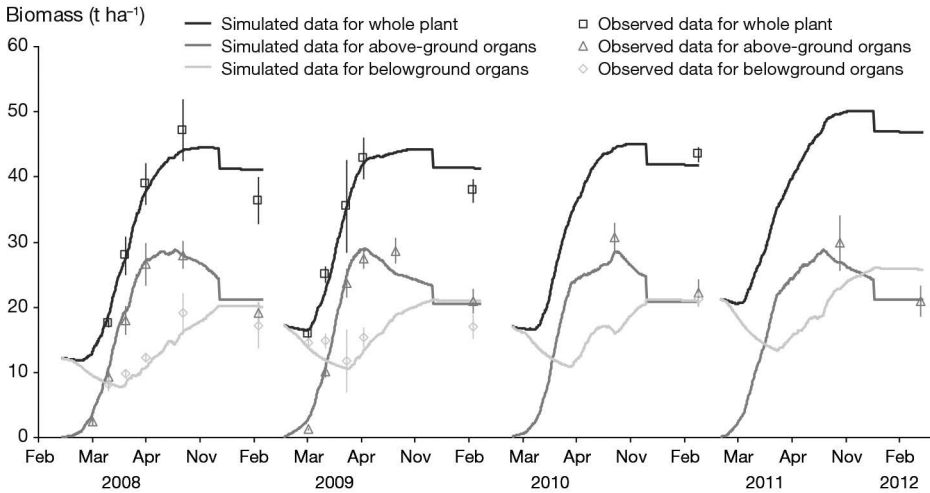


Figure 14.26. Simulation and observation of biomass of *Miscanthus G.*, of unfertilised treatment with early harvest (November) after sowing in spring 2006. Evaluation of the STICS predictions against an independent dataset (Strullu *et al.*, 2014).

14.5.5 Dialogue between stakeholders or disciplines

14.5.5.1 Cognitive role

The collective construction of STICS makes it a good tool for training and synthesising interdisciplinary knowledge at both national and international levels. The numerous parameters in STICS are frequently criticised. However, we would counter this criticism with three arguments: 1) no parameter is written directly in the code and they are all accessible, 2) the model genericity increases the number of options and their associated parameters, and 3) most of the parameters are invariant (general), while only a few must be adjusted by the user (local parameters; § 15). These features can be both scientific assets and operational limitations. The STICS project team is continuing its efforts to optimise the number of parameters.

Predictive performance depends on the quality of local parameter calibration, which must be done by the user. Misunderstandings can arise between disciplinary researchers and agronomists about the meaning of formalisms or parameters because of the functional design of STICS (§ 2). Discussions on the concepts and basis of the

model specifications are encouraged. The STICS project team has been involved in training sessions on modelling and the use of STICS, in order to promote the ‘suitable and reasonable’ use of the model (§ 1 and § 15). Continued discussions about STICS conceptual bases are vital in order to renew the model.

Evaluating an extension of the scope of STICS requires specific efforts with a rigorous collection of input data, observations and metadata. Such efforts are made through a scientific project if the project relates to processes, or as an engineering project (§ 16). A comprehensive generic test was completed based on a large dataset covering 15 single crops and a wide range of agro-pedoclimatic conditions in France (Figure 14.27). STICS was also tested at the crop rotation scale (Beaudoin *et al.*, 2008; Constantin *et al.*, 2012; Jégo *et al.*, 2012b; Plaza-Bonilla *et al.*, 2015), including a comparison with other models (Yin *et al.*, 2020).

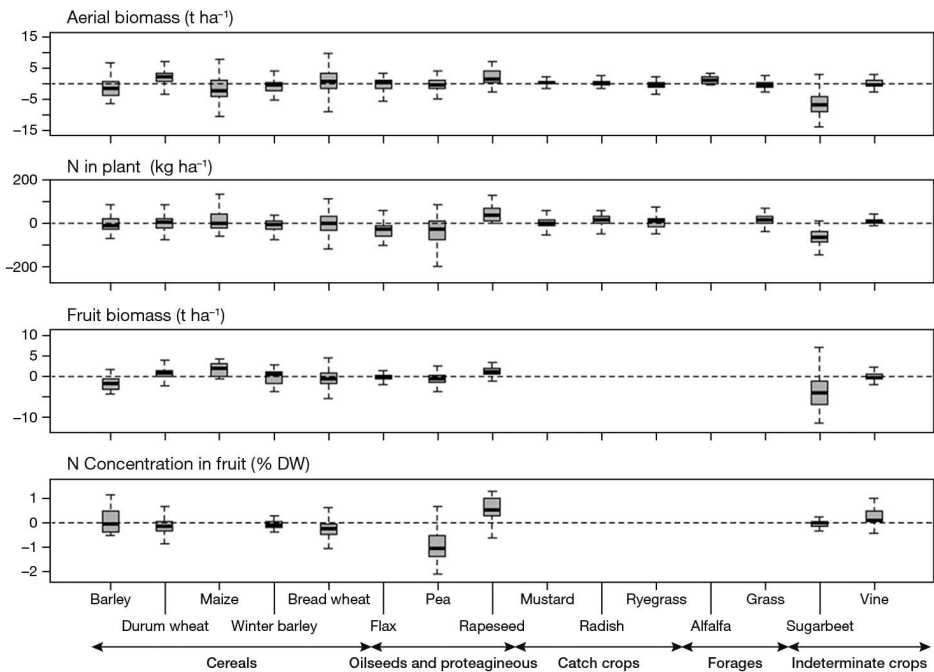


Figure 14.27. Distribution of STICS v8.2.2 prediction discrepancies in four agro-environmental variables for 15 crops of interest, for 1809 plot-year simulation units in France (Coucheny *et al.*, 2015).

14.5.5.2 Contribution to education

STICS has been used in a total of 71 PhD theses until 2020 and numerous master’s internships. Around 20 to 30 people per year attend STICS training courses in France. Overseas training courses were held in 2008 in Argentina, 2013 in Sri Lanka, 2014 in India, and 2017 in India and China. A special STICS open house day was held at the European Society of Agronomy (ESA) Conference in Scotland (2016) and at a joint congress in Montpellier (2020). Recently, STICS courses were produced as webinars.

14.5.5.3 Contribution to the dialogue between partners

STICS has encouraged a dialogue between agricultural development actors (e.g. technical institutes, chambers of agriculture) and scientists. It also contributes to participatory approaches involving farmers, such as when working to identify opportunities for better N management, whether in conventional systems (Bergez *et al.*, 2014) or organic systems (Rakotovololona, 2018).

The aforementioned ANR CLIMATOR (Figure 14.7), PIREN-Seine (Figure 14.12), ATCHA (Figure 14.17) and ISOP (Figure 14.21) projects have interested large audiences about studying behavior and impacts of cropping system.

STICS contributes to international inter-comparison model exercises: in Europe MACSUR (C-yield and C-N balance), and at the global scale with AgMIP (yield) or CN-MIP (N₂O).

►► 14.6 Perspectives for model capacity extension toward agroecology

14.6.1 Context and background

STICS can be used either as a soil-crop model at the crop cycle scale or as a cropping system model at the crop rotation scale (Keating and Thorburn, 2018). Users can assess and/or optimise crop management strategies over the short to long terms based on agro-environmental criteria.

However, the farm scale is insufficiently addressed (3% of the studies in our literature review), considering its important role in driving the agroecological transition. It falls between the field and market levels, and poses the most challenging scale problem when it comes to integrated assessment of agri-environmental systems (Ewert *et al.*, 2011). This challenge stresses on the needs of STICS coupling at farm scale to assess farm variables such as climatic risks or ecosystem services.

New needs related to global climate change mitigation and adaptation for food security emerged from our discussions with students who received STICS training in different countries.

14.6.2 Contribution to the development of agroecology

Agroecology is expected to enhance the efficiency and resilience of cropping systems to extreme climate events, support climate change attenuation and biodiversity enrichment, and therefore bolster food security. Agroecological practices rely on promoting both biological regulations and nutrient recycling. Possible levers include crop rotation diversification, intercropping, cover crops, low- or no-till farming, biological control of weeds and pests, and living mulch. Some agroecological systems, such as agroforestry and crop livestock systems, have also been identified as useful.

The actual ecosystem services of the implemented systems need to be evaluated and compared to conventional systems with regard to their agronomic, economic and environmental dimensions (De Notaris *et al.*, 2018; Mondelaers *et al.*, 2009). Modelling agro-ecological cropping systems requires knowledge engineering and/or model coupling.

STICS can help to quantify the ecosystem services linked to the water, C and N cycles in the soil-crop system. It allows users to test the agronomical and environmental interests of cover crops (Justes *et al.*, 2017; Plaza-Bonilla *et al.*, 2015; Tribouillois *et al.*, 2015) and to lesser extent, intercrops (Bedoussac *et al.*, 2017; Launay *et al.*, 2009; Shili-Touzi *et al.*, 2010) and grasslands (Graux *et al.*, 2020), which are pillars of agro-ecology. STICS has been mostly applied to conventional farming systems but is also now used to simulate low-input and organic farming systems (Figure 14.28). This application makes explicit assumptions about the role of biotic factors, and more specifically, that they are sufficiently controlled to allow STICS to accurately predict crop biomass and N balance. The first studies where STICS was adapted to arboriculture (Demestihis *et al.*, 2018), agroforestry (Dufour *et al.*, 2013; Dupraz *et al.*, 2019) and agrivoltaic systems (Dinesh and Pearce, 2016) were recently conducted, namely by coupling STICS to other models.

Modelling the phosphorus cycle is a new priority for the STICS project team in order to go beyond the current field of application and address questions linked to, for instance, the eutrophication of environments. Other investigations are in progress to i) improve the formalism of crop height kinetics and their consequences on inter-crop behaviour; ii) account for the roles of organic amendments on soil C-N storage (Levavasseur *et al.*, 2021) and iii) better represent the functioning perennial crops (Strullu *et al.*, 2020; Strullu *et al.*, 2015), especially the diversity of grassland types and management strategies (including animal returns at grazing) and grasslands' ability to store C in their soils (Graux *et al.*, 2020).

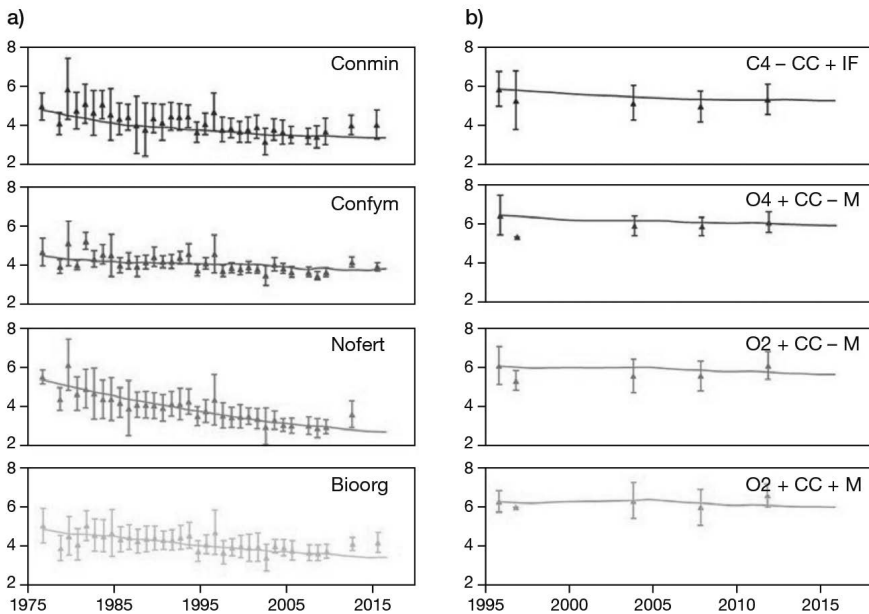


Figure 14.28. Simulation with the research version of STICS (tagged v10) of the evolution of organic N stocks (mg N ha^{-1}) in a) the long-term DOK (Thervil, Switzerland) and b) Organic (Foulum, Denmark) trials, comparing conventional (CONMIN, CONFYM, C4) and agri-biological systems (NOFERT, BIOORG, O2, O4); from Beaudoin *et al.* (2019) and Autret *et al.* (2020).

The desired agroecological transition has called into question the ability of research to build and implement solutions to tackle future climate variations and their abiotic and biotic consequences. Combined practices limiting both input use and the risks of additional stresses on crops have emerged as ways to address today's food security challenges.

14.6.3 Dealing with robustness and capacity extension, at national and international levels

A challenge for the governance of any crop model consists in combining research creativity to renew the conceptual framework with rigorous software engineering to maintain the code and testing model performance, which is a good illustration of the concept of organisational ambidexterity.

Ensuring the robustness of the standard STICS version while increasing the scope of the model and its international reputation as a crop/cropping simulation model remains the project team's priority challenges. This will be done by increasing the number of observed situations used to assess STICS (IDE-STICS dataset), which will be available via open access for users who want to calibrate or evaluate STICS or another model (§ 16).

Increasing the scope of STICS will be mainly based on discussions between the STICS project team members and the STICS community, taking into account possibilities of code management (versioning, modularisation) as explained in § 1.

Chapter 15

Tools for smart use of the standard STICS model version

*DOMINIQUE RIPOCHE-WACHTER, CHRISTINE LE BAS
AND NADINE BRISSON*

REVIEWED BY: NICOLAS BEAUDOIN AND FLORENT LEVAVASSEUR

This chapter aims to guide users in their use of the model. Building the STICS model has always been a twofold scientific and technical challenge, as explained in Beaudoin *et al.* (2019) (§ 2.2.1).

The STICS conceptual scheme is built like a set of modular bricks, which means that many processes are available in the standard version and new ones can be easily added in the research branches (§ 1.5.2). These processes can be activated or deactivated as options to reproduce actual farming practices or to describe soil physics, crop development and growth processes. The first three sections deal with these options: § 15.1 covers the driving options, § 15.2 the strategy options and § 15.3 the formalisms.

As we mentioned above, users must determine the relevant local parameters, but we do provide some tips in § 15.4 to help users fill in these values. In the last part of the chapter, we present a brief overview of the STICS software tools (the JavaStics interface and Stics R packages) and the STICS forum where users can get additional support and information.

» 15.1 Driving use options

Like most dynamic crop models, STICS is driven by the weather, but several options are available to calculate evapotranspiration. The different options are explained below. The final choice will depend on available climatic data as well as the formalisation used for the simulated crop or cropping system.

It is also possible to drive the model with observed values in order to force the model to use values for certain state variables measured in the field or via remote sensing (e.g. observed phenological stages or leaf area index - LAI).

15.1.1 Regular weather driving variables

STICS is driven by the weather on a daily time step. The minimal set of weather variables required to run the model comprises the minimum and maximum temperatures

(°C), global radiation ($\text{MJ m}^{-2} \text{d}^{-1}$) and rainfall (mm d^{-1}). There are four possible ways of estimating evapotranspiration ($\text{tetp}(t)$), for which additional variables are required. The least demanding option is to use the calculation developed by Priestley and Taylor (1972) (§ 15.1.1.2), followed by the calculation that imposes a pre-calculated value (§ 15.1.1.1). The other two options require two additional primary weather variables: wind speed (m s^{-1}) and vapour pressure (mbars). The first one is to use the Penman formula (§ 15.1.1.3) and the second does not rely on evapotranspiration but directly calculates water requirements at the plant level through a resistive approach (§ 15.1.1.4). For the three first options (Priestley-Taylor, pre-calculated value and Penman formula), users should note the close dependence between the reference evapotranspiration value and the \mathbf{kmax}_p value (because \mathbf{kmax}_p is experimentally calculated with a given reference evapotranspiration). A change of option should theoretically lead to a change in \mathbf{kmax}_p . In a comparative work cited by Smith *et al.* (1998), many reference evapotranspiration calculations were compared to lysimeter measurements from 11 locations. The Penman formula exhibits a 0.60-0.70 mm error regardless of the environment, while the Priestley-Taylor formula appears to perform far better in humid environments (0.68 mm) than in arid ones (1.89 mm).

15.1.1.1 Pre-calculated values of evapotranspiration

If potential evapotranspiration (PET) data are available, users can enter them as climatic data inputs. The STICS model has been parameterised for a Penman PET calculation. If the data are not available, then users must choose one of the three options described below to calculate evapotranspiration (in the climatic station file).

15.1.1.2 Calculation of Priestley-Taylor reference evapotranspiration

This calculation (Eq. (15.1)) is recommended if wind speed and humidity measurements are not available, but users should note that it does not take convective factors into account very well. The Priestley-Taylor calculation relies on the site-dependent coefficient $\mathbf{alphapt}_c$, whose value for many soil surface conditions is 1.26, an empirical calculation for the net radiation (rnet_PT) and a constant value of the latent heat of vaporisation (2.5 MJ kg^{-1}). The other variables have already been defined in § 9.4, see Eq. (9.25).

$$\text{tetp}(t) = \mathbf{alphapt}_c \cdot \frac{\text{deltat}(t)}{2.5(\text{deltat}(t)+\text{gamma})} \cdot \text{rnet_PT}(t)$$

with $\text{rnet_PT}(t) = 0.8 \cdot 0.72 \cdot \mathbf{trg}(t) - 0.9504$ (15.1)

15.1.1.3 Calculation of Penman evapotranspiration

The formula shown in Eq. (15.2) is from Penman (1948) and fully described in Brochet and Gerbier (1968).

$$\text{tetp}(t) = \frac{\text{deltat}(t)}{L(t)(\text{deltat}(t)+\text{gamma})} \cdot \text{rnet_PE}(t) + \frac{\text{gamma}}{\text{deltat}(t)+\text{gamma}} \cdot 0.26 \cdot (1 + 0.54 \cdot \text{tvent}(t)) \cdot \text{dsat}(t) \quad (15.2)$$

where rnet_PE is estimated by combining Eq. (9.13) and Eq. (9.17).

15.1.1.4 Use of Shuttleworth-Wallace

This option is based on the energy balance approach (§ 9.3.3). Users should note that:

- This option is mandatory to simulate intercropping systems.
- This option is mandatory to take the CO₂ effect (on stomatal resistance) into account.
- To use this option, the climatic file must contain the wind speed and the vapour pressure.

15.1.2 Driving the model with observed stages

The model can be driven using observed phenological stages. The dates of the different phenological stages are read from the technical file instead of being calculated by the model. The observed stages may be the vegetative stages *ilevs*, *iamfs*, and *ilaxs*, or the harvested organ stages *idrp_s*, *imats* and *irecs*. The phenological stages are described in § 3.2.2. The flowering stage *iflos* is always calculated by the model from a given **stflodrp_p** parameter which corresponds to the thermal duration between flowering and the onset of filling of the harvested organs **idrp_T**. There is no point in driving this flowering stage date *iflos* with observed data, because it does not trigger any calculation in the model. A combination of observed and calculated dates can be used, but the order of the stages is a priori fixed; should there be any disagreement between the calculated and observed dates for consecutive stages, the model will cease to run. The model can be driven also by the **ilan_T** and **isen_T** stages only if the LAI calculation is in the direct LAInet option.

15.1.3 Driving the model with the LAI

In this case, the model uses the observed LAI data as inputs (Ripoche *et al.*, 2001). This driving method can be very useful when developing the model or adapting a new crop. By imposing the LAI, the water and nitrogen requirement levels that are suitable to cope with stress are also imposed.

Because obtaining daily observed LAI data is usually difficult, a tool was developed in the JavaStics interface to interpolate LAI measurements using a statistical relationship representing the LAI time course (Eq. (15.3)). This function is fitted to calculate daily LAI from measurements. These LAI data will be the data prescribed to the model.

$$lai(t) = K_LAI \cdot \left(\frac{1}{1 + \exp(-B_LAI(ST_LAI(t) - TI_LAI))} - \exp(A_LAI \cdot (ST_LAI(t) - TF_LAI)) \right) \quad (15.3)$$

where *ST_LAI* is the growing degree-days since emergence, *K_LAI* is the maximal LAI produced (which is higher than the maximal measured LAI because of the effect of senescence), *TI_LAI* and *TF_LAI* are the growing degree-days for the point of inflexion of the growth curve and complete senescence, respectively, and *A_LAI* and *B_LAI* describe the shapes of the growth and senescence curves (Figure 15.1).

The first term of Eq. (15.3) stands for the green leaf appearance and the second for leaf senescence.

The example in Figure 15.2 shows the three LAI curves for a wheat crop. The daily prescribed LAI data were calculated by fitting the five parameters of Eq. (15.3) to the

LAI measurements. Next, the daily prescribed LAIs were used to drive the model, improving the simulation of above-ground biomass (masec) (Figure 15.3).

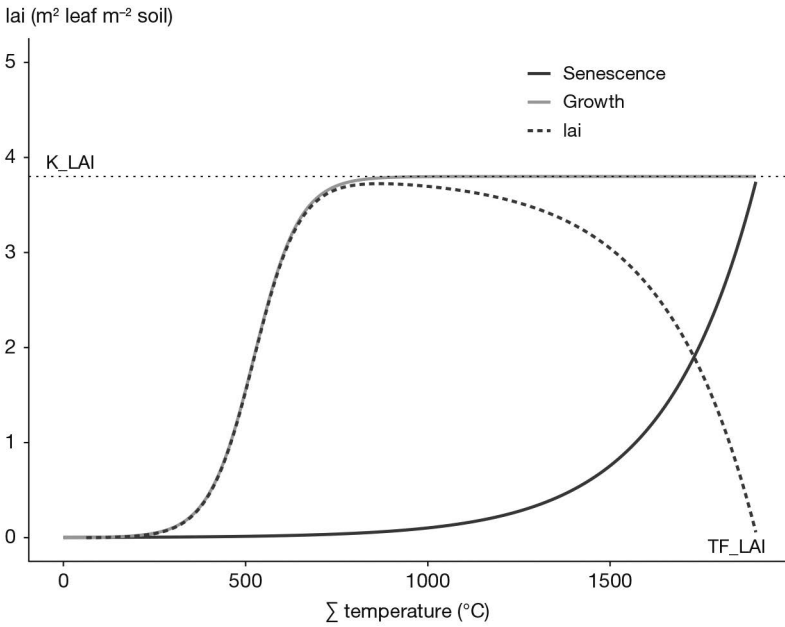


Figure 15.1. Empirical relationship representing the time course of LAI, and its two components, green leaf appearance and leaf senescence.

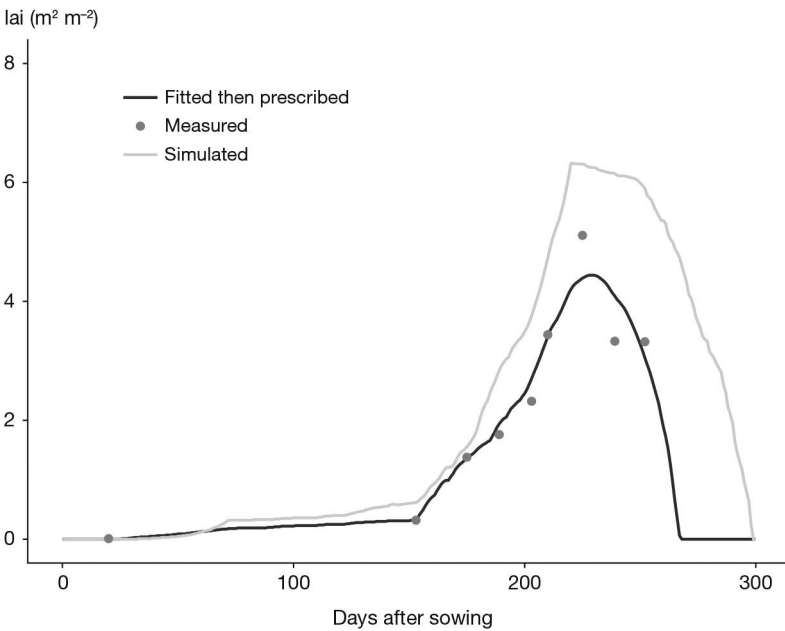


Figure 15.2. Example of simulated LAI versus fitted LAI using this method.

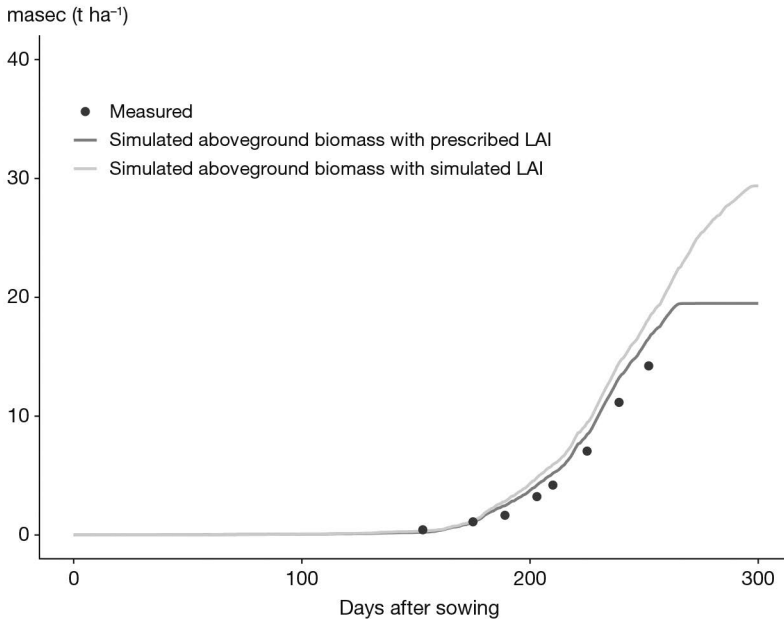


Figure 15.3. Improvement of the above ground biomass values (masec) when the model is run by prescribed LAI versus the free simulation of LAI.

►► 15.2 Strategy use options

The strategy options allow users to activate or deactivate water or nitrogen stresses, or to calculate the initial soil water or nitrogen content with depth.

15.2.1 Activating or deactivating water or nitrogen stress

Users should note that even when deactivated, the stress indices are calculated but may not be considered as ‘actual’ values.

STICS users can deactivate the water and nitrogen stress effects to simulate crop growth and development without water or nitrogen stress (Figure 15.4). With these options, users can predict ‘potential’ yield, for example, or organise these stresses into a hierarchy (by deactivating them separately). It is a tool of diagnosis of crop functioning, namely yield gap analysis (§ 14.5.1). Only water and nitrogen stress effects (Tables 4.1 and 4.2) may be deactivated, while trophic, temperature, waterlogging or stress effects linked to the soil structure remain activated.

However, even if water or nitrogen stress is deactivated and does not influence crop growth and development, the model still calculates these stresses and they are available to users in the model outputs. However, in this case, these stress index values may not be considered as ‘actual’ values because they depend on crop growth, which is calculated as a ‘potential’ value.

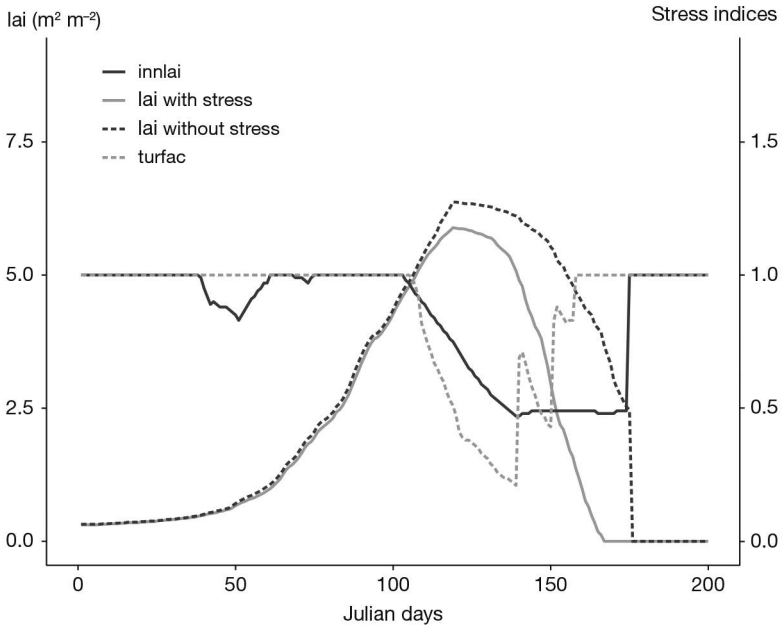


Figure 15.4. Comparison of stressed and unstressed LAI dynamics and the evolution of water and nitrogen stress indices over the cropping season (calculated when influencing crop growth).

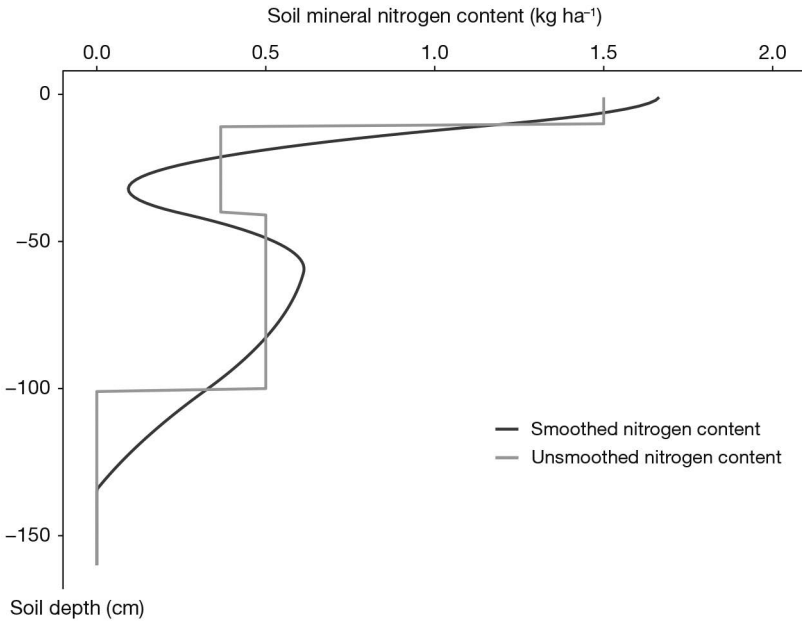


Figure 15.5. Nitrogen content partitioning with soil depth, with or without the smoothing option activated.

15.2.2 Smoothing of initial profiles

To avoid discontinuities of water and nitrogen content between soil layers, a smoothing option may be activated. This option smooths initial profiles of water and nitrogen content (Figure 15.5) using a spline function.

15.2.3 Long-term simulation pathways

STICS is easily able to run monoculture cropping systems as described in the chapter 14.1. There are two ways to do this:

- by chaining the same agricultural configuration (or unit of simulation - USM) over several years with successive weather files (§ 15.2.3.1).
- by taking into account crop rotations by chaining various USMs (§ 15.2.3.2).

With regard to initial conditions, in both cases, the model can either be reset (use the prescribed initial conditions) or run continuously (use the final conditions of the previous simulation as initial conditions of the current one) over the succeeding USM. For crop rotations, the ‘run continuously’ option is generally used, but in some cases, the reset option is chosen, especially when evaluating the predictive performance of a model on the processes at the interface between the USMs, or, for educational purposes, to understand the rotation effects.

We will now briefly explain the methodology for both the climatic succession and crop rotation options. More explanations are available in § 14.2.2, 14.2.3 and § 15.4.4.2.

15.2.3.1 Climatic successions

This option is available to run a climatic succession or climatic serial, such as to simulate the effect of climate change with climate scenarios as in the AgMIP¹ inter-comparison and improvement modelling exercises.

To do this, a single USM is created with the first climatic file as the first year (e.g. 2000) and the second climatic file as the last year of the serial (e.g. 2100, if the model is run with global change climatic scenarios from 2000 to 2100). The crop management is the same for all the climatic years, the climate is the only variant factor. Users can choose to reinitialise the water and nitrogen soil conditions or to simulate a continuous balance (‘climatic series’, `codeinitprecG` = ‘succession’ or ‘reset’).

15.2.3.2 Crop rotations

In this case, several USMs (one crop cycle, with a maximum of one or two calendar years) are chained in a succession of crops, climates and cultural practices.

The time scale in STICS is based on the concept of Julian days (i.e. 1 January = day 1, ..., 31 December = day 365), and by default, the time scale functions over two successive years. From that point, the time is cumulative for the second year (i.e. 366 to 730 days) (Figure 15.6).

1. <https://agmip.org/>

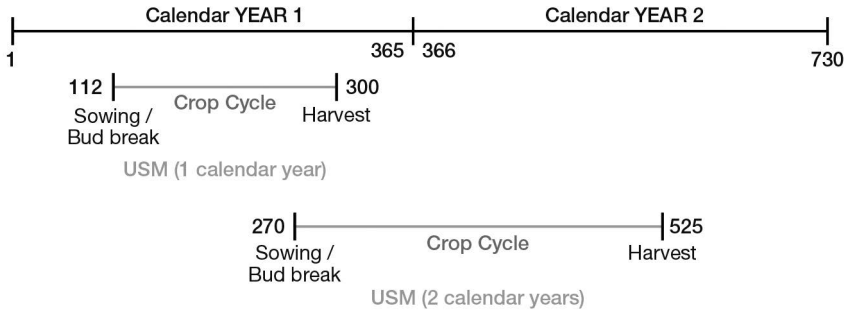


Figure 15.6. Time scale for a single USM (over one or two calendar years).

The beginning time scale could start or end outside the crop period (Figure 15.7).

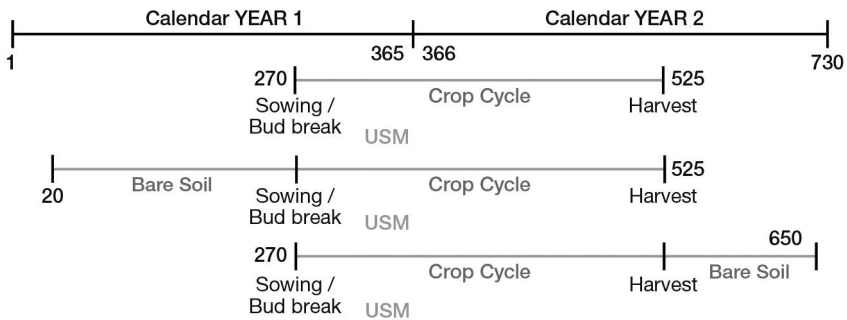


Figure 15.7. Three examples of time scale for a single USM (with or without a bare soil period).

To run over two years (two successive crops), a second USM must be built, as shown in Figure 15.8.

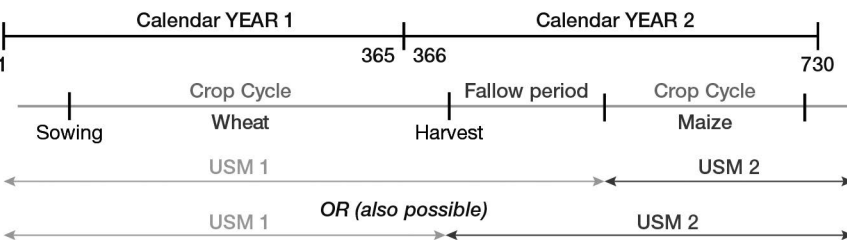


Figure 15.8. Time scale for a crop succession.

For an example of a long-term rotation, see § 14.2.1.

15.2.4 Case of intercropping

As § 2.2.3 explains, the genericity of the STICS model conceptual scheme means users can simulate an intercropping system with two crops on the same field and at the same time. For this situation, the USM is defined as shown in the Figure 15.9. Users choose the plant they consider dominant at the start of the crop cycle (main crop), knowing

that the model handles the inversion of dominance if the height of the associated crop exceeds that of the main crop. The harvest can take place on the same date (maturity of the earliest) or at two different dates (maturity of both) (Table 15.9). The system is described briefly in the § 14.1.3 and a use case is given in § 14.5.4.

For this kind of simulated system, the Shuttleworth-Wallace PET option based on the energy balance approach is mandatory (§ 9.3.3).

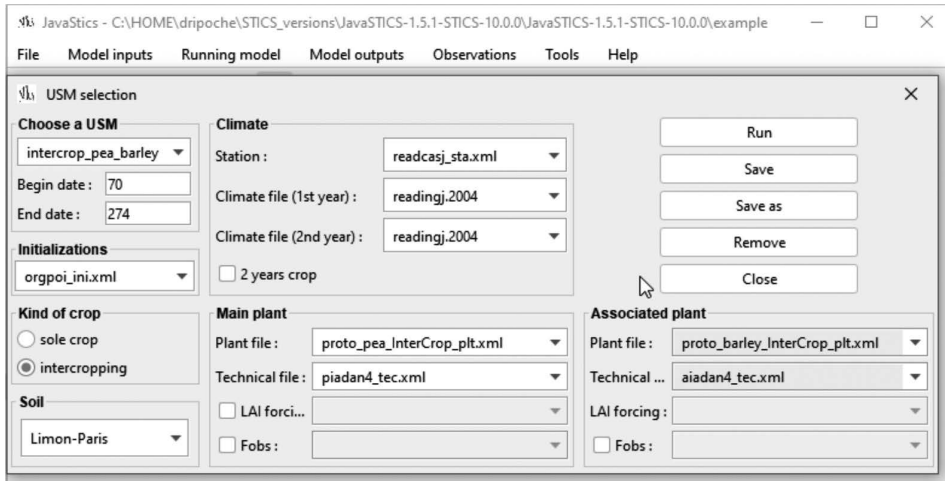


Figure 15.9. Example of an intercropping USM (pea/barley).

►► 15.3 Model formalism options

The model's genericity is made possible mainly because of the availability of formalisation options, some of which must be used exclusively of others. Moreover, some formalisation choices are linked to each other; for example, the option to calculate the foliage amount simply as ground cover precludes the use of the mechanistic option of calculating water balance with a resistive approach. These choices drive the efficient parameter number.

These options address options on simulations (Table 15.1), plant and variety ecophysiology (Tables 15.3 to 15.8), soil biophysics (Table 15.2) or crop management (Tables 15.9 to 15.13). While the plant and variety ecophysiology option is predetermined by species specialists, soil biophysics and crop management options require user input based on descriptions of the local cropping system conditions.

15.3.1 Simulation condition options

Some of the options shown in the Table 15.1 describe the strategy (*) or simulation 'conditions' and are available in the param_gen.xml file. The strategy options are detailed in § 15.2.

Table 15.1. Formalisation options for simulation and strategy conditions.

	Code name: option name	Option choice
Strategy and simulation options	codeinnact (*): Nitrogen stress activation (yes/no)	
	codeh2oact (*): Water stress activation (yes/no)	
	codeminopt: Optimum mineralisation in bare soil (yes/no)	
	iniprofil (*): Smoothing of initial profiles (yes/no)	
	codeprofmes: Depth for mineral N and water stocks calculation	profmes profsol
	codeinitprec (*): Climatic series	reset succession
	codemsfinal: Biomass and yield conservation after harvest (yes/no)	
	codeactimulch: Take account of mulch (yes/no)	
	codefrmur: Fruit load	all fruits (including ripe ones) growing fruits only
	codemicheur: Hourly microclimate (yes/no)	
	codeoutscent: Scientific writing in st2 and report (yes/no)	
	codeserapport: Separator spaces in report (yes/no)	
	codesensibilite: Activation of model sensitivity analysis (yes/no)	

15.3.2 Soil formalisation options

The soil options (Table 15.2) are used to describe soil functioning in terms of heat, water and nitrate transfers in the soil layers. The “*s*” parameters cited in this table are found in the soils.xml file and the “*G*” parameters are found in the param_gen.xml file.

Table 15.2. Formalisation options for soil biophysics.

Chapter	Formalisation	Code name	Option name	Comments
Transfers in soil: water, nitrate and heat fluxes	Transfers	codecailloux _s	pebbles (yes/no)	Pebble type (8 types in param_gen.xml)
		codemacropor _s	macroporosity (yes/no)	See § 10.1.1
		codefente _s	cracks (case of swelling clay soils) (yes/no)	Activation of macroporosity mandatory
		coderemontcap _s	capillary rise (yes/no)	See § 10.1.3
		codrainage _s	artificial drainage (yes/no)	Activation of macroporosity mandatory

Comments	Sub-option code name: sub-option name	Option choice
The stress is always calculated but has no effect if 'no' is chosen		
The stress is always calculated but has no effect if 'no' is chosen		
Mandatory for rotation simulation		
Sub-option code name	Sub-option name	Option choice
codhnappe _G	calculation of groundwater if drainage	average interdrain localisation

Chapter	Formalisation	Code name	Option name	Comments
Transfers in soil: water, nitrate and heat fluxes	Nitrification	codenitrif _s	nitrification (yes/no)	See chap. 12.3
	Denitrification	codedenit _s	denitrification (yes/no)	See chap. 12.4

15.3.3 Plant formalisation options

As explained in § 2.4.3, the modular code development allows for crop genericity by giving users the option to choose ‘strategies’, i.e. to determine whether to activate certain formalisations or not according to the species ecophysiology they want to simulate (Figure 2.5). For example, there is a module dedicated to plant development, which simulates (or not) the action of the photoperiod and the vernalisation require-

Table 15.3. Formalisation options that address plant and variety ecophysiology for development.

Chapter	Formalisation	Code name: option name	Option choice	Comments
		codeplante		Not really an option but a backdoor option which imposes call of functions in the model
	Development driving	codetemp: driving temperature	air temperature temperature within canopy	
Development	Emergence and starting	codeperenne: annual or perennial	annual	
			perennial	
	Aboveground biomass development	codephot: photoperiodic plant	yes	sensiphot, phobase and phosat in genotype parameter
			no	
	coderetflo: delay effect of stress (yes/no)	yes		
		no	vernalisation (herbaceous) jvc in genotype parameter	

Sub-option code name	Sub-option name	Option choice
code_tnit _G	temperature function for nitrification	piecewise linear gaussian
code_vnit _G	nitrification rate dependence on NH ₄	linear Michaelis_Menten
code_hourly_wfps_nit _G	hourly WFPS calculation for nitrification (yes/no)	

ments. There are other formalisation options for each module so, the model can take into account the specific ecophysiology of different crops. These various options are listed in the following tables and grouped by formalisations.

All parameters in these tables are in the '*crop name*'_plt.xml file.

Sub-option code name: sub-option name	Option choice	Sub-option code name: sub option name
codegdh: time scale	daily scale hourly scale	
codegermin: germination or latency (yes/no)		
codehypo: plantlet growth	hypocotyle growth planting	
codgelle: plantlet or emergence frost (yes/no)		
codephot_part: effect of decreasing photoperiod on biomass allocation (yes/no)		

Chapter	Formalisation	Code name: option name	Option choice	Comments
Development	Aboveground biomass development	codebfroid: cold requirements	dormancy (woody)	stdordebour in genotype parameter
			no	

Table 15.4. Formalisation options that address plant and variety ecophysiology for shoot growth.

Chapter	Formalisation	Code name: option name	Option choice
			ground cover
		codelaitr: leaf dynamics	LAI
	Shoot growth		
		codemontaison: Calculation of the stem elongation stage for perennial grasslands (yes/no)	
Shoot growth		codedyntalle: Simulation of tiller dynamics for grasslands	yes no
	Shoot biomass growth	codetransrad: radiation interception	Beer's law radiation transfers
		codeclchange _c : climate change, effect on atmospheric concentration (yes/no)	
	Senescence	codestrphot: effect of photoperiod on senescence (yes/no)	
	N nutrition	codeINN: calculation nitrogen nutrition index (NNI)	NNI cumulative NNI instantaneous
Biomass and nitrogen partitioning	Partitioning of biomass in organs	code_acti_reserve: Simulation of nitrogen and carbon reserves (yes/no)	

Sub-option code name: sub-option name	Option choice	Sub-option code name: sub option name
codedormance: dormancy calculation	forcing	
	Richardson	
	Bidabe	
codegdhdeb: post dormancy calculation	daily temperatures	code_WangEngel: Wang and Engel (yes/no)
	hourly temperatures	

Comments	Sub-option code name: sub-option name	Option choice
Radiation transfers, trophic stress, resistive & energy balances approaches are forbidden		
Trophic stress for codindetermin = indeterminate growing plant	codlainet: LAI calculation option	direct LAInet LAInet = LAibrut-senes
	codgeljuv: leaf frost at juvenile phase (till AMF) (no/yes)	
	codgelveg: leaf frost at adult phase (no/yes)	
	codetranspitale: choice of the ratio used to calculate tiller mortality	et/etm ep/eop
Mandatory with resistive & energy balance approaches		
In link with resistive approach		
Link to the option codeperenne = perennial or codeindetermin = indeterminate growing plant		

Table 15.5. Formalisation options that address plant and variety ecophysiology for yield

Chapter	Formalisation	Code name: option name	Option choice
Yield formation	Yield	codeindetermin: growing dynamics	determinate growing plant
			indeterminate growing plant
		codetrempr: thermal stress on filling (yes/no)	
		codgelflo (yes/no)	
		codazofruit: nitrogen stress on fruit/grain number	no yes (inns)

Table 15.6. Formalisation options that address plant and variety ecophysiology for root growth.

Chapter	Formalisation	Code name: option name	Option choice
Root growth	Root front growth	codetemprac: driving temperature	temperature within the canopy
			soil (threshold TGMIN)
	Root death for grassland	codemortalracine: calculation of the root death at cutting date for grasslands	function of dry matter production between two successive cuts
			no specific root death at cutting
		standard profile	
	Growth in root density	coderacine: root density	true density

Comments	Sub-option code name: sub-option name	Option choice
	codeir: unit Harvest Index	days
		degree days
	codcalinfo: number of inflorescences	prescribed
		trophic status function

Comments	Sub-option code name: sub-option name	Option choice	Sub-option code name: sub option name
	codedisrac: standard root distribution (yes/no)		
	codazorac: N effect on root distribution (yes/no)		
	codtrophrac: trophic-linked production	continuous link	
		threshold	
		no	
	code_stress_root: deactivation of the effect of NNI on biomass allocation to roots (yes/no)		
	code_rootdeposition: rootdeposition activation	yes	code_diff_root: simulation of 2 root classes (yes/no)
		no	

Table 15.7. Formalisation options that address plant and variety ecophysiology for water balance.

Chapter	Formalisation	Code name: option name	Option choice
			crop coefficient
Water balance	Water balance	codebeso: water requirements	resistance approach
Canopy microclimate	Water persistence on foliage	codeintercept: interception of water by foliage (yes/no)	

Table 15.8. Formalisation options that address plant and variety ecophysiology for nitrogen transform

Chapter	Formalisation	Code name: option name	Option choice
Nitrogen acquisition by plants	Nitrogen uptake by plant	codeplisoleN: calculation nitrogen requirements	dense canopies (initial)
			isolated plants (new calculation)
	Nitrogen fixation	codelegume: leguminous	yes no

15.3.4 Crop management formalisation options

This set of tables summarises the options that allow users to describe their cropping system, from crop establishment to harvest.

Table 15.9. Formalisation options for crop management and crop environment through the effect on plants (crop design and cover crop regulation).

Chapter	Sub chapter	Formalisation	Code name: option name
Soil-crop management effects	Crop management	Planting design and simulation of the decision to sow	crop establishment

Comments	Sub-option code name: sub-option name	Option choice	Sub-option code name: sub option name
Mandatory for intercropping. Has to be chosen with radiation interception = radiation transfers & calculation of crop temperature = Energy balance approach. In link with climate change, effect on atmospheric concentration = yes			

mations.

Comments	Sub-option code name: sub-option name	Option choice	Sub-option code name: sub option name
Classical dilution curve			
	codefixpot: maximal fixation capacity	constant growth function	

Option choice	Comments	Sub-option code name: sub-option name	Option choice
sole crop	Define at the usm level		
intercrop			
sowing grains	Define by the initialisation (starting on bare soil)	codedecisemis: rules to prescribe the sowing date (sowing delay depending on the physical soil conditions)	yes/ no
planting plantlets			

Chapter	Sub chapter	Formalisation	Code name: option name
			no establishment (perennial plants)
		Planting design and simulation of the decision to sow	codetradtec: planting structure (if radiative transfer)
			codepalissage: trellis system
Soil-crop management effects	Crop management		codrognage: topping
		Yield regulation	codeffeuil: leaf removal
			codeclaircie: thinning
		Pruning	codetaille: pruning

Table 15.10. Formalisation options for crop management, in particular for the harvest.

Chapter	Sub.Chapter	Formalisation	Code name: option name
			codcueille: method of harvest
Soil-crop management effects	Crop management	Harvest policy	codefauche: cut crop (particular case of forage crop)

Option choice	Comments	Sub-option code name: sub-option name	Option choice
	The starting stage and the crop status have to be filled in		
yes	Has to be chosen with radiation transfer		
no			
yes	Has to be chosen for vineyard		
no			
yes		codcalrogne: topping calendar	fixed date automatic calculation
no			
yes		codhauteff: location of leaf removal	bottom of the canopy top of the canopy
no		codcalefeuille: leaf removal calculation	automatic calculation fixed date
yes			
no			
yes			
no			
yes			
no			
Option choice	Comments	Sub-option code name: sub-option name	Option choice
cutting			
picking		nbcueille: number of pickings	one at the end many during the cycle
yes		codemodfauche: method of cutting	automatic calendar in days calendar in degree days (physiological calendar)
no			

Chapter	Sub.Chapter	Formalisation	Code name: option name
			codrecolte: harvest decision
Soil-crop management effects	Crop management	Decision of harvest	codedecirecolte: rules of harvest/moisture status of the soil harvest delay (depending on the soil physical conditions)
			coderecolteassoc: decision of harvest for associated crops
			codejourdes: date of plant destruction

Table 15.11. Formalisation options for crop management and crop environment through soil water s

Chapter	Sub.Chapter	Formalisation	Code name: option name	Option choice
Soil-crop management effects	Irrigation	Irrigation amount and date	codecalirrig: automatic calculation of irrigations	yes
				no
		Irrigation system	codlocirrig: location of irrigation	above foliage under foliage in the soil
Canopy microclimate	Water persistence on foliage	Interception of water by foliage	codeintercept _p : interception of water by foliage	yes/no

Option choice	Comments	Sub-option code name: sub-option name	Option choice
physiological maturity			
water content (in harversted organs)		codeaumin: minimum or maximum	minimum maximum
sugar content (in harversted organs)			
nitrogen content (in harversted organs)			
oil content (in harversted organs)			
buffer date of harvest			
yes/no			
maturity of the earliest crop	Has to be chosen for the Intercrop simulation		
maturity of both (2 dates)			
	Only for perennial crops		
supply.			
Comments	Sub-option code name: sub-option name	Option choice	Comments
	codate_irrigauto: dates to drive automatic irrigations (start and end)	dates stages	
	amounts calculated		Depending on the water stress, recharges the soil water content to field capacity
	codateappH2O: date of irrigation	in sum of upvt (physiological dates) in Julian days	
	amounts fixed		
Available in the plant file			

Chapter	Sub.Chapter	Formalisation	Code name: option name	Option choice
Transfers in soil: water, nitrate and heat fluxes	Management of snow and its consequences	Modification of rainfall by snow	codesnow: Snow activation	yes/no

Table 15.12. Formalisation options for crop management and crop environment through net nitrogen

Chapter	Sub.Chapter	Formalisation	Code name: option name	Option choice
	N inputs from rain and irrigations			
		Nitrogen use efficiency	type of mineral fertiliser (7 different given types + 1 "blank" type)	
Soil-crop management effects	N inputs from mineral fertiliser	Fertilisation calendar	codecalcfer _G : automatic calculation of fertilisation	yes no
		Localisation	codlocfer _T : location of mineral nitrogen inputs	at soil surface below soil surface
	N and C inputs from organic residues		type of organic residues (9 different given types + rhizomes + roots)	
	N and C inputs from aboveground and belowground residues		types of crop residues (whole_crop / straw / stubble / prunings / stubbleveg / roots)	

Comments	Sub-option code name: sub-option name	Option choice	Comments
Available in general parameter file			

n supply.

Comments	Sub-option code name: sub-option name	Option choice	Comments
Mean concentration to define in crop management file for irrigations in general parameter file for rainfall			
	impose fertiliser efficiency		Only available with the type number 8
	calculated fertiliser efficiency		Only available with the 7 first types
Use with care, because very dependent on the water supply	automatic N fertilisation (1 = based on rainfall, 2 = based on soil water content)	minimum rainfall threshold	
	automatic N fertilisation (1 = based on rainfall, 2 = based on soil water content)	threshold	
	codedateappN: date of fertilisation	sum of upvt (physiological dates)	
	codedateappN: date of fertilisation	Julian days (calendar dates)	
	daily amounts fixed		

Table 15.13. Formalisation options for crop management and crop environment through physical so

Chapter	Sub.Chapter	Formalisation	Code name: option name	Option choice
Soil-crop management effects	Plastic mulch	Presence of plastic cover	codepaillage: mulch	no plastic mulch plastic mulch
	Fragmentation induced by tillage operations	Soil structure modification	codeDST: activation of fragmentation	yes/no
	Compaction induced by sowing and harvesting operations		codeDSTtass: activation of compaction at sowing/harvest	yes/no
Canopy microclimate	Calculation of net radiation	Microclimate	codernet _C : calculation of net radiation	Brunt Brutsaert
	Calculation of crop temperature		codecaltemp: calculation of crop temperature	empirical relation energy balance
	Estimation of microclimate under shelter		codabri: no/yes	

►► 15.4 Parameterisation

This chapter presents some examples of plant, soil and crop management parameters. The methodology for plant parameterisation (formalisation choice and parameter values) is discussed in detail in the § 16.2.

15.4.1 Example of plant parameters

The following tables (15.14 to 15.15) provide examples of plant parameterisation with plant parameter values for five different crops: two perennial crops, *Miscanthus sinensis* and grapevine (*Vitis vinifera* L.), and three annual crops, spring pea (*Pisum sativum* L.), wheat (*Triticum aestivum* L.) and corn (*Zea mays* L.). In these tables, some parameter values are not indicated if the equations for which they are needed have not yet been formulated or used for the relevant species. Others are given for different varieties when they are variety dependent.

il surface conditions, soil structure modification and microclimate.

Comments	Sub-option code name: sub-option name	Option choice	Comments
The plant mulch is taking account by the organic residues (voir Table15.13)			
Mandatory when water requirements = crop coefficient			

Table 15.14. Plant parameters for development.

Chapter/formalism	Parameter	Corn	Wheat
Development/Phasic development	tdmin	6.000	0.000
	tdmax	32.000	28.000
	codetemp	1.000	2.000
	codegdh	1.000	1.000
	coeflevamf		1.000
	coefamflax		1.000
	coeflaxsen		1.000
	coefsenlan		1.000
	coeflevdrp		1.000
	coefdrpmat		1.000
	coefflodrp		1.000
	codephot	2.000	1.000
	codephot_part	2.000	2.000
	coderetflo	2.000	1.000
	stressdev		0.200
	codebfroid	1.000	2.000
	jvcmini		7.000
	julvernal		274.000
	tfroid		6.500
	ampfroid		10.000
	tdmindeb		
	tdmaxdeb		
	codedormance	3.000	3.000
	ifindorm		
	q10		
	idebdorm		
	codegdhdeb	2.000	2.000
code_WangEngel	2.000	2.000	
tdoptdeb			
Development/ Phasic development*	stlevamf	225.000	275.000
	stamflax	450.000	375.000
	stlevdrp	995.000	837.000
	stflodrp	250.000	0.000
	stdrpdcs	650.000	700.000
	jvc		55.000

Pea	Miscanthus	Grapevine (Chardonnay)	Grapevine (Cabernet)
0.0000	6.0		10.00
25.0000	35.0		37.00
2.0000	1.0		1.00
1.0000	1.0		1.00
1.0000			
1.0000			
1.0000			
1.0000			
1.0000			
1.0000			
1.0000			
2.0000	2.0		2.00
2.0000	2.0		2.00
2.0000	1.0		2.00
	0.1		
1.0000	3.0		3.00
	0.0		5.00
	50.0		25.00
3.0000	1.0		3.00
	15.0		
			2.17
			213.00
2.0000	1.0		2.00
2.0000	1.0		2.00
	11.7		
230.0000	150.0		25.00
418.0000	2,400.0	1,123.00	926.60
900.0000	2,550.0	363.30	304.90
216.0000	0.0	50.00	51.00
700.0000	50.0	96.00	95.00

Chapter/formalism	Parameter	Corn	Wheat
Development/ Phasic development*	stdordebour		
	sensiphot		0.000
	phobase		6.300
	phosat		20.000
Development/ Emergence and starting	tgmin	8.000	0.000
	codeperenne	1.000	1.000
	codegermin	1.000	1.000
	stpltger	35.000	50.000
	potgermi	-1.600	-1.600
	nbjgerlim	50.000	50.000
	propjgermin	1.000	1.000
	codehypo	1.000	1.000
	belong	0.022	0.012
	celong	2.040	3.200
	elmax	8.000	8.000
	nlevlim1	50.000	10.000
	nlevlim ²	50.000	50.000
	vigueurbat	1.000	1.000
	laiplantule		
nbfeuilplant			
masecplantule			
zracplantule			

The * in this table indicates genotype parameters.

Table 15.15. Shoot growth parameters.

Chapter/formalism	Parameter	Corn	Wheat
Leaves	phyllotherme	70.0000	120.00000
	laicomp	0.0000	0.30400
	tcmmin	8.0000	0.00000
	tcmmax	32.0000	40.00000
	tcxstop	35.0000	100.00000
	codelaitr	1.0000	1.00000
	vlaimax	2.2000	2.20000
	pentlaimax	5.5000	5.50000
	udlaimax	3.0000	3.00000
	ratiodurviel	1.0000	0.80000
	ratiosen	0.8000	0.80000

Pea	Miscanthus	Grapevine (Chardonnay)	Grapevine (Cabernet)
	70.0	9,174.30	6,576.70
0.0000	6.0		10.00
1.0000	2.0		2.00
1.0000	2.0		2.00
60.0000			
-1.6000			
50.0000			
1.0000			
1.0000	2.0		1.00
0.0115			0.00
4.5701			0.00
7.2100			0.00
10.0000			0.00
50.0000			0.00
1.0000			1.00
	0.0		
	0.0		
	0.0		
	1.0		

Pea	Miscanthus	Grapevine (Chardonnay)	Grapevine (Cabernet)
120.00000	70.0000		25.000
0.00000	3.0000		0.000
0.00000	6.0000		10.000
30.00000	35.0000		37.000
100.00000	40.0000		100.000
1.00000	1.0000		1.000
2.20000	1.5000		2.200
5.50000	10.0000		5.000
3.00000	2.0000		3.000
0.80000	0.5000		1.000
0.25000	0.3000		0.800

Chapter/formalism	Parameter	Corn	Wheat
Leaves	abscission	0.0000	0.00000
	parazofmorte	13.0000	13.00000
	innturgmin	0.3000	-0.65000
	dlaimin	0.0000	0.00000
	codlaint	2.0000	2.00000
	tustressmin		
	durviesupmax	0.4000	0.40000
	codestrphot	2.0000	2.00000
	phobasesen		
	dltamsmaxsen		
	dltamsminsen		
	alphaphot		
	tauxrecouvmax		
	tauxrecouvmax		
	pentrecouv		
infrecouv			
Leaves*	adens	-0.1200	-0.60000
	bdens	5.0000	7.00000
	hautbase	0.0000	0.00000
	hautmax	2.5000	1.20000
	khaut	0.7000	0.70000
	durvieF	200.0000	200.00000
	stlaxsen		
	stsenlan		
	dlaimax		
	dlaimaxbrut	0.0016	0.00047
	innsen	1.0000	0.17000
	rapsenturg	0.0000	0.50000
Shoot biomass growth	temax	32.0000	40.00000
	teoptbis	32.0000	17.00000
	efcroijuv	1.9000	2.20000
	efcroiveg	3.8000	4.25000
	efcroirepro	3.8000	4.25000
	remobres	0.2000	0.20000
	coefmshaut	0.0000	0.00000
Shoot biomass growth*	temin	8.0000	0.00000
	teopt	24.0000	12.00000

The * in this table indicates genotype parameters.

Pea	Miscanthus	Grapevine (Chardonnay)	Grapevine (Cabernet)
0.00000	0.8500		1.000
13.00000	120.0000		13.000
0.30000	-2.0000		0.300
0.00000	0.0100		0.000
1.00000	2.0000		2.000
0.70000			
	0.0000		0.100
2.00000	1.0000		1.000
	12.0000		12.000
	0.1000		0.010
	0.0100		0.150
	0.2500		200.000
-0.45000	-1.5000		0.000
10.00000	1.5000		1.000
0.00000	0.1000	0.600	0.300
0.65000	4.0000		2.500
0.70000	0.7000		0.700
160.00000	150.0000		400.000
350.00000			1.000
280.00000			0.000
0.00047			0.000
	0.0175		0.015
	1.0000		0.870
	0.0000		0.050
30.00000	35.0000		37.000
20.00000	30.0000		25.000
1.20000	2.6000		1.200
2.70000	5.2000		1.040
3.30000	2.6000		2.250
0.20000	0.1000		0.073
0.00000	7.5000		0.000
0.00000	6.0000		10.000
15.00000	25.0000		25.000

Table 15.16. Radiation interception parameters.

Chapter/formalism	Parameter	Corn	Wheat
Radiation interception	codetransrad	1.0	1.0
	forme		
	rapforme		
	adfol		
	dfolbas		
	dfolhaut		
Radiation interception*	extin	0.7	0.5
	ktrou		

The * in this table indicates genotype parameters.

Table 15.17. Yield formation parameters.

Chapter/formalism	Parameter	Corn	Wheat
Yield formation	codeindetermin	1.0000	1.0000
	cgrain	0.0500	0.0360
	cgrainv0	0.1110	0.0000
	irazomax	0.0000	0.0000
	codeir	2.0000	1.0000
	irmax		0.5500
	nboite		
	allocfrmax		
	afpf		
	bfpf		
	cfpf		
	dfpf		
	spfrmin		
	spfrmax		
	splaimin		
	splaimax		
	codcalinfo	1.0000	1.0000
	codetrem	1.0000	1.0000
	tminrem	0.0000	0.0000
	tmaxrem	40.0000	38.0000
Yield formation*	pgrainmaxi	0.3130	0.0397
	vitprosucre	0.0000	0.0000
	vitprophuile	0.0000	0.0000

Pea	Miscanthus	Grapevine (Chardonnay)	Grapevine (Cabernet)
1.00	1.0		2.00
			2.00
			1.50
			3.16
			1.50
			11.50
0.85	0.7		1.70
Pea	Miscanthus	Grapevine (Chardonnay)	Grapevine (Cabernet)
1.000	1		2.00000
0.031	0		
0.000	0		
0.000	0		
1.000	2		1.00000
0.650			
			10.00000
			1.00000
			0.55000
			18.00000
			15.00000
			0.20000
			0.75000
			1.00000
			0.63000
			1.00000
1.000	2		1.00000
1.000	2		1.00000
8.000			0.00000
40.000			37.00000
0.350	0	1.96000	2.00000
0.000	0		0.00290
0.000	0		0.00000

Chapter/formalism	Parameter	Corn	Wheat
Yield formation*	vitirazo	0.0110	0.0145
	deshydbase	0.0080	0.0080
	nbjgrain	20.0000	30.0000
	nbgrmin	1,500.0000	6,000.0000
	nbgrmax	4,000.0000	30,000.0000
	stdrpmat	640.0000	700.0000
	vitircarb		0.0107
	vitircarbT	0.0011	
	afruitpot		
	dureefruit		
	stdrpnou		
	nbinflo		
	inflomax		
	pentinflores		

The * in this table indicates genotype parameters.

Table 15.18. Root parameters.

Chapter/formalism	Parameter	Corn	Wheat
Roots	sensanox	0	1
	stoprac	lax	sen
	sensrsec	0	0.5
	contrdamax	0	0.3
	rayon	0.02	0.02
	codetemprac	2	1
	codemortalracine	2	2
	coefracoupe		
	coderacine	2	2
	zlabour		
	zpenite		
	zprlim		
	draclong	5000	80
	debsenrac	1500	1000
	lvfront	0.05	0.05
	longsperac	11000	18182
	codedisrac	2	2
	kdisrac		
alloperirac			

Pea	Miscanthus	Grapevine (Chardonnay)	Grapevine (Cabernet)
0.022	0		0.00400
0.008	0	0.00159	0.00132
15.000	0		
447.000	0		
3,500.000	1,000		
490.000	1,000		
0.022			0.00000
	0		
		1.15000	2.12000
		1,472.00000	1,280.00000
		91.00000	90.00000
		15.00000	22.00000

Pea	Miscanthus	Grapevine (Chardonnay)	Grapevine (Cabernet)
0	0		0
lax	lax		lax
0.4	1		0
0.34	0		0.3
0.02	0.025		0.02
2	2		1
2	2		2
2	2		2
30	400		40
1000	2250		2000
0.05	0.075		0.005
3300	1553		1021
2	1		2
	0.002		
	0		

Chapter/formalism	Parameter	Corn	Wheat
Roots	codazorac	2	2
	minefnra		
	minazorac		
	maxazorac		
	codtrophrac	3	3
	repracpermax		
	repracpermin		
	krepracperm		
	repracseumax		
	repracseumin		
	krepracseu		
	code_INN_root	2	2
	code_stress_root	2	2
	parazorac		
	code_diff_root	2	2
	lvmax		
	rapdia		
	RTD		
propracfmax			
Roots*	croirac	0.15	0.12

The * in this table indicates genotype parameters.

Table 15.19. Nitrogen parameters.

Chapter/formalism	Parameter	Corn	Wheat
Nitrogen	Vmax1	0.0018	0.0018
	Kmabs1	50.0000	50.0000
	Vmax2	0.0170	0.0500
	Kmabs2	25,000.0000	25,000.0000
	adil	3.5000	5.3500
	bdil	0.3700	0.4400
	masecNmax	1.0000	1.5400
	INNmin	0.3000	0.3600
	INNimin	-0.5000	-0.5000
	inngrain1	2.0000	0.0300
	inngrain2	2.0000	1.2000

Pea	Miscanthus	Grapevine (Chardonnay)	Grapevine (Cabernet)
2	2		2
3	1		3
	0.1		
	0.15		
	2		
2	1		2
2	1		2
	30		
2	1		2
	2.6		
	2.6		
	0.3		
	0.8		
0.12	0.06		0
Pea	Miscanthus	Grapevine (Chardonnay)	Grapevine (Cabernet)
0.012	0.0025		0.0018
50.000	20.0000		50.0000
0.120	0.0500		0.0058
20,000.000	4,000.0000		25,000.0000
5.080	2.7000		3.3000
0.320	0.4800		0.4400
1.000	0.1000		1.6000
0.300	0.3000		0.3000
-0.500	0.0000		-0.4900
0.300	2.0000		1.0000
0.900	2.0000		1.0000

Chapter/formalism	Parameter	Corn	Wheat
Roots	bdilmax	0.3700	0.4400
	codeplisoleN	2.0000	1.0000
	adilmax		8.5000
	Nmeta	4.8000	
	masecmeta	0.0400	
	Nreserve	1.5000	
	codeINN	1.0000	2.0000
	codelegume	1.0000	1.0000
	stlevdno		
	stdnofno		
	stfnofvino		
	vitno		
	profnod		
	concNnodseuil		
	concNrac0		
	concNrac100		
	tempnod1		
	tempnod2		
	tempnod3		
	tempnod4		
	codefixpot	1.0000	1.0000
	fixmax		
	fixmaxveg		
fixmaxgr			
codazofruit	2.0000	1.0000	

The * in this table indicates genotype parameters.

Table 15.20. Stress parameters.

Chapter/formalism	Parameter	Corn	Wheat
Water	h2ofeuilverte	0.900	0.900
	h2ofeuiljaune	0.150	0.150
	h2otigestruc	0.600	0.600
	h2oreserve	0.700	0.700
	h2ofrvert	0.400	0.400
	tempdeshyd	0.005	0.005
	codebeso	1.000	1.000
	kmax	1.200	1.000

Pea	Miscanthus	Grapevine (Chardonnay)	Grapevine (Cabernet)
0.320	0.4800		0.4400
2.000	1.0000		2.0000
	4.5000		
6.470			6.0000
0.040			0.0400
0.500			1.6000
1.000	1.0000		2.0000
2.000	1.0000		1.0000
0.000			
2,000.000			
0.000			
1.000			
30.000			
6.000			
2.700			
0.040			
0.000			
15.000			
25.000			
35.000			
2.000	2.0000		1.0000
30.000			
9.500			
1.000	1.0000		1.0000

Pea	Miscanthus	Grapevine (Chardonnay)	Grapevine (Cabernet)
0.900	0.630		0.75000
0.150	0.100		0.50000
0.600	0.590		0.70000
0.700	0.620		0.70000
0.550	0.400		0.92500
0.005	0.005		0.00016
1.000	1.000		2.00000
1.300	1.000		

Chapter/formalism	Parameter	Corn	Wheat
Water	rsmin		
	codeintercept	2.000	2.000
	mouillabil		
	stemflowmax		
	kstemflow		
Water*	psisto	12.000	15.000
	psiturg	5.000	4.000
	swfacmin	0.100	0.100
Frost	tletale	-5.000	-25.000
	tdebgel	0.000	-4.000
	codgellev	1.000	2.000
	nbfgelev		2.000
	tgellev90		-20.000
	codgeljuv	1.000	2.000
	tgeljuv90		-20.000
	codgelveg	1.000	2.000
	tgelveg90		-10.000
	codgelflo	1.000	2.000
	tgelflo10		-4.500
tgelflo90		-6.500	
Frost*	tgellev10	-1.000	-4.000
	tgeljuv10	-1.000	-10.000
	tgelveg10	-1.000	-4.500

The * in this table indicates genotype parameters.

The beginning of growth for forage crops and grapevine is usually simulated after the winter rest period (dormancy and budding having being parameterised for grapevine, see García de Cortázar Atauri (2006)), when perennial reserves are remobilised. The root system for grapevine is considered to be already completely established (García de Cortázar Atauri *et al.*, 2009; García de Cortázar Atauri, 2006), whereas the root system for forage crops is partially established and will continue to grow during the cropping period. Forage crop parameterisation was done for a grass mixture with an ecophysiology similar to tall fescue (*Festuca arundinacea* Schreb.) and cocksfoot (*Dactylis glomerata* L.) (Ruget *et al.*, 2006). Sugar beet is considered an annual crop by the model because of how it is grown and despite the fact that it completes its vegetative cycle in two years (Launay and Brisson, 2004). For winter wheat only parameters controlling the photoperiod slowing effect (**phobase_p**, **phosat_p** and **sensiphot_p**) and the vernalisation requirement (**jvcmini_p**, **julvernal_p**, **tfroid_p** and **ampfroid_p**) are activated (Brisson *et al.*, 2002).

Pea	Miscanthus	Grapevine (Chardonnay)	Grapevine (Cabernet)
			250.00000
2.000	2.000		2.00000
10.000	25.000		15.00000
2.000	20.000		6.00000
0.100	0.100		0.10000
-25.000	-30.000		-20.00000
-4.000	-1.000		-1.50000
2.000	2.000		1.00000
2.000	3.000		
-20.000	-8.000		
2.000	2.000		2.00000
-20.000	-8.000		-5.00000
2.000	2.000		2.00000
-10.000	-8.000		-5.00000
2.000	1.000		2.00000
-4.500			-2.00000
-6.500			-5.00000
-4.000			0.00000
-10.000			-2.00000
-4.500			-2.00000

Shoot growth, and especially leaf production, are unrestricted throughout the cropping period for forage crops and sugar beet, which are simulated using a high **stamflax_p** parameter value (Launay and Brisson, 2004). Considering the row-planting arrangement of grapevine and the need to simulate intercropping with peas, these two crops were parameterised in order to use the radiation transfer formalisation (§ 9.2.1.2.1) and the associated resistive approach, involving the estimation of **ktrou_p**, **forme_p**, **rapforme_p**, **adfol_p**, **dfolbas_p**, **dfolhaut_p** and **rsmi_n_p** parameters (Table 15.16).

With regard to yield formation, forage crops, spring pea and winter wheat are simulated as determinate crops, whereas sugar beet and grapevine are simulated as indeterminate (§ 8). The parameterisation for forage crops was not targeted to grain production but rather to the aboveground biomass prediction, since this is the harvested part of the crop (Ruguet *et al.*, 2006). For sugar beet, we assumed that only one tuber (storage and harvested root) was set by each plant (**nbinflo_p**=1), and the trophic stress effects

on tuber setting were cancelled by means of very low **spfrmin_p** and **spfrmax_p** parameter values; storage root growth was assumed to be linear over the growth cycle (**bfpf_p**=1) (Launay and Brisson, 2004).

Finally, root length growth was simulated as trophic linked for spring pea, as demonstrated in trials comparing sole and intercropped pea (Corre-Hellou *et al.*, 2007). Symbiotic N uptake formalisation was also parameterised for this legume (Corre-Hellou *et al.*, 2009). The instantaneous nitrogen nutrition index (INNI) based on the daily accumulation of N (Eq. (4.24); § 4.4.2) was chosen to avoid the notable inertia of the NNI dynamics in grapevine and winter wheat (Mary and Guérif, 2005).

15.4.2 Soil parameterisation

Table 15.21 summarises the various soil parameters, recommends methods to assign these parameters, and provides the default value when available. The hydrodynamic parameters need to be discretised by layers (there can be up to five). A minimum amount of information about the soil functioning must be known to be able to determine which options could be activated if necessary. As mentioned by Léonard (2016), it is preferable to use the default options and settings to test the results before modifying any options, especially with regard to the macroporosity option, which must be used only for soils showing hydromorphy or capillary rise, or for soils with artificial drainage.

Table 15.21. List of soil parameters with recommendations to assign them. PTF stands for pedotransfer functions or rules. The sensitivity levels are only suggestions and depend on the purpose of the simulation.

Parameter	Recommended assigning method	Default value	Links between parameters	Sensitivity level
Mandatory parameters				
albedo _s	Reflectance measurements	Table 15.24		*
argi _s	Soil analysis (with decarbonatation)			**
calc _s	Soil analysis	Non calcareous=1		**
		Limestone=10		
		Chalk=60		
cfes _s	Estimation by fitting to water content profiles during evaporation periods	5		*
concseuil _s	Estimation by fitting to the mineral nitrogen content profile	0.01 in temperate soil 0.20 in tropical soil	epd _s (z)	*
CsurNsol _s	Initial C to N ratio of soil humus	0 (if 0 this value is recalculated by the model = 1./Wh)		

Parameter	Recommended assigning method	Default value	Links between parameters	Sensitivity level
Norg _S	Soil analysis	Vineyard soils=0.06	profhum _S	***
		Arable crop soils=0.14		
		Pasture soils=0.20		
obstarac _S	Observed depth of appearance of mechanical constraints or chemical toxicity for roots	200 cm		*
pH _S	Soil analysis	7		*
profhum _S	Observed depth of soil tilling	30 cm	Norg _S	**
q0 _S	Estimation by fitting to measurements of water reserve on bare soil	Figure 15.12	DAF _S (1)	***
mulchbat _S	Sensitivity to crusting estimated by fitting to emergence in terms of date and density	3 cm: insensitive	q0 _S	**
		1.5 cm: low sensitivity		
		0.5 cm: high sensitivity		
pluiebat _S	Sensitivity to crusting estimated by fitting to emergence in terms of date and density	50 mm: insensitive	q0 _S	**
		10 mm: low sensitivity		
		3 mm: high sensitivity		
penterui _S	Runoff coefficient taken into account for plant mulch	0.33		
ruisolnu _S		Table 15.3		*
zesx _S	Estimation by fitting to water content profiles during evaporation periods	60 cm	DAF _S (1)	**
z0solnu _S	Measurements by a roughness meter. Estimated as 1/10 of the average asperity height	0.001 m for sowed soil	DAF _S (1)	***
		0.01 m for ploughed soil		
epc _S (z)	Soil description	30 cm		
epd _S (z)	Estimation by fitting to soil nitrate contents during infiltration periods	10 cm	concseuil _S	**

Parameter	Recommended assigning method	Default value	Links between parameters	Sensitivity level
$DAF_s(z)$	In situ measurements or PTF			
$hccf_s(z)$	Soil analysis, in situ measurement of water content in winter or PTF			***
$hminf_s(z)$	Soil analysis or PTF			
Parameters linked to soil options				
$capiljour_s$	Capillary rises	0		**
$humcapil_s$	Threshold of soil gravimetric water content under which capillary rises occur	0		*
$ecartdrain_s$	Between drain 1/2 spacing	150		*
$ksol_s$	Hydraulic conductivity in the soil above and below drains	1		**
$profdrain_s$	Drain depth	80		**
$profimper_s$	Upper depth of the impermeable layer (from the soil surface). May be greater than the soil depth.	150		***
$profdenit_s$	Thickness of the denitrifying layer	20		*
$vpotdenit_s$	Potential rate of denitrification for the whole denitrifying layer (profdenit)	2		**
$cailloux_s(z)$	In situ estimation			
$typecailloux_s(z)$	Soil description	Table 15.25		
$infil_s(z)$	Estimation by fitting to the water content profile during rainy events	Table 15.22	$DAF_s(z)$	***

When soil information is missing, some soil parameters, considered as permanent characteristics, can be estimated using pedotransfer functions (PTF) or rules (Bouma, 1989), i.e. their values can be inferred from other available soil data such as texture, particle size distribution, organic matter content, etc. PTF has been used extensively for field capacity and wilting point, and to a lesser extent for bulk density. Many pedotransfer functions exist for estimating the soil hydraulic properties (for example, see reviews by Wösten *et al.* (1999) or Vereecken *et al.* (2010)).

To choose the appropriate pedotransfer function, it is better to use a PTF developed for a region with similar soils and landscape history (Wösten *et al.*, 2001) and with a large number of samples (Pachepsky and Rawls, 2004). McBratney *et al.* (2002) consider two

principles for choosing a PTF. The first is the effort required to measure the predictors: an efficient PTF is one where the predictors are more easily available (i.e. less expensive, less time consuming) than the property to predict. The second principle is to choose a PTF where uncertainty is evaluated (using first-order Taylor analysis or bootstrap method) and with minimum variance. McBratney *et al.* (2002) also suggest avoiding extrapolation and propose a method for determining if data are inside or outside a PTF's training set (the published PTF must include statistics on the training data set).

In France, the choice of which PTF to use could be linked to the availability of input data among the most recent PTFs such as Al Majou *et al.* (2008), Bruand *et al.* (2004) or Román Dobarco *et al.* (2019). Pedotransfer functions have also been established at the European level (Tóth *et al.*, 2015).

To enable STICS users to parameterise their soil (at least roughly for test runs), we have created pedotransfer tables based on well-known literature. The tables mostly use textural information so parameter values are likely to change with soil structure and organic matter content (Figure 15.10 and Table 15.22).

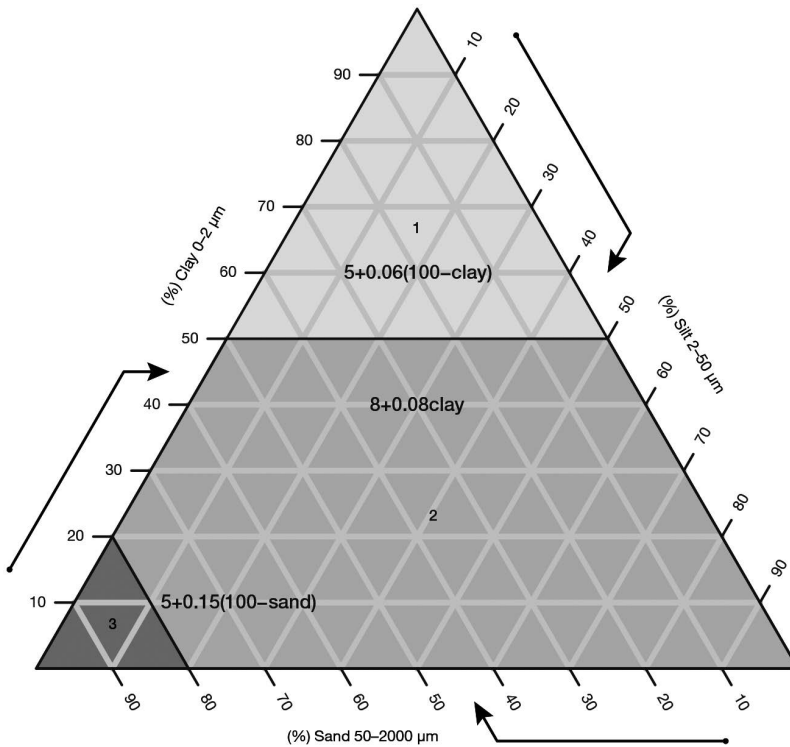


Figure 15.10. Soil transfer functions to assess the Q_0 parameter as a function of clay and sand content.

In Table 15.22, the permeability classes proposed by Ritchie (1985) are arbitrarily associated with textural classes and correspond to a percentage of the amount of water stored in the macroporosity that infiltrates from one day to the next. The calculations show that the effect of layer thickness on \mathbf{infil}_s disappears as permeability decreases.

We can also refer users to the work of Lefebvre (2010), which proposes a method to estimate various soil parameters using the Soil Geographical Data Base for France at 1:1,000,000 (INRA, 2018).

Table 15.22. Pedotransfer table to estimate hydrodynamic parameters according to textural classes based on Wösten *et al.* (1999), Ritchie (1985) and Brisson (Pers. Com.).

	Textural class	HCCF (g/100g dry soil)	HMINF (g/100g dry soil)	DAF (g.cm ⁻³)	INFIL for various layer thickness		
					5 cm	10 cm	15 cm
topsoil	coarse	0.13	0.05	1.30	50.00	50.00	50.00
	medium	0.22	0.12	1.30	22.69	12.66	8.54
	medium fine	0.25	0.10	1.30	8.17	4.29	2.87
	fine	0.31	0.21	1.30	4.22	2.12	1.41
	very fine	0.38	0.26	1.30	1.81	0.91	0.60
subsoil	coarse	0.08	0.03	1.45	50.00	50.00	46.97
	medium	0.19	0.10	1.45	24.43	13.63	9.20
	medium fine	0.22	0.10	1.45	6.94	3.64	2.44
	fine	0.27	0.20	1.50	1.04	0.52	0.43
	very fine	0.33	0.25	1.45	0.27	0.27	0.27

The values of **ruisolnu_s** (Table 15.23), derived from the USDA Runoff Curve Number method, are rather low because they represent only Hortonian (surface) runoff, which only depends on obstacles created by plants and on the water velocity on a slope field. The STICS model takes into account other component of runoff, i.e. resistance to infiltration, as well as the presence of a plant mulch (§ 11.4).

The Table 15.23 provides the values of the parameter **ruisolnu_s** as the proportion of Hortonian runoff to incoming precipitation minus the **pminruis_G** threshold, based on the USDA Runoff Curve Number approach described in Chapman and Lake (2003).

Table 15.23. Values of the parameter **ruisolnu_s**.

Soil cover	Slope classes			
	0-2%	2-5%	5-10%	>10%
Smooth soil	0.05	0.07	0.1	0.13
Ploughed soil	0	0.03	0.06	0.08
Row crop in direction of slope	0.05	0.07	0.1	0.13
Row crop perpendicular to slope	0	0.03	0.06	0.09
Homogeneous crop	0	0.03	0.07	0.1

The **albedo_s** parameter applies to dry soil, with the effect of water content being simulated (Eq. (9.15)). There are two criteria to assign this parameter, texture or colour; the latter is read from a Munsell chart (Table 15.24). The relationship between soil colour and albedo can also be found in Post *et al.* (2000).

INFIL for various layer thicknesses								
20 cm	25 cm	30 cm	40 cm	50 cm	60 cm	80 cm	100 cm	120 cm
50.00	50.00	45.93	34.48	27.59	22.99	17.24	13.79	13.69
6.42	5.13	4.28	4.18	4.18	4.18	4.18	4.18	4.18
2.28	2.28	2.28	2.28	2.28	2.28	2.28	2.28	2.28
1.06	0.85	0.71	0.58	0.58	0.58	0.58	0.58	0.58
0.45	0.36	0.30	0.27	0.27	0.27	0.27	0.27	0.27
36.09	29.10	24.31	18.25	14.60	13.56	13.56	13.56	13.56
6.91	5.53	4.61	3.45	3.33	3.33	3.33	3.33	3.33
1.83	1.66	1.66	1.66	1.66	1.66	1.66	1.66	1.66
0.43	0.43	0.43	0.43	0.43	0.43	0.43	0.43	0.43
0.27	0.27	0.27	0.27	0.27	0.27	0.27	0.27	0.27

Table 15.24. Values of the dry soil albedo using either textural classes or colours, based on Richard and Cellier (1998), Jacquemoud *et al.* (1992).

Soil type	albedo
TEXTURE	
Limestone	0.31
Loamy sand	0.25
Clayey loam	0.18 - 0.22
Loam	0.22 - 0.23
Crusted loam	0.28
Clay	0.28
COLOUR	
Brown soil	0.27
Red soil	0.29
Black soil	0.17
Grey soil	0.29
Yellow soil	0.35

Pebbles are characterised according to their water retention ability. Tetegan *et al.* (2011) assess hydraulic properties for sedimentary pebbles frequently found in French agricultural fields (Table 15.25). For non sedimentary pebbles, we refer to Gras (1994).

Table 15.25. Average values of volumetric mass and gravimetric water content at field capacity for various sedimentary pebbles in France from Tetegan *et al.* (2011) and Gras (1994).

Pebbles type	Volumetric mass in cm g ⁻³	Field capacity in g/100 g
Gaize	1.44	31
Chalk	1.76	21
Chert	2.07	13
Limestone	2.18	9
Flint	2.22	6
Sandstone or unaltered granite	2.65	0
Altered granite	2.3	10
Default types of pebbles of STICS		
Beauce limestone 1	2,2	7
Beauce limestone 2	1,8	16
Lutetian limestone	2,1	11
Lutetian Brackish marl and limestone	2,3	5
Morainic gravels	2,5	3
Unweathered flint, sandstone or granite	2,65	1
Weathered granite	2,3	5
Jurassic limestone	2,2	5
Pebbles from Magneraud	1,5	26

Table 15.26. List of techniques included in the STICS model and the corresponding parameters.

Technique	Compulsory parameters if the technique is applied
Soil tillage and residue incorporation ¹	jultrav, profres, profrav, coderes
	If fragmentation dependent: (codeDST activated) If compaction dependent (codeDStass activated) If sowing date calculated and compaction dependent If codedecirecolte activated and compaction dependent
Sowing ¹	densite
	variete
	If annual: If row crop: If sowing date is calculated:

15.4.3 Crop management parameterisation

While management data are probably the easiest input to provide, the links between practices and the proper state variables in the model can require users to implement transfer rules. For example, the interactions between fertilisers and the soil-crop system are highly dependent on the type of fertiliser, whether organic or mineral, of course, but also within each of these types, their proper biochemical and physical behaviour must be taken into account. As listed in Table 15.26, STICS accounts for practices related to bare soil and cropping periods for industrial crops as well as fruit and vegetables crops. There is no information about the crop health status. The options and parameters for crop management process are described in chapter 13.

Optional parameters if the technique is applied		
	Codification	Dependant parameters
dachisel, dalabour, rugochisel, rugolabour		
dasemis, darecolte, profhumsemoir, profhumrecolteuse prophumtassem	coderes (see Table 13.14)	qres, CsurNres, crespc, nminres, all mineralisation parameters (see Table 13.14)
prophumtassrec		
iplt, profsem interrang, orientrang nbjmaxapressemis, nbj_pr_apres_semis, humirac_decisemis,eau_mini_decisemis, nbjseuiltempref	variete	All varietal parameters

Technique	Compulsory parameters if the technique is applied	
Irrigation ^{1,2}	effirr	If prescribed by dates: If prescribed by phasic stages: If calculated: If in the soil:
Fertilisation ¹	dosen engrais	If fert-irrigation: If calendar application: If phasic application: If in the soil:
Harvesting ¹	ressuite	If non physiological: If water content dependent: If sugar dependent: If nitrogen dependent: If oil dependent: If several pickings: If codecirecolte activated:
Forage cutting ¹		If prescribed cuts: If calendar prescription: If phasic prescription: If calculated:
Mulching		If plastic: If plant (link to the residue properties):
Trellising crops	hautmaxtec largtec	
Tactical shape control ¹	largrogne hautrogne biorognem	If prescribed: If calculated:
Leaf removal ¹	codhauteff	If prescribed: If calculated:
Fruit removal	juleclair, nbfrote	

Optional parameters if the technique is applied		
	Codification	Dependant parameters
julapi, dosei upvttapi, dosei ratiol, dosimx locirrig		
concirr julapn upvttapn locferti	engrais (see Table 13.3)	engamm, orgeng, deneng, voleng
irecbutoir h2ograinmin or h2ograinmax sucrerec cngrainrec huilrec cadencerec nbjmaxaprerecolte		
hautcoupe, lairesiduel, msresiduel, restit, mscoupemini, anitcoupe, engraiscoupe, tauxexportfauche julfauche tempfauche stadecoupedf, haucoupedefault		
couvermulchplastique, albedomulchplastique	codetypres (see Table 15.27)	qmulchruis0, mouillabilmulch, kcouvmlch, albedomulchresidus, Qmulchdec
julrogne margerogne		
juleffeuil, laieffeuil laidebeff, effeuil		

Technique	Compulsory parameters if the technique is applied	
Pruning	jultaille	
Crop destruction	juldes	
Shelter	transplastic	If shelter opened occasionally (3 times maximum):

¹ Several cultivation operations can be planned to bury or mix in residues (of different types) in the soil. These operations include adding new residues or simply modifying the structural and moisture conditions of previously added residues.

² Technique that can either be prescribed or partly calculated using decision rules (Table 15.28). In this table, all the parameters are available in the crop management file excepted for the typology parameters, which are available in the general parameters file.

Table 15.27. Various types of plant mulch and corresponding parameters.

	decomposmulch	qmulchruis0	mouillabilmulch	kcouvmlch	albedomulch
Maize stalk	0.007	1	0.4	0.367	0.10
Sugar cane	0.007	1	0.4	0.367	0.50
Vine stems	0.007	1	0.0	0.050	0.08

Many of the above mentioned techniques can be calculated using simple decision rules (Table 15.28).

Table 15.28. Decision rules to help to implement practices.

Technique	Possible decision rules
Sowing	Date based on soil water status and temperature
Irrigation	Calendar dates or phenological stages and amounts based on water stress
Fertilisation	Calendar dates or phenological stages and amounts based on nitrogen stress and soil surface water status
Harvesting	Date based on plant physiology and soil water status
Forage cutting	Calendar dates or phenological stages with a minimum level of biomass
Tactical shape control	Dates and amounts based on expected shape
Leaf removal	Dates and amounts based on the leaf quantity to remove
Crop destruction	Calendar dates

15.4.4 System initialisations

15.4.4.1 Initialisation parameterisation

To ensure good simulation results, knowledge of the field status at the beginning of the simulation is very important. The simulation start date depends on the knowledge of the system: the date the water and mineral N content was measured, and the date of the first crop intervention (sowing or planting, fertilisation, soil tillage, spreading of organic residues, etc.). When simulating the crop rotation, the start and end date must be successive between two USMs of the rotation as described in § 15.2.3.2.

Optional parameters if the technique is applied

Codification

Dependant parameters

 surfouvre, julouvre

With regard to the crop, if bare soil (i.e. before sowing), is selected as the initial situation, the initial values of the crop can be ignored. This may be desirable if there is uncertainty about the initial crop status, see § 14.2.2

Regarding the water content value, if the status at sowing is unknown, users can start the simulation at a date where it is known (i.e. at the end of the winter when the soil moisture is at field capacity).

More generally, initialisation values of soil water content and mineral N content are those without the pebble compartment (i.e. fine earth only, because the model will integrate the pebble role) whereas the observed values must integrate the pebble compartment.

15.4.4.2 Specific case of succession for perennial crops

For perennial crops like grapevine, miscanthus or sometimes forage, the crop status at the beginning of the simulation must be known:

- phenological stage at the beginning date of simulation (**stade0₁**),
- leaf area index **lai0₁**,
- initial grain dry weight **magrain0₁**,
- initial plant biomass **masec0₁**, initial N amount in the plant **QNplante0₁**, initial value of biomass of storage organs in perennial crops **restemp0₁** (if the option to simulate N and C reserves is not activated),
- initial value of biomass of storage organs in perennial crops **maperenne0₁** and initial aerial biomass **masecnp0₁** (if the option to simulate N and C reserves is activated),
- initial value of nitrogen amount in storage organs in perennial crops **QNperenne0₁** and initial N amount in the plant (if the option to simulate N and C reserves is not activated) **QNplantenp0₁** if the option to simulate N and C reserves is activated).

For **grapevine**, in particular, a recurrent question deals with how to use STICS to simulate several consecutive years with grapevine in order to carry over all the information (N, water, carbon cycles) from the previous year. To use STICS for grapevine, a resistive model (i.e. Shuttleworth-Wallace model) is required. In this case, users will need all the climatic variables (temperature, rainfall, radiation, wind speed and humidity).

Here are the two options available in STICS - with and without dormancy.

Option 1: With dormancy

- In the general parameters file (param_gen.xml), choose ‘Succession’ from the Simulation options/Climatic series
- Open the USM to use with all the information:
 - For the Begin date, introduce the date 345
 - For the End date, introduce the date 710 (pruning date)
 - In the Climate file (first year), select the first year (i.e. 2001)
 - In the Climate file (second year), select the last year (i.e. 2015)
 - Tick the ‘2-year crop’ box.

If the information has been entered correctly, a single balance file will appear with all the information from the first year to the last. Because the simulation is started at day 345 (after the start of dormancy), dormancy break and budbreak will not occur and the first year will not produce anything (no phenology, yield, or anything else): the model will consider the system as having a bare soil. After this first year, the model will consider the succession and take into account the different simulated cycles (C, N, water).

Option 2: Without dormancy

WARNING: All the files provided in the current version of the STICS crop model have been calibrated and validated using the dormancy break model (BRIN model). If a different version of the model is used, results may be strange, so users should keep this risk in mind.

- In the general parameters file (param_gen.xml), choose ‘Succession’ from the Simulation options/Climatic series

Table 15.29. Table of tools uses.

	Launch model	Manage files	Visualise	Evaluate
JavaStics interface	*	*	*	*
JavaStics in command line	*			
Record platform	*			
Batch users	*			
SticsRfiles		*		**
SticsOnR	*			
CroptimizR				
CropPlotR			**	

* available, ** preferable

- In the plant file (the relevant variety file), choose the forcing option in the phasic development/cold requirements/dormancy/dormancy calculation
- Enter a new value for the parameter **stdordebour_p** (the value currently available was calculated using the BRIN model (García de Cortázar Atauri *et al.*, 2005))
- Open the USM to use with all the information:
 - For the Begin date, introduce the date 1
 - For the End date, introduce the date 365 (pruning date)
 - In the Climate file (first year), select the first year (i.e. 2001)
 - In the Climate file (second year), select the last year (i.e. 2015)
 - Untick '2-year crop' box.

If everything has been entered correctly, a single balance file will appear with all the information from the first year to the last.

Please note: The same configuration is used for all the years; It cannot be changed (adaptation). Option 2 is only possible if users do not take into account dormancy. In this case, users must verify if the phenology is correctly simulated. This method is not suited to climate change studies.

►► 15.5 Tools for users

A set of tools are available for the user community. In some cases, the choice of tools can depend on the uses and the knowledge of the development platform, such as for the R Packages. The table below (Table 15.29) can be used as a guide.

Optimise	Starting with the model	Multi-simulation	Calibration	Pre-requisites
*	**	*	*	No
	*	**		No
**		**		Record or web record
				No
				Rstudio
		**		Rstudio
**			**	Rstudio
				Rstudio

15.5.1 The JavaStics interface

JavaStics 1.5.0 is an interface for managing simulations with the STICS crop model on Windows or Linux platforms. This tool provides a user-friendly environment for managing input and output to and from the model and for its operational use.

Users can access the JavaStics interface and STICS model from the STICS web site after a registering². The downloaded .zip file should be unzipped to an independent JavaStics directory. The model executables for Windows and Linux are all included in the zip file.

The main menu items for the JavaStics interface are organised as follows:

- File: select or create a simulation directory. The simulation directory contains the parameter files that can be edited by the user as well as the STICS output files.
- Model inputs: view and edit STICS input files.
- Running model: launch simulations.
- Model outputs: select outputs (before simulation) and view the model outputs when the simulation is complete.
- Observations: process observed data.
- Tools: tools for converting files from earlier STICS versions.
- Help: display the application version.

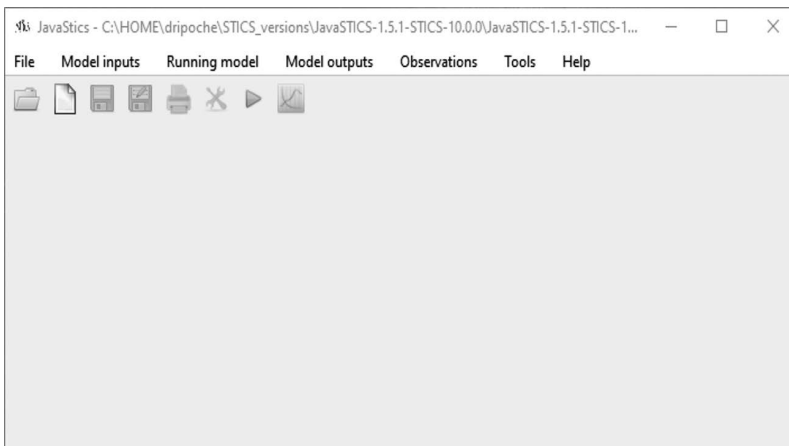


Figure 15.11. JavaStics menus.

Users can use JavaSticsCmd.exe to run the model from a terminal or command prompt. The command options can be used only when executing JavaSticsCmd.exe (users should replace the text below in italics with the name of their own workspace, USM or file path):

- "-run": Use this command to run STICS. The command should be launched in a JavaStics workspace. For example: `-run workspace USM` or `run workspace`
- "-run-successive": Use this command to run successive USMs. The command should be launched in a JavaStics workspace. For example: `-run-successive workspace USM1 USM2` etc.

2. https://www6.paca.inrae.fr/stics_eng/Download

– “-generate-txt”: Use this command to generate Fortran binary input files from JavaStics input files (all the files necessary for the simulation). For example: `-generate-txt workspace USM`

Please note: for use on Linux, replace `JavaSticsCmd.exe` with `java -jar JavaSticsCmd.exe` in the command line. Java version 11 is required for using JavaStics 1.5.0 command line interface as for the graphical interface.

Sample batch files are available in the JavaStics root directory (for Windows: `example_batch.bat`, or for Linux: `example_batch.sh`).

15.5.2 STICS R packages

SticsRPacks is a suite of R packages composed of tools developed to help user during the different steps of using the STICS model:

Some packages are devoted to drive the STICS model from R:

- `SticsRFiles` (Lecharpentier *et al.*, 2021b): this package was designed for reading and writing the input and output files for STICS either from the xml files or directly from the text files (e.g. `ficplt.txt` or `var.mod`).
- `SticsOnR` (Lecharpentier *et al.*, 2021a): this package was designed to control STICS from R, e.g. create USMs and simulation instances, run the STICS model, extract the raw results, etc.

Other packages are generic to link crop models (STICS as well as `ApsimX`, `SiriusQuality` and many others) with mathematical methods such as parameter estimation and model evaluation:

- `CroptimizR` (Buis *et al.*, 2021): a package to estimate parameters of crop models using R.
- `CropPlotR` (Vezy *et al.*, 2021): a package to analyse crop model simulation outputs (plots and statistics).

These packages are developed with an open-source licence and available in the GitHub repository³. They are used for such processes as model calibration (§ 16.2.2.4).

15.5.3 The links and interactions with the users community

The STICS team has established a discussion forum on its web site⁴ as a place to ask questions and get answers from the STICS team and model users.

This forum is organised by items in order to target the right person in charge of the item and is widely used by the STICS community (Figure 15.12). The main thematic approaches are the crop system (44%), followed by software (30%) and soil (16%), with an average of 15 questions per month (117 from 1 January 2021 to the end of august 2021).

3. <https://github.com/SticsRPacks>

4. https://w3.avignon.inra.fr/forge/projects/stics_main_projecu/boards

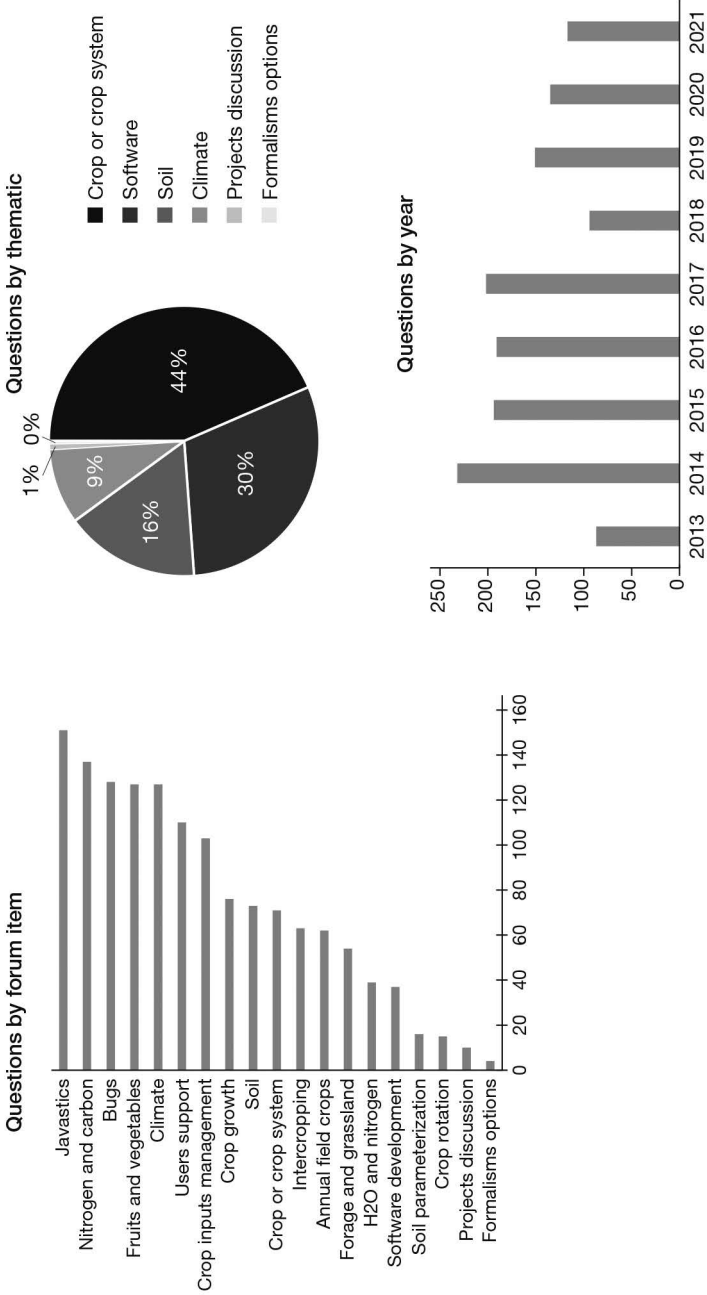


Figure 15.12. Statistics on the use of the STICS user forum.

Chapter 16

Model capacity extension methods

SAMUEL BUIS, GUILLAUME JEGO AND ERIC CASELLAS

*REVIEWED BY: NICOLAS BEAUDOIN, GATIEN FALCONNIER,
FABIEN FERCHAUD, MARIE LAUNAY AND RONAN TREPOS*

►► 16.1 Introduction

A model's domain of validity is the range of conditions for which the model is intended to adequately represent the system under study (see § 2.2).

If the model is to be applied to conditions outside this domain of validity, or if it is not performing to the expected level of accuracy or precision, its capacity can be extended by:

- adapting the model to new plants or cultivars (or re-parameterising existing plant or cultivar adaptations),
- re-parameterising, modifying or adding formalisms, or
- coupling STICS with other models.

This chapter provides information and references on how to do this.

The first section focuses on model evaluation and offers guidelines so users can assess the performance of the model for their particular application. The second and third sections discuss how to adapt STICS to new crops or cultivars as well handle model coupling.

Readers interested in the (re-)parameterisation of formalisms can refer to § 16.3, which provides general guidelines and references on estimating model parameters. Modifying or introducing new formalisms is a vast subject which depends heavily on the type of formalism in question, and requires modifying the STICS code. Information and advice about how to modify the STICS code will be the subject of a new chapter in future versions of this book.

►► 16.2 Evaluating model performances

16.2.1 Introduction

Model evaluation is a crucial step that aims to:

- detect any problem or limit in the model during the model development and improvement process,

- establish the model's overall credibility, and
- ensure the model's use is appropriate for a particular application.

This process therefore concerns both model developers and users.

The term 'model evaluation' has been defined in many ways, and different terminology is found in the literature for similar topics such as verification, validation or assessment. The subject is still under debate and we will not go into further detail about the issue. We will use the general term '**model evaluation**', defined quite broadly by Bellocchi *et al.* (2010) as including 'any action in which the quality of a model is established'.

16.2.2 Objective and dataset

Model quality must be assessed with regard to a given objective, which will determine the way the evaluation is approached. More specifically, the choice of the dataset used to evaluate the model will depend on the objective.

For example, our objective as the STICS model team is to ensure the overall credibility of the model. Accordingly, we must evaluate the model based on a wide range of conditions (e.g. different crops and cultivars, soil types, weather, agricultural practices) and a large set of output variables with final and in-season values (see § 14.5.5.1). Meanwhile, users may be more interested in assessing its credibility for a given crop, perhaps in particular locations in the world or for specific agricultural practices or environmental conditions. This determines the **target population**, i.e. the range of conditions and variables of interest.

The dataset used for model evaluation (and model calibration; § 16.3) should be as representative of this target population as possible. Adequate agro-pedoclimatic indicators can be particularly useful in this context to characterise the variability of conditions represented in a dataset (Ojeda *et al.*, 2021). But if observations of non-targeted variables are available, they can improve understanding of whether the model behaviour is appropriate. They can also be used as a proxy if certain targeted variables are not observed. For example, the water content of the different soil layers (**HR(1)**, **HR(2)**...) can provide information about the distribution of water uptake in the soil profile, and therefore the root system depth (§ 16.3.3.4).

Finally, to ensure an unbiased evaluation, the dataset used for model evaluation should be as independent from the dataset used to calibrate it as possible. At the very least, it should not include situations (called 'simulation units' or 'USMs' in STICS language) nor, if possible, plots or years that have been used to calibrate the model.

16.2.3 Methods

Various complementary model evaluation methods exist:

- **Graphical plots** are often used to compare observations and simulations, as well as to qualitatively assess the agreement between model results and observed data points. When represented in appropriate formats, these plots can yield significant insights into model performance, pinpoint systematic bias or identify specific situations where observations and simulations differ widely. Typical graphical plot examples are scatter plots representing simulated values or residues as a function of observed values for a given variable, together with their linear regressions (Bennett *et al.*, 2013; Vezy *et al.*,

2021). Dynamic plots that display simulated and observed values over time for each variable can also be very useful. Such plots can help identify time lags between simulations and observations or periods that differ considerably.

– **Goodness-of-fit criteria** compute numerical metrics comparing model simulations to corresponding observations. They are the most popular way of evaluating models since they provide a quantitative assessment of model performance. Many different metrics are used in the literature. Mean square error (*MSE*) and its breakdown into different terms, mean absolute error (*MAE*), and model efficiency are among the most popular. Readers can refer to D. Wallach *et al.* (2018) for a comprehensive description of the main criteria used for crop models. Each individual goodness-of-fit criterion provides an image of model performance from a particular point of view. Use of multiple complementary criteria is thus advisable to ensure a good characterisation of the structure of the differences between model simulations and observations. Note also that multiple criteria can be combined in an integrated indicator to rank the performance of different simulated variables or different models (see e.g. Bellocchi *et al.*, 2002).

– **Behavioural analysis** examines the response to changes in key variables or parameters in the model to evaluate whether the model subcomponents behave, at least qualitatively, according to current knowledge about the real physical system being simulated. For example, Coucheney *et al.* (2015) used graphs to compare the relative variations of a set of simulated and observed variables between classes of agro-pedoclimatic indicators (global radiation, fertilisation rate, soil water content at field capacity, etc.). Holzworth *et al.* (2011) referred to this evaluation process as conducting ‘sensitivity tests’. They gave several examples, such as the plot of the predicted response of lupin yield in function of in-season cumulative rainfall and its comparison with a potential yield computed using a simple water use efficiency model. For this example, they verified that the envelope curve of the predicted yield, which takes into account various stresses, was consistent with the variation of the potential yield with respect to the different rainfall conditions.

The behaviour analysis evaluation method is less frequently used and published than the first two methods listed here. However, its importance is recognised because demonstrating that model outputs more or less fit a dataset is a necessary but not sufficient indication of validity. It is nearly impossible to put together a relevant, high-quality dataset that can evaluate most of the model subcomponents on a representative sample of the target population (Sinclair and Seligman, 2000). It is simply not feasible to measure everything in the soil, crop and atmosphere for reasons of cost or technological limitations. Moreover, the target population may also include rare or even future events for which it is very difficult or impossible to have corresponding measured data. This is why many authors advise systematically integrating behavioural analyses into model evaluation to assess whether the model faithfully captures the underlying process driving the system (Bellocchi *et al.*, 2010; Jakeman *et al.*, 2006; Sinclair and Seligman, 2000). We should mention the importance of scrutinising the results obtained for variables for which there are no observations included in the evaluation and calibration datasets used (e.g. harvest index, root characteristics) and the results obtained for synthetic situations (e.g. non-limiting soil and weather), even if doing so does not strictly fall within the behavioural analysis method according to the definition given in the papers cited here. But since such data are not generally taken into account in calibration procedures, they may reveal non-expected behaviours.

The CroPlotR R package (Vezy *et al.*, 2021) can be used to facilitate the application of all these methods on crop models.

16.2.4 Published evaluation of the STICS model

In addition to their own evaluations, users can refer to the many published studies using the STICS model. Coucheney *et al.* (2015) is one of the rare studies to date on crop model evaluation that combines all three of the evaluation methods described above and uses a very large dataset. In this study, version 8.2.2 of the STICS model with its standard set of parameters was evaluated using multiple complementary methods with a large dataset covering 15 crops and a wide range of agro-pedoclimatic conditions in France (see § 14.5.5.1). Evaluation of STICS performance on different crops and environments can also be found in many other articles (see e.g. § 14 for references on various types of applications and contexts).

Furthermore, STICS is automatically evaluated each time its source code or parameter values are modified in its version control system (Buis *et al.*, 2016). This allows the STICS team to preserve and enhance the performance and robustness of future model versions and associated parameters. Evaluation reports per species produced for each distributed version of the model can be found in the doc/evaluations folder of the corresponding JavaStics distribution.

16.2.5 Dealing with poor results

If an evaluation process results in unsatisfactory performances, the following suggestions can be useful to address the issue:

- Verify whether the conditions represented in the dataset used belong to the model's domain of validity:
 - Was the dataset used for model calibration representative of the target population? Simulating conditions that are very different from those used for the model calibration may explain poor performance. In this case, evaluating the behaviour of the main expressed formalisms with respect to the range of conditions explored in both calibration and evaluation datasets may help identify the problem.
 - Are all the important processes expressed in the measured situations included in the model? Some processes may have been overlooked; for example, perhaps there were problems with disease or weeds in the experiment and these processes are not represented in the model. This can be a source of a major discrepancy between simulations and observations.
- Check the evaluation dataset: users must remember that, as the model outputs, the observed datasets also provide imperfect information regarding the true status of the system. Observation errors may affect model inputs (e.g. soil measurements, weather data) and thus model simulation results: rubbish in means rubbish out. Malone *et al.* (2011), for example, showed the large impact of frequent errors in weather data on model simulations and described the commonly recommended quality check and correction procedures for different elements. If some model inputs are likely to be quite uncertain, uncertainty analysis techniques can be used to check the impact of these uncertainties on simulated model outputs. Errors on observations of model outputs may also affect the evaluation process if it is based, at least partly, on the comparison of simulations and observations. Poor-quality data may be eliminated.

Note, however, that if errors have large variances but are unbiased, a large dataset can compensate for large variance (Montesino-San Martin *et al.*, 2018). Quantity and quality issues are especially important when dealing with remote-sensing data and participatory science.

– Post questions and discussion topics on the STICS forum¹: experts are there to try to answer your questions!

Having a detailed knowledge of the system under study, the dataset and the model, is of great help to correctly interpret discrepancies between measured data and simulation outputs.

►► 16.3 Adapting STICS to a new crop or cultivar

16.3.1 Introduction

Adapting STICS to a new crop or cultivar involves i) choosing the appropriate options for the different formalisms implemented in the model (e.g. activate or deactivate) and ii) setting the model parameter values for the crop/cultivar in question.

These two steps must be carefully executed because they determine the simulation model, i.e. the equations that will be used to carry out the simulations. Their impact on the simulated results – and thus on model accuracy, precision and robustness – is therefore decisive.

Often, the choice of formalism options is largely based on agronomic and ecophysiological expertise and the available literature on the crop or cultivar considered. The choice of parameter values is often more difficult.

In STICS, we have adopted the commonly used definitions for parameters and variables: parameters are considered as constant throughout the simulation while variables vary over time (§ 14.5.5.1). The reason parameter values are difficult to set is mainly because generic crop models tend to have many parameters. STICS has 10 to 15 active cultivar parameters and 100 to 150 active specific parameters in the plant files that come with the model. These figures reflect the many proposed formalisms and the STICS team's decision to give users transparent access to all these parameters for the sake of clarity and flexibility: no parameter value is hard coded. The actual number of parameters depends on which formalisms the user activates or deactivates and the associated option codes that determine the set of equations constituting the model (see § 15.3 and § 16.3.2).

Some of these parameters are closely linked to processes and have a well-identified biophysical definition (e.g. the minimum and maximum specific leaf area parameters, **slamin_p** and **slamax_p** or the minimum temperature for photosynthesis, **temin_p**). We can assume that such parameters can be obtained independently from the model through experiments, especially those carried out in controlled environments. However, some parameters have no clear biophysical definition or encompass many processes (e.g. the maximal lifespan of an adult leaf, **durvieF_p** or the interplant competition parameter, **adens_p**). These parameters are difficult or sometimes impossible to measure with experiments and must be set by using mathematical-parameter

1. (https://w3.avignon.inra.fr/forge/projects/stics_main_projecu/boards)

estimation techniques. This typically consists in finding the parameter values which minimise a distance between the results of model simulations obtained on an experimental dataset and the corresponding observations for a given set of variables of interest. We will call this process ‘**model calibration**’ in the remainder of the chapter.

It is difficult to propose a single process to adapt STICS to new crops or cultivars, because it is bound to the user aim, relevant plant, experimental data, available bibliography, and possible analogy between the crop/cultivar of interest and those already parameterised in STICS. Moreover, the crop modelling community is nowhere near a consensus on how to calibrate crop models (Wallach *et al.*, 2021). Thus, this chapter puts forward several methodological elements, guidelines, specific information about STICS, and bibliographic and software references to help users determine their own methodology according to their particular situation. Readers will find more detailed information, especially on statistical methods, in the excellent book by Daniel Wallach *et al.* (2018).

16.3.2 Choosing simulation options

Formalism option choices can depend on several factors. First, they can be based on ecophysiological and agronomical knowledge of the plant to represent: Is it a dicotyledon or monocotyledon? Annual or perennial? Does the stand quickly become homogeneous during growth (e.g. wheat, corn, sugar beet), or should the radiative transfer approach be applied (e.g. in the case of grapevine or intercropping)? Does the plant undergo vernalisation or dormancy? Photoperiodic development? Is there competition between the vegetative and harvested organ growth (e.g. in indeterminate plants, such as sugar beet, tomato or grapevine)? § 15.3 lists the available formalism options. Choices done for different plants are illustrated in Figure 2.5.

The user can also determine some formalism choices: Which choice is best considering the output variable the user is interested in? What is the most or least important process for the case at hand? For example, for leaf coverage, if the user determines that this process is not critical for his/her simulations and that there is not enough information to parameterise a more mechanistic formalism, the user could choose to calculate a coverage rate rather than a leaf area index. In this case, the formalism choices must be adapted to the model use purpose.

Finally, some choices are made by default due to a lack of plant and environmental data. Some more mechanistic formalisms that require more parameters can be replaced with others that are more empirical but easier to configure.

16.3.3 Model calibration

16.3.3.1 Objective and dataset

Just like the preliminary model evaluation process, defining the objective and associated target population for the model calibration process is crucial and helps determine the requirements for the choice of the existing dataset to use or for the dedicated experiment to set-up.

The results of the model calibration process can be highly dependent on the type and quantity of observations of model outputs used (see e.g. Guillaume *et al.* (2011) or He *et al.* (2017)). This raises the question of which data to use for model calibration. The

same principles as outlined for model evaluation can also be applied for model calibration (see § 16.2): more specifically, the selected dataset must be as representative of the target population as possible, i.e. in terms of the variability of conditions and variables to predict.

Should all available variables be used in the calibration process? Two opposite approaches can be considered:

- Use all available observed variables: This would produce the best results if the model were perfect – but it is not. Due to misspecifications in the model and errors in fixed parameters, the parameter values that produce the best predictions for different variables are not the same. This means that using all observed variables for calibration generally results in a sort of compromise rather than the best predictions.
- Use only the observations of the target variable(s): This may produce the best predictions for these variable(s), but may not for others. It could even produce worse predictions than the default parameter values (Guillaume *et al.*, 2011).

When adapting the model to a new crop or cultivar, even if there is only one target variable, we recommend using several observed variables to at least roughly calibrate the different processes involved in the model. The tables given in § 16.3.3.4 describe the list of the main parameters and associated variables for the main model processes. When resetting the parameters to improve the model prediction performance for a particular objective, i.e. if a set of parameter values for the crop and the cultivar considered is already available, then we would instead suggest keeping only observations of the target variable(s).

16.3.3.2 Initial Setting

The chosen formalism options determine the list of active parameters in the model. This list can be displayed in the JavaStics graphical user interface (menu Model inputs > Global parameters > Plant and genotype) or by editing the XML plant file used. For a cultivar adaptation, only cultivar parameters of the considered crop should be changed, i.e. those included in the ‘cultivar parameters’ section of the associated plant file. For a new crop adaptation, it is often advisable to start from an existing plant file of a functionally or ecophysiologicaly related crop to have default values for all parameters. Note, however, that the distinction between species and cultivar parameters is still under debate. If users want to consider a species parameter as a cultivar one, they can create different plant files for different cultivars of the same crop.

The values of some of these parameters can then be estimated either by using experimental data, information from the literature or analogy to other species. For instance, the base temperatures of the development and growth processes are often available in the literature. Experimental measurements of key development stages can then be used to calculate some phenological parameters using the previously estimated base temperature. Regarding yield, maximum grain weight and maximum number of grains can often be determined using the maximal values measured in experiments (providing that treatments not causing water or N stress are available) or available in the literature. The parameter values that are not available in the literature or from experiments can be set by analogy to other crops or cultivars, especially if they are not very sensitive or are quite constant among crops/cultivars. For example, the parameter **idebdorm_p** (day of dormancy start), may be fixed at an early date, such as August 1, which prevents missing out the early cold periods.

16.3.3.3 Choosing the parameters to calibrate

Available datasets often do not allow a robust estimate of all crop model parameters using calibration processes. This often leads to parameter values that make the model well fit the data used for calibration, but not the independent data. Parameters to estimate using calibration processes must thus be chosen, and other parameters set to the default value determined during the initial setting step (see previous section).

In short, if some parameters are not estimated using calibration and are set to erroneous values, and if the observed outputs used in the calibration process are sensitive to the corresponding errors, this will lead to errors in estimated parameters. However, estimating too many parameters with respect to the quantity of information included in the observed dataset will lead to considerable uncertainty in parameter values, and thus in model simulations, due to either compensation between parameters or low sensitivity. This is often referred to as the equifinality problem: different parameter values may lead to an equivalent model fit to observations. A mechanistic model should not be changed into a statistical model, and model calibration must not become a cumbersome method for curve fitting: this is what happens when trying to estimate too many parameters with respect to the information in the dataset using model calibration.

Selecting the parameters to estimate is a major problem in crop model calibration (Seidel *et al.*, 2018), and it is still very difficult to recommend a single selection procedure. Although several methods exist, very few elements in the literature are helpful in making an objective choice. This book does not aim to detail the existing methods, but rather touch on the main options and provide specific information and feedback about the STICS model.

First, expertise on the calibrated model may be extremely useful to select a first set of candidate parameters to estimate. Parameters that should significantly impact the selected observed variables should be candidates. § 16.3.3.4 provides tables that list the main parameters for each model process depending on the type of model calibration application.

Sensitivity analysis may provide elements to further assess the impact of the model parameters on the target and observed outputs for the considered dataset, given the range of uncertainty of the different candidate parameters. If a given parameter does not impact a given observed output variable on the range of observed situations, there is little chance that its estimation using this observed variable will improve model performance. Sensitivity analysis may thus be useful to initially narrow down model parameters by excluding those that do not impact the observed variables. Global sensitivity analysis methods are preferable since they take into account parameter interactions (Saltelli *et al.*, 2019). They can be applied directly to the optimised criterion to simultaneously take into account several variables and situations (Ratto *et al.*, 2001).

Finally, some **model selection** techniques often used in statistical modelling may also be useful. For example, Akaike's or Bayesian information criteria (known by the acronyms AIC or BIC) are a relatively computationally inexpensive way to compare the quality of different models (e.g. a single mechanistic model but with different parameter values) with a given dataset. They compute the trade-off between the goodness

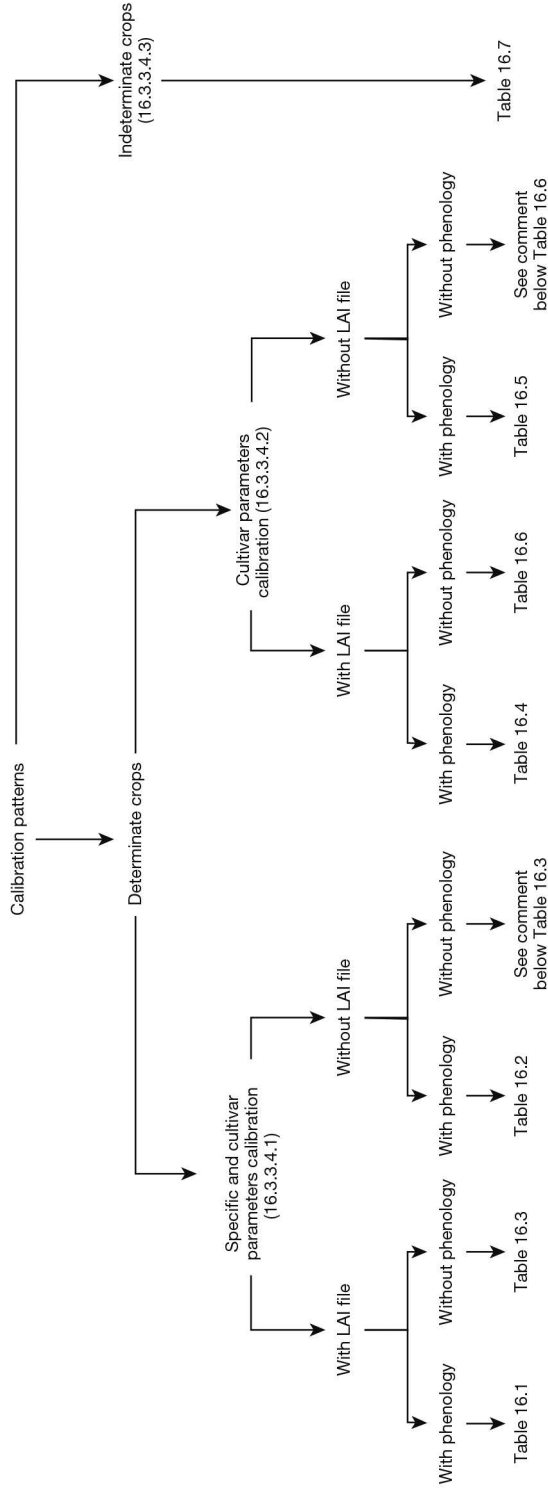


Figure 16.1. Proposed calibration patterns.

of fit and the simplicity of the model, i.e. between the risk of overfitting and underfitting. If users have doubts about including a parameter or set of parameters in the list of parameters to estimate in the calibration process, they can perform the calibration with and without the (set of) parameter(s) and compare the information criterion values obtained to decide which list of parameters should be estimated (see Tremblay and Wallach (2004) for an example of this technique in use).

Parameter values should be adjusted within plausible ranges. It is advisable to gather prior information about the parameter values and to use bound-constraint minimisation or Bayesian methods to include this information in the calibration process.

16.3.3.4 Calibration patterns

Traditionally, multi-step procedures have been used to calibrate the STICS crop model to adapt it to new crops or cultivars. The calibration process is divided into several consecutive steps. Depending on the calibration objective (specific or cultivar), the type of plant and the data available, the following tables propose several series of steps for each step, with a list of parameters to estimate and observed variables to use. This information, resulting from the expertise on the model, can be combined with the methods presented above to determine a calibration scheme adapted to its own case (Figure 16.1). When leaf area index (LAI) and/or phenology information is available, it is possible to use these observations to drive the model during the calibration process. This is called ‘forcing’ in the following tables. Finally, when certain formalism options are activated, additional parameters must be calibrated. When nothing is specified or when ‘in all situations’ is noted, this means that these parameters can be calibrated regardless of the chosen formalism.

16.3.3.4.1 Specific and cultivar: the case of a determinate plant

With *.lai files available and the dates of observed stages (in the following tables, “emergence date” means “emergence date” or “bud burst date” depending on whether the crop is annual or perennial)

Table 16.1. Calibration pattern 1

Step	Forcing	Process	Parameters to calibrate	Targeted variable
1		Root growth	croirac	zrac, HR or resmes
		Standard profile (does not allow soil C simulation)	zlabour, zpente, zprlim	HR, resmes and/or azomes
1a	LAI + phenological stages	Root growth	draclong, debsenrac, lvfront	HR, resmes, azomes, msrac, or LRACH and C&N stocks evolution (under perennial crops)
		True density (required to simulate soil C dynamic)	+ activation of continuous trophic linked production: repracpermax, repracpermin, krepracperm	

Step	Forcing	Process	Parameters to calibrate	Targeted variable
1a	Root growth	True density (required to simulate soil C dynamic)	+ activation of standard Root distribution: kdisrac, alloperirac + activation of simulation of 2 Root classes (recommended for perennial crops): RTD, rapdia, propracfmax	HR, resmes, azomes, msrac, or LRACH and C&N stocks evolution (under perennial crops)
2	Biomass growth	In all situations	efcroijuv, efcroiveg, efcroirepro, teopt, teoptbis, sea, psisto	masec
		Additional parameters for simulation of C reserves	propresP + Propres + tauxmortresp	masecnp, maperenne
3	LAI + phenological stages Nitrogen absorption	In all situations	vmax2, inngrain1, inngrain2, INNmin	QNplante
		Additional parameters for simulation of N partitioning (structural N, reserves and Root)	PropresPN + parazoper + parazorac + parazofmorte, parazotmorte	QNplantenp, QNperenne, QNrnc
		Additional parameters for legumes	fixmaxveg, fixmaxgr, concNrnc0, concNrnc100	Qfix
4	Elaboration of yield		vitircarb/vitircarbT, IRmax, tmaxremp, nbgrmax, pgrainmaxi	mafruit
5	Elaboration of the quality of harvested organs		Vitirazo, stdrpdcs, tempdeshyd, deshydbase, vitprophuile, vitpropsucre	CNgrain, H2Orec, oil, sugar
6	Development		stlevamf, jvc, sensiphot	IAMF
			stamflax, stlevdrp, stdrpmat	ILAX, IDRP, IMAT
7	Emergence date Foliage growth		dlaimaxbrut/dlaimax, tigefeuill, innturgmin, innsen, rapsenturg, psiturg, adens, durvieF	LAI

Remarks:

- We suggest repeating steps 2 and 3 after step 7 to ‘balance’ the effects: 1, 1a, 2, 3, 4, 5, 6, 7, 2, 3.
- Step 1a can be skipped knowing that the resmes and azomes values, from which the root density growth settings are estimated, also depend on foliage growth (important

for calculating transpiration, which affects resmes) and aerial biomass growth (important for calculating nitrogen which affects azomes).

– Step 2 could be divided into two separate steps: one to estimate **efcroijuv_p**, **efcroiveg_p**, **efcroirepro_p**, **teopt_p**, **teoptbis_p**, on masec with USMs in “almost non-limiting” growth conditions, and one to estimate **psisto_p** on the same variable but with limited water conditions. The same approach could be applied for step 3 with the estimation of **Vmax2_p** using USMs without N stress and then the estimation of **inngrain1_p**, **inngrain2_p** and **INNmin_p** using USMs with N stress.

Without *.lai files available but with the dates of observed stages (in italics: information that differs from Table 16.1).

Table 16.2. Calibration pattern 2

Step	Forcing	Process	Parameters to calibrate	Targeted variable
1		Root growth	croirac	zrac, HR or resmes
		Standard profile (does not allow soil C simulation)	zlabour, zpente, zprlim	HR, resmes and/or azomes
			draclong, debsenrac, lvfront	
			+ activation of continuous trophic linked production: repracpermax, repracpermin, krepracperm	HR, resmes, azomes, msrac, or LRACH and C&N stocks evolution (under perennial crops)
1a	Phenological stages	Root growth	+ activation of standard root distribution: kdisrac, alloperirac	
		True density (required to simulate soil C dynamic)	+ activation of simulation of 2 Root classes (recommended for perennial crops): RTD, rapdia, propracfmax	
		In all situations	efcroijuv, efcroiveg, efcroirepro, teopt, teoptbis, sea, psisto	masec
2		Biomass growth	propresP + Propres + tauxmortresp	masecnp, maperenne
		Additional parameters for simulation of C reserves		
3		Nitrogen absorption	vmax2, inngrain1, inngrain2, INNmin	QNplante

Step	Forcing	Process	Parameters to calibrate	Targeted variable	
3		Nitrogen absorption	Additional parameters for simulation of N partitioning (structural N, reserves and Root)	PropresPN + parazorac + parazofmorte, parazotmorte	QNplantenp, QNperenne, QNrac
	Phenological stages		Additional parameters for legumes	fixmaxveg, fixmaxgr, concNrac0, concNrac100	Qfix
4		Elaboration of yield		vitircarb/vitircarbT, IRmax, tmaxremp, nbgmax, pgrainmaxi	mafruit
5		Elaboration of the quality of harvested organs		Vitirazo, stdrpdes, tempdeshyd, deshydbase, vitprophuile, vitpropsucre	CNgrain, H2Orec, oil, sugar
6		Development		stlevamf, jvc, sensiphot	IAMF
	Emergence date			stamflax, stlevdrp, stdrpmat	ILAX, IDRP, IMAT
7		Foliage growth		dlaimaxbrut/dlaimax, tigefeuil, innturgmin, innsen, rapsenturg, psiturg, adens, durvieF	LAI

Remarks:

- We can suggest an iterative process by following the steps in this order: 1, 2, 3, 6, 2, 3, 6, 2, 3, 4, 5, 6, 7 (to 'balance' the compensation effects).
- The same remarks as in Table 16.1 for steps 1a and 2.

With *.lai file available but without the dates of observed stages, except emergence date (in italics: information that differs from Table 16.1).

Table 16.3. Calibration pattern 3

Step	Forcing	Process	Parameters to calibrate	Targeted variable
1		Root growth	croirac	zrac, HR or resmes
		Standard profile (does not allow soil C simulation)	zlabour, zpente, zprlim	HR, resmes and/or azomes
1a		Root growth	draclong, debsenrac, lvfront	
		True density (required to simulate soil C dynamic)	+ activation of continuous trophic linked production: repracpermax, repracpermin, krepracperm	HR, resmes, azomes, msrac, or LRACH and C&N stocks evolution (under perennial crops)
			+ activation of standard root distribution: kdisrac, alloperirac	
			+ activation of simulation of 2 Root classes (recommended for perennial crops): RTD, rapdia, propracrfmax	HR, resmes, azomes, msrac, or LRACH and C&N stocks evolution (under perennial crops)
	LAI + emergence date			
2		Biomass growth	In all situations	efcroijuv, efcroiveg, efcroirepro, teopt, teoptbis, sea, psisto
			Additional parameters for simulation of C reserves	propresP + Propres + tauxmortresp
				masecnp, maperenne
3		Nitrogen absorption	In all situations	vmax2, inngrain1, inngrain2, INNmin
			Additional parameters for simulation of N partitioning (structural N, reserves and Root)	PropresPN + parazoper + parazorac + parazofmorte, parazotmorte
			Additional parameters for leguminous	fixmaxveg, fixmaxgr, concNrac0, concNrac100
				QNplante
				QNplantenp, QNperenne, QNrac
4		Elaboration of yield	vitircarb/vitircarbT, IRmax, tmaxremp, nbgmax, pgrainmaxi	mafruit
			<i>stlevdrp, stdrpmat</i>	

Step	Forcing	Process	Parameters to calibrate	Targeted variable
5	LAI + emergence date	Elaboration of the quality of harvested organs	Vitirazo, stdrpdes, tempdeshyd, deshydbase, vitprophuile, vitpropsucre	CNgrain, H2Orec, oil, sugar
6	Emergence date	Foliage growth	dlaimaxbrut/dlaimax, tigefeuill, innturgmin, innsen, rapsenturg, psiturg, adens, durvieF <i>stlevamf, stamflax, jvc (annual crops), sensiphot</i>	LAI

Without *.lai files available and without the dates of observed stages (except emergence date): we recommend starting with step 6 and then proceeding with steps 1, 2, 3, 4 and 5.

16.3.3.4.2 cultivar calibration schemes: the case of a determinate plant

The calibration patterns presented here can be used in the case of adding a new cultivar or recalibrating an existing cultivar and when the specific parameters have been previously calibrated.

With *.lai files available and the dates of observed stages

Table 16.4. Calibration pattern 4

Step	Forcing	Process	Parameters to calibrate	Targeted variable
1		Root growth	croirac	zrac, HR or resmes
2		Biomass growth	temin, teopt, extin, ktrou, psisto ¹	masec
3	LAI + Phenological stages	Biomass partitioning	slamax, tigefeuill	mafeuilverte, matigestruc
4		Elaboration of yield	vitircarb/vitircarbT, nbgrmax, pgrainmaxi	mafruit
5		Quality elaboration of harvested organs	vitirazo, stdrpdes, deshydbase, vitprophuile, vitpropsucre	CNgrain, H2Orec, oil, sugar
6	Emergence date	Development	stlevamf, jvc(annual crops), sensiphot stamflax, stlevdrp, stdrpmat	IAMF ILAX, IDRP, IMAT
7		Foliage growth	adens, bdens, durvieF, dlaimax, dlaimaxbrut, innsen, rapsenturg, psiturg ¹	LAI

¹ In the event of situations with and without water stress.

Without *.lai files available but with the dates of observed stages (in italics: information that differs from the first cultivar calibration scheme Table (Table 16.4).

Table 16.5. Calibration pattern 5

Step	Forcing	Process	Parameters to calibrate	Targeted variable
1		Root growth	croirac	zrac, HR or resmes
2		Biomass growth	temin, teopt, extin, ktrou, psisto ¹	masec
3	<i>Phenological stages</i>	Biomass partitioning	slamax, tigefeuill	mafeuilverte, matigestruc
4		Elaboration of yield	vitircarb/vitircarbT, nbgrmax, pgrainmaxi	mafruit
5		Quality elaboration of harvested organs	vitirazo, stdrpd, deshydbase, vitprophuile, vitpropsucre	CNgrain, H2Orec, oil, sugar
6	Emergence date	Development	stlevamf, jvc(annual crops), sensiphot	IAMF
			stamflax, stlevdrp, stdrpmat	ILAX, IDRP, IMAT
7		Foliage growth	adens, bdens, durvieF, dlaimax, dlaimaxbrut, innsen, rapsenturg, psiturg ¹	LAI

¹ In the event of situations with and without water stress.

Remarks:

– We can suggest an iterative process by following the steps in this order: 1, 2, 6, 2, 6, 2, 3, 4, 5, 6, 7.

With *.lai files available and without the dates of observed stages, except emergence date (or bud burst date) (in italics:: information that is different from the first cultivar calibration scheme Table (Table 16.4).

Table 16.6. Calibration pattern 6

Step	Forcing	Process	Parameters to calibrate	Targeted variable
1		Root growth	croirac	zrac, HR or resmes
2		Biomass growth	temin, teopt, extin, ktrou, psisto ¹	masec
3	<i>LAI + emergence date</i>	Biomass partitioning	slamax, tigefeuill	mafeuilverte, matigestruc
4		Elaboration of yield	vitircarb/vitircarbT, nbgrmax, pgrainmaxi stlevdrp, stdrpmat	mafruit
5		<i>Quality elaboration of harvested organs</i>	<i>vitirazo, stdrpd, deshydbase, vitprophuile, vitpropsucre</i>	<i>CNgrain, H2Orec, oil, sugar</i>
6		Roots growth	croirac	zrac, HR or resmes
7	Emergence date	Foliage growth	<i>adens, bdens, durvieF, dlaimax, dlaimaxbrut, innsen, rapsenturg, psiturg¹</i> stlevamf, stamflax, jvc (annual crops), sensiphot	LAI

¹ In the event of situations with and without water stress.

Without *.lai files available and without the dates of observed stages, except emergence date: adapt the process to this specific case.

Table 16.7. Calibration pattern 7

Step	Forcing	Process	Parameters to calibrate	Targeted variable
1		Root growth	croirac	zrac or resmes
1a	LAI + Phenological stages	Standard profile (does not allow soil C simulation)	zlabour, zpente, zprlim	resmes and/or azomes
		Root growth True density (required to simulate soil C dynamic)	draclong, debsenrac, lvfront + activation of continuous trophic linked production: repracpermax, repracpermin, krepracpermin + activation of standard root distribution: kdisrac, alloverirac + activation of simulation of 2 Root classes (recommended for perennial crops): RTD, rapdia, propracfmax	resmes, azomes, msrac, or LRACH and C&N stocks evolution (under perennial crops)
2		In all situations	efcroijuv, efcroiveg, efcroirepro, teopt, teoptbis, remobres, abscission, psisto	masec
		Biomass growth Additional parameters for simulation of C reserves	propresP + Propres + tauxmortresp	masecnp, maperenne
3		In all situations	vmax2, INNmin	QNplante
		Nitrogen absorption Additional parameters for simulation of N reserves Additional parameters for legumes	PropresPN + parazoper fixmaxveg, fixmaxgr, concNrac0, concNrac100	QNplantenp, QNperenne Qfix
4	Phenological stages	Foliage growth, elaboration of yield and nitrogen absorption	Innimin, innsen, rapsenturg, dlaimaxbrut/dlaimax, slamax, spfirmin, splaimin, rsmin, tigefeuill, durvieF, afruitpot, pgrainmaxi	LAI, mafruit, QNplante, nbfruit
5		Elaboration of the quality of harvested organs	Vitirazo, stdrpdes, tempdeshyd, deshydbase, vitprophuille, vitpropsucre	CNgrain, H2Orec, oil, sugar
6	Emergence date	Development	stlevamf, jvc (annual crops), sensiphot	IAMF
			stamflax, stlevdrp	ILAX, IDRP

16.3.3.4.3 Specific and cultivar calibration schemes: the case of an indeterminate plant

With *.lai files available and the dates of observed stages

Same remarks as for determinate plants:

- We suggest repeating step 2 after step 6 to ‘balance’ the effects: 1, 1a, 2, 3, 4, 5, 6, 2.
- Step 1a can be skipped if necessary, knowing that resmes and azomes values depend on foliage and aerial biomass growth.
- Step 2 could be divided into two steps: one to estimate **efcroijuv_p**, **efcroiveg_p**, **efcroirepro_p**, **teopt_p**, **teoptbis_p**, **Vmax2_p** on masec and QNplante with USMs in “almost non-limiting” growth conditions, and one to estimate **inngrain1_p**, **inngrain2_p**, **INNmin_p**, **psisto_p** on the same variables but with water and nitrogen limited.

The same main patterns can be used for indeterminate crops (with LAI and without stages, or with stages but without LAI, for cultivar calibration only).

16.3.3.5 Methods and tools

Two different families of methods are often considered for parameter estimation: **frequentist** and **Bayesian** methods.

Frequentist methods involve minimising a goodness-of-fit criterion, i.e. trying to find a single set of parameter values that minimise a distance between the selected model variables and the corresponding observations on the given dataset. These methods are often iterative: starting from initial parameter values, they sequentially propose new values until they (hopefully) converge toward the global minimum value of the criterion. Often, crop models have discontinuities and are coded in single-precision format, which make it difficult to use well-known gradient-based minimisation methods such as Gauss–Newton or Levenberg–Marquardt. A common approach is thus to use the Nelder–Mead simplex algorithm, which is adapted to non-smooth functions because the search for the optimum value is not based on the computation of the function’s gradient. Although few theoretical results are available (Lagarias *et al.*, 1998), this algorithm is very popular because it can be used for multidimensional minimisation for essentially any function. As it may be sensitive to the presence of local minima, it is often advisable to repeat the minimisation from different initial values of the parameters (including their default values). Examples using the STICS model are numerous and can be found in the literature (e.g. Guillaume *et al.* (2011); Jégo *et al.* (2012a) or Falconnier *et al.* (2019)).

Bayesian methods consider the estimated parameters as random variables and seek to assess their joint probability distribution, called the posterior distribution. The uncertainty in the estimated parameters is thus central to this approach. Another advantage of the Bayesian approach is that it uses prior information about the parameter values that may provide substantial information. Markov Chain Monte Carlo (MCMC) methods are iterative methods that are classically used to estimate posterior distributions. Among them, the DREAM_(ZS) algorithm is recognised as an efficient method for estimating complex, high-dimensional and multi-modal posterior distributions. It is extensively described in Vrugt (2016) and has been used in Dumont *et al.* (2014) for estimating STICS parameters. GLUE is another popular method for estimating posterior distributions on crop models (Makowski *et al.* (2002), Varella *et al.* (2010b), He *et al.* (2009), Sheng *et al.* (2019)) and has the advantage of being easily parallelised compared to MCMC methods.

Estimates from all these methods are based on the computation of a distance between the selected model variables and corresponding observations on the given dataset. Wallach *et al.* (2011) and He *et al.* (2010) selected different distances adapted for crop models.

The CROPTIMIZR R package (Buis *et al.*, 2021) is dedicated to crop model calibration and includes different types of methods and goodness-of-fit criteria. It has been interfaced with the STICS model through the SticsOnR (Lecharpentier *et al.*, 2021a) and SticsRFiles (Lecharpentier *et al.*, 2021b) packages (see § 15.5.2). Examples of use with STICS are described in the CROPTIMIZR documentation.

16.3.3.6 Evaluating the results

How can the quality of the calibration results be evaluated?

First, the method used must be checked for solution convergence for the mathematical problem posed:

- Frequentist iterative methods often use a statistical criterion to assess how well the estimated parameters converged toward the solution to stop the minimisation process. However, they also often integrate other stopping criteria (e.g. based on the number of iterations or detection of numerical problems). This means that after the calibration, users must check that the method stopped using a convergence criterion. If the minimisation process is repeated based on different initial values, and if the different repetitions produce very different final parameter values, users can run the calibration again by increasing the number of repetitions based on different initial values to check if the global minimum of the minimised criterion has been reached.
- MCMC methods are often applied on a predetermined number of iterations. Specific convergence criteria can then be used a posteriori to check if the Markov Chain(s) converged to the posterior distribution (Vehtari *et al.*, 2021). If not, the method should be run again from the point it had stopped to increase the number of iterations and reach convergence.

Next, users must check that the calibration method did indeed minimise the distance between the simulations and observations, i.e. that the simulations using the estimated parameter values are closer to the observations than the simulations using the initial values, as computed from the goodness-of-fit criterion used in the calibration process.

Evaluating the estimated parameter values is also often advisable. In particular, users should systematically check that the estimated parameter values lie within accepted physiological ranges. If not, or if they stick to their bounds, this is often due to error compensation: either the model is missing a process to adequately represent the system under study, or some of the (non-estimated) input parameters are set to inadequate values or there are errors in observed values. In addition, compensations between estimated parameter values may lead to a good fit to observations used in the calibration process but to a poor fit on independent datasets. Such compensations can be identified using correlation matrices.

Finally, the results of the calibrated model must be evaluated based on a dataset that is:

- representative of the target population,
- not used in the calibration process, and which is as independent as possible from that process.

One part of the original dataset is often used for the calibration process and another for evaluation. The evaluation process is then similar to the one described in § 16.2. There are, however, many ways to divide the dataset into two parts, and doing so means that a significant part of the dataset will not be used for the parameter estimation step. Cross-validation techniques can be used to avoid these drawbacks, but they are much more computationally expensive (see e.g. Daniel Wallach *et al.* (2018) for more details).

►► 16.4 Tools and rules for model coupling

This section explains several technical aspects of the methods to extend the current STICS model version beyond its initial scope. Applications of such coupling approaches are extensively described in § 14.4.

16.4.1 Overview of STICS model software architecture

The STICS Fortran 90 source code base can be viewed as a two-part software application: the modelling modules (where all the sub-model equations are defined), and a simulation engine (handling simulation time and communication management among the modules).

The execution steps for a single simulation in the program are as follows (and illustrated in Figure 16.2):

- First, several initialisation steps, where the user parameters are read in their respective input files, and additional initialisation validations and computations are made (such as the reference evapotranspiration estimation - see § 15.1.1.2 or § 15.1.1.3, or parameters forcing using *param.sti* files - see § 16.4.3).
- Next, two nested loops (yearly and daily), where the main computations are performed to estimate the evolution of the system modelled.
- Finally, the finalisation steps to produce output files.

16.4.2 IT view on typology of model coupling approaches

There are two main model coupling approaches: **internal** and **external** coupling. By ‘internal coupling’, we mean the integration of new code within the STICS model (including both its simulation engine as well as all existing modelling modules). For example, the MILA-STICS coupling described in § 14.4.2 is an example of internal coupling. By ‘external coupling’, we mean the use and extension of all or part of the STICS modelling modules with a different alternative simulation engine, such as with the FLORSYS and Hi-sAFe coupling described in § 14.4.2. For details on how to integrate new code within the STICS model, see § 1.5.2.

Coupling approaches can also be described as **tight** or **loose**. Here, ‘tight coupling’ is where the information exchanged between the different parts is done at the daily time step, as with the MouSTICS coupling described in § 14.4.2. ‘Loose coupling’ is typically done at the whole USM scale (generally using input and output files).

When using an external and tight coupling approach, users must take into consideration the specificity of the simulation engine architecture of STICS. When using an external and loose coupling approach, users must take into consideration the content and structure of the input and output files (§ 1.4.1).

16.4.3 Things to consider when coupling models with STICS

To a certain extent, the STICS model can be considered as a ‘big leaf’ model - it simulates an homogeneous surface (STICS does nonetheless take into account some spatial heterogeneity, such as the light interception of row crops, or intercroops - see § 9, or the discretisation of soil and root functioning in the soil profile - see § 5). This means that to represent more spatial heterogeneity in a coupled model, users will probably need to have several separate instances of the STICS model to manage the corresponding heterogeneity.

The use of STICS for large-scales applications requires some expertise on the soil and technical input data. For a detailed discussion of this issue, see § 14.3.

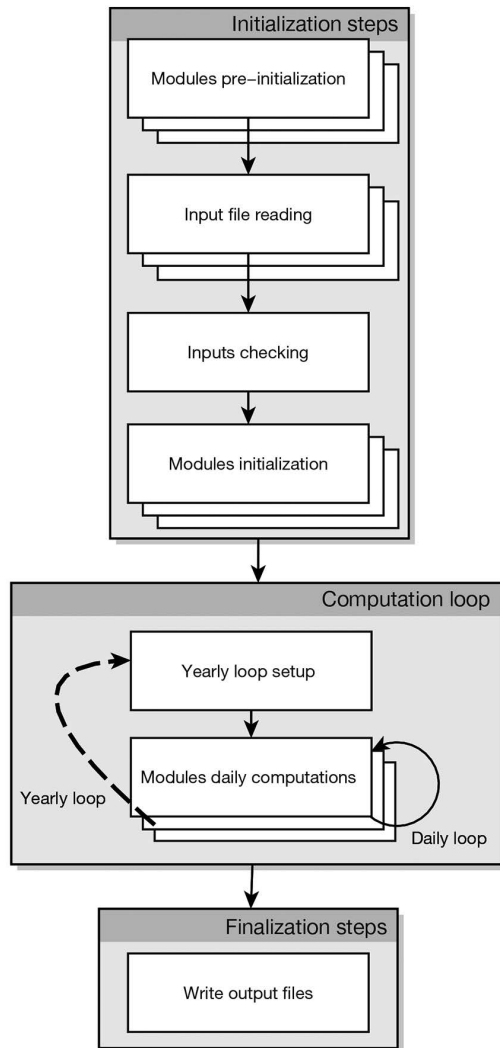


Figure 16.2. Schematic view of the STICS source code architecture.

The STICS software expects all its input files to be in the same working directory with fixed names. As such, if users want to manage a parallel use of the model, they will need to either manage separate directories for each individual simulation or tell the model where to find those files with different locations or names.

A STICS simulation using consecutive USMs (§ 14.1) is computed as several separate simulations (with the internal state stored and/or restored from a *recup.tmp* file when changing the USM).

When using **codeetp_C** options involving calculations (options 2, 3 and 4), the calculations are performed during the input checking part of initialisation step. Accordingly, to integrate climate external data directly into the computation loop, users must have also performed those potential evapotranspiration (ETP) calculations externally and provided ETP as forced Penman (option 1).

One aspect to consider carefully can be an ‘off by one’ error when using a variable value (a large number of variables holds only a single value corresponding to the variable calculation performed in the previous daily step or the current day depending on when you try to access these values). Some variables correspond to daily state variables and others are integrated on various time spans. The *CorrespondanceVariablesDeSorties* subroutine can be used to get access to the variable values. The *SticsRFiles* R package can also be used to handle STICS output files extraction (§ 15.5.2).

Forcing parameters without modifying the main STICS input files can be done by using the *param.sti* file read by the subroutine *Lecture_Optimisation* between the main input files read and inputs checking steps. This *param.sti* file is a text file that must contain the list and associated values of the STICS parameters to force (the name of the parameter on one line and its value on the following line). Any type of parameters (soil, plant, technical, option codes, etc.) can be forced using this file. The *SticsRFiles* R package (§ 15.5.2) can also be used to handle STICS input files modifications.

References

- Abbad H., El Jaafari S., Bort J., Araus J., 2004. Comparison of flag leaf and ear photosynthesis with biomass and grain yield of durum wheat under various water conditions and genotypes. *Agronomie* 24, 19–28. <https://doi.org/10.1051/agro:2003056>
- Abiven S., Recous S., Reyes V., Oliver R., 2005. Mineralisation of C and N from root, stem and leaf residues in soil and role of their biochemical quality. *Biology and Fertility of Soils* 42, 119–128. <https://doi.org/10.1007/s00374-005-0006-0>
- Addiscott T.M., Wagenet R.J., 1985. Concepts of solute leaching in soils: A review of modelling approaches. *European Journal of Soil Science* 36, 411–424. <https://doi.org/10.1111/j.1365-2389.1985.tb00347.x>
- Adiku S.G.K., Ozier-Lafontaine H., Bajazet T., 2001. Patterns of root growth and water uptake of a maize-cowpea mixture grown under greenhouse conditions. *Plant and Soil* 235, 85–94. <https://doi.org/10.1023/A:1011847214706>
- Affholder F., Poeydebat C., Corbeels M., Scopel E., Tiftonell P., 2013. The yield gap of major food crops in family agriculture in the tropics: Assessment and analysis through field surveys and modeling. *Field Crops Research* 143, 106–118. <https://doi.org/10.1016/j.fcr.2012.10.021>
- Affholder F., Scopel E., Neto J.M., Capillon A., 2003. Diagnosis of the productivity gap using a crop model. Methodology and case study of small-scale maize production in central Brazil. *Agronomie* 23, 305–325. <https://doi.org/10.1051/agro:2003004>
- Al Majou H., Bruand A., Duval O., Le Bas C., Vautier A., 2008. Prediction of soil water retention properties after stratification by combining texture, bulk density and the type of horizon. *Soil Use and Management* 24, 383–391. <https://doi.org/10.1111/j.1475-2743.2008.00180.x>
- Allaire J., Xie Y., McPherson J., Luraschi J., Ushey K., Atkins A., Wickham H., Cheng J., Chang W., Iannone R., 2021. Rmarkdown: Dynamic documents for r.
- Allen R.G., Pereira L.S., Raes D., Smith M., 1998. Crop evapotranspiration-Guidelines for computing crop water requirements-. *Fao, Rome* FAO Irrigation and drainage paper, 300 pages.
- Allen R.G., Smith M., Perrier A., Pereira L.S., 1994. An update for the definition of reference evapotranspiration. *ICID bulletin* 43, 1–34.
- Allen W.A., Richardson A.J., 1968. Interaction of light with a plant canopy. *Journal of the Optical Society of America* 58, 1023. <https://doi.org/10.1364/JOSA.58.001023>
- Alm D.M., Stoller E.W., Wax L.M., 1993. An index model for predicting seed germination and emergence rates. *Weed Technology* 7, 560–569. <https://doi.org/10.1017/S0890037X00037349>
- Amir J., Sinclair T.R., 1991. A model of the temperature and solar-radiation effects on spring wheat growth and yield. *Field Crops Research* 28, 47–58. [https://doi.org/10.1016/0378-4290\(91\)90073-5](https://doi.org/10.1016/0378-4290(91)90073-5)
- Angus J.F., Mackenzie D.H., Morton R., Schafer C.A., 1981. Phasic development in field crops II. Thermal and photoperiodic responses of spring wheat. *Field Crops Research* 4, 269–283. [https://doi.org/10.1016/0378-4290\(81\)90078-2](https://doi.org/10.1016/0378-4290(81)90078-2)
- Antonioletti R., 1986. Contribution à l'étude du climat du MontVentoux (Document interne INRA). Station de Bioclimatologie (INRA), Montfavet (FRA).
- Araus J.L., Brown H.R., Febrero A., Bort J., Serret M.D., 1993. Ear photosynthesis, carbon isotope discrimination and the contribution of respiratory CO₂ to differences in grain mass in durum wheat. *Plant, Cell and Environment* 16, 383–392. <https://doi.org/10.1111/j.1365-3040.1993.tb00884.x>

- Araya S., Lyle G., Lewis M., Ostendorf B., 2016. Phenologic metrics derived from MODISNDVI as indicators for PlantAvailableWater-holding Capacity. *Ecological Indicators* 60, 1263–1272. <https://doi.org/10.1016/j.ecolind.2015.09.012>
- Asseng S., Martre P., Maiorano A., Rötter R.P., O'Leary G.J., Fitzgerald G.J., Girousse C., Motzo R., Giunta E., Babar M.A., Reynolds M.P., Kheir A.M.S., Thorburn P.J., Waha K., Ruane A.C., Aggarwal P.K., Ahmed M., Balkovič J., Basso B., Biernath C., Bindi M., Cammarano D., Challinor A.J., Sanctis G.D., Dumont B., Rezaei E.E., Fereres E., Ferrise R., Garcia-Vila M., Gayler S., Gao Y., Horan H., Hoogenboom G., Izaurralde R.C., Jabloun M., Jones C.D., Kassie B.T., Kersebaum K.-C., Klein C., Koehler A.-K., Liu B., Minoli S., Martin M.M.S., Müller C., Kumar S.N., Nendel C., Olesen J.E., Palosuo T., Porter J.R., Priesack E., Ripoche D., Semenov M.A., Stöckle C., Stratonovitch P., Streck T., Supit I., Tao F., Velde M.V. der, Wallach D., Wang E., Webber H., Wolf J., Xiao L., Zhang Z., Zhao Z., Zhu Y., Ewert F., 2019. Climate change impact and adaptation for wheat protein. *Global Change Biology* 25, 155–173. <https://doi.org/10.1111/gcb.14481>
- Aura E., 1996. Modelling non-uniform soil water uptake by a single plant root. *Plant and Soil* 186, 237–243. <https://doi.org/10.1007/BF02415519>
- Autret B., Mary B., Strullu L., Chlebowski F., Mäder P., Mayer J., Olesen J.E., Beaudoin N., 2020. Long-term modelling of crop yield, nitrogen losses and GHG balance in organic cropping systems. *Science of The Total Environment* 710. <https://doi.org/10.1016/j.scitotenv.2019.134597>
- Avicé J.C., Ourry A., Lemaire G., Boucaud J., 1996. Nitrogen and carbon flows estimated by ¹⁵N and ¹³C pulse-chase labeling during regrowth of alfalfa. *Plant Physiology* 112, 281–290. <https://doi.org/10.1104/pp.112.1.281>
- Baier W., 1969. Concepts of soil moisture availability and their effect on soil moisture estimates from a meteorological budget. *Agricultural Meteorology* 6, 165–178. [https://doi.org/10.1016/0002-1571\(69\)90002-8](https://doi.org/10.1016/0002-1571(69)90002-8)
- Baldocchi D.D., Luxmoore R.J., Hatfield J.L., 1991. Discerning the forest from the trees: An essay on scaling canopy stomatal conductance. *Agricultural and Forest Meteorology* 54, 197–226. [https://doi.org/10.1016/0168-1923\(91\)90006-C](https://doi.org/10.1016/0168-1923(91)90006-C)
- Balesdent J., Recous S., 1997. Les temps de résidence du carbone et le potentiel de stockage de carbone dans quelques sols cultivés français. *Canadian Journal of Soil Science* 77, 187–193. <https://doi.org/10.4141/S96-109>
- Barber S.A., Silberbush M., 2015. Plant root morphology and nutrient uptake, in: Barber, S.A., Bouldin, D.R. (Eds.), *Roots, Nutrient and Water Influx, and Plant Growth*, ASA Special Publications. American Society of Agronomy, Crop Science Society of America; Soil Science Society of America, Madison, WI, USA, pp. 65–87. <https://doi.org/10.2134/asaspecpub49.c4>
- Barbottin A., Lecomte C., Bouchard C., Jeuffroy M.-H., 2005. Nitrogen remobilization during grain filling in wheat: Genotypic and environmental effects. *Crop Science* 45, 1141–1150. <https://doi.org/10.2135/cropsci2003.0361>
- Baret F., 1986. Contribution au suivi radiométrique de cultures de céréales (Thèse de doctorat). Université de Paris XI.
- Baret F., Andrieu B., Folmer J.C., Hanocq J.F., Sarrouy C., 1993. Gap fraction measurement from hemispherical infrared photography and its use to evaluate PAR interception efficiency, in: Varlet-Grancher, C., Bonhomme, R., Sinoquet, H. (Eds.), *Crop Structure and Light Microclimate. Characterization and Applications*, Science Update. INRA Editions, Versailles, France, pp. 359–372.
- Baret F., Houles V., Guérif M., 2007. Quantification of plant stress using remote sensing observations and crop models: The case of nitrogen management. *Journal of Experimental Botany* 58, 869–880. <https://doi.org/10.1093/jxb/erl231>
- Baret F., Olioso A., Luciani J.L., 1992. Root biomass fraction as a function of growth degree days in wheat. *Plant and Soil* 140, 137–144. <https://doi.org/10.1007/BF00012815>
- Beaudoin N., 2006. Experimental analysis and modelling of the effects of cropping practices on nonpoint nitrate pollution of a deep aquifer in an arable farming area (Thèse de doctorat). Institut National Agronomique Paris-Grignon.

- Beaudoin N., Gallois N., Viennot P., Le Bas C., Puech T., Schott C., Buis S., Mary B., 2018. Evaluation of a spatialized agronomic model in predicting yield and N leaching at the scale of the Seine-Normandie Basin. *Environmental Science and Pollution Research* 25, 23529–23558. <https://doi.org/10.1007/s11356-016-7478-3>
- Beaudoin N., Launay M., Ripoche D., Buis S., Justes E., Ruget F., Jégo G., García de Cortázar Atauri I., Léonard J., Raynal H., de Noblet-Ducoudre N., Seguin B., Lescouret F., Aubertot J.-N., Habets F., Jayet P.A., Gate P., Mary B., 2019. Modélisation du fonctionnement des agro-écosystèmes: L'épopée STICS, in: Richard, G., Stengel, P., Lemaire, G., Cellier, P., Valceschini, E. (Eds.), *Une Agronomie Pour Le XXIe Siècle*. Editions Quae, pp. 138–149.
- Beaudoin N., Launay M., Sauboua E., Ponsardin G., Mary B., 2008. Evaluation of the soil crop model STICS over 8 years against the "on farm" database of Bruyeres catchment. *European Journal of Agronomy* 29, 46–57. <https://doi.org/10.1016/j.eja.2008.03.001>
- Beaudoin N., Venet E., Maucorps J., Vandenberghe C., Pugeaux N., Viennot P., Gourcy L., Brayer C., Machet J.-M., Couturier A., Billy C., Vigour N., Hulin G., Dorel G., Mary B., 2021. Long term response of water and nitrogen fluxes to Good Agricultural Practices at field and catchment scales. *Science of The Total Environment* 776. <https://doi.org/10.1016/j.scitotenv.2021.145954>
- Beaujouan V., Durand P., Ruiz L., Aurousseau P., Cotteret G., 2002. A hydrological model dedicated to topography-based simulation of nitrogen transfer and transformation: Rationale and application to the geomorphology-denitrification relationship. *Hydrological Processes* 16, 493–507.
- Beblik A., Kersebaum K.C., 2001. Performance of a nitrogen dynamics model applied to evaluate agricultural management practices, in: Shaffer, M.J., Ma, L., Hansen, S. (Eds.), *Modeling Carbon and Nitrogen Dynamics for Soil Management*. CRC Press, Boca Raton, USA, pp. 550–569.
- Bedoussac L., Tribouillois H., Plaza Bonilla D., Journet E.-P., Justes E., 2017. Designing and evaluating arable cropping systems with cash and cover crop legumes in sole crop and intercrop to improve nitrogen use efficiency. *Agricultural Research & Technology Open Access Journal* 12. <https://doi.org/10.19080/ARTOAJ.2017.12.555842>
- Bélangier G., Rochette P., Castonguay Y., Bootsma A., Mongrain D., Ryan D.A.J., 2002. Climate change and winter survival of perennial forage crops in Eastern Canada. *Agronomy Journal* 94, 1120–1130. <https://doi.org/10.2134/agronj2002.1120>
- Bellocchi G., Acutis M., Fila G., Donatelli M., 2002. An indicator of solar radiation model performance based on a fuzzy expert system. *Agronomy Journal* 94, 1222–1233. <https://doi.org/10.2134/agronj2002.1222>
- Bellocchi G., Rivington M., Donatelli M., Matthews K., 2011. Validation of biophysical models: Issues and methodologies, in: Lichtfouse, E., Hamelin, M., Navarrete, M., Debaeke, P. (Eds.), *Sustainable Agriculture*. Springer, Dordrecht, The Netherlands, pp. 577–603. https://doi.org/10.1007/978-94-007-0394-0_26
- Bellocchi G., Rivington M., Donatelli M., Matthews K., 2010. Validation of biophysical models: Issues and methodologies. A review. *Agronomy for Sustainable Development* 30, 109–130. <https://doi.org/10.1051/agro/2009001>
- Bennett N.D., Croke B.F.W., Guariso G., Guillaume J.H.A., Hamilton S.H., Jakeman A.J., Marsili-Libelli S., Newham L.T.H., Norton J.P., Perrin C., Pierce S.A., Robson B., Seppelt R., Voinov A.A., Fath B.D., Andreassian V., 2013. Characterising performance of environmental models. *Environmental Modelling & Software* 40, 1–20. <https://doi.org/10.1016/j.envsoft.2012.09.011>
- Benoit M., Garnier J., Beaudoin N., Billen G., 2016. A participative network of organic and conventional crop farms in the Seine Basin (France) for evaluating nitrate leaching and yield performance. *Agricultural Systems* 148, 105–113. <https://doi.org/10.1016/j.agsy.2016.07.005>
- Bergez J.E., Chabrier P., Gary C., Jeuffroy M.N., Makowski D., Quesnel G., Ramat E., Raynal H., Rousse N., Wallach D., Debaeke P., Durand P., Duru M., Dury J., Faverdin P., Gascuel-Oudou C., Garcia F., 2013. An open platform to build, evaluate and simulate integrated models of farming and agro-ecosystems. *Environmental Modelling & Software* 39, 39–49. <https://doi.org/10.1016/j.envsoft.2012.03.011>
- Bergez J.E., Charron M.H., Leenhardt D., Poupa J.C., 2012. MOUSTICS: A generic dynamic plot-based biodecisional model. *Computers and Electronics in Agriculture* 82, 8–14. <https://doi.org/10.1016/j.compag.2011.12.006>

- Bergez J.E., Raynal H., Launay M., Beaudoin N., Casellas E., Caubel J., Chabrier P., Coucheney E., Dury J., García de Cortázar Aauri I., Justes E., Mary B., Ripoche D., Ruget F., 2014. Evolution of the STICS crop model to tackle new environmental issues: New formalisms and integration in the modelling and simulation platform RECORD. *Environmental Modelling & Software*. <https://doi.org/10.1016/j.envsoft.2014.07.010>
- Bertin N., Gary C., 1993. Évaluation d'un modèle dynamique de croissance et de développement de la tomate (*Lycopersicon esculentum* Mill), TOMGRO, pour différents niveaux d'offre et de demande en assimilats. *Agronomie* 13, 395–405. <https://doi.org/10.1051/agro:19930504>
- Bessou C., Mary B., Leonard J., Roussel M., Grehan E., Gabrielle B., 2010. Modelling soil compaction impacts on nitrous oxide emissions in arable fields. *European Journal of Soil Science* 61, 348–363.
- Bethlenfalvay G.J., Abu-Shakra S.S., Fishbeck K., Phillips D.A., 1978. The effect of source-sink manipulations on nitrogen fixation in peas. *Physiologia Plantarum* 43, 31–34. <https://doi.org/10.1111/j.1399-3054.1978.tb01562.x>
- Bethlenfalvay G.J., Phillips D.A., 1977. Ontogenetic interactions between photosynthesis and symbiotic nitrogen fixation in legumes. *Plant Physiology* 60, 419–421. <https://doi.org/10.1104/pp.60.3.419>
- Beutier D., Renon H., 1978. Gas solubilities near the solvent critical point. *AIChE Journal* 24, 1122–1125. <https://doi.org/10.1002/aic.690240628>
- Bidabe B., 1965. L'action des températures sur l'évolution des bourgeons de l'entrée en dormance à la floraison. *Congr. Pom.(96 sess) Paris*.
- Bindi M., Sinclair T.R., Harrison J., 1999. Analysis of SeedGrowth by LinearIncrease in HarvestIndex. *Crop Science* 39, 486–493. <https://doi.org/10.2135/cropsci1999.0011183X0039000200031x>
- Bingham I.J., 1995. A comparison of the dynamics of root growth and biomass partitioning in wild oat (*Avena fatua* L.) and spring wheat. *Weed Research* 35, 57–66. <https://doi.org/10.1111/j.1365-3180.1995.tb02017.x>
- Blum A., 1996. Crop responses to drought and the interpretation of adaptation, in: Bellassen, E. (Ed.), *Drought Tolerance in Higher Plants: Genetical, Physiological and Molecular Biological Analysis*. Springer, Dordrecht, The Netherlands, pp. 57–70. https://doi.org/10.1007/978-94-017-1299-6_8
- Boesten J.J.T.I., Stroosnijder L., 1986. Simple model for daily evaporation from fallow tilled soil under spring conditions in a temperate climate. *Netherlands Journal of Agricultural Science* 34, 75–90. <https://doi.org/10.18174/njas.v34i1.16818>
- Bonachela S., 1996. Root growth of triticale and barley grown for grain or for forage-plus-grain in a Mediterranean climate. *Plant and Soil* 183, 239–251. <https://doi.org/10.1007/BF00011439>
- Bonhomme R., Derieux M., Edmeades G.O., 1994. Flowering of Diverse Maize Cultivars in Relation to Temperature and Photoperiod in Multilocation Field Trials. *Crop Science* 34, 156–164. <https://doi.org/10.2135/cropsci1994.0011183X003400010028x>
- Bonhomme R., Ruget F., Derieux M., Vincourt P., 1982. Relations entre production de matière sèche aérienne et énergie interceptée chez différents génotypes de maïs. *Comptes rendus de l'Académie des sciences. Série III, Sciences de la vie* 294, 393–398.
- Boote K.J., Jones J.W., 1987. Equations to define canopy photosynthesis from quantum efficiency, maximum leaf rate, light extinction, leaf area index, and photon flux density, in: Biggins, J. (Ed.), *Progress in Photosynthesis Research*. Springer, Dordrecht, The Netherlands, pp. 415–418. https://doi.org/10.1007/978-94-017-0519-6_85
- Boote K.J., Jones J.W., Hoogenboom G., 2018. Simulation of crop growth: CROPGRO model, in: Peart, R.M., Curry, R.B. (Eds.), *Agricultural Systems Modeling and Simulation*. CRC Press, pp. 651–692. <https://doi.org/10.1201/9781482269765-18>
- Boote K.J., Pickering N.B., 1994. Modeling photosynthesis of row crop canopies. *HortScience* 29, 1423–1434. <https://doi.org/10.21273/HORTSCI.29.12.1423>
- Bouaziz A., Bruckler L., 1989. Modeling wheat seedling growth and emergence: I. Seedling growth affected by soil water potential. *Soil Science Society of America Journal* 53, 1832–1838. <https://doi.org/10.2136/sssaj1989.03615995005300060036x>

- Boulard T., Wang S., 2000. Greenhouse crop transpiration model from external climate conditions. *Acta Horticulturae* 235–244. <https://doi.org/10.17660/ActaHortic.2000.534.27>
- Bouma J., 1989. Using soil survey data for quantitative land evaluation, in: Stewart, B.A. (Ed.), *Advances in Soil Science*. Springer, New York, NY, pp. 177–213. https://doi.org/10.1007/978-1-4612-3532-3_4
- Boyer J.S., 1970. Leaf enlargement and metabolic rates in corn, soybean, and sunflower at various leaf water potentials. *Plant Physiology* 46, 233–235. <https://doi.org/10.1104/pp.46.2.233>
- Bradford K.J., 2002. Applications of hydrothermal time to quantifying and modeling seed germination and dormancy. *Weed Science* 50, 248–260. [https://doi.org/10.1614/0043-1745\(2002\)050\[0248:AOHT TQ\]2.0.CO;2](https://doi.org/10.1614/0043-1745(2002)050[0248:AOHT TQ]2.0.CO;2)
- Bradford K.J., 1990. A Water relations analysis of seed germination rates. *Plant Physiology* 94, 840–849. <https://doi.org/10.1104/pp.94.2.840>
- Bradford K.J., Hsiao T.C., 1982. Physiological responses to moderate water stress, in: Lange, O.L., Nobel, P.S., Osmond, C.B., Ziegler, H. (Eds.), *Physiological Plant Ecology II*, Encyclopedia of Plant Physiology (NewSeries). Springer, Berlin, Heidelberg, pp. 263–324. https://doi.org/10.1007/978-3-642-68150-9_10
- Brilli L., Bechini L., Bindi M., Carozzi M., Cavalli D., Conant R., Dorich C.D., Doro L., Ehrhardt F., Farina R., Ferrise R., Fitton N., Francaviglia R., Grace P., Iocola I., Klumpp K., Léonard J., Martin R., Massad R.S., Recous S., Seddaiu G., Sharp J., Smith P., Smith W.N., Soussana J.-F., Bellocchi G., 2017. Review and analysis of strengths and weaknesses of agro-ecosystem models for simulating C and N fluxes. *Science of The Total Environment* 598, 445–470. <https://doi.org/10.1016/j.scitotenv.2017.03.208>
- Brisson N., Bonhomme R., Ameglio T., Gautier H., Oliosio A., Drouet J.-L., 1996. Modèle de culture : Simulation sous contraintes à partir d'un potentiel de production, in: Cruiziat, P., Lagouarde, J.-P. (Eds.), *Actes. Tome 2 : Du Couvert Végétal à La Région*. INRA Editions, Le Croisic, France, pp. 39–51.
- Brisson N., Bussièrre F., Ozier-Lafontaine H., Tournebize R., Sinoquet H., 2004. Adaptation of the crop model STICS to intercropping. Theoretical basis and parameterisation. *Agronomie* 24, 409–421. <https://doi.org/10.1051/agro:2004031>
- Brisson N., Delécolle R., 1992. Développement et modèles de simulation de cultures. *Agronomie* 12, 253–263. <https://doi.org/10.1051/agro:19920305>
- Brisson N., Gary C., Justes E., Roche R., Mary B., Ripoche D., Zimmer D., Sierra J., Bertuzzi P., Burger P., Bussièrre F., Cabidoche Y.M., Cellier P., Debaeke P., Gaudillère J.P., Hénault C., Maraux F., Seguin B., Sinoquet H., 2003. An overview of the crop model STICS. *European Journal of Agronomy* 18, 309–332. [https://doi.org/10.1016/S1161-0301\(02\)00110-7](https://doi.org/10.1016/S1161-0301(02)00110-7)
- Brisson N., Gate P., Gouache D., Charmet G., Oury F.-X., Huard F., 2010. Why are wheat yields stagnating in Europe? A comprehensive data analysis for France. *Field Crops Research* 119, 201–212. <https://doi.org/10.1016/j.fcr.2010.07.012>
- Brisson N., Itier B., L'Hotel J.C., Lorendeau J.Y., 1998a. Parameterisation of the Shuttleworth-Wallace model to estimate daily maximum transpiration for use in crop models. *Ecological Modelling* 107, 159–169. [https://doi.org/10.1016/S0304-3800\(97\)00215-9](https://doi.org/10.1016/S0304-3800(97)00215-9)
- Brisson N., Launay M., Mary B., Beaudoin N. (Eds.), 2009. Conceptual basis, formalisations and parameterization of the Stics crop model. Editions Quae.
- Brisson N., Levraut F., 2010. Livre vert du projet Climator 2007-2010. Changement climatique, agriculture et forêt en France : Simulations d'impacts sur les principales espèces. ADEME Editions.
- Brisson N., Mary B., Ripoche D., Jeuffroy M.H., Ruget F., Nicoulaud B., Gate P., Devienne-Barret F., Antonioletti R., Durr C., Richard G., Beaudoin N., Recous S., Tayot X., Plenet D., Cellier P., Machet J.-M., Meynard J.M., Delécolle R., 1998b. STICS: A generic model for the simulation of crops and their water and nitrogen balances. I. Theory and parameterization applied to wheat and corn. *Agronomie* 18, 311–346. <https://doi.org/10.1051/agro:19980501>
- Brisson N., Oliosio A., Clastre P., 1993. Daily transpiration of field soybeans as related to hydraulic conductance, root distribution, soil potential and midday leaf potential. *Plant and Soil* 154, 227–237. <https://doi.org/10.1007/BF00012528>
- Brisson N., Perrier A., 1991. A semiempirical model of bare soil evaporation for crop simulation models. *Water Resources Research* 27, 719–727. <https://doi.org/10.1029/91WR00075>

- Brisson N., Rebière B., Zimmer D., Renault P., 2002. Response of the root system of a winter wheat crop to waterlogging. *Plant and Soil* 243, 43–55. <https://doi.org/10.1023/A:1019947903041>
- Brisson Nadine, Ruget F., Gate P., Lorgeou J., Nicoullaud B., Tayot X., Plenet D., Jeuffroy M.-H., Bouthier A., Ripoche D., Mary B., Justes E., 2002. STICS: A generic model for simulating crops and their water and nitrogen balances. II. Model validation for wheat and maize. *Agronomie* 22, 69–92. <https://doi.org/10.1051/agro:2001005>
- Brisson N., Seguin B., Bertuzzi P., 1992. Agrometeorological soil water balance for crop simulation models. *Agricultural and Forest Meteorology* 59, 267–287. [https://doi.org/10.1016/0168-1923\(92\)90097-N](https://doi.org/10.1016/0168-1923(92)90097-N)
- Brisson N., Wery J., Boote K.J., 2006. Fundamental concepts of crop models illustrated by a comparative approach, in: Wallach, D., Makowski, D., Jones, J.W. (Eds.), *Working with Dynamic Crop Models: Evaluation, Analysis, Parameterization, and Applications*. Elsevier, pp. 257–277.
- Brochet P., Gerbier N., 1968. L'évapotranspiration. Aspect agrométéorologique. Evaluation pratique de l'évapotranspiration potentielle. Direction de la météorologie nationale.
- Bronson K.F., Touchton J.T., Hauck R.D., Kelley K.R., 1991. Nitrogen-15 recovery in winter wheat as affected by application timing and dicyandiamide. *Soil Science Society of America Journal* 55, 130–135. <https://doi.org/10.2136/sssaj1991.03615995005500010023x>
- Brougham R.W., 1956. Effect of intensity of defoliation on regrowth of pasture. *Australian Journal of Agricultural Research* 7, 377–387. <https://doi.org/10.1071/AR9560377>
- Bruand A., Duval O., Cousin I., 2004. Estimation des propriétés de rétention en eau des sols à partir de la base de données SOLHYDRO: Une première proposition combinant le type d'horizon, sa texture et sa densité apparente. *Etude et Gestion des Sols* 11, 323–334.
- Brunt D., 2007. Notes on radiation in the atmosphere. I. *Quarterly Journal of the Royal Meteorological Society* 58, 389–420. <https://doi.org/10.1002/qj.49705824704>
- Brutsaert W., 1982. Evaporation into the atmosphere. Theory, history and applications, Environmental Fluid Mechanics. Springer, Dordrecht, The Netherlands. <https://doi.org/10.1007/978-94-017-1497-6>
- Buchi L., Valsangiacomo A., Burel E., Charles R., 2016. Integrating simulation data from a crop model in the development of an agri-environmental indicator for soil cover in Switzerland. *European Journal of Agronomy* 76, 149–159. <https://doi.org/10.1016/j.eja.2015.11.004>
- Buis S., Coucheney E., Launay M., Lecharpentier P., Mary B., Ripoche D., Beaudoin N., Ruget F., García de Cortázar Aauri I., Justes E., Constantin J., Andrianarisoa K.-S., Le Bas C., Léonard J., 2016. Multicriteria evaluation of the stics soil-crop model and implementation of an automated evaluation system, in: Ewert, F., Boote, K.J., Rötter, R.P., Thorburn, P., Nendel, C. (Eds.), *International Crop Modelling Symposium "Crop Modelling for Agriculture and Food Security Under Global Change" 2016, 15-17/03/2016*. Berlin, Germany, pp. 214–215.
- Buis S., Lecharpentier P., Vezy R., Giner M., 2021. CroptimizR: A package to estimate parameters of crop models. <https://doi.org/10.5281/ZENODO.4066451>
- Buis S., Wallach D., Guillaume S., Varella H., Lecharpentier P., Launay M., Guérif M., Bergez J.E., Justes E., 2011. The STICS crop model and associated software for analysis, parameterization, and evaluation, in: Ahuja, L.R., Ma, L. (Eds.), *Methods of Introducing System Models into Agricultural Research*, Advances in Agricultural Systems Modeling. John Wiley & Sons, Ltd, pp. 395–426. <https://doi.org/10.2134/advagricsystemodel2.c14>
- Burch G.J., Smith R.C.G., Mason W.K., 1978. Agronomic and Physiological Responses of Soybean and Sorghum Crops to Water Deficits II. Crop Evaporation, Soil Water Depletion and Root Distribution. *Functional Plant Biology* 5, 169–177. <https://doi.org/10.1071/PP9780169>
- Burger P., 2001. Analyse de la variabilité de la teneur en protéines de la graine de soja : Approche par voie d'enquête et étude expérimentale de conduites de cultures visant de hautes teneurs en protéines (Thèse de doctorat). Institut National Agronomique Paris-Grignon.
- Bussière F., 1995. Rainfall interception by plant canopies, consequences for water partitioning in intercropping systems, in: Sinoquet, H., Cruz, P. (Eds.), *Ecophysiology of Tropical Intercropping*, Science Update. INRA Editions, Versailles, pp. 163–174.

- Buvaneshwari S., Riotte J., Sekhar M., Sharma A.K., Helliwell R., Kumar M.S.M., Braun J.J., Ruiz L., 2020. Potash fertilizer promotes incipient salinization in groundwater irrigated semi-arid agriculture. *Scientific Reports* 10, 3691. <https://doi.org/10.1038/s41598-020-60365-z>
- Buvaneshwari S., Sekhar M., Riotte J., Raynal H., Casellas E., Mohan Kumar M.S., Troldborg M., Ruiz L., 2018. Modelling the impact of nutrient recycling on groundwater resource quantity and quality in an irrigated semi-arid tropical catchment, in: *Geophysical Research Abstracts, EGU General Assembly 2018, 8-13/04/2018*. p. 17226.
- Caldwell R.M., 1995. Simulation models for intercropping systems, in: Sinoquet, H., Cruz, P. (Eds.), *Ecophysiology of Tropical Intercropping*. INRA Editions, Pointe à Pitre, France, pp. 353–358.
- Caldwell R.M., Hansen J.W., 1993. Simulation of multiple cropping systems with CropSys, in: de Vries, F.P., Teng, P., Metselaer, K. (Eds.), *Systems Approaches for Agricultural Development*. Springer, Dordrecht, The Netherlands, pp. 397–412. https://doi.org/10.1007/978-94-011-2842-1_24
- Casals M.L., 1996. Introduction des mécanismes de résistance à la sécheresse dans un modèle dynamique de croissance et de développement, du blé dur (Thèse de doctorat). Institut National Agronomique Paris-Grignon.
- Caubel J., Launay M., García de Cortázar Atauri I., Ripoche D., Huard F., Buis S., Brisson N., 2014. A new integrated approach to assess the impacts of climate change on grapevine fungal diseases: The coupled MILA-STICS model. *Journal International des Sciences de la Vigne et du Vin* 45–54.
- Caubel J., Launay M., Lannou C., Brisson N., 2012. Generic response functions to simulate climate-based processes in models for the development of airborne fungal crop pathogens. *Ecological Modelling* 242, 92–104. <https://doi.org/10.1016/j.ecolmodel.2012.05.012>
- Caubel J., Launay M., Ripoche D., Gouache D., Buis S., Huard F., Huber L., Brun F., Bancal M.O., 2017. Climate change effects on leaf rust of wheat: Implementing a coupled crop-disease model in a French regional application. *European Journal of Agronomy* 90, 53–66. <https://doi.org/10.1016/j.eja.2017.07.004>
- Cellier P., Richard G., Robin P., 1996. Partition of sensible heat fluxes into bare soil and the atmosphere. *Agricultural and Forest Meteorology* 82, 245–265. [https://doi.org/10.1016/0168-1923\(95\)02328-3](https://doi.org/10.1016/0168-1923(95)02328-3)
- Cellier P., Ruget F., Chartier M., Bonhomme R., 1993. Estimating the temperature of a maize apex during early growth stages. *Agricultural and Forest Meteorology* 63, 35–54. [https://doi.org/10.1016/0168-1923\(93\)90021-9](https://doi.org/10.1016/0168-1923(93)90021-9)
- Chantigny M.H., Rochette P., Angers D.A., Massé D., Côté D., 2004. Ammonia Volatilization and Selected Soil Characteristics Following Application of Anaerobically Digested Pig Slurry. *Soil Science Society of America Journal* 68, 306–312. <https://doi.org/10.2136/sssaj2004.3060>
- Chapman D.C., Lake D.W., 2003. Computing runoff, in: *New York Standards and Specifications for Erosion and Sediment Control*. New York State Soil, Water Conservation Committee, New York, USA, pp. 16 p.
- Chapman S.C., Hammer G.L., Palta J.A., 1993. Predicting leaf area development of sunflower. *Field Crops Research* 34, 101–112. [https://doi.org/10.1016/0378-4290\(93\)90114-3](https://doi.org/10.1016/0378-4290(93)90114-3)
- Chuine I., 2010. Why does phenology drive species distribution? *Philosophical Transactions of the Royal Society of London B: Biological Sciences* 365, 3149–3160. <https://doi.org/10.1098/rstb.2010.0142>
- Clapp R.B., Hornberger G.M., 1978. Empirical equations for some soil hydraulic properties. *Water Resources Research* 14, 601–604. <https://doi.org/10.1029/WR014i004p060601>
- Clivot H., Mary B., Valé M., Cohan J.-P., Champolivier L., Piraux F., Laurent F., Justes E., 2017. Quantifying in situ and modeling net nitrogen mineralization from soil organic matter in arable cropping systems. *Soil Biology and Biochemistry* 111, 44–59. <https://doi.org/10.1016/j.soilbio.2017.03.010>
- Clivot H., Mouny J.-C., Duparque A., Dinh J.-L., Denoroy P., Houot S., Vertès F., Trochard R., Bouthier A., Sagot S., Mary B., 2019. Modeling soil organic carbon evolution in long-term arable experiments with AMG model. *Environmental Modelling & Software* 118, 99–113. <https://doi.org/10.1016/j.envsoft.2019.04.004>
- Cockborne A.-M. de, Jauzein M., Stengel P., Guennelon R., 1988. Variation du coefficient de diffusion de NO_3^- dans les sols : Influence de la teneur en eau et de la porosité. *Agronomie* 8, 905–914. <https://doi.org/10.1051/agro:19881010>

- Coleman K., Jenkinson D.S., 1996. RothC-26.3 - A Model for the turnover of carbon in soil, in: Powlson, D.S., Smith, P., Smith, J.U. (Eds.), *Evaluation of Soil Organic Matter Models*. Springer, Berlin, Heidelberg, pp. 237–246. https://doi.org/10.1007/978-3-642-61094-3_17
- Confalonieri R., Orlando F., Paleari L., Stella T., Gilardelli C., Movedi E., Pagani V., Cappelli G., Vertemara A., Alberti L., Alberti P., Atanassiu S., Bonaiti M., Cappelletti G., Ceruti M., Confalonieri A., Corgatelli G., Corti P., Dell'Oro M., Ghidoni A., Lamarta A., Maghini A., Mambretti M., Manchia A., Massoni G., Mutti P., Pariani S., Pasini D., Pesenti A., Pizzamiglio G., Ravasio A., Rea A., Santorsola D., Serafini G., Slavazza M., Acutis M., 2016. Uncertainty in crop model predictions: What is the role of users? *Environmental Modelling & Software* 81, 165–173. <https://doi.org/10.1016/j.envsoft.2016.04.009>
- Constantin J., Beaudoin N., Launay M., Duval J., Mary B., 2012. Long-term nitrogen dynamics in various catch crop scenarios: Test and simulations with STICS model in a temperate climate. *Agriculture Ecosystems & Environment* 147, 36–46. <https://doi.org/10.1016/j.agee.2011.06.006>
- Constantin J., Durr C., Tribouillois H., Justes E., 2015a. Catch crop emergence success depends on weather and soil seedbed conditions in interaction with sowing date: A simulation study using the SIMPLE emergence model. *Field Crops Research* 176, 22–33. <https://doi.org/10.1016/j.fcr.2015.02.017>
- Constantin J., Le Bas C., Justes E., 2015b. Large-scale assessment of optimal emergence and destruction dates for cover crops to reduce nitrate leaching in temperate conditions using the STICS soil-crop model. *European Journal of Agronomy* 69, 75–87. <https://doi.org/10.1016/j.eja.2015.06.002>
- Constantin J., Raynal H., Casellas E., Hoffmann H., Bindi M., Doro L., Eckersten H., Gaiser T., Grosz B., Haas E., Kersebaum K.-C., Klatt S., Kuhnert M., Lewan E., Maharjan G.R., Moriondo M., Nendel C., Roggero P.P., Specka X., Trombi G., Villa A., Wang E., Weihermüller L., Yeluripati J., Zhao Z., Ewert F., Bergez J.-E., 2019. Management and spatial resolution effects on yield and water balance at regional scale in crop models. *Agricultural and Forest Meteorology* 275, 184–195. <https://doi.org/10.1016/j.agrformet.2019.05.013>
- Constantin Julie, Willaume M., Murgue C., Lacroix B., Therond O., 2015. The soil-crop models STICS and AqYield predict yield and soil water content for irrigated crops equally well with limited data. *Agricultural and Forest Meteorology* 206, 55–68. <https://doi.org/10.1016/j.agrformet.2015.02.011>
- Cordery I., Graham A., 1989. Forecasting wheat yields using a water budgeting model. *Australian Journal of Agricultural Research* 40, 715–728. <https://doi.org/10.1071/AR9890715>
- Corre-Hellou G., Brisson N., Launay M., Fustec J., Crozat Y., 2007. Effect of root depth penetration on soil nitrogen competitive interactions and dry matter production in pea-barley intercrops given different soil nitrogen supplies. *Field Crops Research* 103, 76–85. <https://doi.org/10.1016/j.fcr.2007.04.008>
- Corre-Hellou G., Faure M., Launay M., Brisson N., Crozat Y., 2009. Adaptation of the STICS intercrop model to simulate crop growth and N accumulation in pea-barley intercrops. *Field Crops Research* 113, 72–81. <https://doi.org/10.1016/j.fcr.2009.04.007>
- Corwin D.L., Wagenet R.J., 1996. Applications of GIS to the Modeling of NonPointSourcePollutants in the VadoseZone: AConferenceOverview. *Journal of Environmental Quality* 25, 403–411. <https://doi.org/10.2134/jeq1996.00472425002500030004x>
- Coucheny E., Buis S., Launay M., Constantin J., Mary B., García de Cortázar Atauri I., Ripoche D., Beaudoin N., Ruget F., Andrianarisoa K.S., Le Bas C., Justes E., Léonard J., 2015. Accuracy, robustness and behavior of the STICS soil-crop model for plant, water and nitrogen outputs: Evaluation over a wide range of agro-environmental conditions in France. *Environmental Modelling & Software* 64, 177–190. <https://doi.org/10.1016/j.envsoft.2014.11.024>
- Courault D., Hadria R., Ruget F., Olioso A., Duchemin B., Hagolle O., Dedieu G., 2010. Combined use of FORMOSAT-2 images with a crop model for biomass and water monitoring of permanent grassland in Mediterranean region. *Hydrology and Earth System Sciences* 14, 1731–1744. <https://doi.org/10.5194/hess-14-1731-2010>
- Cousin R., 1997. Peas (*Pisum sativum*L.). *Field Crops Research* 53, 111–130. [https://doi.org/10.1016/S0378-4290\(97\)00026-9](https://doi.org/10.1016/S0378-4290(97)00026-9)
- Cowan I.R., 1968. The Interception and Absorption of Radiation in PlantStands. *The Journal of Applied Ecology* 5, 367. <https://doi.org/10.2307/2401567>

- Cruz P., Duru M., Therond O., Theau J.-P., Ducourtieux C., Jouany C., Al Haj Khaled R., Ansquer P., 2002. Une nouvelle approche pour caractériser les prairies naturelles et leur valeur d'usage. *Fourrages* 172, 335–354.
- Cruz P., Theau J.-P., Lecloux E., Jouany C., Duru M., 2010. Typologie fonctionnelle de graminées fourragères pérennes : Une classification multitraits. *Fourrages* 201, 11–17.
- Dale R.F., Coelho D.T., Gallo K.P., 1980. Prediction of DailyGreenLeafAreaIndex for Corn. *Agronomy Journal* 72, 999–1005. <https://doi.org/10.2134/agronj1980.00021962007200060032x>
- de Willigen P., Heinen M., Mollier A., Van Noordwijk M., 2002. Two-dimensional growth of a root system modelled as a diffusion process. I. Analytical solutions. *Plant and Soil* 240, 225–234. <https://doi.org/10.1023/A:1015744529454>
- de Wit C.T. (Ed.), 1978. Simulation of assimilation, respiration and transpiration of crops, Centre for Agricultural Publishing and Documentation., Simulation monographs. Pudoc, Wageningen, The Netherlands.
- de Wit C.T., Brouwer R., Penning de Vries F.W.T., 1970. The simulation of photosynthetic systems, in: Setlik, I. (Ed.), *Prediction and Measurement of Photosynthetic Productivity*, Proceeding IBP/PPTechnicalMeetingTrebou 1969. Pudoc, Wageningen, The Netherlands, pp. 47–70.
- De Notaris C., Rasmussen J., Sorensen P., Olesen J.E., 2018. Nitrogen leaching: A crop rotation perspective on the effect of N surplus, field management and use of catch crops. *Agriculture Ecosystems & Environment* 255, 1–11. <https://doi.org/10.1016/j.agee.2017.12.009>
- De Tourdonnet S., 1999. Control of quality and N pollution in greenhouse lettuce production: A modelling study. *Acta Horticulturae* 263–270. <https://doi.org/10.17660/ActaHortic.1999.507.30>
- De Villele O., 1974. Besoins en eau des cultures sous serre - Essai de conduite des arrosages en fonction de l'ensoleillement. *Acta Horticulturae* 123–135. <https://doi.org/10.17660/ActaHortic.1974.35.16>
- Debaeke P., Aboudrar A., 2004. Adaptation of crop management to water-limited environments. *European Journal of Agronomy* 21, 433–446. <https://doi.org/10.1016/j.eja.2004.07.006>
- Debaeke P., Burger P., Brisson N., 2001. A simple model to simulate N₂ symbiotic fixation of annual grain legumes: Application to soybean, in: *Proceedings of the Second International Symposium on Modelling Cropping System*. Florence (Italy), pp. 17–18.
- Defossez P., Richard G., Boizard H., O'Sullivan M.F., 2003. Modeling change in soil compaction due to agricultural traffic as function of soil water content. *Geoderma* 116, 89–105. [https://doi.org/10.1016/S0016-7061\(03\)00096-X](https://doi.org/10.1016/S0016-7061(03)00096-X)
- Deleens E., Gregory N., Bourdu R., 1984. Transition between seed reserve use and photosynthetic supply during development of maize seedlings. *Plant Science Letters* 37, 35–39.
- Demestihis C., Plenet D., Genard M., García de Cortázar Aauri I., Launay M., Ripoché D., Beaudoin N., Simon S., Charreyron M., Raynal C., Lescourret F., 2018. Analyzing ecosystem services in apple orchards using the STICS model. *European Journal of Agronomy* 94, 108–119. <https://doi.org/10.1016/j.eja.2018.01.009>
- Denmead O.T., 1973. Relative significance of soil plant evaporation in estimating evapotranspiration, in: Slatyer, R.O. (Ed.), *Plant Response to Climatic Factors. Proceedings of the UNESCO Uppsala Symposium 1970*. UNESCO, Uppsalla, Sweden, pp. 505–511.
- Denmead O.T., Shaw R.H., 1962. Availability of SoilWater to Plants as Affected by SoilMoistureContent and MeteorologicalConditions. *Agronomy Journal* 54, 385–390. <https://doi.org/10.2134/agronj1962.00021962005400050005x>
- Desclaux D., Roumet P., 1996. Impact of drought stress on the phenology of two soybean (*Glycine max*L. Merr) cultivars. *Field Crops Research* 46, 61–70. [https://doi.org/10.1016/0378-4290\(95\)00086-0](https://doi.org/10.1016/0378-4290(95)00086-0)
- Devienne-Barret F., Justes E., Machet J.M., Mary B., 2000. Integrated Control of NitrateUptake by CropGrowthRate and SoilNitrateAvailability under FieldConditions. *Annals of Botany* 86, 995–1005. <https://doi.org/10.1006/anbo.2000.1264>
- Diaz S., Cabido M., 1997. Plant functional types and ecosystem functions in relation to global change. *Journal of Vegetation Science* 8, 463–474. <https://doi.org/10.2307/3237198>

- Dimassi B., Cohan J.-P., Labreuche J., Mary B., 2013. Changes in soil carbon and nitrogen following tillage conversion in a long-term experiment in Northern France. *Agriculture Ecosystems & Environment* 169, 12–20. <https://doi.org/10.1016/j.agee.2013.01.012>
- Dimassi B., Mary B., Wylleman R., Labreuche J., Couture D., Piraux F., Cohan J.-P., 2014. Long-term effect of contrasted tillage and crop management on soil carbon dynamics during 41 years. *Agriculture Ecosystems & Environment* 188, 134–146. <https://doi.org/10.1016/j.agee.2014.02.014>
- Dinesh H., Pearce J.M., 2016. The potential of agrivoltaic systems. *Renewable & Sustainable Energy Reviews* 54, 299–308. <https://doi.org/10.1016/j.rser.2015.10.024>
- Donohue R.J., Lawes R.A., Mata G., Gobbett D., Ouzman J., 2018. Towards a national, remote-sensing-based model for predicting field-scale crop yield. *Field Crops Research* 227, 79–90. <https://doi.org/10.1016/j.fcr.2018.08.005>
- Doorenbos K., Kassam A.H., Bentvelsen C., Uittenbogaard G., 1980. Yield response to water, in: Johl, S.S. (Ed.), *Irrigation and Agricultural Development*. Pergamon, pp. 257–280. <https://doi.org/10.1016/B978-0-08-025675-7.50021-2>
- Dorsainvil F., 2002. Evaluation, par modélisation, de l'impact environnemental des modes de conduite des cultures intermédiaires sur les bilans d'eau et d'azote dans les systèmes de culture (Thèse de doctorat). Institut National Agronomique Paris-Grignon.
- Douguedroit A., 1986. Les topoclimats thermiques de moyenne montagne. *Agrométéorologie des régions de moyenne montagne, Les colloques de l'INRA, Toulouse* 198–213.
- Drouet J.-L., Pagès L., 2003. GRAAL: A model of GRowth, Architecture and carbon ALlocation during the vegetative phase of the whole maize plant. *Ecological Modelling* 165, 147–173. [https://doi.org/10.1016/S0304-3800\(03\)00072-3](https://doi.org/10.1016/S0304-3800(03)00072-3)
- Ducharne A., Baubion C., Beaudoin N., Benoit M., Billen G., Brisson N., Garnier J., Kieken H., Lebonvallet S., Ledoux E., Mary B., Mignolet C., Poux X., Sauboua E., Schott C., Théry S., Viennot P., 2007. Long term prospective of the SeineRiver system: Confronting climatic and direct anthropogenic changes. *Science of The Total Environment* 375, 292–311. <https://doi.org/10.1016/j.scitotenv.2006.12.011>
- Dufour L., Metay A., Talbot G., Dupraz C., 2013. Assessing LightCompetition for CerealProduction in TemperateAgroforestrySystems using Experimentation and CropModelling. *Journal of Agronomy and Crop Science* 199, 217–227. <https://doi.org/10.1111/jac.12008>
- Dumont B., Leemans V., Mansouri M., Bodson B., Destain J.-P., Destain M.-F., 2014. Parameter identification of the STICS crop model, using an accelerated formal MCMC approach. *Environmental Modelling & Software* 52, 121–135. <https://doi.org/10.1016/j.envsoft.2013.10.022>
- Duncan W.G., 1971. Leaf Angles, LeafArea, and CanopyPhotosynthesis. *Crop Science* 11, 482–485. <https://doi.org/10.2135/cropsci1971.0011183X001100040006x>
- Dupraz C., Wolz K.J., Lecomte I., Talbot G., Vincent G., Mulia R., Bussière F., Ozier-Lafontaine H., Andrianarisoa S., Jackson N., Lawson G., Dones N., Sinoquet H., Lusiana B., Harja D., Domenicano S., Reyes F., Gosme M., Van Noordwijk M., 2019. Hi-sAFe: A3DAgroforestryModel for IntegratingDynamicTree–CropInteractions. *Sustainability* 11. <https://doi.org/10.3390/su11082293>
- Durand J.-L., Delusca K., Boote K., Lizaso J., Manderscheid R., Weigel H.J., Ruane A.C., Rosenzweig C., Jones J., Ahuja L., Anapalli S., Basso B., Baron C., Bertuzzi P., Biernath C., Deryng D., Ewert F., Gaiser T., Gayler S., Heinlein F., Kersebaum K.C., Kim S.-H., Müller C., Nendel C., Olioso A., Priesack E., Villegas J.R., Ripoche D., Rötter R.P., Seidel S.L., Srivastava A., Tao F., Timlin D., Twine T., Wang E., Webber H., Zhao Z., 2018. How accurately do maize crop models simulate the interactions of atmospheric CO₂ concentration levels with limited water supply on water use and yield? *European Journal of Agronomy*, Recent advances in crop modelling to support sustainable agricultural production and food security under global change 100, 67–75. <https://doi.org/10.1016/j.eja.2017.01.002>
- Durand R., 1967. Action de la temperature et du rayonnement sur la croissance. *Annales de Physiologie Végétale* 9, 5.
- Dürr C., Aubertot J.-N., Richard G., Dubrulle P., Duval Y., Boiffin J., 2001. Simple: A model for simulation of plant emergence predicting the effects of soil tillage and sowing operations. *Soil Science Society of America Journal* 65, 414–423. <https://doi.org/10.2136/sssaj2001.652414x>

- Duru M., Ducrocq H., Tirilly V., 1995. Modeling growth of cocksfoot (*Dactylis glomerata*L.) And tall fescue (*Festuca arundinacea* schreb.) At the end of spring in relation to herbage nitrogen status. *Journal of Plant Nutrition* 18, 2033–2047. <https://doi.org/10.1080/01904169509365042>
- Duru M., Justes E., Langlet A., Tirilly V., Rouziès S., Sos L., Viard R., 1993. Comparaison des dynamiques d'apparition et de mortalité des organes de fétuque élevée, dactyle et luzerne (feuilles, talles et tiges). *Agronomie* 13, 237–252.
- Duru M., Tallowin J., Cruz P., 2005. Functional diversity in low-input grassland farming systems: Characterisation, effect and management. *Agronomy research* 3, 125–138.
- Duval Y., Boiffin J., 1990. Influence of soil crusting on the emergence of sugar beet seedlings, in: *Proceedings of the First Congress of the European Society of Agronomy, 5-7/12/1990*. ESA, Colmar, France, p. 311.
- Dwyer L.M., Stewart D.W., 1986. Leaf Area Development in Field-Grown Maize. *Agronomy Journal* 78, 334–343. <https://doi.org/10.2134/agronj1986.00021962007800020024x>
- Eagleman J.R., 1971. An experimentally derived model for actual evapotranspiration. *Agricultural Meteorology* 8, 385–394. [https://doi.org/10.1016/0002-1571\(71\)90124-5](https://doi.org/10.1016/0002-1571(71)90124-5)
- Ehrhardt F., Soussana J.-F., Bellocchi G., Grace P., McAuliffe R., Recous S., Sándor R., Smith P., Snow V., de Antoni Migliorati M., Basso B., Bhatia A., Brill L., Doltra J., Dorich C.D., Doro L., Fitton N., Giacomini S.J., Grant B., Harrison M.T., Jones S.K., Kirschbaum M.U.F., Klumpp K., Laville P., Léonard J., Liebig M., Lieffering M., Martin R., Massad R.S., Meier E., Merbold L., Moore A.D., Myrgeiotis V., Newton P., Patey E., Rolinski S., Sharp J., Smith W.N., Wu L., Zhang Q., 2018. Assessing uncertainties in crop and pasture ensemble model simulations of productivity and N₂O emissions. *Global Change Biology* 24, e603–e616. <https://doi.org/10.1111/gcb.13965>
- Ewert F., van Ittersum M.K., Bezlepina I., Therond O., Andersen E., Belhouchette H., Bockstaller C., Brouwer F., Heckelet T., Janssen S., Knapen R., Kuiper M., Louhichi K., Olsson J.A., Turpin N., Wery J., Wien J.E., Wolf J., 2009. A methodology for enhanced flexibility of integrated assessment in agriculture. *Environmental Science & Policy* 12, 546–561. <https://doi.org/10.1016/j.envsci.2009.02.005>
- Ewert F., van Ittersum M.K., Heckelet T., Therond O., Bezlepina I., Andersen E., 2011. Scale changes and model linking methods for integrated assessment of agri-environmental systems. *Agriculture Ecosystems & Environment* 142, 6–17. <https://doi.org/10.1016/j.agee.2011.05.016>
- Faivre R., Leenhardt D., Voltz M., Benoit M., Papy F., Dedieu G., Wallach D.D., 2004. Spatialising crop models. *Agronomie* 24, 205–217. <https://doi.org/10.1051/agro:2004016>
- Falconnier G.N., Corbeels M., Boote K.J., Affholder F., Adam M., MacCarthy D.S., Ruane A.C., Nendel C., Whitbread A.M., Justes E., Ahuja L.R., Akinseye F.M., Alou I.N., Amouzou K.A., Anapalli S.S., Baron C., Basso B., Baudron F., Bertuzzi P., Challinor A.J., Chen Y., Deryng D., Elsayed M.L., Faye B., Gaiser T., Galdos M., Gayler S., Gerardeaux E., Giner M., Grant B., Hoogenboom G., Ibrahim E.S., Kamali B., Kersebaum K.C., Kim S.-H., van der Laan M., Leroux L., Lizaso J.L., Maestrini B., Meier E.A., Mequanint F., Ndoli A., Porter C.H., Priesack E., Ripoche D., Sida T.S., Singh U., Smith W.N., Srivastava A., Sinha S., Tao F., Thorburn P.J., Timlin D., Traore B., Twine T., Webber H., 2020. Modelling climate change impacts on maize yields under low nitrogen input conditions in sub-Saharan Africa. *Global Change Biology* 26, 5942–5964. <https://doi.org/10.1111/gcb.15261>
- Falconnier G.N., Journet E.P., Bedoussac L., Vermue A., Chlebowski F., Beaudoin N., Justes E., 2019. Calibration and evaluation of the STICS soil-crop model for faba bean to explain variability in yield and N-2 fixation. *European Journal of Agronomy* 104, 63–77. <https://doi.org/10.1016/j.eja.2019.01.001>
- Fan J., McConkey B., Wang H., Janzen H., 2016. Root distribution by depth for temperate agricultural crops. *Field Crops Research* 189, 68–74. <https://doi.org/10.1016/j.fcr.2016.02.013>
- Farquhar G.D., von Caemmerer S., Berry J.A., 1980. A biochemical model of photosynthetic CO₂ assimilation in leaves of C₃ species. *Planta* 149, 78–90. <https://doi.org/10.1007/BF00386231>
- Feddes R.A., Hooghart J.C., 1987. Crop factors in relation to Makkink reference-crop evapotranspiration, in: *Evaporation and Weather. Proceedings and Informations / Committee for Hydrological Research T.N.O.* The Hague, The Netherlands, pp. 33–47.

- Ferchaud F., Mary B., 2016. Drainage and Nitrate Leaching Assessed During 7 Years Under Perennial and Annual Bioenergy Crops. *Bioenergy Research* 9, 656–670. <https://doi.org/10.1007/s12155-015-9710-2>
- Ferrant S., Gascoin S., Veloso A., Salmon-Monviola J., Claverie M., Rivalland V., Dedieu G., Demarez V., Ceschia E., Probst J.L., Durand P., Bustillo V., 2014. Agro-hydrology and multi-temporal high-resolution remote sensing: Toward an explicit spatial processes calibration. *Hydrology and Earth System Sciences* 18, 5219–5237. <https://doi.org/10.5194/hess-18-5219-2014>
- Finn G.A., Brun W.A., 1982. Effect of Atmospheric CO₂ Enrichment on Growth, Nonstructural Carbohydrate Content, and Root Nodule Activity in Soybean. *Plant Physiology* 69, 327–331. <https://doi.org/10.1104/pp.69.2.327>
- Fisher D.K., Elliot R.L., 1996. Modelling rangeland/pasture evapotranspiration using the Shuttleworth-Wallace approach, in: Camp, C.R., Sadler, E.J., Yoder, R.E. (Eds.), *Evapotranspiration and Irrigation Scheduling Proceedings of the International Conference, 3-6/11/1996*. American Society of Agricultural Engineers, San Antonio, USA, pp. 664–672.
- Flood J., 2010. The importance of plant health to food security. *Food Security* 2, 215–231. <https://doi.org/10.1007/s12571-010-0072-5>
- Fontaine S., Barot S., Barré P., Bdioui N., Mary B., Rumpel C., 2007. Stability of organic carbon in deep soil layers controlled by fresh carbon supply. *Nature* 450, 277–280. <https://doi.org/10.1038/nature06275>
- Friend A.D., 1991. Use of a model of photosynthesis and leaf microenvironment to predict optimal stomatal conductance and leaf nitrogen partitioning. *Plant, Cell and Environment* 14, 895–905. <https://doi.org/10.1111/j.1365-3040.1991.tb00958.x>
- Gabrielle B., Mary B., Roche R., Smith P., Gosse G., 2002. Simulation of carbon and nitrogen dynamics in arable soils: A comparison of approaches. *European Journal of Agronomy* 18, 107–120. [https://doi.org/10.1016/S1161-0301\(02\)00099-0](https://doi.org/10.1016/S1161-0301(02)00099-0)
- García de Cortázar Atauri I., 2006. Adaptation du modèle STICS à la vigne (*Vitis vinifera*L.) : Utilisation dans le cadre d'une étude d'impact du changement climatique à l'échelle de la France (Thèse de doctorat). École nationale supérieure agronomique de Montpellier.
- García de Cortázar Atauri I., Brisson N., Gaudillere J.P., 2009a. Performance of several models for predicting budburst date of grapevine (*Vitis vinifera*L.). *International Journal of Biometeorology* 53, 317–326. <https://doi.org/10.1007/s00484-009-0217-4>
- García de Cortázar Atauri I., Brisson N., Ollat N., Jacquet O., Payan J.C., 2009b. Asynchronous dynamics of grapevine ("*Vitis vinifera*") maturation: Experimental study for a modelling approach. *Journal International des Sciences de la Vigne et du Vin* 43, 83–97. <https://doi.org/10.20870/oeno-one.2009.43.2.801>
- García de Cortázar Atauri I., Brisson N., Seguin B., Gaudillère J.P., Baculat B., 2005. Simulation of budbreak date for vine. TheBRIN model. Some applications in climate change study, in: Schultz, H.R. (Ed.), *Proceedings of the XIV International GESCO Viticulture Congress 2005, 23-27/08/2005*. Geisenheim, Germany, pp. 485–490.
- Gardner W.R., 1991. Modeling water uptake by roots. *Irrigation Science* 12, 109–114. <https://doi.org/10.1007/BF00192281>
- Gary C.C., Daudet F.A., Cruiziat P., Brisson N., Ozier Lafontaine H., Bréda N., 1995. Le concept de facteur limitant, in: *Actes. Tome 1: De La Plante Au Couvert Végétal*. INRA Editions, Le Croisic, France, pp. 121–128.
- Gary C., Jones J.W., Longuenesse J.J., 1993. Modelling daily changes in specific leaf area of tomato: The contribution of the leaf assimilate pool. *Acta Horticulturae* 205–210. <https://doi.org/10.17660/ActaHortic.1993.328.19>
- Gateau C., Granger S., Kockmann F., Ruget F., Novak S., 2006. Evaluation du potentiel herbager et de sa variabilité en élevage allaitant. Régionalisation de la démarche ISOP en Saône-et-Loire. *Fourrages* 186, 257–269.
- Génermont S., Cellier P., 1997. A mechanistic model for estimating ammonia volatilization from slurry applied to bare soil. *Agricultural and Forest Meteorology* 88, 145–167. [https://doi.org/10.1016/S0168-1923\(97\)00044-0](https://doi.org/10.1016/S0168-1923(97)00044-0)

- Gervois S., Noblet-Ducoudre N. de, Viovy N., Ciais P., Brisson N., Seguin B., Perrier A., 2004. Including Croplands in a GlobalBiosphereModel: Methodology and Evaluation at Specific Sites. *Earth Interactions* 8, 1–25. [https://doi.org/10.1175/1087-3562\(2004\)8<1:ICLAGB>2.0.CO;2](https://doi.org/10.1175/1087-3562(2004)8<1:ICLAGB>2.0.CO;2)
- Gerwitz A., Page E.R., 1974. An EmpiricalMathematicalModel to DescribePlantRootSystems. *Journal of Applied Ecology* 11, 773–781. <https://doi.org/10.2307/2402227>
- Giacomini S.J., Recous S., Mary B., Aita C., 2007. Simulating the effects of N availability, straw particle size and location in soil on C and N mineralization. *Plant and Soil* 301, 289–301. <https://doi.org/10.1007/s11104-007-9448-5>
- Giauffret C., Derieux M., 1991. Variabilité génétique de la croissance de la jeune racine en fonction de la température, in: Picard, D. (Ed.), *Physiologie Et Production Du Maïs. Pau (France), 13-15 Nov. 1990*. INRA Editions, pp. 69–74.
- Girard M.L., 1997. Modélisation de l'accumulation de biomasse et d'azote dans les grains de blé tendre d'hiver (*Triticum aestivum*L.) ; simulation de leur teneur en protéines à la récolte (Thèse de doctorat). Institut National Agronomique Paris-Grignon.
- Gonzalez-Camacho J.M., Mailhol J.C., Ruget F., 2008. Impacts locaux attendus de l'augmentation du CO₂ dans l'atmosphère sur la productivité de l'eau du maïs dans la Drôme, France. *Irrigation and Drainage* 57, 229–243. <https://doi.org/10.1002/ird.332>
- Gonzalez-Dugo V., Durand J.-L., Gastal F., 2010. Water deficit and nitrogen nutrition of crops. A review. *Agronomy for Sustainable Development* 30, 529–544. <https://doi.org/10.1051/agro/2009059>
- Gordon A.J., Ryle G.J.A., Mitchell D.F., Powell D.C.E., 1985. The Flux of ¹⁴C-LabeledPhotosynthate through SoyabeanRootNodules during N₂ Fixation. *Journal of Experimental Botany* 36, 756–769. <https://doi.org/10.1093/jxb/36.5.756>
- Goudriaan J., Gurney W.S.C., Nisbet R.M., Blythe S.P., 1986. Numerical approaches, in: Metz, J.A.J., Diekmann, O. (Eds.), *The Dynamics of Physiologically Structured Populations*, Lecture Notes in Biomathematics. Springer, Berlin, Heidelberg, pp. 453–473.
- Gras R., 1994. Sols caillouteux et production végétale, Mieux comprendre. INRA Editions, Versailles, France.
- Graux A.-I., 2005. Etude des mécanismes de remobilisation d'assimilats chez la betterave sucrière en réponse aux stress abiotiques : Expérimentation et modélisation (Mémoire de DEA). ENSAIA.
- Graux A.I., Resmond R., Casellas E., Delaby L., Faverdin P., Le Bas C., Ripoche D., Ruget F., Therond O., Vertes F., Peyraud J.L., 2020. High-resolution assessment of French grassland dry matter and nitrogen yields. *European Journal of Agronomy* 112, 125952. <https://doi.org/10.1016/j.eja.2019.125952>
- Grebet P., 1993. Functions, subroutines and a program for easy computation of commonly required data related to the sun, in: Varlet-Grancher, C., Bonhomme, R., Sinoquet, H. (Eds.), *Crop Structure and Light Microclimate*. pp. 501–511.
- Greenwood D.J., Gastal F., Lemaire G., Draycott A., Millard P., Neeteson J.J., 1991. Growth Rate and % N of FieldGrownCrops: Theory and Experiments. *Annals of Botany* 67, 181–190. <https://doi.org/10.1093/oxfordjournals.aob.a088118>
- Grosz B., Dechow R., Gebbert S., Hoffmann H., Zhao G., Constantin J., Raynal H., Wallach D., Coucheney E., Lewan E., Eckersten H., Specka X., Kersebaum K.-C., Nendel C., Kuhnert M., Yeluripati J., Haas E., Teixeira E., Bindi M., Trombi G., Moriondo M., Doro L., Roggero P.P., Zhao Z., Wang E., Tao F., Rötter R., Kassie B., Cammarano D., Asseng S., Weihermüller L., Siebert S., Gaiser T., Ewert F., 2017. The implication of input data aggregation on up-scaling soil organic carbon changes. *Environmental Modelling & Software* 96, 361–377. <https://doi.org/10.1016/j.envsoft.2017.06.046>
- Guérif M., Beaudoin N., Durr C., Houles V., Machel J.-M., Mary B., Moulin S., Richard G., 2001. Designing a field experiment for assessing soil and crop spatial variability and defining site-specific management strategies, in: *Proceedings of the 3rd European Conference on Precision Agriculture, 18-20/06/2001*. ENSAM, Montpellier, France, pp. 677–682.
- Guérif M., Houlès V., Mary B., Beaudoin N., Machel J.-M., Moulin S., Nicoulaud B., 2007. Modulation intra-parcellaire de la fertilisation azotée du blé fondée sur le modèle de culture Stics. Intérêt de la démarche et méthodes de spatialisation, in: Guérif, M., King, D. (Eds.), *Agriculture de Précision*, Update Sciences and Technologies. Editions Quae, pp. 225–248.

- Guérin V., Pladys D., Trinchant J.-C., Rigaud J., 1991. Proteolysis and nitrogen fixation in faba-bean (*Vicia faba*) nodules under water stress. *Physiologia Plantarum* 82, 360–366. <https://doi.org/10.1111/j.1399-3054.1991.tb02918.x>
- Guillaume S., Bergez J.E., Wallach D., Justes E., 2011. Methodological comparison of calibration procedures for durum wheat parameters in the STICS model. *European Journal of Agronomy* 35, 115–126. <https://doi.org/10.1016/j.eja.2011.05.003>
- Guyot G., 1997. Climatologie de l'environnement. De la plante aux écosystèmes. Masson.
- Hallaire M., 1964. Le potentiel efficace de l'eau dans le sol en régime de dessèchement, in: *L'eau Et La Production Végétale*. INRA, Paris, France, pp. 27–62.
- Hammer G.L., Muchow R.C., 1994. Assessing climatic risk to sorghum production in water-limited subtropical environments I. Development and testing of a simulation model. *Field Crops Research* 36, 221–234. [https://doi.org/10.1016/0378-4290\(94\)90114-7](https://doi.org/10.1016/0378-4290(94)90114-7)
- Hansen S., Jensen H.E., Nielsen N.E., Svendsen H., 1990. DAISY: A SoilPlantSystemModel. Danish simulation model for transformation and transport of energy and matter in the soil plant atmosphere system (NPO No. A10). Copenhagen.
- He D., Wang E., 2019. The potential of using LAI time series to predict plant available water capacity (PAWC) of soils, in: *Agronomy Australia Conference*. Agronomy Australia, Wagga Wagga.
- He D., Wang E., Wang J., Robertson M.J., 2017. Data requirement for effective calibration of process-based crop models. *Agricultural and Forest Meteorology* 234–235, 136–148. <https://doi.org/10.1016/j.agrformet.2016.12.015>
- He J., Dukes M.D., Jones J.W., Graham W.D., Judge J., 2009. Applying GLUE for Estimating CERES-Maize Genetic and Soil Parameters for Sweet Corn Production. *Transactions of the ASABE* 52, 1907–1921. <https://doi.org/10.13031/2013.29218>
- He J., Jones J.W., Graham W.D., Dukes M.D., 2010. Influence of likelihood function choice for estimating crop model parameters using the generalized likelihood uncertainty estimation method. *Agricultural Systems* 103, 256–264. <https://doi.org/10.1016/j.agsy.2010.01.006>
- Heinen M., Mollier A., De Willigen P., 2003. Growth of a root system described as diffusion. II. Numerical model and application. *Plant and Soil* 252, 251–265. <https://doi.org/10.1023/A:1024749022761>
- Hidayat T., Koesmaryono Y., Impron, Ghulamahdi M., 2019. Intensifying of reflected radiation under oil palm canopy and its effect on growth and production of soybean. *IOP Conference Series: Earth and Environmental Science* 365, 012001. <https://doi.org/10.1088/1755-1315/365/1/012001>
- Hoffmann H., Enders A., Siebert S., Gaiser T., Ewert F., 2016a. Climate and soil input data aggregation effects in crop models. <https://doi.org/10.7910/DVN/C0J5BB>
- Hoffmann H., Zhao G., Asseng S., Bindi M., Biernath C., Constantin J., Coucheny E., Dechow R., Doro L., Eckersten H., Gaiser T., Grosz B., Heinlein F., Kassie B.T., Kersebaum K.-C., Klein C., Kuhnert M., Lewan E., Moriondo M., Nendel C., Priesack E., Raynal H., Roggero P.P., Rötter R.P., Siebert S., Specka X., Tao F., Teixeira E., Trombi G., Wallach D., Weihermüller L., Yeluripati J., Ewert F., 2016b. Impact of Spatial Soil and Climate Input Data Aggregation on Regional Yield Simulations. *PLOS ONE* 11, e0151782. <https://doi.org/10.1371/journal.pone.0151782>
- Hoffmann H., Zhao G., van Bussel L.G.J., Enders A., Specka X., Sosa C., Yeluripati J., Tao F., Constantin J., Raynal H., Teixeira E., Grosz B., Doro L., Zhao Z., Wang E., Nendel C., Kersebaum K.C., Haas E., Kiese R., Klatt S., Eckersten H., Vanuytrecht E., Kuhnert M., Lewan E., Rotter R., Roggero P.P., Wallach D., Cammarano D., Asseng S., Krauss G., Siebert S., Gaiser T., Ewert F., 2015. Variability of effects of spatial climate data aggregation on regional yield simulation by crop models. *Climate Research* 65, 53–69. <https://doi.org/10.3354/cr01326>
- Holzworth D.P., Huth N.I., deVoil P.G., 2011. Simple software processes and tests improve the reliability and usefulness of a model. *Environmental Modelling & Software* 26, 510–516. <https://doi.org/10.1016/j.envsoft.2010.10.014>
- Holzworth D.P., Snow V., Janssen S., Athanasiadis I.N., Donatelli M., Hoogenboom G., White J.W., Thorburn P., 2015. Agricultural production systems modelling and software: Current status and future prospects. *Environmental Modelling & Software* 72, 276–286. <https://doi.org/10.1016/j.envsoft.2014.12.013>

- Hooghoudt S.B., 1940. General consideration of the problem of field drainage by parallel drains, ditches, watercourses and channels, in: *Contribution to the Knowledge of Some Physical Parameters of the Soil*. Bodemkundig Instituut, Groningen, The Netherlands.
- Hucl P., 1993. Effects of temperature and moisture stress on the germination of diverse common bean genotypes. *Canadian Journal of Plant Science* 73, 697–702. <https://doi.org/10.4141/cjps93-091>
- Humblot P., Leconte-Demarsy D., Clerino P., Szopa S., Castell J.-F., Jayet P.A., 2013. Assessment of ozone impacts on farming systems: A bio-economic modeling approach applied to the widely diverse French case. *Ecological Economics* 85, 50–58. <https://doi.org/10.1016/j.ecolecon.2012.10.012>
- Hungria M., Vargas M.A.T., 2000. Environmental factors affecting N₂ fixation in grain legumes in the tropics, with an emphasis on Brazil. *Field Crops Research* 65, 151–164. [https://doi.org/10.1016/S0378-4290\(99\)00084-2](https://doi.org/10.1016/S0378-4290(99)00084-2)
- Hunt L.A., Pararajasingham S., 1995. CROPSIM — WHEAT: A model describing the growth and development of wheat. *Canadian Journal of Plant Science* 75, 619–632. <https://doi.org/10.4141/cjps95-107>
- Huth N.I., Carberry P.S., Poulton P.L., Brennan L.E., Keating B.A., 2002. A framework for simulating agroforestry options for the low rainfall areas of Australia using APSIM. *European Journal of Agronomy* 18, 171–185. [https://doi.org/10.1016/S1161-0301\(02\)00103-X](https://doi.org/10.1016/S1161-0301(02)00103-X)
- Hyvönen R., Ågren G., Linder S., Persson T., Cotrufo M., Ekblad A., Freeman M., Grelle A., Janssens I., Jarvis P., Kellomäki S., Lindroth A., Lundmark T., Norby R., Oren R., Pilegaard K., Ryan M., Sigurdsson B., Strömberg M., van Oijen M., Wallin G., 2007. The likely impact of elevated [CO₂], nitrogen deposition, increased temperature and management on carbon sequestration in temperate and boreal forest ecosystems: A literature review. *New Phytologist* 173, 463–480. <https://doi.org/10.1111/j.1469-8137.2007.01967.x>
- Idso S.B., 1991. A general relationship between CO₂-induced increases in net photosynthesis and concomitant reductions in stomatal conductance. *Environmental and Experimental Botany* 31, 381–383. [https://doi.org/10.1016/0098-8472\(91\)90035-M](https://doi.org/10.1016/0098-8472(91)90035-M)
- Idso S.B., Jackson R.D., Reginato R.J., 1978. Extending the "DegreeDay" Concept of Plant Phenological Development to Include Water Stress Effects. *Ecology* 59, 431–433. <https://doi.org/10.2307/1936570>
- INRA, 2018. Base de Données Géographique des Sols de France à 1/1 000 000 version 3.2.8.0, 10/09/1998. <https://doi.org/10.15454/BPN57S>
- IPCC, 2007. Climate Change 2007: The physical science basis. Contribution of working group I to the fourth assessment report of the intergovernmental panel on climate change. Cambridge University Press, Cambridge, United Kingdom ; New York, USA.
- Itabari J.K., Gregory P.J., Jones R.K., 1993. Effects of Temperature, Soil Water Status and Depth of Planting on Germination and Emergence of Maize (*Zea mays*) Adapted to Semi-Arid Eastern Kenya. *Experimental Agriculture* 29, 351–364. <https://doi.org/10.1017/S0014479700020913>
- Itier B., Brisson N., Doussan C., Tournebise R., 1997. Bilan hydrique en agrométéorologie, in: Cruiziat, P. (Ed.), *Actes. Tome 2: Du Couvert Végétal à La Région*. INRA Editions, Le Croisic, France, pp. 383–397.
- Jacquemoud S., Baret F., Hanocq J.F., 1992. Modeling spectral and bidirectional soil reflectance. *Remote Sensing of Environment* 41, 123–132. [https://doi.org/10.1016/0034-4257\(92\)90072-R](https://doi.org/10.1016/0034-4257(92)90072-R)
- Jakeman A.J., Letcher R.A., Norton J.P., 2006. Ten iterative steps in development and evaluation of environmental models. *Environmental Modelling & Software* 21, 602–614. <https://doi.org/10.1016/j.envsoft.2006.01.004>
- Jakku E., Thorburn P.J., 2010. A conceptual framework for guiding the participatory development of agricultural decision support systems. *Agricultural Systems* 103, 675–682. <https://doi.org/10.1016/j.agsy.2010.08.007>
- Jamieson P.D., Brooking I.R., Porter J.R., Wilson D.R., 1995. Prediction of leaf appearance in wheat: A question of temperature. *Field Crops Research* 41, 35–44. [https://doi.org/10.1016/0378-4290\(94\)00102-1](https://doi.org/10.1016/0378-4290(94)00102-1)
- Jayasundara H.P.S., Thomson B.D., Tang C., 1997. Responses of cool season grain legumes to soil abiotic stresses, in: Sparks, D.L. (Ed.), *Advances in Agronomy*. Academic Press, pp. 77–151. [https://doi.org/10.1016/S0065-2113\(08\)60242-4](https://doi.org/10.1016/S0065-2113(08)60242-4)

- Jayet P.A., Petsakos A., 2013. Evaluating the Efficiency of a UniformN-InputTax under DifferentPolicyScenarios at DifferentScales. *Environmental Modeling & Assessment* 18, 57–72. <https://doi.org/10.1007/s10666-012-9331-5>
- Jégo G., Chantigny M., Pattey E., Bélanger G., Rochette P., Vanasse A., Goyer C., 2014. Improved snow-cover model for multi-annual simulations with the STICS crop model under cold, humid continental climates. *Agricultural and Forest Meteorology* 195–196, 38–51. <https://doi.org/10.1016/j.agrformet.2014.05.002>
- Jégo G., Pattey E., Liu J., 2012a. Using LeafAreaIndex, retrieved from optical imagery, in the STICS crop model for predicting yield and biomass of field crops. *Field Crops Research* 131, 63–74. <https://doi.org/10.1016/j.fcr.2012.02.012>
- Jégo G., Sánchez-Pérez J.M., Justes E., 2012b. Predicting soil water and mineral nitrogen contents with the STICS model for estimating nitrate leaching under agricultural fields. *Agricultural Water Management* 107, 54–65. <https://doi.org/10.1016/j.agwat.2012.01.007>
- Jensen E.S., 1987. Seasonal patterns of growth and nitrogen fixation in field-grown pea. *Plant and Soil* 101, 29–37. <https://doi.org/10.1007/BF02371027>
- Jeuffroy M.H., Barre C., Bouchard C., Demotes-Mainard S., Devienne-Barret F., Girard M.L., Recous S., 2000. Fonctionnement d'un peuplement de blé en conditions de nutrition azotée sub-optimale, in: Bonhomme, R., Maillard, P. (Eds.), *Fonctionnement Des Peuplements Végétaux Sous Contraintes Environnementales*, Colloques de l'INRA. INRA Editions, Paris, France, pp. 289–304.
- Jeuffroy M.-H., Recous S., 1999. Azodyn: A simple model simulating the date of nitrogen deficiency for decision support in wheat fertilization. *European Journal of Agronomy* 10, 129–144. [https://doi.org/10.1016/S1161-0301\(98\)00059-8](https://doi.org/10.1016/S1161-0301(98)00059-8)
- Jeuffroy M.-H., Warembourg F.R., 1991. Carbon Transfer and Partitioning between Vegetative and ReproductiveOrgans in *Pisum sativum*L. *Plant Physiology* 97, 440–448. <https://doi.org/10.1104/pp.97.1.440>
- Jing Q., Huffman T., Shang J., Liu J., Pattey E., Morrison M., Jégo G., Qian B., 2017. Modelling soybean yield responses to seeding date under projected climate change scenarios. *Canadian Journal of Plant Science* 97, 1152–1164. <https://doi.org/10.1139/cjps-2017-0065>
- Johnson I., Clark D., Clothier B., Giltrap D., Rissman C., Roskrug N., Thorburn P., White R., 2021. Overseer whole-model review- Assessment of the model approach (MPI Technical Paper No. 2021/12). Ministry for Primary Industries; the Ministry for the Environment, Wellington New Zealand.
- Jones H.G., 2013. *Plants and microclimate: A quantitative approach to environmental plant physiology*, 3rd edition. Cambridge University Press, Cambridge. <https://doi.org/10.1017/CBO9780511845727>
- Jones J.W., Antle J.M., Basso B., Boote K.J., Conant R.T., Foster I., Godfray H.C.J., Herrero M., Howitt R.E., Janssen S., Keating B.A., Munoz-Carpena R., Porter C.H., Rosenzweig C., Wheeler T.R., 2017. Brief history of agricultural systems modeling. *Agricultural Systems* 155, 240–254. <https://doi.org/10.1016/j.agsy.2016.05.014>
- Jones J.W., Dayan E., Allen L.H., van Keulen H., Challa H., 1991. A dynamic tomato growth and yield model (TOMGRO). *Transactions of the ASAE* 34, 0663–0672. <https://doi.org/10.13031/2013.31715>
- Jones J.W., Hoogenboom G., Porter C.H., Boote K.J., Batchelor W.D., Hunt L.A., Wilkens P.W., Singh U., Gijsman A.J., Ritchie J.T., 2003. The DSSAT cropping system model. *European Journal of Agronomy* 18, 235–265. [https://doi.org/10.1016/S1161-0301\(02\)00107-7](https://doi.org/10.1016/S1161-0301(02)00107-7)
- Justes E., Beaudoin N., Bertuzzi P., Charles R., Constantin J., Durr C., Hermon C., Joannon A., Le Bas C., Mary B., Mignolet C., Montfort F., Ruiz L., Sarthou J.-P., Souchère V., Tournebize J., Rechauchère O., Savini I., Barbier M., Leiser H., 2013. Les cultures intermédiaires pour une production agricole durable, Matière à débattre et décider. Editions Quae.
- Justes E., Beaudoin N., Bertuzzi P., Charles R., Constantin J., Dürr C., Hermon C., Joannon A., Le Bas C., Mary B., Mignolet C., Montfort F., Ruiz L., Sarthou J.-P., Souchère V., Tournebize J., Savini I., Réchauchère O., 2012. The use of cover crops to reduce nitrate leaching. Effect on the water and nitrogen balance and other ecosystem services, in: *Proceedings n°719, 7-8/12/2012*. The International Fertiliser Society, Leek, United Kingdom, pp. 27 p.

- Justes E., Constantin J., Beaudoin N., Dürr C., Mary B., Ruiz L., 2017. Main lessons drawn from the simulation study, in: Justes, E. (Ed.), *Cover Crops for Sustainable Farming*. Springer, Dordrecht, The Netherlands. https://doi.org/10.1007/978-94-024-0986-4_3
- Justes E., Jeuffroy M.H., Mary B., 1997. Wheat, barley, and durum wheat, in: Lemaire, G. (Ed.), *Diagnosis of the Nitrogen Status in Crops*. Springer, Berlin, Heidelberg, pp. 73–91. https://doi.org/10.1007/978-3-642-60684-7_4
- Justes E., Mary B., Meynard J.M., Machet J.M., Thelier-Huche L., 1994. Determination of a Critical Nitrogen Dilution Curve for Winter Wheat Crops. *Annals of Botany* 74, 397–407. <https://doi.org/10.1006/anbo.1994.1133>
- Justes E., Mary B., Nicolardot B., 2009. Quantifying and modelling C and N mineralization kinetics of catch crop residues in soil: Parameterization of the residue decomposition module of STICS model for mature and non mature residues. *Plant and Soil* 325, 171–185. <https://doi.org/10.1007/s11104-009-9966-4>
- Kage H., Ehlers W., 1996. Does transport of water to roots limit water uptake of field crops? *Zeitschrift für Pflanzenernährung und Bodenkunde* 159, 583–590. <https://doi.org/10.1002/jpln.1996.3581590609>
- Keating B.A., Thorburn P.J., 2018. Modelling crops and cropping systems—Evolving purpose, practice and prospects. *Recent advances in crop modelling to support sustainable agricultural production and food security under global change* 100, 163–176. <https://doi.org/10.1016/j.eja.2018.04.007>
- Kersebaum K.C., Richter J., 1991. Modelling nitrogen dynamics in a plant-soil system with a simple model for advisory purposes, in: Groot, J.J.R., De Willigen, P., Verberne, E.L.J. (Eds.), *Nitrogen Turnover in the Soil-Crop System*, Developments in Plant and Soil Sciences. Springer, Dordrecht, The Netherlands, pp. 273–281. https://doi.org/10.1007/978-94-011-3434-7_12
- Khalil K., Mary B., Renault P., 2004. Nitrous oxide production by nitrification and denitrification in soil aggregates as affected by O₂ concentration. *Soil Biology and Biochemistry* 36, 687–699. <https://doi.org/10.1016/j.soilbio.2004.01.004>
- Kiniry J.R., Williams J.R., Gassman P.W., Debaeke P., 1992. A general, process-oriented model for two competing plant species. *Transactions of the ASAE* 35, 801–810. <https://doi.org/10.13031/2013.28665>
- Kirschbaum M., 2006. The temperature dependence of organic-matter decomposition—still a topic of debate. *Soil Biology and Biochemistry* 38, 2510–2518. <https://doi.org/10.1016/j.soilbio.2006.01.030>
- Kizza T., Sekhar M., Rao S.M., Ruiz L., 2016. Model based estimation of turmeric yield response to saline groundwater irrigation. *International Journal of Scientific Research and Engineering Studies (IJSRES)* 3, 8–12.
- Kollas C., Kersebaum K.C., Nendel C., Manevski K., Müller C., Palosuo T., Armas-Herrera C.M., Beaudoin N., Bindi N., Charfeddine M., Conradt T., Constantin J., Eitzinger J., Ewert F., Ferrise R., Gaiser T., García de Cortázar Aauri I., Giglio L., Hlavinka P., Hoffmann H., Hoffmann M.P., Launay M., Manderscheid R., Mary B., Mirschel W., Moriondo M., Olesen J.E., Öztürk I., Pacholski A., Ripoche-Wachter D., Roggero P.P., Roncossek S., Rötter R.P., Ruget F., Sharif B., Trnka M., Ventrella D., Waha K., Wegehenkel M., Weigel H.-J., Wu L., 2015. Crop rotation modelling—A European model intercomparison. *European Journal of Agronomy* 70, 98–111. <https://doi.org/10.1016/j.eja.2015.06.007>
- Kouchi H., Nakaji K., 1985. Utilization and Metabolism of Photoassimilated ¹³C in Soybean Roots and Nodules. *Soil Science and Plant Nutrition* 31, 323–334. <https://doi.org/10.1080/00380768.1985.10557440>
- Kuhnert M., Yeluripati J., Smith P., Hoffmann H., van Oijen M., Constantin J., Coucheney E., Dechow R., Eckersten H., Gaiser T., Grosz B., Haas E., Kersebaum K.-C., Kiese R., Klatt S., Lewan E., Nendel C., Raynal H., Sosa C., Specka X., Teixeira E., Wang E., Weihermüller L., Zhao G., Zhao Z., Ogle S., Ewert F., 2017. Impact analysis of climate data aggregation at different spatial scales on simulated net primary productivity for croplands. *European Journal of Agronomy* 88, 41–52. <https://doi.org/10.1016/j.eja.2016.06.005>
- Kvakić M., Pellerin S., Ciais P., Achat D.L., Augusto L., Denoroy P., Gerber J.S., Goll D., Mollier A., Mueller N.D., Wang X., Ringeval B., 2018. Quantifying the Limitation to World Cereal Production Due To Soil Phosphorus Status. *Global Biogeochemical Cycles* 32, 143–157. <https://doi.org/10.1002/2017GB005754>

- Lacape M.J., Wery J., Annerose D.J.M., 1998. Relationships between plant and soil water status in five field-grown cotton (*Gossypium hirsutum*L.) cultivars. *Field Crops Research* 57, 29–43. [https://doi.org/10.1016/S0378-4290\(97\)00111-1](https://doi.org/10.1016/S0378-4290(97)00111-1)
- Laгарias J.C., Reeds J.A., Wright M.H., Wright P.E., 1998. Convergence Properties of the Nelder–MeadSimplexMethod in LowDimensions. *SIAM Journal on Optimization* 9, 112–147. <https://doi.org/10.1137/S1052623496303470>
- Lammoglia S.-K., Makowski D., Moeys J., Justes E., Barriuso E., Mamy L., 2017. Sensitivity analysis of the STICS-MACRO model to identify cropping practices reducing pesticides losses. *Science of The Total Environment* 580, 117–129. <https://doi.org/10.1016/j.scitotenv.2016.10.010>
- Launay C., Constantin J., Chlebowski F., Houot S., Graux A.-I., Klumpp K., Martin R., Mary B., Pellerin S., Therond O., 2021. Estimating the carbon storage potential and greenhouse gas emissions of French arable cropland using high-resolution modeling. *Global Change Biology* 27, 1645–1661. <https://doi.org/10.1111/gcb.15512>
- Launay M., Brisson N., 2004. STICS' adaptability to a novel crop as an application of modularity in crop modelling: Example of sugar beet, in: Jacobsen, S.E., Jensen, C.R., Porter, J.R. (Eds.), *European Agriculture in a Global Context, 8th ESA Congress, 11-15/07/2004*. Royal Veterinary; Agricultural University, Copenhagen, Denmark, pp. 283–284.
- Launay M., Brisson N., Satger S., Hauggaard-Nielsen H., Corre-Hellou G., Kasynova E., Ruske R., Jensen E.S., Gooding M.J., 2009. Exploring options for managing strategies for pea-barley intercropping using a modeling approach. *European Journal of Agronomy* 31, 85–98. <https://doi.org/10.1016/j.eja.2009.04.002>
- Lawrie A.C., Wheeler C.T., 1974. The effects of flowering and fruit formation on the supply of photosynthetic assimilates to the nodules of *Pisum sativum* l. In relation to the fixation of nitrogen. *New Phytologist* 73, 1119–1127. <https://doi.org/10.1111/j.1469-8137.1974.tb02141.x>
- Le Bas C., 2016. Impact des incertitudes des paramètres sols estimés à partir de la Base de DonnéesGéographique des Sols de France sur les sorties du modèle de culture Stics. Approche méthodologique (Thèse de doctorat). AgroParisTech.
- Lecharpentier P., Vezy Rémi, Buis S., Giner M., 2021b. SticsRFiles: Read and modify STICS input/output files. <https://doi.org/10.5281/ZENODO.4443206>
- Lecharpentier P., Vezy Rémi, Buis S., Giner M., 2021a. SticsOnR: Manage STICS simulations running the executable orJavaStics. <https://doi.org/10.5281/ZENODO.4443130>
- Lecharpentier P., Vezy Remi, SticsRPacks, 2021c. SticsRFiles: Read and modify STICS input/output files.
- Leclère D., Jayet P.A., Noblet-Ducoudré N. de, 2013. Farm-level AutonomousAdaptation of EuropeanAgriculturalSupply to ClimateChange. *Ecological Economics* 87, 1–14. <https://doi.org/10.1016/j.ecolecon.2012.11.010>
- Lecoœur J., Sinclair T.R., 2001. Analysis of nitrogen partitioning in field pea resulting in linear increase in nitrogen harvest index. *Field Crops Research* 71, 151–158. [https://doi.org/10.1016/S0378-4290\(01\)00151-4](https://doi.org/10.1016/S0378-4290(01)00151-4)
- Ledoux E., Gomez E., Monget J.M., Viavattene C., Viennot P., Ducharne A., Benoit M., Mignolet C., Schott C., Mary B., 2007. Agriculture and groundwater nitrate contamination in the Seine basin. TheSTICS-MODCOU modelling chain. *Science of The Total Environment* 375, 33–47. <https://doi.org/10.1016/j.scitotenv.2006.12.002>
- Leenhardt D., Voltz M., Rambal S., 1995. A survey of several agroclimatic soil water balance models with reference to their spatial application. *European Journal of Agronomy* 4, 1–14. [https://doi.org/10.1016/S1161-0301\(14\)80012-9](https://doi.org/10.1016/S1161-0301(14)80012-9)
- Lefebvre M.-P., 2010. Spatialisation de modèles de fonctionnement hydromécanique des sols appliquée à la prévision des risques de tassement à l'échelle de la France (Thèse de doctorat). Université d'Orléans.
- Lemaire G., Gastal F., 1997. N uptake and distribution in plant canopies, in: Lemaire, G. (Ed.), *Diagnosis of the Nitrogen Status in Crops*. Springer, Berlin, Heidelberg, pp. 3–43. https://doi.org/10.1007/978-3-642-60684-7_1

- Lemaire G., Salette J., Sigogne M., Terrasson J.-P., 1984. Relation entre dynamique de croissance et dynamique de prélèvement d'azote pour un peuplement de graminées fourragères. I. — Etude de l'effet du milieu. *Agronomie* 4, 423–430. <https://doi.org/10.1051/agro:19840503>
- Léonard J., 2016. Nitrification, denitrification and N₂O emissions in STICS.
- Levasseur F., Mary B., Houot S., 2021. C and N dynamics with repeated organic amendments can be simulated with the STICS model. *Nutrient Cycling in Agroecosystems*. <https://doi.org/10.1007/s10705-020-10106-5>
- Limaux F., Recous S., Meynard J.-M., Guckert A., 1999. Relationship between rate of crop growth at date of fertiliser N application and fate of fertiliser N applied to winter wheat. *Plant and Soil* 214, 49–59. <https://doi.org/10.1023/A:1004629511235>
- Loague K., Corwin D.L., 1996. Uncertainty in regional-scale assessments of non-point source pollutants, in: Corwin, D.L., Loague, K. (Eds.), *Applications of GIS to the Modeling of Non-Point Source Pollutants in the Vadose Zone*, SSSASpecialPublication. pp. 131–152. <https://doi.org/10.2136/sssaspecpub48.c7>
- Loague K., Green R., 1991. Statistical and graphical methods for evaluating solute transport models: Overview and application. *Journal of Contaminant Hydrology* 7, 51–73. [https://doi.org/10.1016/0169-7722\(91\)90038-3](https://doi.org/10.1016/0169-7722(91)90038-3)
- Ludwig B., John B., Ellerbrock R., Kaiser M., Flessa H., 2003. Stabilization of carbon from maize in a sandy soil in a long-term experiment. *European Journal of Soil Science* 54, 117–126. <https://doi.org/10.1046/j.1365-2389.2003.00496.x>
- Ludwig B., Schulz E., Rethemeyer J., Merbach I., Flessa H., 2007. Predictive modelling of C dynamics in the long-term fertilization experiment at BadLauchstädt with the RothamstedCarbonModel. *European Journal of Soil Science* 58, 1155–1163. <https://doi.org/10.1111/j.1365-2389.2007.00907.x>
- Luo Z., Wang E., Sun O.J., 2010. Can no-tillage stimulate carbon sequestration in agricultural soils? A meta-analysis of paired experiments. *Agriculture Ecosystems & Environment* 139, 224–231. <https://doi.org/10.1016/j.agee.2010.08.006>
- Maas S.J., 1993. Parameterized Model of GramineousCropGrowth: I. LeafArea and DryMassSimulation. *Agronomy Journal* 85, 348–353. <https://doi.org/10.2134/agronj1993.00021962008500020034x>
- MacDuff J.H., Jarvis S.C., Davidson I.A., 1996. Inhibition of N₂ fixation by white clover (*Trifolium repens*L.) at low concentrations of NO₃⁻ in flowing solution culture. *Plant and Soil* 180, 287–295. <https://doi.org/10.1007/BF00015312>
- Magid J., De Neergaard A., Brandt M., 2006. Heterogeneous distribution may substantially decrease initial decomposition, long-term microbial growth and N-immobilization from high C-to-N ratio resources. *European Journal of Soil Science* 57, 517–529. <https://doi.org/10.1111/j.1365-2389.2006.00805.x>
- Maharjan G.R., Hoffmann H., Webber H., Srivastava A.K., Weihermueller L., Villa A., Coucheny E., Lewan E., Trombi G., Moriondo M., Bindi M., Grosz B., Dechow R., Kuhnert M., Doro L., Kersebaum K.-C., Stella T., Specka X., Nendel C., Constantin J., Raynal H., Ewert F., Gaiser T., 2019. Effects of input data aggregation on simulated crop yields in temperate and Mediterranean climates. *European Journal of Agronomy* 103, 32–46. <https://doi.org/10.1016/j.eja.2018.11.001>
- Mailhol J.C., Ruelle P., Revol P., Delage L., Lescot J.M., 1996. Operative modelling for actual evapotranspiration assessment: Calibration methodology, in: *Proceedings of the International Conference on Evaporation and Irrigation Scheduling*, 3-6/11/1996/. American Society of Agricultural Engineers, San Antonio, Texas, USA, pp. 474–479.
- Makowski D., Wallach D., Tremblay M., 2002. Using a Bayesian approach to parameter estimation; comparison of the GLUE and MCMC methods. *Agronomie* 22, 191–203. <https://doi.org/10.1051/agro:2002007>
- Malone R.W., Meek D.W., Ma L., Jaynes D.B., Nolan B.T., Karlen D.L., Ahuja L.R., Ma L., 2011. Quality assurance of weather data for agricultural system model input: A case study using the walnut creek watershed in central Iowa, in: *Methods of Introducing System Models into Agricultural Research*. John Wiley & Sons, Ltd, pp. 283–295. <https://doi.org/10.2134/advagricsystem2.c10>
- Mary B., Beaudoin N., Justes E., Mchet J.M., 1999. Calculation of nitrogen mineralization and leaching in fallow soil using a simple dynamic model. *European Journal of Soil Science* 50, 549–566. <https://doi.org/10.1046/j.1365-2389.1999.00264.x>

- Mary B., Clivot H., Blaszczyk N., Labreuche J., Ferchaud F., 2020. Soil carbon storage and mineralization rates are affected by carbon inputs rather than physical disturbance: Evidence from a 47-year tillage experiment. *Agriculture Ecosystems & Environment* 299, 106972. <https://doi.org/10.1016/j.agee.2020.106972>
- Mary B., Guérif M., 2005. Effet du stress azoté sur la plante : Définition d'un indice de nutrition instantané. Carry-le-Rouet, pp. 23–27.
- McBratney A.B., Minasny B., Cattle S.R., Vervoort R.W., 2002. From pedotransfer functions to soil inference. *Geoderma* 109, 41–73. [https://doi.org/10.1016/S0016-7061\(02\)00139-8](https://doi.org/10.1016/S0016-7061(02)00139-8)
- McCann R., McFarland M.J., Witz J.A., 1991. Near-surface bare soil temperature model for biophysical models. *Transactions of the ASAE* 34, 0748–0755. <https://doi.org/10.13031/2013.31726>
- McMaster G.S., Klepper B., Rickman R.W., Wilhelm W.W., Willis W.O., 1991. Simulation of shoot vegetative development and growth of unstressed winter wheat. *Ecological Modelling* 53, 189–204. [https://doi.org/10.1016/0304-3800\(91\)90156-U](https://doi.org/10.1016/0304-3800(91)90156-U)
- McMillan W.D., Burgy R.H., 1960. Interception loss from grass. *Journal of Geophysical Research* 65, 2389–2394. <https://doi.org/10.1029/JZ065i008p02389>
- Mesbah M., Pattey E., Jégo G., 2017. A model-based methodology to derive optimum nitrogen rates for rainfed crops - a case study for corn using STICS in Canada. *Computers and Electronics in Agriculture* 142, 572–584. <https://doi.org/10.1016/j.compag.2017.11.011>
- Meurer K.H.E., Haddaway N.R., Bolinder M.A., Katterer T., 2018. Tillage intensity affects total SOC stocks in boreo-temperate regions only in the topsoil-A systematic review using an ESM approach. *Earth-Science Reviews* 177, 613–622. <https://doi.org/10.1016/j.earscirev.2017.12.015>
- Meyer W.S., Green G.C., 1981. Plant indicators of wheat and soybean crop water stress. *Irrigation Science* 2, 167–176. <https://doi.org/10.1007/BF00257978>
- Mignolet C., Schott C., Benoit M., 2004. Spatial dynamics of agricultural practices on a basin territory: A retrospective study to implement models simulating nitrate flow. The case of the Seine basin. *Agronomie* 24, 219–236. <https://doi.org/10.1051/agro:2004015>
- Mignolet C., Schott C., Benoit M., 2007. Spatial dynamics of farming practices in the Seine basin: Methods for agronomic approaches on a regional scale. *Science of The Total Environment* 375, 13–32. <https://doi.org/10.1016/j.scitotenv.2006.12.004>
- Milroy S.P., Goyné P.J., 1995. Leaf area development in barley—model construction and response to soil moisture status. *Australian Journal of Agricultural Research* 46, 845–860. <https://doi.org/10.1071/AR9950845>
- Mondelaers K., Aertsens J., Van Huylenbroeck G., 2009. A meta-analysis of the differences in environmental impacts between organic and conventional farming. *British Food Journal* 111, 1098–1119. <https://doi.org/10.1108/00070700910992925>
- Monteith J.L., 1972. Solar Radiation and Productivity in Tropical Ecosystems. *The Journal of Applied Ecology* 9, 747–766. <https://doi.org/10.2307/2401901>
- Monteith J.L., 1965. Evaporation and environment. Cambridge University Press, pp. 205–234.
- Montesino-San Martín M., Wallach D., Olesen J.E., Challinor A.J., Hoffman M.P., Koehler A.K., Rötter R.P., Porter J.R., 2018. Data requirements for crop modelling—Applying the learning curve approach to the simulation of winter wheat flowering time under climate change. *European Journal of Agronomy* 95, 33–44. <https://doi.org/10.1016/j.eja.2018.02.003>
- Moore A.D., Eckard R.J., Thorburn P.J., Grace P.R., Wang E., Chen D., 2014. Mathematical modeling for improved greenhouse gas balances, agro-ecosystems, and policy development: Lessons from the Australian experience. *WIREs Climate Change* 5, 735–752. <https://doi.org/10.1002/wcc.304>
- Moreau D., Pointurier O., Perthame L., Beaudoin N., Villerd J., Colbach N., 2021. Integrating plant-plant competition for nitrogen into a 3D individual-based model simulating the effects of cropping systems on weed dynamics. *Field Crops Research* 268. <https://doi.org/10.1016/j.fcr.2021.108166>
- Moreau P., Ruiz L., Mabon F., Raimbault T., Durand P., Delaby L., Devienne S., Vertes F., 2012. Reconciling technical, economic and environmental efficiency of farming systems in vulnerable areas. *Agriculture Ecosystems & Environment* 147, 89–99. <https://doi.org/10.1016/j.agee.2011.06.005>

- Moreau P., Viaud V., Parnaudeau V., Salmon-Monviola J., Durand P., 2013. An approach for global sensitivity analysis of a complex environmental model to spatial inputs and parameters: A case study of an agro-hydrological model. *Environmental Modelling & Software* 47, 74–87. <https://doi.org/10.1016/j.envsoft.2013.04.006>
- Morvan T., 1999. Quantification et modélisation des flux d'azote résultant de l'épandage de lisier (Thèse de doctorat). Université de Paris VI.
- Morvan T., Leterme P., 2001. Vers une prévision opérationnelle des flux d'azote résultant de l'épandage de lisier : Paramétrage d'un modèle dynamique de Simulation des transformations de l'azote des lisiers (STAL). *Ingénieries eau-agriculture-territoires* 26, 17–26.
- Muchow R.C., Carberry P.S., 1990. Phenology and leaf-area development in a tropical grain sorghum. *Field Crops Research* 23, 221–237. [https://doi.org/10.1016/0378-4290\(90\)90056-H](https://doi.org/10.1016/0378-4290(90)90056-H)
- Muchow R.C., Sinclair T.R., Bennett J.M., 1990. Temperature and Solar Radiation Effects on Potential Maize Yield across Locations. *Agronomy Journal* 82, 338–343. <https://doi.org/10.2134/agronj.1990.00021962008200020033x>
- Mulder V., Lacoste M., Richer-De-Forges A., Arrouays D., 2016. Global Soil Map France: High-resolution spatial modelling the soils of France up to two meter depth. *Science of The Total Environment* 573, 1352–1369. <https://doi.org/10.1016/j.scitotenv.2016.07.066>
- Mumen M., 2006. Caractérisation du fonctionnement hydrique des sols à l'aide d'un modèle mécaniste de transferts d'eau et de chaleur mis en œuvre en fonction des informations disponibles sur le sol (Thèse de doctorat). Université d'Avignon et des Pays de Vaucluse.
- Munier-Jolain N.G., Munier-Jolain N.M., Roche R., Ney B., Duthion C., 1998. Seed growth rate in grain legumes I. Effect of photoassimilate availability on seed growth rate. *Journal of Experimental Botany* 49, 1963–1969. <https://doi.org/10.1093/jxb/49.329.1963>
- Nelder J.A., 1961. The Fitting of a Generalization of the Logistic Curve. *Biometrics* 17, 89–110. <https://doi.org/10.2307/2527498>
- Nesme T., Brisson N., Lescouret F., Bellon S., Crete X., Plenet D., Habib R., 2006. Epistics: A dynamic model to generate nitrogen fertilisation and irrigation schedules in apple orchards, with special attention to qualitative evaluation of the model. *Agricultural Systems* 90, 202–225. <https://doi.org/10.1016/j.agry.2005.12.006>
- Nicolardot B., Parnaudeau V., Chabalier P., 2006. Effet de la température sur la minéralisation de différents produits organiques apportés dans les sols, in: Findeling, A., Marlet, S., Montange, D., Saint Macary, H. (Eds.), *Impacts Du Recyclage Des Déchets Agro-Industriels : Actes de l'atelier de Clôture de l'ATP, 1-2/07/2004*. Cirad, Montpellier, France.
- Nicolardot B., Recous S., Mary B., 2001. Simulation of C and N mineralisation during crop residue decomposition: A simple dynamic model based on the C:N ratio of the residues. *Plant and Soil* 228, 83–103. <https://doi.org/10.1023/A:1004813801728>
- Nicoullaud B., Couturier A., Beaudoin N., Mary B., Coutadeur C., King D., 2004. Modélisation spatiale à l'échelle parcellaire des effets de la variabilité des sols et des pratiques culturales sur la pollution nitrique agricole, in: Monestiez, P., Lardon, S., Seguin, B. (Eds.), *Organisation Spatiale Des Activités Agricoles Et Processus Environnementaux*, Science Update. INRA Editions, Paris, France, pp. 143–161.
- Nicoullaud B., King D., Tardieu F., 1994. Vertical distribution of maize roots in relation to permanent soil characteristics. *Plant and Soil* 159, 245–254. <https://doi.org/10.1007/BF00009287>
- Novak V., 1989. Determination of critical moisture contents of soils in the course of evapotranspiration. *Sov. Soil Sci.* 122–126.
- Ojeda J.J., Huth N., Holzworth D., Raymundo R., Zyskowski R.F., Sinton S.M., Michel A.J., Brown H.E., 2021. Assessing errors during simulation configuration in crop models – A global case study using APSIM-Potato. *Ecological Modelling* 458, 109703. <https://doi.org/10.1016/j.ecolmodel.2021.109703>
- Ong C.K., 1983. Response to Temperature in a Stand of Pearl Millet (*Pennisetum typhoides* S. & H.). *Journal of Experimental Botany* 34, 322–336. <https://doi.org/10.1093/jxb/34.3.322>
- Oorts K., Laurent F., Mary B., Thiébeau P., Labreuche J., Nicolardot B., 2007. Experimental and simulated soil mineral N dynamics for long-term tillage systems in northern France. *Soil and Tillage Research* 94, 441–456. <https://doi.org/10.1016/j.still.2006.09.004>

- Otegui M.E., Nicolini M.G., Ruiz R.A., Dodds P.A., 1995. Sowing Date Effects on Grain Yield Components for Different Maize Genotypes. *Agronomy Journal* 87, 29–33. <https://doi.org/10.2134/agronj1995.00021962008700010006x>
- Ozier-Lafontaine H., Lecompte F., Sillon J.F., 1999. Fractal analysis of the root architecture of *Gliricidia sepium* for the spatial prediction of root branching, size and mass: Model development and evaluation in agroforestry. *Plant and Soil* 209, 167–179. <https://doi.org/10.1023/A:1004461130561>
- Pachepsky Y., Rawls W.J., 2004. Preface: Status of pedotransfer functions, in: Pachepsky, Y., Rawls, W.J. (Eds.), *Development of Pedotransfer Functions in Soil Hydrology*, Developments in Soil Science. Elsevier, Amsterdam, The Netherlands, p. 512.
- Pagès L., Bécel C., Boukcim H., Moreau D., Nguyen C., Voisin A.-S., 2014. Calibration and evaluation of ArchiSimple, a simple model of root system architecture. *Ecological Modelling* 290, 76–84. <https://doi.org/10.1016/j.ecolmodel.2013.11.014>
- Palacios E., Quevedo A.N., 1996. Irrigation scheduling using small evaporation pan and computer program for developing countries, in: *Proceedings of the International Conference on Evapotranspiration and Irrigation Scheduling, 3-6/11/1996*. American Society of Agricultural Engineers, San Antonio, Texas, USA, pp. 1029–1034.
- Pararajasingham S., Hunt L.A., 1991. Wheat Spike Temperature in Relation to Base Temperature for Grain Filling Duration. *Canadian Journal of Plant Science* 71, 63–69. <https://doi.org/10.4141/cjps91-007>
- Parton W.J., Schimel D.S., Cole C.V., Ojima D.S., 1987. Analysis of Factors Controlling Soil Organic Matter Levels in Great Plains Grasslands. *Soil Science Society of America Journal* 51, 1173–1179. <https://doi.org/10.2136/sssaj1987.03615995005100050015x>
- Passioura J.B., 1996. Simulation Models: Science, Snake Oil, Education, or Engineering? *Agronomy Journal* 88, 690–694. <https://doi.org/10.2134/agronj1996.00021962008800050002x>
- Peart R.M., Jones J.W., Curry R.B., Boote K., Allen L.H., 1989. Impact of climate change on crop yield in the southwestern USA: A simulation study, in: Smith, J.B., Tirpak, D.A. (Eds.), *The Potential Effects of Global Climate Change on the United States. Report to Congress*. United States Environmental Protection Agency, Washington, DC, USA, pp. 1–54.
- Pellegrino A., Wery J., Lebon E., 2002. Crop management adaptation to water-limited environments, in: Villalobos, F.J., Testi, L. (Eds.), *Proceedings of the VII ESA Congress, 15-18/07/2002*. Junta de Andalucía, Consejería de Agricultura y Pesca, Cordoba, Spain, pp. 313–314.
- Pellerin S., Bamière L., Launay C., Martin R., Schiavo M., Angers D., Augusto L., Balesdent J., Basile-Doelsch I., Bellassen V., Cardinael R., Cécillon L., Ceschia E., Chenu C., Constantin J., Daroussin J., Delacote P., Delame N., Gastal F., Gilbert D., Graux A.-I., Guenet B., Houot S., Klumpp K., Letort E., Litrico I., Martin M., Menasseri-Aubry S., Meziere D., Morvan T., Mosnier C., Roger-Estrade J., Saint-André L., Sierra J., Therond O., Viaud V., Grateau R., Le Perchec S., Savini I., Rechauchère O., 2020. Stocker du carbone dans les sols français. Quel potentiel au regard de l'objectif 4 pour 1000 et à quel coût ? (Other). INRA.
- Peña-Cabriaes J.J., Castellanos J.Z., 1993. Effects of water stress on N₂ fixation and grain yield of *Phaseolus vulgaris* L. *Plant and Soil* 152, 151–155. <https://doi.org/10.1007/BF00016345>
- Penman H.L., 1948. Natural evaporation from open water, bare soil and grass. *Proceedings of the Royal Society of London. Series A. Mathematical and Physical Sciences* 193, 120–145. <https://doi.org/10.1098/rspa.1948.0037>
- Perarnaud V., Seguin B., Malezieux E., Deque M., Loustau D., 2005. Agrometeorological research and applications needed to prepare agriculture and forestry to 21st century climate change. *Climatic Change* 70, 319–340. <https://doi.org/10.1007/s10584-005-5953-9>
- Perfect E., Sukop M.C., Haszler G.R., 2002. Prediction of Dispersivity for Undisturbed Soil Columns from Water Retention Parameters. *Soil Science Society of America Journal* 66, 696–701. <https://doi.org/10.2136/sssaj2002.6960>
- Perrin A., Basset-Mens C., Huat J., Gabrielle B., 2017. The variability of field emissions is critical to assessing the environmental impacts of vegetables: A Benin case-study. *Journal of Cleaner Production* 153, 104–113. <https://doi.org/10.1016/j.jclepro.2017.03.159>

- Peyrard C., Ferchaud F., Mary B., Grehan E., Leonard J., 2017. Management Practices of *miscanthus x giganteus* Strongly Influence Soil Properties and N₂O Emissions Over the Long Term. *Bioenergy Research* 10, 208–224. <https://doi.org/10.1007/s12155-016-9796-1>
- Plaza-Bonilla D., Nolot J.-M., Raffaillac D., Justes E., 2015. Cover crops mitigate nitrate leaching in cropping systems including grain legumes: Field evidence and model simulations. *Agriculture Ecosystems & Environment* 212, 1–12. <https://doi.org/10.1016/j.agee.2015.06.014>
- Porter C.H., Villalobos C., Holzworth D., Nelson R., White J.W., Athanasiadis I.N., Janssen S., Ripoche D., Cufi J., Raes D., Zhang M., Knapen R., Sahajpal R., Boote K., Jones J.W., 2014. Harmonization and translation of crop modeling data to ensure interoperability. *Environmental Modelling & Software* 62, 495–508. <https://doi.org/10.1016/j.envsoft.2014.09.004>
- Post D.F., Fimbres A., Matthias A.D., Sano E.E., Accioli L., Batchily A.K., Ferreira L.G., 2000. Predicting soil albedo from soil color and spectral reflectance data. *Soil Science Society of America Journal* 64, 1027–1034. <https://doi.org/10.2136/sssaj2000.6431027x>
- Powlson D.S., Hart P.B.S., Poulton P.R., Johnston A.E., Jenkinson D.S., 1992. Influence of soil type, crop management and weather on the recovery of ¹⁵N-labelled fertilizer applied to winter wheat in spring. *The Journal of Agricultural Science* 118, 83–100. <https://doi.org/10.1017/S0021859600068040>
- Powlson D.S., Pruden T.L.G., Johnston A.E., Jenkinson D.S., 1986. The nitrogen cycle in the BroadbalkWheatExperiment: Recovery and losses of ¹⁵N-labelled fertilizer applied in spring and inputs of nitrogen from the atmosphere. *The Journal of Agricultural Science* 107, 591–609. <https://doi.org/10.1017/S0021859600069768>
- Priestley C.H.B., Taylor R.J., 1972. On the assessment of surface heat flux and evaporation using large-scale parameters. *Monthly Weather Review* 100, 81–92. [https://doi.org/10.1175/1520-0493\(1972\)100%3C0081:OTAOSH%3E2.3.CO;2](https://doi.org/10.1175/1520-0493(1972)100%3C0081:OTAOSH%3E2.3.CO;2)
- Puech T., Schott C., Mignolet C., 2015. Modélisation de la pollution nitrique d'origine agricole des grands aquifères du bassin de Seine-Normandie à l'échelle des masses d'eau. Vol. 1. Évolution des systèmes de culture sur le bassin Seine- Normandie depuis les années 2000 : Construction d'une base de données spatialisée sur les pratiques agricoles (Contract). Agence de l'Eau Seine Normandie (AESN).
- Puntel L.A., Sawyer J.E., Barker D.W., Thorburn P.J., Castellano M.J., Moore K.J., VanLoocke A., Heaton E.A., Archontoulis S.V., 2018. A Systems Modeling Approach to Forecast Corn Economic Optimum Nitrogen Rate. *Frontiers in Plant Science* 9, 436. <https://doi.org/10.3389/fpls.2018.00436>
- Queyrel W., Habets F., Blanchoud H., Ripoche D., Launay M., 2016. Pesticide fate modeling in soils with the crop model STICS: Feasibility for assessment of agricultural practices. *Science of The Total Environment* 542, Part A, 787–802. <https://doi.org/10.1016/j.scitotenv.2015.10.066>
- Quintana Segui P., Martin E., Habets F., Noilhan J., 2009. Improvement, calibration and validation of a distributed hydrological model over France. *Hydrology and Earth System Sciences* 13, 163–181. <https://doi.org/10.5194/hess-13-163-2009>
- R Core Team, 2020. R: A language and environment for statistical computing. R Foundation for Statistical Computing, Vienna, Austria.
- Rakotovololona L., 2018. Quantification expérimentale et modélisation de la production, des flux d'eau et d'azote en systèmes de culture biologiques (Thèse de doctorat). Institut agronomique, vétérinaire et forestier de France.
- Rao Kanneganti V., Fick G.W., 1991. A warm-season annual grass growth model parameterized for maize and sudangrass. *Agricultural Systems* 36, 439–470. [https://doi.org/10.1016/0308-521X\(91\)90071-H](https://doi.org/10.1016/0308-521X(91)90071-H)
- Ratto M., Tarantola S., Saltelli A., 2001. Sensitivity analysis in model calibration: GSA-GLUE approach. *Computer Physics Communications* 136, 212–224. [https://doi.org/10.1016/S0010-4655\(01\)00159-X](https://doi.org/10.1016/S0010-4655(01)00159-X)
- Rebière B., 1996. Effet d'un excès d'eau sur la croissance d'une culture de blé d'hiver. Identification d'une variable de stress et analyse de la réponse de la culture (Thèse de doctorat). Université Louis Pasteur de Strasbourg, Strasbourg.
- Recous S., Fresneau C., Faurie G., Mary B., 1988. The fate of labelled ¹⁵N urea and ammonium nitrate applied to a winter wheat crop: I. Nitrogen transformations in the soil. *Plant and Soil* 112, 205–214. <https://doi.org/10.1007/BF02139997>

- Recous S., Machet J.-M., 1999. Short-term immobilisation and crop uptake of fertiliser nitrogen applied to winter wheat: Effect of date of application in spring. *Plant and Soil* 206, 137–149. <https://doi.org/10.1023/A:1004377006602>
- Recous S., Machet J.M., Mary B., 1992. The partitioning of fertilizer-N between soil and crop: Comparison of ammonium and nitrate applications. *Plant and Soil* 144, 101–111. <https://doi.org/10.1007/BF00018850>
- Recous S., Robin D., Darwis D., Mary B., 1995. Soil inorganic N availability: Effect on maize residue decomposition. *Soil Biology and Biochemistry* 27, 1529–1538. [https://doi.org/10.1016/0038-0717\(95\)00096-W](https://doi.org/10.1016/0038-0717(95)00096-W)
- Refsgaard J.C., Henriksen H.J., Harrar W.G., Scholten H., Kassahun A., 2005. Quality assurance in model based water management - review of existing practice and outline of new approaches. *Environmental Modelling & Software* 20, 1201–1215. <https://doi.org/10.1016/j.envsoft.2004.07.006>
- Rennie R.J., Kemp G.A., 1981. Dinitrogen fixation in pea beans (*Phaseolus vulgaris*) as affected by growth stage and temperature regime. *Canadian Journal of Botany* 59, 1181–1188. <https://doi.org/10.1139/b81-161>
- Richard G., Brisson N., Lebonvallet S., Ripoche D., Boizard H., Défossez P., Chanzy A., Roger-Estrade J., 2007. Eléments de description de la structure du sol introduits dans Stics, in: *Séminaire Stics. Annales 2007. 20-22/03/2007*. INRA, Reims, France, pp. 152–155.
- Richard G., Cellier P., 1998. Effect of tillage on bare soil energy balance and thermal regime: An experimental study. *Agronomie* 18, 163–181. <https://doi.org/10.1051/agro:19980301>
- Richardson E.A., Seeley S.D., Walker D.R., 1974. A model for estimating the completion of rest for 'Redhaven' and 'Elberta' peach trees. *HortScience* 9, 331–332.
- Richardson E.A., Seeley S.D., Walker D.R., Anderson J.L., Ashcroft G.L., 1975. Pheno-climatography of spring peach bud development. *HortScience* 10, 236–237.
- Rickman R.W., Waldman S.E., Klepper B., 1996. MODWht3: A Development-Driven Wheat Growth Simulation. *Agronomy Journal* 88, 176–185. <https://doi.org/10.2134/agronj1996.00021962008800020010x>
- Riou C., Itier B., Seguin B., 1988. The influence of surface roughness on the simplified relationship between daily evaporation and surface temperature. *International Journal of Remote Sensing* 9, 1529–1533. <https://doi.org/10.1080/01431168808954957>
- Ripoche D., Weiss M., Prevot L., 2001. Driving the STICS crop model by exogeneous values of leaf area index. Application of remote sensing, in: *Proceedings of the Second International Symposium on Modelling Cropping System*. Florence, Italy, pp. 169–170.
- Ritchie J.T., 1985. A user-orientated model of the soil water balance in wheat, in: Day, W., Atkin, R.K. (Eds.), *Wheat Growth and Modelling*, NATO ASI Science (Series A: Life Sciences). Springer, Boston, USA, pp. 293–305. https://doi.org/10.1007/978-1-4899-3665-3_27
- Ritchie J.T., 1972. Model for predicting evaporation from a row crop with incomplete cover. *Water Resources Research* 8, 1204–1213. <https://doi.org/10.1029/WR008i005p01204>
- Ritchie J.T., Otter S., 1985. Description and performance of CERESWheat: A user-oriented wheat yield model, in: *ARS Wheat Yield Project*, ARS. Natural Technology Information Service, Springfield, USA, pp. 159–175.
- Robert M., Thomas A., Sekhar M., Raynal H., Casellas E., Casel P., Chabrier P., Joannon A., Bergez J.E., 2018. A dynamic model for water management at the farm level integrating strategic, tactical and operational decisions. *Environmental Modelling & Software* 100, 123–135. <https://doi.org/10.1016/j.envsoft.2017.11.013>
- Robertson M.J., Fukai S., Ludlow M.M., Hammer G.L., 1993. Water extraction by grain sorghum in a sub-humid environment. II. Extraction in relation to root growth. *Field Crops Research* 33, 99–112. [https://doi.org/10.1016/0378-4290\(93\)90096-6](https://doi.org/10.1016/0378-4290(93)90096-6)
- Rodrigo A., Recous S., Neel C., Mary B., 1997. Modelling temperature and moisture effects on C–N transformations in soils: Comparison of nine models. *Ecological Modelling* 102, 325–339. [https://doi.org/10.1016/S0304-3800\(97\)00067-7](https://doi.org/10.1016/S0304-3800(97)00067-7)

- Román Dobarco M., Cousin I., Le Bas C., Martin M.P., 2019. Pedotransfer functions for predicting available water capacity in French soils, their applicability domain and associated uncertainty. *Geoderma* 336, 81–95. <https://doi.org/10.1016/j.geoderma.2018.08.022>
- Rosenthal W.D., Arkin G.F., Shouse P.J., 1985. Water deficit effects on sorghum transpiration, in: *Proceedings of National Conference on Advances in Evapotranspiration. 16-17/12/1985*. ASAE publication, Chicago, USA, pp. 159–169.
- Rotter R.P., Palosuo T., Kersebaum K.C., Angulo C., Bindi M., Ewert F., Ferrise R., Hlavinka P., Moriondo M., Nendel C., Olesen J.E., Patil R.H., Ruget F., Takac J., Trnka M., 2012. Simulation of spring barley yield in different climatic zones of Northern and Central Europe: A comparison of nine crop models. *Field Crops Research* 133, 23–36. <https://doi.org/10.1016/j.fcr.2012.03.016>
- RStudio Team, 2021. RStudio: Integrated development environment for r. RStudio, PBC, Boston, MA.
- Ruguet F., Bethenod O., Combe L., 1996. Repercussions of increased atmospheric CO₂ on maize morphogenesis and growth for various temperature and radiation levels. *Maydica* 41, 181–191.
- Ruguet F., Brisson N., 2007. Modéliser l'impact de la sécheresse sur la production fourragère par le modèle STICS, in: *Journées AFPF 2007 – Productions Fourragères Et Adaptations 48 à La Sécheresse, 27-28/03/2007*. Association Francophone pour les Prairies et les Fourrages, Rennes, France.
- Ruguet F., Clastre P., Moreau J.-C., Cloppet E., Souverain F., Lacroix B., Lorgeou J., 2012. Conséquences possibles des changements climatiques sur la production fourragère en France. II. Exemples de quelques systèmes d'élevage. *Fourrages* 211, 243–251.
- Ruguet F., Novak S., Granger S., 2006. Du modèle STICS au système ISOP pour estimer la production fourragère. Adaptation à la prairie, application spatialisée. *Fourrages* 186, 241–256.
- Saffih-Hdadi K., Mary B., 2008. Modeling consequences of straw residues export on soil organic carbon. *Soil Biology and Biochemistry* 40, 594–607. <https://doi.org/10.1016/j.soilbio.2007.08.022>
- Saltelli A., Aleksankina K., Becker W., Fennell P., Ferretti F., Holst N., Li S., Wu Q., 2019. Why so many published sensitivity analyses are false: A systematic review of sensitivity analysis practices. *Environmental Modelling & Software* 114, 29–39. <https://doi.org/10.1016/j.envsoft.2019.01.012>
- Sau E., Boote K.J., McNair Bostick W., Jones J.W., Inés Mínguez M., 2004. Testing and Improving Evapotranspiration and Soil Water Balance of the DSSAT Crop Models. *Agronomy Journal* 96, 1243–1257. <https://doi.org/10.2134/agronj2004.1243>
- Savary S., Ficke A., Aubertot J.-N., Hollier C., 2012. Crop losses due to diseases and their implications for global food production losses and food security. *Food Security* 4, 519–537. <https://doi.org/10.1007/s12571-012-0200-5>
- Sawyer J., Nafziger E., Randall G., Bundy L., Rehm G., Joern B., 2006. Concepts and Rationale for Regional Nitrogen Rate Guidelines for Corn (Departmental Report). Iowa State University Extension, Ames.
- Schnebelen N., Nicoulaud B., Bourennane H., Couturier A., Verbeque B., Revalier C., Bruand A., Ledoux E., 2004. The STICS model to predict nitrate leaching following agricultural practices. *Agronomie* 24, 423–435. <https://doi.org/10.1051/agro:2004039>
- Schott C., Mimet A., Mignolet C.C., 2010. Création d'une base de données sur les pratiques agricoles de Basse-Normandie de 1970 à 2006 (Rapport de contrat). INRA.
- Schwartz M.D. (Ed.), 2013. Phenology: An integrative environmental science. Springer, Dordrecht, The Netherlands.
- Scopel E., Muller B., Arreola Tostado J.M., Chavez Guerra E., Maraun F., 1998. Quantifying and modeling the effects of a light crop residue mulch on the water balance: An application to rainfed maize in western Mexico, in: *Proceedings of XVI World Congress of Soil Science, 20-26/08/1998*. Montpellier, France.
- Seghier J., Floret Ch., Pontanier R., 1995. Plant phenology in relation to water availability: Herbaceous and woody species in the savannas of northern Cameroon. *Journal of Tropical Ecology* 11, 237–254. <https://doi.org/10.1017/S0266467400008713>
- Seguin B., Antonioletti R., 1988. Quelques éléments sur le climat du Mont Ventoux. *Bulletin Climatologique et Agroclimatologique du Vaucluse* 17, 26–34.

- Seguin B., Itier B., 1983. Using midday surface temperature to estimate daily evaporation from satellite thermal IR data. *International Journal of Remote Sensing* 4, 371–383. <https://doi.org/10.1080/01431168308948554>
- Seidel S.J., Palosuo T., Thorburn P., Wallach D., 2018. Towards improved calibration of crop models – Where are we now and where should we go? *European Journal of Agronomy* 94, 25–35. <https://doi.org/10.1016/j.eja.2018.01.006>
- Sellers W.D., 1965. Physical climatology. *University of Chicago Press*.
- Sene K., 1994. Parameterisations for energy transfers from a sparse vine crop. *Agricultural and Forest Meteorology* 71, 1–18. [https://doi.org/10.1016/0168-1923\(94\)90097-3](https://doi.org/10.1016/0168-1923(94)90097-3)
- Sheng M., Liu J., Zhu A.-X., Rossiter D.G., Liu H., Liu Z., Zhu L., 2019. Comparison of GLUE and DREAM for the estimation of cultivar parameters in the APSIM-maize model. *Agricultural and Forest Meteorology* 278, 107659. <https://doi.org/10.1016/j.agrformet.2019.107659>
- Shili-Touzi I., Tourdonnet S. de, Launay M., Doré T., 2010. Does intercropping winter wheat (*Triticum aestivum*) with red fescue (*Festuca rubra*) as a cover crop improve agronomic and environmental performance? A modeling approach. *Field Crops Research* 116, 218–229. <https://doi.org/10.1016/j.fcr.2009.11.007>
- Shuttleworth W.J., Wallace J.S., 1985. Evaporation from sparse crops-an energy combination theory. *Quarterly Journal of the Royal Meteorological Society* 111, 839–855. <https://doi.org/10.1002/qj.49711146910>
- Sierra J., Brisson N., Ripoche D., Deque M., 2010. Modelling the impact of thermal adaptation of soil microorganisms and crop system on the dynamics of organic matter in a tropical soil under a climate change scenario. *Ecological Modelling* 221, 2850–2858. <https://doi.org/10.1016/j.ecolmodel.2010.08.031>
- Sierra J., Brisson N., Ripoche D., Noël C., 2003. Application of the STICS crop model to predict nitrogen availability and nitrate transport in a tropical acid soil cropped with maize. *Plant and Soil* 256, 333–345. <https://doi.org/10.1023/A:1026106208320>
- Silva F.A.M., Naudin K., Corbeels M., Scopel E., Affholder F., 2019. Impact of conservation agriculture on the agronomic and environmental performances of maize cropping under contrasting climatic conditions of the Brazilian Cerrado. *Field Crops Research* 230, 72–83. <https://doi.org/10.1016/j.fcr.2018.10.009>
- Silva J.V., Giller K.E., 2020. Grand challenges for the 21st century: What crop models can and can't (yet) do. *The Journal of Agricultural Science* 158, 794–805. <https://doi.org/10.1017/S0021859621000150>
- Sinclair T.R., 1986. Water and nitrogen limitations in soybean grain production I. Model development. *Field Crops Research* 15, 125–141. [https://doi.org/10.1016/0378-4290\(86\)90082-1](https://doi.org/10.1016/0378-4290(86)90082-1)
- Sinclair T.R., de Wit C.T., 1976. Analysis of the Carbon and Nitrogen Limitations to Soybean Yield. *Agronomy Journal* 68, 319–324. <https://doi.org/10.2134/agronj1976.00021962006800020021x>
- Sinclair T.R., Mosca G., Bona S., 1993. Simulation Analysis of Variation among Seasons in Winter Wheat Yields in Northern Italy. *Journal of Agronomy and Crop Science* 170, 202–207. <https://doi.org/10.1111/j.1439-037X.1993.tb01076.x>
- Sinclair T.R., Seligman N., 2000. Criteria for publishing papers on crop modeling. *Field Crops Research* 68, 165–172. [https://doi.org/10.1016/S0378-4290\(00\)00105-2](https://doi.org/10.1016/S0378-4290(00)00105-2)
- Sinclair T.R., Seligman N.G., 1996. Crop Modeling: From Infancy to Maturity. *Agronomy Journal* 88, 698–704. <https://doi.org/10.2134/agronj1996.00021962008800050004x>
- Singels A., de Jager J.M., 1991. Refinement and validation of the PUTU wheat crop growth model 3. Grain growth. *South African Journal of Plant and Soil* 8, 73–77. <https://doi.org/10.1080/02571862.1991.10634583>
- Smith M., Allen R., Pereira L., 1998. Revised FAO methodology for crop-water requirements, in: *Consultants Meeting on Management of Nutrients and Water in Rainfed Arid and Semi-Arid Areas, 26-29/05/1997*, IAEA-TECDOC. International Atomic Energy Agency (IAEA), Vienne, Austria, pp. 51–58.
- Sonohat G., Sinoquet H., Varlet-Grancher C., Rakocevic M., Jacquet A., Simon J.-C., Adam B., 2002. Leaf dispersion and light partitioning in three-dimensionally digitized tall fescue-white clover mixtures. *Plant, Cell and Environment* 25, 529–538. <https://doi.org/10.1046/j.1365-3040.2002.00833.x>

- Spaeth S.C., Sinclair T.R., 1985. Linear Increase in SoybeanHarvestIndex during Seed-Filling. *Agronomy Journal* 77, 207–211. <https://doi.org/10.2134/agronj1985.00021962007700020008x>
- Spitters C.J.T., Toussaint H.A.J.M., Goudriaan J., 1986. Separating the diffuse and direct component of global radiation and its implications for modeling canopy photosynthesis PartI. Components of incoming radiation. *Agricultural and Forest Meteorology* 38, 217–229. [https://doi.org/10.1016/0168-1923\(86\)90060-2](https://doi.org/10.1016/0168-1923(86)90060-2)
- Sprent J.I., Stephens J.H., Rupela O.P., 1988. Environmental effects on nitrogen fixation, in: Bliss, F.A., Summerfield, R.J. (Eds.), *World Crops: Cool Season Food Legumes*, Current PlantScience and Biotechnology in Agriculture. Springer, Dordrecht, The Netherlands, pp. 801–810. https://doi.org/10.1007/978-94-009-2764-3_64
- Sreelash K., Buis S., Sekhar M., Ruiz L., Tomer S.K., Guerif M., 2017. Estimation of available water capacity components of two-layered soils using crop model inversion: Effect of crop type and water regime. *Journal of Hydrology* 546, 166–178. <https://doi.org/10.1016/j.jhydrol.2016.12.049>
- Sreelash K., Sekhar M., Ruiz L., Tomer S.K., Guerif M., Buis S., Durand P., Gascuel-Oudou C., 2012. Parameter estimation of a two-horizon soil profile by combining crop canopy and surface soil moisture observations using GLUE. *Journal of Hydrology* 456, 57–67. <https://doi.org/10.1016/j.jhydrol.2012.06.012>
- Stockle C.O., Kjølgaard J., 1996. Parameterizing Penman-Monteith surface resistance for estimating daily crop ET, in: Camp, C.R., Sadler, E.J., Yoder, R.E. (Eds.), *Proceedings of the International Conference on Evapotranspiration and Irrigation Scheduling*, 3-6/11/1996. American Society of Agricultural Engineers, San Antonio, Texas, USA, pp. 632–638.
- Stockle C.O., Williams J.R., Rosenberg N.J., Jones C.A., 1992. A method for estimating the direct and climatic effects of rising atmospheric carbon dioxide on growth and yield of crops: PartI—Modification of the EPIC model for climate change analysis. *Agricultural Systems* 38, 225–238. [https://doi.org/10.1016/0308-521X\(92\)90067-X](https://doi.org/10.1016/0308-521X(92)90067-X)
- Stöckle C.O., Donatelli M., Nelson R., 2003. CropSyst, a cropping systems simulation model. *European Journal of Agronomy* 18, 289–307. [https://doi.org/10.1016/S1161-0301\(02\)00109-0](https://doi.org/10.1016/S1161-0301(02)00109-0)
- Strullu L., Beaudoin N., García de Cortázar Atauri I., Mary B., 2014. Simulation of Biomass and NitrogenDynamics in PerennialOrgans and Shoots of *Miscanthus* × *Giganteus* Using the STICSModel. *BioEnergy Research* 7, 1253–1269. <https://doi.org/10.1007/s12155-014-9462-4>
- Strullu L., Beaudoin N., Thiébeau P., Julier B., Mary B., Ruget F., Ripoché D., Rakotovololona L., Louarn G., 2020. Simulation using the STICS model of C&N dynamics in alfalfa from sowing to crop destruction. *European Journal of Agronomy* 112. <https://doi.org/10.1016/j.eja.2019.125948>
- Strullu L., Ferchaud F., Yates N., Shield I., Beaudoin N., García de Cortázar Atauri I., Besnard A., Mary B., 2015. Multisite YieldGapAnalysis of *Miscanthus* × *giganteus* Using the STICSModel. *BioEnergy Research* 8, 1735–1749. <https://doi.org/10.1007/s12155-015-9625-y>
- Tao F., Rötter R.P., Palosuo T., DíazNANA Ambrona C.G.H., Mínguez M.I., Semenov M.A., Kersebaum K.C., Nendel C., Specka X., Hoffmann H., Ewert F., Dambreville A., Martre P., Rodríguez L., Ruiz-Ramos M., Gaiser T., Höhn J.G., Salo T., Ferrise R., Bindi M., Cammarano D., Schulma A.H., 2018. Contribution of crop model structure, parameters and climate projections to uncertainty in climate change impact assessments. *Global Change Biology* 24, 1291–1307. <https://doi.org/10.1111/gcb.14019>
- Tardieu F., Granier C., Muller B., 1999. Modelling leaf expansion in a fluctuating environment: Are changes in specific leaf area a consequence of changes in expansion rate. *New Phytologist* 143, 33–43. <https://doi.org/10.1046/j.1469-8137.1999.00433.x>
- Tavakoly A.A., Habets F., Saleh F., Yang Z.-L., Bourgeois C., Maidment D.R., 2019. An integrated framework to model nitrate contaminants with interactions of agriculture, groundwater, and surface water at regional scales: TheSTICS–EauDyssée coupled models applied over the SeineRiverBasin. *Journal of Hydrology* 568, 943–958. <https://doi.org/10.1016/j.jhydrol.2018.11.061>
- Teittinen M., Karvonen T., Peltonen J., 1994. A DynamicModel for Water and NitrogenLimitedGrowth in SpringWheat to PredictYield and Quality. *Journal of Agronomy and Crop Science* 172, 90–103. <https://doi.org/10.1111/j.1439-037X.1994.tb00534.x>

- Tetegan M., Nicoullaud B., Baize D., Bouthier A., Cousin I., 2011. The contribution of rock fragments to the available water content of stony soils: Proposition of new pedotransfer functions. *Geoderma* 165, 40–49. <https://doi.org/10.1016/j.geoderma.2011.07.001>
- Texeira J.L., Liu Y., Zhang H.J., Pereira L.S., 1996. Evaluation of the ISAREG irrigation scheduling model in north China plain, in: Camp, C.R., Sadler, E.J., Yoder, R.E. (Eds.), *Proceedings of the International Conference on Evapotranspiration and Irrigation Scheduling, 3-6/11/1996*. American Society of Agricultural Engineers, San Antonio, Texas, USA, pp. 632–638.
- Theau J.-P., Coléno F.C., Duru M., Rauzy Y., 1998. L'utilisation de l'herbe paturée et fauchée en référence au potentiel de production des prairies. *Fourrages* 156, 589–601.
- Therond O., Tichit M., Tibi A., Accatino F., Biju-Duval L., Bockstaller C., Bohan D., Bonaudo T., Boval M., Cahuzac E., Casellas E., Chauvel B., Cholier P., Constantin J., Cousin I., Daroussin J., David M., Delacote P., Derocles S., Sousa L. de, Domingues J.P., Dross C., Duru M., Eugène M., Fontaine C., Garcia B., Geizendorffer I.R., Girardin A., Graux A.-I., Jouven M., Langlois B., Le Bas C., Le Bissonnais Y., Lelievre V., Lifran R., Maigne E., Martin G., Martin R., Martin-Laurent F., Martinet V., McLaughlin O., Meillet A., Mignolet C., Mouchet M., Nozieres-Petit M.-O., Ostermann O.P., Paracchini M.L., Pellerin S., Peyraud J.-L., Michaut S.P., Picaut C., Plantureux S., Poméon T., Porcher E., Puech T., Puillet L., Rambonilaza T., Raynal H., Resmond R., Ripoché D., Ruget F., Rulleau B., Rush A., Salles J.-M., Sauvant D., Schott C., Tardieu L., 2017. Volet "écosystèmes agricoles" de l'Evaluation Française des Ecosystèmes et des Services Ecosystémiques (Rapport d'expertise). INRA.
- Thornley J., 1996. Modelling Water in Crops and Plant Ecosystems. *Annals of Botany* 77, 261–275. <https://doi.org/10.1006/anbo.1996.0030>
- Thorsen S.M., Roer A.-G., Oijen M. van, 2010. Modelling the dynamics of snow cover, soil frost and surface ice in Norwegian grasslands. *Polar Research* 29, 110–126. <https://doi.org/10.3402/polar.v29i1.6057>
- Tolk J.A., Howel T.A., Steiner J.L., 1996. Corn canopy resistance determined from whole plant transpiration, in: Camp, C.R., Sadler, E.J., Yoder, R.E. (Eds.), *Proceedings of the International Conference on Evapotranspiration and Irrigation Scheduling, 3-6/11/1996*. American Society of Agricultural Engineers, San Antonio, Texas, USA, pp. 664–672.
- Toreti A., Deryng D., Tubiello F.N., Müller C., Kimball B.A., Moser G., Boote K., Asseng S., Pugh T.A.M., Vanuytrecht E., Pleijel H., Webber H., Durand J.-L., Dentener F., Ceglar A., Wang X., Badeck F., Lecerf R., Wall G.W., van den Berg M., Hoegy P., Lopez-Lozano R., Zampieri M., Galmarini S., O'Naleary G.J., Manderscheid R., Mencos Contreras E., Rosenzwei C., 2020. Narrowing uncertainties in the effects of elevated CO₂ on crops. *Nature Food* 1, 775–782. <https://doi.org/10.1038/s43016-020-00195-4>
- Tóth B., Weynants M., Nemes A., Makó A., Bilas G., Tóth G., 2015. New generation of hydraulic pedotransfer functions for Europe. *European Journal of Soil Science* 66, 226–238. <https://doi.org/10.1111/ejss.12192>
- Tournebize J., Kao C., Nikolic N., Zimmer D., 2004. Adaptation of the STICS model to subsurface drained soils. *Agronomie* 24, 305–313. <https://doi.org/10.1051/agro:2004030>
- Trapani N., Hall A.J., Sadras V.O., Vilella F., 1992. Ontogenetic changes in radiation use efficiency of sunflower (*Helianthus annuus*L.) crops. *Field Crops Research* 29, 301–316. [https://doi.org/10.1016/0378-4290\(92\)90032-5](https://doi.org/10.1016/0378-4290(92)90032-5)
- Tremblay M., Wallach D., 2004. Comparison of parameter estimation methods for crop models. *Agronomie* 24, 351–365. <https://doi.org/10.1051/agro:2004033>
- Tribouillois H., Constantin J., Justes E., 2018b. Cover crops mitigate direct greenhouse gases balance but reduce drainage under climate change scenarios in temperate climate with dry summers. *Global Change Biology* 24, 2513–2529. <https://doi.org/10.1111/gcb.14091>
- Tribouillois H., Constantin J., Justes E., 2018a. Analysis and modeling of cover crop emergence: Accuracy of a static model and the dynamic STICS soil-crop model. *European Journal of Agronomy* 93, 73–81. <https://doi.org/10.1016/j.eja.2017.12.004>
- Tribouillois H., Cruz P., Cohan J.-P., Justes E., 2015. Modelling agroecosystem nitrogen functions provided by cover crop species in bispecific mixtures using functional traits and environmental factors. *Agriculture, Ecosystems & Environment* 207, 218–228. <https://doi.org/10.1016/j.agee.2015.04.016>

- Trnka M., Kocmánková E., Balek J., Eitzinger J., Ruget F., Formayer H., Hlavinka P., Schaumberger A., Horáková V., Možný M., Žalud Z., 2010. Simple snow cover model for agrometeorological applications. *Agricultural and Forest Meteorology* 150, 1115–1127. <https://doi.org/10.1016/j.agrformet.2010.04.012>
- Valé M., 2006. Quantification et prédiction de la minéralisation nette de l'azote du sol in situ, sous divers pédoclimats et systèmes de culture français (Thèse de doctorat). Institut National Polytechnique de Toulouse.
- van Bavel C.H.M., 1953. A drought criterion and its application in evaluating drought incidence and hazard. *Agronomy Journal* 45, 167–172. <https://doi.org/10.2134/agronj1953.00021962004500040009x>
- van Keulen H., Seligman N.G., 1987. Simulation of water use, nitrogen nutrition and growth of a spring wheat crop, Simulation monographs. Pudoc, Wageningen, The Netherlands.
- Van Der Ploeg R.R., Ringe H., Machulla G., 1995. Late Fall Site-Specific Soil Nitrate Upper Limits for Groundwater Protection Purposes. *Journal of Environmental Quality* 24, 725–733. <https://doi.org/10.2134/jeq1995.00472425002400040025x>
- Van Ittersum M.K., Leffelaar P.A., van Keulen H., Kropff M.J., Bastiaans L., Goudriaan J., 2003. On approaches and applications of the Wageningen crop models. *European Journal of Agronomy* 18, 201–234. [https://doi.org/10.1016/S1161-0301\(02\)00106-5](https://doi.org/10.1016/S1161-0301(02)00106-5)
- Varella H., Guérif M., Buis S., 2010a. Global sensitivity analysis measures the quality of parameter estimation: The case of soil parameters and a crop model. *Environmental Modelling & Software* 25, 310–319. <https://doi.org/10.1016/j.envsoft.2009.09.012>
- Varella H., Guérif M., Buis S., Beaudoin N., 2010b. Soil properties estimation by inversion of a crop model and observations on crops improves the prediction of agro-environmental variables. *European Journal of Agronomy* 33, 139–147. <https://doi.org/10.1016/j.eja.2010.04.005>
- Varlet-Grancher C., Bonhomme R., 1979. Application aux couverts végétaux des lois de rayonnement en milieu diffusant. II - Interception de l'énergie solaire par une culture. *Annales Agronomiques* 30, 1.
- Varlet-Grancher C., Bonhomme R., Chartier M., Artis P., 1982. Efficience de la conversion de l'énergie solaire par un couvert végétal. *Acta Oecologica Oecologia Plantarum* 3, 3–26.
- Varlet-Grancher C., Bonhomme R., Chartier M., Artis P., 1981. Évolution de la réponse photosynthétique des feuilles et efficience théorique de la photosynthèse brute d'une culture de canne à sucre (*Saccharum officinarum* L.). *Agronomie* 1, 473–481. <https://doi.org/10.1051/agro:19810607>
- Varlet-Grancher C., Bonhomme R., Sinoquet H. (Eds.), 1993. Crop structure and light microclimate. Characterization and applications, Science Update. INRA Editions.
- Varlet-Grancher C., Gosse G., Chartier M., Sinoquet H., Bonhomme R., Allirand J.M., 1989. Mise au point : Rayonnement solaire absorbé ou intercepté par un couvert végétal. *Agronomie* 9, 419–439. <https://doi.org/10.1051/agro:19890501>
- Vehtari A., Gelman A., Simpson D., Carpenter B., Bürkner P.-C., 2021. Rank-Normalization, Folding, and Localization: An Improved R for Assessing Convergence of MCMC. *Bayesian Analysis* 16, 667–718. <https://doi.org/10.1214/20-BA1221>
- Vereecken H., Weynants M., Javaux M., Pachepsky Ya.A., Schaap M.G., van Genuchten M.Th., 2010. Using Pedotransfer Functions to Estimate the van Genuchten-Mualem Soil Hydraulic Properties: A Review. *Vadose Zone Journal* 9, 795–820. <https://doi.org/10.2136/vzj2010.0045>
- Vezy R., Buis S., Lecharpentier P., Giner M., 2021. CroPlotR: A package to analyse crop model simulations outputs with plots and statistics.
- Vinten A.J.A., Redman M.H., 1990. Calibration and validation of a model of non-interactive solute leaching in a clay-loam arable soil. *Journal of Soil Science* 41, 199–214. <https://doi.org/10.1111/j.1365-2389.1990.tb00057.x>
- Voisin A.S., 2003. Symbiotic N₂ fixation activity in relation to C economy of *Pisum sativum* L. As a function of plant phenology. *Journal of Experimental Botany* 54, 2733–2744. <https://doi.org/10.1093/jxb/erg290>
- Voisin A.-S., Salon C., Munier-Jolain N.G., Ney B., 2002. Quantitative effects of soil nitrate, growth potential and phenology on symbiotic nitrogen fixation of pea (*Pisum sativum* L.). *Plant and Soil* 243, 31–42. <https://doi.org/10.1023/A:1019966207970>

- Vrugt J.A., 2016. Markov chain MonteCarlo simulation using the DREAM software package: Theory, concepts, and MATLAB implementation. *Environmental Modelling & Software* 75, 273–316. <https://doi.org/10.1016/j.envsoft.2015.08.013>
- Wagenet R.J., Hutson J.L., 1996. Scale-dependency of solute transport modeling/GIS applications. *Journal of Environmental Quality* 25, 499–510. <https://doi.org/10.2134/jeq1996.00472425002500030015x>
- Wallace J.S., 1995. Towards a coupled light partitioning and transpiration model for use in intercrops and agroforestry.
- Wallach D., Buis S., Lecharpentier P., Bourges J., Clastre P., Launay M., Bergez J.E., Guéris M., Soudais J., Justes E., 2011. A package of parameter estimation methods and implementation for the STICS crop-soil model. *Environmental Modelling & Software* 26, 386–394. <https://doi.org/10.1016/j.envsoft.2010.09.004>
- Wallach D., Makowski D., Jones J.W., Brun F., 2018. Model evaluation, in: Wallach, D., Makowski, D., Jones, J.W., Brun, F. (Eds.), *Working with Dynamic Crop Models: Methods, Tools and Examples for Agriculture and Environment*. Academic Press, San Diego, CA, USA, pp. 311–373.
- Wallach Daniel, Makowski D., Jones J.W., Brun F., 2018. Working with dynamic crop models: Methods, tools and examples for agriculture and environment, Third edition. Academic Press, London San Diego, CA Cambridge, MA Oxford.
- Wallach D., Palosuo T., Thorburn P., Hochman Z., Gourdain E., Andrianasolo F., Asseng S., Basso B., Buis S., Crout N., Dibari C., Dumont B., Ferrise R., Gaiser T., Garcia C., Gayler S., Ghahramani A., Hiremath S., Hoek S., Horan H., Hoogenboom G., Huang M., Jabloun M., Jansson P.-E., Jing Q., Justes E., Kersebaum K.C., Klosterhalfen A., Launay M., Lewan E., Luo Q., Maestrini B., Mielenz H., Moriondo M., Nariman Zadeh H., Padovan G., Olesen J.E., Poyda A., Priesack E., Pullens J.W.M., Qian B., Schütze N., Shelia V., Souissi A., Specka X., Srivastava A.K., Stella T., Streck T., Trombi G., Wallor E., Wang J., Weber T.K.D., Weihermüller L., de Wit A., Wöhling T., Xiao L., Zhao C., Zhu Y., Seidel S.J., 2021. The chaos in calibrating crop models: Lessons learned from a multi-model calibration exercise. *Environmental Modelling & Software* 145, 105206. <https://doi.org/10.1016/j.envsoft.2021.105206>
- Warembourg F.R., 1983. Estimating the true cost of dinitrogen fixation by nodulated plants in undisturbed conditions. *Canadian Journal of Microbiology* 29, 930–937. <https://doi.org/10.1139/m83-149>
- Warren-Wilson J., 1972. Control of crop processes, in: Rees, A.R., Cockshull, K.E., Hand, D.W., Hurd, R.G. (Eds.), *Crop Processes in Controlled Environments*. Academic Press, London; New York, pp. 7–30.
- Waterer J.G., Vessey J.K., 1993. Effect of low static nitrate concentrations on mineral nitrogen uptake, nodulation, and nitrogen fixation in field pea. *Journal of Plant Nutrition* 16, 1775–1789. <https://doi.org/10.1080/01904169309364649>
- Weaich K., Cass A., Bristow K.L., 1996. Pre-emergent shoot growth of maize (*Zea mays*, L.) As a function of soil strength. *Soil and Tillage Research* 40, 3–23. [https://doi.org/10.1016/S0167-1987\(96\)80003-1](https://doi.org/10.1016/S0167-1987(96)80003-1)
- Weir A.H., Bragg P.L., Porter J.R., Rayner J.H., 1984. A winter wheat crop simulation model without water or nutrient limitations. *The Journal of Agricultural Science* 102, 371–382. <https://doi.org/10.1017/S0021859600042702>
- Whisler F.D., Acock B., Baker D.N., Fye R.E., Hodges H.F., Lambert J.R., Lemmon H.E., McKinion J.M., Reddy V.R., 1986. Crop simulation models in agronomic systems, in: Brady, N.C. (Ed.), *Advances in Agronomy*. Academic Press, pp. 141–208. [https://doi.org/10.1016/S0065-2113\(08\)60282-5](https://doi.org/10.1016/S0065-2113(08)60282-5)
- Williams J., C. A. Jones, P. T. Dyke, 1984. A modeling approach to determining the relationship between erosion and soil productivity. *Transactions of the ASAE* 27, 0129–0144. <https://doi.org/10.13031/2013.32748>
- Williams J.R., Jones C.A., Kiniry J.R., Spindel D.A., 1989. The EPIC crop growth model. *Transactions of the ASAE* 32, 0497–0511. <https://doi.org/10.13031/2013.31032>
- Wilson J.B., 1988. A Review of Evidence on the Control of Shoot: RootRatio, in Relation to Models. *Annals of Botany* 61, 433–449. <https://doi.org/10.1093/oxfordjournals.aob.a087575>
- Wösten J.H.M., Lilly A., Nemes A., Le Bas C., 1999. Development and use of a database of hydraulic properties of European soils. *Geoderma* 90, 169–185. [https://doi.org/10.1016/S0016-7061\(98\)00132-3](https://doi.org/10.1016/S0016-7061(98)00132-3)

- Wösten J.H.M., Pachepsky Ya.A., Rawls W.J., 2001. Pedotransfer functions: Bridging the gap between available basic soil data and missing soil hydraulic characteristics. *Journal of Hydrology* 251, 123–150. [https://doi.org/10.1016/S0022-1694\(01\)00464-4](https://doi.org/10.1016/S0022-1694(01)00464-4)
- Wu X., Vuichard N., Ciais P., Viovy N., Noblet-Ducoudre N. de, Wang X., Magliulo V., Wattenbach M., Vitale L., Tommasi P.D., Moors E.J., Jans W., Elbers J., Ceschia E., Talleg T., Bernhofer C., Gruenwald T., Moureaux C., Manise T., Ligne A., Cellier P., Loubet B., Larmanou E., Ripoche D., 2016. ORCHIDEE-CROP (v0), a new process-based agro-land surface model: Model description and evaluation over Europe. *Geoscientific Model Development* 9, 857–873. <https://doi.org/10.5194/gmd-9-857-2016>
- Xie Y., 2021. Bookdown: Authoring books and technical documents with r markdown.
- Xie Y., 2016. Bookdown: Authoring books and technical documents with R markdown. Chapman; Hall/CRC, Boca Raton, Florida.
- Yin X., Beaudoin N., Ferchaud F., Mary B., Strullu L., Chlébowski F., Clivot H., Herre C., Duval J., Louarn G., 2020. Long-term modelling of soil N mineralization and N fate using STICS in a 34-year crop rotation experiment. *Geoderma* 357, 113956. <https://doi.org/10.1016/j.geoderma.2019.113956>
- Yin X.G., Kersebaum K.C., Beaudoin N., Constantin J., Chen F., Louarn G., Manevski K., Hoffmann M., Kollas C., Armas-Herrera C.M., Baby S., Bindi M., Dibari C., Ferchaud F., Ferrise R., García de Cortázar Atauri I., Launay M., Mary B., Moriondo M., Ozturk I., Ruget F., Sharif B., Wachter-Ripoche D., Olesen J.E., 2020. Uncertainties in simulating N uptake, net N mineralization, soil mineral N and N leaching in European crop rotations using process-based models. *Field Crops Research* 255. <https://doi.org/10.1016/j.fcr.2020.107863>
- Zhao G., Hoffmann H., van Bussel L.G.J., Enders A., Specka X., Sosa C., Yeluripati J., Tao F., Constantin J., Raynal H., Teixeira E., Grosz B., Doro L., Zhao Z., Nendel C., Kiese R., Eckersten H., Haas E., Vanuytrecht E., Wang E., Kuhnert M., Trombi G., Moriondo M., Bindi M., Lewan E., Bach M., Kersebaum K.-C., Roetter R., Roggero P.P., Wallach D., Cammarano D., Asseng S., Krauss G., Siebert S., Gaiser T., Ewert F., 2015. Effect of weather data aggregation on regional crop simulation for different crops, production conditions, and response variables. *Climate Research* 65, 141–157. <https://doi.org/10.3354/cr01301>
- Zhao G., Hoffmann H., Yeluripati J., Xenia S., Nendel C., Coucheney E., Kuhnert M., Tao F., Constantin J., Raynal H., Teixeira E., Grosz B., Doro L., Kiese R., Eckersten H., Haas E., Cammarano D., Kassie B., Moriondo M., Trombi G., Bindi M., Biernath C., Heinlein F., Klein C., Priesack E., Lewan E., Kersebaum K.-C., Rotter R., Roggero P.P., Wallach D., Asseng S., Siebert S., Gaiser T., Ewert F., 2016. Evaluating the precision of eight spatial sampling schemes in estimating regional means of simulated yield for two crops. *Environmental Modelling & Software* 80, 100–112. <https://doi.org/10.1016/j.envsoft.2016.02.022>

Chapter 17

Definition of symbols

►► 17.1 Definition of parameters

Name	Definition	Unit
aangst_C	Coefficient of the Angstrom relationship for extraterrestrial radiation	ND
abscission_p	Fraction of senescent leaves falling to the soil	ND
aclim_C	Climatic component to calculate actual soil evaporation (Brisson & Perrier, 1991)	mm
adens_p	Interplant competition parameter	ND
adfol_p	Parameter determining the leaf density evolution within the chosen shape	m ⁻¹
adil_p	Parameter of the critical dilution curve [Nplante]=adil MS [^] (-bdil)	%
adilmax_p	Parameter of the maximum dilution curve [Nplante]=adilmax MS [^] (-bdilmax)	%
afpf_p	Parameter of the logistic function defining sink strength of fruits (indeterminate growth): relative fruit age at which growth is maximal	ND
afruitpot_p	Maximal number of set fruits per inflorescence and per degree day (indeterminate growth)	fruits inflorescence ⁻¹ degree days ⁻¹
ahres_G	Parameter of organic residues humification: hres=1-ahres*CsurNres/(bhres+CsurNres)	ND
akres_G	Parameter of organic residues decomposition: kres=akres+bkres/CsurNres	day ⁻¹
aks_C	Parameter of calculation of the energetic loss between the inside and the outside of a greenhouse	W m ⁻² K ⁻¹
albedo_s	Albedo of the bare dry soil	ND
albedomulchplastique_T	Albedo of plastic cover	ND
albedomulchresidus_G	Albedo of plant mulch	ND
albveg_C	Albedo of the vegetation	ND
allocfmax_p	Maximal daily allocation to fruits	ND

Nome	Definition	Unit
alloperirac_p	Allocation rate of the seed reserves (perisperm) to the rootlet growth	ND
alphaCO_{2p}	Coefficient accounting for the modification of radiation use efficiency in case of atmospheric CO ₂ increase	ND
alphaph_G	Maximal soil pH variation per unit of inorganic N added with slurry	kg ⁻¹ ha
alphaphot_p	Parameter of photoperiodic effect on leaf lifespan	ND
alphapt_C	Parameter of Priestley-Taylor formula	ND
altinversion_C	Altitude of inversion of the thermal gradient	m
altisimul_C	Altitude of simulated site	m
altistation_C	Altitude of the input meteorological station	m
ampfroid_p	Semi thermal amplitude for vernalising effect	°C
anitcoupe_T	Amount of mineral N added by fertiliser application at each cut of a forage crop	kg ha ⁻¹
argi_s	Clay content after decarbonation	%
awb_G	Parameter determining C/N ratio of biomass during organic residues decomposition: CsurNbio=awb+bwb/CsurNres	g g ⁻¹
bangst_C	Coefficient of the Angstrom s relationship for extraterrestrial radiation	ND
bdens_p	Minimal plant density above which interplant competition starts	m ⁻²
bdil_p	Parameter of the critical dilution curve [Nplante]=adil MS ⁻¹ (-bdil)	ND
bdilmax_p	Parameter of the maximum dilution curve [Nplante]=adilmax MS ⁻¹ (-bdilmax)	ND
belong_p	Parameter of the curve of coleoptile elongation	degree days ⁻¹
beta_G	Parameter of increase of maximal transpiration when a water stress occurs	ND
bformnappe_G	Coefficient for the water table shape (artificially drained soil)	ND
bfpf_p	Parameter of the logistic curve defining sink strength of fruits (indeterminate growth): maximum growth rate relative to maximum fruit weight	ND
bhres_G	Parameter of organic residues humification: hres=1-ahres*CsurNres/(bhres+CsurNres)	g g ⁻¹

Name	Definition	Unit
biorognem_T	Minimal crop biomass removed when topping (automatic calculation)	t ha ⁻¹
bkres_G	Potential rate of decomposition of organic residues: $kres=akres+bkres/CsurNres$	g g ⁻¹
bks_C	Parameter of calculation of the energetic lost between the inside and the outside of a greenhouse	W m ⁻² K ⁻¹
bwb_G	Parameter determining C/N ratio of biomass during organic residues decomposition: $CsurNbio=awb+bwb/CsurNres$	g g ⁻¹
cadencerec_T	Number of days between two harvests	days
cailloux_S	Volumetric content of pebbles per soil layer	%
calc_S	Total carbonate content	%
capiljour_S	Capillary rise upward water flux	mm day ⁻¹
celong_p	Parameter of the plantlet elongation curve	ND
cfes_S	Parameter defining the soil contribution to evaporation versus depth	ND
cfpf_p	Parameter of the first potential growth phase of fruit, corresponding to an exponential type function describing the cell division phase	ND
cgrain_p	Slope of the relationship between grain number and growth rate	t ⁻¹ m ² d
cgrainv0_p	Fraction of the maximal number of grains when growth rate is zero	ND
cielclair_C	Fraction of sunny hours allowing the inversion of thermal gradient with altitude	ND
cmax_pdenit_G	Soil organic carbon concentration above which denitrification potential is constant and maximum	g kg ⁻¹
cmin_pdenit_G	Soil organic carbon concentration below which denitrification potential is constant and minimum	g kg ⁻¹
CNgrainrec_T	Minimal N content of grain at harvest	g g ⁻¹
CNresmax_G	Maximum value of C/N ratio of organic residue	g g ⁻¹
CNresmin_G	Minimum value of C/N ratio of organic residue	g g ⁻¹
codabri_T	Option to activate cropping under shelter: 1 = no, 2 = yes	code, 1 to 2
codadret_C	Option to calculate mountain climate taking into account the orientation: 1 = south, 2 = north	code, 1 to 2

Nam_e	Definition	Unit
codaltitude_C	Option to activate the calculation of the climate in altitude: 1 = no, 2 = yes	code, 1 to 2
codazofruit_p	Option to activate the direct effect of N plant status on the fruit/grain number: 1 = no, 2 = yes	code, 1 to 2
codazorac_p	Option to activate the effect of N stress on root partitioning within the soil profile: 1 = yes, 2 = no	code, 1 to 2
codcaleffeuil_T	Option to calculate leaf removal by thinning: 1 = proportion of leaf removed (effeuil), 2 = lai minimal (laieffeuil)	code, 1 to 2
codcalinfo_p	Option to calculate the inflorescences number: 1 = read in param.par, 2 = calculated at the amf stage	code, 1 to 2
codcalrogne_T	Option to calculate topping: 1 = forced topping, 2 = automatic calculation	code, 1 to 2
codcueille_T	Option to define harvest type: 1 = single harvest (cutting), 2 = multiple harvests (picking)	code, 1 to 2
code_acti_reserve_p	Option to activate the simulation of Nitrogen and Carbon reserves: 1 = yes, 2 = no	code, 1 to 2
code_auto_profres_T	Option to define profres: 1 = profres read in tec file, 2 = profres calculated as proftrav *(1-exp(-resk.(proftrav-resz))	code, 1 to 2
code_CsurNsol_dynamic_G	Option to activate the dynamic calculation of CsurNsol: 1 = yes, 2 = no	code, 1 to 2
code_diff_root_p	Option to activate the simulation of 2 root classes: 1 = yes, 2 = no	code, 1 to 2
code_hautfauche_dyn_T	Option to activate dynamic calculation of residual LAI, biomass and N content after cutting: 1 = yes, 2 = no	code, 1 to 2
code_hourly_wfps_denit_G	Option to activate hourly WFPS calculation for denitrification: 1 = yes, 2 = no	code, 1 to 2
code_hourly_wfps_nit_G	Option to activate hourly WFPS calculation for nitrification: 1 = yes, 2 = no	code, 1 to 2
code_pdenit_G	Option to define the denitrification potential: 1 = read in soil parameter, 2 = calculated from soil organic carbon concentration	code, 1 to 2
code_ratiodenit_G	Option to define the N ₂ O/(N ₂ +N ₂ O) ratio of denitrification: 1 = constant, 2 = variable	code, 1 to 2
code_rationit_G	Option to define the N ₂ O/(N ₂ +N ₂ O) ratio of nitrification: 1 = constant, 2 = variable	code, 1 to 2

Nam_e	Definition	Unit
code_rootdeposition_p	Code to simulate N demand and allocation to roots and their turn-over during crop growth cycle: 1 = daily deposition, 2 = deposition only at harvest	code, 1 to 2
code_stress_root_p	Option to activate the preferential allocation of biomass to roots in case of water or N stress: 1 = yes, 2 = no	code, 1 to 2
code_tnit_G	Option to define the temperature function for nitrification: 1 = piecewise linear, 2 = gaussian	code, 1 to 2
code_vnit_G	Option to define the nitrification rate dependence on NH ₄ : 1 = first order, 2 = Michaelis-Menten	code, 1 to 2
code_WangEngel_p	Option to activate the effect of temperature on development units for emergence according to Wang et Engel (1998): 1 = yes, 2 = no	code, 1 to 2
codeactimulch_G	Option to activate the mulch effect at soil surface: 1 = yes, 2 = no	code, 1 to 2
codeaumin_T	Option to activate the harvest according to grain/fruit water content: 1 = water content > minimum threshold, 2 = water content < maximum threshold	code, 1 to 2
codebeso_p	Option to calculate water requirements: 1 = k.ETP approach, 2 = resistive method	code, 1 to 2
codebfroid_p	Option to calculate chilling requirements: 1 = no need, 2 = vernalising days, 3 = development stage	code, 1 to 3
codecailloux_S	Option to take into account pebbles in the water and N balances: 1 = yes, 2 = no	code, 0 to 1
codecaferti_G	Option to activate the automatic calculation of fertilisation rate: 1 = yes, 2 = no	code, 1 to 2
codecalirrig_T	Option to activate the automatic calculation of irrigation requirements: 1 = yes, 2 = no	code, 1 to 2
codecaltemp_C	Option to activate the use of crop temperature for phasic development calculation: 1 = empirical relation, 2 = energy balance	code, 1 to 2
codeclaircie_T	Option to simulate fruit removal: 1 = no, 2 = yes (for smallest fruits)	code, 1 to 2
codeclichange_C	Option to activate climate change: 1 = no, 2 = yes	code, 1 to 2
codedate_irrigauto_T	Option to activate the beginning and the ending dates in case of automatic irrigation: 1 = dates, 2 = crop stages, 3 = nothing	code, 1 to 3

Nam_e	Definition	Unit
codedateappH2O_T	Option to calculate irrigation dates according to sum of temperatures: 1 = yes, 2 = no	code, 1 to 2
codedateappN_T	Option to calculate mineral fertilizer application dates according to sum of temperatures: 1 = yes, 2 = no	code, 1 to 2
codedecirecolte_T	Option to activate moisture and frost effects on harvest decision: 1 = yes, 2 = no	code, 1 to 2
codedecisemis_T	Option to activate the moisture effect on harvest decision: 1 = yes, 2 = no	code, 1 to 2
codedenit_S	Option to activate the calculation of denitrification model: 1 = yes, 2 = no	code, 1 to 2
codedisrac_p	Option to define root profile in soil: 1 = standard root distribution, 2 = root emission proportional to root biomass	code, 1 to 2
codedormance_p	Option to calculate dormancy and chilling requirements: 1 = forcing, 2 = Richardson, 3 = Bidabe	code, 1 to 3
codeDST_T	Option to activate the variations in physical soil conditions due to tillage: 1 = yes, 2 = no	code, 1 to 2
codeDSTnbcouche_T	Option to define the number of compacted soil layers: 1 = one layer, 2 = two layers	code, 1 to 2
codeDSTtass_T	Option to activate the soil compaction at sowing and harvest: 1 = yes, 2 = no	code, 1 to 2
codedyntalle_p	Option to activate the module simulating tillers dynamics: 1 = yes, 2 = no	code, 1 to 2
codeetp_C	Option to calculate PET: 1 = forced Penman, 2 = calculated Penman, 3 = Shuttleworth & Wallace, 4 = Priestley & Taylor	code, 1 to 4
codefauche_T	Option to activate cuts of forage crops: 1 = yes, 2 = no	code, 1 to 2
codefente_S	Option to activate an additional water compartment for swelling soils: 1 = yes, 2 = no	code, 0 to 1
codefeuille_T	Option to activate plant thinning: 1 = no, 2 = yes	code, 1 to 2
codefixpot_p	Option to calculate the maximal symbiotic fixation: 1 = fixed value read in the plant file, 2 = depends on growth rate	code, 1 to 2
codefracappN_T	Option to activate split applications of N fertiliser: 1 = absolute value, 2 = fraction of total N application	code, 1 to 2

Name	Definition	Unit
codefrmur_G	Option to define the maturity status of the fruits in the variable CHARGEFRUIT: 1 = including ripe fruits (last box N), 2 = excluding ripe fruits (first N-1 boxes)	code, 1 to 2
codefxn_G	Option to define the effect of soil nitrate on N fixation: 1 = no effect, 2 = effect of nitrate amount, 3 = effect of nitrate concentration	code, 1 to 3
codegdh_p	Option to define the time step used for calculating development units: 1 = hourly, 2 = daily	code, 1 to 2
codegdhdeb_p	Option to define the time step used for calculating bud break date: 1 = daily, 2 = hourly growing degrees	code, 1 to 2
codegermin_p	Option to simulate germination: 1 = germination phase, 2 = immediate germination	code, 1 to 2
codeh2oact_G	Option to activate water stress effect on crop growth: 1 = yes, 2 = no	code, 1 to 2
codehypo_p	Option to simulate plant emergency: 1 = phase of hypocotyl growth (sown crops), 2 = plantation of plantlets	code, 1 to 2
codeindetermin_p	Option to simulate the type of leaf growth and fruit growth: 1 = determinate, 2 = undeterminate	code, 1 to 2
codeinitprec_G	Option to activate reset of initial conditions in case of chained simulations: 1 = yes, 2 = no	code, 1 to 2
codeINN_p	Option to compute NNI: 1 = cumulative NNI, 2 = instantaneous NNI	code, 1 to 2
codeinnact_G	Option to activate N stress effect on root length growth: 1 = yes, 2 = no	code, 1 to 2
codeintercept_p	Option to simulate rainfall interception by leaves: 1 = yes, 2 = no	code, 1 to 2
codeir_p	Option to calculate the ratio grain weight/ total biomass: 1 = proportional to time, 2 = proportional to thermal time	code, 1 to 2
codejourdes_T	Option to simulate perennial crops destruction	code, 1 to 2
codelair_p	Option to calculate the intercepted radiation according to: 1 = LAI, 2 = soil cover	code, 1 to 2
codelegume_p	Option to define if the crop is a legume fixing N: 1 = yes, 2 = no	code, 1 to 2
codemacropor_S	Option to activate calculation of water flux in soil macroporosity: 1 = yes, 2 = no	code, 1 to 2

Nam_e	Definition	Unit
codemicheur_G	Option to calculate hourly microclimatic outputs (output file humidite.sti): 1 = yes, 2 = no	code, 1 to 2
codeminopt_G	Option to simulate a bare soil with a constant water content: 1 = yes, 2 = no	code, 0 to 1
codemodfauche_T	Option to define the cutting mode: 1 = automatic calculation depending on phenologic and trophic state, 2 = pre-established calendar in days, 3 = pre-established calendar in degree-days	code, 1 to 3
codemodlsnow_C	Option to calculate snow variables: 1 = unused, 2 = unused, 3 = Snow model 3	code, 1 to 3
codemonocot_p	Option to define the type of plant: 1 = monocot, 2 = dicot	code, 1 to 2
codemontaison_p	Option to stop the reserve limitation after stem elongation in grassland: 1 = yes, 2 = no	code, 1 to 2
codemortalracine_p	Option to calculate the mass of dead roots after a cut: 1 = based on masec, 2 = based on masecot	code, 1 to 2
codemsfinal_G	Option to define if the biomass and yield are conserved after harvest: 1 = yes, 2 = no (values set at 0)	code, 1 to 2
codenitrif_s	Option to activate the nitrification model: 1 = yes, 2 = no	code, 1 to 2
codeNmindec_G	Option to activate the limitation of residues decomposition due lack of mineral N: 1 = yes, 2 = no	code, 1 to 2
codeoutscent_G	Option to write outputs files with scientific format: 1 = yes, 2 = no	code, 1 to 2
codepailage_T	Option to define soil cover: 1 = no cover, 2 = plastic cover partly covering the soil	code, 1 to 2
codepalissage_T	Option to define if the plant is fixed onto a vertical support: 1 = no, 2 = yes	code, 1 to 2
codeperenne_p	Option to define the crop perennality: 1 = annual crop, 2 = perennial crop	code, 1 to 2
codephot_p	Option to define plant photoperiodism: 1 = yes, 2 = no	code, 1 to 2
codephot_part_p	Simulation of the effect of decreasing photoperiod on biomass allocation: 1 = yes, 2 = no	code, 1 to 2
codeplante_p	Option to define the coding name of the plant (3 characters)	ND
codeplisoleN_p	Option to define N requirements at the beginning of the cycle: 1 = dense plant population, 2 = isolated plants	code, 1 to 2

Nam_e	Definition	Unit
codepluiepoquet_G	Option to replace rainfall by irrigation at poquet depth in the case of poquet sowing: 1 = yes, 2 = no	code, 1 to 2
codeprofmes_G	Option of soil depth for calculating water and N stocks (1 = profmes, 2 = soil depth)	code, 1 to 2
coderacine_p	Option to define the calculation of root growth and extension: 1 = standard profile, 2 = root length density	code, 1 to 2
coderecolteassoc_T	Option to harvest intercrop species simultaneously, at the physiological maturity date of the earliest one: 1 = no, 2 = yes	code, 1 to 2
coderemontcap_S	Option to activate capillary rise: 1 = yes, 2 = no	code, 1 to 2
coderes_T	Residue type: 1 = mature crop, 2 = cover crop, 3 = Manure, 4 = Green compost, 5 = Sewage sludge, 6 = Vinasse, 7 = Horn, 8 = vineyard prunings, 9 = pig slurry, 10 = rhizomes	code, 1 to 10
coderes_pature_G	Residue type used to simulate bovine feces: 1-10	code, 1 to 10
coderetflo_p	Option to activate the effect of water stress on development before the stage DRP (filling of harvested organs): 1 = yes, 2 = no	code, 1 to 2
codernet_C	Option to calculate net radiation: 1 = Brunt method, 2 = Cellier method	code, 1 to 2
codesensibilite_G	Option to activate the sensitivity analysis version of the model: 1 = yes, 2 = no	code, 1 to 2
codeserapport_G	Option to select the column separator in the rapport.sti output file: 1 = space separator, 2 = separator indicated in the file rapport.sti	code, 1 to 2
codesimul_U	Option to define the type of crop simulation: culture or 0 (LAI calculated by the model), feuille or 1 (LAI forced)	code, 0 to 1
codesnow_G	Option to activate the snow module: 1 = yes, 2 = no	code, 1 to 2
codestade_T	Option to force one or several development stages: 1 = yes, 2 = no	code, 1 to 2
codestrphot_p	Option to activate the photoperiodic stress on lifespan (1 = yes, 2 = no)	code, 1 to 2
codesuite_U	Option to simulate several successive USM: 0 = no, 1 = yes	code, 0 to 1
codeSWDRH_G	Optin to calculate the duration of surface wetness: 1 = yes , 2 = no	code, 1 to 2

Nam_e	Definition	Unit
codesymbiose_G	Option to calculate symbiotic N fixation: 1 = based on critical dilution curve, 2 = specific calculation of N fixation	code, 1 to 2
codetaille_T	Option to activate pruning: 1 = no, 2 = yes	code, 1 to 2
codetemp_p	Option to calculate thermal time for plant growth: 1 = based on air temperature, 2 = based on crop temperature	code, 1 to 2
codetempfauche_T	Option to define the reference temperature to compute cutting sum of temperatures: 1 = upvt, 2 = udevair	code, 1 to 2
codetemprac_p	Option to calculate thermal time for root growth: 1 = crop temperature, 2 = soil temperature	code, 1 to 2
codetesthum_{N_G}	Option to define automatic N fertilisation calculation: 1 = based on rainfall, 2 = based on soil water content	code, 1 to 2
codetradtec_T	Option to activate the effect of crop structure on radiation transfer: 1 = yes, 2 = no	code, 1 to 2
codetranspalle_p	Option to choose the ratio used to calculate tiller mortality: 1 = et/etm, 2 = epc2/eopC	code, 1 to 2
codetransrad_p	Option to calculate radiation interception: 1 = Beer law, 2 = radiative transfer	code, 1 to 2
codetrem_p	Option to activate heat effect on grain filling: 1 = yes, 2 = no	code, 1 to 2
codetrosee_G	Option to calculate hourly dew temperature: 1 = linear interpolation, 2 = sinusoidal interpolation (Debele Bekele et al, 2007)	code, 1 to 2
codetycailloux_G	Code for pebble type	code, 1 to 10
codetypeng_G	Code for fertiliser type	code, 1 to 8
codetypres_G	Code for organic residue	code, 1 to 10
codevar_p	Code for cultivar name	ND
codgelflo_p	Option to activate the frost effect at anthesis: 1 = no, 2 = yes	code, 1 to 2
codgeljuv_p	Option to activate the frost effect on LAI at the juvenile stage: 1 = no, 2 = yes	code, 1 to 2
codgellev_p	Option to activate the frost effect on plantlet growth: 1 = no, 2 = yes	code, 1 to 2
codgelveg_p	Option to activate the frost effect on LAI at adult stage: 1 = no, 2 = yes	code, 1 to 2

Na_me	Definition	Unit
codhauteff_T	Option to define the height of leaf removal (if the thinning option is activated): 1 = bottom of the canopy, 2 = top of the canopy	code, 1 to 2
codhnappe_G	Option to calculate the watertable level: 1 = mean height, 2 = height at the distance distrain	code, 1 to 2
codlaine_p	Option to calculate the LAI: 1 = net LAI, 2 = difference between gross LAI and senescent LAI	code, 1 to 2
codlocferti_T	Option to define localized fertilisation: 1 = at soil surface, 2 = deeper in the soil	code, 1 to 2
codlocirrig_T	Option to define localized irrigation: 1 = above the foliage, 2 = below the foliage above the soil, 3 = in the soil	code, 1 to 3
codoptim_U	Option to activate the optimisation code: 0 = no, 1 = optimisation for the main crop, 2 = optimisation for the associated crop	code, 0 to 2
codrainage_S	Option to simulate artificial drainage: 1 = yes, 2 = no	code, 1 to 2
codrecolte_T	Option to define harvest strategy: 1 = at physiological maturity, 2 = according to water content, 3 = according to sugar content, 4 = according to nitrogen content, 5 = according to oil content	code, 1 to 5
codrognage_T	Option to activate foliage control by trimming: 1 = no, 2 = yes	code, 1 to 2
codtrophrac_p	Option to activate a trophic effect on root length growth: 1 = permanent link, 2 = link by thresholds, 3 = no effect	code, 1 to 3
coef_calcul_doseN_G	Crop N concentration below which there is no N return to the soil through animal urine	g kg ⁻¹
coef_calcul_qres_G	Crop N concentration used to calculate animal feces from animal grass dry matter intake	g kg ⁻¹
coefamflax_p	Multiplier coefficient applied to the thermal time requirement between stages AMF and LAX	ND
coefb_G	Parameter defining the radiation saturation effect on biomass conversion efficiency	g MJ ⁻¹
coefdevil_C	Multiplier coefficient of the outdoor radiation to calculate PET inside of a greenhouse	ND

Nam_e	Definition	Unit
coefdrpmat_p	Multiplier coefficient applied to the thermal time requirement between stages DRP and MAT	ND
coefflodrp_p	Multiplier coefficient applied to the thermal time requirement between stages FLO and DRP	ND
coeflaxsen_p	Multiplier coefficient applied to the thermal time requirement between stages LAX and SEN	ND
coeflevamf_p	Multiplier coefficient applied to the thermal time requirement between stages LEV and AMF	ND
coeflevdrp_p	Multiplier coefficient applied to the thermal time requirement between stages LEV and DRP	ND
coefmshaut_p	Ratio of crop biomass to useful cutting height of crops	t ha ⁻¹ m ⁻¹
cofracoupe_p	Proportion of roots dying after a cut of a forage crop	ND
coefrnet_C	Coefficient applied to the (outdoor) net radiation to calculate the net radiation under a greenhouse	ND
cofsenlan_p	Multiplier coefficient applied to the thermal time requirement between stages SEN and LAN	ND
concirr_T	Concentration of mineral N (NH ₄ +NO ₃ -N) in irrigation water	kg ha ⁻¹ mm ⁻¹
concNnodseuil_p	Maximal concentration of mineral N in soil for nodule onset	kg ha ⁻¹ mm ⁻¹
concNrac0_p	Nitrate-N concentration (if codefxN=3) or nitrate-N amount (if codefxN=2) above which N fixation is totally inhibited	kg ha ⁻¹ mm ⁻¹ or kg ha ⁻¹ cm ⁻¹
concNrac100_p	Nitrate-N concentration (if codefxN=3) or nitrate-N amount (if codefxN=2) below which N fixation is maximum	kg ha ⁻¹ mm ⁻¹ or kg ha ⁻¹ cm ⁻²
concr_C	Concentration of mineral N (NH ₄ +NO ₃ -N) in the rain	kg ha ⁻¹ mm ⁻¹
concseuil_S	Minimum concentration of NO ₃ -N in soil (unavailable for leaching and for uptake)	kg ha ⁻¹ mm ⁻¹
contrdamax_p	Maximal reduction factor applied to root growth rate due to soil strengthness (high bulk density)	ND
corecTrosee_C	Temperature to subtract to Tmin to estimate dew point temperature (in case of missing air humidity data)	°C

Nam_e	Definition	Unit
couvermulchplastique_T	Fraction of soil covered by the plastic mulch	ND
Crespc_T	C content in organic residue (DW)	%
Crespc_pature_G	C content in animal feces (FW)	%
CroCo_G	Fraction of organic residue which is decomposable	ND
croirac_P	Elongation rate of the root apex	cm degree days ⁻¹
CsurNres_T	C/N ratio of residue	g g ⁻¹
CsurNsolO_S	Initial C to N ratio of soil humus	g g ⁻¹
culturean_U	Number of calendar years involved in the crop cycle (1 = 1 year e.g. for spring crops, 2 = two years, e.g. for winter crops)	ND
cvent_C	Parameter of the climate calculation under shelter	ND
cwb_G	Minimum ratio C/N of microbial biomass decomposing organic residues	g g ⁻¹
dachisel_T	Bulk density of soil after soil tillage (Chisel)	g cm ⁻³
dacohes_G	Bulk density of soil below which root growth is reduced due to a lack of soil cohesion	g cm ⁻³
DAF_S	Bulk density of fine earth fraction in each soil layer	g cm ⁻³
dalabour_T	Bulk density of soil after full inversion tillage (plough)	g cm ⁻³
darecolte_T	Bulk density of soil after harvest	g cm ⁻³
dasemis_T	Bulk density of soil after sowing	g cm ⁻³
daseuilbas_G	Bulk density of soil above which root growth is maximal	g cm ⁻³
daseuilhaut_G	Bulk density of soil above which root growth becomes impossible	g cm ⁻³
datedeb_irrigauto_T	Starting date of automatic irrigations	julian day
datedebut_U	Starting date of simulation	julian day
datefin_U	Ending date of simulation	julian day
datefin_irrigauto_T	Ending date of automatic irrigations	julian day
debsenrac_P	Thermal time units defining the beginning of root senescence (root life time)	degree days
deneng_G	Maximal fraction of the mineral fertilizer that can be denitrified (used if codedenit is not activated)	ND
densinitial_I	Initial root density in each of the five soil layers	cm cm ⁻³
densitesem_T	Plant sowing density	pl m ⁻²

Nam_e	Definition	Unit
deshydbase_p	Rate of change of water content in fruits (FW) vs thermal time (>0 or <0)	g g ⁻¹ degree days ⁻¹
dfolbas_p	Minimal foliar density within the considered shape	m ² m ⁻³
dfolhaut_p	Maximal foliar density within the considered shape	m ² m ⁻³
dfpf_p	Parameter of the first potential growth phase of fruit, corresponding to an exponential type function describing the cell division phase	ND
difN_G	Diffusion coefficient of nitrate in soil at field capacity	cm ² day ⁻¹
diftherm_G	Soil thermal diffusivity	cm ² s ⁻¹
distdrain_G	Distance between mole drains	cm
DKmax_C	Difference between the maximum and the minimum melting rates for snow	mm °C ⁻¹ day ⁻¹
dlaimax_p	Maximum rate of net daily increase of LAI	m ² pl ⁻¹ degree days ⁻¹
dlaimaxbrut_p	Maximum rate of gross daily increase of LAI	m ² pl ⁻¹ degree days ⁻¹
dlaimin_p	Accelerating parameter for the lai growth rate	ND
dltamsmaxsen_p	Growth rate above which there is no more photoperiodic effect on senescence	t ha ⁻¹ day ⁻¹
dltamsminsen_p	Growth rate below which the photoperiodic effect on senescence is maximal	t ha ⁻¹ day ⁻¹
doseI_T	Daily amount of irrigation water	mm day ⁻¹
doseirrigmin_T	Minimal amount of daily irrigation	mm day ⁻¹
doseN_T	Daily amount of N added through fertilizers	kg ha ⁻¹ day ⁻¹
dosimx_T	Maximum amount of irrigation water applied daily (mode automatic irrigation)	mm day ⁻¹
dosimxN_G	Maximum amount of fertiliser N applied daily (mode automatic fertilisation)	kg ha ⁻¹ day ⁻¹
dpHvolmax_G	Maximal pH increase following the application of slurry	ND
draclong_p	Maximum rate of root length production per plant	cm pl ⁻¹ degree days ⁻¹
dureefruit_p	Duration of the fruit between onset and physiological maturity	degree days
durvieF_p	Maximal lifespan of an adult leaf expressed in summation of Q10=2 (2**(T-Tbase))	ND

Nam_e	Definition	Unit
durviesupmax_p	Relative additional lifespan due to N excess in plant (INN > 1)	ND
E_C	Snow compaction parameter	mm mm ⁻¹ day ⁻¹
eau_mini_decisemis_T	Minimum amount of rainfall required to start sowing (when codesemis is activated)	mm
eaures_T	Water content of organic residue (FW)	%
eaures_pature_G	Water content of animal feces deposited on soil during grazing (FW)	%
ecardrain_S	Distance between mole drains	cm
efcroijuv_p	Maximum radiation use efficiency during the juvenile phase (LEV-AMF)	g MJ ⁻¹
efcroirepro_p	Maximum radiation use efficiency during the grain filling phase (DRP-MAT)	g MJ ⁻¹
efcroiveg_p	Maximum radiation use efficiency during the vegetative stage (AMF-DRP)	g MJ ⁻¹
effeuil_T	Fraction of leaf removed by plant thinning	ND
effirr_T	Irrigation efficiency	ND
efremobil_p	Efficiency of use of carbohydrates in storage organs of perennials	ND
elmax_p	Maximum elongation of the coleoptile in darkness condition	cm
engamm_G	Fraction of ammonium in the N fertilizer	ND
engrais_T	Fertilizer type (1 = ammonium nitrate, 2 = UAN solution, 3 = urea, 4 = anhydrous ammonia, 5 = ammonium sulfate, 6 = ammonium phosphate, 7 = calcium nitrate, 8 = fixed efficiency fertiliser)	ND
engrais_pature_G	Fertilizer type used to mimic urine excretion (1 = ammonium nitrate, 2 = UAN solution, 3 = urea, 4 = anhydrous ammonia, 5 = ammonium sulfate, 6 = ammonium phosphate, 7 = calcium nitrate, 8 = fixed efficiency fertiliser)	ND
engraiscoupe_T	Fertilizer type (1 = ammonium nitrate, 2 = UAN solution, 3 = urea, 4 = anhydrous ammonia, 5 = ammonium sulfate, 6 = ammonium phosphate, 7 = calcium nitrate, 8 = fixed efficiency fertiliser)	ND
envfruit_p	Fraction of envelop in grainmaxi	ND
epc_S	Thickness of each soil layer	cm
epd_S	Thickness of mixing cells in each soil layer (= 2 * dispersion length)	cm
extin_p	Extinction coefficient of photosynthetic active radiation in the canopy	ND

Na_m_e	Definition	Unit
fclim1_U	Name of the first climate file	ND
fclim2_U	Name of the second climate file	ND
fhminsat_G	Relative soil mineralisation rate at water saturation	ND
finert_S	Initial fraction of inert pool in the soil organic pool (= stable SON/ total SON)	ND
finit_U	Name of the initialisation file	ND
fixmax_P	Maximal N symbiotic fixation rate	kg ha ⁻¹ day ⁻¹
fixmaxgr_P	Maximal N symbiotic fixation rate per unit of grain growth rate	kg t ⁻¹
fixmaxveg_P	Maximal N symbiotic fixation rate per unit of vegetative growth rate	kg t ⁻¹
flagecriture_G	Option for writing the output files (1 = mod_history.sti, 2 = daily outputs, 4 = report outputs, 8 = balance outputs, 16 = profile outputs, 32 = debug outputs, 64 = screen outputs) sum them to have several types of outputs	ND
flai_U	Name of the LAI file	ND
fNcbiomin_G	Minimal value for the ratio N/C of the microbial biomass when N limits decomposition	g g ⁻¹
fNmindecmin_G	Minimal fraction of mineral N available for residues decomposition (if codeNmindec is activated)	ND
fnx_G	Maximum fraction of NH4 nitrified each day (first order model)	ND
fobs_U	Name of the observed file	ND
forme_P	Option to define the shape of leaf density profile: 1 = rectangle, 2 = triangle	code, 1 to 2
fplt_U	Name of the plant file	ND
fracN_T	Proportion of fertiliser N applied at each application	%
fredkN_G	Reduction factor of decomposition rate of organic residues when mineral N is limiting	ND
fredlN_G	Reduction factor of decomposition rate of microbial biomass when mineral N is limiting	ND
fredNsup_G	Additional reduction factor of residues decomposition rate when mineral N is highly limiting	ND
fstation_U	Name of the weather station file	ND

Nam_e	Definition	Unit
ftec_U	Name of the technical file	ND
ftemh_G	Parameter (1/2) of the temperature function on humus decomposition rate	K ⁻¹
ftemha_G	Parameter (2/2) of the temperature function on humus decomposition rate	ND
ftemr_G	Parameter (1/2) of the temperature function on decomposition rate of organic residues	K ⁻¹
ftemra_G	Parameter (2/2) of the temperature function on decomposition rate of organic residues	ND
GMIN1_G	Parameter (1/7) of the new mineralization function (Clivot et al, 2017)	day ⁻¹
GMIN2_G	Parameter (2/7) of the new mineralization function (Clivot et al, 2017)	-1%
GMIN3_G	Parameter (3/7) of the new mineralization function (Clivot et al, 2017)	-1%
GMIN4_G	Parameter (4/7) of the new mineralization function (Clivot et al, 2017)	pH ⁻¹
GMIN5_G	Parameter (5/7) of the new mineralization function (Clivot et al, 2017)	pH
GMIN6_G	Parameter (6/7) of the new mineralization function (Clivot et al, 2017)	g g ⁻¹
GMIN7_G	Parameter (7/7) of the new mineralization function (Clivot et al, 2017)	g g ⁻¹
gradtn_C	Thermal gradient in altitude for minimal temperatures	°C 100m ⁻¹
gradtninv_C	Thermal gradient in altitude for minimal temperatures under the inversion level	°C 100m ⁻¹
gradtx_C	Thermal gradient in altitude for maximal temperatures	°C 100m ⁻¹
h2ofeuiljaune_p	Water content of yellow leaves (FW)	g g ⁻¹
h2ofeuilverte_p	Water content of green leaves (FW)	g g ⁻¹
h2ofrvert_p	Water content of fruits before the beginning of dehydration (FW)	g g ⁻¹
h2ograinmax_T	Maximal water content of fruits at harvest (FW)	g g ⁻¹
h2ograinmin_T	Minimal water content of fruits at harvest (FW)	g g ⁻¹
h2oreserve_p	Water content of crop reserve (FW)	g g ⁻¹
h2otigestruc_p	Water content of structural stem part (FW)	g g ⁻¹
hautbase_p	Basal height of crop	m

Nam_e	Definition	Unit
hautcoupe_T	Cut height for forage crops (calendar fixed)	m
hautcoupedefault_T	Cut height for forage crops (calendar calculated)	m
hautmax_P	Maximum height of crop	m
hautmaxtec_T	Maximal height of the plant allowed by the management	m
hautrogne_T	Cutting height for trimmed plants	m
hccc_G	Gravimetric water content at field capacity of each type of pebble (dry soil)	%
hccf_S	Gravimetric water content at field capacity of each soil layer (in fine earth, dry soil)	%
Hinitf_I	Initial gravimetric water content of each soil layer (in fine earth, dry soil)	%
hminf_S	Gravimetric water content at wilting point of each soil layer (in fine earth, dry soil)	%
hminm_G	Relative water content (fraction of field capacity) below which mineralisation rate is nil	ND
hminn_G	Relative water content (fraction of field capacity) below which nitrification rate is nil	ND
hoptm_G	Relative water content (fraction of field capacity) above which mineralisation rate is maximum	ND
hoptn_G	Relative water content (fraction of field capacity) above which nitrification rate is maximum	ND
huilerec_T	Minimal oil content of fruits at harvest (FW)	g g ⁻¹
humcapil_S	Threshold of soil gravimetric water content under which capillary rise occurs (dry soil)	%
humirac_G	A revoir: 1 = la fonction F_humirac atteint un plateau (ancien code) / 2 = la fonction n atteint pas de plateau (identique a la phase germination-levee)	ND
humirac_decisemis_T	Relative soil moisture threshold above which sowing is possible (0 = no sensitivity to drought, 1 = highly sensitive)	ND
iamf_T	Day when the stage AMF is reached (999 if not reached)	julian day
ichsl_U	Soil number in the param.soil file	ND
idebdorm_P	Day of the dormancy entrance	julian day
idor_J	Day of the dormancy entrance	julian day

Name	Definition	Unit
idrp_T	Day of the stage DRP (beginning of grain filling) when the stage is observed (else 999)	julian day
ifindorm_p	Day of dormancy break	julian day
iflo_T	Day of anthesis	julian day
ifwater_U	Day of the end of simulation	julian day
ilan_T	Day when the stage LAN is reached (999 if not observed)	julian day
ilax_T	Day when the stage LAX is reached (999 if not observed)	julian day
ilev_T	Day when the stage LEV is reached (999 if not observed)	julian day
imat_T	Day when the stage MAT is reached (999 if not observed)	julian day
infil_s	Infiltrability rate at the base of each soil layer (if codemacropor = 1)	mm day ⁻¹
inflomax_p	Maximal number of inflorescences per plant	ND
infrecouv_p	Ulai at the stage AMF (maximal rate of leaf growth)	ND
inilai_p	Initial value of lai for cotyledons	m ² m ⁻²
iniprofil_G	Option of smoothing out the initial mineral N and water profiles (spline function): 0 = no, 1 = yes	ND
inngrain1_p	NNI below which net absorption of N during grain filling is maximal	ND
inngrain2_p	NNI above which net absorption of N during grain filling is nil	ND
INNimin_p	INNI (instantaneous NNI) corresponding to INNmin	ND
INNmin_p	Minimum value of NNI possible for the crop	ND
innsen_p	Parameter of the N stress function active on senescence (INNsenes)	ND
innturgmin_p	Parameter of the N stress function active on leaf expansion (INNLAJ)	ND
interrang_T	Width of the crop interrow	m
iplt_j	Date of sowing	julian day
iplt0_T	Date of sowing	julian day
irazomax_p	Maximum nitrogen harvest index	ND
irec_T	Date of harvest	julian day
irecbutoir_T	Latest date of harvest (imposed if the crop cycle is not finished at this date)	julian day

Na_m_e	Definition	Unit
irmax_p	Maximum harvest index	ND
irrlev_G	Amount of irrigation applied automatically on the sowing day to allow germination when the model calculates irrigation	mm
isen_T	Day when the stage SEN is reached (999 if not observed)	julian day
isnu_j	Date when the soil is bare	julian day
iwater_U	Starting day of the simulation	julian day
julapl_T	Date(s) of irrigation	julian day
julapN_T	Date(s) of fertilizer application	julian day
juldes_T	Day of perennial crop destruction	julian day
juleclair_T	Day of fruits removal	julian day
juleffeuil_T	Day of leaf removal	julian day
julfauche_T	Date(s) of each cut for forage crops	julian day
julouvre2_T	Day (1/2) of opening the shelter	julian day
julouvre3_T	Day (2/2) of opening the shelter	julian day
julres_T	Date(s) of organic residue addition to soil	julian day
julrogne_T	Day of plant trimming	julian day
jultaille_T	Day of pruning	julian day
jultrav_T	Date(s) of soil tillage	julian day
julvernal_p	Day of initiation of vernalisation in perennial crops (between 1 and 365)	julian day
jvc_p	Number of vernalising days or dormancy units	days
jvcmini_p	Minimum number of vernalising days	days
Kamm_G	Affinity constant for NH ₄ in nitrification (if Michaelis_Menten formalism is used)	mg L ⁻¹
kbio_G	Potential decay rate of microbial biomass decomposing organic residues	day ⁻¹
kcouvmlch_G	Extinction coefficient connecting the soil cover to the amount of plant mulch	ND
Kd_G	Affinity constant for nitrate in denitrification	mg L ⁻¹
kdesat_G	Rate constant of de-saturation	day ⁻¹
kdisrac_p	Rate constant defining root length distribution throughout the profile	cm ⁻²
khaut_p	Extinction coefficient connecting LAI to crop height	ND
Kmabs1_p	Affinity constant of N uptake by roots for the fast uptake system	micromole L ⁻¹

Na_m_e	Definition	Unit
Kmabs_{2p}	Affinity constant of N uptake by roots for the low uptake system	micromole L ⁻¹
kmax_p	Maximum crop coefficient for water requirements (= MET/PET)	ND
Kmin_C	Minimum snow melting rate on 21 December	mm °C ⁻¹ day ⁻¹
krepracperm_p	Parameter of biomass root partitioning: evolution of the ratio root/total (permanent trophic link)	ND
krepracseu_p	Parameter of biomass root partitioning: evolution of the ratio root/total (trophic link by thresholds)	ND
ksol_S	Soil hydraulic conductivity in the vicinity of mole drains	ND
kstemflow_p	Extinction coefficient connecting LAI to stemflow	ND
ktrou_p	Extinction coefficient of PAR through the crop (used in the radiative transfer module)	ND
lai0_I	Initial leaf area index	m ² m ⁻²
laicomp_p	LAI above which competition between plants starts	m ² m ⁻²
laidebeff_T	LAI at the beginning of leaf removal	m ² m ⁻²
laieffeuil_T	LAI removed from the crop at day juleffeuil	m ² m ⁻²
laiplantule_p	LAI of plantlet at the plantation	m ² m ⁻²
lairesiduel_T	Residual LAI after each cut of forage crop	m ² m ⁻²
largrogne_T	Trimmed width	m
largtec_T	Technical width	m
latitude_C	Latitude of the site	degree
locferti_T	Soil depth at which fertiliser is applied	cm
locirrig_T	Soil depth at which irrigation is applied	cm
longsperac_p	Specific root length	cm g ⁻¹
lvfront_p	Root density at the root apex	cm cm ⁻³
lvmax_p	Maximum root length density in the top soil (used to calculate root mass)	cm cm ⁻³
lvopt_G	Root length density (RLD) above which water and N uptake are maximum and independent of RLD	cm cm ⁻³
magrain0_I	Initial grain dry weight	g m ⁻²
maperenne0_I	Initial value of biomass of storage organs in perennial crops	t ha ⁻¹

Nome	Definition	Unit
margerogne_T	Topping occurs when plant height exceeds (hautrogne+margerogne) when automatic trimming is activated	m
masec0_I	Initial plant biomass (if the option to simulate N and C reserves is not activated)	t ha ⁻¹
masecmeta_p	Biomass of the plantlet supposed to be composed of metabolic N	t ha ⁻¹
masecNmax_p	Aerial biomass above which N dilution occurs (critical and maximal curves)	t ha ⁻¹
masecnp0_I	Initial aerial biomass	t ha ⁻¹
masecplantule_p	Initial shoot biomass of plantlet	t ha ⁻¹
masvolcx_G	Bulk density of each type of pebble	g cm ⁻³
max_pdenit_G	Maximal value of the denitrification potential (if code_pdenit = 2)	kg ha ⁻¹ cm ⁻¹ day ⁻¹
maxazorac_p	Mineral N concentration in soil above which root growth is maximum	kg ha ⁻¹ cm ⁻¹
maxtalle_p	Maximum tillers density per soil area	nb m ⁻²
min_pdenit_G	Minimal value of the denitrification potential (if code_pdenit = 2)	kg ha ⁻¹ cm ⁻¹ day ⁻¹
minazorac_p	Mineral N concentration in soil below which root growth is reduced	kg ha ⁻¹ cm ⁻¹
minefnra_p	Reduction factor on root growth when soil mineral N is limiting (< minazorac)	ND
mouillabil_p	Maximum wettability of leaves	mm m ⁻²
mouillabilmulch_G	Maximum wettability of crop mulch	mm t ⁻¹ ha
mscoupemini_T	Minimum value of aerial biomass required to make a cut of forage crop	t ha ⁻¹
msresiduel_T	Residual aerial biomass after a cut of a forage crop	t ha ⁻¹
mulchbat_S	Mulch depth at which a crust occurs (a value must be given but if in the plt.xml the vigueurbat parameter is equal to 1 then the parameter is inactive)	cm
nbans_U	Number of years for a simulation	years
nbcueille_T	Number of fruit harvests during the crop cycle: 1 = one harvest, 2 = several harvests	code, 1 to 2
nbfeuilplant_p	Leaf number per plant when planting	pl ⁻¹
nbfgellev_p	Leaf number at the end of the juvenile phase (frost sensitivity)	pl ⁻¹
nbgrmax_p	Maximum number of fruits per surface area	m ⁻²
nbgrmin_p	Minimum number of fruits per surface area	m ⁻²

Nam_e	Definition	Unit
nbinfo_p	Imposed number of inflorescences per plant	pl ⁻¹
nbinfoecl_T	Number of inflorescences or fruits removed at fruit removal	pl ⁻¹
nbj_pr_apres_semis_T	Number of days used to calculate rainfall requirement to start sowing (if codesemis is activated)	days
nbjgerlim_p	Maximum number of days after grain imbibition allowing full germination	days
nbjgrain_p	Number of days used to compute the number of viable grains	days
nbjmaxapresrecolte_T	Maximum number of days allowed for harvest (if the soil compaction option is activated)	days
nbjmaxapressemis_T	Maximum number of days allowed for sowing (if the soil compaction option is activated)	days
nbjournrrversirrig_G	Number of days during which rainfall is replaced by irrigation in the soil after a sowing poquet	days
nbjres_T	Number of residue additions	ND
nbjseuiltempref_T	Number of days without frost for sowing (if sowing decision option is activated)	days
nbjtrav_T	Number of tillage operations	ND
nboite_p	Number of boxes or age classes of fruits used to calculate fruit growth for undeterminate crops	ND
nbplantes_U	Number of simulated plants	ND
NH3ref_C	NH3 concentration in the atmosphere	microgram m ⁻³
nh4_min_G	Minimum (fixed ?) NH4 concentration found in soil	mg kg ⁻¹
NH4initf_I	Initial amount of NH4-N in each of the soil layers (in fine earth)	kg ha ⁻¹
nlevlim1_p	Number of days after germination after which plant emergence is reduced	days
nlevlim2_p	Number of days after germination after which plant emergence is impossible	days
Nmeta_p	Proportion of metabolic N in the plantlet	%
Nminres_T	Proportion of mineral N content in organic residues (FW)	%
Nminres_pature_G	Proportion of N mineral content in animal feces (FW)	%
NO3initf_I	Initial amount of NO3-N in each of the soil layers (in fine earth)	kg ha ⁻¹

Nam_e	Definition	Unit
nom_U	Name of the USM	ND
nomsol_U	Name of the soil	ND
Norg_S	Soil organic N content in the first soil layer (constant down to the depth profhum, dry soil)	%
Nreserve_p	Maximal proportion of N in plant reserves (difference between the maximal and critical dilution curves)	%
numsol	Soil number	ND
obstarac_S	Soil depth at which root growth is stopped due to physical constraints	cm
ombragetx_C	Change in air temperature in the northern hillslope of mountains (activated if codadret=2)	°C
option_pature_G	Option to activate grazing in pastures: 1 = yes, 2 = no	code, 1 to 2
orgeng_G	Maximal amount of fertilizer N that can be immobilized in the soil (fraction for type 8)	kg ha ⁻¹
orientrang_T	Direction of crop rows (relative to north)	rad
parazofmorte_p	C/N ratio of dead leaves when crop NNI = 1	g g ⁻¹
Parazoper_p	C/N ratio of perennial organs when crop NNI = 1	g g ⁻¹
parazorac_p	C/N ratio of roots when crop NNI = 1	g g ⁻¹
ParazoTmorte_p	C/N ratio of dead stems when crop NNI = 1	g g ⁻¹
parsurg_G	Fraction of photosynthetically active radiation in global radiation (PAR/RG)	ND
patm_C	Atmospheric pressure	hPa
penterui_S	Runoff coefficient taking into account the plant mulch	ND
pentinflores_p	Parameter used to calculate the inflorescences number	kg ⁻¹
pentlaimax_p	Parameter of the logistic curve of LAI growth	ND
pentrecouv_p	Parameter of the logistic curve of soil cover rate	ND
pertes_restit_ext_G	Fraction of animal feces and urine not returned in grazed paddocks (e.g. in resting area, milking parlour, housing and paths/roads)	ND
pgrainmaxi_p	Maximum grain weight (at 0% water content)	g

Na_m_e	Definition	Unit
pH0_S	Initial soil pH (water solution)	pH
phiv0_C	Parameter allowing the calculation of the climate under shelter	ND
pHmaxden_G	pH beyond which the N ₂ O molar fraction in the denitrification process is minimum (<= ratiodenit)	pH
pHmaxnit_G	Soil pH above which nitrification rate is maximum	pH
pHmaxvol_G	Soil pH above which NH ₃ volatilisation derived from fertiliser is maximum	pH
pHminden_G	pH below which the N ₂ O molar fraction in the denitrification process is maximum (100%)	pH
pHminnit_G	Soil pH below which nitrification is nil	pH
pHminvol_G	Soil pH below which NH ₃ volatilisation derived from fertiliser is nil	pH
phobase_p	Basal photoperiod	hours
phobasesen_p	Photoperiod under which the photoperiodic stress affects the lifespan of leaves	hours
phosat_p	Saturating photoperiod	hours
pHvols_G	Parameter used to calculate the variation of soil pH after the addition of slurry	pH
phyllotherme_p	Thermal duration between the apparition of two successive leaves on the main stem	degree days
plNmin_G	Minimal amount of rain required to start an automatic N fertilisation	mm day ⁻¹
pluibat_S	Minimal amount of rain required to create a soil crust (a value must be given but if in the plt.xml the vigurebat parameter is equal to 1 then the parameter is inactive)	mm day ⁻¹
pminruis_G	Minimal amount of rain required to produce runoff	mm day ⁻¹
Pns_C	Density of the new snow	kg m ⁻³
potgermi_p	Soil water potential below which seed imbibition is impeded	MPa
primingmax_G	Maximum priming ratio (relative to SOM decomposition rate)	ND
prof_C	Snow cover threshold for snow insulation	cm
profdenit_S	Soil depth at which denitrification is active (if codedenit is activated)	cm
profdrain_S	Depth of mole drains	cm

Nam_e	Definition	Unit
profhum_S	Maximum soil depth with an active biological activity	cm
profhumrecolteuse_T	Soil depth at which moisture is considered to allow harvesting (if soil compaction is activated)	cm
profhumsemoir_T	Soil depth at which moisture is considered to allow sowing (if soil compaction is activated)	cm
profimper_S	Upper depth of the impermeable layer (from the soil surface)	cm
proflabour_G	Minimal soil depth for ploughing (if soil compaction is activated)	cm
profmes_T	Depth of measurement of the soil water reserve	cm
profnod_p	Maximum depth at which N ₂ fixation by legume crops is possible	cm
profres_T	Upper depth of organic residue incorporation	cm
profsem_T	Depth of sowing	cm
proftrav_T	Maximum depth affected by soil tillage	cm
proftravmin_G	Minimal soil depth for chisel tillage (if soil compaction is activated)	cm
prophumtassrec_G	Soil moisture content (fraction of field capacity) above which compaction may occur and delay harvest	ND
prophumtasse_G	Soil moisture content (fraction of field capacity) above which compaction may occur and delay sowing	ND
propjgermin_p	Minimal fraction of the duration nbjgerlim when the temperature is higher than the temperature threshold Tdmax	%
proprac_G	Ratio of root mass to aerial mass at harvest	ND
propracfmax_p	Fraction of fine roots emitted in the layer 0-1 cm (in length, maximum value over the root profile)	ND
Propres_p	Maximal fraction of the biomass reserves that can be mobilized from aerial organs in all crops	ND
propresP_p	Maximal fraction of the biomass reserves that can be mobilized from storage organs in perennials	ND
PropresPN_p	Maximal fraction of the N reserves that can be mobilized from storage organs in perennials	ND

Na_me	Definition	Unit
ps _{0_I}	Initial density of the snow cover	kg m ⁻³
psihucc _G	Soil water potential corresponding to field capacity	MPa
psihumin _G	Soil water potential corresponding to wilting point	MPa
psisto _p	Potential of stomatal closing (absolute value)	bars
psiturg _p	Potential of the beginning of decrease of the cellular extension (absolute value)	bars
q _{0_S}	Cumulative soil evaporation above which evaporation rate is decreased	mm
q _{10_P}	Q10 used for the dormancy break calculation	ND
qmulchdec _G	Maximal amount of decomposable mulch	t ha ⁻¹
qmulchrui _{0_G}	Amount of mulch above which runoff is suppressed	t ha ⁻¹
QNperenne _{0_I}	Initial value of nitrogen amount in storage organs in perennial crops	kg ha ⁻¹
QNplante _{0_I}	Initial N amount in the plant (if the option to simulate N and C reserves is not activated)	t ha ⁻¹
QNplantenp _{0_I}	Initial N amount in non-perennial organs of the plant	kg ha ⁻¹
QNpltminINN _G	Minimal amount of N in the plant required to compute INN	kg ha ⁻¹
qres _T	Mass of organic residues added to soil (fresh weight)	t ha ⁻¹
Qtot_N _T	Total amount of mineral N fertilizer applications	kg ha ⁻¹
ra _C	Aerodynamic resistance (used in volatilization module with the PET approach)	s m ⁻¹
rapdia _p	Ratio of coarse roots diameter to fine roots diameter	ND
rapforme _p	Ratio of thickness to width of the crop shape (negative when the base of the form < top)	ND
rapNmindec _G	Slope of the linear relationship between the fraction of mineral N available for residue decomposition and the amount of C in decomposing residues	g g ⁻¹
rapsenturg _p	Threshold soil water content active to simulate water senescence stress as a proportion of the turgor stress	ND

Nam_e	Definition	Unit
ratiodenit_G	Fraction of N ₂ O emitted per unit of N denitrified	ND
ratiodurviel_p	Life span of early leaves expressed as a fraction of the life span of the last leaves emitted DURVIEF	ND
ratiol_T	Water stress index below which irrigation is started in automatic mode (0 in manual mode)	ND
ratioN_G	Nitrogen stress index below which fertilisation is started in automatic mode (0 in manual mode)	ND
rationit_G	Fraction of N ₂ O emitted per unit of N nitrified	ND
ratiosen_p	Fraction of senescent biomass (relative to total biomass)	ND
rayon_p	Average radius of the roots	cm
rdrain_G	Radius of the mole drains	cm
remobres_p	Fraction of daily remobilisable C reserves	day ⁻¹
repracpermax_p	Maximum root biomass relative to total biomass (permanent trophic link)	ND
repracpermin_p	Minimum root biomass relative to total biomass (permanent trophic link)	ND
repracseumax_p	Maximum root biomass relative to total biomass (trophic link by thresholds)	ND
repracseumin_p	Minimum root biomass relative to total biomass (trophic link by thresholds)	ND
resk_T	Parameter 1/2 used to calculate profres (if code_auto_profres = 2): profres = proftrav * (1 - exp(-resk.(proftrav-resz)))	cm ⁻¹
resplmax_p	Maximal reserve of biomass	t ha ⁻¹
ressuite_T	Type of crop residue: roots / whole_crop / straw+roots / stubble+roots / prunings	ND
restemp0_l	Initial biomass of metabolic reserves in the perennial organs	t ha ⁻¹
restit_T	Option of restitution in case of pasture yes (1), no (2)	code, 1 to 2
resz_T	Parameter 2/2 used to calculate profres (if code_auto_profres = 2): profres = proftrav * (1 - exp(-resk.(proftrav-resz)))	cm
rsmin_p	Minimal stomatal resistance of leaves	s m ⁻¹
RTD_p	Root tissue density	g cm ⁻³
rugochisel_T	Roughness length of bare soil after chisel tillage (if soil compaction is activated)	m

Nam_e	Definition	Unit
rugolabour_T	Roughness length of bare soil after mouldboard ploughing (if soil compaction is activated)	m
ruisolnu_S	Fraction of runoff (relative to total rainfall) in a bare soil	ND
scale_tdenitopt_G	Parameter related to the range of optimum temperature for denitrification	ND
scale_tnitopt_G	Parameter related to the range of optimum temperature for nitrification	ND
Sdepth0_I	Initial snow cover depth	m
Sdry0_I	Initial water in solid state in the snow cover	mm
sea_p	Specific area of fruit envelops	cm ² g ⁻¹
sensanox_p	Index of anoxia sensitivity (0 = insensitive, 1 = highly sensitive)	ND
sensiphot_p	Index of photoperiod sensitivity (1 = insensitive, 0 = highly sensitive)	ND
sensrsec_p	Index of root sensitivity to drought (1 = insensitive, 0 = highly sensitive)	ND
separateurrapport_G	Column separator in rapport.sti file	ND
seuilLAlapex_p	Maximal value of LAI+LAlapex when LAlapex is > 0	m ² m ⁻²
seuilmortalle_p	Relative transpiration threshold to calculate tiller mortality	mm day ⁻¹
seuilreconspeupl_p	Tiller density below which the entire population will not be regenerated	m ⁻²
sigmadistalle_p	Parameter used for calculating tiller mortality (gamma law)	ND
slamax_p	Maximum SLA (specific leaf area) of green leaves	cm ² g ⁻¹
slamin_p	Minimum SLA (specific leaf area) of green leaves	cm ² g ⁻¹
spfrmax_p	Maximal sources/sinks value allowing the trophic stress calculation for fruit onset	ND
spfrmin_p	Minimal sources/sinks value allowing the trophic stress calculation for fruit onset	ND
splaimax_p	Maximal sources/sinks value allowing the trophic stress calculation for leaf growing	ND
splaimin_p	Minimal value of ratio sources/sinks for the leaf growth	ND
stade0_I	Crop stage at the beginning of simulation	ND
stadebbchamf_p	Equivalent stage in BBCH-scale (amf = maximum acceleration of leaf growth, end of juvenile phase)	ND

Nam_e	Definition	Unit
stadebbchdebdes_p	Equivalent stage in BBCH-scale (debdes = date of onset of water dynamics in harvested organs)	ND
stadebbchdrp_p	Equivalent stage in BBCH-scale (drp = starting date of filling of harvested organs)	ND
stadebbchfindorm_p	Equivalent stage in BBCH-scale (end of dormancy)	ND
stadebbchflo_p	Equivalent stage in BBCH-scale (flowering)	ND
stadebbchger_p	Equivalent stage in BBCH-scale (germination)	ND
stadebbchlax_p	Equivalent stage in BBCH-scale (lax = maximum leaf area index, end of leaf growth)	ND
stadebbchlev_p	Equivalent stage in BBCH-scale (emergence)	ND
stadebbchmat_p	Equivalent stage in BBCH-scale (maturity)	ND
stadebbchnou_p	Equivalent stage in BBCH-scale (fruit set)	ND
stadebbchplt_p	Equivalent stage in BBCH-scale (sowing)	ND
stadebbchrec_p	Equivalent stage in BBCH-scale (harvest)	ND
stadebbchsen_p	Equivalent stage in BBCH-scale (senescence)	ND
stadecoupdf_T	Stage of automatic cut for forage crops	ND
stage_end_irrigauto_T	Phenological stage for ending automatic irrigations (plt, ger, lev, amf, lax, drp ,flo, sen, rec, mat, debdorm, findorm)	ND
stage_start_irrigauto_T	Phenological stage for starting automatic irrigations (plt, ger, lev, amf, lax, drp ,flo, sen, rec, mat, debdorm, findorm)	ND
stamflax_p	Cumulative thermal time between the stages AMF (maximum acceleration of leaf growth, end of juvenile phase) and LAX (maximum leaf area index, end of leaf growth)	degree days
stdnofno_p	Cumulative thermal time between the beginning and the end of nodulation	degree days
stdordebou_p	Cumulative thermal time between the dormancy break and the bud break	degree days
stdrpd_p	Cumulative thermal time between the DRP stage (starting date of filling of harvested organs) and DEBDES (date of onset of water dynamics in harvested organs)	degree days
stdrpmat_p	Cumulative thermal time between the stages DRP (starting date of filling of harvested organs) and MAT (maturity)	degree days

Na_m_e	Definition	Unit
stdrpnou_p	Cumulative thermal time between the stages DRP (starting date of filling of harvested organs) and NOU (end of setting)	degree days
stemflowmax_p	Maximal fraction of rainfall flowing down along the stems	ND
stfloodrp_p	Cumulative thermal time between FLO (anthesis) and DRP (starting date of filling of harvested organs) (only for indication)	degree days
stfnofvino_p	Cumulative thermal time between the end of the nodulation and the end of the nodule life	degree days
stlaxsen_p	Cumulative thermal time between the stages LAX (maximum leaf area index, end of leaf growth) and SEN (beginning of leaf senescence)	degree days
stlevamf_p	Cumulative thermal time between the stages LEV (emergence) and AMF (maximum acceleration of leaf growth, end of juvenile phase)	degree days
stlevdno_p	Cumulative thermal time between emergence and the beginning of nodulation	degree days
stlevdrp_p	Cumulative thermal time between the stages LEV (emergence) and DRP (starting date of filling of harvested organs)	degree days
stoprac_p	Stage when root growth stops (LAX = maximum leaf area index, end of leaf growth or SEN=beginning of leaf senescence)	ND
stpltger_p	Cumulative thermal time allowing germination	degree days
stressdev_p	Maximum phasic delay allowed due to stresses	ND
stsenlan_p	Cumulative thermal time between the stages SEN (beginning of leaf senescence) and LAN	degree days
stubblevegratio_T	Fraction of unharvested biomass stubble to vegetative biomass at harvest	ND
sucrerec_T	Minimal sugar concentration at harvest (/ fresh matter)	g g ⁻¹ FW
surfapex_p	Equivalent surface of a transpiring apex	m ²
surfouvre1_T	Relative area of the shelter opened the first day of opening	ND
surfouvre2_T	Relative area of the shelter opened the second day of opening	ND

Nam_e	Definition	Unit
surfouvre_{3T}	Relative area of the shelter opened the third day of opening	ND
Swet_{0I}	Initial water in liquid state in the snow cover	mm
swfactmin_p	Minimal value for drought stress index (turfac, swfac, senfac)	ND
SWrf_C	Degree day temperature index for snow refreezing	mm °C ⁻¹ day ⁻¹
tauxexportfauche_T	Fraction of cut which is exported	ND
tauxmortes_{Pp}	Mortality rate of perennial organs	day ⁻¹
tauxrecouv_{kmaxp}	Soil cover rate corresponding to the maximal crop coefficient for water requirement (plant surface / soil surface)	m ² m ⁻²
tauxrecouv_{maxp}	Maximal soil cover rate (plant surface / soil surface)	m ² m ⁻²
tcm_{axp}	Maximum temperature at which growth ceases	°C
tcm_{inp}	Minimum temperature at which growth ceases	°C
tcxstop_p	Temperature beyond which foliar growth stops	°C
tdebgel_p	Temperature below which frost affects plant growth	°C
tdenitopt_gauss_G	Optimum temperature for denitrification	°C
tdmax_p	Maximum temperature above which development stops	°C
tdmaxdeb_p	Maximal temperature for hourly calculation of phasic duration between dormancy and bud breaks	°C
tdmin_p	Minimum temperature below which development stops	°C
tdmindeb_p	Minimal thermal threshold for hourly calculation of phasic duration between dormancy and bud breaks	°C
tdoptdeb_p	Optimal temperature for calculation of phasic duration between dormancy and bud breaks	°C
tem_{axp}	Maximal temperature above which plant growth stops	°C
tem_{inp}	Minimum temperature for development	°C
tempdeshyd_p	Increase in fruit dehydration rate due to the increase in crop temperature (Tcult-Tair)	% °C ⁻¹

Nam_e	Definition	Unit
tempfauche_T	Cumulative thermal time between two cuts of forage crops	degree days
tempnod1_p	Temperature parameter (1/4) used to calculate N fixation by legumes	°C
tempnod2_p	Temperature parameter (2/4) used to calculate N fixation by legumes	°C
tempnod3_p	Temperature parameter (3/4) used to calculate N fixation by legumes	°C
tempnod4_p	Temperature parameter (4/4) used to calculate N fixation by legumes	°C
teopt_p	Optimal temperature (1/2) for plant growth	°C
teoptbis_p	Optimal temperature (2/2) for plant growth	°C
tfroid_p	Optimal temperature for vernalisation	°C
tgelflo10_p	Temperature resulting in 10% of frost damages on flowers and fruits	°C
tgelflo90_p	Temperature resulting in 90% of frost damages on flowers and fruits	°C
tgeljuv10_p	Temperature resulting in 10% of frost damage on LAI (juvenile stage)	°C
tgeljuv90_p	Temperature resulting in 90% of frost damage on LAI (juvenile stage)	°C
tgellev10_p	Temperature resulting in 10% of frost damages on plantlet	°C
tgellev90_p	Temperature resulting in 90% of frost damages on plantlet	°C
tgelveg10_p	Temperature resulting in 10% of frost damage on LAI (adult stage)	°C
tgelveg90_p	Temperature resulting in 90% of frost damage on LAI (adult stage)	°C
tgmin_p	Minimum temperature below which emergence is stopped	°C
tigefeuil_p	Ratio stem (structural part)/leaf	ND
tigefeuilcoupe_p	Ratio stem (structural part)/leaf on the cutting day	ND
tletale_p	Lethal temperature for the plant	°C
tmaxremp_p	Maximal temperature above which grain filling stops	°C
tmaxseuil_C	Maximum temperature when snow cover is higher than prof	°C
Tmf_C	Threshold temperature for snow melting	°C

Nome	Definition	Unit
tmin_mineralisation_G	Minimal temperature for decomposition of humified organic matter	°C
tminremp_p	Minimal temperature below which grain filling stops	°C
tminseuil_C	Minimum temperature when snow cover is higher than prof	°C
tmitmax_G	Maximal temperature above which nitrification stops	°C
tmitmin_G	Minimal temperature below which nitrification stops	°C
tmitopt_G	Optimal temperature (1/2) for nitrification	°C
tmitopt_gauss_G	Optimal temperature (1/2) for nitrification	°C
tmitopt2_G	Optimal temperature (2/2) for nitrification	°C
transplastic_T	Transmission coefficient of the plastic shelter	ND
trefh_G	Reference temperature for decomposition of humified organic matter	°C
trefr_G	Reference temperature for decomposition of organic residues	°C
trmax_C	Maximum air temperature (tmax) above which all precipitation is assumed to be rain	°C
tymax_C	Maximum air temperature (tmax) below which all precipitation is assumed to be snow	°C
tustressmin_p	Water stress index (min(turfac, inns)) below which there is an extra LAI senescence	ND
typecailloux_S	Pebbles type: 1 = Beauce limestone, 2 = Beauce limestone, 3 = Lutetian limestone, 4 = Lutetian Brackish marl and limestone, 5 = morainic gravels, 6 = unweathered flint, sandstone or granite, 7 = weathered granite, 8 = Jurassic limestone 9 = Pebbles from Magneraud	ND
typsol_S	Soil type	ND
udlaimax_p	Ulai from which the rate of leaf growth decreases	ND
upvttapl_T	Thermal time from emergence (UPVT units) driving irrigation	degree days
upvttapN_T	Thermal time from emergence (UPVT units) driving fertilization	degree days
usm_U	Name of the USM	ND

Nam_e	Definition	Unit
Vabs_{2G}	N uptake rate at which fertilizer loss is divided by 2	kg ha ⁻¹ day ⁻¹
variete_T	Cultivar number corresponding to the cultivar name in the plant file	ND
vigueurbat_p	Plant vigor index allowing to emerge through a soil crust	ND
vitirazo_p	Rate of increase of the N harvest index vs time	g g ⁻¹ day ⁻¹
vitircarb_p	Rate of increase of the C harvest index vs time	g g ⁻¹ day ⁻¹
vitircarbT_p	Rate of increase of the C harvest index vs thermal time	g g ⁻¹ degree days ⁻¹
vitno_p	Rate of increase of the potential biological fixation rate after nodule onset, per unit of thermal time	nb degree days ⁻¹
vitprophuile_p	Rate of increase of oil harvest index vs time	g g ⁻¹ day ⁻¹
vitpropsucre_p	Rate of increase of sugar harvest index vs time	g sugar g ⁻¹ day ⁻¹
vitreconspeupl_p	Rate of regeneration of the tiller population	°C ⁻¹
vlaimax_p	Ulai at the inflexion point of the function DELTAI=f(ULAI)	ND
Vmax1_p	Maximum specific N uptake rate with the low affinity transport system	micromole cm ⁻¹ h ⁻¹
Vmax2_p	Maximum specific N uptake rate with the high affinity transport system	micromole cm ⁻¹ h ⁻¹
vnitmax_G	Maximum nitrification rate (if Michaelis-Menten formalism is used)	mg kg ⁻¹ day ⁻¹
voleng_G	Maximal fraction of mineral fertilizer that can be volatilized	ND
vpotdenit_s	Potential rate of denitrification for the whole denitrifying layer	kg ha ⁻¹ day ⁻¹
wdata1_U	Name of the first climate file	ND
wdata2_U	Name of the last climate file	ND
wfpsc_G	WFPS (Water filled porosity space) threshold above which denitrification occurs	ND
Wh_G	N/C ratio of soil humus	g g ⁻¹
Xorgmax_G	Maximal amount of N immobilised in soil derived from the mineral fertilizer	kg ha ⁻¹
y0msrac_G	Minimal amount of root mass at harvest (when aerial biomass is nil)	t ha ⁻¹
yres_G	Carbon assimilation yield by the microbial biomass during crop residues decomposition	ND

Na_m_e	Definition	Unit
z0solnu_s	Roughness length of bare soil	m
zesx_s	Maximal soil depth affected by soil evaporation	cm
zlabour_p	Depth of ploughing (reference profile)	cm
zpen_p	Depth at which root density is 50% of the surface root density (reference profile)	cm
zprlim_p	Maximum depth of the root profile (reference profile)	cm
zr_C	Reference height of meteorological data measurement	m
zrac0_i	Initial depth of root apex of the crop	cm
zracplantule_p	Initial depth of root apex of the plantlet	cm

►► 17.2 Definition of output variables

Name	Definition	Unit
abso(n)	N uptake rate by the crop	kg ha ⁻¹ day ⁻¹
age_prairie	Age of the forage crop since sowing	year
airg(n)	Daily amount of irrigation water	mm day ⁻¹
albedolai	Albedo of the crop including soil and vegetation	ND
allocfruit	Allocation ratio of assimilates to the fruits	0 to 1
amm_1_30	Amount of NH4-N in the soil layer 1 to 30 cm	kg ha ⁻¹
amm_31_60	Amount of NH4-N in the soil layer 31-60 cm	kg ha ⁻¹
amm_61_90	Amount of NH4-N in the soil layer 61-90 cm	kg ha ⁻¹
ammomes	Amount of NH4-N in soil over the depth profmes	kg ha ⁻¹
amptcultmat	Mean daily temperature range (tcult) during the reproductive phase (stages lax - rec)	°C
anit(n)	Daily amount of fertiliser-N added to crop	kg ha ⁻¹ day ⁻¹
anit_engrais(n)	Daily nitrogen provided by fertiliser	kgN ha ⁻¹ j ⁻¹
anit_uree(n)	Amount of animal urine returned to the soil	kgN ha ⁻¹ j ⁻¹
anoxmoy	Index of anoxia over the root depth	0 to 1
AZamm(1)	Amount of NH4-N in soil layer 1	kg ha ⁻¹
AZamm(2)	Amount of NH4-N in soil layer 2	kg ha ⁻¹
AZamm(3)	Amount of NH4-N in soil layer 3	kg ha ⁻¹

Name	Definition	Unit
AZamm(4)	Amount of NH ₄ -N in soil layer 4	kg ha ⁻¹
AZamm(5)	Amount of NH ₄ -N in soil layer 5	kg ha ⁻¹
azlesd	Daily amount of NO ₃ -N leached in mole drains	kg ha ⁻¹ day ⁻¹
AZnit(1)	Amount of NO ₃ -N in soil layer 1	kg ha ⁻¹
AZnit(2)	Amount of NO ₃ -N in soil layer 2	kg ha ⁻¹
AZnit(3)	Amount of NO ₃ -N in soil layer 3	kg ha ⁻¹
AZnit(4)	Amount of NO ₃ -N in soil layer 4	kg ha ⁻¹
AZnit(5)	Amount of NO ₃ -N in soil layer 5	kg ha ⁻¹
azomes	Amount of NO ₃ -N in soil over the depth profmes	kg ha ⁻¹
azsup_by_horizon(1)	Lixiviation under the horizon 1	kgN ha ⁻¹
azsup_by_horizon(2)	Lixiviation under the horizon 2	kgN ha ⁻¹
azsup_by_horizon(3)	Lixiviation under the horizon 3	kgN ha ⁻¹
azsup_by_horizon(4)	Lixiviation under the horizon 4	kgN ha ⁻¹
azsup_by_horizon(5)	Lixiviation under the horizon 5	kgN ha ⁻¹
azsup_under_profmes	Lixiviation under the depth of measurement profmes	kgN ha ⁻¹
bouchon	Index showing if the shrinkage slots are opened (0) or closed (1)	code, 0 to 1
Cb	Amount of C in the microbial biomass decomposing organic residues mixed with soil	kg ha ⁻¹
Cbmulch	Amount of C in the microbial biomass decomposing organic residues at soil surface (mulch)	kg ha ⁻¹
cdemande	Cumulative amount of N needed by the plant (plant needs)	kg ha ⁻¹
cEdirect	Total evaporation (water evaporated by the soil + intercepted by leaves and mulch) integrated over the cropping season	mm
cEdirecttout	Total evaporation (water evaporated by the soil + intercepted by leaves and mulch) integrated over the simulation period	mm
cep	Cumulative transpiration over the cropping season of plant 1	mm
cep2	Cumulative transpiration over the cropping season of plants 1 and 2	mm
ces	Cumulative evaporation over the cropping season	mm
cestout	Cumulative evaporation over the simulation period	mm

Name	Definition	Unit
cet_from_lev	Cumulative evapotranspiration over the cropping season (from emergence or budbreak)	mm
cet_from_plt	Cumulative evapotranspiration over the cropping season (from planting or budbreak)	mm
cet	Cumulative evapotranspiration over the cropping season	mm
cetm	Cumulative maximum evapotranspiration over the cropping season	mm
Cetmtout	Cumulative maximum evapotranspiration over the simulation period	mm
cetp	Cumulative potential evapotranspiration (PET) over the cropping season	mm
chargefruit	Number of filling grains or ripe fruits	m ⁻²
Chuma	Amount of active C in humified organic matter	kg ha ⁻¹
Chumi	Amount of inert C in humified organic matter	kg ha ⁻¹
Chumt	Amount of C in humified organic matter (active + inert fractions)	kg ha ⁻¹
cintermulch	Cumulative amount of rain intercepted by the mulch	mm
cinterpluie	Cumulative amount of rain intercepted by the leaves	mm
Cmulch	Amount of C in the whole plant mulch	kg ha ⁻¹
Cmulchdec	Amount of C in the decomposable mulch	kg ha ⁻¹
Cmulchnd	Amount of C in the non decomposable mulch	kg ha ⁻¹
CNgrain	N concentration in fruits	% dry weight
Cnondec(1)	Amount of C in the undecomposable mulch made of residues of type 1	kg ha ⁻¹
Cnondec(10)	Amount of C in the undecomposable mulch made of residues of type 10	kg ha ⁻¹
Cnondec(2)	Amount of C in the undecomposable mulch made of residues of type 2	kg ha ⁻¹
Cnondec(3)	Amount of C in the undecomposable mulch made of residues of type 3	kg ha ⁻¹
Cnondec(4)	Amount of C in the undecomposable mulch made of residues of type 4	kg ha ⁻¹
Cnondec(5)	Amount of C in the undecomposable mulch made of residues of type 5	kg ha ⁻¹
Cnondec(6)	Amount of C in the undecomposable mulch made of residues of type 6	kg ha ⁻¹

Name	Definition	Unit
Cnondec(7)	Amount of C in the undecomposable mulch made of residues of type 7	kg ha ⁻¹
Cnondec(8)	Amount of C in the undecomposable mulch made of residues of type 8	kg ha ⁻¹
Cnondec(9)	Amount of C in the undecomposable mulch made of residues of type 9	kg ha ⁻¹
CNplante	N concentration in the aboveground plant	% dry weight
CO2(n)	Atmospheric CO2 concentration above 330 ppm	ppm
CO2hum	Daily amount of CO2-C emitted due to the mineralisation of soil humus	kg ha ⁻¹ day ⁻¹
CO2res	Daily amount of CO2-C emitted due to the mineralisation of organic residues	kg ha ⁻¹ day ⁻¹
CO2sol	Daily amount of CO2-C emitted due to soil mineralisation (humus and organic residues)	kg ha ⁻¹ day ⁻¹
codebbch_output	Code of the bbch stage (see plant file)	0 to 99
concN_W_drained	Daily nitrate concentration in drainage water	mg NO3 l ⁻¹ day
concNO3les	Nitrate concentration in drained water	mg NO3 l ⁻¹
concNO3sol(1)	Nitrate concentration in soil layer 1	mg NO3 l ⁻¹
concNO3sol(2)	Nitrate concentration in soil layer 2	mg NO3 l ⁻¹
concNO3sol(3)	Nitrate concentration in soil layer 3	mg NO3 l ⁻¹
concNO3sol(4)	Nitrate concentration in soil layer 4	mg NO3 l ⁻¹
concNO3sol(5)	Nitrate concentration in soil layer 5	mg NO3 l ⁻¹
condenit	Ratio of actual to potential denitrifying rate	0 to 1
couvermulch	Cover ratio of mulch	0 to 1
cpluie	Cumulative amount of rain over the simulation period	mm
cprecip	Cumulative water supply over the cropping season (precipitation + irrigation)	mm
cprecipout	Cumulative water supply over the simulation period (precipitation + irrigation)	mm
Cr	Amount of C in organic residues mixed with soil in the profhum layer	kg ha ⁻¹
Cresiduprofil(1)	Amount of C in residues over the soil depth profhum in the residue type 1	kg ha ⁻¹
Cresiduprofil(10)	Amount of C in residues over the soil depth profhum in the residue type 10	kg ha ⁻¹
Cresiduprofil(2)	Amount of C in residues over the soil depth profhum in the residue type 2	kg ha ⁻¹
Cresiduprofil(3)	Amount of C in residues over the soil depth profhum in the residue type 3	kg ha ⁻¹

Name	Definition	Unit
Cresiduprofil(4)	Amount of C in residues over the soil depth profhum in the residue type 4	kg ha ⁻¹
Cresiduprofil(5)	Amount of C in residues over the soil depth profhum in the residue type 5	kg ha ⁻¹
Cresiduprofil(6)	Amount of C in residues over the soil depth profhum in the residue type 6	kg ha ⁻¹
Cresiduprofil(7)	Amount of C in residues over the soil depth profhum in the residue type 7	kg ha ⁻¹
Cresiduprofil(8)	Amount of C in residues over the soil depth profhum in the residue type 8	kg ha ⁻¹
Cresiduprofil(9)	Amount of C in residues over the soil depth profhum in the residue type 9	kg ha ⁻¹
crg	Cumulative global radiation over the cropping season	MJ m ⁻²
crgtout	Cumulative global radiation over the simulation period	MJ m ⁻²
Crprof	Amount of C in deep organic residues mixed with soil (below the profhum depth)	kg ha ⁻¹
Crtout	Total amount of C in organic residues present over the whole soil profile	kg ha ⁻¹
CsurNrac	C/N ratio of living roots	g g ⁻¹
CsurNracmort	C/N ratio of dead roots (cumulative)	g g ⁻¹
CsurNres_pature	C/N ratio of residues in case of pasture	g g ⁻¹
CsurNsol	C/N ratio of soil organic matter in the profhum layer	g g ⁻¹
ctairtout	Cumulative air temperature (tair) over the simulation period	°C
ctcult	Cumulative crop temperature (tcult) over the cropping season	°C
ctculttout	Cumulative crop temperature (tcult) over the simulation period	°C
ctetptout	Cumulative potential evapotranspiration (pet) over the simulation period	mm
ctmoy	Cumulative air temperature over the cropping season	°C
cum_et0_from_lev	Cumulative maximum evapotranspiration over the cropping season from germination or budbreak (eop+eos)	mm
cum_et0	Cumulative maximum evapotranspiration over the cropping season (eop+eos)	mm
cum_immob_positif	Cumulative amount of N immobilised by the microbial biomass decomposing residues (positive value)	kg ha ⁻¹

Name	Definition	Unit
cum_immob	Cumulative amount of N immobilised by the microbial biomass decomposing residues	kg ha ⁻¹
cumlracz	Cumulative length of active roots per soil surface	cm cm ⁻²
cumraint	Cumulative intercepted radiation	MJ m ⁻²
cumrg	Cumulative global radiation during the stage sowing-harvest	MJ m ⁻²
cumvminh	Daily amount of N mineralised from humus	kg ha ⁻¹ day ⁻¹
cumvminr	Daily amount of N mineralised from organic residues	kg ha ⁻¹ day ⁻¹
da(1)	Bulk density of the layer 1 (recalculated by the model if codeDSTass is 1)	g cm ⁻³
da(2)	Bulk density of the layer 2 (recalculated by the model if codeDSTass is 1)	g cm ⁻³
date_irrigations(1)	Date of irrigation	julian day
date_irrigations(10)	Date of irrigation	julian day
date_irrigations(11)	Date of irrigation	julian day
date_irrigations(12)	Date of irrigation	julian day
date_irrigations(13)	Date of irrigation	julian day
date_irrigations(14)	Date of irrigation	julian day
date_irrigations(15)	Date of irrigation	julian day
date_irrigations(16)	Date of irrigation	julian day
date_irrigations(17)	Date of irrigation	julian day
date_irrigations(18)	Date of irrigation	julian day
date_irrigations(19)	Date of irrigation	julian day
date_irrigations(2)	Date of irrigation	julian day
date_irrigations(20)	Date of irrigation	julian day
date_irrigations(21)	Date of irrigation	julian day
date_irrigations(22)	Date of irrigation	julian day
date_irrigations(23)	Date of irrigation	julian day
date_irrigations(24)	Date of irrigation	julian day
date_irrigations(25)	Date of irrigation	julian day
date_irrigations(26)	Date of irrigation	julian day
date_irrigations(27)	Date of irrigation	julian day
date_irrigations(28)	Date of irrigation	julian day
date_irrigations(29)	Date of irrigation	julian day
date_irrigations(3)	Date of irrigation	julian day

Name	Definition	Unit
date_irrigations(30)	Date of irrigation	julian day
date_irrigations(4)	Date of irrigation	julian day
date_irrigations(5)	Date of irrigation	julian day
date_irrigations(6)	Date of irrigation	julian day
date_irrigations(7)	Date of irrigation	julian day
date_irrigations(8)	Date of irrigation	julian day
date_irrigations(9)	Date of irrigation	julian day
day_after_begin_simul	Number of days from the beginning of simulation	days
day_after_emergence	Number of days after emergence	days
day_after_sowing	Days after sowing or planting	days
day_cut	Cut day	julian day
DCbmulch	Change in C amount in microbial biomass decomposing mulch between the beginning and the end of simulation	kg ha ⁻¹
DChumt	Change in humified organic C in soil between beginning and end of simulation	kg ha ⁻¹
DCmulch	Change in mulch C between the beginning and end of simulation	kg ha ⁻¹
DCr	Change in C of organic residues between beginning and end of simulation	kg ha ⁻¹
DCrprof	Change in deep root C between the beginning and end of simulation	kg ha ⁻¹
deltai(n)	Daily increase in green leaf index per soil surface	m ² m ⁻² day ⁻¹
deltaz	Rate of deepening of the root front	cm day ⁻¹
demande	Daily N requirement of the plant to maximise crop growth	kg ha ⁻¹ day ⁻¹
demandeper	Daily N requirement of the perennial organs to maximise crop growth	kg ha ⁻¹ day ⁻¹
demande rac	Daily N requirement of the roots to maximise crop growth	kg ha ⁻¹ day ⁻¹
demandetot	Daily N requirement of the plant to maximise crop growth after subtracting N fixation	kg ha ⁻¹ day ⁻¹
densite	Actual sowing density	plants m ⁻²
densiteequiv	Equivalent plant density for the understorey crop	plants m ⁻²
dfol	Within the shape leaf density	m ² m ⁻³
diftemp1intercoupe	Mean difference between crop and air temperatures during the vegetative phase (emergence - maximum LAI)	°C

Name	Definition	Unit
diftemp2intercoupe	Mean difference between crop and air temperatures during the reproductive phase (maximum LAI - maturity)	°C
dltags	Daily growth rate of the plantlets	t ha ⁻¹ day ⁻¹
dltaisen	Daily change in the senescent leaf area index	m ² m ⁻² day ⁻¹
dltams(n)	Daily growth rate of the plant	t ha ⁻¹ day ⁻¹
dltamsen	Daily senescence rate of the plant	t ha ⁻¹ day ⁻¹
dltaremobil	Daily amount of perennial reserves remobilised	t ha ⁻¹ day ⁻¹
dltaremobilN	Daily amount of perennial N reserves remobilised	kg ha ⁻¹ day ⁻¹
dltmsrac_plante	Pour sorties ArchiSTICS: biomasse journaliere allowee aux racines	g m ² sol
DNbmulch	Change in biomass N associated with the mulch between beginning and end of simulation	kg ha ⁻¹
DNhumt	Change in humified organic N in soil between beginning and end of simulation	kg ha ⁻¹
DNmulch	Change in mulch N between beginning and end of simulation	kg ha ⁻¹
DNr	Change in N of organic residues between begining and end of simulation	kg ha ⁻¹
DNrprof	Change in N of deep dead roots between begining and end of simulation	kg ha ⁻¹
DQNtot2	Change in N content of the two plants (aerial + root + perennial organs) between beginning and end of simulation	kg ha ⁻¹
drain_from_lev	Cumulative amount of water drained at the base of the soil profile during the crop cycle (emergence or budbreak to harvest)	mm
drain_from_plt	Cumulative amount of water drained at the base of the soil profile during the crop cycle (planting to harvest)	mm
drain	Daily amount of water drained at the base of the soil profile	mm day ⁻¹
drat	Cumulative amount of water drained at the base of the soil profile during the simulation period	mm
drlsenmortalle	Root biomass corresponding to dead tillers	t ha ⁻¹ day ⁻¹
DSMN	Change in soil mineral N between beginning and end of simulation	kg ha ⁻¹
DSOC	Change in soil organic C (without residues) between beginning and end of simulation	kg ha ⁻¹

Name	Definition	Unit
DSOtot	Change in total soil organic C (with residues) between beginning and end of simulation	kg ha ⁻¹
DSON	Change in soil organic N (without residues) between beginning and end of simulation	kg ha ⁻¹
DSONtot	Change in total soil organic N (with residues) between beginning and end of simulation	kg ha ⁻¹
DSTN	Change in total soil N (mineral + organic) between beginning and end of simulation	kg ha ⁻¹
dtj(n)	Thermal time for root growth	°C d
dureehumec	Number of hours which are wet (rainy days or days when tcult < dew point)	hour
dureeRH	Number of night hours during which relative humidity exceeds a 90% threshold	hour
durvie(n)	Actual life span of the leaf surface	°C
eai	Equivalent leaf area for ear	m ² m ⁻²
ebmax_gr	Maximum radiation use efficiency during the vegetative stage (AMF-DRP)	g MJ ⁻¹
ebmax	Maximum value of radiation use efficiency	cg MJ ⁻¹
Edirect	Daily amount of water evaporated by the soil + intercepted by leaves and mulch	mm day ⁻¹
efda	Reduction factor on root growth due to physical constraint (through bulk density)	0 to 1
efdensite_rac	Density factor on root growth	0 to 1
efdensite	Density factor on leaf area growth	0 to 1
efNrac_mean	Reduction factor on root growth rate due to mineral N concentration	0 to 1
em_N2O	Daily amount of N2O-N emitted from soil	kg ha ⁻¹ day ⁻¹
em_N2Oden	Daily amount of N2O-N emitted from soil by denitrification	kg ha ⁻¹ day ⁻¹
em_N2Onit	Daily amount of N2O-N emitted from soil by nitrification	kg ha ⁻¹ day ⁻¹
Emd	Daily amount of water directly evaporated after leaves interception	mm day ⁻¹
emulch	Daily amount of water directly evaporated after mulch interception	mm day ⁻¹
eo	Intermediary variable for the computation of evapotranspiration	mm day ⁻¹
eop	Daily maximum transpiration flux	mm day ⁻¹
eos	Daily maximum evaporation flux	mm day ⁻¹

Name	Definition	Unit
ep	Daily actual transpiration flux	mm day ⁻¹
epc_recal(1)	Thickness of the soil layer 1 (recalculated by the model if codeDStass is 1)	cm
epc_recal(2)	Thickness of the soil layer 2 (recalculated by the model if codeDStass is 1)	cm
epc_recal(3)	Thickness of the soil layer 3 (recalculated by the model if codeDStass is 1)	cm
epc_recal(4)	Thickness of the soil layer 4 (recalculated by the model if codeDStass is 1)	cm
epc_recal(5)	Thickness of the soil layer 5 (recalculated by the model if codeDStass is 1)	cm
epsib	Radiation use efficiency	t ha ⁻¹ MJ ⁻¹ m ²
esol	Daily actual soil evaporation flux	mm day ⁻¹
et	Daily evapotranspiration (esol + ep)	mm day ⁻¹
et0	Daily maximum evapotranspiration flux (transpiration + soil evaporation)	mm
etm_etr1moy	Etm/etr ratio on the vegetative phase	0 to 1
etm_etr2moy	Etm/etr ratio on the reproductive phase	0 to 1
etm	Daily maximum evapotranspiration (esol + eop)	mm day ⁻¹
etpp(n)	Daily potential evapotranspiration as given by the formula of Penman	mm day ⁻¹
etr_etm1moy	Etr/etm ratio on the vegetative phase	0 to 1
etr_etm2moy	Etr/etm ratio on the reproductive phase	0 to 1
exces(1)	Amount of water in the macroporosity of the layer 1	mm
exces(2)	Amount of water in the macroporosity of the layer 2	mm
exces(3)	Amount of water in the macroporosity of the layer 3	mm
exces(4)	Amount of water in the macroporosity of the layer 4	mm
exces(5)	Amount of water in the macroporosity of the layer 5	mm
exobiom	Reduction factor on biomass growth due to water excess	0 to 1
exofac	Waterlogging index	0 to 1
exofac1moy	Mean value of the waterlogging index during the vegetative stage (emergence - fruit establishment)	0 to 1
exofac2moy	Mean value of the waterlogging index during the reproductive stage (fruit establishment - maturity)	0 to 1

Name	Definition	Unit
exolai	Reduction factor on leaf growth due to water excess	0 to 1
fapar	Proportion of the radiation intercepted	0 to 1
fco2	Specie-dependant CO2 effect on radiation use efficiency	ND
fco2s	Specie-dependant CO2 effect on stomate closure	ND
fgelflo	Reduction factor on the number of fruits due to frost	0 to 1
fixmaxvar	Maximal rate of BNF (symbiotic fixation)	kg ha ⁻¹ day ⁻¹
fixpot	Potential rate of BNF (symbiotic fixation)	kg ha ⁻¹ day ⁻¹
fixreel	Actual rate of BNF (symbiotic fixation)	kg ha ⁻¹ day ⁻¹
flurac	Daily amount of N taken up by the plant when N uptake is limited by the plant capacity absorption	kg ha ⁻¹ day ⁻¹
flusol	Daily amount of N taken up by the plant when N uptake is limited by the transfer from soil to root	kg ha ⁻¹ day ⁻¹
fpari_gr	Radiation factor on the calculation of conversion efficiency	g MJ ⁻¹
fpari	Radiation effect on conversion efficiency	g MJ ⁻¹
fpft	Daily sink capacity of fruits	g m ⁻² day ⁻¹
fpv(n)	Daily sink capacity of growing leaves	g m ⁻² day ⁻¹
FsNH3	Daily amount of NH3-N emitted from soil by volatilisation	micro g m ⁻² day ⁻¹
fstressgel	Reduction factor on leaf growth due to frost	0 to 1
ftemp	Reduction factor on biomass growth due to temperature-related epsibmax	0 to 1
fxa	Reduction factor on BNF (symbiotic fixation) due to soil anoxia	0 to 1
fxn	Reduction factor on BNF (symbiotic fixation) due to mineral N concentration	0 to 1
fxt	Reduction factor on BNF (symbiotic fixation) due to soil temperature	0 to 1
fxw	Reduction factor on BNF (symbiotic fixation) due to soil water content	0 to 1
gel1_percent	Proportion of leaves damaged by frost before amf stage (end of juvenile phase)	%
gel1	Stress factor on leaves damaged by frost before amf stage (end of juvenile phase)	0 to 1

Name	Definition	Unit
gel2_percent	Proportion of leaves damaged by frost after amf stage (end of juvenile phase)	%
gel2	Stress factor on leaves damaged by frost after amf stage (end of juvenile phase)	0 to 1
gel3_percent	Proportion of flowers or fruits damaged by frost	%
gel3	Stress factor on flowers or fruits damaged by frost	0 to 1
GHG	Greenhouse Gas emission (CO ₂ + N ₂ O) expressed in CO ₂ eq/ha = $Qem_{N2O44/28296} - DSOC^{*44/12}$	kg ha ⁻¹
grain_dry_weight_mg	Grain unit dry weight	mg
H2Orec_percent	Water content of harvested organs	% fresh weight
H2Orec	Water content of harvested organs	0 to 1
hauteur	Height of canopy	m
HI_C	Harvest index for carbon	0 to 1
HI_N	Harvest index for nitrogen	0 to 1
Hmax	Maximum height of water table between drains	cm
Hnappe	Height of water table affecting plant growth	cm
Hpb	Minimum depth of perched water table	cm
Hph	Maximum depth of perched water table	cm
HR(1)	Water content of the soil layer 1	% dry weight
HR(2)	Water content of the soil layer 2	% dry weight
HR(3)	Water content of the soil layer 3	% dry weight
HR(4)	Water content of the soil layer 4	% dry weight
HR(5)	Water content of the soil layer 5	% dry weight
HR_mm(1)	Water content of the soil layer 1	mm
HR_mm(2)	Water content of the soil layer 2	mm
HR_mm(3)	Water content of the soil layer 3	mm
HR_mm(4)	Water content of the soil layer 4	mm
HR_mm(5)	Water content of the soil layer 5	mm
HR_mm_1_30	Water content of the layer 1-30 cm	mm
HR_mm_31_60	Water content of the layer 31-60 cm	mm
HR_mm_61_90	Water content of the layer 61-90 cm	mm
HR_vol_1_10	Water content of the layer 1-10 cm	mm ⁻³ mm ⁻³
HR_vol_1_30	Water content of the layer 1-30 cm (table)	mm ⁻³ mm ⁻³

Name	Definition	Unit
HR_vol_121_150	Water content of the layer 121-150 cm (table)	mm ⁻³ mm ⁻³
HR_vol_151_180	Water content of the layer 151-180 cm (table)	mm ⁻³ mm ⁻³
HR_vol_31_60	Water content of the layer 31-60 cm (table)	mm ⁻³ mm ⁻³
HR_vol_61_90	Water content of the layer 61-90 cm (table)	mm ⁻³ mm ⁻³
HR_vol_91_120	Water content of the layer 91-120 cm (table)	mm ⁻³ mm ⁻³
huile_percent	Oil content of harvested organs	% fresh weight
huile	Oil content of harvested organs	0 to 1
humair_percent	Air moisture content	% saturation
humair	Air moisture content	0 to 1
humidite_percent	Air moisture content in the canopy	% saturation
humidite	Air moisture content in the canopy	0 to 1
humirac_mean	Reduction factor on root growth due to soil water content (mean value over the root profile)	0 to 1
hur_10_vol	Soil water content in the soil at 10 cm	cm/cm
husup_by_horizon(1)	Drainage under the horizon 1	mm
husup_by_horizon(2)	Drainage under the horizon 2	mm
husup_by_horizon(3)	Drainage under the horizon 3	mm
husup_by_horizon(4)	Drainage under the horizon 4	mm
husup_by_horizon(5)	Drainage under the horizon 5	mm
husup_under_profmes	Drainage under the depth of measurement profmes	mm
iamfs	Date of amf stage (maximum acceleration of leaf growth, end of juvenile phase)	julian day
idebdebs	Date of onset of water dynamics in harvested organs	julian day
idebdorms	Date of entry into dormancy	julian day
idrps	Starting date of filling of harvested organs	julian day
ifindorms	Date of emergence from dormancy	julian day
iflos_minus_150	Date of flowering minus 150 degrees day	julian day
iflos_plus_150	Date of flowering plus 150 degrees day	julian day
iflos	Date of flowering	julian day
igers	Date of germination	julian day
ilans	Date of lan stage (leaf index nil)	julian day
ilaxs	Date of lax stage (leaf index maximum)	julian day
ilevs	Date of emergence	julian day
imats	Date of start of physiological maturity	julian day

Name	Definition	Unit
imontaisons	Date of start of stem elongation	julian day
infil_recal(1)	Infiltrability parameter at the base of the layer 1	mm day ⁻¹
infil_recal(2)	Infiltrability parameter at the base of the layer 2	mm day ⁻¹
infil_recal(3)	Infiltrability parameter at the base of the layer 3	mm day ⁻¹
infil_recal(4)	Infiltrability parameter at the base of the layer 4	mm day ⁻¹
infil_recal(5)	Infiltrability parameter at the base of the layer 5	mm day ⁻¹
inn	Nitrogen nutrition index (NNI)	0 to 2
inn1intercoupe	Average NNI during the cut (cut crop vegetative phase: emergence to maximum LAI)	0 to 2
inn1moy	Average NNI during the vegetative stage	0 to 2
inn2intercoupe	Average NNI during the cut (cut crop reproductive phase: maximum LAI to maturity)	0 to 2
inn2moy	Average NNI during the reproductive stage	0 to 2
innlai	Reduction factor on leaf growth due to NNI (nitrogen deficiency)	innmin to 1
inns	Reduction factor on biomass growth due to NNI (nitrogen deficiency)	innmin to 1
innsenes	Nitrogen stress index affecting leaves death	innmin to 1
inous	Ending date for setting of harvested organs	julian day
intermulch	Daily amount of water intercepted by the mulch (vegetal)	mm day ⁻¹
interpluie	Daily amount of water intercepted by leaves	mm day ⁻¹
iplts	Date of sowing or planting	julian day
irazo(n)	Nitrogen harvest index	0 to 1
ircarb(n)	Carbon harvest index	0 to 1
irecs	Date of harvest (first if several)	julian day
irrigjN	Daily amount of mineral N added by irrigation	kg ha ⁻¹ day ⁻¹
irrigN	Cumulative amount of mineral N added by irrigation	kg ha ⁻¹
isens	Date of beginning leaf senescence stage	julian day
izrac	Water excess stress index on roots	0 to 1
lai(n)	Leaf area index (table)	m ² m ⁻²

Name	Definition	Unit
lai_mx_av_cut	LAI before cut (for cut crops , for others = lai(n))	ND
laimax	Maximum leaf area index	m ² m ⁻²
laisen(n)	Leaf area index of senescent leaves (table)	m ² m ⁻²
largeur	Width of the plant shape	m
leaching_from_lev	Cumulative amount of NO ₃ -N leached at the base of the soil profile during the crop cycle (emergence or budbreak to harvest)	kg ha ⁻¹
leaching_from_plt	Cumulative amount of NO ₃ -N leached at the base of the soil profile during the crop cycle (planting to harvest)	kg ha ⁻¹
leai	Leaf+ear area index = lai +eai	m ² m ⁻²
lessiv	Daily amount of NO ₃ -N leached at the base of the soil profile	kg ha ⁻¹ day ⁻¹
lracf(1)	Root length density of fine roots in layer 1	cm cm ⁻³
lracf(2)	Root length density of fine roots in layer 2	cm cm ⁻³
lracf(3)	Root length density of fine roots in layer 3	cm cm ⁻³
lracf(4)	Root length density of fine roots in layer 4	cm cm ⁻³
lracf(5)	Root length density of fine roots in layer 5	cm cm ⁻³
lracg(1)	Root length density of coarse roots in layer 1	cm cm ⁻³
lracg(2)	Root length density of coarse roots in layer 2	cm cm ⁻³
lracg(3)	Root length density of coarse roots in layer 3	cm cm ⁻³
lracg(4)	Root length density of coarse roots in layer 4	cm cm ⁻³
lracg(5)	Root length density of coarse roots in layer 5	cm cm ⁻³
LRACH(1)	Root length density in soil layer 1	cm cm ⁻³
LRACH(2)	Root length density in soil layer 2	cm cm ⁻³
LRACH(3)	Root length density in soil layer 3	cm cm ⁻³
LRACH(4)	Root length density in soil layer 4	cm cm ⁻³
LRACH(5)	Root length density in soil layer 5	cm cm ⁻³
lracsentotf	Cumulative length of senescent roots	cm root cm ⁻² soil
lracsentotg	Cumulative length of senescent roots	cm root cm ⁻² soil
mabois	Biomass removed by pruning	t ha ⁻¹
maenfruit	Biomass of harvested organ envelops	t ha ⁻¹
mafauche	Biomass of forage cuts	t ha ⁻¹
mafauchetot	Cumulative biomass of forage cuts	t ha ⁻¹

Name	Definition	Unit
mafeuille_kg_ha	Dry matter of leaves	kg ha ⁻¹
mafeuille	Biomass of leaves	t ha ⁻¹
mafeuillejaune	Biomass of yellow leaves	t ha ⁻¹
mafeuilletombe	Biomass of fallen leaves	t ha ⁻¹
mafeuilletombefauche	Biomass of fallen leaves between two cuts	t ha ⁻¹
mafeuilleverte	Biomass of green leaves	t ha ⁻¹
mafou	Biomass of harvested organs for cut crops	t ha ⁻¹
mafrais	Aboveground fresh matter	t ha ⁻¹
mafruit_kg_ha	Dry matter of harvested organs	kg ha ⁻¹
mafruit	Biomass of harvested organs	t ha ⁻¹
maperenne	Biomass of perennial organs	t ha ⁻¹
maperennemort	Biomass of dead perennial organs	t ha ⁻¹
masec(n)	Biomass of aboveground plant (table)	t ha ⁻¹
masec_kg_ha	Aboveground dry matter	kg ha ⁻¹
masec_mx_av_cut	Aboveground dry matter before cut (for cut crops, for others = masec(n))	t ha ⁻¹
masecneo	Biomass of newly-formed organs	t ha ⁻¹
masecnp	Biomass of aerals and non perennial organs	t ha ⁻¹
masectot	Total plant biomass (aerials + roots + perennial organs)	t ha ⁻¹
masecveg	Biomass of vegetative organs	t ha ⁻¹
matigestruc_kg_ha	Dry matter of stems (only structural parts)	kg ha ⁻¹
matigestruc	Biomass of stems (only structural parts)	t ha ⁻¹
matuber	Biomass of tuber (harvested organs, only calculated for sugarbeet)	t ha ⁻¹
mean_swfac_flo_p_m_150	Swfac mean on the period flowering minus 150 degrees day to flowering plus 150 degrees days	0 to 1
mortalte	Daily number of dying tillers	day ⁻¹
mortmasec	Cumulative biomass of dead tillers	t ha ⁻¹
mortreserve	Biomass of reserves corresponding to dead tillers	t ha ⁻¹ day ⁻¹
MSexporte	Cumulative amount of harvested biomass	t ha ⁻¹
msjaune	Senescent biomass of the plant	t ha ⁻¹
msneojaune	Newly-formed senescent biomass	t ha ⁻¹
msrac(n)	Biomass of roots	t ha ⁻¹
msracf(1)	Biomass of fine roots in layer 1	t ha ⁻¹
msracf(2)	Biomass of fine roots in layer 2	t ha ⁻¹

Name	Definition	Unit
msracf(3)	Biomass of fine roots in layer 3	t ha ⁻¹
msracf(4)	Biomass of fine roots in layer 4	t ha ⁻¹
msracf(5)	Biomass of fine roots in layer 5	t ha ⁻¹
msracg(1)	Biomass of coarse roots in layer 1	t ha ⁻¹
msracg(2)	Biomass of coarse roots in layer 2	t ha ⁻¹
msracg(3)	Biomass of coarse roots in layer 3	t ha ⁻¹
msracg(4)	Biomass of coarse roots in layer 4	t ha ⁻¹
msracg(5)	Biomass of coarse roots in layer 5	t ha ⁻¹
msracmort	Biomass of dead roots	t ha ⁻¹
msracmortf(1)	Cumulative biomass of dead fine roots in layer 1	t ha ⁻¹
msracmortf(2)	Cumulative biomass of dead fine roots in layer 2	t ha ⁻¹
msracmortf(3)	Cumulative biomass of dead fine roots in layer 3	t ha ⁻¹
msracmortf(4)	Cumulative biomass of dead fine roots in layer 4	t ha ⁻¹
msracmortf(5)	Cumulative biomass of dead fine roots in layer 5	t ha ⁻¹
msracmortg(1)	Cumulative biomass of dead coarse roots in layer 1	t ha ⁻¹
msracmortg(2)	Cumulative biomass of dead coarse roots in layer 2	t ha ⁻¹
msracmortg(3)	Cumulative biomass of dead coarse roots in layer 3	t ha ⁻¹
msracmortg(4)	Cumulative biomass of dead coarse roots in layer 4	t ha ⁻¹
msracmortg(5)	Cumulative biomass of dead coarse roots in layer 5	t ha ⁻¹
msrec_fou_coupe	Dry matter of harvested organs for forages at cutting	t ha ⁻¹
msrec_fou_tot	Dry matter of harvestable organs for forages cumulated over the USM	t ha ⁻¹
msrec_fou	Biomass of harvested forage	t ha ⁻¹
MSrecycle	Cumulative amount of biomass returned to soil (unexported at harvest + fallen leaves)	t ha ⁻¹
msresjaune	Senescent residual dry matter	t ha ⁻¹
mstot	Biomass of whole plant (aerial + root + perennial organs)	t ha ⁻¹
N_mineralisation	Cumulative amount of N mineralized from humus and organic residues	kg ha ⁻¹

Name	Definition	Unit
n_tot_irrigations	Total number of irrigations	ND
N_volatilisation	Cumulative amount of N volatilised from fertilizer and organic inputs	kg ha ⁻¹
nb_days_frost_amf_120	Number of days of tcultmin < tdebgel from amf stage to amf+120 degrees day	days
nb_days_humair_gt_90_percent1	Number of days when humair_percent >=90% between amf and lax	days
nb_days_humair_gt_90_percent2	Number of days when humair_percent >=90% between lax and drp	days
Nb	Amount of N in the microbial biomass decomposing organic residues mixed with soil	kg ha ⁻¹
nbfeuille	Number of leaves on main stem	ND
nbinflo_recal	Number of inflorescences per plant	ND
nbj0remp	Number of shrivelling days	days
nbjechaudage	Number of shrivelling days between lax and rec	days
nbjgel	Number of frosting days active on the plant	days
nbjpourdecirecolte	Number of days until harvest is launched when it is postponed by the harvest decision option	days
nbjpourdecisemis	Number of days until sowing is launched when it is postponed by the sowing decision option	days
Nbmulch	Amount of N in microbial biomass decomposing the decomposable mulch	kg ha ⁻¹
NCbio	N/C ratio of biomass decomposing organic residues	ND
Ndenit	Daily denitrification rate in soil (if option denitrification is activated)	kg ha ⁻¹ day ⁻¹
Ndfa	Proportion of total plant N issued from N fixation	0 to 1
Nexporte	Cumulative amount of N removed by crop harvests	kg ha ⁻¹
nfruit(1)	Number of fruits in box 1	ND
nfruit(2)	Number of fruits in box 2	ND
nfruit(3)	Number of fruits in box 3	ND
nfruit(4)	Number of fruits in box 4	ND
nfruit(5)	Number of fruits in box 5	ND
nfruit(nboite-1)	Number of fruits in last but one box	ND
nfruit(nboite)	Number of fruits in last box	ND

Name	Definition	Unit
nfruitnou	Number of set fruits	fruits m ⁻²
Nhuma	Amount of N in active soil organic matter	kg ha ⁻¹
Nhumi	Amount of N in inert soil organic matter	kg ha ⁻¹
Nhumt	Amount of N in humus soil organic matter (active + inert fractions)	kg ha ⁻¹
nit_1_30	Amount of NO ₃ -N in the soil layer 1 to 30 cm	kg ha ⁻¹
nit_31_60	Amount of NO ₃ -N in the soil layer 31 to 60 cm	kg ha ⁻¹
nit_61_90	Amount of NO ₃ -N in the soil layer 61 to 90 cm	kg ha ⁻¹
nitcult(n)	Number of iterations to calculate tcult	ND
nitrijf	Daily nitrification rate in soil (if option nitrification is activated)	kg ha ⁻¹
Nmineral_from_lev	Cumulative amount of N mineralized during the crop cycle (emergence or budbreak-harvest)	kg ha ⁻¹
Nmineral_from_plt	Cumulative amount of N mineralized during the crop cycle (sowing-harvest)	kg ha ⁻¹
Nmulch	Amount of N in the plant mulch	kg ha ⁻¹
Nmulchdec	Amount of N in the decomposable mulch	kg ha ⁻¹
Nmulchnd	Amount of N in the non decomposable mulch	kg ha ⁻¹
Nnondec(1)	Amount of N in the undecomposable mulch derived from residues type 1	kg ha ⁻¹
Nnondec(10)	Amount of N in the undecomposable mulch derived from residues type 10	kg ha ⁻¹
Nnondec(2)	Amount of N in the undecomposable mulch derived from residues type 2	kg ha ⁻¹
Nnondec(3)	Amount of N in the undecomposable mulch derived from residues type 3	kg ha ⁻¹
Nnondec(4)	Amount of N in the undecomposable mulch derived from residues type 4	kg ha ⁻¹
Nnondec(5)	Amount of N in the undecomposable mulch derived from residues type 5	kg ha ⁻¹
Nnondec(6)	Amount of N in the undecomposable mulch derived from residues type 6	kg ha ⁻¹
Nnondec(7)	Amount of N in the undecomposable mulch derived from residues type 7	kg ha ⁻¹
Nnondec(8)	Amount of N in the undecomposable mulch derived from residues type 8	kg ha ⁻¹
Nnondec(9)	Amount of N in the undecomposable mulch derived from residues type 9	kg ha ⁻¹

Name	Definition	Unit
nodn	Reduction factor on nodulation establishment (potential BNF) due to mineral N stress	0 to 1
Norgeng	Daily amount of N immobilized from fertiliser	kg ha ⁻¹ day ⁻¹
Nr	Amount of N in the decomposing organic residues mixed with soil	kg ha ⁻¹
Nrecycle	Cumulative amount of N returned to soil (unexported at harvest + fallen leaves)	kg ha ⁻¹
Nresiduprofil(1)	Amount of N in organic residues over the profhum depth, derived from residues type 1	kg ha ⁻¹
Nresiduprofil(10)	Amount of N in organic residues over the profhum depth, derived from residues type 10	kg ha ⁻¹
Nresiduprofil(2)	Amount of N in organic residues over the profhum depth, derived from residues type 2	kg ha ⁻¹
Nresiduprofil(3)	Amount of N in organic residues over the profhum depth, derived from residues type 3	kg ha ⁻¹
Nresiduprofil(4)	Amount of N in organic residues over the profhum depth, derived from residues type 4	kg ha ⁻¹
Nresiduprofil(5)	Amount of N in organic residues over the profhum depth, derived from residues type 5	kg ha ⁻¹
Nresiduprofil(6)	Amount of N in organic residues over the profhum depth, derived from residues type 6	kg ha ⁻¹
Nresiduprofil(7)	Amount of N in organic residues over the profhum depth, derived from residues type 7	kg ha ⁻¹
Nresiduprofil(8)	Amount of N in organic residues over the profhum depth, derived from residues type 8	kg ha ⁻¹
Nresiduprofil(9)	Amount of N in organic residues over the profhum depth, derived from residues type 9	kg ha ⁻¹
Nrprof	Amount of N in deep organic residues mixed with soil (below the profhum depth)	kg ha ⁻¹
Nrtout	Total amount of N in organic residues present over the whole soil profile	kg ha ⁻¹
Nsurplus_min	Difference between N inputs and outputs to the soil, without organic fertilizer inputs	kg ha ⁻¹

Name	Definition	Unit
Nsurplus	Difference between N inputs and outputs to the soil, including organic fertilizer inputs	kg ha ⁻¹
numcoupe	Cut number	ND
numcult	Crop season number	ND
Nvolat_from_lev	Cumulative amount of N volatilised during the crop cycle(emergence or budbreak-harvest)	kg ha ⁻¹
Nvolat_from_plt	Cumulative amount of N volatilised during the crop cycle (planting-harvest)	kg ha ⁻¹
Nvoleng	Daily amount of N volatilised from fertiliser	kg ha ⁻¹ day ⁻¹
Nvolorg	Daily amount of N volatilised from organic inputs	kg ha ⁻¹ day ⁻¹
offrenod	Daily amount of N fixed symbiotically (BNF)	kg ha ⁻¹ day ⁻¹
p1000grain	1000 grains weight (dry weight)	g
pdsfruit(1)	Weight of fruits in box 1	g m ⁻²
pdsfruit(2)	Weight of fruits in box 2	g m ⁻²
pdsfruit(3)	Weight of fruits in box 3	g m ⁻²
pdsfruit(4)	Weight of fruits in box 4	g m ⁻²
pdsfruit(5)	Weight of fruits in box 5	g m ⁻²
pdsfruit(nboite-1)	Weight of fruits in last but one box	g m ⁻²
pdsfruit(nboite)	Weight of fruits in last box	g m ⁻²
pdsfruitfrais	Weight of fresh fruits	g m ⁻²
penfruit	Ratio of fruit envelops to plant biomass	0 to 1
pfeuil(n)	Ratio of leaves to plant biomass	0 to 1
pfeuiljaune	Ratio of yellow leaves to plant biomass	0 to 1
pfeuilverte(n)	Ratio of green leaves to non-senescent plant biomass	0 to 1
phoi	Photoperiod	hour
pHvol	PH of soil surface as affected by organic residues application (slurry)	ND
pousfruit	Number of fruits transferred from one box to the next	ND
poussracmoy	Mean reduction factor on the root growth due to soil constraints (option true density)	0 to 1
precip	Daily amount of water added to soil (precipitation + irrigation - mulch interception - runoff at the surface)	mm day ⁻¹
precipjN	Daily amount of mineral N added to soil due to precipitation	kg ha ⁻¹ day ⁻¹

Name	Definition	Unit
precipN	Cumulative amount of mineral N added to soil due to precipitation	kg ha ⁻¹
preciprec(n)	Recalculated daily precipitation	mm day ⁻¹
preserve	Proportion of reserve in total plant biomass	0 to 1
profexteau	Average depth of water absorption by plant	cm
profextN	Average depth of N absorption by plant	cm
profnappe	Depth of water table	cm
psibase	Predawn leaf water potential	MPa
ptigestruc	Proportion of structural stems in total plant biomass	0 to 1
q_irrigations(1)	Amount of irrigation	mm
q_irrigations(10)	Amount of irrigation	mm
q_irrigations(11)	Amount of irrigation	mm
q_irrigations(12)	Amount of irrigation	mm
q_irrigations(13)	Amount of irrigation	mm
q_irrigations(14)	Amount of irrigation	mm
q_irrigations(15)	Amount of irrigation	mm
q_irrigations(16)	Amount of irrigation	mm
q_irrigations(17)	Amount of irrigation	mm
q_irrigations(18)	Amount of irrigation	mm
q_irrigations(19)	Amount of irrigation	mm
q_irrigations(2)	Amount of irrigation	mm
q_irrigations(20)	Amount of irrigation	mm
q_irrigations(21)	Amount of irrigation	mm
q_irrigations(22)	Amount of irrigation	mm
q_irrigations(23)	Amount of irrigation	mm
q_irrigations(24)	Amount of irrigation	mm
q_irrigations(25)	Amount of irrigation	mm
q_irrigations(26)	Amount of irrigation	mm
q_irrigations(27)	Amount of irrigation	mm
q_irrigations(28)	Amount of irrigation	mm
q_irrigations(29)	Amount of irrigation	mm
q_irrigations(3)	Amount of irrigation	mm
q_irrigations(30)	Amount of irrigation	mm
q_irrigations(4)	Amount of irrigation	mm
q_irrigations(5)	Amount of irrigation	mm
q_irrigations(6)	Amount of irrigation	mm

Name	Definition	Unit
q_irrigations(7)	Amount of irrigation	mm
q_irrigations(8)	Amount of irrigation	mm
q_irrigations(9)	Amount of irrigation	mm
QCapp	Cumulative amount of organic C added to soil	kg ha ⁻¹
QCO2hum	Cumulative amount of CO ₂ -C emitted due to mineralisation of humus	kg ha ⁻¹
QCO2mul	Cumulative amount of CO ₂ -C emitted due to mineralisation of residues in the mulch	kg ha ⁻¹
QCO2res	Cumulative amount of CO ₂ -C emitted due to mineralisation of residues (including mulch)	kg ha ⁻¹
QCO2sol	Cumulative amount of CO ₂ -C emitted due to heterotrophic respiration (QCO ₂ res + QCO ₂ hum)	kg ha ⁻¹
QCperennemort	Cumulative amount of C in dead perennial organs	kg ha ⁻¹
QCperennemort2	Cumulative amount of C in dead perennial organs of the two plants	kg ha ⁻¹
QCplantetombe	Cumulative amount of C added to soil by fallen leaves due to senescence	kg ha ⁻¹
QCplantetombe2	Cumulative amount of C added to soil by fallen leaves due to senescence for the two plants	kg ha ⁻¹
QCprimed	Cumulative amount of C mineralised by priming effect	kg ha ⁻¹
QCrac	Amount of C in roots	kg ha ⁻¹
QCrac	Amount of C in living roots	kg ha ⁻¹
QCracmort	Cumulative amount of C added to soil by dead roots	kg ha ⁻¹
QCracmort2	Cumulative amount of C added to soil by dead roots of the two plants	kg ha ⁻¹
QCresorg	Cumulative amount of C added to soil through organic exogenous residues	kg ha ⁻¹
QCressuite_tot	Cumulative amount of C added to soil by aerial residues from all harvests	t ha ⁻¹
QCressuite_tot2	Cumulative amount of C added to soil by aerial residues from all harvests of the two plants	kg ha ⁻¹
QCressuite	Cumulative amount of C added to soil due to aerial residues at harvest	kg ha ⁻¹
QCressuite2	Cumulative amount of C added to soil due to aerial residues at harvest for the two plants	kg ha ⁻¹

Name	Definition	Unit
QCrogne	Cumulative amount of C added to soil by fallen leaves due to trimming	kg ha ⁻¹
QCrogne2	Cumulative amount of C added to soil by fallen leaves due to trimming of the two plants	kg ha ⁻¹
Qdrain	Water flow rate in mole drains	mm day ⁻¹
Qdraincum	Cumulative amount of water flowing in mole drains	mm
Qem_N2O	Cumulative amount of N2O-N emitted from soil	kg ha ⁻¹
Qem_N2Oden	Cumulative amount of N2O-N emitted from soil by denitrification	kg ha ⁻¹
Qem_N2Onit	Cumulative amount of N2O-N emitted from soil by nitrification	kg ha ⁻¹
qexport	Biomass exported out of the field	t ha ⁻¹
Qfix	Amount of N fixed symbiotically (BNF) between two cuts	kg ha ⁻¹
Qfixtot	Cumulative amount of N fixed symbiotically (BNF)	kg ha ⁻¹
Qfixtot2	Cumulative amount of N fixed symbiotically (BNF) by the two plants	kg ha ⁻¹
Qles	Cumulative amount of NO3-N leached at the base of the soil profile	kg ha ⁻¹
Qlesd	Cumulative amount of NO3-N leached into mole drains	kg ha ⁻¹
Qmin	Cumulative amount of mineralized N from soil	kg ha ⁻¹
Qminh	Cumulative amount of mineralized N derived from humus decomposition	kg ha ⁻¹
Qminr	Cumulative amount of mineralized N derived from organic residues decomposition	kg ha ⁻¹
qmulch	Biomass of plant mulch	t ha ⁻¹
QNabso	Cumulative N absorbed by the crop (fixation not included)	kg ha ⁻¹
QNabso2	Cumulative N absorbed by the two crops (fixation not included)	kg ha ⁻¹
QNabsoaer	Cumulative N absorbed by the crop and allocated to the aerals	kg ha ⁻¹
QNabsoper	Cumulative N absorbed by the crop and allocated to the perennial organs	kg ha ⁻¹
QNabsorac	Cumulative N absorbed by the crop and allocated to the roots	kg ha ⁻¹

Name	Definition	Unit
QNabsotot	Cumulative N taken up by the crop, including N fixation	kg ha ⁻¹
QNapp	Cumulative amount of organic N added to soil (straw + roots + fallen leaves + organic fertilisers)	kg ha ⁻¹
QNdenit_from_lev	Cumulative amount of N denitrified during the crop cycle (emergence or budbreak-harvest)	kg ha ⁻¹
QNdenit_from_plt	Cumulative amount of N denitrified during the crop cycle	kg ha ⁻¹
QNdenit	Cumulative amount of N denitrified during the simulation period	kg ha ⁻¹
QNexport	Amount of nitrogen exported at harvest (harvested and removed parts)	kg ha ⁻¹
QNexport2	Amount of nitrogen exported at harvest from the two plants	kg ha ⁻¹
QNfauche	Amount of N exported in each cut	kg ha ⁻¹
QNfauchetot	Cumulative amount of N exported by all cuts	kg ha ⁻¹
QNfauchetot2	Cumulative amount of N exported by all cuts of the two plants	kg ha ⁻¹
QNfeuille	N content of structural part of the leaves	kg ha ⁻¹
QNgaz	Cumulative amount of gaseous N losses (through volatilisation and denitrification)	kg ha ⁻¹
QNgrain	Amount of N in harvested organs (grains / fruits)	kg ha ⁻¹
Qnitrif	Cumulative amount of N nitrified in soil (if option nitrification is activated)	kg ha ⁻¹
QNorgeng	Cumulative amount of N immobilized from fertiliser	kg ha ⁻¹
QNperenne	Amount of N in perennial organs	kg ha ⁻¹
QNperennemort	Cumulative amount of N in dead perennial organs	kg ha ⁻¹
QNperennemort2	Cumulative amount of N in dead perennial organs of the two plants	kg ha ⁻¹
QNplante_mx_av_cut	Amount of nitrogen taken up by the plant before cut (for cut crops, for others = QNplante)	kg ha ⁻¹
QNplante	Amount of N in plants (aerial + perennial organs), without roots	kg ha ⁻¹
QNplantenp	Amount of N in non perennial organs (aerials + roots)	kg ha ⁻¹
QNplantetombe	Cumulative amount of N added to soil by fallen leaves	kg ha ⁻¹

Name	Definition	Unit
QNplantetombe2	Cumulative amount of N added to soil by fallen leaves of the two plants	kg ha ⁻¹
QNprimed	Cumulative amount of N mineralised by priming effect	kg ha ⁻¹
QNrac	Amount of N in roots	kg ha ⁻¹
QNracmort	Cumulative amount of N added to soil by dead roots	kg ha ⁻¹
QNracmort2	Cumulative amount of N added to soil by dead roots of the two plants	kg ha ⁻¹
QNresorg	Cumulative amount of organic exogenous N added to soil	kg ha ⁻¹
QNresperenne	Amount of N in perennial reserves	kg ha ⁻¹
QNresperennestruc	Amount of N in the structural pool of perennial organs	kg ha ⁻¹
QNressuite_tot	Cumulative amount of N added to soil by aerial residues from all harvests	kg ha ⁻¹
QNressuite_tot2	Cumulative amount of N added to soil by aerial residues from all harvests of the two plants	kg ha ⁻¹
QNressuite	Cumulative amount of N added to soil by aerial residues at harvest	kg ha ⁻¹
QNressuite2	Cumulative amount of N added to soil by aerial residues of the two plants	kg ha ⁻¹
QNrestemp	Amount of N in temporary reserves of vegetative organs that can be remobilised	kg ha ⁻¹
QNrogne	Cumulative amount of N added to soil due to trimming	kg ha ⁻¹
QNrogne2	Cumulative amount of N added to soil due to trimming of the two plants	kg ha ⁻¹
QNtige	Structural nitrogen content in stems	kg ha ⁻¹
QNtot	Amount of N in whole plant (aerial + root + perennial organs)	kg ha ⁻¹
QNtot2	Amount of N in whole plant (aerial + root + perennial organs) of the two plants	kg ha ⁻¹
QNveg	Amount of N in vegetative organs	kg ha ⁻¹
QNvegstruc	Amount of N in the structural part of vegetative organs	kg ha ⁻¹
QNvoleng	Cumulative amount of N volatilised from fertiliser	kg ha ⁻¹
QNvolorg	Cumulative amount of N volatilised from organic inputs	kg ha ⁻¹
qres_pature	Amount of crop residue by pasture applied to the soil (fresh weight)	t MF ha ⁻¹

STICS soil-crop model

Name	Definition	Unit
Qressuite_tot	Amount of total harvest residues (aerials + roots)	t ha ⁻¹
Qressuite	Biomass of residues from the previous crop returned to soil at harvest (without fallen leaves)	t ha ⁻¹
ra_recal	Aerodynamic resistance between the canopy and the reference level zr	s m ⁻¹
raint	Photosynthetic active radiation intercepted by the canopy	MJ m ⁻²
ras	Aerodynamic resistance between the soil and the canopy	s m ⁻¹
ratioFT	Leaves to stem ratio	ND
Ratm	Atmospheric radiation	MJ m ⁻²
rc	Resistance of canopy	s m ⁻¹
rdif	Ratio of diffuse radiation to global radiation	0 to 1
remobilj	Daily amount of biomass remobilized for growth	kg ha ⁻¹ day ⁻¹
remontee	Capillary uptake from the base of the soil profile	mm day ⁻¹
rendementsec	Biomass of harvested organs (0% moisture)	t ha ⁻¹
resmes	Amount of soil water integrated on the measurement depth	mm
resperenne	Biomass of metabolic reserves in the perennial organs	t ha ⁻¹
resrac	Soil water reserve in the root zone	mm
restemp	Biomass reserves (carbohydrates) in shoots that can be accumulated or mobilized for crop growth	t ha ⁻¹
rfpi	Reduction factor on plant development due to photoperiod	0 to 1
rfvi	Reduction factor on plant development due to vernalization	0 to 1
rlj	Rate of root length growth	m day ⁻¹
rltot	Total root length (accounting for senescent roots)	cm cm ⁻²
rltotf	Total root length (accounting for senescent roots)	cm cm ⁻²
rltotg	Total root length (accounting for senescent roots)	cm cm ⁻²
rmaxi	Maximum water reserve used	mm
rnet	Net radiation	MJ m ⁻²
rnetS	Net radiation at the soil surface	MJ m ⁻²

Name	Definition	Unit
rombre	Fraction of the total radiation in the shade	0 to 1
rsoleil	Fraction of the total radiation in the full sun	0 to 1
RsurRU	Fraction of plant available water over the soil profile	0 to 1
RsurRUrac	Fraction of plant available water over the root profile	0 to 1
RU	Plant available water content over the soil profile	mm
ruissel	Daily amount of water in total runoff (surface + overflow)	mm day ⁻¹
ruisselsurf	Daily amount of water in runoff at soil surface	mm day ⁻¹
ruisselt	Cumulative amount of water in total runoff (surface + overflow)	mm
runoff_from_lev	Cumulative amount of water in runoff (surface + overflow) during the crop cycle (emergence or budbreak-harvest)	mm
runoff_from_plt	Cumulative amount of water in runoff (surface + overflow) during the crop cycle (sowing-harvest)	mm
RUrac	Maximum plant available water content over the root profile	mm
saturation	Amount of water in the soil macroporosity	mm
Sdepth(n)	Snow cover depth	m
senfac	Reduction factor on leaf life span due to water stress (increasing senescence rate)	0 to 1
sla	Specific leaf area	cm ² g ⁻¹
SMN	Amount of soil mineral N content over the soil profile	kg ha ⁻¹
SMNmes	Amount of soil mineral N content over the depth profiles	kg ha ⁻¹
Snowaccu(n)	Daily snowfall accumulation (mm water equivalent)	mm day ⁻¹
Snowmelt(n)	Daily snowmelt (mm water equivalent)	mm day ⁻¹
SOC	Amount of soil organic C (= Chumt + Cb) over the profile depth	kg ha ⁻¹
SOC0	Amount of soil organic C (= Chumt + Cb) over the profile depth at time 0	kg ha ⁻¹
SOCbalance	Soil organic C balance (inputs-outputs) over the whole soil profile	kg ha ⁻¹
SOCinputs	Soil organic C inputs to the whole soil profile	kg ha ⁻¹

STICS soil-crop model

Name	Definition	Unit
SOCL(1)	Amount of soil organic C (= Chumt + Cb) in the layer 1	kg ha ⁻¹
SOCL(2)	Amount of soil organic C (= Chumt + Cb) in the layer 2	kg ha ⁻¹
SOCL(3)	Amount of soil organic C (= Chumt + Cb) in the layer 3	kg ha ⁻¹
SOCL(4)	Amount of soil organic C (= Chumt + Cb) in the layer 4	kg ha ⁻¹
SOCL(5)	Amount of soil organic C (= Chumt + Cb) in the layer 5	kg ha ⁻¹
SOCtot	Amount of soil organic C (all organic pools) over the whole soil profile	kg ha ⁻¹
SoilAvW_by_layers(1)	Amount of plant available water in soil for layer 1	mm
SoilAvW_by_layers(2)	Amount of plant available water in soil for layer 2	mm
SoilAvW_by_layers(3)	Amount of plant available water in soil for layer 3	mm
SoilAvW_by_layers(4)	Amount of plant available water in soil for layer 4	mm
SoilAvW_by_layers(5)	Amount of plant available water in soil for layer 5	mm
SoilAvW	Amount of plant available water in soil over the depth profmes	mm
soilN_rootdepth	Amount of NO3-N in soil in the maximum root depth	kg ha ⁻¹
SoilN	Amount of mineral N in soil over the depth profmes	kg ha ⁻¹
SoilNM	Amount of NO3-N in soil over the depth profmesN	kg ha ⁻¹
SoilWatM	Amount of plant available water in soil over the depth profmesW	mm
som_HUR	Cumulative water content of the soil microporosity	mm
som_sat	Cumulative amount of water in the soil macroporosity	mm
somcour	Cumulative units of development (upvt) between two stages	°C d
somcourdp	Cumulative units of development (upvt) between two reproductive stages	°C d
somcourfauche	Sum of temperature beetwen 2 cuts of forage crop	°C d
somcourmont	Cumulative units of development from the start of vernalisation	°C d

Name	Definition	Unit
somdiffculttair	Cumulative temperature difference (tcult-tair) during the simulation period	°C
somtemp	Sum of temperatures (expressed in Q10 = sum (2.0 ** (udevair ou udevcult / 10.))	°C d
somudevair	Sum of air temperature (udevair) from sowing to harvest	°C
somudevcult	Sum of crop temperature (udevcult) from sowing to harvest	°C
somupvtsem	Sum of development units (upvt) from sowing to harvest	°C
SON	Amount of soil organic N (= Nhumt + Nb) over the profhum depth	kg ha ⁻¹
SON0	Amount of soil organic N (= Nhumt + Nb) over the profhum depth at time 0	kg ha ⁻¹
SONbalance	Soil organic N balance (inputs-outputs) over the whole soil profile	kg ha ⁻¹
SONinputs	Soil organic N inputs to the whole soil profile	kg ha ⁻¹
SONL(1)	Amount of soil organic N (= Nhumt + Nb) in the layer 1	kg ha ⁻¹
SONL(2)	Amount of soil organic N (= Nhumt + Nb) in the layer 2	kg ha ⁻¹
SONL(3)	Amount of soil organic N (= Nhumt + Nb) in the layer 3	kg ha ⁻¹
SONL(4)	Amount of soil organic N (= Nhumt + Nb) in the layer 4	kg ha ⁻¹
SONL(5)	Amount of soil organic N (= Nhumt + Nb) in the layer 5	kg ha ⁻¹
SONtot	Amount of soil organic N (all organic pools) over the whole soil profile	kg ha ⁻¹
sourcepuits	Source to sink ratio of assimilates in the plant	ND
spfruit	Reduction factor on the fruits number due to trophic stress	0 to 1
splai	Source to sink ratio of assimilates in the leaves	ND
stemflow	Daily amount of water runoff along the stem	mm day ⁻¹
STN	Total soil N (mineral + organic)	kg ha ⁻¹
str1intercoupe	Average stomatal water stress index during the vegetative phase (emergence - maximum LAI) of forage crops	0 to 1
str2intercoupe	Average stomatal water stress index during the reproductive phase (maximum LAI - maturity) of forage crops	0 to 1

STICS soil-crop model

Name	Definition	Unit
stu1intercoupe	Average turgescence water stress index during the vegetative phase (emergence - maximum LAI) of forage crops	0 to 1
stu2intercoupe	Average turgescence water stress index during the reproductive phase (maximum LAI - maturity) of forage crops	0 to 1
sucre_percent	Sugar content of harvested organs	% fresh weight
sucre	Sugar content of harvested organs	0 to 1
surf(ao)	Fraction of the soil surface in the shade	0 to 1
surf(as)	Fraction of the soil surface in the sun	0 to 1
swfac	Stomatic water stress index	0 to 1
swfac1moy	Average stomatic water stress index over the vegetative stage	0 to 1
swfac2moy	Average stomatic water stress index over the reproductive stage	0 to 1
tairveille	Mean air temperature at the previous day	°C
taucouv(n)	Cover rate of the canopy	ND
tcult_tairveille	Difference between canopy temperature and air temperature	°C
tcult	Crop surface temperature (daily average)	°C
tcultmax	Crop surface temperature (daily maximum)	°C
tcultmin	Crop surface temperature (daily minimum)	°C
tempeff	Efficient temperature for growth	°C
tetp(n)	Efficient potential evapotranspiration (entered or calculated)	mm day ⁻¹
tetstomate	Threshold of soil water content limiting transpiration and photosynthesis	% vol
teturg	Threshold of soil water content limiting the growth of leaves (in surface area)	% vol
tmax(n)	Maximum active temperature of atmosphere	°C
tmaxext(n)	Maximum temperature of external atmosphere	°C
tmaxrec(n)	Recalculated daily maximum temperature (with presence of a snow cover)	°C
tmin(n)	Minimum active temperature of atmosphere	°C
tminext(n)	Minimum temperature of external atmosphere	°C
tminrec(n)	Recalculated daily minimum temperature (with presence of a snow cover)	°C

Name	Definition	Unit
tmoy(n)	Mean active temperature of atmosphere	°C
tmoyext(n)	Mean temperature of external atmosphere	°C
tmoy pltJuin	Mean temperature from sowing or planting (iplt stage) until June 30	°C
tmoy pltSept	Mean temperature from sowing or planting (iplt stage) until September 30	°C
tncultmat	Average of minimum crop temperatures (tcultmin) between the stages lax and rec	°C
tnhc	Cumulative normalised time for the mineralisation of humus	days
tnrc	Cumulative normalised time for the mineralisation of organic residues	days
totapN	Cumulative amount of mineral N added by mineral fertilisers and organic fertilisers	kg ha ⁻¹
totapNres	Cumulative amount of mineral N added by organic fertilisers	kg ha ⁻¹
totir	Cumulative amount of irrigation water	mm
tpm(n)	Water vapour pressure in air	hPa
trg(n)	Active radiation (entered or calculated)	MJ m ⁻²
trgext(n)	Exterior radiation	MJ m ⁻²
trr(n)	Daily rainfall	mm day ⁻¹
TS(1)	Mean soil temperature (in layer 1)	°C
TS(2)	Mean soil temperature (in layer 2)	°C
TS(3)	Mean soil temperature (in layer 3)	°C
TS(4)	Mean soil temperature (in layer 4)	°C
TS(5)	Mean soil temperature (in layer 5)	°C
tsol(10)	Temperature in the soil at 10 cm	degrees
tsol_mean_0_profsem	Daily min soil temperature on the layer 1 to sowing depth	days
tsol_mean_ger_lev_0_dpthsow	Mean soil temperature on the layer 1 to sowing depth from germination date to emergence	°C d
tsol_mean_plt_ger_0_dpthsow	Mean soil temperature on the layer 1 to sowing depth from sowing date to germination	°C d
tsol_min_0_profsem	Daily mean soil temperature on the layer 1 to sowing depth	days
tsol_min_ger_lev_0_dpthsow	Min soil temperature on the layer 1 to sowing depth from germination date to emergence	°C d
tsol_min_plt_ger_0_dpthsow	Min soil temperature on the layer 1 to sowing depth from sowing date to germination	°C d

Name	Definition	Unit
turfac	Turgescence water stress index	0 to 1
turfac1moy	Average turgescence water stress index during the vegetative stage	0 to 1
turfac2moy	Average turgescence water stress index during the reproductive stage	0 to 1
tustress	Reduction factor on leaf growth due to the effective water stress (= min(turfac, innlai))	0 to 1
tvent(n)	Mean daily wind speed at 2 m high above soil	m s ⁻¹
udevair	Effective temperature for crop development, computed with tair	°C d
udevcult	Effective temperature for crop development, computed with tcult	°C d
ulai(n)	Relative development unit for LAI	0 to 3
upvt(n)	Development unit	°C d
urac	Daily relative development unit for root growth	1 to 3
vitmoy	Mean canopy growth rate	g m ⁻² day ⁻¹
xmlch1	Thickness of the dry layer created by evaporation from the soil and mulch	cm
zrac	Maximum depth reached by root system	cm
zracmax	Maximum rooting depth	cm

►► 17.3 Internal variables definition

Name	Definition	Unit
A_LAI	Shapes of the senescence curve	ND
absoaer	Daily N absorbed by the crop and allocated to the aerals	kg N ha ⁻¹
absodrp	Variable relecting the nitrogen status of the crop from the starting date of filling of harvested organs	ND
absorac	Daily N absorbed by the crop and allocated to the roots	kg N ha ⁻¹
absotot	Daily N taken up by the crop, including N fixation	kg N ha ⁻¹
absz	Actual N uptake in each elementary soil layer	kg N ha ⁻¹ day ⁻¹
aevap	Soil evaporation parameter combining climatic and soils aspects	mm
albsol	Albedo of the soil	ND
alloresp	Daily coefficient of allocation of remobilised biomass between structural and reserves pools of perennial organs	ND

Name	Definition	Unit
amplsurf	Daily thermal amplitude at the surface	°C
amplz	Daily thermal amplitude	°C
anox	Daily index of anoxia over the root depth	0 to 1
azorac	Amount of mineral nitrogen in the rooting zone	kg N ha ⁻¹
B_LAI	Shapes of the growth curve	ND
biorgne	Topped biomass	t ha ⁻¹
bpsisol	Retention curve parameter 2	ND
CCper	Carbon concentration in perennial organs	g C kg ⁻¹ DM
CCrac	Carbon concentration in roots	g C kg ⁻¹ DM
code_diff_rac	1 two types of roots (fine and coarse roots or 2 a single mean type of root	ND
codeinstal	Technical code to describe either seedling or already installed crop	ND
coeflev	Ratio between the emerged and the germinated density depending on non-optimal water content and temperature conditions	ND
coeflevb	Ratio between the emerged and the germinated density depending on the crust layer	ND
concN	Mean nitrate concentration in each elementary soil layer	kg N ha ⁻¹ mm ⁻¹ water
conv	Daily convection flow of N in each elementary soil layer	kg N ha ⁻¹ day ⁻¹
croifruit	Fruit growth	g m ⁻²
crust	Indicator of crust conditions at the soil surface	0/1
CsurNper	C/N ratio of the storage organs	ND
CsurNresid	C/N ratio of falling leaves	ND
CsurNressuite	C/N ratio of calculated crop residue for the next crop	ND
CsurNsol	C to N ratio of soil throughout time	ND
cuh	Chilling hourly units	°C
cumoffrN	Sum of nitrogen soil supply over the profile	kg N ha ⁻¹
da	Bulk soil density	g cm ⁻³
debsenracf	Thermal time units defining the beginning of root senescence for fine roots	°C day ⁻¹
debsenracg	Thermal time units defining the beginning of root senescence for coarse roots	°C day ⁻¹
deltabso	Nitrogen dependant biomass growth	t ha ⁻¹ day ⁻¹

Name	Definition	Unit
deltai_	Daily increase of the green leaf index for determinate crops	m ² leaf m ⁻² soil
deltai_	Daily increase of the green leaf index for indeterminate crops	m ² leaf m ⁻² soil
deltai_dens	Density component of deltai	plant m ⁻²
deltai_dev	Phasic development component of deltai	m ² plant ⁻¹ degree day ⁻¹
deltai_stress	Stress component of deltai	ND
deltai_T	Thermal component of deltai	degree days
deltaimax	Maximum increase in leaf expansion	m ² leaf m ⁻² soil
deltamsresen	Senescence rate of residual dry matter after forage crop cutting	t DM ha ⁻¹ day ⁻¹
deltat	Gradient of the relationship between saturation pressure and temperature	mbars
deltatemp	Difference in mean daily temperature inside and outside a greenhouse	°C
deltaz_stress	Stress component of deltaz	ND
deltaz_T	Thermal component of deltaz	cm day ⁻¹
densite_d	Density of dominant plant	plants m ⁻²
densite_u	Density of understorey plant	plants m ⁻²
densiteger	Density of germinated plants	plants m ⁻²
densitelev	Density of emerged plants	plants m ⁻²
devjour	Daily development rate	ND
dfr	Fruit development stage of each age class	ND
dh	Displacement height	m
difdewmin		
diff	Diffusion flow of N in each elementary soil layer	kg N ha ⁻¹ day ⁻¹
diffcult	Is the variation of tcult between two successive days	°C
difNe	Effective diffusion coefficient of nitrate in soil	cm ² day ⁻¹
dis	A voir avec Nicolas	?
dltafv	Daily biomass partitioning to the structural part of green leaves	t DM ha ⁻¹
dltamsrac	Daily root growth	t DM ha ⁻¹ day ⁻¹
dtamsracmort	Daily dead root biomass on the root depth	t DM ha ⁻¹ day ⁻¹
dltacQCracmort	Cumulative amount of C lost by dead roots over the soil profile	kg N ha ⁻¹ day ⁻¹
dltacQNracmort	Cumulative amount of N lost by dead roots over the soil profile	kg N ha ⁻¹ day ⁻¹

Name	Definition	Unit
dltaremobsen	Daily biomass remobilised during leaves senescence	t DM ha ⁻¹
dltares	Daily biomass partitioning to the temporary reserves	t DM ha ⁻¹
dltaresper	Daily biomass remobilised from temporary reserves allocated to perennial organs reserves	t DM ha ⁻¹
dltarestemp	Daily biomass remobilised from temporary reserves to perennial organs	t DM ha ⁻¹
dltarestemp	Daily biomass remobilised from temporary reserves to perennial organs	t DM ha ⁻¹
dltat	Daily biomass partitioning to the structural part of stems	t DM ha ⁻¹
dltazo	Daily increase of grain nitrogen content	kgN ha ⁻¹ day ⁻¹
dNdWc		
dos	Saturation deficit within the canopy	mbars
dpHvol	Increase of soil pH after manure application	ND
dpHvolm	Maximum pH increase following the application of slurry (taking into account the amount of inorganic N applied)	ND
drliz	Daily root length emission per elementary layer	cm root cm ⁻³ soil
drlsenf	Length of dead fine roots in layer iz on day n	cm cm ⁻² soil
drlseng	Length of dead coarse roots in layer iz on day n	cm cm ⁻² soil
dsat	Air saturation deficit	mbars
durage	Natural lifespan of leaves	Q10
durviel	Lifespan of a young leal (at the AMF stage) expressed as a proportion of DURVIEF	Q10
durviesup	Increase of lifespan in case of high availability of nitrogen	Q10
E	Snow compaction parameter	mm mm ⁻¹ day ⁻¹
Edirectm	Maximum value of Edirect	mm day ⁻¹
effN	Nitrogen use efficiency	ND
elong	Elongation of the coleoptile	cm
emissa	Emissivity of the atmosphere	0 to 1
Empd	Evaporation from free water on leaves	mm
ePTt	Potential evapotranspiration according to Priestley-Taylor formula	mm day ⁻¹

Name	Definition	Unit
epz	Daily transpiration flow in each elementary soil layer	mm day ⁻¹
estimet	Evapotranspiration estimated from the water balance for the previous day and the climatic demand of the day in case of greenhouse	mm day ⁻¹
esz	Evaporation soil profile	mm day ⁻¹ cm ⁻¹
etmax	Maximum value of daily evaporation flux	W m ⁻²
etmin	Minimum value of daily evaporation flux	W m ⁻²
EVAP	Accumulation of evaporative fluxes (esol, Emd, emulch)	mm
fgeljuv	Frost index acting on LAI during the juvenile phase	ND
fgellev	Frost index acting on plant density during the plantlet phase	ND
fgelveg	Frost index acting on LAI during the vegetative phase	ND
fh	Moisture factor on humus and residue decomposition rates	ND
fluxrac	Potential N uptake rate in each elementary soil layer	kg N ha ⁻¹ day ⁻¹
fluxsol	Daily soil N supply in each elementary soil layer	kg N ha ⁻¹ day ⁻¹
FPH	Soil pH effect on the volatilisation	pH
Fr	Ratio of rain in repartition between rain and snow rain	0 to 1
fracinsol	Insolation fraction	0 to 1
fruis	Proportion of run-off water above the activation threshold (pminruis)	ND
Fs	Ratio of snow in repartition between rain and snow rain	0 to 1
FsNH	Potential ammonia volatilization rate	microgram m ⁻² day ⁻¹
ftemprem	Thermal stress index as a function of temperature using cardinal temperatures (tminrem et tmaxrem)	0 to 1
fth	Temperature factor on humus mineralisation rate	ND
fttr	Temperature factor on residue decomposition rate	ND
gamma	Psychrometric constant	mb °C ⁻¹
gmax	Maximum value of daily soil heat flux	W m ⁻²
gmin	Minimum value of daily soil heat flux	W m ⁻²
grainsnb	Number of grains per square meter	grains m ⁻²

Name	Definition	Unit
ha	Residual soil water content in the sed bed	mm water cm soil ⁻¹
HB	Soil layer between the seedbe and the root front	cm
HCUM	Available water over the rooting zone	mm water g soil ⁻¹ x 100
hmin	Water content at permanent wilting point of macro layer	%weight
hn	Wilting point mean in the seed bed	mm water cm soil ⁻¹
hucc	Elementary layer soil water content at field capacity	mm water cm soil ⁻¹
Hum	Hourly humidity	mm
humin	Elementary layer soil water content at wilting point	mm water cm soil ⁻¹
humirac	Influence of soil water content on germination and root growth	ND
humsol	Soil moisture	mm water cm soil ⁻¹
hur	Microporosity elementary layer soil water content	mm water cm soil ⁻¹
hx	Mean water content at field capacity in the sed bed	mm water cm soil ⁻¹
ilets	Date of the plantlet stage	days
IMB	Date of the beginning of seed moistening	days
inni	Instantaneous nitrogen index	ND
jvi	Vernalizing contribution of a given day	nb days
k	Growth compartment	ND
K	Melting rate	mm °C ⁻¹ day ⁻¹
K_LAI	Maximal LAI produced	m ² m ⁻²
K	Actual mineralisation rate of humus	day ⁻¹
Khum	Potential mineralisation rate of humus	day ⁻¹
kgdiffus	Proportion of diffusive radiation reaching the soil	ND
kgdirect	Proportion of direct radiation reaching the soil	ND
kh	Coefficient of heat transfer in the cold shelter	W m ⁻² K ⁻¹
ks	Coefficient of energy losses between the outside and inside of the shelter	W m ⁻² K ⁻¹
L	Latent heat of vaporization	MJ kg ⁻¹
laieffcum	LAI removed	ND
lairogne	Lai topped	ND

Name	Definition	Unit
lairognecum	Sum of topped leaf area index	m ² m ⁻²
longsperacf	Specific fine root length	cm g ⁻¹
longsperacg	Specific coarse root length	cm g ⁻¹
lracsentot	Total length of senescent roots	cm root cm ⁻² soil
lracsenz	Death root length density at depth z	cm root cm ⁻³ soil
lracz	Efficient root length density	cm root cm ⁻³ soil
M	Snow in the process of melting	mm day ⁻¹
mafraislefeuille	Leaf fresh matter	t ha ⁻¹
mafraisle	Reserve fresh matter	t ha ⁻¹
mafraislestige	Structural stem fresh matter	t ha ⁻¹
masecabso	Biomass accounting for nitrogen absorption	t DM ha ⁻¹
mouill	Water retained on the foliage	mm
mouillmulch	Water retained by the vegetal mulch	mm
Mrf	Liquid water in the snow cover in the process of refreezing	mm day ⁻¹
msracmort	Dead root biomass on the root depth	t ha ⁻¹
nbgraingel	Number of frozen grains per square meter	grains m ⁻²
nbgrains	Number of grains per square meter	grains m ⁻²
nbjgrauto	Days of autotrophy for a moistened seed	days
nbjhumec	Maximal period that seed can be in a moist status without seed death occurs	days
NC	Critical nitrogen content	%
newrac	Root length growth thanks to seed reserve remobilization during germination	m day ⁻¹
NHg	Ammonia concentration in the gaseous soil phase	mol l ⁻¹
NHsurf	Ammonia concentration at the soil surface	microgram N m ⁻³
nhet	Number of days of heterotrophy during germination	day
nit	Amount of NO ₃ -N in an elementary layer	kg N ha ⁻¹
nodn	Coefficient used to take into account the effect of the soil mineral N content on the potential N fixation	ND
Nvolatorg	Volatilizable NH ₄	kg N ha ⁻¹
Nvolorg	Actual ammonia volatilization rate	kg N ha ⁻¹ day ⁻¹
offrN	Mineral N available for root uptake in each elementary soil layer	kg N ha ⁻¹
pgrain	Weight of grains per square meter	g m ⁻²
pgraingel	Weight of frozen grains per square meter	g m ⁻²

Name	Definition	Unit
pHvol	Soil surface pH varying after organic residue application (such as slurry)	ND
potcrofruit	Potential growth of a fruit	g fruit ⁻¹ day ⁻¹
propfixpot	Phenology-dependent coefficient used to calculate potential N fixation	ND
propvolat	Proportion of the volatilizable N fraction of the residue	ND
ps	Density of the snow cover	kg m ⁻³
psisol	Soil potential of the elementary layer	Mpa
psisols	Retention curve parameter 1	MPa
QNplantule	Amount of nitrogen in the plantlet	kg N ha ⁻¹
QNplmax	Maximal amount of N possible in the crop	kg N ha ⁻¹
raa	Aerodynamic resistance between the canopy and the reference height of weather measurements	s m ⁻¹
raamax	Maximum daily value of the aerodynamic resistance between the cover et the reference level zr	W m ⁻²
raamin	Minimum daily value of the aerodynamic resistance between the cover et the reference level zr	W m ⁻²
rac	Resistance of the canopy boundary layer	s m ⁻¹
racinepsi	Efficient root length density participating in predawn potential, located in the moist layers (PSISOL < -1.5 Mpa), else = 0.	cm root cm ⁻³ soil
Ratm	Atmospheric component of the long wave radiation	MJ m ⁻² day ⁻¹
rc	Resistance of canopy	s m ⁻¹
rdiffus	Diffusive radiation	MJ m ⁻² day ⁻¹
rdirect	Direct radiation	MJ m ⁻² day ⁻¹
rdroit	Radiation not intercepted by the crop	MJ m ⁻² day ⁻¹
reprac	Underground/total biomass partitioning coefficient	ND
resperenne	Initial biomass reserve	t ha ⁻¹
rgex	Extraterrestrial radiation	MJ m ⁻² day ⁻¹
Rglo	Long wave radiation	MJ m ⁻² day ⁻¹
rgmax	Maximum daily value of the global radiation	W m ⁻²
rgmin	Minimum daily value of the global radiation	W m ⁻²
rl	Root length density at depth z	cm root cm ⁻³ soil
rlf	Length of fine roots in layer iz on day n	cm cm ⁻² soil

Name	Definition	Unit
rlg	Length of coarse roots in layer iz on day n	cm cm ⁻² soil
rlj_dens	Plant density component of rlj	plant m ⁻²
rlj_dev	Plant density component of rlj	m root plant ⁻¹ degree-day ⁻¹
rlj_stress	Stress component of root length growth rlj	ND
rlj_T	Thermal component of root length growth rlj	°C day ⁻¹
rljfront	Root length growth at the root front	m root m ⁻² day ⁻¹
rnet_PE	Net radiation for Brunt formula	MJ m ⁻²
rnet_PT	Net radiation for Priestley-Taylor evapotranspiration calculation	MJ m ⁻²
rnetmax	Maximum value of daily net radiation	W m ⁻²
rnetmin	Minimum value of daily net radiation	W m ⁻²
rnetP	Net radiation affecting the crop	MJ m ⁻²
RNETP	Net radiation affecting the crop (use for direct evaporation)	MJ m ⁻² day ⁻¹
RNETP	Net radiation affecting the crop (use for transpiration)	MJ m ⁻² day ⁻¹
Rsol	Surface component of the long wave radiation	MJ m ⁻² day ⁻¹
RsRso	Total to extraterrestrial radiation ratio	ND
rtransmis	Radiation transmitted through the crop	MJ m ⁻² day ⁻¹
S_WE	Ratio between the snow water equivalent	mm
sat	Macroporosity elementary layer soil water content	mm water cm soil ⁻¹
SB	Seed bed	cm
sbv	Specific surface area of biomass	cm ² g ⁻¹
sbvmax	Leaf expansion allowed per unit of biomass accumulated	cm ² g ⁻¹
Sdry	Water in solid state in the snow cover	mm
senstress	Effect of the stresses (water and Nitrogen) on the lidespan	0 to 1
sla	Maximum SLA (specific leaf area) of green leaves	cm ² g ⁻¹
somger	Growing degree-days from planting in the seed bed	°C
somsen	Current thermal time for senescence	Q10
ST_LAI	Growing degree-days since emergence	°C
stdebsenrac_p	Life span of roots	°C day ⁻¹
sum_eos	Sum of daily maximum evaporation flux	mm

Name	Definition	Unit
SURFAO	Fraction of surface in the shade	ND
SURFAS	Fraction of surface in the sun	ND
surfouvre	Proportion of vents related to the total surface area of the greenhouse	0 to 1
Swet	Water in liquid state in the snow cover	mm
tair	Mean air temperature (measured)	°C
tdevelop	Sum of temperature for the senescence calculation	Q10
TDEW	Dewpoint temperature	°C
tdewmin		
teaugrain	Water content of (harvested) organs	g g ⁻¹
teta	Available water content in the root zone	cm ³ water cm ⁻³ soil
tetsen	Threshold soil water content accelerating senescence	cm ³ water cm ⁻³ soil
TF_LAI	Growing degree-days for the point of inflexion of the complete senescence	°C
theta_sat	Volumic soil water content at saturation	cm ³ cm ⁻³
TI_LAI	Growing degree-days for the point of inflexion of the growth curve	°C
tmin	Minimum temperature	°C
tnh	Normalised time (day) for humus mineralization	ND
tpm	Vapour pressure in air	mbars
TRECOUVMAXp	Proportion of the soil covered by isolated plant	ND
tsol	Soil temperature	°C
tursla	Mean water stress TURFAC experienced since emergence	ND
TVAR	Saturating vapour pressure as a function of temperature	mbars
Vabs	Specific N absorption capacity of the roots	micromole N h ⁻¹ cm ⁻¹ root
vabsmoy	Nitrogen uptake rate	Kg N ha ⁻¹ day ⁻¹
VABSN	Nitrogen accumulation rate in the plant (uptake and fixation)	kg N ha ⁻¹ day ⁻¹
vnit	Nitrification rate	mg N kg ⁻¹ day ⁻¹
vnitpot	Potential nitrification rate	mg N kg ⁻¹ day ⁻¹
wfps	Water filled pore space	ND
wfpsc	Water filled pore space at field capacity	ND
Wi	Index of soil water availability (0-1)	ND

STICS soil-crop model

Name	Definition	Unit
wsat	Total porosity	ND
XMULCH	Thickness of mulch created by evaporation from the soil	cm
z	Soil elementary layer of 1 cm	cm
z	Crop roughness	m
zs	Soil or understorey crop roughness	m
zdemi	Root depth that ensures at least an extraction near the soil surface of 20% of the water available	cm
znonli	Root depth if no obstacle	cm

Authors list

François Affholder

CIRAD, AIDA
34398, Montpellier cedex 5,
FRANCE
francois.affholder@cirad.fr

Nicolas Beaudoin

INRAE/ retired, BioEcoAgro
2000, Barenton-Bugny
FRANCE
nicolas.beaudoin@inrae.fr

Patrick Bertuzzi

INRAE/ retired, Agroclim
84914, Avignon Cedex 9
FRANCE
patrick.bertuzzi@inrae.fr

Samuel Buis

INRAE, Emmah
84914, Avignon Cedex 9
FRANCE
samuel.buis@inrae.fr

Eric Casellas

INRAE, MIAT
31326, Castanet-Tolosan
FRANCE
eric.casellas@inrae.fr

Florent Chlebowski

INRAE, BioEcoAgro
02000, Barenton-Bugny
FRANCE
florent.chlebowski@outlook.fr

Hugues Clivot

Reims University, FARE
51686, Reims cedex 2
FRANCE
hugues.clivot@univ-reims.fr

Julie Constantin

INRAE, AGIR
31326, Castanet-Tolosan
FRANCE
julie.constantin@inrae.fr

Benjamin Dumont

Liege University, Gembloux Agro-Bio Tech
NA, Gembloux
BELGIUM
benjamin.dumont@ulg.ac.be

Jean-Louis Durand

INRAE, P3F
86600, Lusignan
FRANCE
jean-louis.durand@inrae.fr

Gatien Falconnier

CIRAD, UPR Aida
34398, Montpellier Cedex 5
FRANCE
gatien.falconnier@cirad.fr

Fabien Ferchaud

INRAE, BioEcoAgro
02000, Barenton-Bugny
FRANCE
fabien.ferchaud@inrae.fr

Iñaki García de Cortázar Atauri

INRAE, Agroclim
84914, Avignon Cedex 9
FRANCE
inaki.garciadecortazar@inrae.fr

Anne-Isabelle Graux

INRAE, UMR Pegase
35590, Saint-Gilles
FRANCE
anne-isabelle.graux@inrae.fr

Guillaume Jégo

Agriculture and Agri-Food Canada,
Quebec Research and Development Centre
QC G1V 2J3, Québec, QC
CANADA
guillaume.jego@agr.gc.ca

Eric Justes

CIRAD, Département PERSYST
34060, Montpellier Cedex 2
FRANCE
eric.justes@cirad.fr

Marie Launay

INRAE, Agroclim
84914, Avignon Cedex 9
FRANCE
marie.launay@inrae.fr

Christine Le Bas

INRAE, Infosol
45075, Orleans Cedex
FRANCE
christine.le-bas@inrae.fr

Patrice Lecharpentier

INRAE, Agroclim
84914, Avignon Cedex 9
FRANCE
patrice.lecharpentier@inrae.fr

Joël Léonard

INRAE, BioEcoAgro
02000, Barenton-Bugny
FRANCE
joel.leonard@inrae.fr

Gaetan Louarn

INRAE, P3F
86600, Lusignan
FRANCE
gaetan.louarn@inrae.fr

Bruno Mary

INRAE/ retired, BioEcoAgro
02000, Barenton-Bugny
FRANCE
bruno.mary@inrae.fr

Alain Mollier

INRAE, ISPA
33882, Villenave d'Ornon cedex
FRANCE
alain.mollier@inrae.fr

Dominique Ripoché-Wachter

INRAE, Agroclim
84914, Avignon Cedex 9
FRANCE
dominique.ripoche@inrae.fr

Françoise Ruget

INRAE/ retired, Emmah
84914, Avignon Cedex 9
FRANCE
francoise.ruget@inrae.fr

Laurent Ruiz

INRAE, SAS
35042, Rennes Cedex
FRANCE
laurent.ruiz@inrae.fr

Loïc Strullu

Strullu company
51460, Courtisols
FRANCE
lstrullu@gmail.com

Peter Thorburn

CSIRO Agriculture & Food, Systems program
Qld 4067, St Lucia
AUSTRALIA
peter.thorburn@csiro.au

Remi Vezy

CIRAD, AMAP
34398, Montpellier
FRANCE
remi.vezy@cirad.fr

Cover illustrations: © Brigitte Cauvin, INRAE; © Guy Trébuil, CIRAD

Edition : Teri Jones-Villeneuve
Layout: H  l  ne Bonnet, Studio 9
Printed in June 2023 by IsiPrint
139 rue Rateau – 93120 La Courneuve (France)
Legal deposit: June 2023

The STICS soil-crop model simulates the production and environmental impacts of cropping systems under current and changing climatic conditions. It synthesises a significant share of agronomic knowledge about field and cropping system behaviour. The model algorithms presented in this book mainly draw from literature references in the bioclimatology, soil and crop sciences; the model also considers most management practices. The book is structured to reflect how the crop-soil system is modelled according to weather conditions and farming practices. Each chapter focuses on a set of important functions, such as plant functioning (development initiation, growth, yield formation, water uptake and transpiration) and soil processes of the water cycle and organic matter transformation and associated fluxes.

This new edition integrates all the STICS updates that have been developed, evaluated and published over the last decade. Thanks to the innovative editorial design of this digital format, modellers can develop a research version of the model and users can track changes in the current version. While this book is primarily intended for soil-crop modellers and agronomists using STICS, its many illustrative examples of the processes involved and case studies of crops and cropping systems may be of interest to a wider audience.

Nicolas Beaudoin is an agronomist at INRAE. He evaluated the model prediction for the short and long terms and coordinated the STICS team (2012–2016).

Patrice Lecharpentier is a developer at INRAE. He handles STICS maintenance and tools as well as testing and evaluation of STICS performances.

Dominique Ripoche-Wachter is a computer engineer at INRAE. She has been in charge of developing the source code for the STICS model since the first versions of the model were released.

Loïc Strullu is a freelance researcher who has developed new STICS model formalisms to improve the simulation of perennial crop production and environmental impacts.

Bruno Mary is a senior scientist at INRAE. He developed the STICS modules on crop and soil nitrogen balance.

Joël Léonard is a research scientist at INRAE. His research activities focus on soil N₂O emissions. He developed the N₂O module for the STICS model.

Marie Launay is an agronomist at INRAE. She is involved in climate change impact and adaptation studies. She supervised the development of the STICS module on airborne fungal pathogens.

Éric Justes is a senior scientist and agronomist who spent three decades at INRAE and is currently at CIRAD. He helped develop the model and was also a STICS team coordinator (2016–2022).



MINISTÈRE
DE L'ENSEIGNEMENT
SUPÉRIEUR
ET DE LA RECHERCHE

*Liberté
Égalité
Fraternité*

éditions
Quæ

Éditions Cirad, Ifremer, INRAE
www.quae.com

INRAE

59 €

ISBN : 978-2-7592-3678-7



9 782759 236787

Réf. : 02881